

# **DESIGN AND SYNTHESIS OF INHIBITORS OF THE ANTI-INFECTIVE TARGET ENZYME ISPE**

**DISSERTATION**

zur Erlangung des Grades  
des Doktors der Naturwissenschaften  
der Naturwissenschaftlich-Technischen Fakultät  
der Universität des Saarlandes

von

**Henni-Karoliina Ropponen**

Saarbrücken

2021



**Tag des Kolloquiums:** 01. Juli 2021

**Dekan:** Prof. Dr. Jörn Eric Walter

**Berichterstatter/in:** Prof. Dr. Anna K. H. Hirsch  
Prof. Dr. Uli Kazmaier

**Vorsitzende/r:** Prof. Dr. Christian Ducho

**Akad. Mitarbeiter/in:** Dr. Jennifer Herrmann





Die vorliegende Arbeit wurde von September 2018 bis Februar 2021 unter Anleitung von Frau Prof. Dr. Anna K. H. Hirsch in der Fachrichtung Pharmazeutische und Medizinische Chemie der Naturwissenschaftlich-Technischen Fakultät der Universität des Saarlandes sowie am Helmholtz-Institut für Pharmazeutische Forschung Saarland (HIPS) in der Abteilung Drug Design and Optimization (DDOP) angefertigt.

*“One sometimes finds what one is not looking for.”*

- Sir Alexander Fleming

## Preface

*First of all, I would like to thank Prof. Dr. Anna K. H. Hirsch for welcoming me to her DDOP group. This PhD journey has been full of learnings and I will be forever grateful for your encouragement and trust during this time. Following your previous findings, we have managed to make the next step in IspE research. Special thanks also belong to the Chemical Industry Fund of the German Chemical Industry Association for the Kekulé Mobility Fellowship. Additionally, I would like to express my gratitude for my PhD thesis committee; Prof. Dr. Uli Kazmaier for providing chemistry views and inspiring lectures and Dr. Jennifer Herrmann for giving important biological insights.*

*The IspD/IspE team has grown recently and there is someone, who keeps it all together – my warmest thanks go to Dr. Eleonora Diamanti for the help and guidance in the past years and always remembering the details when needed. The projects have involved many bacterial assays and there Dr. Jörg Haupenthal deserves a big thank for always happily scheduling the wish lists, Jeannine Jung, Dennis-Thomas Jener and Simone Amann, whom I will forever be thankful. I would also like to pass my sincerest thank you for our interns Laura Lucaroni, Miriam Jaki and Johannes Brandstätter and warmly thank the latest IspD/IspE team members, in particular Spyridon Bousis, Dr. Mostafa Hamed and Zhoor Hamid for their contributions to the continuing projects.*

*From the MEP consortium, I would like to warmly thank the MEP enzyme experts Dr. Boris Illarionov, Prof. Dr. Markus Fischer and Prof. Dr. Adelbert Bacher, the malaria expert Dr. Matthias Rottmann and the compound resource and chemistry expert Dr. Matthias Witschel for a smooth collaboration beside their other main duties. In remembrance of Prof. Dr. François Diederich, thank you for connecting the pieces together.*

*From the HIPS collaborations, I would like to thank the drug delivery experts Prof. Dr. Claus-Michael Lehr and Dr. Robert Richter from DDEL. Thank you very much for the uncountable hours of discussions and re-editing – I learnt a lot from you and will hold on to the positivity of you both for keeping always the look ahead. Additionally, I would like to thank Chantal Bader from MINS for the continuous help with the decomposition manuscript. We will both for sure remember the pink fraction.*

*Many great memories and friendships were created during this journey that I will surely remember with a smile; Jelena and the +186, Sandra and the Scheidt talks after Aerial Yoga with Cansu and Christina, Federica and the Zumba classes, Alaa and the walks to German classes, Alwin and the trip to Groningen, Chris and the early mornings, Ravi & Spyros and the virtual screening licenses, Andreas and the COVID plates, Vlad and the happy birthday played on harmonica, Alex and the crave for salt liquorice, Robin and the focusmate sessions, Office 2.29 and the colleagues as well as many others... Thank you for these memories! Here, I would also like to thank the whole DDOP/CBCH team for the friendly atmosphere. Additionally, my extended thanks belong to the DDOP-office and HIPS-IT for all your help and support.*

*Beside the PhD journey, a special thank you goes to the EXPERIO team for all the support, bringing other perspectives and most importantly reminding me of the essentials of research – entdecke & erlebe.*

*This year 2021 marks ten years since I moved abroad. The journey in Scotland, Switzerland and Germany has been filled with many people, who have welcomed me warmly and made the journey unforgettable. Cheerio, merci vielmol and danke schön! This would not have been possible without the support, encouragement and love from my family in Finland. Kiitos paljon! The distance has sometimes been hard but as much as you would had enjoyed me being closer, you have enjoyed visiting the numerous places with long car tours around Europe. Last but not least, the biggest thank you belong to Stephan for always being there for me and ready to explore Saarbrücken and the world together.*

## Short Summary

Global health is facing a serious threat due to increasing multi-drug resistance in microorganisms, making most of the current therapeutic agents ineffective to treat infectious diseases. This study aims to revert this trend by focusing on the discovery of inhibitors of the underexplored enzyme IspE of the 2-C-methyl-D-erythritol 4-phosphate (MEP) pathway.

*Chapter A:* A structure-based virtual screening campaign using *Escherichia coli* IspE afforded a fragment-like hit after filtering based on the eNTRY rules to ensure bacterial accumulation. Multi-parameter optimisation with the support of biophysical assays and structure-based design yielded a novel class of inhibitors, exhibiting activity against the more pathogenic bacteria *Pseudomonas aeruginosa* and *Acinetobacter baumannii*.

*Chapter B:* The known accumulation rules into Gram-negative bacteria were assessed by implementing them to an amino acid modified series. This study reports the expression and purification of *Plasmodium falciparum* IspE, enabling the discovery of its first inhibitors.

*Chapter C:* A prior inhibitor of *Pf*IspE was discovered to suffer from decomposition. Substantial analytical efforts were taken to unravel the real chemical composition for the cause of antimalarial activity.

Overall, this study adds novel chemical entities inhibiting the corresponding IspE enzymes with new molecular insights for structure–permeation relationships and provides key learnings about rule-based design and chemical decomposition.

## Zusammenfassung

Die zunehmende Multiresistenz von Mikroorganismen macht die meisten der heutigen Behandlungsmethoden für Infektionskrankheiten unwirksam und stellt somit eine globale Bedrohung dar. Um dieser Entwicklung entgegenzuwirken, befasst sich diese Studie mit der Entdeckung von Inhibitoren für das Enzym IspE des 2-C-Methyl-D-Erythritol-4-Phosphat-Stoffwechselweges (MEP).

*Kapitel A:* Mittels der eNTRY-Regeln zur Verbesserung der bakteriellen Akkumulation, lieferte ein strukturbasiertes virtuelles Screening an *Escherichia coli* IspE einen fragmentartigen Treffer. Durch eine Multiparameter-Optimierung wurde eine neuartige Inhibitorklasse abgeleitet, die auch gegen die gefährlicheren *Pseudomonas aeruginosa* und *Acinetobacter baumannii* wirksam ist.

*Kapitel B:* Die bekannten Akkumulationsregeln für Gram-negative Bakterien wurden überprüft, indem sie auf Verbindungen mit Aminosäuren angewandt wurden. Hier wird die Expression und Reinigung von *Plasmodium falciparum* IspE beschrieben, welche die Entdeckung erster *PfIspE*-Inhibitoren ermöglichte.

*Kapitel C:* Bei einem *PfIspE*-Inhibitor wurde eine Zersetzungsreaktion festgestellt. Durch eine umfassende Analyse wurde die chemische Zusammensetzung entschlüsselt, die zu der Antimalaria-Aktivität führte.

Insgesamt wurden neue Inhibitoren der verschiedenen IspE-Enzyme entwickelt sowie neue Erkenntnisse über die Struktur-Permeationsbeziehung gewonnen. Außerdem liefert die Studie „Key Learnings“ zu regelbasiertem Wirkstoffdesign und chemischen Zersetzungsreaktionen.

## **Publications Included in this Thesis**

### **Publication 1**

Mastering the Gram-Negative Bacterial Barrier – Chemical Approaches to Increase Bacterial Bioavailability of Antibiotics

H.-K. Ropponen\*, R. Richter\*, A. K. H. Hirsch and C.-M. Lehr,  
*Advanced Drug Delivery Reviews*, **2021**, DOI:10.1016/j.addr.2021.02.014, in press.

\* these authors contributed equally

### **Publication 2**

Assessment of the Rules Related to Gaining Activity against Gram-Negative Bacteria

H.-K. Ropponen, E. Diamanti, A. Siemens, B. Illarionov, J. Hauptenthal, M. Fischer, M. Rottmann, M. Witschel and A. K. H. Hirsch,  
*RSC Medicinal Chemistry*, **2021**, DOI:10.1039/d0md00409j, in press.

### **Publication 3 – under review**

Search for the Active Ingredients from a 2-Aminothiazole DMSO Stock Solution with Antimalarial Activity

H.-K. Ropponen, C. D. Bader, E. Diamanti, B. Illarionov, M. Rottmann, M. Fischer, M. Witschel, R. Müller and A. K. H. Hirsch, *ChemMedChem*, submitted. (Later published as *ChemMedChem*, **2021**, DOI: 10.1002/cmdc.202100067)

*The publications included in this thesis are as their status at the time of the submission of this thesis.*

## Contribution Report

**Introduction - Publication 1:** The author played a key role in conceiving the initial review proposal. She contributed equally with R. Richter for the literature research and thereafter, writing and editing, focusing on the chemical part. She also performed the computational calculations.

**Chapter A:** The author performed the virtual screening, further computational calculations and molecular modelling. She performed the majority of the chemical syntheses and selected the compounds to be purchased. She established the MST protocol and performed the analysis. She contributed to the establishment of TSA as well as STD-NMR assays. She was actively involved in broadening the mutant strain collection and thereby, designing the bacterial assays to exploit the structure–permeation relationships. She analysed the SAR and designed the new derivatives with the support of molecular modelling and computational calculations. She conceived and wrote the manuscript until this point.

**Chapter B - Publication 2:** The author designed the class of compounds and performed the majority of syntheses. She interpreted and summarised the SAR from enzymatic and bacterial assays. She performed the computational calculations and compared them to the literature values, being the foundation for this manuscript. She conceived and wrote the manuscript.

**Chapter C - Publication 3 – *under review*:** The author designed and carried out the analytical investigations of the decompositions using HRMS and NMR. She traced down, characterised the active ingredients and correlated them to enzyme and cellular activities. She helped with the purification of the compounds and performed the computational analysis. She conceived and wrote the manuscript.

## Abbreviations

<b>Aa</b>	<i>Aquifex aeolicus</i> , <i>A. aeolicus</i>
<b>AA</b>	amino acid
<b>ACN</b>	acetonitrile
<b>AMP</b>	adenosine monophosphate
<b>AMR</b>	antimicrobial resistance
<b>ANN</b>	artificial neural networks
<b>aq.</b>	aqueous
<b>ATP</b>	adenosine triphosphate
<b>BBB</b>	blood brain barrier
<b>Bs</b>	<i>Bacillus subtilis</i> , <i>B. subtilis</i>
<b>CDP-ME</b>	4-diphosphocytidyl-2-C-methyl-D-erythritol
<b>CDP-MEP</b>	4-diphosphocytidyl-2-C-methyl-D-erythritol 2-phosphate
<b>clogD<sub>7.4</sub></b>	computationally generated logarithmic partition coefficient of octanol/water at pH 7.4
<b>clogP</b>	computationally generated logarithmic partition coefficient of octanol/water
<b>DBO</b>	diazabicyclooctane
<b>DCM</b>	dichloromethane
<b>DIPEA</b>	<i>N,N</i> -diisopropylethylamine
<b>DMADP</b>	dimethyl allyl diphosphate
<b>DMF</b>	<i>N,N</i> -dimethylformamide
<b>DMSO</b>	dimethylsulfoxide
<b>Ec</b>	<i>Escherichia coli</i> , <i>E. coli</i>
<b>ENR</b>	enoyl-acyl carrier protein reductase
<b>eNTRy-rules</b>	structural rules for accumulation: N = ionisable amine, T = three-dimensionality, R = rigidity
<b>eq.</b>	equivalent
<b>ESBL</b>	extended spectrum $\beta$ -lactamase
<b>ESI</b>	electrospray ionisation
<b>EtOAc</b>	ethyl acetate
<b>EtOH</b>	ethanol
<b>EU/EEA</b>	European Union/Economic European Area
<b>FA</b>	formic acid
<b>FCC</b>	flash column chromatography
<b>FDA</b>	Food and Drug Administration
<b>Fsp<sup>3</sup></b>	the fraction of sp <sup>3</sup> carbon atoms
<b>h</b>	hour
<b>HBTU</b>	hexafluorophosphate benzotriazole tetramethyl uronium
<b>HATU</b>	hexafluorophosphate azabenzotriazole tetramethyl uronium
<b>hERG</b>	human <i>Ether-à-go-go</i> -Related Gene
<b>HMBC</b>	heteronuclear multiple bond correlation



<b>HRMS</b>	high resolution mass spectrometry
<b>HSQC</b>	heteronuclear single quantum coherence
<b>HTS</b>	high-throughput screening
<b>IPDP</b>	isopentenyl diphosphate
<b>IC<sub>50</sub></b>	inhibition concentration 50
<b>IM</b>	inner membrane
<b>GARDP</b>	Global Antibiotic Research and Development Partnership
<b>GBT</b>	gradient boosted trees
<b>GHMP</b>	galactose, homoserine, mevalonate and phosphomevalonate
<b>LCMS</b>	liquid chromatography mass spectrometry
<b>LHS</b>	left-hand side
<b>LogP</b>	common logarithm of the octanol-water partition coefficient
<b>LPS</b>	lipopolysaccharides
<b>M</b>	molar concentration
<b>MALDI-TOF MS</b>	matrix assisted laser desorption ionisation — time of flight mass spectrometry
<b>MD</b>	molecular dynamics
<b>MBL</b>	metallo-β-lactamases
<b>MEP</b>	2-C-methyl-D-erythritol 4-phosphate
<b>MeOH</b>	methanol
<b>MIC</b>	minimum inhibition concentration
<b>min</b>	minute
<b>mL</b>	milliliter
<b>MS</b>	mass spectrometry
<b>MST</b>	microscale thermophoresis
<b>N/A</b>	not applicable
<b>NB</b>	Naïve Bayes
<b>n.d.</b>	not determined
<b>nsp</b>	non-structural protein
<b>NMR</b>	nuclear magnetic resonance
<b>OM</b>	outer membrane
<b>OMVs</b>	outer membrane vesicles
<b>Omp</b>	outer membrane protein
<b>on</b>	overnight
<b>PA</b>	<i>Pseudomonas aeruginosa</i> , <i>P. aeruginosa</i>
<b>PE</b>	phosphatidylethanolamine
<b>Pf</b>	<i>Plasmodium falciparum</i> , <i>P. falciparum</i>
<b>P-gp</b>	p-glycoprotein
<b>PM</b>	plasma membrane
<b>PPI</b>	protein–protein interaction
<b>prep. HPLC</b>	preparative high-performance liquid chromatography
<b>PS</b>	periplasmic space

<b>RdRp</b>	RNA-dependent RNA polymerase
<b>PSA</b>	polar surface area
<b>RF</b>	random forest analysis
<b>RHS</b>	right-hand side
<b>RND</b>	resistance-nodulation-division
<b>rpm</b>	rounds per minute
<b>RT</b>	room temperature
<b>SBDD</b>	structure-based drug design
<b>SBL</b>	serine- $\beta$ -lactamase
<b>SAR</b>	structure–activity relationship
<b>SARS-CoV-2</b>	severe acute respiratory syndrome coronavirus 2
<b>SERF</b>	susceptibility to efflux random forest
<b>SICAR</b>	structure intracellular concentration activity relationship
<b>S-layer</b>	surface layer
<b>SPARK</b>	Shared Platform for Antibiotic Research and Knowledge
<b>SPE</b>	solid-phase extraction
<b>SPR</b>	surface plasmon resonance
<b>STD-NMR</b>	saturation transfer difference-nucleomagnetic resonance
<b>SuFEx</b>	sulfur(VI) fluoride exchange
<b>TBAF</b>	tetrabutylammonium fluoride
<b>TBAI</b>	tetrabutylammonium iodide
<b>TBDT</b>	TonB-dependent transporters
<b>TEA</b>	triethylamine
<b>TOMAS</b>	titrable outer membrane permeability assay system
<b>TFA</b>	trifluoroacetic acid
<b>THF</b>	tetrahydrofuran
<b>TLC</b>	thin layer chromatography
<b>TSA</b>	thermal shift assay
<b>VS</b>	virtual screening
<b>vsurf_A</b>	amphiphilic moment
<b>WaterLOGSY</b>	water-ligand observed <i>via</i> gradient spectroscopy
<b>WHO</b>	World Health Organisation

# Table of Contents

<b>Preface</b> .....	<b>i</b>
<b>Short Summary</b> .....	<b>ii</b>
<b>Zusammenfassung</b> .....	<b>iii</b>
<b>Publications Included in this Thesis</b> .....	<b>iv</b>
<b>Contribution Report</b> .....	<b>v</b>
<b>Abbreviations</b> .....	<b>vi</b>
<b>Table of Contents</b> .....	<b>ix</b>
<b>1.) Introduction</b> .....	<b>1</b>
1.1 The Urge for Increasing Anti-Infective Research.....	1
1.2 MEP Pathway and the Enzyme IspE.....	4
1.3 Mastering the Gram-Negative Bacterial Barrier – Chemical Approaches to Increase Bacterial Bioavailability of Antibiotics <sup>Publication 1</sup> .....	8
<b>2.) Aims of the Thesis</b> .....	<b>55</b>
<b>3.) Results</b> .....	<b>56</b>
3.1 Chapter A: Novel Class Inhibitors of <i>Escherichia coli</i> IspE Originating from a Virtual Screening.....	56
3.2 Chapter B: Assessment of the Rules Related to Gaining Activity against Gram- Negative Bacteria <sup>Publication 2</sup> .....	76
3.3 Chapter C: Search for the Active Ingredients from a 2-Aminothiazole DMSO Stock Solution with Antimalarial Activity <sup>Publication 3 – under review</sup> .....	86
<b>4.) Conclusions and Outlook</b> .....	<b>95</b>
<b>5.) Supplementary Material</b> .....	<b>99</b>
5.1 Supplementary Material of Introduction .....	99
5.1.1 Section 1.2 .....	99
5.1.2 Section 1.3 .....	103
5.2 Supplementary Material of Chapter A .....	105
5.3 Supplementary Material of Chapter B.....	160
5.4 Supplementary Material of Chapter C.....	177

<b>6, Appendix: Extra Projects .....</b>	<b>217</b>
6.1 Appendix I - MS-MEP .....	217
6.2 Appendix II - Field-Based Screening with CDP-ME .....	220
6.3 Appendix III - COVID-19 Virtual Screenings .....	221
<b>7.) References.....</b>	<b>226</b>
<b>8.) Conference Contributions .....</b>	<b>241</b>
<b>9.) Curriculum Vitae .....</b>	<b>242</b>

All references, except the ones embedded directly in the publications, are included in Chapter 7.

All compound codes and sections in embedded publications refer to the respective publication.

Style of the embedded publications are as per the journal.

# 1. Introduction

## 1.1 The Urge for Increasing Anti-Infective Research

Already in 1945, the discoverer of penicillin, Sir Alexander Fleming, stated:

*“the public will demand [the drug and] ... then will begin an era...of abuses. The microbes are educated to resist penicillin and a host of penicillin-fast organisms is bred out which can be passed to other individuals and perhaps from there to others until they reach someone who gets a septicaemia or a pneumonia which penicillin cannot save. In such a case, the thoughtless person playing with penicillin treatment is morally responsible for the death of the man who finally succumbs to infection with the penicillin-resistant organism. I hope the evil can be averted.”<sup>1</sup>*

Here, nearly a century after the discovery of penicillin, we are living the luxury of antibiotics, for instance penicillins, aminoglycosides and sulfanomides, to treat common bacterial infections and guarantee safe organ transplantation. The development of antibiotics is well reviewed by Chellat *et al.*<sup>2</sup> However, the increasing antimicrobial resistance (AMR) without a concomitant increase in numbers of novel antibiotic therapies are starting to leave us armless.<sup>3</sup> Although AMR does not yet affect most of us in our daily life, a study by the European Antimicrobial Resistance Surveillance Network (EARS-Net) reported 671,689 infections caused by antibiotic-resistant bacteria in 2015 within the EU/EEA. More than half of them (64%) were health care-associated and about 5% were lethal. For example, in Germany, 54,509 infections caused by antibiotic-resistant bacteria were reported and out of these 2,363 (4.3%) were lethal.<sup>4</sup> These results were only published in January 2019, underlining that we are in the midst of an AMR crisis. Although caused by a virus, the current COVID-19 pandemic reminds us of the consequences of an unexpected outbreak of any infectious disease.<sup>5</sup>

Ever since the antibiotic golden age between the 1940s and 1960s, the antibiotic pipeline has been missing numerous chemical entities addressing novel targets. Why have the efforts to continuously fill the antibiotic pipeline been limited? The current business model, the sheer complexity of antibiotic drug discovery and antibiotic overuse are often provided as answers.<sup>3</sup> In 2008, L. Rice defined threatening nosocomial pathogens as ESKAPE pathogens (*Enterococcus faecium*, *Staphylococcus aureus*, *Klebsiella pneumoniae*, *Acinetobacter baumannii*, *Pseudomonas aeruginosa* and *Enterobacter* species).<sup>6</sup> Here, it is also necessary to mention that bacteria are categorised into Gram-positive and Gram-negative bacteria based on their cell envelope structure, (more detailed in Section 1.3).<sup>7</sup> Following on this, the “10 x ‘20 Initiative” by Infectious Diseases Society of America (IDSA) was launched to support the release of ten new antibiotics by 2020.<sup>8</sup> The overall summary results are not published after a last progress report since 2013.<sup>9</sup> Comparably, only three novel antibiotics and eleven antibiotics based on old classes were approved by the Food and

Drug Administration (FDA) between 2014–2019.<sup>10</sup> Meanwhile, one of the ticking time bombs was addressed by J. O’Neill in 2016, stating that 10 million people could die due to an untreatable infection in 2050.<sup>11</sup> Now, the World Health Organisation (WHO) has played an active role by defining the priority pathogens, most of them being Gram-negative bacteria, for which new antibiotics are needed, as announced in 2017, and additionally, innovative criteria to aid the development of new antibiotics were reported in 2019.<sup>12,13</sup> Many new initiatives have also been formed, to name for example the Global Antibiotic Research and Development Partnership (GARDP), the Combating Antibiotic-Resistance Bacteria (CARB-X) and the AMR Action Fund.<sup>14–16</sup> GARDP for example aims to bring five new antibiotics to the markets by 2025 and AMR Action Fund two to four novel antibiotics by 2030.<sup>14,16</sup> The efforts are not limited to the scientific communities only, the general awareness has also been raised by initiating for example a World Antimicrobial Awareness Week, taking place yearly in November since 2015.<sup>17</sup> Along this line, the WHO has recently published a technical guideline to strengthen the actions for better water, sanitation and hygiene (WASH) and wastewater management to reduce the spread of AMR. This includes for example better leadership and coordination of the needed hygiene principles with increased attention for households, health-care facilities and animal farming as well as an overall reduction of antibiotic use to the essential cases. In addition, the wastewater management plays an important role to avoid them becoming the spreader of superbugs resistant to the current antibiotic treatment options.<sup>18</sup>

In the first place, it is important to raise the awareness of the AMR, antibiotic (mis)usage, the importance of hygiene to hinder the resistance development to gain extra time for the research of new treatment options, although this should not be taken for granted. Evidently, faster diagnostic tools to detect (resistant) infections are also crucial in order to enhance treatment efficacy.<sup>19</sup> Here, it is fundamentally important to look at the synergies of chemical and biological approaches to answer the question how to design successful antibiotics. Chapter 1.3 in this thesis introduces the concept of bacterial bioavailability that it brings alternative views to antibiotic drug discovery. It is time to start thinking about designing antibacterial compounds in a similar fashion as aiming for high oral bioavailability as well as to benefit from the assays to measure bacterial bioavailability. In another recent review, K. Lewis addresses these overall difficulties of antibiotic drug discovery more broadly and urges the community to change from an artistic to a more scientific manner of antibiotic development.<sup>20</sup>

How to achieve selectivity over mammalian cells and also against the largely important gut microbiota represents one of the challenges of antibiotic discovery.<sup>21</sup> Especially, the side effects of previously often prescribed fluoroquinolones are being debated after warnings about their safety.<sup>22</sup> The human microbiome also suffers from the use of conventional antibiotics lacking selectivity between “good and bad” bugs. C. Ribeiro *et al.* review the negative effects of conventional antibiotics on the human microbiome, possibly resulting in an irreversible physiological imbalance.<sup>23</sup> Therefore,

non-traditional therapy strategies selectively targeting pathogenic bacteria are welcome, including for instance antibodies, bacteriophages and antimicrobial peptides.<sup>23,24</sup> Where possible, defining the bacterial bioavailability specifically for the target pathogens with the definition of Gram-negative and Gram-positive bacteria will hopefully support the drug-discovery efforts. Although until now the focus here has been on antibiotics, it is important to mention that the term anti-infectives or antimicrobials may fit better for future approaches. Boldly defined, an antibiotic is “*a compound that inhibits the growth or kills bacteria. In recent years, ‘antibiotic’ has become synonymous with ‘antibacterial’*”, as defined by a recent encyclopaedia by the GARDP REVIVE platform.<sup>25</sup> On the other hand, anti-infective or antimicrobial may refer to “*a drug, chemical or other substance that kills, inactivates or slows the growth of microbes, including bacteria, viruses, fungi and parasites*”.<sup>25</sup> Therefore, novel approaches targeting for example virulence agents would not strictly classify here due to their mode of action.<sup>26</sup> The antibiotic discovery is at the bridging point, where novel approaches and targets, like the MEP pathway and the underexplored target enzyme IspE, are highly sought after.

The term anti-infective covers also the term antimalarials, playing another important role in this thesis. Yearly, over 200 million people suffer from malaria and out of them, 400,000 cases being deadly.<sup>27</sup> Malaria is another major global health problem, occurring mainly in tropical zones with ideal humidity and temperature for transmission.<sup>28</sup> Malaria is caused by a stitch of an infected mosquito carrying *Plasmodium* parasites.<sup>29</sup> There are five identified *Plasmodium* species; *P. vivax*, *P. knowlesi*, *P. ovale*, *P. malariae* and *P. falciparum*.<sup>28,30</sup> *P. falciparum* exists predominantly in Africa and *P. vivax* outside of Africa.<sup>31</sup> High fever is a frequent symptom of malaria, but non-specific symptoms may also occur. Fast parasitological diagnosis is key for survival. Substantial efforts have been made to provide rapid diagnostic tools in the highly affected areas, also often with limited infrastructure and finance.<sup>32</sup> Therapies exist to treat malaria, for example quinolone derivatives, artemisinin and antifolates, however, there are concerns about their safety profile, dosing and resistance development.<sup>30,31</sup> In this light, the open access platform “Guide to Pharmacology” was created for continuous exchange about antimalarials and particularly about their pharmacology studies.<sup>33</sup>

In similar fashion to AMR, the WHO has played an active role by defining the assets against malaria; control, elimination and eradication, reinforcing further engagement from research and communities.<sup>27</sup> The WHO also encourages for novel malaria medication as one of the eradication methods with their “test, treat and track” philosophy, being also applicable to AMR to prevent infectious diseases spreading.<sup>32</sup>

## 1.2 MEP Pathway and the Enzyme IspE

The 2-C-methyl-D-erythritol 4-phosphate (MEP) pathway was first discovered in the early 1990s.<sup>34</sup> There are overall seven enzymatic steps resulting in the biosynthesis of the vitally important structural building blocks, isopentenyl diphosphate (IPDP) and dimethyl allyl diphosphate (DMADP). They are essential for example for cell-wall synthesis and internal signalling. Most bacteria, parasites and plants rely on the MEP pathway, whereas humans rely on the mevalonate pathway, both shown in Figure 1.2:1.<sup>35,36</sup> Amongst bacteria, Gram-negative bacteria use the MEP pathway, whereas the Gram-positive mainly rely on the mevalonate pathway.<sup>37</sup> The MEP pathway consists of several interesting drug targets in clinically relevant pathogens, avoiding selectivity issues with human cells. Additionally, the MEP pathway has been validated as a successful target by fosmidomycin, being a clinical candidate as a novel antimalarial. It inhibits the second enzyme IspC, which is located in the unique organelle apicoplast that hosts the MEP pathway enzymes in parasites.<sup>38</sup>

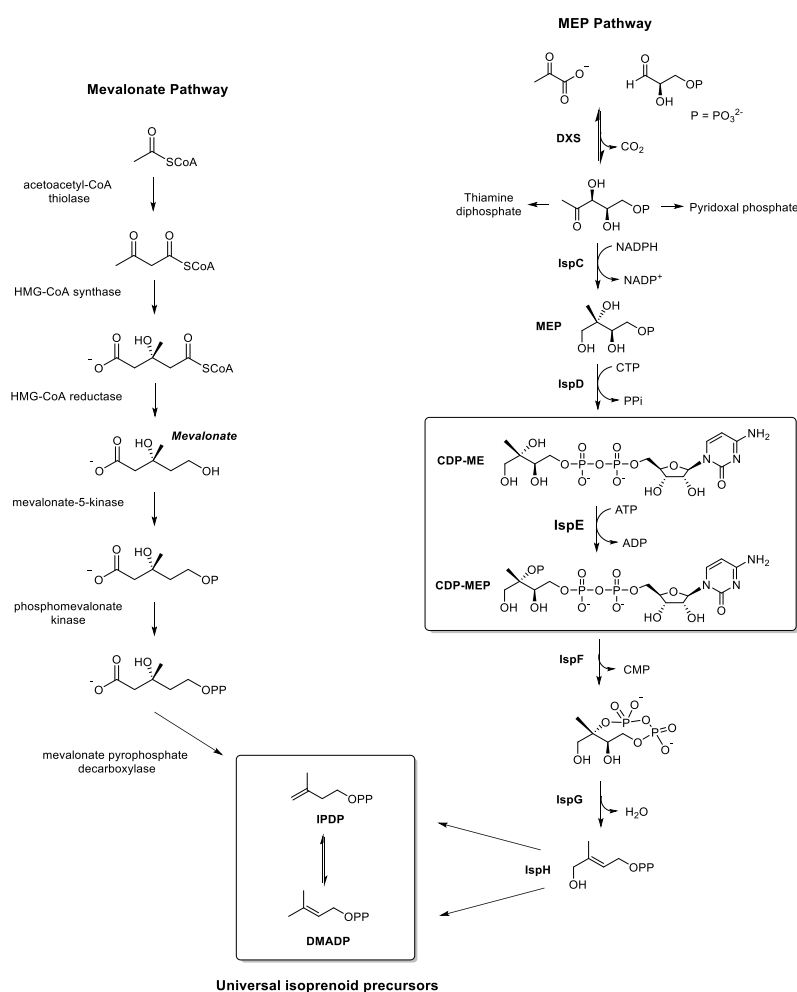


**Figure 1.2:1** - The mevalonate pathway vs the 2-C-methyl-D-erythritol 4-phosphate (MEP) pathway.



Several medicinal-chemistry projects have been conducted and in the course of them, a new understanding of the MEP enzyme functions has emerged, as reviewed in detail by A. DeColli *et al.*, A. Frank *et al.* and T. Masini *et al.*<sup>39-41</sup> The specific target of this thesis is the fourth enzyme IspE, which phosphorylates 4-diphosphocytidyl-2-C-methyl-D-erythritol (CDP-ME) into 4-diphosphocytidyl-2-C-methyl-D-erythritol-2-phosphate (CDP-MEP) by ATP-dependant catalysis (Figure 1.2:1). IspE is a kinase-like enzyme, belonging to the galactose, homoserine, mevalonate and phosphomevalonate (GHMP) kinase superfamily, some also being present in humans.<sup>42,43</sup> Considering the potential of the enzyme IspE as a promising anti-infective drug target, rather little efforts have been taken hitherto. Substantial efforts have been made within the MEP consortium of this thesis to establish high-throughput functional assays.<sup>44</sup> Co-crystallisation attempts of inhibitors with *EcIspE* have been unsuccessful until date, but successful co-crystals of the non-pathogenic homologue *Aquifex aeolicus* have provided the needed X-ray structures to support structure-based drug design (SBDD). For example, the cytidine mimic **1** (*EcIspE* IC<sub>50</sub> = 590 ± 10 µM) was successfully co-crystallised with *A. aeolicus* (PDB 2VF3).<sup>45</sup> More cytidine and non-cytidine derivatives were published by the Diederich group (ETH Zürich) with a focus on inhibition of the target enzyme rather than cellular activity for the hits.<sup>46,47</sup> Alternatively, N. Tidten-Luksch *et al.* identified compounds **2** (*EcIspE* IC<sub>50</sub> = 160 µM) and **3** (*EcIspE* IC<sub>50</sub> = 1.5 mM) from a simultaneous virtual screening with *AaIspE* (PDB 2V8P) and two high-throughput screening (HTS) hits **4** (*EcIspE* IC<sub>50</sub> = 19 µM) and **5** (*EcIspE* IC<sub>50</sub> = 2.5 µM) against *EcIspE*.<sup>48</sup> Similarly, M. Tang *et al.* performed structure-based virtual screenings with *EcIspE* (PDB 1OJ4), identifying for instance compound **6** (*EcIspE* %-inh. = 40%) and a couple of its derivatives to show *EcIspE* inhibition. M. Tang *et al.* also implemented a selectivity screening against the human galactokinases in the light of potential off-target kinases from the GMPH superfamily. For example compound **7** originated from a previous human galactokinase (GALK1) screening and proved also to cross-inhibit IspE enzymes (*EcIspE* IC<sub>50</sub> = 18 µM and *Yersinia pestis* IspE IC<sub>50</sub> = 9 µM).<sup>49-51</sup> As an alternative strategy, pharmacophore-based virtual screenings focusing on the protein-protein interaction (PPI) and the water-mediated dimer formation of *EcIspE*, identified novel scaffold **8** showing binding to *EcIspE* based on measurements with matrix assisted laser desorption/ionisation time-of-flight mass spectrometry (MALDI-TOF MS).<sup>52</sup> Similarly, a pharmacophore-based virtual screening study focusing on the dimer interface resulted in compound **9** and cyclic peptide **10**, which were confirmed to interact with *EcIspE* by surface plasmon resonance (SPR) studies.<sup>53</sup> It is still debated, how the enzyme IspE, in particular *E. coli*, exists in solution.<sup>39,54</sup>

The research around IspE has been heavily focused on *EcIspE* that is often considered as the model organism. Compound **11** is shown to bind Gram-negative *Burkholderia thailandensis* IspE using saturation transfer difference (STD)-NMR, also demonstrating antibacterial activity in Kirby-Bauer disk diffusion susceptibility tests against its close relative *P. aeruginosa* (*P. aeruginosa* inhibitory activity at 0.5 mM vs *B. thailandensis* at 0.1 mM).<sup>55,56</sup> Prior to this thesis, the *PfIspE*

enzyme became available within the MEP consortium (the Fischer Group, University of Hamburg). Compound **12** and its derivatives were tested against *PfIspE* showing no inhibition.<sup>57,58</sup> The crystal structure of the homologue *PfIspE* still remains unsolved, but homology models for various *Plasmodium* species were reported in 2018, showing high conservation amongst *Plasmodium* species but differing substantially from the other IspE enzymes.<sup>59</sup>

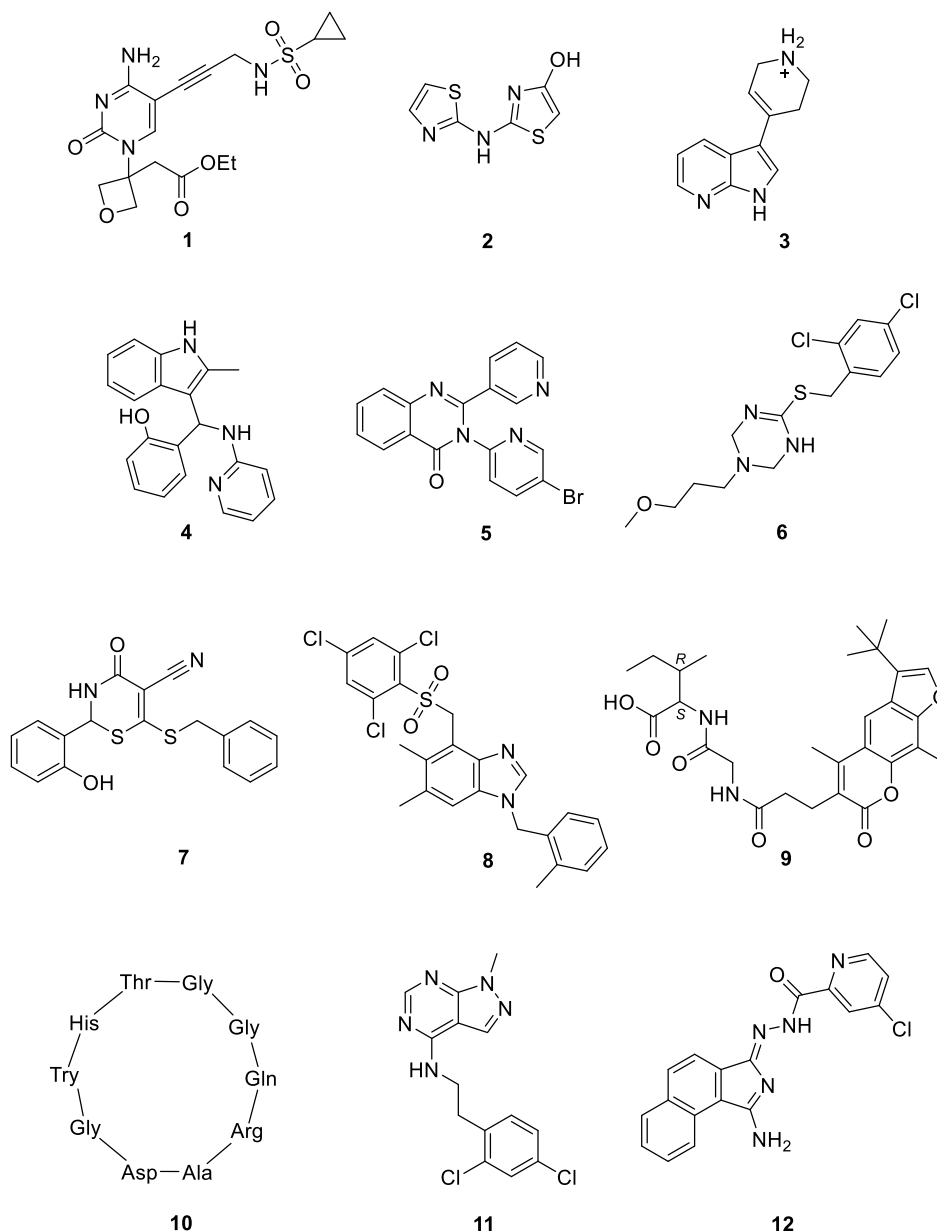


**Figure 1.2:2** - Summary of the reported inhibitors and binders of the enzyme IspE.

A comparison of the sequence similarity amongst the Gram-negative ESKAPE pathogens against *EcIspE* shows high similarity and offers a promising space for broad-spectrum inhibitors (Table 1.2:1). In particular, *Klebsiella pneumoniae* and *Enterobacter* spp. belonging to Enterobacterales show a high sequence similarity (~92%). In comparison, *P. aeruginosa* and its less pathogenic derivative *B. thailandensis*, as examples of Pseudomonales, show lower similarity in comparison to *EcIspE*, but still significant conservation in the catalytic site (Supplementary Material, Section 5.1). On the other hand, *M. tuberculosis*, the causative agent of tuberculosis, *P. falciparum* and *B. subtilis* as a collective sample of other organisms than Gram-negative show about 50% sequence similarity.

**Table 1.2:1.** Sequence comparison of the Gram-negative ESKAPE pathogens, *Mycobacterium tuberculosis* and *Plasmodium falciparum* against the *Escherichia coli* IspE (PDB 1OJ4). The codes refer to UniProt ID and the matching was done via EMBOSS.<sup>60-62</sup>

<i>EcIspE</i> (Strain from PDB 1OJ4) vs.	Percentage Identity (%)	Sequence Similarity (%)
<i>Pseudomonas aeruginosa</i> (P42805)	54.6	68.1
<i>Burkholderia thailandensis</i> (Q2T1B6)	46.1	60.3
<i>Acinetobacter baumannii</i> (B7GYQ7)	43.6	63.7
<i>Klebsiella pneumoniae</i> (A6TAP2)	85.2	91.9
<i>Enterobacter</i> spp. (A4WBC9)	85.2	91.5
<i>Mycobacterium tuberculosis</i> (P9WKG7)	36.7	53.2
<i>Plasmodium falciparum</i> (A0A1B1TK84)	33.3	52.8
<i>Bacillus subtilis</i> (P37550)	34.6	53.7

This provides a promising starting point for broad-spectrum inhibitors, or even the possibility for a design of tool compounds to further examine the function of IspE. The significance of inhibiting the function of IspE in cell-based assays remains a subject for future research. In rice plants, however, the shutdown of IspE has cross-effects influencing various genes, for example mevalonate pathway genes, photosynthetic genes and mitochondrial genes (Chen *et al.*, *Plant Cell Physiol.* **2018**, 59(9), 1905–1917). To fill the translational gap between the cellular activity and enzyme inhibitory activity, an *in vitro* metabolomics assay was conducted (Appendix I). In the ideal case, one would be able to quantify the enzyme inhibition as well as cellular inhibition from a single well. Where successful, this would allow fast translation across the species. For example, throughout the series we used Gram-positive bacteria *Bacillus subtilis* as a positive control for the first indication of target engagement, since it relies on both the MEP and the mevalonate pathway.<sup>37</sup> For instance, the hydrolytic conversion rate of the third MEP enzyme IspD is twice as fast as in *B. subtilis* than in *E. coli*, suggesting that different dependencies on the MEP pathway exist across the strains.<sup>63</sup> This opens also another discussion point for further approaches targeting the MEP pathway, and its essentiality across the different species.

### 1.3 Mastering the Gram-Negative Bacterial Barrier – Chemical Approaches to Increase Bacterial Bioavailability of Antibiotics<sup>Publication 1</sup>

H.-K. Ropponen\*, R. Richter\*, A. K. H. Hirsch and C.-M. Lehr

\* these authors contributed equally

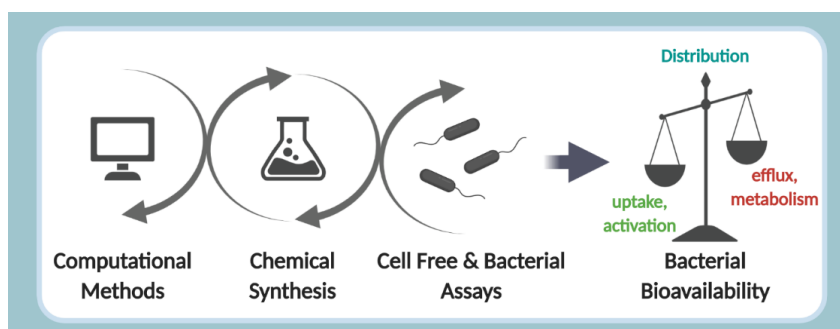
This part of the thesis was accepted for publishing in *Advanced Drug Delivery Reviews*, DOI:10.1016/j.addr.2021.02.014, in press.

Copyright retained by the authors and reused here acceptably in accordance to Elsevier guidelines.

**Abstract:** To win the battle against resistant, pathogenic bacteria, novel classes of anti-infectives and targets are urgently needed. Bacterial uptake, distribution, metabolic and efflux pathways of antibiotics in Gram-negative bacteria determine what we here refer to as bacterial bioavailability. Understanding these mechanisms from a chemical perspective is essential for anti-infective activity and hence, drug discovery as well as drug delivery. A systematic and critical discussion of *in bacterio*, *in vitro* and *in silico* assays reveals that a sufficiently accurate holistic approach is still missing. We expect new findings based on Gram-negative bacterial bioavailability to guide future anti-infective research.

**Keywords:** Antibiotic Drug Design & Discovery • Accumulation Rules • Permeability • *In silico* & *in vitro* Assays • Medicinal Chemistry • Drug Delivery • Antimicrobial Resistance

#### Graphical Abstract:



## 1. Introduction

Currently, the treatment of bacterial infections faces a crisis since the current portfolio of antibiotics is impaired by increasing numbers of resistant pathogens and simultaneously limited number of efforts to find new antibiotics [1,2]. Being not only transported across continents due to the movement of people, animals and trading, but also found in wastewater, it becomes clear that multidrug-resistant bacteria are unnoticeably surrounding us in daily life [3–6]. In 2017, the World Health Organisation (WHO) initiated a wake-up call by announcing a priority list for bacteria running out of treatment options – most of them being Gram-negative (Table 1) [7]. Although the widely used model organism *Escherichia coli* is associated with less severe infections, 58% of the clinical isolates in the EU/EEA were resistant to the current treatment options in 2018 [6].

A more recent report by the WHO states that the current antibiotic pipeline is drying out as most of them are “traditional” antibiotics, such as  $\beta$ -lactams, tetracyclines or fluoroquinolones, targeting pathogens not found on the priority list [8,9]. In the course of the past decades, the concepts that antibiotic drug researchers have followed (e.g., target-based drug design while neglecting membrane permeability, screening of growth inhibition, search for broad-spectrum activity) turned out to be inappropriate to find structures promising to overcome the preclinical phase [10]. In a rather recent evaluation of the (preclinical) pipeline, it was shown that some innovative approaches are emerging (e.g., phages, antivirulence agents, antibodies and vaccines). Interestingly, out of these, 40% are pathogen-specific rather than broad-spectrum and comparatively large compounds [11–13]. Furthermore, the WHO has defined innovative criteria for novel antibiotics, urging that a candidate should represent a new class addressing a new target, display a new mode of action and absence of within-class cross-resistance [9]. In practice, these claims are difficult to achieve and require a thorough understanding. With a likelihood of only one in five phase-1 clinical candidates for infectious diseases to be marketed, more (cost)-efficient antibiotic research and stronger cross-disciplinary collaboration along the classical development pipeline between academia and industry are required. Keeping this pipeline better filled and fostering translational science are pivotal to avoid the next antibiotic discovery void [14–16].

Especially, Gram-negative bacteria are known for their intrinsic resistance to a wide range of antibiotics being often related to drug uptake and efflux [17]. Additionally, antibiotic resistance occurs as a result of different more or less adaptive mechanisms caused by mutations and exchange of genetic information, requiring constantly need new antibiotic treatment options. These adaptive mechanisms are modifications on the target biomacromolecule, enzymatic modifications of the anti-infective compound, or decreased uptake and increased expression and activity of efflux pumps [18,19]. The decrease of uptake can be caused by the production of biofilm, reduction of certain membrane proteins, or by changes in the composition of other membrane components, such as

phospholipids or lipopolysaccharides [17]. Having mentioned the aspect of antibiotic uptake, one can easily see, how many factors must be taken into account for optimal drug design.

Hence, we will first give a brief overview on the underlying biological principles of the Gram-negative cell envelope and then discuss chemical approaches that have been undertaken to utilise them for drug design. As recently pinpointed by A. L. Parkes, the most burning question in antibiotic research is “what can we design for?” [20] In order to answer this, we would like to introduce the concept of bacterial bioavailability, which will be further detailed in Section 2. A thorough understanding of bacterial bioavailability would strongly support antibiotic research from early stages up to the clinic. All molecules employed to kill bacteria, hamper their growth or lower their virulence are discussed as antibiotics in this review.

**Table 1.** The WHO priority pathogens with their commonly associated infections [3,6,21–23]. ESBL = extended spectrum  $\beta$ -lactamase

Level of urgency	Pathogen (Gram-type +/-)	Resistance	Infections
Critical	<i>Acinetobacter baumannii</i> (-)	carbapenem-resistant	pneumonia, urinary tract, bloodstream, wound
Critical	<i>Pseudomonas aeruginosa</i> (-)	carbapenem-resistant	pneumonia, urinary tract, bloodstream, surgical site
Critical	Enterobacteriaceae (-)	carbapenem-resistant, ESBL-producing	medical devices, long-term antibiotic users
High	<i>Enterococcus faecium</i> (+)	vancomycin-resistant	bloodstream, endocarditis, urinary tract
High	<i>Staphylococcus aureus</i> (+)	methicillin-resistant, vancomycin-intermediate and resistant	bloodstream, skin, soft tissue, bone
High	<i>Helicobacter pylori</i> (-)	clarithromycin-resistant	gastritis, duodenal, gastric ulcer
High	<i>Campylobacter</i> spp. (-)	fluoroquinolone-resistant	diarrhoea, fever, abdominal cramps
High	<i>Salmonella</i> spp. (-)	fluoroquinolone-resistant	diarrhoea, fever, abdominal cramps, bloodstream

High	<i>Neisseria gonorrhoeae</i> (-)	cephalosporin-resistant, fluoroquinolone-resistant	gonorrhoea
Medium	<i>Streptococcus pneumoniae</i> (+)	penicillin-non-susceptible	pneumonia, meningitis, bloodstream, ear, sinus
Medium	<i>Haemophilus influenzae</i> (-)	ampicillin-resistant	pneumonia, meningitis, bloodstream
Medium	<i>Shigella</i> spp. (-)	fluoroquinolone-resistant	diarrhoea, fever, abdominal pain

---

### 1.1. The Gram-negative cell envelope

Bacteria are categorised into Gram-negative or Gram-positive based on their different cell envelope structures that H. Gram observed with different dye labelling [24,25]. A comparative overview of membrane structures in Gram-positive, Gram-negative and eukaryotic cells is given in Fig. 1. [24]. Shown that a major reason for antibiotic inactivity against Gram-negative bacteria is the barrier function of their cell envelope, its profound understanding is essential for successful anti-infective drug development [26].

For Gram-negative bacteria, in particular the outer membrane (OM) delimits the intracellular access of antibiotics [27]. The OM is asymmetric and features lipopolysaccharides (LPS) on the outer leaflet and phospholipids on the inner leaflet. The vicinity of divalent cations leads to the reduction of the permeability across LPS, since the cations act as a linker between adjacent phosphorylated glucosamine disaccharides of the Lipid A [28]. OM protein channels act as molecular sieves (“porins”) and can be subdivided into non-specific and specific ones [26].

As shown in Table 2, the most abundant porins in *Acinetobacter baumannii*, *E. coli*, *Klebsiella pneumoniae* and *Salmonella typhimurium* seem to have a molecular weight cut-off of 500–700 Da. However, even within a single porin, the cut-off should never be considered as an absolute limit, since various physicochemical properties of the permeating molecule as well as the electrostatic interactions with the porin and its fluctuations in diameter also play a significant role [29]. *E. coli* porins OmpC and OmpF and *K. pneumoniae* porins OmpK35 and 36 have an hourglass-shaped cavity. At their narrowest part (constriction region) opposed negatively and positively charged residues of amino acids create a strong transverse electric field influencing drug permeation [29].

**Table 2.** Selection of outer membrane proteins with channel function (“porins”). n.r.: not reported.

Species	Porin	Molecular weight cut-off	Selectivity
<i>Acinetobacter baumannii</i>	OmpA <sub>AB</sub>	~500 Da [30]	Non-selective [30]
<i>Escherichia coli</i>	OmpF	~600–700 [31]	Slightly cation selective [32]
	OmpC	~600–700 [31]	Non-selective [32]
	PhoE	n.r.	Anion selective [32]
<i>Klebsiella pneumoniae</i>	OmpK35	Similar to OmpF [33]	Similar to OmpF, less selective towards larger, lipophilic molecules [33]
	OmpK36	Similar to OmpC [33]	Similar to OmpC [33]
<i>Pseudomonas aeruginosa</i>	OprF	~3000 [34]	Non-selective [35]
	OprD	n.r.	Basic amino acids, small peptides, carbapenems [36]
	OprP	n.r.	Phosphate anions [34]
<i>Salmonella enterica ser. typhimurium</i>	OmpF	~600 [37]	Non-selective [28]

Besides, it is important to realise that cut-off numbers not always provide an indication of the degree of molecular translocation across porins. Although OprF in *P. aeruginosa* is known to be the most abundant OM protein, which even allows for compounds as large as 3 kDa to permeate, it was found that the permeation speed is generally low [38]. OmpA<sub>ab</sub> in *A. baumannii* also shows remarkably slow permeation [30]. Notably, both of these bacterial species belong to order of Pseudomonadales. In contrast, *E. coli*, *K. pneumoniae* and *S. typhimurium* belong to Enterobacterales. Furthermore, Gram-negative bacteria can also acquire resistance by downregulating porin expression, as has been reported for OmpF in *E. coli* [39], OprD in *P. aeruginosa* [36] and OmpK35 and OmpK36 in *K. pneumoniae* [40]. It must be mentioned that these discussed porins despite their general selectivity



for rather small and hydrophilic molecules are regarded as non-specific porins. Porins, such as LamB (passive transport of maltose, malto-oligosaccharides) and Tsx (passive transport of nucleosides, deoxynucleosides) in *E. coli* have a much higher substrate specificity and are thus termed “specific porins”. Among those, so-called ligand-gated channels, for example FadL (passive transport of long fatty acids, *E. coli* and others) and CymA (passive transport of  $\alpha$ -cyclodextrins, *K. oxytoca*) only open in the presence of their substrate [26].

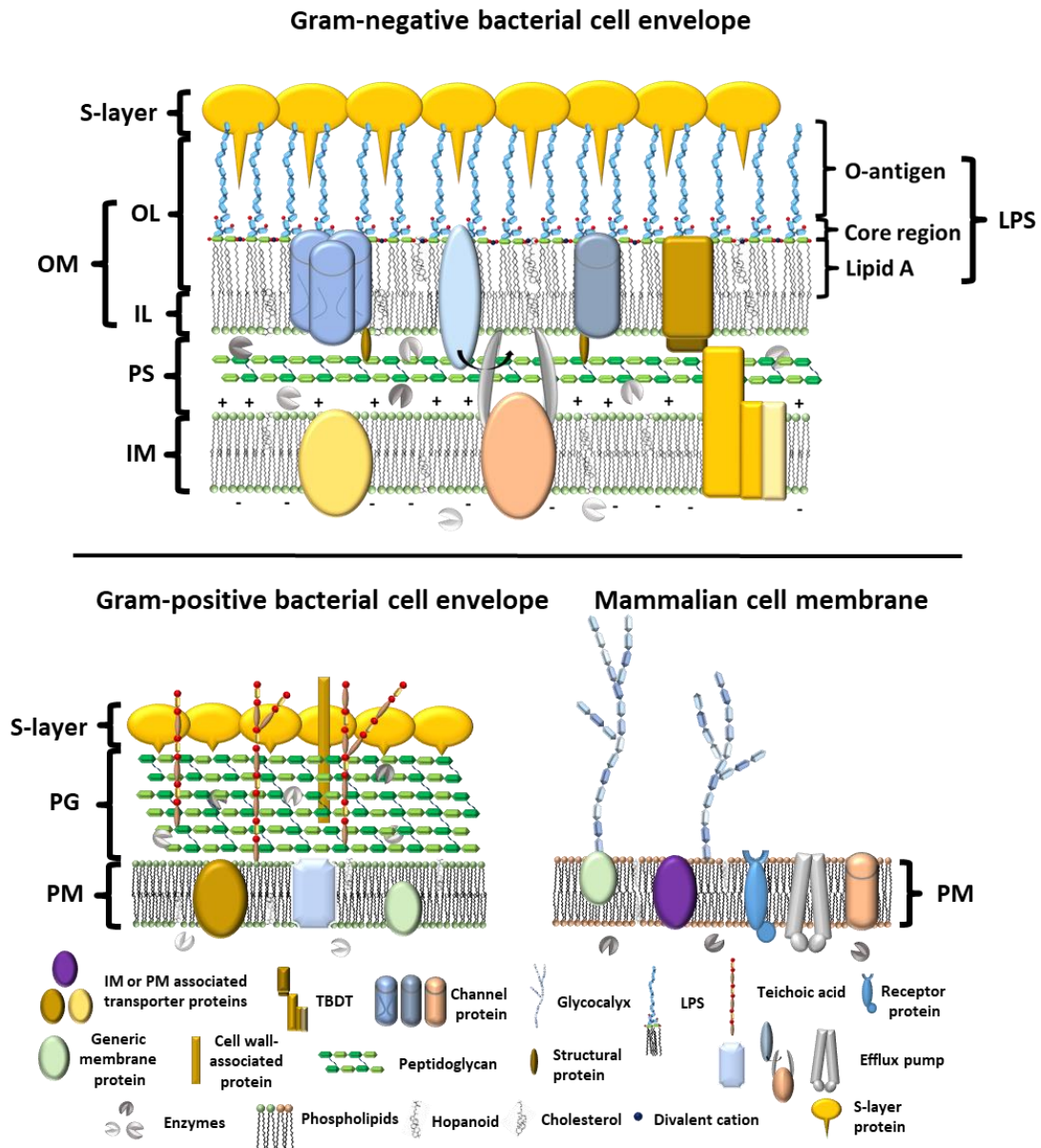


**Fig. 1. Membrane structure of Gram-negative, Gram-positive and mammalian cells.** The Gram-negative bacterial cell envelope comprises three major compartments: outer membrane (OM), inner membrane (IM), murein-containing periplasmic space (PS). Gram-positive bacteria have a thicker murein layer surrounding the more permeable plasma membrane (PM), featuring polymers (e.g., teichoic acids) and cell-wall-associated proteins. A surface-layer (S-layer) of proteins covers some Gram-positive and -negative species with sieving effects for macromolecules [41]. Mammalian membranes consist of a PM with transport, receptor and efflux proteins and polysaccharide-protein or -phospholipid conjugates.

TonB-dependent transporters (TBDT) are a long-known active uptake pathway that depends on adenosine triphosphate (ATP) for chelators of iron (siderophores), cobalt (Vitamin B<sub>12</sub>), nickel and some carbohydrates [42]. Like TBDT, efflux pumps span over the entire envelope and are the major excretion pathway of antibiotics. The AcrAB-TolC complex is the most prominent efflux system in *E. coli*. MexAB-OprM, MexCD-OprJ and MexXY-OprM are the dominant efflux pumps in *P. aeruginosa*, whereas AdeABC are typically found in *A. baumannii* [43]. All of these pumps belong to the resistance-nodulation-division (RND) family and span across the IM, OM and periplasm [28]. They require energy for compound secretion, which is provided by the proton-motive-force – a force that is created as a result of membrane potential and a proton gradient along the inner membrane (IM). Apart from those, also ATP-binding cassette transporters were found to efflux macrolides [44]. Efflux pumps are also known for mammalian cells (e.g., P-gp) and Gram-positive bacteria (e.g., TetK) [45,46]. While efflux pumps of Gram-positive bacteria obtain their energy from the proton-motive force or ATP [47], respectively, mammalian efflux pumps work only under supply of ATP [48]. Like for porins, bacteria can adjust efflux pump function and expression by mutational or adaptive changes [49].

While the OM has become much better understood during the past 30 years, knowledge about the IM has been stagnating. Facilitated diffusion systems, as for glycerol translocation, secondary active transport systems, such as proton symporters or phosphoenolpyruvate-dependent phosphotransferase systems for sugar transport as well as primary active binding protein-dependent transport systems energised by ATP are known. The latter type transports sugars, amino acids and ions [50].

Whereas mammalian cell membranes contain cholesterol, the membranes of Gram-negative bacteria feature structurally similar sterol compounds so-called hopanoids, affecting the permeability and fluidity of the cell envelope [51]. The exact functions of hopanoids, however, are still under investigations and could relate to bacterial membrane permeability in the same way as cholesterol in mammalian cells or liposomes. Moreover, mammalian membranes are mainly composed of phosphatidylcholine, while the predominant phospholipid of Gram-negative bacteria is commonly phosphatidylethanolamine (PE). Gram-positive cell envelopes have balanced amounts of PE and cardiolipin [52].

## **2. Bacterial bioavailability – a new concept for antibiotic research**

Previously, different concepts have emerged to describe the amount of drug within the bacterial cell. The term “accumulation” has been used in several publications. However, no clear definition exists, making it difficult for the reader to understand which factors contribute to intrabacterial accumulation [53–56]. For example, does a drug that was enzymatically modified within the bacterium still account for the overall accumulation? While results from mass-spectrometric methods would likely exclude

these modifications, fluorimetric and UV-vis-spectroscopic methods, due to their lesser selectivity, would likely include them.

Lately, the concept of SICAR (“Structure Intracellular Concentration Activity Relationship”) has been created referring to the interplay between compound uptake and efflux and the compound’s structure [57]. In addition, another recent review reports ongoing efforts to create a cheminformatics-based prediction tool for permeation and efflux in Gram-negative bacteria [58]. Here, it seems that the factor of enzymatic degradation has been explicitly excluded.

As a complementary term, we want to introduce “bacterial bioavailability”, which can be understood as an extension of the concept mentioned above that takes enzymatic degradation and distribution into account. The term bioavailability refers to the rate and extent at which a drug is available at the target site. In a patient, it is determined by absorption, distribution, metabolism and excretion, but these mechanisms also apply to the compartment of bacterial cells. Moreover, the distribution between different bacterial compartments may be of importance, especially in Gram-negative bacteria [54,59]. Hence, we regard “bacterial bioavailability” as an appropriate term to describe the time-dependent aspects of antibiotic accumulation in bacteria. In classical pharmacokinetics, bioavailability calculations are based on plasma concentrations of the host organism. For bacteria, the amount of substance per colony forming unit could be used and translated into concentrations since the average volume of bacteria can be calculated [60–62].

Since the biological basis of antibiotic uptake, degradation and efflux in Gram-negative bacteria has been extensively reviewed elsewhere [28,63–68], we aim in this section for a better understanding, which molecular properties may be beneficial or limiting bacterial bioavailability as a whole. We first summarise the key understanding of the physicochemical properties related to bacterial uptake and metabolism, distribution and efflux reported until now. In this light, we then compare clinically approved antibiotic classes against Gram-negative infections (based on a representative selection of antibiotics, see Supplementary Material, Table S1) and discuss the opportunities and risks associated with the “rule”-based design. Finally, we report recent approaches from antibiotic drug-discovery campaigns with comparison to their physicochemical criteria.

### **2.1.1 Bacterial uptake**

Non-ionisable lipophilicity, logP, was first observed during the antibiotic “golden age” between the 1940s and 1960s to correlate with observed activity differences of antibacterial compounds between Gram-negative and Gram-positive bacteria [69,70]. As a result, the ideal logP of compounds against Gram-negative bacteria was found to be around 4 and against Gram-positive around 6 [69].

Later, O’Shea *et al.* performed a statistical analysis, concluding that physicochemical properties of antibiotics targeting Gram-negative bacteria, in comparison to other drugs, are on average more

hydrophilic ( $\text{clogD}_{7.4} -2.8$  vs  $1.6$ ) and have a greater polar surface area (PSA) ( $165 \text{ \AA}^2$  vs  $70 \text{ \AA}^2$ ). Particularly compared to antibiotics against Gram-positive bacteria, they are two log units more polar but half as large [71]. Similar trends for  $\text{clogD}_{7.4}$  were also observed at AstraZeneca [72]. Although target distribution or accumulation were not directly taken into account in these studies, the results were in agreement with previous findings by Nikaido and co-workers [32,73]. High hydrophilicity favours water-gated porin (e.g., *E. coli* OmpF) uptake with a size limit of 600 Da [71]. On the other hand, they conclude that the uptake of zwitterionic synthetic fluoroquinolones are favourable for porin uptake as well as for oral availability due to (un)charged forms. We generally tend to optimise for the highest activity in *in vitro* settings. Environmental settings, such as pH, influence not only the state of the compound but also the bacterial behaviour under stress as well as under varying physiological conditions at the site of infection [74,75]. These are factors that need to be taken into account in the bacterial bioavailability concept.

Further statistical attempts were undertaken by binning compounds based on their translocation pathway into the cytoplasm as passive diffusion or energy-dependent versus their physicochemical properties. Compounds taken up by passive diffusion have a lower molecular weight and higher  $\text{clogD}_{7.4}$  values than actively transported compounds [76].

A new direction was given by the so-called “eNTRY rules”: an ionisable amine (N), low globularity ( $\leq 0.25$ ) as parameter for three-dimensionality (T) and high rigidity (R) in terms of a low number of rotatable bonds ( $\leq 5$ ) favour accumulation in *E. coli* [53,77]. M. Richter *et al.*, pointed towards the importance of the 3D shape as the measure of globularity (e.g., benzene = 0.0 and adamantane = 1.0). By following these rules, the spectrum of several antibiotics was extended towards other Gram-negative bacteria (see Sections 2.3.4 and 2.3.6) [78,79]. The rules also highlight the need of an amphiphilic moment. Amphiphilic moment accounts for hydrophilicity and hydrophobicity as well the distance between the hydrophobic part and charged part. It had already previously been used to predict ideal conformations and orientations of molecules in biological membranes, using a programme called CAFCA (CALculated Free energy of amphiphilicity of small Charged Amphiphiles) [80]. Nikaido *et al.* also already partially referred to amphiphilic moment earlier, highlighting charge as an important factor for OM uptake and hydrophobicity for accumulation through the IM [81]. Based on the eNTRY rules, the ionisable amine together with a low globularity is needed for the charge–charge interactions in *E. coli* OmpF porin [53]. Notably, the eNTRY rules do not feature any physicochemical parameter related to molecular size. The compounds the group selected for their analysis have a molecular weight of  $<500$  Da. Hence, all tested compounds were potentially eligible for OmpF-mediated permeation, making the impact of molecular size negligible. A platform to check if compounds fulfil eNTRY rules is freely available online (“eNTRY-way”) [82]. Calculating these properties using different software may lead to inconsistencies because of different underlying settings, such as how rotatable bonds are defined.

Whereas eNTRy-way only indirectly suggests good or bad accumulation by showing if eNTRy rules are fulfilled, the platform “Open Drug Discovery” by Idorsia employs a machine-learning algorithm to predict the permeability of the submitted molecule structures [83]. This machine-learning model suggests that compound accumulation in *E. coli* is determined by a combination of physicochemical properties (e.g., symmetric atoms, basic  $pK_a$ /nitrogens, solubility clogS and non H-atoms) [84]. The model was built on data of 13.000 compounds tested on TolC-deficient *E. coli*, which may give false indications in comparison to wild-type *E. coli*. Comparing favoured physicochemical properties in both *E. coli* strains, may in reverse, help to understand governing properties for efflux. The practical use of this submission platform, however, still needs to be demonstrated.

More recently, Acosta-Gutiérrez *et al.* used molecular dynamics (MD) to include the 3D shape of the compound as well as the porin channel creating a model taking into account electric field and electrostatic potential, media osmolarity and the energy barriers of molecules. This new scoring function defines if a molecule can permeate through the restriction area of the hourglass-shaped porins. This is determined based on molecule’s partial atomic charges, as the count of charge and dipole and its minimal projection area, as the measure of size. The higher the partial atomic charge and the lower the size, the better the permeability through the dynamic porins [29,85]. The attractiveness of the scoring function lies in its transferability across species and mutated porins, although the cut-off rules for porin uptake are not clearly listed and not all structures of bacterial porins are known [63]. To note, this scoring function defines no functional group specificity in contrast to the eNTRy rules.

A future avenue may be driven by 3D properties. A good example of this was demonstrated by an antibacterial compound with a relatively high molecular weight of ca. 700 Da that would normally be considered as too large for porin uptake. The antibacterial activity could be explained by its favourable 3D volume and shape for permeability [86]. 2D NOESY NMR spectroscopy provided experimental support for the minimal rectangle dimensions that would ideally match with the eyelet of the *E. coli* OmpF porin [28]. Cheminformatic methods could reveal the angle for diffusion between the dipole moment along the theoretical diffusion axis. This enforces the further evaluation of the 3D shapes of anti-infectives, but also evaluation of the permeability or accumulation data in 3D rather than in 2D benefitting from the modern computational capabilities. In particular, 3D approaches would be of use to examine the favoured pathway of permeation depending on the state of charge. For example, zwitterionic compounds might permeate fast across non-specific porins. On the other hand, compounds with a single positive charge may follow the same route, but without at least an electron-dense counterpart located at a certain distance to the positive charge, their uptake is likely to be poor. Hence, fast computational predictions would be welcome to support the design based on bacterial bioavailability. However, the concept of the 3D shape needs the support of computational methods and it is important to note that the 3D-descriptors have not been in the toolbox of medicinal

chemists until today and are rarely used. For simple 3D-parameter calculations, one requires first the access to computational programmes as well as know-how of the more advanced cheminformatics. The same holds true even for  $\text{clogD}_{7.4}$  calculations that are nowadays more often computed rather than determined experimentally.

### **2.1.2 Intrabacterial distribution**

Since overall subcellular quantification of chemical compounds is possible only very recently [54,59], not much data are available to draw general conclusions. Hence, we would like to use this section for postulations. Uncharged and non-polar compounds are known to show better partition into phospholipid bilayers, and therefore also into the Gram-negative IM and OM [87–90]. However, it will be discussed in “2.2.2. Distribution” that this topic might be more complex. Throughout most of the compounds investigated so far, it seems that the highest amount is found in the cytoplasm rather than the periplasm. This can be rationalised by the larger distribution volume of the cytoplasm leading to a sustained concentration gradient between both compartments and hence an extensive transport towards the cytoplasm. For small, charged and hydrophilic compounds that take the porin-mediated pathway or for compounds that are taken up actively across the outer membrane, it can be expected that the concentration in the periplasm is much higher than in the cytoplasm. Compared to their facilitated translocation across the OM, their translocation across the IM will happen more slowly, if facilitated transport mechanisms do not play a significant role. This difference in concentration between periplasm and cytoplasm, even though less pronounced, should be found also among compounds that are more lipophilic and uncharged, which follow non-facilitated transmembrane diffusion across OM and IM. An inverse gradient, showing the highest concentration in the periplasm could probably be found, when active transporters are significantly involved in translocation across the IM. Since sugars undergo such mechanism [50,91], compounds with sugar moieties as for example aminoglycosides or macrolides could show this phenomenon. Thus, looking at the membrane distribution may also help to evaluate if compounds follow substantial passive (non-facilitated) diffusion or active uptake.

### **2.1.3 Bacterial metabolism**

After passing the OM of Gram-negative bacteria, antibiotics can become exposed to degrading enzymes (destructases). Although it is occasionally suggested to consider antibiotic degradation as a mechanism that is separate from bacterial metabolism, it seems more plausible to consider also destructases as one specialised part of it. After all, also in humans the degradation of toxins is carried out by metabolic enzymes and names such as “penicillinase” or “aminoglycoside modifying enzymes” may just reflect on our current ignorance to other potential substrates. It is important to be aware that not only the commonly known  $\beta$ -lactam structures can become subjected to metabolism, but also for example amino groups, hydroxyl groups, esters, lactones and quinoid structures

(Table 3). These enzymes usually have a low substrate specificity, which decreases their efficiency [92]. Hence, also here, the key could be to design highly permeating compounds with a low efflux rate, which may overwhelm these destructases and in this way decrease the impact on this resistance mechanism. However, apart from  $\beta$ -lactamases, the quantitative impact destructases have on the overall bioavailability is still largely unknown and urgently deserves more research. Simply avoiding the structures mentioned above will possibly render it impossible to design new antibiotics. Since systematic overviews are so far missing and in order to avoid redundancy, we here refer to the extensive set of examples given in section “2.2.3 Metabolism”.

#### 2.1.4 Bacterial efflux

Efflux pumps are currently considered to be mainly responsible for the elimination of the compounds [63,93]. The most common *E. coli* multidrug efflux pump is AcrAB-TolC (Fig. 1). AcrB is located in the IM and AcrA is an elongated channel from the AcrB that pumps the compounds through the periplasm to TolC that is located in the OM. This RND-system was thought to exist continuously integrated, however, recent studies show that TolC is only recruited when AcrAB is actively pumping something out [94]. The presence of AcrAB-TolC is also the key to allow cell-to-cell transfer of resistant genes as shown in recent real-time analysis [95,96]. Perhaps there is something about the efflux system that we do not yet understand, but something worth further investigating in the search of novel efflux pump inhibitors [97]. In spite of recent findings related to efflux-system integrity and cell-to-cell transfer of resistant genes [94–96], a general rule-based optimisation of avoiding efflux remains difficult.

Earlier studies suggest that hydrophobic compounds are pumped out ( $\text{clogD}_{7.4} > 3$ ), whereas hydrophilic, highly charged compounds with a low molecular weight ( $< 400$  Da) and polar zwitterions with a high molecular weight ( $\sim 400$ – $600$  Da), would avoid efflux, although with some discrepancies between *E. coli* and *P. aeruginosa* [98]. Machine-learning-based analyses of antibacterial compounds in different OM-porin or efflux-deficient *E. coli* and *P. aeruginosa* mutants by Cooper *et al.* also show that favoured compound properties differ between pathogens. In *P. aeruginosa*, compounds are more likely to be effluxed, if they are rigid, more lipophilic and bear a high partial positive charge. In comparison, lipophilic uncharged compounds are favourably pumped out by *E. coli*. Cooper *et al.* also showed that a negative partial charge arising from the dipole moment may enhance porin permeability in *P. aeruginosa* and suggests that it may be possible to simultaneously avoid efflux and enhance porin-mediated uptake. Optimisation of compounds targeting *P. aeruginosa* should therefore focus on electrostatic properties and surface area, whereas for *E. coli*, topology, physical properties and atom or bond count should be taken into account [99]. The limitation of the study is that no clear cut-off limits are given. Earlier studies by the same group indicate that chemical properties favourable for different Gram-negative bacteria are so inconsistent

that the permeation of compounds is not chemically but biologically driven, as demonstrated by hyperporination studies in *A. baumannii*, *P. aeruginosa* and *Burkholderia* spp. [100].

Based on different machine learning techniques, a very recent publication reports molecular properties leading to increased susceptibility to efflux in *E. coli* [101,102]. Their so-called Susceptibility to Efflux Random Forest (SERF) tool reveals that hydrophobic (clogD 1–5), planar (the fraction of sp<sup>3</sup> carbon atoms, Fsp<sup>3</sup> 0–0.5), unbranched, compact molecules (hyper-Wiener index) with “low” molecular stability (the resonant structure count at pH 7.0 is <4) have greater susceptibility to efflux. These parameters are rather unconventional, although for example Fsp<sup>3</sup> is gaining more attention as a new parameter for drug-likeness [103]. Thus, it will be interesting to see if these new parameters prove to be successful also against other Gram-negative bacteria.

## **2.2. Application of this concept to clinically approved antibiotic classes**

### **2.2.1 Uptake**

Relevant antibiotic classes for Gram-negative bacterial infections - except for polymyxins - have an intracellular target. Most of them follow passive porin-mediated permeation (Table 3). Already in 1988, R. E. W. Hancock gave an overview about the uptake of the major antibiotic classes into Gram-negative bacteria [104]. In this review,  $\beta$ -lactams, tetracyclines and some quinolones follow mainly passive permeation across porins. These antibiotics have a zwitterionic structure in common, usually feature an ionisable amine, are relatively flat, rigid and hence, often fulfil the proposed eNTRY rules. Fluoroquinolones tended to become larger in size over the generations, which may have compromised permeability. The group of Gameiro showed that 1:1:1 complexation of certain fluoroquinolones such as ciprofloxacin and enrofloxacin with Cu<sup>2+</sup> and phenanthroline, a commonly used coordination ligand, enhances their activity in resistant Gram-negative *E. coli* strains [105]. Since the target remains the same, the enhanced activity should result from enhanced bioavailability. The underlying mechanism remains unclear.

Most fluoroquinolones and also tetracyclines exist to some extent in uncharged form at pH 7.4, which enables these compounds to permeate passively across the lipid layer of the OM [106,107]. Nalidixic acid, the progenitor of fluoroquinolones, has a pK<sub>a</sub> of 6 for its strongest acidic moiety [108]. This leads to a comparatively high amount of roughly 4% uncharged molecules at pH 7.4 resulting in a substantial uptake through phospholipid layers [109].

Lately, an alternative route was successfully utilised for  $\beta$ -lactam antibiotics. Cefiderocol, a bulky cephem featuring a Fe<sup>3+</sup>-chelating catechol group, was the first FDA-approved  $\beta$ -lactam that was especially designed for enhanced active uptake via TBDT [110,111]. The rifamycin derivative,



CGP4832, featuring a morpholino moiety at position 3 of its naphthofuran ring system and a terminal piperidine-containing sidechain in exchange for its acetic acid ester, was also reported to have an enhanced uptake across FhuA – an *E. coli*-specific siderophore receptor [112]. The dependency on a specific OM, however, makes these antibiotics prone to resistance development.

Regarding  $\beta$ -lactamase inhibitors, only few investigations were undertaken, but without elucidating the uptake pathway [113]. Due to their small size, polarity and anionic or zwitterionic nature, respectively, as well as further structural similarity to  $\beta$ -lactam antibiotics, we assume a porin-mediated pathway to be the dominant one.

Notably, the neutral chloramphenicol and negatively charged fosfomycin are also assumed to permeate via porins [104,114,115]. For fosfomycin, MD simulations on OmpF revealed that this very small molecule moves along a group of positively charged residues (“basic ladder”) to pass the constriction region. Chloramphenicol has a nitro group, which might enable it to pass in a similar manner. However, MD simulations would provide stronger evidence. Recent experimental studies suggest that an uptake pathway exists that is independent of OmpF, OmpC and LamB [86]. Due to the small size and the lack of a permanent charge, this molecule might also permeate well across the LPS and phospholipid layers. Sulfonamides, as another important compound class for the treatment of Gram-negative infections, still completely lack a defined permeation pathway. Closing this gap of knowledge is highly desired. A long-known alternative pathway, which is taken by polycationic molecules, such as aminoglycosides, is the self-promoted uptake [104]. Polymyxins are assumed to use the same mechanism [116]. The presence of neighbouring amine groups enables these molecules to displace divalent cations from the outer leaflet and hence, destabilises the barrier of LPS, which enhances membrane permeability. The introduction of additional primary amines to circumvent porin-dependent uptake may broaden the spectrum of activity also towards *P. aeruginosa* [117]. As for polymyxins, their amphiphilic character may additionally contribute to membrane destabilisation. In the case of kanamycin, very recently evidence was provided that it also follows passive permeation across non-specific porins significantly contributing to its activity [118]. Liposome-swelling assays suggest that also other aminoglycosides may follow this pathway, but further experiments are required to confirm this hypothesis [32,119].

### **2.2.2. Distribution**

When taking the data by Prochnow *et al.* and calculating the concentrations of tetracycline, trimethoprim in addition to ciprofloxacin, it seems that their concentration in the periplasm is higher than in the cytoplasm, which due to their porin-mediated uptake is plausible, as detailed in 2.1.2. Interestingly, erythromycin, which accumulates very slowly in Gram-negative bacteria, shows a higher concentration in the cytoplasm [54]. One may speculate whether this could be due to active

transport mechanisms in the IM. Additionally, tetracycline and ciprofloxacin seem to enrich in the bacterial membranes, which was not observed for trimethoprim and erythromycin. Considering the high polarity and its mainly positive charge ( $pK_a \sim 8.9$ ) at the physiological bacterial pH of 7.2–7.8 [120], the behaviour of erythromycin is understandable. However, the absence of significant amounts of the aniline-like trimethoprim ( $pK_a \sim 7.4$ ) [121] remains unclear, since a considerable amount of this substance should also exist uncharged. The enhanced membrane partition of the largely zwitterionic tetracycline and ciprofloxacin ( $pK_a \sim 6.0, 8.8$ ) [121] can occur either because a considerable uncharged amount exists at the intrabacterial pH range or, as in the particular case of ciprofloxacin, additional molecular stacking reduces their polarity [107,122,123]. The absence of efflux pumps usually increased the compound concentration in every compartment, but more data regarding the extent of enzymatic degradation will be necessary to understand these first systematic data better.

### 2.2.3 Metabolism

The most well-known class subjected to enzymatic degradation is the  $\beta$ -lactams, where especially penicillins undergo the enzymatically catalysed  $\beta$ -lactam ring opening. Cephamycins and cephalosporins of the third generation are also susceptible to enzymatic hydrolysis of the  $\beta$ -lactam ring [124]. Cephamycins feature a 7-  $\beta$ -methoxy moiety that together with the amino acyl sidechain provides a steric protection of the  $\beta$ -lactam ring on both sides. Third-generation cephalosporins feature an oxime ether instead of this methoxy group. Monobactams feature *N*-substituents and methyl groups in addition to their aminoacyl chain, while carbapenems sterically avoid  $\beta$ -lactam hydrolysis by *trans*-configuration of the hydrogens in the  $\alpha$  and  $\beta$  positions of the  $\beta$ -lactam ring [125]. All these features lead to the same protective effect. However, extended spectrum  $\beta$ -lactamases (ESBL) can open this ring. Notably, except for carbapenems, the molecular size and number of substituents increased over the course of  $\beta$ -lactam generations, making them less susceptible to enzymatic inactivation whilst limiting their access via porins. One solution to this limitation is currently extensively worked on: with the development co-administration of further small  $\beta$ -lactamase inhibitors similar to tazobactam or clavulanic acid,  $\beta$ -lactams can be designed in a less sterically demanding way and still avoid enzymatic degradation. The application of two small molecules rather than one larger molecule would enhance translocation of both compounds and possibly also reduce their efflux.

Currently,  $\beta$ -lactamase inhibitors can be divided into three generations. Inhibitors of the first-generation feature a  $\beta$ -lactam ring and irreversibly inhibit certain classes of serine- $\beta$ -lactamases (SBLs; class A and D according to the Ambler classification system of  $\beta$ -lactamases) [126,127]. Inhibitors of the second-generation feature a diazabicyclooctane (DBO) scaffold. They inhibit all SBLs, by reversible acylation of the serine group under loss of the cyclooctane structure [128]. The

*Klebsiella* SBL KPC-2, however, is also capable of irreversibly hydrolysing the DBO structure. Metallo-  $\beta$ -lactamases (MBL; class B) remain unaffected by second-generation  $\beta$ -lactamase inhibitors [129]. Regarding  $\beta$ -lactam inhibitors of the third-generation, the carbonyl oxygen of the lactam group was replaced by a boronic acid. They are effective inhibitors of all classes of SBLs (A and C). The inhibition of SBLs works by nucleophilic attack of the serine hydroxyl group on the boron leading to a highly stable  $sp^3$ -hybridised intermediate [130]. Third-generation  $\beta$ -lactamase inhibitors hold potential to inhibit  $\beta$ -lactamases of all classes (“pan-spectrum”  $\beta$ -lactamases). For example, taniborbactam has shown to inhibit all SBLs (A, C, D) but also MBLs [131]. It is assumed that two features in addition to the boronic acid ester moiety are responsible: An annulated benzoic acid cycle (Table 3, highlighted in orange) to the oxaborinane scaffold and a substituent on the amide group with a hydrophobic linker (Table 3, highlighted in pink) and polar moiety with a terminal amine group (Table 3, highlighted in green) [127].

Hydroxyl groups, as present in aminoglycosides or chloramphenicol, are also prone to enzymatic modification. While acetylation was reported for chloramphenicol, conjugation with adenosine monophosphate (AMP) or phosphoric acid was reported for aminoglycosides. In addition, aminoglycosides and fluoroquinolones are known to undergo inactivation by *N*-acetylation. The methylation of the amino group as done for example for levofloxacin or ofloxacin might prevent the molecule from this enzymatic modification, (perhaps at the expense of permeability). The enzyme FosA, whose genes were identified in *P. aeruginosa*, *K. pneumoniae* and *A. baumannii*, catalyses the conjugation of thiol group-containing compounds with fosfomycin. Tetracycline-inactivating enzymes, as for example TetX, are known to oxidise tetracyclines at different positions leading to various products. Especially, positions C1, C2, C3, C11a and C12 are targets for enzymes. These are parts of vinylogous carboxylic acid groups. Like for  $\beta$ -lactams, a possible approach could be to co-administer enzyme inhibitors, such as anhydrotetracycline. Chelocardins, which have been lately rediscovered as a basis of novel antibiotic structures, may profit from structural similarities to anhydrotetracycline. Both structures share an annulated aromatic ring system and a methyl group on C6. For tetracyclines, however, chemical modifications do not seem clinically relevant [110]. Sulfonamides were reported to undergo enzymatic degradation in *Escherichia* spp., *Acinetobacter* spp. and *Pseudomonas* spp. These data, however, do not originate from clinical strains [132].

For polymyxins, enzymatic peptide hydrolysis was only reported for Gram-positive *Bacillus* spp. The sequence of some serine proteases in Gram-negative bacteria seems similar to that of Gram-positives. The clinical relevance for Gram-negative species is, however, questionable, since these enzymes would need to be secreted to prevent bacterial killing early enough [133].

Notably, all currently relevant antibiotics for Gram-negative bacteria, are potentially prone to enzymatic degradation. A critical evaluation of the clinical relevance of antibiotic inactivation, depending on the bacterial species and molecular entities, is still needed. In the ideal case, one would be able to predict functional groups prone for bacterial metabolism and avoid thus synthesising them unnecessarily by running a quick predictive calculation beforehand - as commonly done for human metabolites of drug candidates.

#### 2.2.4 Efflux

As mentioned previously in Section 2.2, Gram-negative bacteria like *E. coli*, *P. aeruginosa*, *S. enterica ser. typhimurium*, *K. pneumoniae* and *A. baumannii* possess multidrug efflux pumps, which have structural similarities, but can have different substrate preferences.  $\beta$ -Lactams, fluoroquinolones and tetracyclines are efflux substrates in Enterobacterales (*E. coli*, *Salmonella* spp.) and Pseudomonadales (*A. baumannii* and *P. aeruginosa*), excluding imipenem [65,134]. For  $\beta$ -lactams, it has been shown that lipophilic side chains increase the efflux rate. Glycylcyclines – a subclass of tetracyclines – feature a glycyl sidechain in the position C9 of the tetracycline scaffold, which is supposed to prevent efflux. Despite of this, *A. baumannii* and *P. aeruginosa* still succeed in eliminating tigecycline by this pathway [65].

The accumulation of quinolones of the first-generation (e.g., nalidixic acid, flumequine), second-generation (e.g., ciprofloxacin, fleroxacin, norfloxacin) and fourth-generation (e.g., gatifloxacin, gemifloxacin) seems less affected by efflux activity, while fluoroquinolones of the third-generation (e.g., sparfloxacin, balofloxacin) are more susceptible. Moreover, an aminopyrrolidine at the C7 position of the quinolone scaffold instead of a piperazine substituent seems to lower the efflux rate of fluoroquinolones in *E. coli* [64].

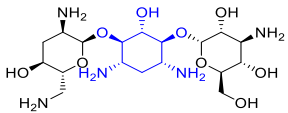
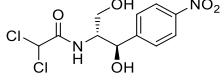
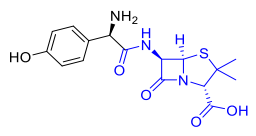
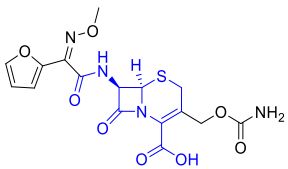
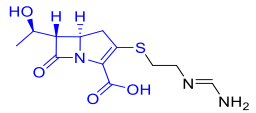
Aminoglycosides are known efflux substrates in *A. baumannii*, *P. aeruginosa*, *N. gonorrhoeae* and *E. coli* [65,135]. In *Pseudomonas* spp. the impact of the MexXY multidrug efflux pump on microbial resistance against aminoglycosides can be assumed as moderate [136]. More detailed structure–efflux relationships are still missing.

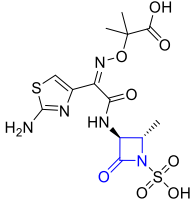
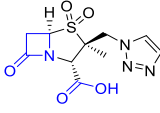
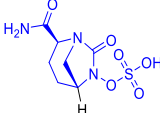
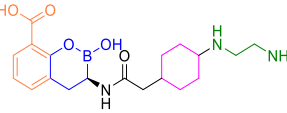
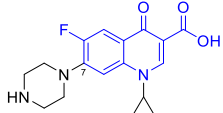
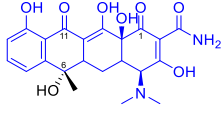
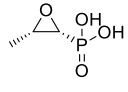
Regarding fosfomicin, not many studies suggest a significant impact of efflux on accumulation. It might play a role in *A. baumannii* [137]. This is in agreement with findings mentioned in Section 2.1.4, where small, highly charged molecules are less prone to undergo efflux.

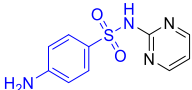
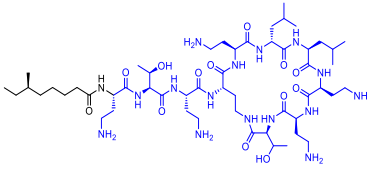
Generally, for many antibiotics uptake, degradation and efflux mechanisms are known to occur. Their interplay on a quantitative level, however, is still largely unknown. Prospectively, analogously

to  $\beta$ -lactamase inhibitors the development and co-application of efflux blockers can be a way to further enhance bacterial bioavailability. However, currently available compounds are only applicable for experimental purposes *in vitro* [49].

**Table 3.** Main classes of antibiotics for the treatment of Gram-negative infections.

Name	Example with the key structural motif highlighted	Physicochemical properties	Uptake	Metabolism in bacterio
Aminoglycosides	 Tobramycin	- polycationic - clogD $-8.1^{[a]}$ - MW 526 Da <sup>[a]</sup> - N <sup>[b]</sup>	Self-promoted uptake [104], Porin [118]	N-acetylation, O-AMP-conjugation, O-phosphorylation [66]
Chloramphenicol		- non-ionic - clogD 0.86 <sup>[c]</sup> - MW 323 Da - T <sup>[b]</sup>	Porin [104,138]	O-acetylation [139]
Penicillins	 Amoxicillin	- anionic, zwitterionic - clogD $-2.4^{[a]}$ - MW 413 Da <sup>[a]</sup> - (N), T, (R) <sup>[b]</sup>	Porin [73]	$\beta$ -lactam hydrolysis [140]
Cephems	 Cefuroxim	- anionic, zwitterionic - clogD $-3^{[a]}$ - MW 452 Da <sup>[a]</sup> - (N), T, (R) <sup>[b]</sup>	Porin [49]	$\beta$ -lactam hydrolysis [140]
Carbapenems	 Imipenem	- zwitterionic - clogD $-5.8^{[a]}$ - MW 397 Da <sup>[a]</sup> - (N), T, (R) <sup>[b]</sup>	Porin [49]	$\beta$ -lactam hydrolysis [140]

<b>Monobactams</b>		<ul style="list-style-type: none"> <li>- anionic, zwitterionic</li> <li>- clogD -2.8<sup>[c]</sup></li> <li>- MW 423 Da<sup>[a]</sup></li> <li>- (N), T<sup>[b]</sup></li> </ul>	(Porin) [141]	<ul style="list-style-type: none"> <li><math>\beta</math>-lactam</li> <li>hydrolysis</li> <li>[142]</li> </ul>
	Aztreonam			
		<ul style="list-style-type: none"> <li>- anionic, zwitterionic</li> <li>- clogD -3.0<sup>[d]</sup></li> <li>- MW 262<sup>[c]</sup></li> <li>- (T), R<sup>[b]</sup></li> </ul>	n.r. (porin likely)	<ul style="list-style-type: none"> <li>(<math>\beta</math>-lactam</li> <li>hydrolysis)</li> <li>[143]</li> </ul>
	Tazobactam (1 <sup>st</sup> Gen.)			
<b><math>\square</math>-Lactamase inhibitors</b>		<ul style="list-style-type: none"> <li>- anionic, zwitterionic</li> <li>- clogD -2.2<sup>[d]</sup></li> <li>- MW 312<sup>[c]</sup></li> <li>- (N), (T), (R)<sup>[b]</sup></li> </ul>	n.r. (porin likely)	<ul style="list-style-type: none"> <li>Carbamate</li> <li>hydrolysis</li> <li>[129]</li> </ul>
	Avibactam (2 <sup>nd</sup> Gen.)			
		<ul style="list-style-type: none"> <li>- anionic, zwitterionic</li> <li>- clogD -1.9<sup>[d]</sup></li> <li>- MW 343<sup>[c]</sup></li> <li>- (N), T, (R)<sup>[b]</sup></li> </ul>	n.r. (porin likely)	n.r.
	Taniborbactam (3 <sup>rd</sup> Gen.)			
<b>Fluoroquinolones<sup>[d]</sup></b>		<ul style="list-style-type: none"> <li>- zwitterionic</li> <li>- clogD -0.8<sup>[a]</sup></li> <li>- MW 371 Da<sup>[a]</sup></li> <li>- (N), T, R<sup>[b]</sup></li> </ul>	Porin, OM lipids [26]	N-acetylation [139]
	Ciprofloxacin			
<b>Tetracyclines</b>		<ul style="list-style-type: none"> <li>- zwitterionic</li> <li>- clogD -3.6<sup>[a]</sup></li> <li>- MW 481 Da<sup>[a]</sup></li> <li>- (N), T, (R)<sup>[b]</sup></li> </ul>	Porin, OM lipids [26,104]	Oxidation [92,144]
	Tetracycline			
<b>Fosfomicin</b>		<ul style="list-style-type: none"> <li>- anionic</li> <li>- clogD -3.2<sup>[c]</sup></li> <li>- MW 138 Da<sup>[c]</sup></li> <li>- R<sup>[b]</sup></li> </ul>	(Porin) [145]	<ul style="list-style-type: none"> <li>Nucleophilic addition of water,</li> <li>glutathione,</li> <li>L-cysteine or bacillithiol</li> <li>[146]</li> </ul>

Sulfonamides <sup>[e]</sup>	 Sulfadiazine	- non-ionic - clogD -0.1 <sup>[a]</sup> - MW 273 Da <sup>[a]</sup> - T, R <sup>[b]</sup>	Passive, not further specified [147]	oxidation of sulfanilic acid moiety, hydrolysis of sulfamate ester [132]
Polymyxins	 Colistin A	- polycationic - clogD 2.9 <sup>[c]</sup> - MW 1176 Da - N <sup>[b]</sup>	Self-promoted uptake, membrane permeabilisation [32,116,148]	(proteolysis) [149]

[a] Average values reported by O'Shea and Moser [71]. [b] The fulfilment of eNTRY rules [53,82], N = ionisable amine, T = low three dimensionality, R = rigidity. [c] Values generated by StarDrop v. 6.6.1.22652. [d] Values generated by StarDrop version 6.6.4.23412; the antibiotic panel used for [b] and [c] shown in the Supplementary Material, Table S1. [e] Fully synthetic. MW = molecular weight, n.r. = not reported

### 2.3. Novel chemical classes with anti-Gram-negative activity

New chemical entities, also addressing novel targets, are entering the clinical development. However, with the exception of zoliflodacin (against resistant *N. gonorrhoea*) all of them tend to focus on Gram-positive bacteria [150,151]. We therefore just highlighted some recent approaches used in antibacterial drug discovery (Table 4) and evaluate how these compounds match the rules discussed in Chapter 2.1. We review them with a focus on bacterial bioavailability; further exploration of their safety profile is still needed.

#### 2.3.1 Zoliflodacin

Being investigated in clinical phase III trials, zoliflodacin is currently the most advanced candidate among the compounds with anti-Gram-negative activity and is a representative of a novel antibiotic class called spiropyrimidinetrione. Although the structure is new, the target protein is not, since it inhibits the DNA synthesis by binding to the GyrB-subunit of bacterial Topoisomerase II (Gyrase) as well as Topoisomerase IV, which holds true also for novobiocin, flavonoids and so-called "novel bacterial topoisomase inhibitors" [152,153]. However, studies on drug-resistant mutants showed no cross-resistance between zoliflodacin and any other gyrase targeting agent, as the mode-of-inhibition is different [154,155]. Regarding bacterial bioavailability, no specific studies have been performed. Neither the way of uptake is known (although the PorB is assumed to be potentially involved), nor any metabolic pathways. Susceptibility studies on *Neisseria* efflux pump mutants, revealed that especially MtrCDE, but also MacAB and NorM play a significant role in decreasing the bioavailability [156]. Considering the properties of the molecule with its medium molecular size, without charged groups and low globularity, it is likely that it mainly takes the PorB porin pathway

as well as to some extent the passive non-facilitated uptake across the OM, which is known to be rather unselective and seems to determine the efficacy of other antimicrobials [28,157].

### 2.3.2 Halicin

A recent study based on a computational deep learning model using a library from Drug Repurposing Hub [158,159] resulted in the discovery of nitrothiazole halicin, c-Jun N-terminal kinase inhibitor SU3327, as a potential antibacterial compound [160]. With respect to the physicochemical parameters, halicin complies with the rules, although it lacks an ionisable amine and is rather non-drug like, as shown in Table 4. No antibacterial activity was observed for *P. aeruginosa* and the authors in fact refer to possible permeability issues. This pinpoints need for bacteria-specific models not only to predict antibiotic activity but also bacterial bioavailability. Where such a model is successful, lengthy experimental high-throughput screenings (HTS) may in future be driven using computational settings. When repurposing substances, however, it will be of utmost important to investigate their history and question why research has been previously discontinued. As for halicin, there is some evidence that it may affect mitochondrial function [161].

### 2.3.3 Compound “13e”

An application of fragment-based drug design was recently illustrated by Ushiyama *et al.*, where DNA gyrase inhibitor 8-(methylamino)-2-oxo1,2-dihydroquinoline compound “13e” was reassembled successfully from an HTS hit [162]. In general, fragment-based design (compounds with molecular weight <300 Da) provides the freedom to design and introduce desired physicochemical parameters to the scaffold [163]. However, in this case the design was driven by enzymatic activity. The study represents a good example, how difficult it is to balance enzymatic and cellular activity. Compound 13e only displays a weak antibacterial activity profile in *E. coli* (MIC = 64 µg/mL) and is potentially prone for efflux, as demonstrated with an increased minimum inhibitory concentration (MIC) in presence of an efflux pump inhibitor Phe-Arg-β-naphthylamide (*E. coli* = MIC ≤ 0.03 µg/mL with PAβN (200 µL)). Compound 13e has a low molecular weight (337 Da) but is only negatively charged with one carboxylic acid and thus, the observations by Brown *et al.* could predict efflux issues [98].

### 2.3.4 Debio-1452-NH3

Debio-1452-NH3 is also a recent example of the application of the eNTRY rules, where its non-amine derivative Debio-1452 was converted into a compound active against Gram-negative with the introduction of a primary amine. Both inhibitors represent a novel class of benzofuran naphthyridines targeting a novel target, namely the enoyl-acyl carrier protein reductase FabI. This study demonstrates the power of the eNTRY rules, or particularly the primary amine, by expanding the activity profile from Gram-positive into Gram-negative. However, Debio-1452-NH3 shows activity



against *A. baumannii*, *K. pneumoniae* and *E. coli*, but not against *P. aeruginosa* [78]. Several factors may be responsible for this, highlighting again the need for bacteria-specific rules of compound properties. The non-amine derivative Debio-1452 is already in phase-2 clinical studies to treat skin infections caused by Gram-positive *Staphylococcus aureus* [150]. Time will tell, whether the amine-modified Debio-1452-NH<sub>3</sub> will also make it to clinical studies. An interactive tool by the PEW trust can be used to trace the clinical candidates by the Food and Drug Administration (FDA) [150,164].

### 2.3.5 Quorum-sensing inhibitors

Quorum-sensing inhibitors interfere with the interbacterial communication and thus, inhibit bacterial growth and virulence. Since they do not act bacteriostatically or bactericidally, the selection pressure is reduced, and resistance formation decelerated. Since substances of many different structural classes belong to this group, we will here mainly focus on furanone derivatives, a compound class that interfere with quorum sensing of various bacterial species as for example *P. aeruginosa* and *S. enterica*. One target is the intracellular Quorum-sensing control repressor (QscR). Its inhibition indirectly leads to a decrease in the expression of virulence genes.

Quorum sensing inhibitors of the furanone class are rather small, mostly uncharged and less hydrophilic molecules, such as Fur-5 in Table 4 [165–167]. One might question at first glance if such compounds can accumulate enough to interact with their intracellular target. It is, however, important to consider that for *P. aeruginosa* the porin pathway is highly challenging due to the low number of these OM proteins and their increased specificity. It is likely that such small and less polar compounds substantially permeate porin-independently across the OM, as has been previously indicated by PqsD inhibitors [109]. Bearing this in mind, the design of small, flat, rigid and amphiphilic molecules could lead to better bioavailability and hence activity in *P. aeruginosa* than strictly following the current dogma, which includes enhanced polarity and positive charge.

Rosmarinic acid has also been shown to inhibit quorum sensing in *P. aeruginosa*. Notably, this molecule features two Fe<sup>3+</sup> complexing catechol groups, which may enhance active uptake via TonB-dependent receptors [168].

### 2.3.6 Peptide antibiotics

Arylomycins are partially cyclic hexapeptides featuring an *N*-terminal fatty acid. They are primarily active against Gram-positive species. In a recent publication structural changes were reported, which broadened the spectrum of activity of Arylomycin A-C<sub>16</sub>. By replacing the linear peptide-fatty acid structure by a 2-(4-(*tert*-butyl)phenyl)-4-methylpyrimidine-5-carboxylic acid – linked diaminobutyric acid the compound G0775 was obtained, which showed antimicrobial activity was achieved against *E. coli* and *K. pneumoniae*. Target molecule is the LepB enzyme located in the IM. By adding a nitrile function to the C-terminus, the target affinity was enhanced leading to a further

gain of potency. Further addition of ethylene amine groups to its two phenolic OH-functions led to significant activity also against *P. aeruginosa* and *A. baumannii* [79]. Notably, the activity was enhanced by introduction of several primary amine moieties and a more rigid aromatic system. The authors reported a porin-independent uptake of this compound, which may be partially facilitated by its polycationic nature enabling it for self-promoted uptake. With a molecular mass of 890 Da, it seems unlikely that this compound shows fast accumulation. It might rather be the synergism of enhanced bioavailability and target affinity, making this compound active and opening the door for new potent representatives of this class.

### 2.3.7 Nucleic acids and analogues

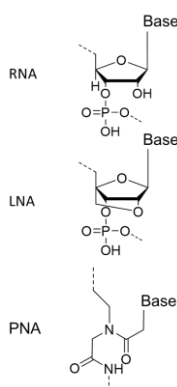
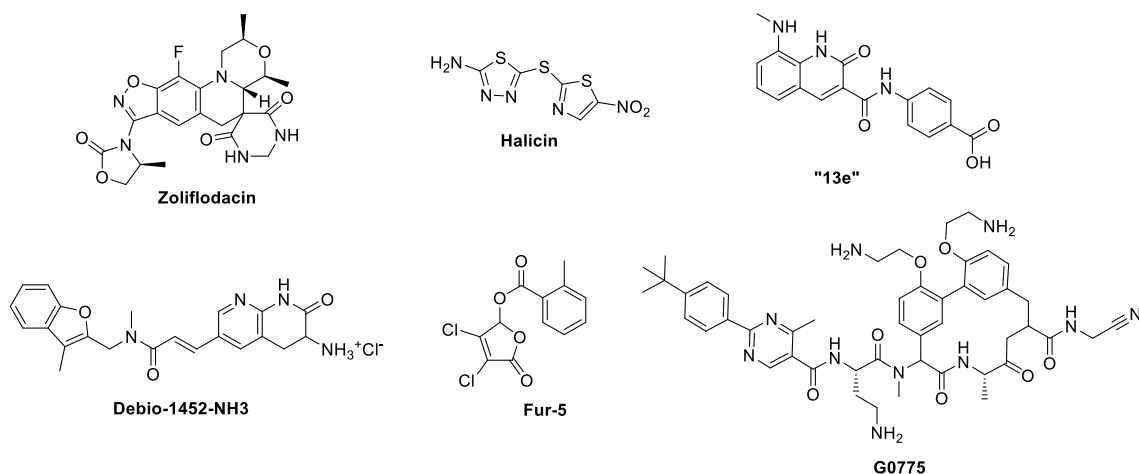


**Fig. 2. Key motifs of RNA and of other polynucleotide analogue**

(Poly-)nucleotide and nucleoside analogues are an emerging antibiotic class with high potential. Some compounds inhibit enzymes while others interfere with gene expression [169,170]. Especially, in the latter case antisense nucleic acids can be tailor-made for virtually every type of target mRNA and hence, inhibit the biosynthesis of the respective protein. Apart from designing RNAs, novel analogous structures with different backbones such as locked nucleic acids (LNAs) and peptide nucleic acids (PNAs) are emerging (Fig. 2) [171]. These are more resistant to nucleases and heat. While single nucleotides may still have access to the cell through porins, entire sequences of nucleic acids commonly violate many currently considered rules for good bacterial bioavailability, since they possess too many H-bond donors and acceptors, are polyanions and exceed upper limits of globularity, flexibility and size. Hence, a big issue for nucleic acid activity in Gram-negative bacteria is indeed their uptake. Co-administration with membrane-perturbing agents, such as polymyxins or cell penetrating peptides as well as conjugation with siderophores, may help to increase bacterial bioavailability.

**Table 4.** Recent examples of antibacterial compounds against Gram-negative bacteria



	<b>Zoliflodacin</b> [155]	<b>Halicin</b> [160]	<b>"13e"</b> [162]	<b>Debio-1452-NH3</b> [78]	<b>Fur-5</b> [165]	<b>G0775</b> [79]
<b>Target Enzyme or Mode of Action</b>	DNA gyrase and topoisomerase IV inhibitor	Dissipator of the $\Delta$ pH Component of the Proton Motive Force	DNA gyrase inhibitor	FabI inhibitor	Inhibition of QscR Reduction of virulence factor production	Inhibition of LepB Blockage of protein translocation across IM
<b>Molecular Weight<sup>[a]</sup></b>	487.4	261.3	337.3	390.4	287.1	889.1
<b>clogD<sub>7.4</sub><sup>[a]</sup></b>	1.7	0.9	0.3	0.8	1.9	2.3
<b>Ionisable Amine<sup>[b]</sup></b>	no	no	no	yes	no	yes
<b>Rotatable Bonds<sup>[b]</sup></b>	1	3	4	4	3	16
<b>Globularity<sup>[b]</sup></b>	0.095	0.073	0.006	0.033	0.073	0.062
<b>Minimal Projection Area (<math>\text{\AA}^2</math>)<sup>[c]</sup></b>	62.52	33.11	29.87	48.02	38.15	116.93

[a] Values generated by StarDrop v. 6.6.1.22652. [b] Calculated in the eNTRY-way [53,82]. [c] Values generated by MarvinSketch 20.8 [172].

## 2.4. Opportunities and risks of antibiotic drug design

It is important to note that most of the antibiotics are natural products, which normally have properties that differ largely from synthetic small molecules. On the one hand, these differences give a strong hint that some physicochemical features are rather specific to achieve an enhanced bacterial bioavailability. On the other hand, producers of natural antibiotics are usually found outside a living host (*Streptomyces* spp. [173,174], *Micromonospora* spp. [175], *Penicillium* spp. [176]), which means that secreted structures are not adapted to the mammalian organism and hence, some unexpected binding or metabolites may lead to adverse effects.

However, it is necessary to mention that despite the physicochemical differences between antibiotics and other drugs with human targets also many similarities can be found. This can be exploited towards better oral uptake of antibiotics into the human body, but can bear also a downside, since we may unintentionally be tuning our compounds to a higher risk of side effects when focussing too much on necessary parameters for Gram-negative uptake. There is evidence that mitochondria have evolved from Gram-negative  $\alpha$ -proteobacteria, which cannot only be observed by genome analysis, but also by several features of their membranes (e.g., presence of porins or phospholipid composition) [177]. When juxtaposing currently discussed favourable properties for compound uptake to “Lipinski’s rules of five” and other properties known to be advantageous for mammalian membrane permeability and oral systemic bioavailability (Table 5), it becomes obvious that similarities exist, which can affect the selectivity of antibiotic accumulation. As seen in Table 5, anti-infective compounds with low molecular weight, zwitterionic state, high rigidity and a low number of H-bond donors or acceptors, respectively, can potentially also cross mammalian membranes. If such compounds also bind to mammalian intracellular structures, this can lead to side effects. In addition, aiming for low globularity and high rigidity can enhance the risk for DNA intercalation [178], whereas the presence of amines can increase the risk for the human *Ether-à-go-go*-Related Gene (hERG) inhibition and unspecific receptor binding, affected also by 3D shape [179–181]. Flat molecules are also often associated with poor solubility [182]. Keeping this in mind, compound polarity, charge and the number of H-bond acceptors and donors appear as most crucial physicochemical properties to guarantee Gram-negative selectivity and hence, reduce the likelihood of side effects. Wisely selecting these limits for compounds may allow to find a compromise between sufficient bacterial and oral bioavailability and low, unspecific accumulation in mammalian cells. This understanding could also be integrated into computational programmes to support antibiotic drug discovery. Especially, zwitterions could be advantageous since they permeate well across unspecific bacterial porins, but poorly across phospholipid bilayers. Moreover, they have a good bioavailability due to paracellular uptake in the intestine and may avoid hERG inhibition [183].

**Table 5.** Physicochemical properties empirically found to be associated with enhanced accumulation in Gram-negative bacteria or mammalian cells, respectively.

Physicochemical property	Favoured accumulation in Gram-negative bacteria	Favoured accumulation in mammalian cells
Molecular weight (Da)	<600–900 [31,37,71,86,184]	<500 [185,186] (questioned by Mazák <i>et al.</i> [187])
State of charge	Zwitterionic [63,73], positive (ionisable amine) [53,77]	Uncharged [183]
Rotatable bonds	≤5 [77]	≤10 [186]
PSA	~ 165 Å <sup>2</sup> [71]	~ 70 Å <sup>2</sup> [71]; <140 Å <sup>2</sup> [187]
logP	~ 4.1 [69]	<5 [185]
clogP	– 0.1 [71]	2.7 [71]
clogD <sub>7.4</sub>	– 2.8 [71]	1.6 [71]
H-bond donors	5.1 [71]	1.6 [71], ≤5 [185]
H-bond acceptors	9.4 [71]	4.9 [71], ≤10 [185]
Globularity	≤0.25 [77]	Flat molecules associated with membrane partition rather than permeation [183]

In contrast to bacterial efflux, the selectivity of mammalian P-gp-mediated efflux is more thoroughly understood. P-gp removes a wide range of substances from cancer cells, but also from normal cells, such as hepatic cells, endothelial cells along the blood brain barrier (BBB), and the placenta as well as cells of the intestinal epithelium [188]. Functional groups, such as primary and secondary amides, alcohols, phenols, carboxylic acids and sulfonamides, are often recognised by P-gp. In general, rather hydrophobic compounds in a size range of approx. 300 to 4000 Da are recognised by P-gp [189,190]. Furthermore, a compound should have H-bond donors (<2) and total PSA below 90 Å<sup>2</sup>, or ideally below 70 Å<sup>2</sup>, to avoid P-gp efflux [190]. Predictive models exist to support drug design [191]. In the ideal case, we would reach the same level of understanding of bacterial efflux. Based on that knowledge, compounds could be designed with sufficiently high molecular size, PSA (~165 Å<sup>2</sup>) and an optimal number of H-bond donors to be substrate of P-gp leading to low accumulation in host cells but avoid efflux in Gram-negative bacteria to render the drug safer for the host and more active

against the pathogen. A recent attempt in this direction was made by the multiparameter optimisation software StarDrop releasing an antibacterial scoring profile in 2018. The properties of compounds active against Gram-negative bacteria were compared to other marketed drugs defining the following set of limits, where the resulting score should ideally be in the range of 0.4–0.6; total PSA > 65.68, flexibility < 0.3656, log solubility (logS) > 0.8232, logD < 1.793, hERG pIC<sub>50</sub> < 4.938, molecular weight > 237.1 and BBB category: negative [192].

### 3. How about combining oral and bacterial bioavailability?

Notably, there is the tendency that rather recently introduced antibiotic compounds against Gram-negative bacteria (cefiderocol, evaracycline, carbapenems, monobactams) need to be administered *intravenously* since they are too polar to undergo sufficient uptake via the intestinal mucosa. Also rifamycin, which is available as oral dosage form against non-invasive *E. coli* infections, has an oral bioavailability of less than 0.1% [193]. Nanoisation and many nanoformulations of drugs (e.g., dendrimers [194,195], nanoemulsions [196], liposomes [197]) usually enhance oral bioavailability by increasing the solubility, but cannot solve the problem of low trans- or paracellular transport across eucaryotic epithelia due to high polarity. The application of (bioadhesive) liposomes or chitosan nanoparticles; however, can enhance the dwelling time of the drug at mucosal surfaces and hence allow for a better bioavailability [198–201].

Moreover, the application of penetration enhancers is one possible way to enhance uptake through the intestinal mucosa. Even though many of these excipients are known to harm the mucosa, there are also more biocompatible approaches, such as the use of derivatised bile acids in combination with nano-sized delivery systems [202]. Direct ion-pairing of bile acids with positively charged drug molecules also reportedly increased oral bioavailability [203]. This strategy can be particularly useful for compounds, such as aminoglycosides or the above-mentioned compounds halicin, Debio-1452-NH<sub>3</sub> and G0775.

It is also worth pointing out that several -lactam antibiotics - although being either an- or zwitterions - have a high oral bioavailability. For 3<sup>rd</sup> to 5<sup>th</sup> generation cephalosporins (e.g., cefpodoxime proxetil, ceftriaxone, ceftazidime) this could be achieved by conjugating them with hydrophobic moieties leading to enhanced passive transmembrane diffusion.  $\beta$ -Amino-benzyl-penicillins, older cephalosporins (e.g., cefaclor, cefalexin, cefadroxil), but also some 3<sup>rd</sup> generation cephalosporins (e.g., cefixime, cefibuten) profit from their dipeptide-like structure and take a specific dipeptide-carrier mediated active route across the intestinal mucosa [204–207].

Instead of directly mimicking nutrient-like structures, antibiotic compounds can also be conjugated with substrates of active transporters actively taken up moieties, such as vitamins [208], amino acids (e.g., glycine, lysine, valine) [209,210] and sugars (glycosylation) [67,211]. At the same time, such moieties can also act as “recognition handles” for bacteria and hence, enhance both bacterial and oral bioavailability. If the conjugated moieties are natural, the release of them into systematic circulation may have a fewer side-effects [209].

When optimising drug design for non-facilitated passive diffusion across the bacterial envelope, which means the decrease of hydrophilicity and size compared to drugs taking the porin-mediated route, the issue of low oral bioavailability may be solved at the same time. Furthermore, it can be worthwhile to convert antibiotic compounds with low bioavailability into siderophores, as has been done for rifamycin [112]. It must, however, be carefully assessed to what extent these iron chelators interfere with the iron metabolism of the patient.

Additionally, the design of the compound should address the potentially difficulties to be faced at the site of bacterial infection. One of the problems are biofilms that are often, for example, associated with lung infections. Biofilms are even more difficult to penetrate than the planktonic bacteria. Within biofilm, bacterial colonies are dormant and have different mode of growth [212].

Overall, we think that a fine balance of the chemical design for ideal bacterial and oral bioavailability is needed in future antibiotic discovery. Evidently, it is difficult to address all these points in the current *in vitro* settings. Considering that critical Gram-negative pathogens such as Enterobacteriaceae and *P. aeruginosa* cause nosocomial infections of the gastrointestinal tract or the lung, respectively, it is worth considering if novel antibiotics should be administered locally rather than systemically. Additionally, hospitalised patients generally have some venous access. In order to support the design of antibacterial compounds, we first need more robust assays with meaningful assay read-outs to quantify bacterial bioavailability (Section 4).

#### **4. Assays for determining bacterial bioavailability**

We have not yet reached the ideal set of rules to design compounds that successfully cross any Gram-negative barrier. Whether the starting molecular entity is a decorated HTS hit or a small fragment, such rules may be difficult to realise without meaningful reference assays. Standard MIC assays will be partially indicative in this case; however, the activity read-out cannot specify where the problem may be. The ideal set of rules would consider the location of the target protein so that the compound has the highest chance to accumulate in the needed compartment. Importantly, they would also include environmental settings, such as pH, that influence not only the state of the compound but

also the bacterial behaviour and physiological conditions at the site of infection [74,75]. It is common practice in drug development to assess permeability across mammalian barriers at an early stage. Whilst several assays are routinely used to predict oral bioavailability (e.g., PAMPA, Caco-2), analogous fast, high-throughput membrane model methods for bacterial bioavailability are urgently needed with meaningful parameters for drug optimisation. Over the years, several groups have developed cell-based or cell-free assays to understand fundamental bacterial transport processes, of which the most important are listed in Table 6.

#### **4.1. Whole-cell assays**

Nikaido pioneered the accumulation time course of different antibiotics indirectly by incubating bacteria with an antibiotic solution and determined the decrease of antibiotic concentration in the supernatant by simple spectrophotometry (Fig. 3A) [213]. This easy procedure has been adapted also to LC-MS quantification [214] and deserves still further validation and upscaling. Direct compound quantification from the bacterium is possible using LC-MS after bacterial lysis [53,109,215], fluorimetry [56], RAMAN spectroscopy [216] or radiometry [217]. Especially LC-MS-based methods gained popularity and have become considerably quick [218]. LC-MS can be regarded as a gold standard to study accumulation, however, the effort in experimental preparation and sample purification, must still not be underestimated.

Beside quantifying general accumulation, it is already possible to detect accumulation in a subcellular manner either by detecting fluorescence using biorthogonal probes [59] or probe free by LC-MS [54]. While the former concept so far only works for compounds with azide moieties, the latter method is much more broadly applicable.

Microspectrofluorometry, enabling to study antibiotic accumulation in living bacteria and spheroplasts [56,219] may allow in situ colocalisation and uptake studies on upcoming larger antibiotic agents, such as peptides, phages, antibodies, nucleic acids and nanoparticles.

Systematic knock-out and stimulus-triggered expression of proteins involved in specific uptake and efflux can also make it possible to compare minimum inhibitory concentrations of different antibiotics and allow for studies on structure-permeation relationships, as shown by the so-called Titrable Outer Membrane Permeability Assay System (TOMAS) [220].

Overall, whole-cell assays are recommended as reference systems to directly measure the accumulation of antibiotics, because they also cover active uptake and efflux processes. Studies can be performed on specific strains and clinical isolates. Blocking or knock-out of diverse uptake, degradation and efflux mechanisms moreover allows investigation of the specific factors involved in antimicrobial accumulation. Assays with living bacteria, however, are prone to a number of errors



[221]. For example, genetic modifications may lead to a general shift in protein expression, as shown for  $\Delta$ TolC mutants [222]. The wide use of this strain, however, gives the impression that for translocation studies the outcome appears plausible, at least for *E. coli*, as it is often used to account for efflux-issues [169,215,223,224]. Chemosensitisers (e.g., carbonyl cyanide *m*-chlorophenylhydrazine,  $\beta$ -lactamase inhibitors) can either lack specificity and/or unintentionally interfere with other bacterial processes. Moreover, living organisms undergo continuous adaptation to their environment. Small deviations in the performance of the experiments may have severe effects on reproducibility. Lastly, working with living pathogens requires specific safety measures and classification.

#### **4.2. Vesicle-swelling assays**

Alternative cell-free approaches emerged to study specific pathways and to make investigations more distinct, faster and easier. Nikaido followed the hypothesis that the access of most anti-infective compounds is controlled by porins [32]. He investigated porin-mediated permeation by proteoliposomes containing *E. coli* OmpF [73]. The osmosis-driven compound uptake into the liposomes was investigated indirectly by measuring the increase of vesicle size (Fig. 3B). Ferreira *et al.* performed similar studies employing OM vesicles (OMVs) of *E. coli* K-12 instead [225]. Transferring this approach to other species, however, cannot be generally recommended as the membrane composition of OMVs does not always represent the original OM composition [226].

#### **4.3. Electrophysiology**

Nestorovich *et al.* studied the interactions of ampicillin with OmpF by electrophysiological methods (Fig. 3C) [227]. However, such studies lack evidence whether blocking events on the membrane channels are indeed reflecting molecular translocation across the membrane [85]. Recently, Wang *et al.* introduced OmpF channels featuring a cysteine moiety to quantify permeating molecules [228].

#### **4.4. Membrane-permeation assays**

To predict bacterial accumulation measuring the transport rates across surrogate membranes can be used. Permeable well-plate inserts can be coated with phospholipids [229] or multiple layers of biomaterials [109] resembling the overall Gram-negative bacterial envelope (Fig. 3D). For molecules <300 Da, these models seem to deliver results consistent with intrabacterial activity. Permeation data obtained for compounds >300 Da were only consistent for antibiotics following porin-independent passive permeation. A more recent approach employs a slightly acid-degraded starch hydrogel coating to mimic mainly porin-dependent drug permeation. Interestingly, permeation data obtained from this simple approach correlated quite well with intrabacterial accumulation data for a variety of representatives from different antibiotic classes [215].

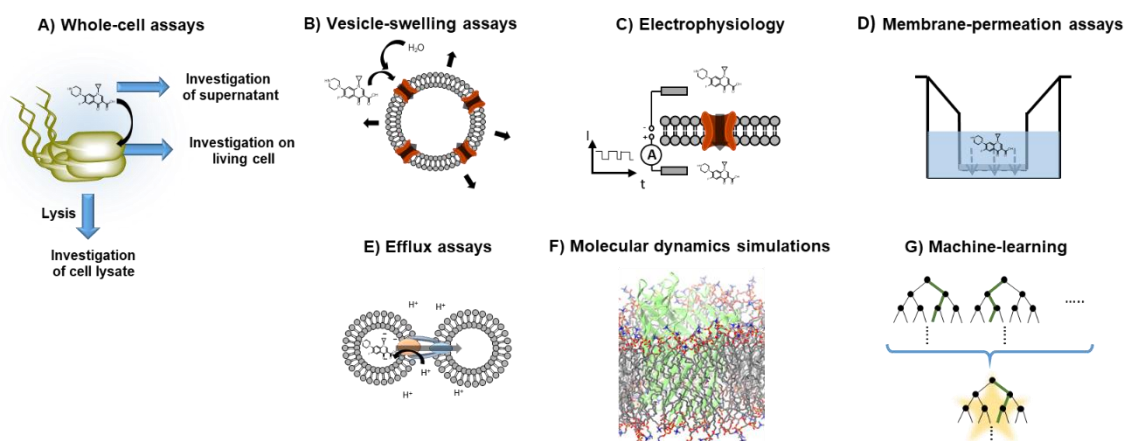


**Fig. 3. Overview over approaches to study compound accumulation, uptake or efflux.**

## 4.5 Efflux assays

Notably, efflux studies are much more challenging, since it is an active transport driven by the proton-motive force and depends on a complex of proteins. Zgurskaya *et al.* created proteoliposomes of *E. coli* AcrAB (Fig. 1) and embedded fluorescent phospholipids [230]. These proteoliposomes were assembled with unlabelled, unloaded liposomes. By creating a proton gradient across the liposomal membrane, they could activate the pumping complex, which then pumped fluorescent cargo from proteoliposomes into plain liposomes. Verchère *et al.* expanded this approach to two *P. aeruginosa* efflux pump subunits inserted in separated groups of liposomes (Fig. 3E) [231].

## 4.6. *In silico* methods

### 4.6.1 Molecular dynamics (MD) simulations

MD simulations describe atom movements within a system of molecules based on laws of classical mechanics [232]. As a result, this method can be used not only to study conformational changes, ligand binding and (macro-)molecular folding, but also membrane permeation. Regarding drug permeation in particular, it is possible to predict interactions between the permeating compound and various membrane structures, such as phospholipids, porins or membrane receptors (Fig. 3F) [233]. First MD simulations on parts of porins were reported as early as in 1994 [234], while first MD studies between OmpF and antibiotic molecules were published in 2002 [227]. Since then, the translocation of numerous antibiotics was studied across different porins [235]. Cramariuc *et al.* studied the permeation of ciprofloxacin across a phospholipid bilayer using MD simulations and confirmed energetically that the uncharged species of fluoroquinolones is the major permeating species across phospholipid membranes. Moreover, they proposed a mechanism of permeation where the loss of polarity, resulting from molecular stack formation among zwitterionic fluoroquinolones, favours the penetration into the membrane followed by neutralisation due to intermolecular transfer

of protons [107]. Furthermore, models of the asymmetric outer membrane [236], LPS [237], IM proteins [238] and also of TBDT [239] have been developed. These could be optimised towards a better understanding of antibiotic permeability.

MD can be considered sophisticated in several ways: it requires an abstract understanding of underlying simulation processes and the adequate adjustment of parameters (number of simulated molecules, starting conformation, molecular parameterisation, equations for intermolecular interactions, etc.). Moreover, high performing graphic processors are required. Depending on the size of the simulated system, the size of the permeating molecule and the computer infrastructure, a full analysis of a permeation process may take weeks to months. Coarse-grained models, where groups of atoms are merged to one “grain” can improve the computational performance [240], but lead to a loss of atomistic details about molecular interactions. To further reduce processing time of a permeation event, enhanced sampling techniques can be employed, such as metadynamics or umbrella sampling [235,241]. MD is a complementary method to experimental investigations, as for example electrophysiological assays, X-ray crystallography or Foerster resonance energy transfer (FRET) and can either be used to develop hypothesis to be experimentally investigated or explain experimental data [221,242].

#### **4.6.2 Machine-learning**

As previously mentioned in Sections 2.1.1 and 2.1.4, different types of machine-learning or deep learning have not only been employed to identify compounds with antibacterial activity [160,243,244], but also for investigations of bacterial membrane permeability [245], accumulation [53] and efflux [99,101]. Here, we want to give a brief introduction to the commonly used approaches:

Naïve Bayes (NB) is a rather simple supervised machine-learning method, which is used by the later mentioned Shared Platform for Antibiotic Research (SPARK). This method assumes independency of the training parameters (“dimensions”). Hence, it is less affected by the so-called “curse of dimensionality” and can also deal well with data sets that feature only a small overall sample number or a small number of “good” samples. This is of great advantage, since regarding Gram-negative bacterial bioavailability one can expect a much larger number of compounds with low bioavailability (“bad samples”) than there are with good bioavailability. As a drawback, it cannot detect synergistic patterns of physicochemical parameters.

Random-forest (RF) analysis is another example for supervised machine-learning and so far the most often reported technique to resolve chemical questions on antibiotic translocation phenomena [53,99,215]. RF analysis works by creation of multiple decision trees by applying a training data set.

When performing the analysis on a test set of data, these decision trees “vote” for the outcome (Fig. 3G). Depending on the selection of RF classification or regression, qualitative or quantitative predictions are possible. The results are comparatively easily interpretable. It is advantageous that RF also allows for the analysis of data sets, which contain incomplete information and parameters of different nature (e.g., shift between logP and logD or logD and molecular weight). This is helpful, since data sets from different groups were usually generated under different conditions while investigating different parameters.

More sophisticated than NB and RF is the use of Gradient Boosted Trees (GBT) as offered by the website “Open Drug Discovery” by Idorsia [84]. GBT work by sequential building of a high number of small decision trees. Each newly built tree is created based on the prediction error of the previous ones. As in RF, data sets may be incomplete. However, also as in RF the number of sample data must be exponentially larger than the number of training parameters. Comparatively high computational power is required.

Deep artificial neural networks (ANN) belong to the most complex machine-learning approaches. To the best of our knowledge these have not been reported so far for investigating aspects of bacterial bioavailability, but rather antibacterial activity [160]. An overview of the various types of ANN and current applications in drug discovery, design and delivery is given by Puri *et al.* [245]. Their current lack of application with respect to bacterial drug delivery is understandable, since deep ANN require a large amount of sample data, usually millions; a sophisticated computer infrastructure and comparatively long learning time. Once sufficiently large amounts of data are available, deep ANN can become the most powerful tools to predict antibiotic permeability and to elucidate structure-accumulation relationships, however at the same time resilience to noisy data and overfitting still needs to be improved [246].

Generally, the performance of machine-learning models is only as good as their training data set: the higher the quality, quantity and versatility the better.

#### **4.6.3 Shared Platform for Antibiotic Research and Knowledge (SPARK)**

The interactive and free SPARK platform, created by the PEW charitable trusts, holds high potential for future research on enhanced bacterial drug permeation, efflux, bioavailability and efficacy [247]. Researchers are invited to share their data on antibacterial activity or bacterial bioavailability on this platform. The platform provides statistical and visual applications. In addition, it offers a Bayesian statistical modelling option [248], where models can be trained using structural fingerprints (FCFP6) of the selected compounds to predict biological parameters as for example mean inhibitory concentration or accumulation [249–251]. Although the platform features a large master set of IC<sub>50</sub> and MIC data for example from Novartis, it would still profit from more physicochemical properties

provided along with the biological data. The database also features information on marketed drugs; however, comparability of different data sets and structures is currently complicated. For future antibiotic discovery, this platform can become a powerful tool. It can help to overcome the publication bias towards active compounds. In return, the platform can benefit from old clinical data, including for example insights of resistance development.

**Table 6.** Selection of assays for studies on bacterial accumulation and related processes.

Assay class	Method	Advantages	Disadvantages	Applicable for
<b>Whole-cell assays</b>	Indirect compound quantification via supernatant [213,252]	+ low equipment requirements + easy quantification	- no distinction between molecule accumulation, adhesion, partition - more extensive validation	Accumulation, (permeability)
	Intracellular quantification by -LC-MS [53,54]	+ highly specific + suitable for automation	- compound purification - sophisticated equipment - comparably slow	Accumulation
	-Spectrofluorimetry [56]	As in LC-MS, but + less sophisticated equipment	- only fluorescent compounds	Accumulation, (permeability)
	-Fluorescence microscopy [56]	+ accumulation-time course + upscalable/automation	- only fluorescent compounds - high resolution required	Accumulation, partition studies, (permeability)
	Titration Outer Membrane Permeability Assay System (TOMAS) [220]	+ upscalable + information about efficacy + less sophisticated equipment	- does not monitor accumulation directly - sophisticated biotechnological preparation of bacterial strains	Accumulation, permeability studies
<b>Vesicle-swelling assays</b>	Liposome-[253]/OMV-[225] swelling assay	+ less sophisticated equipment + covers lots of aspects of passive permeation across OM (using OMV's) or specific ones (using proteoliposomes)	- only for known membrane proteins - isolation of membrane proteins/OMV's necessary - only highly soluble compounds - lack of precision	Permeability

<b>Electrophysiology</b>	Black lipid membrane-based [221]	+ translocation of single molecules + adjustable to different bacterial strains by OMV	- migration along electric field instead of concentration gradient - susceptible to disturbances	Structure–permeability relationship studies on single substances
<b>Membrane-permeation assays</b>	Lipid-coated filter supports [109,229]	+ upscalable + easy-to-handle	- unspecific - expensive reagents	Direct measurement of permeability
<b>Efflux assay</b>	Liposome assembly [230,254]	+ study of efflux pump function + mimicry of active transport mechanisms	- preparation and loading of proteoliposomes	Characterisation of single efflux systems
<b><i>In silico</i></b>	Molecular dynamics [235]	+ detailed elucidation of structure–membrane interaction in course of permeation + strain and structure specific	- computation is time consuming and resource-demanding - requires background in physics and experience with simulation programs	Hypothesis testing regarding different uptake routes
	Machine-learning [53]	+ fast + mechanistic insights + predictive	- large experimental data sets - expertise in statistics and programming required	Prediction of accumulation and related factors; investigation of structural relations

## 5. Conclusions

Our current knowledge reveals that over the past five decades, overall findings of different generations of scientists have been complementary and consistent. Discrepancies, however, do appear when neglecting the individuality of Gram-negative species, their cell envelope, compound-dependent uptake pathways and other important aspects of bacterial bioavailability. Species belonging to Enterobacterales (*Escherichia*, *Salmonella* and *Klebsiella* spp.) usually feature “non-specific” porins as major Omp class, which allow for fast drug translocation. Here, designing drugs for porin-dependent uptake is a promising strategy. Favourable properties are low molecular weight, low minimal projection area, a strong dipole moment or zwitterionic structure, hydrophilicity, high rigidity and low globularity. This optimisation may, however, lead to limited oral bioavailability.

Until today, most rules are based on the structure of approved, active compounds. Would a second look at the many compounds, discontinued either for lacking activity or prohibitive adverse effects,

provide additional insights? Sources to obtain these data could be the Community for Open Antimicrobial Drug Discovery (CO-ADD) [255], SPARK [247] and the REVIVE hub by the Global Antibiotic Research & Development Partnership (GARDP) [256].

To characterise and better understand bacterial bioavailability of new antibiotics, we propose to define a small set of standardised assays, which preferably provide kinetic data, as for example permeability coefficients or concentration per colony forming units over time. Data obtained from these assays could be used to train machine-learning models, which could then accurately predict antibiotic accumulation in different bacterial compartments over time without further experimental effort and help the translation of effective antibiotics to the market. Clinical data should also be considered for future validation of bacterial bioavailability assays, also enabling the translation of the concept to Gram-positive bacteria. We envision that more candidates will make it to the clinics, if we master the early discovery stages and understand why we often fail to “translate” the activity from the bacterial assays to animal models and beyond. To achieve this goal, we need to work even more closely together by bridging chemistry, biology, microbiology, bio/cheminformatics and pharmaceutical sciences.

## Acknowledgements

H.-K.R. thanks Stiftung Stipendien-Fonds des Verbandes der Chemischen Industrie for the Kekulé Mobility Fellowship. A.K.H.H. gratefully acknowledges the Helmholtz-Association’s Initiative and Networking Fund. Moreover, the authors thank Carla Filipa Sousa and Olga Kalinina (both Helmholtz Institute for Pharmaceutical research Saarland, HIPS) for helpful advice and supply of images in the field of MD or machine-learning, respectively. The graphical abstract was created with BioRender.com.

## References

- [1] N.Q. Balaban, S. Helaine, K. Lewis, M. Ackermann, B. Aldridge, D.I. Andersson, M.P. Brynildsen, D. Bumann, A. Camilli, J.J. Collins, C. Dehio, S. Fortune, J.M. Ghigo, W.D. Hardt, A. Harms, M. Heinemann, D.T. Hung, U. Jenal, B.R. Levin, J. Michiels, G. Storz, M.W. Tan, T. Tenson, L. Van Melderen, A. Zinkernagel, Definitions and guidelines for research on antibiotic persistence, *Nat. Rev. Microbiol.* 17 (2019) 441–448. <https://doi.org/10.1038/s41579-019-0196-3>.
- [2] M.A.T. Blaskovich, The Fight Against Antimicrobial Resistance Is Confounded by a Global Increase in Antibiotic Usage, *ACS Infect. Dis.* 4 (2018) 868–870. <https://doi.org/10.1021/acscinfecdis.8b00109>.
- [3] U.S. Centers for Disease Control, Antibiotic Resistance Threats in the United States, 2019, [www.cdc.gov/DrugResistance/Biggest-Threats.html](http://www.cdc.gov/DrugResistance/Biggest-Threats.html). (accessed January 27, 2020).
- [4] S. Mukerji, M. Stegger, A.V. Truswell, T. Laird, D. Jordan, R.J. Abraham, A. Harb, M. Barton, M. O’Dea, S. Abraham, Resistance to critically important antimicrobials in Australian silver gulls (*Chroicocephalus novaehollandiae*) and evidence of anthropogenic origins, *J. Antimicrob. Chemother.* 74 (2019) 2566–2574. <https://doi.org/10.1093/jac/dkz242>.
- [5] K.M.M. Pärnänen, C. Narciso-Da-Rocha, D. Kneis, T.U. Berendonk, D. Cacace, T.T. Do, C. Elpers, D. Fatta-Kassinos, I. Henriques, T. Jaeger, A. Karkman, J.L. Martinez, S.G. Michael, I. Michael-Kordatou, K. O’Sullivan, S. Rodriguez-Mozaz, T. Schwartz, H. Sheng, H. Sørum, R.D. Stedtfeld, J.M. Tiedje, S.V. Della Giustina, F. Walsh, I. Vaz-Moreira, M. Virta, C.M. Manaia, Antibiotic resistance in European wastewater treatment plants mirrors the pattern of clinical antibiotic resistance prevalence, *Sci. Adv.* 5 (2019). <https://doi.org/10.1126/sciadv.aau9124>.
- [6] ECDC, Surveillance of antimicrobial resistance in Europe 2018, [www.ecdc.europa.eu](http://www.ecdc.europa.eu) (accessed January 27, 2020).
- [7] E. Tacconelli, N. Magrini, Global Priority List of Antibiotic-Resistant Bacteria to Guide Research, Discovery, and Development of New Antibiotics, WHO. (2017). <https://doi.org/10.1590/S0100-15742013000100018>.

- [8] K.M. Lehman, M. Grabowicz, Countering Gram-Negative Antibiotic Resistance: Recent Progress in Disrupting the Outer Membrane with Novel Therapeutics, *Antibiotics*. 8 (2019) 163. <https://doi.org/10.3390/antibiotics8040163>.
- [9] WHO, Antibacterial agents in clinical development: an analysis of the antibacterial clinical development pipeline, 2019.
- [10] E.D. Brown, G.D. Wright, Antibacterial drug discovery in the resistance era, *Nature*. 529 (2016) 336–343. <https://doi.org/10.1038/nature17042>.
- [11] U. Theuretzbacher, K. Outtersson, A. Engel, A. Karlén, The global preclinical antibacterial pipeline, *Nat. Rev. Microbiol.* (2019) 1–11. <https://doi.org/10.1038/s41579-019-0288-0>.
- [12] M. Lakemeyer, W. Zhao, F.A. Mandl, P. Hammann, S.A. Sieber, Thinking Outside the Box—Novel Antibacterials To Tackle the Resistance Crisis, *Angew. Chemie - Int. Ed.* 57 (2018) 14440–14475. <https://doi.org/10.1002/anie.201804971>.
- [13] WHO, Antibacterial agents in preclinical development: an open access database, 2019. WHO/EMP/IAU/2019.12.
- [14] M. Hay, D.W. Thomas, J.L. Craighead, C. Economides, J. Rosenthal, Clinical development success rates for investigational drugs, *Nat. Biotechnol.* 32 (2014) 40–51. <https://doi.org/10.1038/nbt.2786>.
- [15] M.A. Fischbach, C.T. Walsh, Antibiotics for emerging pathogens, *Science* (80-. ). 325 (2009) 1089–1093. <https://doi.org/10.1126/science.1176667>.
- [16] It's time to fix the antibiotic market, <https://wellcome.ac.uk/what-we-do/our-work/drug-resistant-infections/its-time-fix-broken-antibiotics-market> (accessed August 10, 2020).
- [17] M.O. A Sommer, C. Munck, R. Vendler Toft-Kehler, D.I. Andersson, Prediction of antibiotic resistance: time for a new preclinical paradigm?, *Nat. Rev. Microbiol.* 15 (2017) 689–696. <https://doi.org/10.1038/nrmicro.2017.75>.
- [18] G. Kapoor, S. Saigal, A. Elongavan, Action and resistance mechanisms of antibiotics: A guide for clinicians, *J Anaesthesiol Clin Pharmacol.* 33 (2017) 300–305. [https://doi.org/10.4103/joacp.JOACP\\_349\\_15](https://doi.org/10.4103/joacp.JOACP_349_15).
- [19] W. C Reygaert, An overview of the antimicrobial resistance mechanisms of bacteria, *AIMS Microbiol.* 4 (2018) 482–501. <https://doi.org/10.3934/microbiol.2018.3.482>.
- [20] A.L. Parkes, Antibacterial medicinal chemistry—what can we design for?, *Expert Opin. Drug Discov.* 00 (2020) 1–9. <https://doi.org/10.1080/17460441.2020.1767065>.
- [21] WHO, Priorization of Pathogens to Guide Discovery, Research and Development of New Antibiotics for Drug-Resistant Bacterial Infections, Including Tuberculosis, 2017. WHO/EMP/IAU/2017.12.
- [22] Press release: The 2005 Nobel Prize in Physiology or Medicine to Barry J. Marshall and J. Robin Warren, <https://www.nobelprize.org/prizes/medicine/2005/press-release/> (accessed February 16, 2020).
- [23] Haemophilus influenzae | Hib | Types of Infection and Causes | CDC, <https://www.cdc.gov/hi-disease/about/types-infection.html> (accessed February 16, 2020).
- [24] H. Gram, Ueber die isolirte Faerbung der Schizomyceten: in Schnitt- und Trockenpraeparaten, *Dtsch Med Wochenschr.* 10 (1884) 234–235. <https://doi.org/10.1055/s-0029-1209285>.
- [25] T. Sandle, Gram's Stain: History and Explanation of the Fundamental Technique of Determinative Bacteriology, *IST Sci. Technol. J.* (2004) 3–4.
- [26] R.S. Santos, C. Figueiredo, N.F. Azevedo, K. Braeckmans, S.C. De Smedt, Nanomaterials and molecular transporters to overcome the bacterial envelope barrier: Towards advanced delivery of antibiotics, *Adv. Drug Deliv. Rev.* 136–137 (2018) 28–48. <https://doi.org/10.1016/j.addr.2017.12.010>.
- [27] R.E.W. Hancock, The bacterial outer membrane as a drug barrier, *Trends Microbiol.* 5 (1997) 37–42. [https://doi.org/10.1016/S0966-842X\(97\)81773-8](https://doi.org/10.1016/S0966-842X(97)81773-8).
- [28] H. Nikaido, Molecular Basis of Bacterial Outer Membrane Permeability Revisited, *Microbiol. Mol. Biol. Rev.* 67 (2003) 593–656. <https://doi.org/10.1128/mbr.67.4.593-656.2003>.
- [29] S. Acosta-Gutiérrez, L. Ferrara, M. Pathania, M. Masi, J. Wang, I. Bodrenko, M. Zahn, M. Winterhalter, R.A. Stavenger, J.-M. Pagès, J.H. Naismith, B. Van Den Berg, M.G.P. Page, M. Ceccarelli, Getting Drugs into Gram-Negative Bacteria: Rational Rules for Permeation through General Porins, *ACS Infect. Dis.* 4 (2018) 1487–1498. <https://doi.org/10.1021/acsinfecdis.8b00108>.
- [30] E. Sugawara, H. Nikaido, OmpA is the principal nonspecific slow porin of *Acinetobacter baumannii*, *J. Bacteriol.* 194 (2012) 4089–4096. <https://doi.org/10.1128/JB.00435-12>.
- [31] A.G. Moat, J.W. Foster, M.P. Spector, *Microbial physiology*, Wiley-Liss Inc. 4 (2002) 383. <https://doi.org/10.1038/266092a0>.
- [32] H. Nikaido, M. Vaara, Molecular basis of bacterial outer membrane permeability, *Microbiol. Rev.* 49 (1985) 1–32.
- [33] E. Sugawara, S. Kojima, H. Nikaido, Klebsiella pneumoniae Major Porins OmpK35 and OmpK36 Allow More Efficient Diffusion of beta-Lactams than Their Escherichia coli Homologs OmpF and OmpC, 198 (2016) 3200–3208. <https://doi.org/10.1128/JB.00590-16.Editor>.
- [34] R.E.W. Hancock, R. Siehnell, N. Martin, Outer membrane proteins of *Pseudomonas*, *Mol. Microbiol.* 4 (1990) 1069–1075. <https://doi.org/10.1111/j.1365-2958.1990.tb00680.x>.



- [35] E. Sugawara, K. Nagano, H. Nikaido, Alternative folding pathways of the major porin OprF of *Pseudomonas aeruginosa*, *FEBS J.* 279 (2012) 910–918. <https://doi.org/10.1111/j.1742-4658.2012.08481.x>.
- [36] H. Li, Y.-F. Luo, B.J. Williams, T.S. Blackwell, C.-M. Xie, Structure and function of OprD protein in *Pseudomonas aeruginosa*: From antibiotic resistance to novel therapies Hui, *Int J Med Microbiol.* 302 (2012) 1–13. <https://doi.org/10.1016/j.ijmm.2011.10.001>.Structure.
- [37] T. Nakae, Outer Membrane of *Salmonella Typhimurium*: Reconstitution of Sucrose-Permeable Membrane Vesicles, *Biochem. Biophys. Res. Commun.* 64 (1975) 1224–1230.
- [38] E. Sugawara, E.M. Nestorovich, S. M. Bezrukov, H. Nikaido, *Pseudomonas aeruginosa* Porin OprF Exists in Two Different Conformations, *J Biol Chem.* 281 (2006) 16220–16229. <https://doi.org/10.1074/jbc.M600680200>.
- [39] Y. Fei, V. Ma, N. Maerkl, P. You, The down regulation of *E. coli* OmpF in response to sub-inhibitory concentrations of kanamycin is not mediated by MarA, *J. Exp. Microbiol. Immunol.* 16 (2012) 101–107.
- [40] L. Martínez-Martínez, S. Hernández-Allés, S. Albertí, J.M. Tomás, V.J. Benedi, G.A. Jacoby, In vivo selection of porin-deficient mutants of *Klebsiella pneumoniae* with increased resistance to cefoxitin and expanded-spectrum cephalosporins, *Antimicrob. Agents Chemother.* 40 (1996) 342–348. <https://doi.org/10.1128/aac.40.2.342>.
- [41] U.B. Sleytr, B. Schuster, E.M. Egelseer, D. Pum, S-layers: Principles and applications, *FEMS Microbiol. Rev.* 38 (2014) 823–864. <https://doi.org/10.1111/1574-6976.12063>.
- [42] N. Noinaj, M. Guillier, T.J. Barnard, S.K. Buchanan, TonB-dependent transporters: regulation, structure, and function., *Annu. Rev. Microbiol.* 64 (2010) 43–60. <https://doi.org/10.1146/annurev.micro.112408.134247>.
- [43] J.M.A. Blair, G.E. Richmond, L.J.V. Piddock, Multidrug efflux pumps in Gram-negative bacteria and their role in antibiotic resistance, *Future Microbiol.* 9 (2014) 1165–1177. <https://doi.org/10.2217/FMB.14.66>.
- [44] N.P. Greene, E. Kaplan, A. Crow, V. Koronakis, Antibiotic resistance mediated by the MacB ABC transporter family: A structural and functional perspective, *Front. Microbiol.* 9 (2018) 950. <https://doi.org/10.3389/fmicb.2018.00950>.
- [45] R.L. Juliano, V. Ling, A surface glycoprotein modulating drug permeability in Chinese hamster ovary cell mutants, *BBA - Biomembr.* 455 (1976) 152–162. [https://doi.org/10.1016/0005-2736\(76\)90160-7](https://doi.org/10.1016/0005-2736(76)90160-7).
- [46] B.D. Schindler, G.W. Kaatz, Multidrug efflux pumps of Gram-positive bacteria, *Drug Resist. Updat.* 27 (2016) 1–13. <https://doi.org/10.1016/j.drup.2016.04.003>.
- [47] J.M. Munita, C.A. Arias, Mechanisms of antibiotic resistance, *Microbiol. Spectr.* 4 (2016). <https://doi.org/10.1128/microbiolspec.VMBF-0016-2015>.
- [48] E.C.M. De Lange, Multi Drug Resistance P Glycoprotein and other Transporters, *Encycl. Stress.* (2007) 774–783. <https://doi.org/10.1016/B978-012373947-6.00562-6>.
- [49] L. Fernández, R.E.W. Hancock, Adaptive and mutational resistance: Role of porins and efflux pumps in drug resistance, *Clin. Microbiol. Rev.* 25 (2012) 661–681. <https://doi.org/10.1128/CMR.00043-12>.
- [50] H. Nikaido, M.H.J. Saier, Transport Proteins in Bacteria: Common Themes in Their Design, *Science* (80-. ). 258 (1992) 936–942.
- [51] B.J. Belin, N. Busset, E. Giraud, A. Molinaro, A. Silipo, Di.K. Newman, Hopanoid lipids: From membranes to plant-bacteria interactions, *Nat. Rev. Microbiol.* 16 (2018) 304–315. <https://doi.org/10.1038/nrmicro.2017.173>.
- [52] R.F. Epand, P.B. Savage, R.M. Epand, Bacterial lipid composition and the antimicrobial efficacy of cationic steroid compounds (Ceragenins), *Biochim. Biophys. Acta - Biomembr.* 1768 (2007) 2500–2509. <https://doi.org/10.1016/j.bbmem.2007.05.023>.
- [53] M.F. Richter, B.S. Drown, A.P. Riley, A. Garcia, T. Shirai, R.L. Svec, P.J. Hergenrother, Predictive compound accumulation rules yield a broad-spectrum antibiotic, *Nature.* 545 (2017) 299–304. <https://doi.org/10.1038/nature22308>.
- [54] H. Prochnow, V. Fetz, S.K. Hotop, M.A. García-Rivera, A. Heumann, M. Brönstrup, Subcellular Quantification of Uptake in Gram-Negative Bacteria, *Anal. Chem.* 91 (2019) 1863–1872. <https://doi.org/10.1021/acs.analchem.8b03586>.
- [55] J. Bedard, S. Wong, L.E. Bryan, Accumulation of enoxacin by *Escherichia coli* and *Bacillus subtilis*, *Antimicrob. Agents Chemother.* 31 (1987) 1348–1354. <https://doi.org/10.1128/AAC.31.9.1348>.
- [56] J. Vergalli, E. Dumont, J. Pajović, B. Cinquin, L. Maigre, M. Masi, M. Réfrégiers, J.M. Pagès, Spectrofluorimetric quantification of antibiotic drug concentration in bacterial cells for the characterization of translocation across bacterial membranes, *Nat. Protoc.* 13 (2018) 1348–1361. <https://doi.org/10.1038/nprot.2018.036>.
- [57] M. Masi, M. Réfrégiers, K.M. Pos, J.M. Pagès, Mechanisms of envelope permeability and antibiotic influx and efflux in Gram-negative bacteria, *Nat. Microbiol.* 2 (2017) 17001. <https://doi.org/10.1038/nmicrobiol.2017.1>.
- [58] S. Zhao, J.W. Adamiak, V. Bonifay, J. Mehla, H.I. Zgurskaya, D.S. Tan, Defining new chemical space for drug penetration into Gram-negative bacteria, *Nat. Chem. Biol.* 16 (2020) 1293–1302. <https://doi.org/10.1038/s41589-020-00674-6>.
- [59] B. Spangler, D. Dovala, W.S. Sawyer, K. V. Thompson, D.A. Six, F. Reck, B.Y. Feng, Molecular Probes for the Determination of Subcellular Compound Exposure Profiles in Gram-Negative Bacteria, *ACS Infect. Dis.* 4 (2018) 1355–1367. <https://doi.org/10.1021/acsinfectdis.8b00093>.

- [60] M. Campos, S.K. Govers, I. Irnov, G.S. Dobihal, F. Cornet, C. Jacobs-Wagner, Genomewide phenotypic analysis of growth, cell morphogenesis, and cell cycle events in *Escherichia coli*, *Mol. Syst. Biol.* 14 (2018) 1–21. <https://doi.org/10.15252/msb.20177573>.
- [61] N. Ojkic, D. Serbanescu, S. Banerjee, Universal surface-to-volume scaling and aspect ratio homeostasis in rod-shaped bacteria, *BioRxiv.* 3 (2019) 1–11. <https://doi.org/10.1101/583989>.
- [62] H.E. Kubitschek, J.A. Friske, Determination of bacterial cell volume with the Coulter Counter, *J. Bacteriol.* 168 (1986) 1466–1467. <https://doi.org/10.1128/jb.168.3.1466-1467.1986>.
- [63] J. Vergalli, I. V. Bodrenko, M. Masi, L. Moynié, S. Acosta-Gutiérrez, J.H. Naismith, A. Davin-Regli, M. Ceccarelli, B. van den Berg, M. Winterhalter, J.-M. Pagès, Porins and small-molecule translocation across the outer membrane of Gram-negative bacteria., *Nat. Rev. Microbiol.* 18 (2020) 164–176. <https://doi.org/10.1038/s41579-019-0294-2>.
- [64] J. Vergalli, A. Atzori, J. Pajovic, E. Dumont, G. Mallocci, M. Masi, A.V. Vargiu, M. Winterhalter, M. Réfrégiers, P. Ruggerone, J.M. Pagès, The challenge of intracellular antibiotic accumulation, a function of fluoroquinolone influx versus bacterial efflux, *Commun. Biol.* 3 (2020) 1–12. <https://doi.org/10.1038/s42003-020-0929-x>.
- [65] D. Du, X. Wang-Kan, A. Neuberger, H.W. van Veen, K.M. Pos, L.J.V. Piddock, B.F. Luisi, Multidrug efflux pumps: structure, function and regulation, *Nat. Rev. Microbiol.* 16 (2018) 523–539. <https://doi.org/10.1038/s41579-018-0048-6>.
- [66] M.S. Ramirez, M.E. Tolmasky, Aminoglycoside Modifying Enzymes Maria, *Drug Resist. Updat.* 13 (2010) 151–171. <https://doi.org/10.1016/j.drug.2010.08.003>.Aminoglycoside.
- [67] L. Guan, H.R. Kaback, Glucose/Sugar Transport in Bacteria, in: *Encycl. Biol. Chem. Second Ed.*, Elsevier Inc., 2013: pp. 387–390. <https://doi.org/10.1016/B978-0-12-378630-2.00580-6>.
- [68] G.D. Wright, Bacterial resistance to antibiotics: Enzymatic degradation and modification, *Adv. Drug Deliv. Rev.* 57 (2005) 1451–1470. <https://doi.org/10.1016/j.addr.2005.04.002>.
- [69] E.J. Lien, C. Hansch, S.M. Anderson, Structure-Activity Correlations for Antibacterial Agents on Gram-Positive and Gram-Negative Cells, *J. Med. Chem.* 11 (1968) 430–441. <https://doi.org/10.1021/jm00309a004>.
- [70] K. Gould, Antibiotics: from prehistory to the present day, *J. Antimicrob. Chemother.* 71 (2016) 572–575. <https://doi.org/10.1093/jac/dkv484>.
- [71] R. O’Shea, H.E. Moser, Physicochemical properties of antibacterial compounds: Implications for drug discovery, *J. Med. Chem.* 51 (2008) 2871–2878. <https://doi.org/10.1021/jm700967e>.
- [72] R. Tommasi, D.G. Brown, G.K. Walkup, J.I. Manchester, A.A. Miller, ESKAPEing the labyrinth of antibacterial discovery, *Nat. Rev. Drug Discov.* 14 (2015) 529–542. <https://doi.org/10.1038/nrd4572>.
- [73] F. Yoshimura, H. Nikaido, Diffusion of  $\beta$ -lactam antibiotics through the porin channels of *Escherichia coli* K-12, *Antimicrob. Agents Chemother.* 27 (1985) 84–92. <https://doi.org/10.1128/AAC.27.1.84>.
- [74] T. Ferenci, K. Phan, How Porin Heterogeneity and Trade-Offs Affect the Antibiotic Susceptibility of Gram-Negative Bacteria, *Genes (Basel).* 6 (2015) 1113–1124. <https://doi.org/10.3390/genes6041113>.
- [75] J. van der Heijden, L.A. Reynolds, W. Deng, A. Mills, R. Scholz, K. Imami, L.J. Foster, F. Duong, B.B. Finlay, *Salmonella* rapidly regulates membrane permeability to survive oxidative stress, *MBio.* 7 (2016) e01238-16. <https://doi.org/10.1128/mBio.01238-16>.
- [76] L.L. Silver, A Gestalt approach to Gram-negative entry, *Bioorganic Med. Chem.* 24 (2016) 6379–6389. <https://doi.org/10.1016/j.bmc.2016.06.044>.
- [77] M.F. Richter, P.J. Hergenrother, The challenge of converting gram-positive-only compounds into broad-spectrum antibiotics, *Ann. N. Y. Acad. Sci.* 1435 (2019) 18–38. <https://doi.org/10.1111/nyas.13598>.
- [78] E.N. Parker, B.S. Drown, E.J. Geddes, H.Y. Lee, N. Ismail, G.W. Lau, P.J. Hergenrother, Implementation of permeation rules leads to a FabI inhibitor with activity against Gram-negative pathogens, *Nat. Microbiol.* 5 (2020) 67–75. <https://doi.org/10.1038/s41564-019-0604-5>.
- [79] P.A. Smith, M.F.T. Koehler, H.S. Girgis, D. Yan, Y. Chen, Y. Chen, J.J. Crawford, M.R. Durk, R.I. Higuchi, J. Kang, J. Murray, P. Paraselli, S. Park, W. Phung, J.G. Quinn, T.C. Roberts, L. Rougé, J.B. Schwarz, E. Skipington, J. Wai, M. Xu, Z. Yu, H. Zhang, M.W. Tan, C.E. Heise, Optimized arylomycins are a new class of Gram-negative antibiotics, *Nature.* 561 (2018) 189–194. <https://doi.org/10.1038/s41586-018-0483-6>.
- [80] H. Fischer, M. Kansy, D. Bur, CAFCA: A novel tool for the calculation of amphiphilic properties of charged drug molecules, *Chimia (Aarau).* 54 (2000) 640–645.
- [81] H. Nikaido, An.G. David Thanassi, Penetration of Lipophilic Agents with Multiple Protonation Sites into Bacterial Cells: Tetracyclines and Fluoroquinolones as Examples, *Antimicrob. Agents Chemother.* 37 (1993) 1393–1399.
- [82] Entryway, <http://www.entry-way.org/> (accessed January 28, 2020).
- [83] Open Drug Discovery, <https://opendrugdiscovery.com/> (accessed August 5, 2020).
- [84] F. Le Goff, L. Christen, G. Bourquin, J. Hazemann, M. Von Korff, G. Pierlot, G. Rueedi, O. Peter, D. Ritz, Poster: Measurement and prediction of small molecule retention by Gram-negative bacteria based on a large-scale LC / MS screen, 2017.

- [85] H. Bajaj, S. Acosta Gutierrez, I. Bodrenko, G. Mallocci, M.A. Scorciapino, M. Winterhalter, M. Ceccarelli, Bacterial Outer Membrane Porins as Electrostatic Nanosieves: Exploring Transport Rules of Small Polar Molecules, *ACS Nano*. 11 (2017) 5465–5473. <https://doi.org/10.1021/acsnano.6b08613>.
- [86] F. Ruggiu, S. Yang, R.L. Simmons, A. Casarez, A.K. Jones, C. Li, J.M. Jansen, H.E. Moser, C.R. Dean, F. Reck, M. Lindvall, Size Matters and How You Measure It: A Gram-Negative Antibacterial Example Exceeding Typical Molecular Weight Limits, *ACS Infect. Dis.* 5 (2019) 1688–1692. <https://doi.org/10.1021/acinfecdis.9b00256>.
- [87] Q. Zhu, Y. Lu, X. He, T. Liu, H. Chen, F. Wang, D. Zheng, H. Dong, J. Ma, Entropy and Polarity Control the Partition and Transportation of Drug-like Molecules in Biological Membrane, *Sci. Rep.* 7 (2017) 1–10. <https://doi.org/10.1038/s41598-017-18012-7>.
- [88] P. Plésiat, H. Nikaido, Outer membranes of Gram-negative bacteria are permeable to steroid probes, *Mol. Microbiol.* 6 (1992) 1323–1333. <https://doi.org/10.1111/j.1365-2958.1992.tb00853.x>.
- [89] J.L. MacCallum, D.P. Tieleman, Chapter 8 Interactions between Small Molecules and Lipid Bilayers, *Curr. Top. Membr.* 60 (2008) 227–256. [https://doi.org/10.1016/S1063-5823\(08\)00008-2](https://doi.org/10.1016/S1063-5823(08)00008-2).
- [90] J.L. MacCallum, W.F. Drew Bennett, D. Peter Tieleman, Distribution of amino acids in a lipid bilayer from computer simulations, *Biophys. J.* 94 (2008) 3393–3404. <https://doi.org/10.1529/biophysj.107.112805>.
- [91] K. Shimizu, Metabolic Regulation of a Bacterial Cell System with Emphasis on Escherichia coli Metabolism, *ISRN Biochem.* 2013 (2013) 1–47. <https://doi.org/10.1155/2013/645983>.
- [92] J.L. Markley, T.A. Wencewicz, Tetracycline-inactivating enzymes, *Front. Microbiol.* 9 (2018) 1–22. <https://doi.org/10.3389/fmicb.2018.01058>.
- [93] H.I. Zgurskaya, C.A. López, S. Gnanakaran, Permeability Barrier of Gram-Negative Cell Envelopes and Approaches to Bypass It, *ACS Infect. Dis.* 1 (2015) 512–522. <https://doi.org/10.1021/acinfecdis.5b00097>.
- [94] X. Shi, M. Chen, Z. Yu, J.M. Bell, H. Wang, I. Forrester, H. Villarreal, J. Jakana, D. Du, B.F. Luisi, S.J. Ludtke, Z. Wang, In situ structure and assembly of the multidrug efflux pump AcrAB-TolC, *Nat. Commun.* 10 (2019) 1–6. <https://doi.org/10.1038/s41467-019-10512-6>.
- [95] S. Nolivos, J. Cayron, A. Dedieu, A. Page, F. Delolme, C. Lesterlin, Role of AcrAB-TolC multidrug efflux pump in drug-resistance acquisition by plasmid transfer, *Science*. 364 (2019) 778–782. <https://doi.org/10.1126/science.aav6390>.
- [96] V.R. Povolov, M. Ackermann, Disseminating antibiotic resistance during treatment, *Science*. 364 (2019) 737–738. <https://doi.org/10.1126/science.aax6620>.
- [97] N. Abdali, J.M. Parks, K.M. Haynes, J.L. Chaney, A.T. Green, D. Wolloscheck, J.K. Walker, V. V Rybenkov, J. Baudry, J.C. Smith, H.I. Zgurskaya, Reviving Antibiotics: Efflux Pump Inhibitors That Interact with AcrA, a Membrane Fusion Protein of the AcrAB-TolC Multidrug Efflux Pump, *ACS Infect. Dis.* 3 (2017) 89–98. <https://doi.org/10.1021/acinfecdis.6b00167>.
- [98] D.G. Brown, T.L. May-Dracka, M.M. Gagnon, R. Tommasi, Trends and Exceptions of Physical Properties on Antibacterial Activity for Gram-Positive and Gram-Negative Pathogens, *J. Med. Chem.* 57 (2014) 10144–10161. <https://pubs.acs.org/sharingguidelines> (accessed January 29, 2020).
- [99] S.J. Cooper, G. Krishnamoorthy, D. Wolloscheck, J.K. Walker, V. V. Rybenkov, J.M. Parks, H.I. Zgurskaya, Molecular Properties That Define the Activities of Antibiotics in Escherichia coli and Pseudomonas aeruginosa, *ACS Infect. Dis.* 4 (2018) 1223–1234. <https://doi.org/10.1021/acinfecdis.8b00036>.
- [100] G. Krishnamoorthy, I. V Leus, J.W. Weeks, D. Wolloscheck, V. V Rybenkov, H.I. Zgurskaya, Synergy between Active Efflux and Outer Membrane Diffusion Defines Rules of Antibiotic Permeation into Gram-Negative Bacteria, *MBio*. 8 (2017) 1–16. <https://doi.org/10.1128/mBio>.
- [101] S.S. El Zahed, S. French, M.A. Farha, G. Kumar, E.D. Brown, Physicochemical and Structural Parameters Contributing to the Antibacterial Activity and Efflux Susceptibility of Small Molecule Inhibitors of Escherichia coli, *Antimicrob. Agents Chemother.* (2021). <https://doi.org/10.1128/aac.01925-20>.
- [102] GitHub - sfrench007/serf: Code and example data from a synthetic compound phenotypic screen identifying efflux substrates in E. coli, <https://github.com/sfrench007/serf> (accessed February 1, 2021).
- [103] W. Wei, S. Cherukupalli, L. Jing, X. Liu, P. Zhan, Fsp3: A new parameter for drug-likeness, *Drug Discov. Today*. 25 (2020) 1839–1845. <https://doi.org/10.1016/j.drudis.2020.07.017>.
- [104] R.E.W. Hancock, A. Bell, Antibiotic Uptake into Gram-Negative Bacteria, *Eur. J. Clin. Microbiol. Infect. Dis.* 7 (1988) 713–720. <https://doi.org/10.1007/BF01975036>.
- [105] M. Ferreira, L.J. Bessa, C.F. Sousa, P. Eaton, D. Bongiorno, S. Stefani, F. Campanile, P. Gameiro, Fluoroquinolone metalloantibiotics: A promising approach against methicillin-resistant staphylococcus aureus, *Int. J. Environ. Res. Public Health*. 17 (2020) 1–18. <https://doi.org/10.3390/ijerph17093127>.
- [106] A. Sigler, P. Schubert, W. Hillen, M. Niederweis, Permeation of tetracyclines through membranes of liposomes and Escherichia coli, *Eur. J. Biochem.* 267 (2000) 527–534. <https://doi.org/10.1046/j.1432-1327.2000.01026.x>.
- [107] O. Cramariuc, T. Rog, M. Javanainen, L. Monticelli, A. V. Polishchuk, I. Vattulainen, Mechanism for translocation of fluoroquinolones across lipid membranes, *Biochim. Biophys. Acta - Biomembr.* 1818 (2012) 2563–2571. <https://doi.org/10.1016/j.bbamem.2012.05.027>.

- [108] P.E. Grubb, Nalidixic Acid, *Anal. Profiles Drug Subst. Excipients*. 8 (1979) 371–397. [https://doi.org/10.1016/S0099-5428\(08\)60124-0](https://doi.org/10.1016/S0099-5428(08)60124-0).
- [109] F. Graef, R. Richter, V. Fetz, X. Murgia, C. De Rossi, N. Schneider-Daum, G. Allegretta, W. Elgaher, J. Hauptenthal, M. Empting, F. Beckmann, M. Brönstrup, R. Hartmann, S. Gordon, C.M. Lehr, In Vitro Model of the Gram-Negative Bacterial Cell Envelope for Investigation of Anti-Infective Permeation Kinetics, *ACS Infect. Dis.* 4 (2018) 1188–1196. <https://doi.org/10.1021/acinfecdis.7b00165>.
- [110] G.G. Zhanel, A.R. Golden, S. Zelenitsky, K. Wiebe, C.K. Lawrence, H.J. Adam, T. Idowu, R. Domalaon, F. Schweizer, M.A. Zhanel, P.R.S. Lagacé-Wiens, A.J. Walky, A. Noreddin, J.P. Lynch, J.A. Karlowsky, Cefiderocol: A Siderophore Cephalosporin with Activity Against Carbapenem-Resistant and Multidrug-Resistant Gram-Negative Bacilli, *Drugs*. 79 (2019) 271–289. <https://doi.org/10.1007/s40265-019-1055-2>.
- [111] FDA approves new antibacterial drug to treat complicated urinary tract infections as part of ongoing efforts to address antimicrobial resistance, (2019). <https://www.fda.gov/news-events/press-announcements/fda-approves-new-antibacterial-drug-treat-complicated-urinary-tract-infections-part-ongoing-efforts> (accessed January 26, 2021).
- [112] W. Wehrli, W. Zimmermann, W. Kump, W. Tosch, W. Vlscher, O. Zak, Cgp 4832, A New Semisynthetic Rifamycin Derivative Highly Active Against Some Gram-Negative Bacteria, *J. Antibiot. (Tokyo)*. 40 (1987) 1733–1739. <https://doi.org/10.7164/antibiotics.40.1733>.
- [113] S. Satake, T. Nakae, Outer membrane permeability of  $\beta$ -lactamase inhibitors in *Pseudomonas aeruginosa*, *FEMS Microbiol. Lett.* 129 (1995) 251–254. [https://doi.org/10.1016/0378-1097\(95\)00166-3](https://doi.org/10.1016/0378-1097(95)00166-3).
- [114] M. Zahn, S.P. Bhamidimarri, A. Baslé, M. Winterhalter, B. Van Den Berg, Structural Insights into Outer Membrane Permeability of *Acinetobacter baumannii*, *Structure*. 24 (2016) 221–231. <https://doi.org/10.1016/j.str.2015.12.009>.
- [115] F. Citak, I. Ghai, F. Rosenkötter, L. Benier, M. Winterhalter, R. Wagner, Probing transport of fosfomycin through substrate specific OprO and OprP from *Pseudomonas aeruginosa*, *Biochem. Biophys. Res. Commun.* 495 (2018) 1454–1460. <https://doi.org/10.1016/j.bbrc.2017.11.188>.
- [116] R.E.W. Hancock, Alterations in structure of the cell envelope, *Ann. Rev. Microbiol.* 38 (1984) 237–264.
- [117] C.K. Skepper, D. Armstrong, C.J. Balibar, D. Bauer, C. Bellamacina, B.M. Benton, D. Bussiere, G. De Pascale, J. De Vicente, C.R. Dean, B. Dhumale, L.M. Fisher, J. Fuller, M. Fulsunder, L.M. Holder, C. Hu, B. Kantariya, G. Lapointe, J.A. Leeds, X. Li, P. Lu, A. Lvov, S. Ma, S. Madhavan, S. Malekar, D. McKenney, W. Mergo, L. Metzger, H.E. Moser, D. Mutnick, J. Noeske, C. Osborne, A. Patel, D. Patel, T. Patel, K. Prajapati, K.R. Prosen, F. Reck, D.L. Richie, A. Rico, M.R. Sanderson, S. Satasia, W.S. Sawyer, J. Selvarajah, N. Shah, K. Shanghavi, W. Shu, K. V. Thompson, M. Traebert, A. Vala, L. Vala, D.A. Veselkov, J. Vo, M. Wang, M. Widya, S.L. Williams, Y. Xu, Q. Yue, R. Zang, B. Zhou, A. Rivkin, Topoisomerase Inhibitors Addressing Fluoroquinolone Resistance in Gram-Negative Bacteria, *J. Med. Chem.* 63 (2020) 7773–7816. <https://doi.org/10.1021/acs.jmedchem.0c00347>.
- [118] J.A. Bafna, E. Sans-Serramitjana, S. Acosta-Gutiérrez, I. V. Bodrenko, D. Hörömpöli, A. Berscheid, H. Brötz-Oesterhelt, M. Winterhalter, M. Ceccarelli, Kanamycin Uptake into *Escherichia coli* Is Facilitated by OmpF and OmpC Porin Channels Located in the Outer Membrane, *ACS Infect. Dis.* 6 (2020) 1855–1865. <https://doi.org/10.1021/acinfecdis.0c00102>.
- [119] R. Nakae, T. Nakae, Diffusion of aminoglycoside antibiotics across the outer membrane of *Escherichia coli*, *Antimicrob. Agents Chemother.* 22 (1982) 554–559. <https://doi.org/10.1128/AAC.22.4.554>.
- [120] J.W. McFarland, C.M. Berger, S.A. Froshauer, S.F. Hayashi, S.J. Hecker, B.H. Jaynes, M.R. Jefson, B.J. Kamicker, C.A. Lipinski, K.M. Lundy, C.P. Reese, C.B. Vu, Quantitative structure–activity relationships among macrolide antibacterial agents: In vitro and in vivo potency against *Pasteurella multocida*, *J. Med. Chem.* 40 (1997) 1340–1346. <https://doi.org/10.1021/jm960436i>.
- [121] J. Aagaard, P.O. Madsen, P. Rhodes, T. Gasser, MICs of ciprofloxacin and trimethoprim for *Escherichia coli*: Influence of pH, inoculum size and various body fluids, *Infection*. 19 (1991) S167–S169. <https://doi.org/10.1007/BF01643691>.
- [122] I. Chopra, M. Roberts, Tetracycline Antibiotics: Mode of Action, Applications, Molecular Biology, and Epidemiology of Bacterial Resistance, *Microbiol. Mol. Biol. Rev.* 65 (2001) 232–260. <https://doi.org/10.1128/MMBR.65.2.232>.
- [123] T.H. Grossman, Tetracycline antibiotics and resistance, *Cold Spring Harb. Perspect. Med.* 6 (2016) 1–24. <https://doi.org/10.1101/cshperspect.a025387>.
- [124] E.P. Abraham, E. Chain, An Enzyme from Bacteria able to, *Nature*. 146 (1940) 837.
- [125] M.J. Basker, R.J. Boon, P.A. Hunter, Comparative antibacterial properties in vitro of seven olivanic acid derivatives: Mm 4550, MM 13902, MM 17880, MM 22380, MM 22381, MM 22382 and MM 22383, *J. Antibiot. (Tokyo)*. 33 (1980) 878–884. <https://doi.org/10.7164/antibiotics.33.878>.
- [126] R.P. Ambler, The structure of beta-lactamases, *Philos Trans R Soc L. B Biol Sci.* 289 (1980) 312–331. <https://doi.org/10.1098/gsm/146/03>.
- [127] J. Schmitz, Alte und neue beta-Lactamase Inhibitoren – Old and new beta-lactamase inhibitors, *Pharmakon*. 8 (2020) 231–239. <https://doi.org/10.1691/pn.20200022>.
- [128] D.E. Ehmman, H. Jahić, P.L. Ross, R.F. Gu, J. Hu, G. Kern, G.K. Walkup, S.L. Fisher, Avibactam is a covalent, reversible, non- $\beta$ -lactam  $\beta$ -lactamase inhibitor, *Proc. Natl. Acad. Sci. U. S. A.* 109 (2012) 11663–11668. <https://doi.org/10.1073/pnas.1205073109>.
- [129] N.P. Krishnan, N.Q. Nguyen, K.M. Papp-Wallace, R.A. Bonomo, F. Van Den Akker, Inhibition of *Klebsiella*  $\beta$ -lactamases (SHV-1 and KPC-2) by avibactam: A structural study, *PLoS One*. 10 (2015) 1–13. <https://doi.org/10.1371/journal.pone.0136813>.

- [130] A. Krajnc, J. Brem, P. Hinchliffe, K. Calvopiña, T.D. Panduwawala, P.A. Lang, J.J.A.G. Kamps, J.M. Tyrrell, E. Widlake, B.G. Saward, T.R. Walsh, J. Spencer, C.J. Schofield, Bicyclic Boronate VNRX-5133 Inhibits Metallo- And Serine- $\beta$ -Lactamases, *J. Med. Chem.* 62 (2019) 8544–8556. <https://doi.org/10.1021/acs.jmedchem.9b00911>.
- [131] J.C. Hamrick, J.-D. Docquier, T. Uehara, C.L. Myers, D.A. Six, C.L. Chatwin, K.J. John, S.F. Vernacchio, S.M. Cusick, R.E.L. Trout, C. Pozzi, F. De Luca, M. Benvenuti, S. Mangani, B. Liu, R.W. Jackson, G. Moeck, L. Xerri, C.J. Burns, D.C. Pevear, D.M. Daigle, VNRX-5133 (Taniborbactam), a Broad-Spectrum Inhibitor of Serine- and Metallo-beta-Lactamases, Restores Activity of Cefepime in Enterobacterales and *Pseudomonas aeruginosa*, *Antimicrob. Agents Chemother.* 64 (2020) e01963-19, <https://doi.org/10.1128/AAC.01963-19>.
- [132] J. Chen, S. Xie, Overview of sulfonamide biodegradation and the relevant pathways and microorganisms, *Sci. Total Environ.* 640–641 (2018) 1465–1477. <https://doi.org/10.1016/j.scitotenv.2018.06.016>.
- [133] J. Yin, G. Wang, D. Cheng, J. Fu, J. Qiu, Z. Yu, Inactivation of polymyxin by hydrolytic mechanism, *Antimicrob. Agents Chemother.* 63 (2019) 1–10. <https://doi.org/10.1128/AAC.02378-18>.
- [134] S. Coyne, P. Courvalin, B. Périchon, Efflux-mediated antibiotic resistance in *Acinetobacter* spp., *Antimicrob. Agents Chemother.* 55 (2011) 947–953. <https://doi.org/10.1128/AAC.01388-10>.
- [135] E.Y. Rosenberg, D. Ma, H. Nikaido, AcrD of *Escherichia coli* is an aminoglycoside efflux pump, *J. Bacteriol.* 182 (2000) 1754–1756. <https://doi.org/10.1128/JB.182.6.1754-1756.2000>.
- [136] R. Chuanchuen, W. Wannaprasat, K. Ajariyakhajorn, H.P. Schweizer, Role of the MexXY multidrug efflux pump in moderate aminoglycoside resistance in *Pseudomonas aeruginosa* isolates from *Pseudomonas mastitis*, *Microbiol. Immunol.* 52 (2008) 392–398. <https://doi.org/10.1111/j.1348-0421.2008.00051.x>.
- [137] A. Sharma, R. Sharma, T. Bhattacharyya, T. Bhando, R. Pathania, Fosfomycin resistance in *Acinetobacter baumannii* is mediated by efflux through a major facilitator superfamily (MFS) transporter-AbaF, *J. Antimicrob. Chemother.* 72 (2017) 68–74. <https://doi.org/10.1093/jac/dkw382>.
- [138] U. Choi, C.-R. Lee, Distinct Roles of Outer Membrane Porins in Antibiotic Resistance and Membrane Integrity in *Escherichia coli*, *Front. Microbiol.* 10 (2019) 953. <https://doi.org/10.3389/fmicb.2019.00953>.
- [139] A. Robicsek, J. Strahilevitz, G.A. Jacoby, M. Macielag, D. Abbanat, H.P. Chi, K. Bush, D.C. Hooper, Fluoroquinolone-modifying enzyme: A new adaptation of a common aminoglycoside acetyltransferase, *Nat. Med.* 12 (2006) 83–88. <https://doi.org/10.1038/nm1347>.
- [140] K. Bush, P.A. Bradford, Interplay between  $\beta$ -lactamases and new  $\beta$ -lactamase inhibitors, *Nat. Rev. Microbiol.* 17 (2019) 295–306. <https://doi.org/10.1038/s41579-019-0159-8>.
- [141] C.R. Dean, D.T. Barkan, A. Bermingham, J. Blais, F. Casey, A. Casarez, R. Colvin, J. Fuller, A.K. Jones, C. Li, S. Lopez, L.E. Metzger, M. Mostafavi, R. Prathapam, D. Rasper, F. Reck, A. Ruzin, J. Shaul, X. Shen, R.L. Simmons, P. Skewes-Cox, K.T. Takeoka, P. Tamrakar, T. Uehara, J.R. Wei, Mode of action of the monobactam LYS228 and mechanisms decreasing in vitro susceptibility in *Escherichia coli* and *klebsiella pneumoniae*, *Antimicrob. Agents Chemother.* 62 (2018) 1–19. <https://doi.org/10.1128/AAC.01202-18>.
- [142] D. Rawat, D. Nair, Extended-spectrum  $\beta$ -lactamases in gram negative bacteria, *J. Glob. Infect. Dis.* 2 (2010) 263–274. <https://doi.org/10.4103/0974-777x.68531>.
- [143] P.S. Padayatti, M.S. Helfand, M.A. Totir, M.P. Carey, P.R. Carey, R.A. Bonomo, F. Van Den Akker, High resolution crystal structures of the trans-enamine intermediates formed by sulbactam and clavulanic acid and E166A SHV-1  $\beta$ -lactamase, *J. Biol. Chem.* 280 (2005) 34900–34907. <https://doi.org/10.1074/jbc.M505333200>.
- [144] F. Nguyen, A.L. Starosta, S. Arenz, D. Sohmen, A. Dönhöfer, D.N. Wilson, Tetracycline antibiotics and resistance mechanisms, *Biol. Chem.* 395 (2014) 559–575. <https://doi.org/10.1515/hsz-2013-0292>.
- [145] V.K. Golla, E. Sans-Serramitjana, K.R. Pothula, L. Benier, J.A. Bafna, M. Winterhalter, U. Kleinekathöfer, Fosfomycin Permeation through the Outer Membrane Porin OmpF, *Biophys. J.* 116 (2019) 258–269. <https://doi.org/10.1016/j.bpj.2018.12.002>.
- [146] M.K. Thompson, M.E. Keithly, G.A. Sulikowski, R.N. Armstrong, Diversity in fosfomycin resistance proteins, *Perspect. Sci.* 4 (2015) 17–23. <https://doi.org/10.1016/j.pisc.2014.12.004>.
- [147] C. Zarfl, M. Matthies, J. Klasmeier, A mechanistical model for the uptake of sulfonamides by bacteria, *Chemosphere.* 70 (2008) 753–760. <https://doi.org/10.1016/j.chemosphere.2007.07.045>.
- [148] A.P. Zavascki, L.Z. Goldani, J. Li, R.L. Nation, Polymyxin B for the treatment of multidrug-resistant pathogens: A critical review, *J. Antimicrob. Chemother.* 60 (2007) 1206–1215. <https://doi.org/10.1093/jac/dkm357>.
- [149] C.L. Shelton, F.K. Raffel, W.L. Beatty, S.M. Johnson, K.M. Mason, Sap Transporter Mediated Import and Subsequent Degradation of Antimicrobial Peptides in *Haemophilus*, *PLoS Pathog.* 7 (2011) e1002360. <https://doi.org/10.1371/journal.ppat.1002360>.
- [150] Antibiotics Currently in Global Clinical Development | The Pew Charitable Trusts, <https://www.pewtrusts.org/en/research-and-analysis/data-visualizations/2014/antibiotics-currently-in-clinical-development> (accessed August 11, 2020).
- [151] S.N. Taylor, J. Marrazzo, B.E. Batteiger, E.W. Hook, A.C. Seña, J. Long, M.R. Wierzbicki, H. Kwak, S.M. Johnson, K. Lawrence, J. Mueller, Single-Dose Zoliflodacin (ETX0914) for Treatment of Urogenital Gonorrhoea, *N. Engl. J. Med.* 379 (2018) 1835–1845. <https://doi.org/10.1056/nejmoa1706988>.
- [152] G.S. Basarab, G.H. Kern, J. McNulty, J.P. Mueller, K. Lawrence, K. Vishwanathan, R.A. Alm, K. Barvian, P. Doig, V. Galullo, H. Gardner, M. Gowravaram, M. Huband, A. Kimzey, M. Morningstar, A. Kutschke, S.D. Lahiri, M. Perros, R. Singh, V.J.A. Schuck, R.

- Tommasi, G. Walkup, J. V. Newman, Responding to the challenge of untreatable gonorrhoea: ETX0914, a first-in-class agent with a distinct mechanism-of-action against bacterial Type II topoisomerases, *Sci. Rep.* 5 (2015). <https://doi.org/10.1038/srep11827>.
- [153] Y. Fang, Y. Lu, X. Zang, T. Wu, X.J. Qi, S. Pan, X. Xu, 3D-QSAR and docking studies of flavonoids as potent *Escherichia coli* inhibitors, *Sci. Rep.* 6 (2016) 1–13. <https://doi.org/10.1038/srep23634>.
- [154] P.A. Bradford, A.A. Miller, J. O'Donnell, J.P. Mueller, Zoliflodacin: An Oral Spiropyrimidinetrione Antibiotic for the Treatment of *Neisseria gonorrhoeae*, including Multi-Drug-Resistant Isolates, *ACS Infect. Dis.* 6 (2020) 1332–1345. <https://doi.org/10.1021/acscinfecdis.0c00021>.
- [155] G.S. Basarab, G.H. Kern, J. McNulty, J.P. Mueller, K. Lawrence, K. Vishwanathan, R.A. Alm, K. Barvian, P. Doig, V. Galullo, H. Gardner, M. Gowravaram, M. Huband, A. Kimzey, M. Morningstar, A. Kutschke, S.D. Lahiri, M. Perros, R. Singh, V.J.A. Schuck, R. Tommasi, G. Walkup, J. V. Newman, Responding to the challenge of untreatable gonorrhoea: ETX0914, a first-in-class agent with a distinct mechanism-of-action against bacterial Type II topoisomerases, *Sci. Rep.* 5 (2015). <https://doi.org/10.1038/srep11827>.
- [156] S. Foerster, D. Golparian, S. Jacobsson, L.J. Hathaway, N. Low, W.M. Shafer, C.L. Althaus, M. Unemo, Genetic resistance determinants, in vitro time-kill curve analysis and pharmacodynamic functions for the novel topoisomerase II inhibitor ETX0914 (AZD0914) in *Neisseria gonorrhoeae*, *Front. Microbiol.* 6 (2015) 1–14. <https://doi.org/10.3389/fmicb.2015.01377>.
- [157] I.R. Peak, C.D. Jennings, F.E.C. Jen, M.P. Jennings, Role of *neisseria meningitidis* porA and porB expression in antimicrobial susceptibility, *Antimicrob. Agents Chemother.* 58 (2014) 614–615. <https://doi.org/10.1128/AAC.02506-12>.
- [158] S.M. Corsello, J.A. Bittker, Z. Liu, J. Gould, P. McCarren, J.E. Hirschman, S.E. Johnston, A. Vrcic, B. Wong, M. Khan, J. Asiedu, R. Narayan, C.C. Mader, A. Subramanian, T.R. Golub, The Drug Repurposing Hub: A next-generation drug library and information resource, *Nat. Med.* 23 (2017) 405–408. <https://doi.org/10.1038/nm.4306>.
- [159] THE DRUG REPURPOSING HUB, <https://clue.io/repurposing> (accessed June 25, 2020).
- [160] J.M. Stokes, K. Yang, K. Swanson, W. Jin, A. Cubillos-Ruiz, N.M. Donghia, C.R. MacNair, S. French, L.A. Carfrae, Z. Bloom-Ackerman, V.M. Tran, A. Chiappino-Pepe, A.H. Badran, I.W. Andrews, E.J. Chory, G.M. Church, E.D. Brown, T.S. Jaakkola, R. Barzilay, J.J. Collins, A Deep Learning Approach to Antibiotic Discovery, *Cell.* 180 (2020) 688–702.e13. <https://doi.org/10.1016/j.cell.2020.01.021>.
- [161] S. Jang, S. Javadov, Inhibition of JNK Aggravates the Recovery of Rat Hearts after Global Ischemia: The Role of Mitochondrial JNK, *PLoS One.* 9 (2014) e113526. <https://doi.org/10.1371/journal.pone.0113526>.
- [162] F. Ushiyama, H. Amada, T. Takeuchi, N. Tanaka-Yamamoto, H. Kanazawa, K. Nakano, M. Mima, A. Masuko, I. Takata, K. Hitaka, K. Iwamoto, H. Sugiyama, N. Ohtake, Lead Identification of 8-(Methylamino)-2-oxo-1,2-dihydroquinoline Derivatives as DNA Gyrase Inhibitors: Hit-to-Lead Generation Involving Thermodynamic Evaluation, *ACS Omega.* 5 (2020) 10145–10159. <https://doi.org/10.1021/acsomega.0c00865>.
- [163] B. Lamoree, R.E. Hubbard, Using Fragment-Based Approaches to Discover New Antibiotics., *SLAS Discov. Adv. Life Sci. R D.* 23 (2018) 495–510. <https://doi.org/10.1177/2472555218773034>.
- [164] Analysis Shows Continued Deficiencies in Antibiotic Development since 2014 | The Pew Charitable Trusts, <https://www.pewtrusts.org/en/research-and-analysis/data-visualizations/2019/five-year-analysis-shows-continued-deficiencies-in-antibiotic-development> (accessed June 25, 2020).
- [165] J.C.A. Janssens, H. Steenackers, S. Robijns, E. Gellens, J. Levin, H. Zhao, K. Hermans, D. De Coster, T.L. Verhoeven, K. Marchal, J. Vanderleyden, D.E. De Vos, S.C.J. De Keersmaecker, Brominated furanones inhibit biofilm formation by *Salmonella enterica* serovar Typhimurium, *Appl. Environ. Microbiol.* 74 (2008) 6639–6648. <https://doi.org/10.1128/AEM.01262-08>.
- [166] W. Zhao, N. Lorenz, K. Jung, S.A. Sieber, Natürliche Fimbrinole inhibieren Autoinduktorsynthese und Luciferaseaktivität und unterdrücken damit die Biolumineszenz in *Vibrio*, *Angew. Chemie.* 128 (2016) 1203–1207. <https://doi.org/10.1002/ange.201508052>.
- [167] M. Hentzer, K. Riedel, T.B. Rasmussen, A. Heydorn, J.B. Andersen, M.R. Parsek, S.A. Rice, L. Eberl, S. Molin, N. Høiby, S. Kjelleberg, M. Givskov, Inhibition of quorum sensing in *Pseudomonas aeruginosa* biofilm bacteria by a halogenated furanone compound, *Microbiology.* 148 (2002) 87–102. <https://doi.org/10.1099/00221287-148-1-87>.
- [168] V.C. Kalia, Quorum sensing inhibitors: An overview, *Biotechnol. Adv.* 31 (2013) 224–245. <https://doi.org/10.1016/j.biotechadv.2012.10.004>.
- [169] D. Wiegmann, S. Koppermann, M. Wirth, G. Niro, K. Leyerer, C. Ducho, Muraymycin nucleoside-peptide antibiotics: Uridine-derived natural products as lead structures for the development of novel antibacterial agents, *Beilstein J. Org. Chem.* 12 (2016) 769–795. <https://doi.org/10.3762/bjoc.12.77>.
- [170] E.K. Sully, B.L. Geller, Antisense antimicrobial therapeutics, *Curr. Opin. Microbiol.* 33 (2016) 47–55. <https://doi.org/https://doi.org/10.1016/j.mib.2016.05.017>.
- [171] L. Goltermann, N. Yavari, M. Zhang, A. Ghosal, P.E. Nielsen, PNA length restriction of antibacterial activity of peptide-PNA conjugates in *Escherichia coli* through effects of the inner membrane, *Front. Microbiol.* 10 (2019) 1–8. <https://doi.org/10.3389/fmicb.2019.01032>.
- [172] ChemAxon - Software Solutions and Services for Chemistry & Biology, <https://chemaxon.com/> (accessed October 6, 2020).
- [173] P. Sivalingam, K. Hong, J. Pote, K. Prabakar, Extreme environment streptomycetes: Potential sources for new antibacterial and anticancer drug leads?, *Int. J. Microbiol.* (2019) 2019:5283948. <https://doi.org/10.1155/2019/5283948>.
- [174] R.E. de Lima Procópio, I.R. da Silva, M.K. Martins, J.L. de Azevedo, J.M. de Araújo, Antibiotics produced by Streptomycetes, Brazilian J. Infect. Dis. 16 (2012) 466–471. <https://doi.org/10.1016/j.bjid.2012.08.014>.

- [175] M.S. Hifnawy, M.M. Fouda, A.M. Sayed, R. Mohammed, H.M. Hassan, S.F. AbouZid, M.E. Rateb, A. Keller, M. Adamek, N. Ziemert, U.R. Abdelmohsen, The genus *Micromonospora* as a model microorganism for bioactive natural product discovery, *RSC Adv.* 10 (2020) 20939–20959. <https://doi.org/10.1039/d0ra04025h>.
- [176] A.N. Yadav, P. Verma, V. Kumar, P. Sangwan, S. Mishra, N. Panjiar, V.K. Gupta, A.K. Saxena, *New and Future Developments in Microbial Biotechnology and Bioengineering: Penicillium System Properties and Applications*, Elsevier B.T., 2017. <https://doi.org/10.1016/B978-0-444-63501-3.00001-6>.
- [177] M.W. Gray, Establecimiento de un nuevo sistema de cultivo de células en capas profundas. I. Dise no y principios operativos., *Cold Spring Harb. Perspect. Biol.* 4:a011403 (2012). <https://doi.org/10.1101/cshperspect.a011403>.
- [178] A.A. Almaqwashi, T. Paramanathan, I. Rouzina, M.C. Williams, Mechanisms of small molecule-DNA interactions probed by single-molecule force spectroscopy, *Nucleic Acids Res.* 44 (2016) 3971–3988. <https://doi.org/10.1093/nar/gkw237>.
- [179] C. Jamieson, E.M. Moir, Z. Rankovic, G. Wishart, Medicinal chemistry of hERG optimizations: Highlights and hang-ups, *J. Med. Chem.* 49 (2006) 5029–5046. <https://doi.org/10.1021/jm060379l>.
- [180] F. Reck, J.M. Jansen, H.E. Moser, The Free Internet Journal for Organic Chemistry Review Archive for Organic Chemistry Challenges of antibacterial drug discovery, *Arkivoc.* iv (2019) 0–0. <https://doi.org/10.24820/ark.5550190.p010.955>.
- [181] B.C. Doak, J. Zheng, D. Dobritzsch, J. Kihlberg, How Beyond Rule of 5 Drugs and Clinical Candidates Bind to Their Targets, *J. Med. Chem.* 2016., 59 (2016) 2312–2327. <https://doi.org/10.1021/acs.jmedchem.5b01286>.
- [182] C.M. Wassvik, A.G. Holmén, R. Draheim, P. Artursson, C.A.S. Bergström, Molecular Characteristics for Solid-State Limited Solubility, *J. Med. Chem.* 51 (2008) 3035–3039. <https://doi.org/10.1021/jm701587d>.
- [183] A. Avdeef, *Absorption and Drug Development: Solubility Permeability, and Charge State*, 2nd ed., 2012. <https://doi.org/10.1002/9781118286067>.
- [184] R. Koebnik, K.P. Locher, P. Van Gelder, Structure and function of bacterial outer membrane proteins: Barrels in a nutshell, *Mol. Microbiol.* 37 (2000) 239–253. <https://doi.org/10.1046/j.1365-2958.2000.01983.x>.
- [185] C.A. Lipinski, F. Lombardo, B.W. Dominy, P.J. Feeney, Experimental and computational approaches to estimate solubility and permeability in drug discovery and development settings, *Adv. Drug Deliv. Rev.* 23 (1997) 3–25. [https://doi.org/10.1016/S0169-409X\(96\)00423-1](https://doi.org/10.1016/S0169-409X(96)00423-1).
- [186] D.F. Veber, S.R. Johnson, H.Y. Cheng, B.R. Smith, K.W. Ward, K.D. Kopple, Molecular properties that influence the oral bioavailability of drug candidates, *J. Med. Chem.* 45 (2002) 2615–2623. <https://doi.org/10.1021/jm020017n>.
- [187] K. Mazák, B. Noszál, Zwitterions can be predominant in membrane penetration of drugs: Experimental proof, *J. Med. Chem.* 55 (2012) 6942–6947. <https://doi.org/10.1021/jm3007992>.
- [188] S.F. Zhou, Structure, function and regulation of P-glycoprotein and its clinical relevance in drug disposition, *Xenobiotica.* 38 (2008) 802–832. <https://doi.org/10.1080/00498250701867889>.
- [189] S.G. Aller, J. Yu, A. Ward, Y. Weng, S. Chittaboina, R. Zhuo, P.M. Harrell, Y.T. Trinh, Q. Zhang, I.L. Urbatsch, G. Chang, Structure of P-glycoprotein reveals a molecular basis for poly-specific drug binding, *Science* (80-. ). 323 (2009) 1718–1722. <https://doi.org/10.1126/science.1168750>.
- [190] S.A. Hitchcock, Structural modifications that alter the P-glycoprotein efflux properties of compounds, *J. Med. Chem.* 55 (2012) 4877–4895. <https://doi.org/10.1021/jm201136z>.
- [191] P. Crivori, B. Reinach, D. Pezzetta, I. Poggesi, Computational models for identifying potential P-glycoprotein substrates and inhibitors, *Mol. Pharm.* 3 (2006) 33–44. <https://doi.org/10.1021/mp050071a>.
- [192] B. Montefiore, F. Klingler and N. Foster, Poster: A novel scoring profile for the design of antibacterials active against gram-negative bacteria, (2018).
- [193] A.F.D. Di Stefano, A. Rusca, L. Loprete, M.J. Dröge, L. Moro, A. Assandri, Systemic absorption of rifamycin SV MMX administered as modified-release tablets in healthy volunteers, *Antimicrob. Agents Chemother.* 55 (2011) 2122–2128. <https://doi.org/10.1128/AAC.01504-10>.
- [194] Y. Cheng, H. Qu, M. Ma, Z. Xu, P. Xu, Y. Fang, T. Xu, Polyamidoamine (PAMAM) dendrimers as biocompatible carriers of quinolone antimicrobials: An in vitro study, *Eur. J. Med. Chem.* 42 (2007) 1032–1038. <https://doi.org/10.1016/j.ejmech.2006.12.035>.
- [195] M. Ma, Y. Cheng, Z. Xu, P. Xu, H. Qu, Y. Fang, T. Xu, L. Wen, Evaluation of polyamidoamine (PAMAM) dendrimers as drug carriers of anti-bacterial drugs using sulfamethoxazole (SMZ) as a model drug, *Eur. J. Med. Chem.* 42 (2007) 93–98. <https://doi.org/10.1016/j.ejmech.2006.07.015>.
- [196] D.J. McClements, J. Rao, Food-Grade nanoemulsions: Formulation, fabrication, properties, performance, Biological fate, and Potential Toxicity, *Crit. Rev. Food Sci. Nutr.* 51 (2011) 285–330. <https://doi.org/10.1080/10408398.2011.559558>.
- [197] G. Bozzuto, A. Molinari, Liposomes as nanomedical devices, *Int. J. Nanomedicine.* 10 (2015) 975–999. <https://doi.org/10.2147/IJN.S68861>.
- [198] Z. Yang, A. Lu, B. Kwan Wong, X. Chen, Z. Bian, Z. Zhao, W. Huang, G. Zhang, H. Chen, M. Xu, Effect of Liposomes on the Absorption of Water-soluble Active Pharmaceutical Ingredients via Oral Administration, *Curr. Pharm. Des.* 19 (2013) 6647–6654. <https://doi.org/10.2174/1381612811319370008>.

- [199] M. Daeihamed, S. Dadashzadeh, A. Haeri, M. Akhlaghi, Potential of Liposomes for Enhancement of Oral Drug Absorption, *Curr. Drug Deliv.* 13 (2016) 1–1. <https://doi.org/10.2174/1567201813666160115125756>.
- [200] K. Bowman, K.W. Leong, Chitosan nanoparticles for oral drug and gene delivery, *Int. J. Nanomedicine.* 1 (2006) 117–128. <https://doi.org/10.2147/nano.2006.1.2.117>.
- [201] I.W. Jung, H.K. Han, Effective mucoadhesive liposomal delivery system for risedronate: Preparation and in vitro/in vivo characterization, *Int. J. Nanomedicine.* 9 (2014) 2299–2306. <https://doi.org/10.2147/IJN.S61181>.
- [202] C.L. Bowe, L. Mokhtarzadeh, P. Venkatesan, S. Babu, H.R. Axelrod, M.J. Sofia, R. Kakarla, T.Y. Chan, J.S. Kim, H.J. Lee, G.L. Amidon, S.Y. Choe, S. Walker, D. Kahne, Design of compounds that increase the absorption of polar molecules, *Proc. Natl. Acad. Sci. U. S. A.* 94 (1997) 12218–12223. <https://doi.org/10.1073/pnas.94.22.12218>.
- [203] R. Pangeni, J.U. Choi, V.K. Panth, Y. Byun, J.W. Park, Enhanced oral absorption of pemetrexed by ion-pairing complex formation with deoxycholic acid derivative and multiple nanoemulsion formulations: Preparation, characterization, and in vivo oral bioavailability and anticancer effect, *Int. J. Nanomedicine.* 13 (2018) 3329–3351. <https://doi.org/10.2147/IJN.S167958>.
- [204] A.H. Dantzig, L. Bergin, Uptake of the cephalosporin, cephalexin, by a dipeptide transport carrier in the human intestinal cell line, Caco-2, *BBA - Biomembr.* 1027 (1990) 211–217. [https://doi.org/10.1016/0005-2736\(90\)90309-C](https://doi.org/10.1016/0005-2736(90)90309-C).
- [205] D. Steinhilber, M. Schubert-Zsilavecz, H. Josef Roth, *Medizinische Chemie: Targets, Arzneistoffe und Chemische Biologie*, 2010.
- [206] H. Lode, M. Fassbender, T. Schaberg, K. Borner, P. Koeppel, Pharmacokinetics of new oral cephalosporins, including a new carbacephem, *Clin. Infect. Dis.* 16 (1993) 646–653. <https://doi.org/10.1093/clind/16.5.646>.
- [207] A. Tsuji, I. Tamai, H. Hirooka, T. Terasaki, beta-Lactam antibiotics and transport via the dipeptide carrier system across the intestinal brush-border membrane, *Biochem. Pharmacol.* 36 (1987) 565–567.
- [208] Q. Luo, M. Jiang, L. Kou, L. Zhang, G. Li, Q. Yao, L. Shang, Y. Chen, Ascorbate-conjugated nanoparticles for promoted oral delivery of therapeutic drugs via sodium-dependent vitamin C transporter 1 (SVCT1), *Artif. Cells, Nanomedicine Biotechnol.* 46 (2018) 198–208. <https://doi.org/10.1080/21691401.2017.1417864>.
- [209] B. Vig, J. Rautio, Amino acid prodrugs for oral delivery: Challenges and opportunities, *Ther. Deliv.* 2 (2011) 959–962. <https://doi.org/10.4155/tde.11.75>.
- [210] Y. Yang, A.M. Pollard, C. Höfler, G. Poschet, M. Wirtz, R. Hell, V. Sourjik, Relation between chemotaxis and consumption of amino acids in bacteria, *Mol. Microbiol.* 96 (2015) 1272–1282. <https://doi.org/10.1111/mmi.13006>.
- [211] F. Chen, G. Huang, H. Huang, Sugar ligand-mediated drug delivery, *Future Med. Chem.* 12 (2020) 161–171. <https://doi.org/10.4155/fmc-2019-0114>.
- [212] D. Davies, Understanding biofilm resistance to antibacterial agents, *Nat. Rev. Drug Discov.* 2 (2003) 114–122. <https://doi.org/10.1038/nrd1008>.
- [213] H. Nikaïdo, Outer membrane of *Salmonella typhimurium*. Transmembrane diffusion of some hydrophobic substances, *BBA - Biomembr.* 433 (1976) 118–132. [https://doi.org/10.1016/0005-2736\(76\)90182-6](https://doi.org/10.1016/0005-2736(76)90182-6).
- [214] A. Monserrat-Martinez, Y. Gambin, E. Sierecki, Thinking outside the bug: Molecular targets and strategies to overcome antibiotic resistance, *Int. J. Mol. Sci.* 20 (2019) 1255.
- [215] R. Richter, M.A.M. Kamal, M.A. García-Rivera, J. Kaspar, M. Junk, W.A.M. Elgaher, S.K. Srikakulam, A. Gress, A. Beckmann, A. Griebner, C. Meier, M. Vielhaber, O. Kalinina, A.K.H. Hirsch, R.W. Hartmann, M. Brönstrup, N. Schneider-Daum, C.-M. Lehr, A hydrogel-based in vitro assay for the fast prediction of antibiotic accumulation in Gram-negative bacteria, *Mater. Today Bio.* (2020) 100084. <https://doi.org/10.1016/j.mtbio.2020.100084>.
- [216] H. Heidari Torkabadi, C.R. Bethel, K.M. Papp-Wallace, P.A.J. De Boer, R.A. Bonomo, P.R. Carey, Following drug uptake and reactions inside *Escherichia coli* cells by raman microspectroscopy, *Biochemistry.* 53 (2014) 4113–4121. <https://doi.org/10.1021/bi500529c>.
- [217] G.M. Decad, H. Nikaïdo, Outer membrane of gram negative bacteria. XII. Molecular sieving function of cell wall, *J. Bacteriol.* 128 (1976) 325–336.
- [218] M. Widya, W.D. Pasutti, M. Sachdeva, R.L. Simmons, P. Tamrakar, T. Krucker, D.A. Six, Development and Optimization of a Higher-Throughput Bacterial Compound Accumulation Assay, *ACS Infect. Dis.* 5 (2019) 394–405. <https://doi.org/10.1021/acsinfecdis.8b00299>.
- [219] D.M. Figueroa, H.M. Wade, K.P. Montales, D.E. Elmore, L.E.O. Darling, Production and visualization of bacterial spheroplasts and protoplasts to characterize antimicrobial peptide localization, *J. Vis. Exp.* 2018 (2018) 1–8. <https://doi.org/10.3791/57904>.
- [220] R. Iyer, M.A. Sylvester, C. Velez-Vega, R. Tommasi, T.F. Durand-Reville, A.A. Miller, Whole-Cell-Based Assay to Evaluate Structure Permeation Relationships for Carbapenem Passage through the *Pseudomonas aeruginosa* Porin OprD, *ACS Infect. Dis.* 3 (2017) 310–319. <https://doi.org/10.1021/acsinfecdis.6b00197>.
- [221] J. Cama, A.M. Henney, M. Winterhalter, Breaching the Barrier: Quantifying Antibiotic Permeability across Gram-negative Bacterial Membranes, *J. Mol. Biol.* 431 (2019) 3531–3546. <https://doi.org/10.1016/j.jmb.2019.03.031>.
- [222] R. Misra, P.R. Reeves, Role of micF in the tolC-mediated regulation of OmpF, a major outer membrane protein of *Escherichia coli* K-12, *J. Bacteriol.* 169 (1987) 4722–4730. <https://doi.org/10.1128/jb.169.10.4722-4730.1987>.



- [223] H.I. Zgurskaya, G. Krishnamoorthy, A. Ntrel, S. Lu, Mechanism and function of the outer membrane channel TolC in multidrug resistance and physiology of enterobacteria, *Front. Microbiol.* 2 (2011) 1–13. <https://doi.org/10.3389/fmicb.2011.00189>.
- [224] W.A.M. Elgaher, M. Fruth, M. Groh, J. Haupenthal, R.W. Hartmann, Expanding the scaffold for bacterial RNA polymerase inhibitors: Design, synthesis and structure-activity relationships of ureido-heterocyclic-carboxylic acids, *RSC Adv.* 4 (2014) 2177–2194. <https://doi.org/10.1039/c3ra45820b>.
- [225] R.J. Ferreira, P. Kasson, Antibiotic uptake across gram-negative outer membranes: better predictions towards better antibiotics, *ACS Infect. Dis.* 5 (2019) 2096–2104. <https://doi.org/10.1021/acinfeddis.9b00201>.
- [226] J.L. Kadurugamuwa, T.J. Beveridge, Virulence Factors Are Released from *Pseudomonas aeruginosa* in Association with Membrane Vesicles during Normal Growth and Exposure to Gentamicin: a Novel Mechanism of Enzyme Secretion, *Microbiology.* 177 (1995) 3998–4008. <https://doi.org/10.1128/jb.177.14.3998-4008.1995>.
- [227] E.M. Nestorovich, C. Danelon, M. Winterhalter, S.M. Bezrukov, Designed to penetrate: Time-resolved interaction of single antibiotic molecules with bacterial pores, *Proc. Natl. Acad. Sci. U. S. A.* 99 (2002) 9789–9794. <https://doi.org/10.1073/pnas.152206799>.
- [228] J. Wang, J.A. Bafna, S.P. Bhamidimarri, M. Winterhalter, Small-Molecule Permeation across Membrane Channels: Chemical Modification to Quantify Transport across OmpF, *Angew. Chemie - Int. Ed.* 58 (2019) 4737–4741. <https://doi.org/10.1002/anie.201814489>.
- [229] F. Graef, B. Vukosavljevic, J.P. Michel, M. Wirth, O. Ries, C. De Rossi, M. Windbergs, V. Rosilio, C. Ducho, S. Gordon, C.M. Lehr, The bacterial cell envelope as delimiter of anti-infective bioavailability – An in vitro permeation model of the Gram-negative bacterial inner membrane, *J. Control. Release.* 243 (2016) 214–224. <https://doi.org/10.1016/j.jconrel.2016.10.018>.
- [230] H.I. Zgurskaya, H. Nikaido, Bypassing the periplasm: Reconstitution of the AcrAB multidrug efflux pump of *Escherichia coli*, *Proc. Natl. Acad. Sci. U. S. A.* 96 (1999) 7190–7195. <https://doi.org/10.1073/pnas.96.13.7190>.
- [231] A. Verchère, M. Picard, I. Broutin, Functional Investigation of the MexA-MexB-OprM Efflux Pump of *Pseudomonas Aeruginosa*, *Biophys. J.* 104 (2013) 286a. <https://doi.org/10.1016/j.bpj.2012.11.1600>.
- [232] W.F. Van Gunsteren, H.J.C. Berendsen, Molecular dynamics computer simulation. Method, application and perspectives in chemistry., *Sect. Title Phys. Org. Chem.* 102 (1990) 1020–1055.
- [233] F. Di Meo, G. Fabre, K. Berka, T. Ossman, B. Chantemargue, M. Paloncýová, P. Marquet, M. Otyepka, P. Trouillas, In silico pharmacology: Drug membrane partitioning and crossing, *Pharmacol. Res.* 111 (2016) 471–486. <https://doi.org/10.1016/j.phrs.2016.06.030>.
- [234] J. Björkstén, C.M. Soares, O. Nilsson, O. Tapia, On the stability and plastic properties of the interior 13 loop in R.capsulatus porin. A molecular dynamics study, *Protein Eng. Des. Sel.* 7 (1994) 487–493. <https://doi.org/10.1093/protein/7.4.487>.
- [235] K.R. Pothula, C.J.F. Solano, U. Kleinekathöfer, Simulations of outer membrane channels and their permeability, *Biochim. Biophys. Acta - Biomembr.* 1858 (2016) 1760–1771. <https://doi.org/10.1016/j.bbamem.2015.12.020>.
- [236] T.J. Piggot, D.A. Holdbrook, S. Khalid, Electroporation of the *E. coli* and *S. aureus* membranes: Molecular dynamics simulations of complex bacterial membranes, *J. Phys. Chem. B.* 115 (2011) 13381–13388. <https://doi.org/10.1021/jp207013v>.
- [237] E.L. Wu, O. Engström, S. Jo, D. Stuhlsatz, M.S. Yeom, J.B. Klauda, G. Widmalm, W. Im, Molecular dynamics and NMR spectroscopy studies of *E. coli* lipopolysaccharide structure and dynamics, *Biophys. J.* 105 (2013) 1444–1455. <https://doi.org/10.1016/j.bpj.2013.08.002>.
- [238] J. Parkin, M. Chavent, S. Khalid, Molecular Simulations of Gram-Negative Bacterial Membranes: A Vignette of Some Recent Successes, *Biophys. J.* 109 (2015) 461–468. <https://doi.org/10.1016/j.bpj.2015.06.050>.
- [239] S.J. Hickman, R.E.M. Cooper, L. Bellucci, E. Paci, D.J. Brockwell, Gating of TonB-dependent transporters by substrate-specific forced remodelling, *Nat. Commun.* 8 (2017) 1–12. <https://doi.org/10.1038/ncomms14804>.
- [240] R. Menichetti, K.H. Kanekal, T. Bureau, Drug-Membrane Permeability across Chemical Space, *ACS Cent. Sci.* 5 (2019) 290–298. <https://doi.org/10.1021/acscentsci.8b00718>.
- [241] J. Kästner, Umbrella sampling, *Wiley Interdiscip. Rev. Comput. Mol. Sci.* 1 (2011) 932–942. <https://doi.org/10.1002/wcms.66>.
- [242] S.A. Hollingsworth, R.O. Dror, Molecular Dynamics Simulation for All, *Neuron.* 99 (2018) 1129–1143. <https://doi.org/10.1016/j.neuron.2018.08.011>.
- [243] K. Yang, K. Swanson, W. Jin, C. Coley, P. Eiden, H. Gao, A. Guzman-Perez, T. Hopper, B. Kelley, M. Mathea, A. Palmer, V. Settels, T. Jaakkola, K. Jensen, R. Barzilay, Analyzing Learned Molecular Representations for Property Prediction, *J. Chem. Inf. Model.* 59 (2019) 3370–3388. <https://doi.org/10.1021/acs.jcim.9b00237>.
- [244] Chemprop, <http://chemprop.csail.mit.edu/> (accessed June 25, 2020).
- [245] M. Puri, Y. Pathak, V.K. Sutariya, S. Tipparaju, W. Moreno, Artificial Neural network for Drug Design, Delivery and Disposition, Elsevier, 2016. <https://doi.org/10.1016/C2014-0-00253-5>.
- [246] N. Brown, P. Ertl, R. Lewis, T. Luksch, D. Reker, N. Schneider, Artificial intelligence in chemistry and drug design, *J. Comput. Aided. Mol. Des.* 34 (2020) 709–715. <https://doi.org/10.1007/s10822-020-00317-x>.
- [247] J. Thomas, M. Navre, A. Rubio, A. Coukell, Shared Platform for Antibiotic Research and Knowledge: A Collaborative Tool to SPARK Antibiotic Discovery, *ACS Infect. Dis.* 4 (2018) 1536–1539. <https://doi.org/10.1021/acinfeddis.8b00193>.

- [248] X. Xia, E.G. Maliski, P. Gallant, D. Rogers, Classification of kinase inhibitors using a Bayesian model, *J. Med. Chem.* 47 (2004) 4463–4470. <https://doi.org/10.1021/jm0303195>.
- [249] N.M. O’Boyle, R.A. Sayle, Comparing structural fingerprints using a literature-based similarity benchmark, *J. Cheminform.* 8 (2016) 36. <https://doi.org/10.1186/s13321-016-0148-0>.
- [250] D. Rogers, M. Hahn, Extended-connectivity fingerprints, *J. Chem. Inf. Model.* 50 (2010) 742–754. <https://doi.org/10.1021/ci100050t>.
- [251] Open source ECFP/FCFP circular fingerprints in CDK - Collaborative Drug Discovery Inc. (CDD), <https://www.collaborativedrug.com/open-source-ecfpfcfp-circular-fingerprints-in-cdk/> (accessed July 28, 2020).
- [252] Y. Zhou, C. Joubran, L. Miller-Vedam, V. Isabella, A. Nayar, S. Tentarelli, A. Miller, Thinking outside the “bug”: A unique assay to measure intracellular drug penetration in Gram-negative bacteria, *Anal. Chem.* 87 (2015) 3579–3584. <https://doi.org/10.1021/ac504880r>.
- [253] H. Nikaido, E.Y. Rosenberg, Porin channels in *Escherichia coli*: Studies with liposomes reconstituted from purified proteins, *J. Bacteriol.* 153 (1983) 241–252.
- [254] A. Verchère, M. Dezi, V. Adrien, I. Broutin, M. Picard, In vitro transport activity of the fully assembled MexAB-OprM efflux pump from *Pseudomonas aeruginosa*, *Nat. Commun.* 6 (2015) 1–6. <https://doi.org/10.1038/ncomms7890>.
- [255] CO-ADD Community for Open Antimicrobial Drug Discovery, <https://www.co-add.org>, (accessed March 3, 2020).
- [256] L.J.V. Piddock, The global antibiotic research and development partnership (GARDP): Researching and developing new antibiotics to meet global public health needs, *Medchemcomm.* 10 (2019) 1227–1230. <https://doi.org/10.1039/c9md90010a>.

## 2. Aims of the Thesis

There is a high need for novel anti-infective targets and here the target enzyme IspE represents one of the many possibilities in the MEP pathway. A small number of inhibitors of the target enzyme IspE, namely inhibiting *EcIspE*, have been published. However, a chemical class with confirmed target engagement and cellular activity is still missing. Most of the reported inhibitors lack substantial cellular activity or such has not been reported at all for them, making them less attractive starting points for further medicinal-chemistry optimisation. Therefore, to tackle this dilemma, the focus of this thesis was to apply multidisciplinary methods to expand the selection of the inhibitors of the enzyme IspE, ideally also possessing the highly sought-after cellular activity. For this thesis, the isolated IspE enzymes of *E. coli* and *P. falciparum* and their corresponding functional assays were available within the MEP consortium by the Fischer Group, University of Hamburg. The bacterial assays were conducted in-house at HIPS and *P. falciparum* cell-based assays were performed at Swiss TPH by M. Rottmann.

To address the lack of antibacterial activity of the previous *EcIspE* inhibitors, a virtual screening with *EcIspE* (PDB 1OJ4) was completed and as the novelty, the “eNTRY” rules were applied for the filtering (3.1. Chapter A). Here, the aim was to ensure a promising starting point inhibiting *EcIspE* as well as showing antibacterial activity, resulting in the so-called “primary amine series”. After hit selection, the objectives for the newly synthesised derivatives were improving the target engagement, increasing the antibacterial activity and reducing the cytotoxicity, while understanding the overall structure–permeation relationships around the primary amine series.

Prior to the thesis, a first enzymatic high-throughput screening (HTS) with *PfIspE* was completed within the MEP consortium, resulting in a promising 2-aminothiazole series (unpublished results from the consortium). From this series, two amide-modified reference compounds were selected as suitable starting points for amino-acid modifications and thereby the aim was to assess, whether the implementation of the reported Gram-negative rules guarantees antibacterial activity regardless of the starting point, whilst screening for *EcIspE* and *PfIspE in vitro* activity (3.2. Chapter B). Independently from the latter series, the original *PfIspE* 2-aminothiazole lead compound turned out to suffer from decomposition in DMSO stock solution, surprisingly resulting in increased activity against the enzyme *PfIspE* and the cellular target *PfNF54* (3.3. Chapter C). Therefore, rather than expanding the SAR for this series, the objective was to understand the decomposition as well as to isolate and characterise the active decomposition products.

### 3. Results

#### 3.1 Chapter A:

##### **Novel Class Inhibitors of *Escherichia coli* IspE Originating from a Virtual Screening**

This chapter is being prepared as a manuscript for which H.-K. Ropponen is the first author.

With many thanks for active contribution to (in alphabetical order by surname)

E. Diamanti – help with synthesis and supervision

J. Hauptenthal – coordinating biological assays done by J. Jung, D.-T. Jener and S. Amann

A. K. H. Hirsch – overall supervision

B. Illarionov, M. Fischer – enzyme assays and their supervision, respectively

M. Jaki – help with synthesis, SuFEx probe optimisation and TSA/MST measurements

S. Johannsen – STD-NMR measurements

L. Lucaroni – synthesis

P. Sass – *B. subtilis* microscopy experiments with the strains kindly provided by C. Gross

Additionally, thanks to J. Herrmann for kindly providing *E. coli*  $\Delta$ *acrB*, J.-M. Pagés for kindly providing *E. coli* BL21(DE3)*omp8*, S. Bousis for the help in establishing TSA and VS, S. Adam and Z. Hamid for the continuous crystallisation attempts, J. Konstantinović for the help with HRMS measurements, W. Elgaher for the tips with the SuFEx probe and C. D. Bader for the SuFEx probe measurements.

## Introduction

As the globe is facing the COVID-19 pandemic, the severity of the lack of novel antibiotics to treat bacterial infections is also becoming more apparent. Viral and bacterial infections can be difficult to distinguish as they can occur simultaneously, particularly in intensive-care units.<sup>5,64</sup> Up to now, it is still being debated, whether the COVID-19 pandemic worsens or, in fact, slows down the development of the antimicrobial resistance.<sup>65,66</sup> As seen with the COVID-19 pandemic, it is evidently too late to start with the early research steps, when the problem is already present. The bottleneck of discovering new antibiotics already arises from the early research steps with the difficulty to find novel compounds and targets circumventing cross-resistance, as defined by the innovative criteria set by the WHO.<sup>13</sup> Over the past years, several rules have been developed to speed up the discovery of the ideal antibiotic candidates, particularly for Gram-negative pathogens. (Publication 1, H.-K. Ropponen *et al.*, *ADDR*, **2021**, DOI:10.1016/j.addr.2021.02.014) Additionally, in another recent review A. L. Parkers raised the most fundamental question in antibiotic research “*what can we design for?*”<sup>67</sup> There are contradicting opinions on which ones of the rules are of actual importance. Successful antibiotic drug design should be guided by the recently introduced bacterial bioavailability that is a holistic balance of bacterial uptake, distribution, metabolic and efflux pathways. (Publication 1, H.- K. Ropponen *et al.*, *ADDR*, **2021**, DOI:10.1016/j.addr.2021.02.014) The outer membrane of Gram-negative bacteria represents an extra hurdle for compounds to enter the cells in comparison to their Gram-positive bacteria counterparts. Essentially, compounds can be actively transported through membrane porins and pumps or pass passively through the phospholipid layers.<sup>68</sup> In 2017, Richter *et al.* reported the so-called eNTRy rules aiming for a good accumulation into Gram-negative *Escherichia coli*. The eNTRy rules state that a well-accumulating compound needs an ionisable amine (N), preferably a primary amine, low globularity ( $\leq 0.25$ ) (T=three-dimensionality) and rotatable bonds ( $\leq 5$ ) (R=rigidity). Based on the eNTRy rules, the ionisable amines provide better accumulation due to a key salt-salt interaction with the outer membrane porin F (OmpF).<sup>69,70</sup> Although this LC-MS-based accumulation study focused only on Gram-negative *E. coli*, the follow-up studies have also shown the applicability of the rules for other Gram-negative bacteria, namely *Acinetobacter baumannii* and *Klebsiella pneumoniae*.<sup>71-75</sup> The activity against the less permeable *Pseudomonas aeruginosa*, however, is often lacking<sup>76</sup> and we questioned the overall applicability of the rules in an amino acid modified series. (Publication 2, H.-K. Ropponen *et al.*, *RSC Med. Chem.*, **2021**, DOI:10.1039/d0md00409j)

Good accumulation and permeability into the cytoplasm is important in order to achieve good enzymatic activity for intracellular targets. In this study, we focus on evaluating the cytoplasmic 2-C-methyl-D-erythritol 4-phosphate (MEP) pathway that is vital for the biosynthesis of universal isoprenoid precursors.<sup>40</sup> Since the same isoprenoid precursors are synthesised *via* the distinct mevalonate pathway in humans, the bacterial MEP-pathway is a rich source of attractive drug

targets.<sup>41</sup> As validation of the druggability of the MEP-pathway, fosmidomycin, an inhibitor of 1-deoxy-D-xylulose-5-phosphate reductoisomerase (DXR or IspC), is in clinical trials to treat malaria.<sup>77,78</sup> It is also shown to inhibit multi-drug resistant bacterial strains, such as *P. aeruginosa* and *A. baumannii*.<sup>79</sup> However, to the authors' knowledge, as advanced success stories with other compounds targeting the bacterial MEP pathway have not yet been reported.

In the search for novel inhibitors of the MEP pathway, we focused on the fourth enzyme IspE that phosphorylates the natural substrate 4-diphosphocytidyl-2-C-methyl-D-erythritol (CDP-ME) to afford 4-diphosphocytidyl-2-C-methyl-D-erythritol 2-phosphate (CDP-MEP) in the presence of ATP. Most of the previously reported IspE inhibitors against Gram-negative *E. coli* have low-micromolar enzyme activity but report no activity in cell-based assays.<sup>39,41</sup> (+Publication 2, H.-K. Ropponen *et al.*, *RSC Med. Chem.*, **2021**, DOI:10.1039/d0md00409j) To address this translational gap, we embarked on an *in silico* virtual screening (VS) of a SPECS library of 106,801 compounds using the crystal structure of *EcIspE* (PDB 1OJ4) and in particular, applying the eNTRY rules in the filtering process to obtain hits with a high *E. coli* accumulation.

### ***Virtual Screening Workflow***

We selected the catalytic, phosphorylating site of *EcIspE* as the binding pocket for the VS based on the druggability assessment using DogSiteScorer.<sup>80,81</sup> The druggability score accounts for instance for an ideal volume, surface and depth of the binding pocket and it should be in the range of 0.80–1.00.<sup>81</sup> Under this assumption, the selected binding pocket has a good druggability score of 0.81 (Supplementary Material, Section 5.2.1). The hydrophobic pocket extending from CDP-ME had been examined previously but the cavity on the left-hand side remains underexplored (Figure 3.1:1).<sup>45</sup> Previous *EcIspE* inhibitors addressing the same catalytic site have been published within the consortium and other VS campaigns have also been conducted using *EcIspE* (1OJ4).<sup>45,47,48,50</sup> However, most of these inhibitors lack the needed antibacterial cell activity and to best of our knowledge, they have not been further developed. Thus, by implementing the eNTRY rules into the filtering process of the VS, we aimed to find a hit with both cellular activity against *E. coli* and enzymatic inhibitory activity against *EcIspE*.

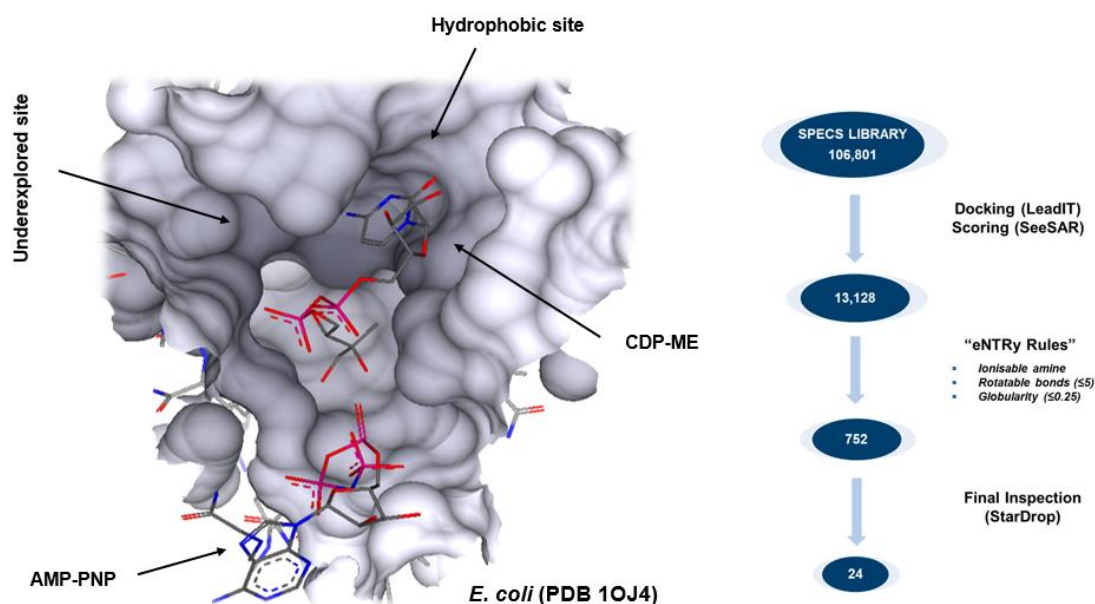


**Figure 3.1:1** - The used binding pocket for the virtual screening with *EcIspE* (PDB 1OJ4) and summary of the workflow. The figure was created with SeeSAR 8.2.<sup>82</sup>

The VS campaign was completed using BioSolveIT software, where LeadIT was used for docking and SeeSAR for scoring (Supplementary Material, Section 5.2.1).<sup>82,83</sup> After scoring, the compounds were filtered and only compounds with estimated HYDE-affinity ( $<1$  mM), torsional angles (green or orange) and a total number of poses ( $\geq 2$ ) were selected further. In total, 13,128 compounds passed through these filters. After the final inspection of the poses and clustering compound classes in StarDrop, we purchased 24 compounds and tested them against *EcIspE*, *E. coli* wild-type K12 and mutant strain  $\Delta tolC$ . The selection included a mixture of compounds with different degrees of ionisation of the ionisable amine (Supplementary Material, Table S5.2.1:1–S5.2.1:6). In addition, we also selected a few compounds simply with the highest estimated HYDE-binding affinities and a few compounds based on a novel antibacterial scoring profile developed by StarDrop.<sup>84</sup>

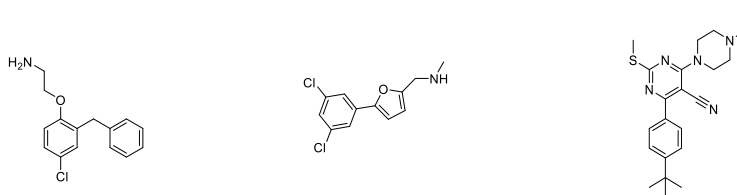
The original research paper of the eNTRY rules pinpoints that most of the commercially available libraries do not contain many primary amines, concluding this to be one of the reasons for unsuccessful screening campaigns in the search for novel antibacterial candidates.<sup>69</sup> Overall, this particular SPECS library consisted of 70 compounds with a primary amine and we decided to test twelve additional primary amines that had not passed through the VS filters. They were also tested against *E. coli* and out of them, three compounds showed moderate inhibition (e.g., **HIPS5407** *E. coli* K12 %-inh. =  $81 \pm 0$  and *E. coli*  $\Delta tolC$  =  $50 \pm 8$ , **HIPS5415** *E. coli* K12 %-inh. =  $76 \pm 16$  and *E. coli*  $\Delta tolC$  MIC =  $98 \pm 11$  and **HIPS5422** *E. coli* K12 %-inh. =  $57 \pm 4$  and *E. coli*  $\Delta tolC$  =  $79 \pm 1$ , Supplementary Material, Table S5.2.2.4:1).

### ***Hit Selection***

Disappointingly, out of the 24 compounds none displayed *E. coli* IspE inhibition and even those showing slight *EcIspE* inhibition also undesirably inhibited the auxiliary enzymes pyruvate kinase and lactate dehydrogenase (PK/LDH) in the coupled enzyme assay (Supplementary Material, Table S5.2.1:1–S5.2.1:6).<sup>44</sup> Nevertheless, we made a top-three hit selection based on the cellular activities. The compounds in the top-three selection were all structurally different and included primary, secondary and tertiary amines, **HIPS5242**, **HIPS5254** and **HIPS5255**, respectively. They all had a promising cellular activity profile inhibiting *E. coli* K12 and  $\Delta tolC$ , measured as percentage inhibition at the highest solubility, where no minimum inhibitory concentration (MIC) could be measured. They were also tested against the more pathogenic and less susceptible Gram-negative strains, *P. aeruginosa* and *A. baumannii*, as well as against Gram-positive *Staphylococcus aureus* and *Bacillus subtilis* (Table 3.1:1).



**Table 3.1:1** - Top-three hits of the virtual screening based on the cellular activities.



	HIPS5242	HIPS5255	HIPS5254
<b>Enzyme activity</b>			
<b>Docking Pose in <i>E. coli</i> IspE 1OJ4<sup>[d]</sup></b>			
<b><i>EcIspE</i> IC<sub>50</sub> (μM)</b>	>500	356*	>500
<b>PK/LDH IC<sub>50</sub> (μM)</b>	n.d.	n.d.	n.d.
<b>T<sub>m</sub>(°C) (ΔT<sub>m</sub> (°C))</b>	50.42 ± 0.09 (-1.1)	50.81 ± 0.09 (-0.7)	51.23 ± 0.09 (-0.3)
<b>MST - K<sub>d</sub></b>	~ 700 μM	n.d.	n.d.
<b>Bacterial Minimum Inhibitory Concentration (MIC) or Percentage Inhibition @ 100 μM</b>			
<i>E. coli</i> Δ <i>tolC</i>	99 ± 2 (MIC)	74 ± 4%	33 ± 16 (MIC)
<i>E. coli</i> K12	97 ± 4 (MIC)	71 ± 6%	>50 (MIC)
<i>P. aeruginosa</i>	52 ± 10%	25 ± 11%	>100 (MIC)
<i>A. baumannii</i>	100 ± 0 (MIC)	41 ± 28%	>50 (MIC)
<i>S. aureus</i>	47 ± 8%	4 ± 1%	>50 (MIC)
<i>B. subtilis</i>	>100 (MIC) <sup>[a]</sup>	>100 (MIC) <sup>[a]</sup>	91 ± 4%
<b>Cytotoxicity Inhibitory Concentration (IC<sub>50</sub>) or Percentage Inhibition</b>			
HepG2	IC <sub>50</sub> = 21 ± 1 μM	IC <sub>50</sub> = 25 ± 2 μM	85 ± 1% @50 μM
Hek293	IC <sub>50</sub> = 14 μM*	IC <sub>50</sub> = 20 μM*	81 ± 0% @50 μM
A549	IC <sub>50</sub> = 29 μM*	IC <sub>50</sub> = 42 ± 2 μM	22 ± 13% @50 μM
<b>Calculated Properties</b>			
<b>clogD (pH 7.4)<sup>[b]</sup></b>	2.5	2.6	4.6
<b>clogP<sup>[b]</sup></b>	3.5	4.0	4.9
<b>Ionisable amine (pK<sub>a</sub>)<sup>[b]</sup></b>	1° amine (9.1)	2° amine (8.4)	3° amine (9.3)
<b>Rotatable bonds<sup>[b]</sup></b>	5	3	5
<b>Globularity<sup>[c]</sup></b>	0.11	0.06	0.08
<b>Amphiphilic moment<sup>[c]</sup></b>	4.7	4.5	2.6
[a] Anomalous kinetics, (Section 5.2.2.5). [b] Calculated with StarDrop v. 6.5.1 or 6.6.7. [c] Calculated with MOE 2018.01 for the docked pose. [d] The poses were generated in SeeSAR 8.1 and the figures were created in StarDrop 6.5.1. <sup>82</sup> *Value of a single measurement.			

The MEP pathway is mainly present in Gram-negative bacteria and only exists in some selected Gram-positive bacteria including for example *B. subtilis*.<sup>37</sup> Therefore, the Gram-positive strains, *S. aureus* and *B. subtilis*, were used as a negative and positive control, respectively, for a first indication of target engagement with the enzyme IspE. Both **HIPS5242** (%-inh. = 47 ± 8%

@100  $\mu\text{M}$ ) and **HIPS5255** (%-inh. =  $4 \pm 1\%$  @100  $\mu\text{M}$ ) showed poorer activities against *S. aureus* than *E. coli* K12. However, with *B. subtilis* we observed anomalous kinetics in overnight cultures for the two hits, **HIPS5242** and **HIPS5255**, and another VS hit **HIPS5250** was included as a negative control, (Figure 3.1:2 and SI, Section 5.2.2.5).

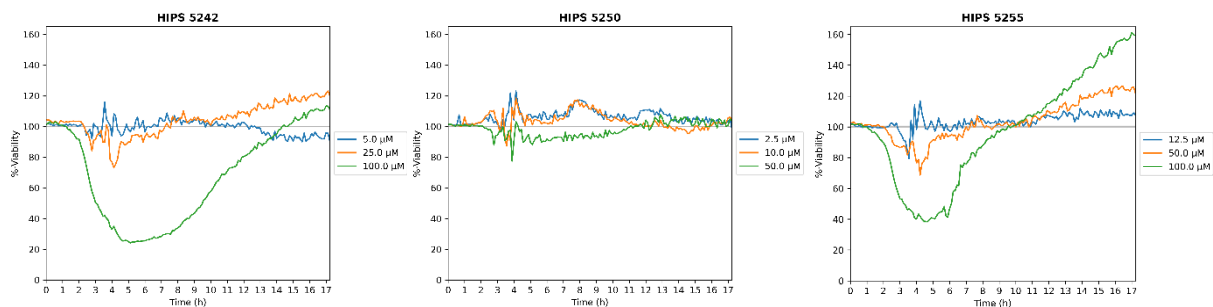


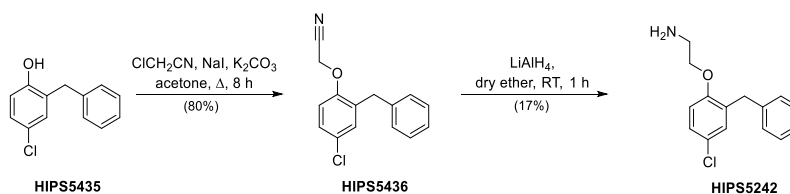
**Figure 3.1:2** - Anomalous growth kinetics of *B. subtilis* overnight cultures treated with **HIPS5242**, **HIPS5250** and **HIPS5255**.

Abnormally, the replication of the cells increased for the first few hours when treated with a compound concentration close to its MIC, but decreased back to the control DMSO levels over time for **HIPS5242** and **HIPS5255**. On the contrary, a similar effect was lacking for **HIPS5250**. Since *B. subtilis* relies on both the MEP and the mevalonate pathways<sup>37</sup>, we hypothesised when the MEP pathway becomes suppressed in the presence of an inhibitor, a “switch-on” mechanism would turn on the mevalonate pathway as a protecting response, resulting in increased cell replication. Similar studies showed for Gram-negative *Chlamydia trachomatis* that inhibition of the MEP pathway by fosmidomycin itself is not lethal, but causes induced persistence by inhibiting the synthesis of the vital isoprenoid bactoprenol disturbing follow-up peptidoglycan precursor assembly and subsequent cell division.<sup>85</sup> **HIPS5242** and **HIPS5255** were therefore tested against mutants with repressed IspC (*kd-dxr*) or IspE (*kd-ispE*) in *B. subtilis*. In the overnight cultures, similar anomalous kinetics were not observed, but the cell morphology examined by phase contrast microscopy suggested some bulging effect (Supplementary Material, Section 5.2.2.5).

### Hit Validation

Overall, the primary amine derivative **HIPS5242** possessed the most promising starting point for further optimisation due to its fragment-likeness (MW=261.7 g/mol). After resynthesis and validation of the hit compound, we evaluated its binding affinity using microscale thermophoresis (MST) showing weak binding to *EcIspE* ( $K_d \sim 700 \mu\text{M}$ ) (Supplementary Material, Section 5.2.3.2). We also confirmed its binding with *EcIspE* using saturated transfer difference (STD)-NMR (Supplementary Material, Section 5.2.3.3). However, it was clear that IspE inhibition was not the

only target based on the lack of *in vitro* activity, although it is still generally unclear how strong target engagement of the MEP pathway is needed for cellular inhibition. Due to its fragment-likeness, we decided to proceed with the primary amine hit **HIPS5242** to evaluate its potential to increase the affinity for *EcIspE* and in parallel, focusing on understanding the structure–permeation relationship for antibacterial activity through subtle handle modifications. The resynthesis of **HIPS5242** began from the corresponding phenolic derivative followed by introduction of the handle via an S<sub>N</sub>2 reaction (Scheme 3.1:1). In order to evaluate the need for the primary amine, we tested all the synthetic derivatives, the phenolic core and the nitrile-handle derivatives, **HIPS5435** and **HIPS5436** respectively, and confirmed that the primary amine indeed boosted the activity against the wild-type *E. coli* K12 (Supplementary Material, Table S5.2.2.4:3). These slight modifications in the handle, hereafter called the “activity handle”, further encouraged us to move on with the series aiming to evaluate the molecular causes leading to differentiating antibacterial activities. This was further supported by similar phenolic compounds reported to show antibacterial activity and used as disinfectants.<sup>86–89</sup> In addition, a similar ethanolamine handle was used for arylomycin derivative G0775 to increase antibacterial activity against a panel of Gram-negative bacteria, also against *P. aeruginosa*.<sup>72</sup>

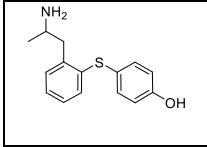
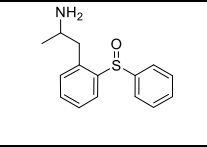
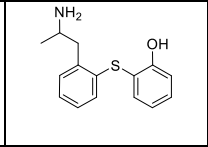


**Scheme 3.1:1** – Resynthesis of the hit **HIPS5242**.

### Follow-up Synthesis

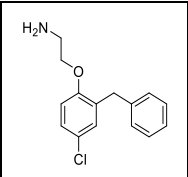
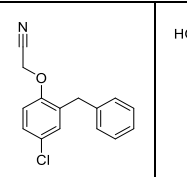
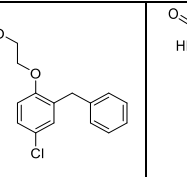
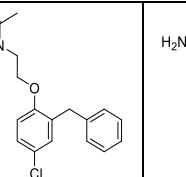
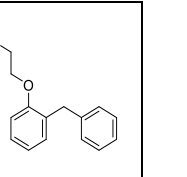
As the next step, we investigated several close derivatives of **HIPS5242** mainly focusing on different modifications of the ethanolamine. The handle modifications were tested against *E. coli* strains as well as the target enzyme *EcIspE* (a comprehensive list given in the Supplementary Material, Table S5.2.2.4:2). None of the handle modifications exhibited *EcIspE* activity, however, thioether compound **HIPS5411** showed slight inhibition (*EcIspE* IC<sub>50</sub> = 447 μM, from a single measurement), whereas its close derivative **HIPS5419** bearing the hydroxy in *ortho*-position showed no inhibitory activity but slight decrease in the melting point (T<sub>m</sub> = 51.10 ± 0.08 (–0.4) °C). Given that the sulfoxide derivative **HIPS5412** showed no activity and also due to the fact that thioether may oxidise to the sulfoxide *in cellulo*, we decided not to pursue in this direction.

**Table 3.1:2** - Summary of the ordered thioether core linkers.

			
	<b>HIPS5411</b>	<b>HIPS5412</b>	<b>HIPS5419</b>
<b>EcIspE</b>			
<b>EcIspE IC<sub>50</sub> (μM)</b>	447*	>500	>500
<b>PK/LDH IC<sub>50</sub> (μM)</b>	n.d.	n.d.	n.d.
<b>T<sub>m</sub>(°C) (ΔT<sub>m</sub> (°C))</b>	50.82 ± 0.12 (-0.7)	51.52 ± 0.10 (0.0)	51.10 ± 0.08 (-0.4)
<b>Bacterial Minimum Inhibitory Concentration (MIC) or Percentage Inhibition @ 100 μM</b>			
<b><i>E. coli</i> Δ<i>tolC</i></b>	47 ± 20%	7 ± 2%	57 ± 7 (MIC)
<b><i>E. coli</i> K12</b>	33 ± 4%	12 ± 1%	48 ± 3%
<b>Cytotoxicity Inhibition Concentration or Percentage Inhibition @ 100 μM</b>			
<b>HepG2</b>	IC <sub>50</sub> = 45 ± 6	-4 ± 20%	91 ± 2%
n.d. = not determined. *Value of a single measurement.			

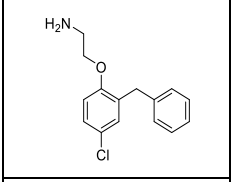
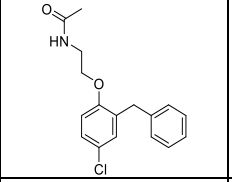
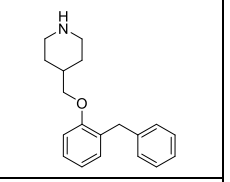
We also screened some of the handle-modified compounds against the *E. coli* mutant strains to identify potential permeability or efflux issues (Table 3.1:3). The nitrile-handle **HIPS5436** and the other activity handle modifications with hydroxyl **HIPS5423** or amide **HIPS5418** could further support the hypothesis that a primary amine is necessary, as all the other derivatives without an ionisable amine proved to be inactive against the *E. coli* K12 wild-type. Most of them only showed *E. coli* Δ*tolC* activity, suggesting efflux issues may account for the lack of activity against *E. coli* K12. In addition, the activities dropped against the lipopolysaccharide (LPS) mutated D22, proposing the overall scaffold also to play key interactions with the LPS layer. Nevertheless, we could demonstrate that the activity against the *E. coli* porin-knockdown mutant *omp8* with **HIPS5242** suffered a 10% decrease in activity (%-inh. = 87 ± 7% @ 100 μM), suggesting that **HIPS5242** finds an alternative uptake mechanism despite the primary amine being present. Interestingly, the drop in activity for the amide derivative **HIPS5418** (%-inh. = -6 ± 7% @ 50 μM) was more drastic, unexpectedly hinting it relies more on porin uptake than the corresponding amine **HIPS5242** in disagreement with the eNTRY rules (Table 3.1:3).

**Table 3.1:3** - Comparison of the different activity handles in different *Escherichia coli* mutant strains.

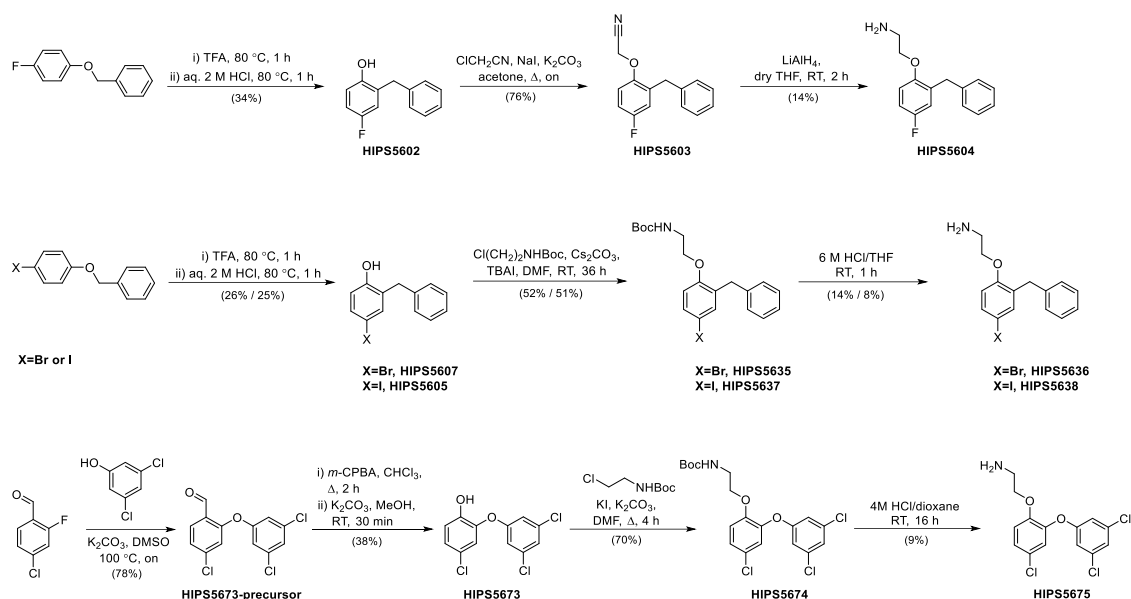
					
	<b>HIPS5242</b>	<b>HIPS5436</b>	<b>HIPS5423</b>	<b>HIPS5418</b>	<b>HIPS5380</b>
<b>Bacterial Minimum Inhibitory Concentration (MIC) or Percentage Inhibition @ 100 μM</b>					
<i>E. coli</i> K12	99 ± 2(MIC)	13 ± 2%	27 ± 3%	8 ± 8%	31 ± 5%
<i>E. coli</i> Δ <i>tolC</i>	97 ± 4(MIC)	38 ± 1 (MIC)	50 ± 0 (MIC)	88 ± 11 (MIC)	41 ± 0%
<i>E. coli</i> Δ <i>acrB</i>	95 ± 0 (MIC)	54 ± 5%	103 ± 3 (MIC)	30 ± 12% @50μM	42 ± 1%
<i>E. coli</i> D22	105 ± 7 (MIC)	35 ± 5	22 ± 4%	34 ± 6% @50 μM	-3 ± 19%
<i>E. coli</i> Omp8	87 ± 7%	n.d.	104 ± 2 (MIC)	-6 ± 7% @50 μM	3 ± 1%
<i>P. aeruginosa</i>	52 ± 10%	9 ± 5%	5 ± 2%	1 ± 4% @50 μM	-2 ± 4%
<i>A. baumannii</i>	100 ± 0	2%* @50 μM	-2 ± 3 @50 μM	2 ± 1% @50 μM	22 ± 1%
<i>S. aureus</i>	47 ± 8%	18 ± 24%	32 ± 21%	13 ± 19%	11 ± 7%
<b>Cytotoxicity Inhibition Concentration or Percentage Inhibition @ 100 μM</b>					
HepG2	IC <sub>50</sub> = 21 ± 1	80 ± 3%	78 ± 13%	48 ± 4%	88 ± 5%
n.d.: not determined, *Value of a single measurement.					

Given that some of the investigated derivatives showed some antibacterial activity, we tested the best handle modifications against the more pathogenic *A. baumannii* and *P. aeruginosa* (Supplementary Material, Table S5.2.2:8). Interestingly, the piperidine handle **HIPS5417** showed slightly better %-inhibition against *P. aeruginosa* wild-type (%-inh. = 43 ± 9 @100 μM) than *E. coli* wild-type (%-inh. = 13 ± 11 @100 μM), although it lacks the chlorine atom in 4-position. The general trend is that most of the compounds active against *E. coli* lose potency when moving to the more pathogenic bacteria. We also had the capability to test the most promising compounds **HIPS5242** and **HIPS5417** and the amide-handle derivative **HIPS5418** as a negative control against other *Pseudomonas* mutant strains to evaluate the potential efflux or permeability issues with outer membrane porin mutants Δ*oprF* and Δ*omph*, and efflux pump mutants Δ*mexB* and Δ*mexA*.<sup>90-92</sup> Surprisingly, we did not observe such striking activity differences as we had seen for the *E. coli* mutants, mainly with Δ*tolC* (Table 3.1:4). This could, however, suggest that there are other molecular properties governing the uptake and efflux ratios in *P. aeruginosa*.

**Table 3.1:4** - Comparison of **HIPS5242**, **HIPS5418** and **HIPS5417** against the panel of mutant strains of *Escherichia coli* and *Pseudomonas aeruginosa*.

				
		<b>HIPS5242</b>	<b>HIPS5418</b>	<b>HIPS5417</b>
<b>Bacterial Minimum Inhibitory Concentration (MIC) or Percentage Inhibition @ 100 μM</b>				
<i>Wild-type</i>	<i>E. coli</i> K12	99 ± 2 (MIC)	8 ± 8%	27 ± 3%
<i>Efflux pump mutant</i>	<i>E. coli</i> Δ <i>tolC</i>	97 ± 4 (MIC)	88 ± 11 (MIC)	85 ± 8%
<i>Efflux pump mutant</i>	<i>E. coli</i> Δ <i>acrB</i>	95 ± 0 (MIC)	30 ± 12% @50 μM	108 ± 4 (MIC)
<i>Porin mutant</i>	<i>E. coli</i> Omp8	87 ± 7%	-6 ± 7% @50 μM	58 ± 8%
<b>Bacterial Minimum Inhibitory Concentration (MIC) or Percentage Inhibition @ 100 μM</b>				
<i>Wild-type</i>	<i>PA 14</i>	52 ± 10%	2 ± 1% @50 μM	43 ± 9%
<i>Porin mutant</i>	<i>PA 14</i> Δ <i>mexB</i>	33 ± 9%	0.2 ± 0.4% @50 μM	35 ± 21%
<i>Porin mutant</i>	<i>PA 14</i> Δ <i>mexA</i>	49 ± 25%	4 ± 1% @50 μM	43 ± 10%
<i>Efflux pump mutant</i>	<i>PA 14</i> Δ <i>oprF</i>	59 ± 27%	20 ± 10% @50 μM	48 ± 8%
<i>Efflux pump mutant</i>	<i>PA 14</i> Δ <i>omph</i>	48 ± 5%	2 ± 7% @50 μM	31 ± 16%
n.d. = not determined				

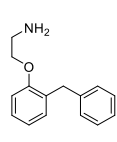
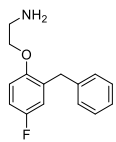
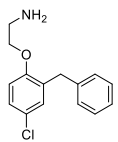
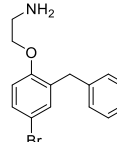
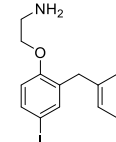
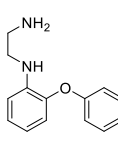
As with the commercially available derivatives we could not see a great increase in activity, neither cellular nor enzymatic, we next focused on altering the amphiphilic moment, as also described in the original eNTRY rules.<sup>93</sup> The amphiphilic moment is the distribution of or distance between the hydrophilic and hydrophobic parts of a compound.<sup>94</sup> In the hit structure **HIPS5242**, there is a high amphiphilic moment between the chlorine and the free amine (vsurf\_A = 7.1). In simplicity, one can consider that charge is necessary to get through the outer membrane porins favourably and lipophilicity for passive uptake through the lipophilic polysaccharide bilayers either in the outer or the inner membrane, as earlier hinted by H. Nikaido *et al.*<sup>95</sup> Therefore, to modify the amphiphilic moment, we synthesised a so-called halogen series, where the chlorine in 4-position was substituted by different halogens. The calculated amphiphilic moment increased when going down the halogen row in the periodic table. The unsubstituted derivative **HIPS5380** was commercially available and we synthesised other halogen derivatives from the diphenylether derivatives *via* an adapted Fries/Duff rearrangement (Scheme 3.1:2)<sup>96</sup>, followed by the handle introduction *via* an S<sub>N</sub>2 reaction with either chloroacetonitrile or the *N*-Boc handle (Scheme 3.1:2). The reduction of the nitrile group failed with the bromine **HIPS5608** and iodine **HIPS5606** derivatives, resulting in the de-halogenated derivative **HIPS5380**. Therefore, we selected the *N*-Boc handle as an alternative for the follow-up synthesis (Scheme 3.1:2).



**Scheme 3.1:2** - Synthetic route to the halogen and dichloro-series.

We confirmed that the increased amphiphilic moment boosted the activity with a very clear trend when moving down the periodic table (Table 3.1:5). The iodine derivative led to a two-fold decreased MIC value against *E. coli* K12 and increased activity against *A. baumannii* and *P. aeruginosa*. The engagement of a possible halogen bonding interaction with *EcIspE* still needs to be confirmed.

**Table 3.1:5** - Summary of the biological results for the halogen series.

						
	<b>HIPS5380</b>	<b>HIPS5604</b>	<b>HIPS5242</b>	<b>HIPS5636</b>	<b>HIPS5638</b>	<b>HIPS5504</b>
<b>Amphiphilic moment<sup>[a]</sup></b>	6.1	6.5	7.1	7.1	7.8	5.0
<b>Most basic pK<sub>a</sub><sup>[b]</sup></b>	9.3	9.3	9.1	9.1	9.1	9.1
<b>Bacterial Minimum Inhibitory Concentration (MIC) or Percentage Inhibition @ 100 μM</b>						
<i>E. coli</i> K12	31 ± 5%	38 ± 2%	99 ± 2 (MIC)	90 ± 0 (MIC)	53 ± 4 (MIC)	29 ± 2%
<i>E. coli</i> Δ <i>tolC</i>	41 ± 0%	48 ± 6%	97 ± 4 (MIC)	93 ± 4 (MIC)	88 ± 4 (MIC)	24 ± 7%
<i>E. coli</i> Δ <i>acrB</i>	42 ± 1%	44 ± 11%	95 ± 0 (MIC)	94 ± 0 (MIC)	84 ± 5 (MIC)	29 ± 20%
<i>E. coli</i> D22	-3 ± 19%	n.d.	105 ± 7 (MIC)	n.d.	n.d.	1 ± 8%
<i>E. coli</i> Omp8	3 ± 1%	8 ± 3%	87 ± 7%	94 ± 1 (MIC)	75 ± 10 (MIC)	-14 ± 0%
<i>P. aeruginosa</i>	-2 ± 4%	n.d.	52 ± 10%	70 ± 3%	52 ± 6%	n.d.
<i>A. baumannii</i>	22 ± 1%	11 ± 1%	100 ± 0 (MIC)	n.d.	28±13@50μM	n.d.
<i>S. aureus</i>	11 ± 7%	10 ± 5%	47 ± 8%	79%*	n.d.	3 ± 2%
<b>Cytotoxicity Inhibition Concentration or Percentage Inhibition @ 100 μM</b>						
HepG2	88 ± 5%	IC <sub>50</sub> = 55 ± 4	IC <sub>50</sub> = 21 ± 1	98 ± 1%	IC <sub>50</sub> = 17 ± 1	48 ± 7%

[a] Calculated with MOE 2018.01. [b] Calculated with StarDrop v. 6.6.7. n.d. = not determined. \* Value of a single measurement.

Next, we evaluated **HIPS5504** with a central diaryl ether linker and an aniline-linked activity handle, but without any halogen. As expected based on the low calculated amphiphilic moment ( $v_{surf\_A} = 5.0$ ), the compound lacked cellular activity. Since the cytotoxicity of the halogen series was another problem, we further opted for a series with the central, diaryl ether linker supported by the previous thioether results (Table 3.1:2). We designed the dichloro derivative **HIPS5675** (Scheme 3.1:2) using structure-based drug design (SBDD) using *E. coli* IspE (PDB 1OJ4). During the VS, several compounds including **HIPS5255** were observed to have a similar dichloro-motif in the hydrophobic site interacting with Arg72 from the other monomer.

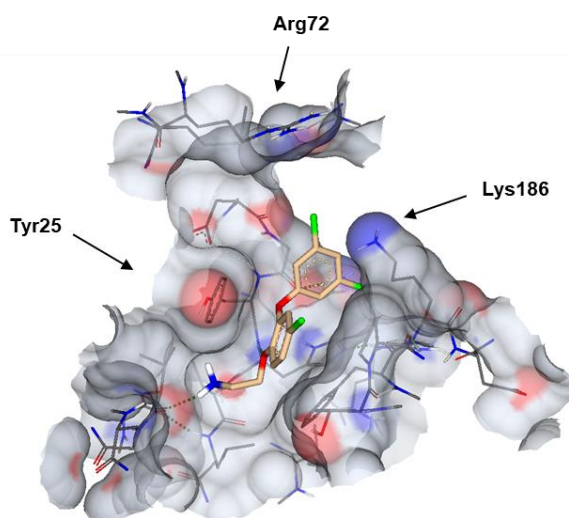


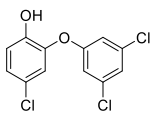
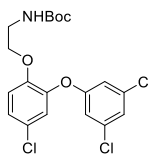
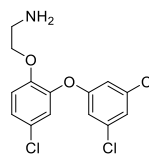
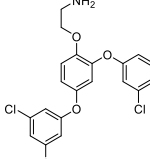
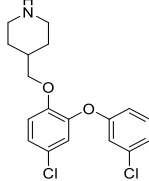
**Figure 3.1:3** - Binding site with **HIPS5675** showing the possible interaction with the Arg72 from the other monomer in its predicted docking pose and demonstrating the possibility for the covalent inhibitor with Lys186 or Tyr25. Molecular modelling was done in SeeSAR 10.3 and the figure was created in StarDrop 6.6.7.<sup>82</sup>

This dichloro-motif was introduced on the right-hand side phenyl ring and for the first time, the series also showed *EcIspE* inhibitory activity ( $IC_{50} = 159 \pm 4 \mu M$ ) with an increased binding affinity determined by MST ( $K_d \sim 60 \mu M$ ). STD-NMR studies further confirmed the binding with *EcIspE*. Based on the SBDD, the interaction of this dichloro-motif could disturb the dimerisation of *EcIspE* by interacting with the residue Arg72 from the other monomer, potentially destabilising the enzyme, which could lead to a decreased melting point in a thermal shift assay (TSA).<sup>97</sup> The ether **HIPS5675** was also tested in TSA, where we in fact observed a decreased melting point ( $\Delta T_m = -1.9 \text{ }^\circ C$ ) in comparison to the native *EcIspE* ( $T_m = 51.52 \pm 0.14 \text{ }^\circ C$ ), being in the previously reported range.<sup>54</sup> In comparison, the natural substrate CDP-ME shows as increased melting point ( $\Delta T_m = +0.8 \text{ }^\circ C$ ). This was the first indication supporting the binding of **HIPS5675** in the hydrophobic pocket, possibly disturbing the dimerisation, although it is not yet fully confirmed, whether *EcIspE* enzyme really exists as a dimer in solution.<sup>39,54</sup>



In the *N*-Boc deprotection step, we observed the formation of a side product **HIPS5676** that turned out to be an even more potent *Ec*IspE inhibitor ( $IC_{50} = 4 \pm 1 \mu\text{M}$ ). The structure suggests that the 4-position of the left-hand side phenyl ring could also be metabolically labile, but also confirms that there is space to grow in this direction. Nevertheless, it shows no inhibition against wild-type *E. coli* K12, pointing to permeability issues. We also tested it against *B. subtilis* showing low micromolar activity ( $MIC = 22 \pm 18 \mu\text{M}$ ). Next, we compared the effect of **HIPS5676** on *B. subtilis* cells with that of IspE (or Dxr) depletion. To this end, exponential *B. subtilis* wild-type cells treated with  $6.25 \mu\text{M}$  **HIPS5676** as well as the *B. subtilis* mutant strains *kd-ispE* or *kd-dxr* with repressed IspE or Dxr expression, respectively, were imaged (Supplementary Material, Section 5.2.2.5). For both **HIPS5676** exposure as well as for IspE (or Dxr) depletion, we observed a reduced cell number due to cell lysis after 90 minutes, which was often preceded by a characteristic bulging phenotype. We also calculated the sequence similarity between *E. coli* and *B. subtilis* IspE to be 54%, being the most conserved in the catalytic site as used for the VS (Supplementary Material, Section 5.2.2.5). All synthetic derivatives of the dichloro-series were tested against *Ec*IspE and we could confirm that the free amine **HIPS5675** selectively inhibits *Ec*IspE, whereas the phenol derivative **HIPS5673** and *N*-Boc handle **HIPS5674** also inhibit the auxiliary enzymes PK/LDH (Table 3.1:6). This was a key information for our further optimisation of the series and to minimise the potential cytotoxicity effects. As we had seen activity changing between *E. coli* and *P. aeruginosa* with different activity handles, **HIPS5242** vs **HIPS5417**, we synthesised the dichloro-derivative using a piperidine handle **HIPS6016** aiming to increase the bacterial activity selectively for *P. aeruginosa*. The piperidine handle **HIPS6016** displays the highest antibacterial of the series against *P. aeruginosa* ( $MIC = 107 \pm 12 \mu\text{M}$ ), showing also activity against *E. coli* wild-type ( $MIC = 98 \pm 6 \mu\text{M}$ ), but suffering simultaneously from efflux (*E. coli*  $\Delta tolC$   $MIC = 41 \pm 2 \mu\text{M}$ ). In comparison, no MIC could be determined for the corresponding primary amine derivative **HIPS5675** against *P. aeruginosa* wild-type (%-inh. =  $63 \pm 8\%$  @  $100 \mu\text{M}$ ).

**Table 3.1:6** - Summary of the dichloro-series.

					
	<b>HIPS5673</b>	<b>HIPS5674</b>	<b>HIPS5675</b>	<b>HIPS5676</b>	<b>HIPS6016</b>
<b>Amphiphilic moment<sup>[a]</sup></b>	5.4	3.1	5.6	5.3	5.7
<b>Most basic pK<sub>a</sub><sup>[b]</sup></b>	n.d.	n.d.	9.0	9.1	9.4
<b>EcIspE</b>					
<b>EcIspE IC<sub>50</sub> (μM)</b>	40 ± 6	130 ± 20	159 ± 4	4 ± 1	n.d.
<b>PK/LDH IC<sub>50</sub> (μM)</b>	46 ± 1	>500	>500	>500	n.d.
<b>T<sub>m</sub> (°C)</b> <b>(ΔT<sub>m</sub> (°C))</b>	n.d.	51.31 ± 0.08 (-0.2)	49.60 ± 0.20 (-1.9)	49.75 ± 0.34 (-1.8)	n.d.
<b>MST - K<sub>d</sub></b>	n.d.	n.d.	~ 60 μM	n.d.	n.d.
<b>Bacterial Minimum Inhibitory Concentration (MIC) or Percentage Inhibition @ 100 μM</b>					
<b><i>E. coli</i> K12</b>	58 ± 6% @50 μM	-2 ± 5% @50 μM	85 ± 6 (MIC)	16 ± 13% @50 μM	98 ± 6 (MIC)
<b><i>E. coli</i> Δ<i>tolC</i></b>	3 ± 0 (MIC)	3 ± 0% @50 μM	41 ± 2 (MIC)	20 ± 6 (MIC)	11 ± 0 (MIC)
<b><i>E. coli</i> Δ<i>acrB</i></b>	n.d.	n.d.	44 ± 1 (MIC)	20 ± 5 (MIC)	n.d.
<b><i>E. coli</i> D22</b>	n.d.	n.d.	86 ± 4 (MIC)	n.d.	n.d.
<b><i>E. coli</i> Omp8</b>	n.d.	n.d.	45 ± 2 (MIC)	n.d.	n.d.
<b><i>P. aeruginosa</i></b>	n.d.	-1 ± 4% @50 μM	63 ± 8%	13%* @50 μM	107 ± 12 (MIC)
<b><i>A. baumannii</i></b>	n.d.	22 ± 0% @50 μM	64 ± 2 (MIC)	21%* @50 μM	33* (MIC)
<b><i>S. aureus</i></b>	5 ± 0 (MIC)	33 ± 8% @50 μM	99 ± 6 (MIC)	n.d.	n.d.
<b><i>B. subtilis</i></b>	n.d.	n.d.	46 ± 1 (MIC)	22 ± 18 (MIC)	n.d.
<b>Cytotoxicity Inhibition Concentration or Percentage Inhibition @ 100 μM</b>					
<b>HepG2</b>	IC <sub>50</sub> = 33 ± 2	55 ± 3%	IC <sub>50</sub> = 15 ± 3	95% @50 μM*	97 ± 0

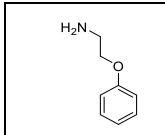
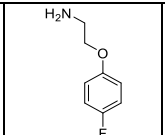
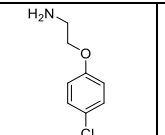
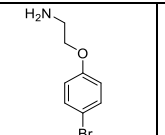
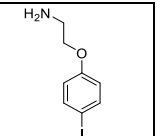
[a] Calculated with MOE 2018.01. [b] Calculated with StarDrop v. 6.6.7. n.d. = not determined. \*Value of a single measurement.

### Attempts to unravel the cytotoxicity issue

With the dichloro-series, we could obtain activity against *EcIspE* and increase the antibacterial activity, without being able to decrease the cytotoxicity. We also tested the mono-halogenated derivatives of the hit **HIPS5242** lacking the right-hand side. They show no antibacterial activity, confirming the right-hand side is essential for the activity, although their amphiphilic moment is rather high, yet increasing going down the halogen derivatives (Table 3.1:7). No toxicity was observed for the chloro-derivative **HIPS5679** (HepG2 %-inh. = 9 ± 1 @100 μM) or iodo-derivative **HIPS5681** (HepG2 %-inh. = -5 ± 3 @100 μM). Therefore, the cytotoxicity seems to stem from the subtle balance between lipophilicity and the basicity of the primary amine. This is slightly surprising, as such diaryl ethers are common building blocks in drug candidates, as shown in a recent review.<sup>98</sup>

Additionally, other halogenated diphenylic structures, such as triclosan, (5-chloro-2-(2,4-dichlorophenoxy)-phenol), and its derivatives, have been described in the literature targeting the enoyl-acyl carrier protein reductase (ENR) essential for the bacterial type II fatty acid biosynthesis.<sup>99,100</sup> One of the other cellular targets for our series could indeed also be related to ENR inhibition. In the best case, our series could dually inhibit two of the key isoprenoid-related biosynthetic pathways, which could be a successful approach to overcome resistance development, as recently seen in cancer research.<sup>101,102</sup>

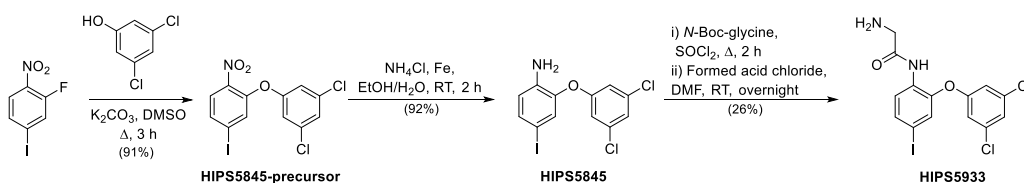
**Table 3.1:7** - Summary of the biological results of the mono-halogenated left-hand side fragments.

					
	<b>HIPS5677</b>	<b>HIPS5678</b>	<b>HIPS5679</b>	<b>HIPS5680</b>	<b>HIPS5381</b>
<b>Amphiphilic moment<sup>[a]</sup></b>	5.6	5.0	6.3	6.4	6.7
<b>Most basic pK<sub>a</sub><sup>[b]</sup></b>	9.6	9.2	9.3	9.3	9.5
<b>Bacterial Minimum Inhibitory Concentration (MIC) or Percentage Inhibition @ 100 μM</b>					
<i>E. coli</i> K12	3 ± 3	4 ± 1	5 ± 0	-1 ± 6	-3 ± 1
<i>E. coli</i> Δ <i>tolC</i>	9 ± 7	9 ± 4	5 ± 3	8 ± 1	10 ± 5
<i>E. coli</i> Δ <i>acrB</i>	n.d.	n.d.	11 ± 3	n.d.	18 ± 2
<b>Cytotoxicity Inhibition Concentration or Percentage Inhibition @ 100 μM</b>					
HepG2	n.d.	n.d.	9 ± 1	n.d.	-5 ± 3

[a] Calculated with MOE 2018.01. [b] Calculated with StarDrop v. 6.6.7. n.d. = not determined.

### Addressing the Cytotoxicity

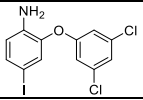
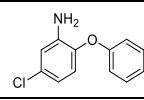
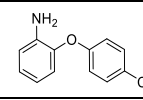
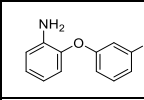
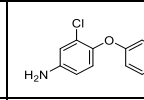
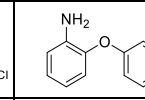
To solve the cytotoxicity issues, we next focused on a series using the central phenolic linker whilst changing the activity handle to an aniline derivative. The best parts including the iodo-motif on the left-hand side of **HIPS5638** and the dichloro-motif on the right-hand side of **HIPS5675** were combined into **HIPS5933** (Scheme 3.1:3). Due to the synthetic accessibility, the activity handle was now introduced *via* a coupling with *N*-Boc-glycine, affording the amide derivative that was kept considering the long-term metabolic stability over the aniline handle. The compound showed a notable increase in binding affinity ( $K_d \sim 20 \mu\text{M}$ ) and a clear drop in the melting point ( $\Delta T_m = -3.9 \text{ }^\circ\text{C}$ ). It also showed better antibacterial profile (*E. coli* K12 MIC =  $47 \pm 2 \mu\text{M}$ ), but disappointingly still suffered from a high cytotoxicity against the HepG2 cell line ( $\text{IC}_{50} = 9 \pm 1 \mu\text{M}$ ).



**Scheme 3.1:3** – Synthetic route to **HIPS5933**.

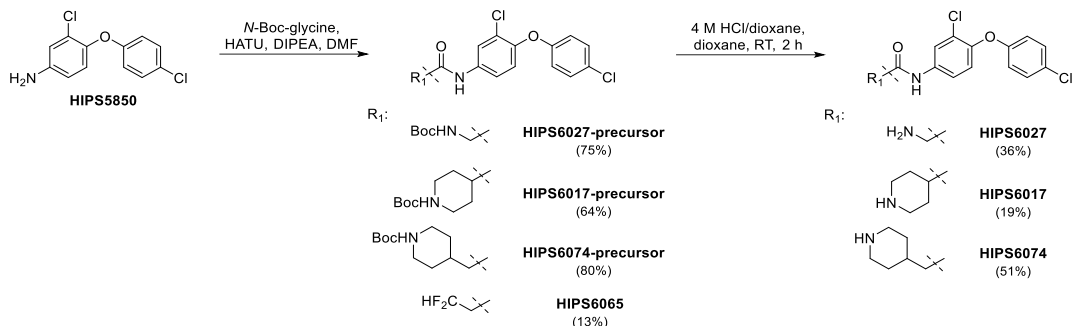
We therefore explored similar commercially available aniline derivatives, having halogens in different substitution patterns. None of the aniline derivatives without the activity handle, even the precursor of **HIPS5933**, **HIPS5845**, however, showed substantial antibacterial activity against *E. coli* K12 (Table 3.1:8).

**Table 3.1:8** - Summary of the core compounds with different substitution patterns.

						
	<b>HIPS5845</b>	<b>HIPS5847</b>	<b>HIPS5848</b>	<b>HIPS5849</b>	<b>HIPS5850</b>	<b>HIPS5502</b>
<b>Bacterial Minimum Inhibitory Concentration (MIC) or Percentage Inhibition @ 100 μM</b>						
<i>E. coli</i> K12	10 ± 7% @50 μM	27 ± 5%	21 ± 0%	4 ± 5%	28 ± 8%	12 ± 6%
<i>E. coli</i> Δ <i>tolC</i>	45 ± 7% @50 μM	100 ± 0 (MIC)	29 ± 5%	27 ± 6%	45 ± 1 (MIC)	13 ± 4%
<b>Cytotoxicity Inhibition Concentration or Percentage Inhibition @ 100 μM</b>						
HepG2	IC <sub>50</sub> = 15 ± 8	20 ± 8%	92 ± 18%	51 ± 7%	-16 ± 9%	45 ± 4%

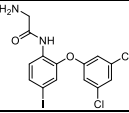
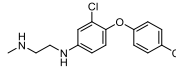
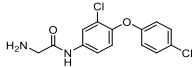
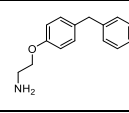
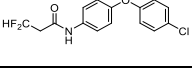
Nevertheless, **HIPS5850** showed a strong activity against *E. coli* Δ*tolC* (MIC = 45 ± 1 μM) and interestingly, no cytotoxicity (HepG2 %-inh. = -16 ± 9 @100 μM), which further encouraged us to introduce the activity handle to this core. Additionally, one of the first commercial compounds **HIPS5425** with a similar substitution pattern to **HIPS5850** showed lower cytotoxicity (HepG2 %-inh. = 51 ± 8 @100 μM). This opened up a new direction to introduce the activity handle *via* amide couplings, (Scheme 3.1:4). The primary amine handle **HIPS6027** showed activity against *E. coli* and the piperidine handles **HIPS6017** and **HIPS6074** against *P. aeruginosa*, as seen with **HIPS6016** in the dichloro-series. Compound **HIPS5990** with the dicationic handle, obtained from a side reaction, however, retained the cytotoxicity issues, reinforcing the high basicity of the primary amine to be the cause of the cytotoxicity (Table 3.1:9). On the contrary, the primary amine handle **HIPS6027** with an ideal p*K*<sub>a</sub> (7.5) and amphiphilic moment (8.2) finally showed a safer cytotoxicity-profile (%- inh. HepG2 = 77 ± 20% @100 μM) *vs E. coli* K12 (MIC = 48 ± 1 μM). As the overall activity loss in the porin mutant *omp8* for the initial hit **HIPS5242** was minimal, we also investigated a replacement of the primary amine bioisosterically with a more metabolically stable difluoromethyl handle, inspired by a recent publication by X. Zeng *et al.*<sup>103</sup> The difluoromethyl-handle modified **HIPS6065** was accessible in a single synthetic step *via* an amide coupling, following the protocol from Scheme 3.1:4. **HIPS6065** improved the cytotoxicity-profile even more than **HIPS6027** (%-inh. HepG2 = 65 ± 6% @100 μM), however, the preliminary results suggest efflux issues (*E. coli* K12 %-inh. 25 @50 μM *vs E. coli* Δ*tolC* MIC = 11 μM, both from single measurements). Further analysis of its influence on bacterial uptake and excretion is ongoing. As **HIPS6065** also showed low MIC against the porin mutated *omp8* (*E. coli* *omp8* MIC = 35 μM, from a single measurement), further

derivatives should be optimised with lower  $\text{clogD}_{7.4}$  to circumvent efflux issues (**HIPS6065**  $\text{clogD}_{7.4} = 4.8$ ) and simultaneously increase the amphiphilic moment (**HIPS6065**  $\text{vsurf\_A} = 5.8$ ).



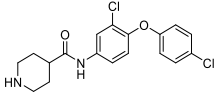
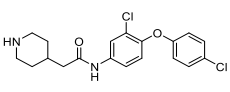
**Scheme 3.1:4** - Summary of the synthesis with the new core **HIPS5850**.

**Table 3.1:9** - Summary of the biological data for the derivatives featuring new core.

					
	<b>HIPS5933</b>	<b>HIPS5990</b>	<b>HIPS6027</b>	<b>HIP5425</b>	<b>HIPS6065</b>
<b>Amphiphilic moment<sup>[a]</sup></b>	6.5	6.1	8.2	7.8	5.8
<b>Most basic <math>\text{pK}_3</math><sup>[b]</sup></b>	7.8	9.3	7.5	9.4	N/A
<b><math>\text{clogD}_{7.4}</math><sup>[b]</sup></b>	2.8	2.2	1.7	0.8	4.8
<b><i>EcIspE</i></b>					
<b><i>EcIspE</i> <math>\text{IC}_{50}</math> (<math>\mu\text{M}</math>)</b>	n.d.	n.d.	n.d.	>500	n.d.
<b>PK/LDH <math>\text{IC}_{50}</math> (<math>\mu\text{M}</math>)</b>	n.d.	n.d.	n.d.	n.d.	n.d.
<b><math>T_m</math> (<math>^{\circ}\text{C}</math>)</b> ( $\Delta T_m$ ( $^{\circ}\text{C}$ ))	48.38 $\pm$ 0.29 (-3.1)	47.58 $\pm$ 0.31 (-3.9)	n.d.	n.d.	n.d.
<b>Bacterial Minimum Inhibitory Concentration (MIC) or Percentage Inhibition @ 100 <math>\mu\text{M}</math></b>					
<b><i>E. coli</i> K12</b>	47 $\pm$ 2 (MIC)	98 $\pm$ 6 (MIC)	48 $\pm$ 1 (MIC)	41 $\pm$ 9%	25%* @ 50 $\mu\text{M}$
<b><i>E. coli</i> <math>\Delta\text{tolC}</math></b>	46 $\pm$ 1 (MIC)	46 $\pm$ 1 (MIC)	36 $\pm$ 11 (MIC)	45 $\pm$ 15%	12* MIC
<b><i>P. aeruginosa</i></b>	64 $\pm$ 7%	n.d.	95* (MIC)	12 $\pm$ 1%	44%* @ 50 $\mu\text{M}$
<b><i>A. baumannii</i></b>	43 $\pm$ 4 (MIC)	n.d.	n.d.	13 $\pm$ 4%	n.d.
<b><i>S. aureus</i></b>	87 $\pm$ 7%	n.d.	100* (MIC)	6 $\pm$ 10%	105* (MIC)
<b>Cytotoxicity Inhibition Concentration or Percentage Inhibition @ 100 <math>\mu\text{M}</math></b>					
<b>HepG2</b>	$\text{IC}_{50} = 9 \pm 1$	96 $\pm$ 2%	77 $\pm$ 20%	51 $\pm$ 8%	65 $\pm$ 6%
<b>Hek293</b>	n.d.	n.d.	92 $\pm$ 6%	n.d.	83 $\pm$ 5%
<b>A549</b>	n.d.	n.d.	91 $\pm$ 6%	n.d.	68 $\pm$ 7%

[a] Calculated with MOE 2018.01. [b] Calculated with StarDrop v. 6.6.7. N/A = not applicable, n.d. = not determined. \* Value of a single measurement.

**Table 3.1:10** - Summary of the biological data for the new core **HIPS5850** with piperidine handles.

		
	<b>HIPS6017</b>	<b>HIPS6074</b>
<b>Amphiphilic moment<sup>[a]</sup></b>	6.9	7.5
<b>Most basic pK<sub>a</sub><sup>[b]</sup></b>	9.6	9.4
<b>clogD<sub>7.4</sub><sup>[b]</sup></b>	2.6	2.8
<b>Bacterial Minimum Inhibitory Concentration (MIC) or Percentage Inhibition @ 100 μM</b>		
<i>E. coli</i> K12	97 ± 2 (MIC)	94* (MIC)
<i>E. coli</i> Δ <i>tolC</i>	45 ± 1 (MIC)	n.d.
<i>P. aeruginosa</i>	86 ± 14%	92* (MIC)
<i>A. baumannii</i>	86%*	n.d.
<i>S. aureus</i>	n.d.	n.d.
<b>Cytotoxicity Inhibition Concentration or Percentage Inhibition @ 100 μM</b>		
HepG2	97 ± 0%	96 ± 0%

[a] Calculated with MOE 2018.01. [b] Calculated with StarDrop v. 6.6.7. n.d. = not determined. \* Value of a single measurement.

### Attempts to Confirm the Binding Site

As the first attempt, a *benzophenone photoaffinity probe* was designed into the core of **HIPS5242**.<sup>104</sup> Due to its reactivity with the presence of formic acid salt after preparative HPLC, the probe reacted *in situ* to a [f][1,4]-oxazepine core. We did not further pursue this route, however, the reaction could be of general interest for the research dealing with oxazepines considered as a privileged scaffold in medicinal chemistry with a broad range of biological activities and continuous attempts to find new synthetic pathways are explored, as listed by S. Shaabani *et al.*<sup>105,106</sup> The equilibrium conditions shall be examined more closely either resulting in synthesis or in an application of dynamic combinatorial chemistry.

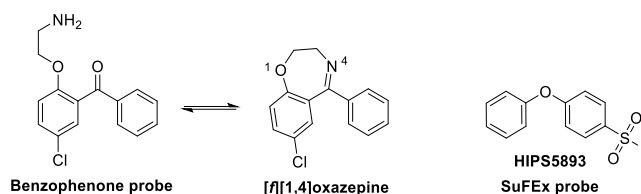


**Figure 3.1:4** - Summary of the designed probes to study the binding site for the series. Benzophenone probe leading to the formation of [f][1,4]oxazepine.

As an alternative approach to confirm the binding site for the series, a commercially available 4-phenoxybenzenesulfonyl fluoride **HIPS5893** warhead was used as a tool compound. In the close proximity of the binding site, residues Lys186 or Tyr25 are ideally located for a nucleophilic attack

using sulfur(VI)-fluoride exchange (SuFEx) chemistry (Figure 3.1:4).<sup>107</sup> Monitoring the reaction by MS, showed covalent addition of the SuFEx probe to *EcIspE* enzyme (Supplementary Material, Section 5.2.4). TSA measurements also revealed the decreasing effect on the melting point ( $\Delta T_m = -1.2$  °C), as seen for the whole series, suggesting a similar binding mode. In parallel to target engagement approach, co-crystallisation attempts are ongoing to confirm the binding site.

### **Conclusions**

We completed a VS using *EcIspE* (PDB 1OJ4) and applied the eNTRY rules in the filtering process. The primary amine hit **HIPS5242** was selected as the hit due to its promising antibacterial profile and its fragment-likeness, although suffering from a low target engagement and cytotoxicity. Follow-up optimisation supported by the amphiphilic moment and SBDD resulted in a diaryl ether compound class with low micromolar binding affinities for *EcIspE*. The frontrunners show an improved cytotoxicity profile and low micromolar MIC values against *E. coli* wild-type strain. In addition, piperidine handles were shown to induce better activity against *P. aeruginosa* than the corresponding primary amine handles. Further optimisation of the series is ongoing, aiming to find the balance between cytotoxicity and antibacterial activity as well as increase the *EcIspE* selectivity and understand the mode of action. Furthermore, we aim to extend the activity of the class to more pathogenic Gram-negative bacteria focusing on the highly conserved catalytic site of the IspE enzymes amongst the other pathogens.

## 3.2 Chapter B:

### Assessment of the Rules Related to Gaining Activity against Gram-Negative Bacteria

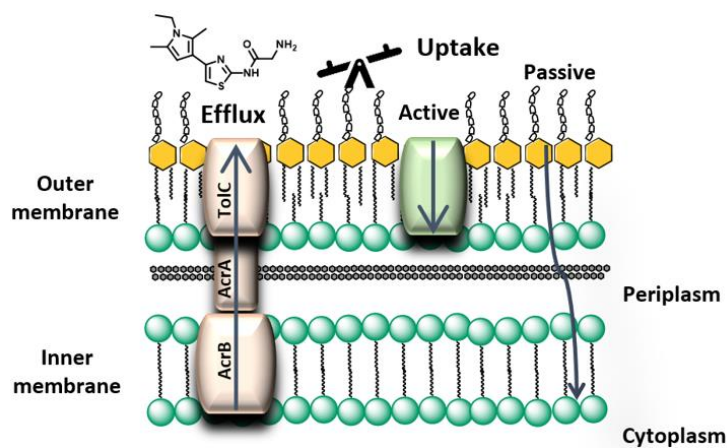
Publication 2

H.-K. Ropponen, E. Diamanti, A. Siemens, B. Illarionov, J. Haupenthal, M. Fischer, M. Rottmann, M. Witschel and A. K. H. Hirsch

This part of the thesis was accepted for publishing in *RSC Medicinal Chemistry*, **2021**, DOI: 10.1039/d0md00409j, in press.

Copyright retained by the authors and reused here acceptably in accordance to RSC guidelines.

#### Graphical Abstract:





## RESEARCH ARTICLE

Assessment of the rules related to gaining activity  
against Gram-negative bacteria†

Cite this: DOI: 10.1039/d0md00409j

Henni-Karoliina Ropponen,<sup>a,b</sup> Eleonora Diamanti,<sup>a</sup> Alexandra Siemens,<sup>c</sup>  
Boris Illarionov,<sup>c</sup> Jörg Hauptenthal,<sup>a</sup> Markus Fischer,<sup>c</sup> Matthias Rottmann,<sup>d,e</sup>  
Matthias Witschel<sup>f</sup> and Anna K. Hirsch<sup>b,\*</sup>

In the search for new antibacterial compounds, we repositioned an antimalarial compound class by designing it based on the so-called “eNTRY” rules for enhanced accumulation into Gram-negative bacteria. We designed, synthesised and evaluated a small library of amino acid modified compounds together with the respective Boc-protected analogues, leading to no substantial improvement in antibacterial activity against *Escherichia coli* wildtype K12, whereas more distinct activity differences were observed in *E. coli* mutant strains  $\Delta$ tolC, D22,  $\Delta$ acrB and BL21(DE3)omp8. A comparison of the activity results of the *E. coli* mutants with respect to the known rules related to enhanced activity against Gram-negative bacteria revealed that applicability of the rules is not always ensured. Out of the four amino acids used in this study, glycine derivatives showed highest antibacterial activity, although still suffering from efflux issues.

Received 4th December 2020,  
Accepted 30th January 2021

DOI: 10.1039/d0md00409j

rsc.li/medchem

## Introduction

The threat of increasing antimicrobial resistance is alarming, which reinforces the need to continuously nourish the antibiotic pipeline.<sup>1</sup> Despite ongoing debates on the “golden set of rules” for antibiotic accumulation into Gram-negative bacteria, the current understanding what makes a molecule a successful antibiotic candidate is still incomplete (H.-K. Ropponen and A. K. H. Hirsch, review in preparation). In another recent review, A. L. Parkes raised the question “*what can we design for?*” – which still needs to be answered in the antibiotic field.<sup>2</sup>

The first correlation of physicochemical properties with antibacterial activity dates back to the 1960s, when low non-ionisable lipophilicity, log*P*, was correlated to enhanced activity against Gram-negative bacteria.<sup>3</sup> Later on, low ionisable lipophilicity, log *D*<sub>7,4</sub>, strict molecular weight (MW)

limit ( $\leq 600$  Da) and high polar surface area (PSA) were found to be characteristic for marketed antibiotics against Gram-negative infections.<sup>4</sup> In 2017, a new direction was given by the so-called “eNTRY” rules. Based on them, a compound needs an ionisable amine (*N*), low globularity as the factor of three-dimensionality (*T*) and high rigidity as the measure of rotatable bonds (*R*) to accumulate into *Escherichia coli*.<sup>5,6</sup> This sparked the research to focus on 3D-properties of the compounds and a scoring function for Gram-negative bacteria was developed based on molecular-dynamics simulations between the outer membrane porins (e.g., *E. coli* OmpF and OmpC) and the passing molecule. A molecule is more likely to go through the porin with lower size, as the measure of minimal projection area, and with high partial charge determined by dipole moment and charge.<sup>7</sup> An alternative scoring profile for Gram-negative bacteria was implemented in the multiparameter software StarDrop in 2018, focusing on physicochemical properties and comparing compounds active against Gram-negative bacteria to other marketed drugs.<sup>8</sup> Antibacterial activity requires, however, a delicate balance between permeation and efflux, which can be achieved by focusing on topology, physical properties and atom/bond count of the compounds.<sup>9</sup>

The eNTRY rules were derived from compound accumulation to *E. coli* and some success stories of their applications have already been published, where an introduction of, in particular, an ionisable amine according to the eNTRY rules has increased the antibacterial activity against other Gram-negative bacteria, such as *Acinetobacter baumannii* and *Klebsiella pneumoniae*.<sup>10–14</sup> In contrast, another recent

<sup>a</sup> Department for Drug Design and Optimization, Helmholtz Institute for Pharmaceutical Research Saarland (HIPS) – Helmholtz Centre for Infection Research (HZI), Campus Building E8.1, 66123 Saarbrücken, Germany.  
E-mail: Anna.Hirsch@helmholtz-hips.de

<sup>b</sup> Department of Pharmacy, Saarland University, Campus Building E8.1, 66123 Saarbrücken, Germany

<sup>c</sup> Hamburg School of Food Science, University of Hamburg, Grindelallee 117, 20146 Hamburg, Germany

<sup>d</sup> Swiss Tropical and Public Health Institute, Socinstrasse 57, 4002 Basel, Switzerland

<sup>e</sup> Universität Basel, Petersplatz 1, 4003 Basel, Switzerland

<sup>f</sup> BASF-SE, Carl-Bosch-Strasse 38, 67056 Ludwigshafen, Germany

† Electronic supplementary information (ESI) available: Synthetic protocols and biological data. See DOI: 10.1039/d0md00409j



**Table 1** Summary of the reported rules for compounds to gain activity against Gram-negative bacteria

Rules	Governing properties
Gram-negative vs. Gram-positive <sup>3</sup>	log <i>P</i> ~ 4 for Gram-negative log <i>P</i> ~ 6 for Gram-positive
Gram-negative vs. other drugs <sup>4</sup>	4-Fold lower log <i>D</i> <sub>7,4</sub> (~2.8) Higher MW (~414, ≤600 Da) Higher PSA (~165 Å <sup>2</sup> )
eNTRY rules <sup>5,6</sup>	Ionisable amine (preferably primary) Rotatable bonds (≤5) Globularity (≤0.25)
Gram-negative scoring function <sup>7</sup>	High partial atomic charge (dipole moment and charge) Low size (minimal projection area)
StarDrop scoring profile <sup>8</sup> (Gram-negative vs. other drugs)	The most active ones in the range of 0.4–0.6 including TPSA >65.68 Å <sup>2</sup> , flexibility <0.3656, log <i>S</i> > 0.8232, log <i>D</i> < 1.79, hERG pIC <sub>50</sub> < 4.938, MW > 237.1 Da, BBB category: negative
Gram-negative permeation & efflux <sup>9</sup>	<i>Escherichia coli</i> : topology, physical properties, atom/bond count

<sup>a</sup> MW: molecular weight, (T) PSA: (total) polar surface area, log *S*: log solubility, hERG: the human *Ether-à-go-go*-related gene, BBB: blood brain barrier.

study argues that there are properties in addition to the ones defined by the eNTRY rules that govern the Gram-negative uptake. Even though the ionisable amine provided the needed activity boost against *E. coli*, the lower effect on the activity against *A. baumannii* and *Pseudomonas aeruginosa* is not yet understood.<sup>15</sup> The downside of most rules (Table 1), however, is that they are always representative for only a certain set of compounds or based on a specific bacterium. Sometimes clear boundaries for the applicability of the rules are missing and most of the reported studies are based on known antibacterial compound classes. However, to the authors' knowledge, the general applicability of the rules for a design of a novel series without previous antibacterial activity is questionable. Therefore, it is necessary to evaluate, whether these rules are applicable for repositioning an antimalarial chemical class originating from inhibitors of *Plasmodium falciparum* (*Pf*) IspE

displaying *Pf* cell-based activity, but lacking antibacterial activity (unpublished results from this consortium). The purification of *Pf*IspE is reported in the present study for the first time. The kinase IspE is the central and fourth enzyme of the 2-*C*-methyl-*D*-erythritol 4-phosphate (MEP) pathway for the biosynthesis of universal isoprenoid precursors.<sup>16</sup> Since most of the reported IspE inhibitors have low-micromolar *in vitro* activity against Gram-negative homologues but lack activity in cell-based assays, we embarked to address this activity gap by designing a small set of compounds in accordance with the eNTRY rules using *L*-amino acids.<sup>17</sup>

## Results and discussion

Compound **1** originated from a previous publication within the consortium and no antibacterial activity was reported back then for this compound and its close derivatives.<sup>18</sup> As it was only used as a reference compound for the *E. coli* IspE inhibition, the focus was not on its antibacterial activity. Even in the presence of the outer membrane permeabiliser polymyxin B nonapeptide (PMBN) ensuring enhanced uptake, no antibacterial activity (*E. coli* K12 % inh. = 6 ± 1@100 μM + 1 μg mL<sup>-1</sup> PMBN) was observed (Table 2). In the search of new *E. coli* IspE inhibitors with antibacterial activity, we selected compounds **2** and **3**, originating from the antimalarial class featuring moderate *E. coli* IspE inhibition as suitable starting points to test the applicability of the rules to compounds with weak antibacterial starting profiles. The heterocycles, furan and thiophene, on the right-hand side (RHS) could be bioisosterically replaced by amino acids, exploiting amide coupling chemistry. As both compounds **2** and **3** also inhibit undesirably the auxiliary enzymes pyruvate kinase and lactate dehydrogenase (PK/LDH) in the coupled enzyme activity assay, we focused more on gaining antibacterial activity by modifying them based on the eNTRY rules, while also monitoring activity changes at the enzymatic level to find new scaffolds selectively inhibiting the *Pf* or *E. coli* IspE enzymes. Under the cellular assay conditions, compounds **2** and **3** are poorly soluble and percentage (%)

**Table 2** Biological-activity results of the reference compounds

	<b>1</b>	<b>2</b>	<b>3</b>
<i>Pf</i> NF54 IC <sub>50</sub> (μM)	n.d.	5 ± 1	6 ± 0
<i>Pf</i> IspE IC <sub>50</sub> (μM)	>500	57 ± 12	39 ± 24
<i>Ec</i> IspE IC <sub>50</sub> (μM)	1 ± 0	91 ± 21	68 ± 13
PK/LDH IC <sub>50</sub> (μM)	>500	65 ± 15	56 ± 11
<i>E. coli</i> Δ <i>tolC</i> (% inh.)	n.d.	30 ± 16@25 μM	33 ± 3@50 μM
<i>E. coli</i> K12 (% inh.)	6 ± 1@100 μM + 1 μg mL <sup>-1</sup> PMBN	5 ± 6@25 μM	2 ± 11@50 μM

<sup>a</sup> *Pf*: *Plasmodium falciparum*, *E. coli* or *Ec*: *Escherichia coli*, PK/LDH: pyruvate kinase/lactate dehydrogenase, n.d.: not determined, PMBN: polymyxin B nonapeptide.

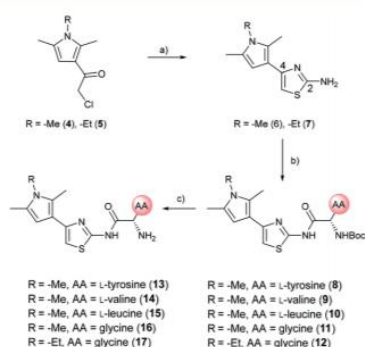


growth inhibition could only be measured at 25 and 50  $\mu\text{M}$ , respectively, showing no substantial activity against *E. coli* K12 wildtype, nor against the  $\Delta\text{tolC}$  efflux-pump mutant (Table 2). Therefore, the compounds 2 and 3 were used to test, whether an application of these eNTRY rules to this series by introducing L-amino acids and glycine will afford the sought-after antibacterial activity. Amino acid modifications were considered a suitable way of evaluating the influence of the free amine vs. the Boc-protected amine on the antibacterial activity. The key interest for the primary amine was influenced by the eNTRY rules and thereby, amino acid modifications opened up a synthetically readily accessible way to introduce them.

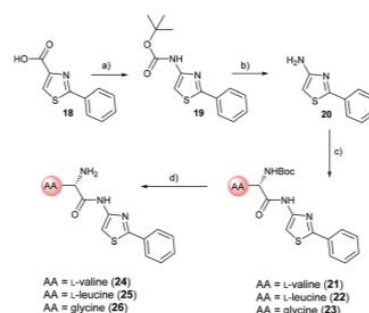
For the synthesis, we selected four readily available *N*-Boc-protected amino acids; L-valine, L-leucine, L-tyrosine and glycine. To obtain derivatives with modifications on the RHS, the 2-aminothiazole building block 6 was accessed via Hantzsch condensation and used for amide couplings followed by Boc-deprotection (Scheme 1).<sup>19</sup> In order to evaluate the influence of an increased number of rotatable bonds in accordance to the eNTRY rules, ethyl-pyrrole derivative 7 was used to synthesise the corresponding glycine derivative 12 with one additional rotatable bond.

The amide moiety of the amino acids was also considered as a suitable bioisosteric replacement of the pyrrole moiety on the left-hand side (LHS). As 2,4-aminothiazoles are known to be unstable and general concerns about the stability of 2-aminothiazoles emerged from the underlying class, we decided to use building block 18 with a direct phenyl-linker in position 2.<sup>20,21</sup> The *N*-Boc protected compound 19 was accessed via a Curtius rearrangement and used for amide couplings followed by Boc-deprotection to afford a small library of LHS-modified compounds (Scheme 2).<sup>22,23</sup>

Out of the new compounds, only RHS amine derivative featuring L-tyrosine 13 showed moderate inhibitory activity against *E. coli* IspE, ( $\text{IC}_{50} = 200 \pm 35 \mu\text{M}$ ), yet selectivity over PK/LDH. In contrast, moderate inhibitory activities selective for *Pf*IspE were observed for the three Boc-derivatives 9, 11



**Scheme 1** Synthetic route for right-hand side modifications. a) Thiourea, EtOH,  $\Delta$ , 16 h. b) *N*-Boc-AA-OH, HBTU, TEA, DMF, RT, 18 h. c) DCM, TFA, RT, 30 min. AA: amino acid side chain.



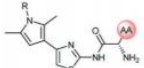
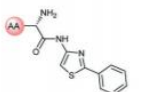
**Scheme 2** Synthetic route for left-hand side modifications. a) DPPA, TEA, tBuOH, 80  $^{\circ}\text{C}$ , 18 h. b) 4M HCl/dioxane, RT, 16 h. c) *N*-Boc-AA-OH, HBTU, TEA, DMF, RT, 18 h. d) DCM, TFA, RT, 30 min. AA: amino acid side chain.

and 12 (Table S2, ESI<sup>†</sup>) and out of them, both *N*-Boc-valine 9 (*Pf*IspE  $\text{IC}_{50} = 61 \pm 7 \mu\text{M}$  and *Pf*NF54  $\text{IC}_{50} = 1.9 \pm 0.4 \mu\text{M}$ ) and *N*-Boc-glycine 11 (*Pf*IspE  $\text{IC}_{50} = 196 \pm 44 \mu\text{M}$  and *Pf*NF54  $\text{IC}_{50} = 5.1 \pm 0.5 \mu\text{M}$ ) showed low micromolar antimalarial activity, being the first inhibitors of *Pf*IspE showing also antimalarial activity. The overall weak enzymatic activities suggested minimal *E. coli* IspE target engagement of the class and we shifted our focus to study how well the reported rules listed in Table 1 apply to this set of compounds. To evaluate antibacterial activity, we screened the compounds primarily against *E. coli* efflux-pump mutated  $\Delta\text{tolC}$  and wildtype K12 strains. Since most of the compounds only showed antibacterial activity against the efflux-pump mutated *E. coli*  $\Delta\text{tolC}$  and not against wildtype K12 (Table S3, ESI<sup>†</sup>), we decided to compare only the  $\Delta\text{tolC}$  results and the respective physicochemical properties to minimise the impact of efflux issues (Table 3). One of the difficulties with the current rules is the lack of clear boundaries of their applicability and therefore, where no reported values were given, we distinguished the physicochemical properties with colour coding (Table 3) to differentiate the *N*-Boc protected compounds from the free base forms, and not in comparison to other known antibiotics.

The applicability of the eNTRY rules was tested by comparing the Boc-protected derivatives 8–12 and 21–23 to the amine derivatives 13–17 and 24–26. As a general trend, we observed that most ionisable amine derivatives have improved cellular activity in comparison to the Boc-protected compounds. This trend is more dominant on the RHS-derivative compounds. This is in line with the eNTRY rules as the Boc-protected compounds generally display a higher number of rotatable bonds and lack the ionisable amine. Interestingly, the ethyl-pyrrole derivatives featuring glycine 17 showed a similar activity profile to its corresponding methyl-pyrrole derivative 16 despite the increased number of rotatable bonds, but still being within the eNTRY limits. All tested compounds respect the limits of low globularity, although the Boc-protected compounds have higher globularity than the corresponding amine derivatives.

Another parameter of rigidity was described by S. Cooper *et al.* as *b\_rotB* (fraction of rotatable bonds), stating that *b\_rotB* should be below 0.2 to achieve higher activities in *E. coli* in the absence of efflux.<sup>9</sup> Using this parameter of rigidity,

**Table 3** Summary of *Escherichia coli*  $\Delta$ tolC growth-inhibition results with their respective calculated properties from the different rules related to antibacterial activity in Gram-negative bacteria

Right-hand side (RHS)	<i>E. coli</i> $\Delta$ tolC (% inh.)	Ionisable amine (Most basic pK <sub>a</sub> )	Globularity	Rotatable bonds	Amphiphilic moment (vsurf_A)	logD <sub>7.4</sub>	MW (Da)	TPSA (Å <sup>2</sup> )	Minimal projection area (Å <sup>2</sup> )	Dipole moment (D)	logP <sub>(0.05)</sub>	b_rotR	SlogP	Antibacterial scoring profile
 Left-hand side (LHS)  AA = amino acid side chain														
<b>Reference</b>														
<b>1</b>	n.d.	no	0.031	4	4.53	0.1	354.4	107.1	49.06	7.9	1.1	0.2	0.6	0.40
<b>2</b>	30 ± 16 (@25 μM)	no	0.029	5	3.58	4.0	329.4	60.1	39.98	0.9	3.3	0.2	4.8	0.00
<b>3</b>	33 ± 3 (@50 μM)	no	0.029	5	3.12	4.4	345.5	46.9	40.33	1.4	4.1	0.2	5.2	0.00
<b>RHS – R = Me</b>														
<b>8</b> N-Boc-L-tyrosine	9 ± 13 (@50 μM)	no	0.060	8	1.92	4.4	470.6	105.5	66.87	4.5	4.3	0.3	4.9	0.05
<b>13</b> L-tyrosine	38 ± 14 (@100 μM)	yes (7.7)	0.153	5	5.01	0.5	370.5	93.2	39.96	5.2	2.6	0.2	3.3	0.25
<b>9</b> N-Boc-L-valine	14 ± 10 (@50 μM)	no	0.077	7	2.29	4.0	406.5	85.3	63.45	3.7	4.0	0.3	4.6	0.07
<b>14</b> L-valine	42 ± 15 (@100 μM)	yes (7.3)	0.046	4	5.18	0.7	306.4	72.9	40.69	4.1	2.4	0.2	3.0	0.06
<b>10</b> N-Boc-L-leucine	5 ± 8 (@50 μM)	no	0.058	8	2.29	4.4	420.6	85.3	62.04	3.8	4.5	0.3	5.0	0.07
<b>15</b> L-leucine	58 ± 17 (@100 μM)	yes (7.8)	0.043	5	5.31	0.8	320.5	72.9	42.62	4.2	2.8	0.3	3.4	0.06
<b>11</b> N-Boc-glycine	46 ± 12 (@100 μM)	no	0.040	6	2.46	3.3	364.5	85.3	51.45	3.2	2.6	0.3	3.6	0.10
<b>16</b> glycine	57 ± 2 (@100 μM)	yes (7.5)	0.016	3	6.58	0.3	264.3	72.9	32.52	4.0	0.9	0.2	2.0	0.08
<b>RHS – R = Et</b>														
<b>12</b> N-Boc-glycine	41 ± 17 (@50 μM)	no	0.021	7	2.99	3.6	378.5	85.3	52.69	3.1	2.9	0.3	4.0	0.10
<b>17</b> glycine	55 ± 14 (@100 μM)	yes (7.5)	0.034	4	5.49	0.0	278.4	72.9	34.21	4.0	1.3	0.3	2.4	0.12
<b>LHS</b>														
<b>21</b> N-Boc-L-valine	21 ± 2 (@100 μM)	no	0.072	7	4.07	3.8	375.5	80.3	58.43	3.9	4.3	0.3	4.3	0.08
<b>24</b> L-valine	17 ± 1 (@100 μM)	yes (8.0)	0.066	4	4.55	1.1	275.4	68.0	40.64	4.1	2.6	0.3	2.7	0.04
<b>22</b> N-Boc-L-leucine	−3 ± 1 (@100 μM)	no	0.107	8	1.92	4.1	389.5	80.3	59.22	3.8	4.7	0.4	4.7	0.08
<b>25</b> L-leucine	32 ± 1 (@100 μM)	yes (8.1)	0.044	5	4.72	1.3	289.4	68.0	38.26	2.5	3.0	0.3	3.1	0.04
<b>23</b> N-Boc-glycine	34 ± 10 (@100 μM)	no	0.062	6	1.83	3.1	333.4	80.3	48.59	3.5	2.8	0.3	3.3	0.11
<b>26</b> glycine	10 ± 5 (@100 μM)	yes (8.1)	0.007	3	5.72	0.1	233.3	68.0	29.49	3.2	1.2	0.2	1.7	0.06

<sup>a</sup> Colour coding was applied for the reported cut-off limits, where possible, and otherwise, arbitrarily chosen cut-off limits were used to differentiate the *N*-Boc protected compounds from the free base forms. The colour coding of the results is as follows, (green: obeys the rule, orange: in between and red: disobeys the rule, not statistically determined): *E. coli*  $\Delta$ tolC % inh.: red (<20%), orange (20–39%) and green (>40%) at the highest compound solubility, ionisable amine: green (yes) and red (no), globularity: green ( $\leq 0.25$ ), rotatable bonds: green ( $\leq 5$ ) and red (>5), amphiphilic moment: red ( $\leq 4.0$ ) and green (>4.0), logD<sub>7.4</sub>: green (<1.5), and red (>1.5), MW: green (<600 Da) and red (>600 Da), TPSA: red (<60 Å<sup>2</sup>) and green (>60 Å<sup>2</sup>), minimal projection area: green (<50 Å<sup>2</sup>) and red (>50 Å<sup>2</sup>), dipole moment: green (>5.5 D) and red (<5.5 D), logP<sub>(0.05)</sub>: green (<1.5) and red (>1.5), b\_rotR: green (<0.2), orange (0.2) and red (>0.2), SlogP: green ( $\leq 0.5$ ) and red ( $\geq 0.5$ ) and antibacterial scoring profile: red (<0.40) and green (>0.40). n.d.: not determined.



all of the compounds would have been predicted not to accumulate well. The Boc-protected compounds also show lower solubility in the bacterial assays, which is supported by the calculated  $\log D_{7.4}$ ,  $\log P_{(o/w)}$  and  $S\log P$  values that are poorer than for the amine derivatives (Table 3). However, the Boc-derivatives have a higher TPSA than the corresponding amine derivatives. In contrast to the antibacterial activity results, the Boc-protected compounds 8–12 are more active in the enzyme assay than the corresponding free amines (Table S2, ESI†). This brings across one of the key challenges in antibiotic research, how to achieve cellular activity and target engagement in a balanced way. For example, it would be expected that the best reference *EclspE* inhibitor 1 would show antibacterial activity based on the overall profile of the calculated properties. Additionally, in contradiction to the experimental results of compound 1 (*E. coli* K12 % inh. with  $1 \mu\text{g mL}^{-1}$  PMBN =  $6 \pm 1\%$ @100  $\mu\text{M}$ ), the antibacterial scoring profile implemented in StarDrop also predicts high antibacterial activity (score = 0.4), but rates the new amino acid derivatives poorly (Tables 2 and 3). On the other hand, the other reference compounds 2 and 3 do not exhibit any antibacterial activity that is supported by the predicted poor antibacterial scoring profile (score = 0.0 for both).

Since the observed antibacterial activities against *E. coli*  $\Delta\text{tolC}$  did not correlate with these against wildtype *E. coli* K12, the most active compounds against *E. coli*  $\Delta\text{tolC}$  were also tested against efflux-pump mutated *E. coli*  $\Delta\text{acrB}$ , lipopolysaccharide-mutated *E. coli* D22 and porin-knockdown mutant (BL21(DE3)omp8) to evaluate potential permeation or efflux issues (Tables 4 and S3, ESI†). Reference compounds 2 and 3, however, do not display any antibacterial activity in

any of the mutant strains (Table 4). Accumulation into Gram-negative bacteria can occur *via* active or passive transport. Recent studies show that molecular uptake through porins is governed by other properties than by a previously-defined, simple MW cut-off ( $\leq 600$  Da).<sup>24,25</sup> Most of the rules given in Table 1 are based on the dominating *E. coli* OmpF. The eNTRY rules demonstrate that the ionisable amine is needed for a key salt-salt interaction within OmpF and the scoring function by S. Acosta-Gutiérrez *et al.* relies on compound passage through outer membrane porins including *E. coli* OmpF and OmpC.<sup>5,7</sup> Therefore, we used the porin-knockdown mutant (BL21(DE3)omp8) to evaluate, whether the primary amine is needed for permeability *via* porins and in fact, none of the tested compounds showed antibacterial activity against the omp8 strain lacking the major *E. coli* porins OmpF, OmpA and OmpC (Table 4).<sup>26</sup> With respect to the eNTRY rules, the glycine derivative 17 showed no inhibition against the omp8 strain, suggesting that the amine could indeed play a role in the uptake *via* the porins. On the other hand, its Boc-derivative 12 also showed no inhibition, thus disagreeing with the necessity of the ionisable amine proposed by the eNTRY rules, leaving the question of the real uptake mechanism of the series (Table S3, ESI†). With respect to the other defining properties for porin passage, the reference compounds 2 and 3 lack ionisable amines and have clearly lower dipole moments than compound 1, but they have smaller minimal projection areas. All amine derivatives have higher dipole moments than the corresponding Boc-protected derivatives, except the LHS derivatives L-leucine 25 and glycine 26. The dipole moments of the amine derivatives are, however, lower than the threshold (5.5 D), which is

Table 4 Summary of the activities of the most active compounds against a panel of *Escherichia coli* strains, *Staphylococcus aureus* and HepG2 cells

		Percentage Inhibition (@100 $\mu\text{M}$ or unless otherwise stated)						
	Compound	<i>E. coli</i>					<i>S. aureus</i> Newman	HepG2
		K12	$\Delta\text{tolC}$	$\Delta\text{acrB}$	D22	(DE3) omp8		
Ref.	2 (@25 $\mu\text{M}$ )	5 $\pm$ 6	30 $\pm$ 16	2 $\pm$ 5	9 $\pm$ 7	-4 $\pm$ 3	6 $\pm$ 1	19 $\pm$ 2
	3 (@50 $\mu\text{M}$ )	2 $\pm$ 11	33 $\pm$ 3	6 $\pm$ 7	3 $\pm$ 4	-22 $\pm$ 19	7 $\pm$ 5	-3 $\pm$ 5
RHS	16 glycine	13 $\pm$ 0	57 $\pm$ 2	4 $\pm$ 8	3 $\pm$ 3	18 $\pm$ 1	6 $\pm$ 3	19 $\pm$ 12 (@50 $\mu\text{M}$ )
	17 glycine	13 $\pm$ 2	55 $\pm$ 14	65 $\pm$ 1	20 $\pm$ 4	16 $\pm$ 10	14 $\pm$ 3 (@50 $\mu\text{M}$ )	23 $\pm$ 5
LHS	24 L-valine	10 $\pm$ 13	17 $\pm$ 1	1 $\pm$ 2	14 $\pm$ 1	-3 $\pm$ 16	5 $\pm$ 3	n.d.
	25 L-leucine	18 $\pm$ 11	32 $\pm$ 1	11 $\pm$ 6	18 $\pm$ 3	30 $\pm$ 7	11 $\pm$ 1	n.d.
	26 glycine	22 $\pm$ 4	10 $\pm$ 5	6 $\pm$ 1	15 $\pm$ 3	-20 $\pm$ 19	-2 $\pm$ 5	17 $\pm$ 17

<sup>a</sup> The colour coding of the results is as follows: bacterial % inh.: red (0–19%), orange (20–39%), and green (>40%) at the highest compound solubility. RHS: right-hand side, LHS: left-hand side, n.d.: not determined.



shown for *P. aeruginosa* for good outer membrane permeability.<sup>9</sup> The minimal projection areas of the amines are also lower compared to their corresponding Boc-derivatives, supporting the general trend seen with the slightly increased antibacterial activities in the efflux-suppressed mutants.

As we observed increased antibacterial activities for glycine derivatives **16** and **17** in the efflux-mutated strains, the lack of activity in the wildtype strain K12 is likely to be linked to efflux issues. The *TolC*-pump is located in the outer membrane, whereas the *AcrB*-pump is in the inner membrane of the *E. coli* transmembrane efflux pump *AcrAB-TolC*.<sup>27</sup> Efflux issues have also been linked to high lipophilicity measured as non-ionisable lipophilicity  $\log P_{(o/w)}$  ( $>1.5$ ) and  $S \log P$  ( $\geq 0.5$ ).<sup>9</sup> Only the glycine derivatives **16** and **17** are within the limits of  $\log P_{(o/w)}$  (0.9 and 1.4, respectively) and therefore, should avoid efflux in the wildtype strain K12 (Table 3). Interestingly, the effect of the increased activity in *E. coli*  $\Delta$ *acrB* is only present for the ethyl-pyrrole derivative **17** and not for the methyl-pyrrole derivative **16**, nor for their corresponding Boc-derivatives **11** and **12**, (Table S3, ESI<sup>†</sup>), nor for the LHS free amine derivatives **24–26**. This may also be due to different concentrations of the compounds being present in different compartments of the cell envelope, which may cause different parts of the efflux pumps being more engaged than others. The accumulation of the compounds into the different bacterial compartments could be confirmed by MS-based methods.<sup>28</sup> However, due to the overall lack of antibacterial activity within the series this path was not followed. Based on the results of the *E. coli* mutants, it is likely that the ionisable amines engage partly with the outer membrane porins and accumulate in, but are later pumped out, seemingly recognised by the efflux-pump units. No clear inhibitory differences for the Boc-derivatives against the mutants were observed, which contradicts the clear single uptake pathway of the primary amine uptake *via* porins. Due to the lipophilicity of Boc-derivatives, passive transport through the phospholipid layers could also occur or alternatively, *via* amino acid specific uptake. Due to the weak target engagement, it is difficult to assess the influence of different amino acids on the antibacterial activities. It is important to remember that amino acids are also important building blocks for bacteria, and specific chemotaxis proteins are linked to different amino acids.<sup>29–31</sup> Particularly out of the amino acids used in this study, glycine is reported as an attractant for *E. coli* growth *via* Tsr receptor engagement, whereas L-valine, L-leucine and L-tyrosine are reported as repellents.<sup>32–35</sup> The most striking difference is that most of the compounds showed no activity against Gram-positive *Staphylococcus aureus*, except L-leucine derivative **15** (% inh. =  $52 \pm 15$ @100  $\mu$ M). This could be related to different chemotaxis mechanisms or slight target engagement, in particular, as the MEP pathway is absent in most Gram-positive bacteria.<sup>36,37</sup> The glycine derivative **17** also weakly inhibited *P. aeruginosa* (% inh. =  $11 \pm 7$ @100  $\mu$ M) and *A. baumannii*, (% inh. =  $31 \pm 17$ @100  $\mu$ M), the latter even

slightly more than *E. coli* K12. Further studies are needed to understand if such bacteria-specific amino acid handles could be used to solve uptake issues or in fact, if they are recognised as toxins resulting in efflux. Such amino acid modified compounds could be implemented as “recognition handles” for chemotaxis-enhanced accumulation or for efflux-pump inhibitors into a class with a clear cellular and target engagement.

## Conclusions

One of the major problems of antibiotic research is to achieve a balance between antibacterial and enzymatic activity, and yet to have a good safety profile. The implementation of L-amino acids in accordance to the eNTRY rules into the old antimalarial class did not result in a highly active antibacterial compound series. Nevertheless, increased antibacterial activity was achieved in comparison to the reference compounds at the expense of efflux issues as demonstrated with the *E. coli* mutants. Modifications with a non-chiral glycine might be a suitable option to enhance antibacterial activity by introducing an ionisable primary amine, as shown by glycine derivative **17**. It might also be worth investigating other amino acids, particularly ones linked to chemotaxis used in Gram-negative bacteria. Eventually, such amino acid-modified compounds could also be used as “recognition probes” for cellular uptake or for efflux pumps inhibitors. One should, however, avoid designing compound series based on only one set of the current rules available in the literature. We hope that the antibiotic community will continue to investigate the underlying chemical and biological principles of antibiotic accumulation and excretion in a holistic way.

## Experimental

### Cloning, expression and purification of *Plasmodium falciparum* IspE

Custom-synthesised DNA fragment coding for IspE of *P. falciparum* was purchased from GenScript (Piscataway, NJ, USA). The purchased plasmid DNA (based on pET22(+) vector) was used as the template for re-cloning of the DNA fragment coding for IspE with simultaneous re-arrangement of the His6-Tag from N terminus to the C terminus of the protein. The DNA fragment coding for IspE of *P. falciparum* was amplified by PCR using primers shown in Table S1.† The amplicate was isolated from agarose gel, digested with restriction endonucleases NcoI and HindIII and ligated into the plasmid pNCO113 that had been treated with the same restriction enzymes. The plasmid pNCO113-PFispE-cHis<sub>6</sub>, containing IspE under control of T5 promoter, was transformed into the *E. coli* XL1 strain. The transformants were plated on LB medium containing Ap (170 mg L<sup>-1</sup>). LB medium (50 mL) containing Ap (170 mg L<sup>-1</sup>) was inoculated with one colony from the plate and incubated for 12 hours at 37 °C in shaking flasks. Preculture (15 mL) was transferred



into 1.5 L of terrific broth medium containing Ap (170 mg L<sup>-1</sup>) and incubated for 3 hours at 37 °C in shaking flasks until the OD<sub>600</sub> reached 0.6. The cultures were cooled down to 25 °C, and the incubation was continued for 72 hours in shaking flasks. The cells were harvested by centrifugation (2000 × g, 4 °C, 30 min). The cell pellet was washed once with saline, centrifuged once again and the supernatant was discarded. The cell paste was stored at -20 °C.

All procedures used for cell disruption and protein isolation and purification were performed at 4 °C. Cell paste (10 g) was resuspended in buffer A (50 mM Tris-HCl pH 9.0, 15 mM imidazole 500 mM NaCl, 5% glycerol; 50 mL). Cell disruption was achieved by passing the cell slurry two times through the French press prechilled to 4 °C. Cell debris was centrifuged down (10 000 × g, 4 °C, 30 min). The supernatant was applied onto a chelating Sepharose column (Ni<sup>2+</sup>-form, 1 cm × 25 cm) equilibrated with buffer A. The column was washed with buffer A (220 mL) and the protein was eluted by a three-step gradient of imidazole concentration (50 mM, 250 mM and 500 mM) in buffer B (50 mM Tris/HCl pH 9.0, 500 mM NaCl, 5% glycerol). Fractions containing IspE were identified with polyacrylamide gel electrophoresis, pooled and applied in 10 mL-aliquots onto a Sephadex G-25 fine cross-linked dextran column (2 cm × 60 cm) equilibrated with buffer C (50 mM Tris/HCl pH 9.0, 100 mM NaCl, 2 mM DTT, 5% glycerol). The column was developed with the same buffer (flow rate, 10 mL min<sup>-1</sup>). The fractions containing IspE were identified with polyacrylamide gel electrophoresis, concentrated using ultrafiltration cell (Merck, Darmstadt, Germany) equipped with the membrane permeable for proteins with molecular weight up to 10 kDa. The final samples of IspE were stored at -80 °C. The nucleotide sequence of the DNA fragment coding for IspE from *P. falciparum* is given in Fig. S1, ESI.†

#### *In vitro* IspE inhibitory assay

For the IspE assay, CDP-ME (1.0 mM and 0.2 mM for the assaying of IspE from *P. falciparum* and *E. coli*, respectively) in 100 mM Tris-HCl, pH 7.6, 0.02% NaN<sub>3</sub> (30 μL) were added to a microplate well preloaded either with DMSO or with test compound dissolved in DMSO (3 μL). *E. coli* IspE was purified as previously described.<sup>18,38</sup> The reaction was started by addition of 100 mM Tris-HCl, pH 7.6, 10 mM MgCl<sub>2</sub>, 60 mM KCl, 10 mM dithiothreitol, 0.02% NaN<sub>3</sub>, 1 mM NADH, 2 mM phosphoenolpyruvate, 2 mM ATP, pyruvate kinase (1 U mL<sup>-1</sup>), lactate dehydrogenase (1 U mL<sup>-1</sup>), and *E. coli* IspE (0.05 U mL<sup>-1</sup>) (27 μL per microplate well). For the pyruvate kinase and lactate dehydrogenase (PK/LDH) assay 1 mM ADP in 100 mM Tris-HCl, pH 7.6 (30 μL) was added to a microplate well that had been preloaded with DMSO or with test compound solved in DMSO (3 μL). The reaction was started by addition of 100 mM Tris-HCl, pH 7.6, 10 mM MgCl<sub>2</sub>, 200 mM KCl, 10 mM dithiothreitol, 0.02% NaN<sub>3</sub>, 1 mM NADH, 2 mM phosphoenolpyruvate, pyruvate kinase (0.05 U mL<sup>-1</sup>) and lactate dehydrogenase (0.05 U mL<sup>-1</sup>) (27

μL per microplate well). The assays were monitored photometrically at room temperature for 30 min. A summary of the results can be found in Table S2, ESI.†

#### *In vitro* antibacterial assays

Assays regarding the determination of the minimum inhibitory concentration (MIC) were performed as described recently.<sup>39</sup> Our experiments were based on a variety of *E. coli* strains/mutants (K12, D22, Δ*tolC*, Δ*acrB*, and BL21(DE3)omp8 as well as *S. aureus* (Newman strains), *P. aeruginosa* (PA14) and *A. baumannii* (DSM30007). For the case that no MIC value could be determined due to activity reasons, percentage (%) inhibition at 100 μM (or lower, depending on the solubility of the compounds) was determined. A summary of the results can be found Tables S3 and S4, ESI.†

#### *In vitro* cytotoxicity assay

Cytotoxicity assays based on the human hepatocellular carcinoma cell line HepG2 were performed as described previously.<sup>40</sup> A summary of the results can be found in Table S3, ESI.†

#### *In vitro* antiplasmodial assay

*Plasmodium falciparum* drug-sensitive NF54 (airport strain from The Netherlands, provided by F. Hoffmann-La Roche Ltd) was cultivated in a variation of the medium consisting of RPMI 1640 supplemented with 0.5% ALBUMAX® II, 25 mM Hepes, 25 mM NaHCO<sub>3</sub> (pH 7.3), 0.36 mM hypoxanthine, and 100 μg mL<sup>-1</sup> neomycin, as previously described.<sup>41,42</sup> Human erythrocytes served as host cells. Cultures were maintained in an atmosphere of 3% O<sub>2</sub>, 4% CO<sub>2</sub>, and 93% N<sub>2</sub> in humidified modular chambers at 37 °C. Compounds were dissolved in DMSO (10 mM), diluted in hypoxanthine-free culture medium and titrated in duplicate over a 64-fold range in 96 well plates. Infected erythrocytes (1.25% final hematocrit and 0.3% final parasitemia) were added into the wells. After 48 h incubation, 0.25 μCi of [<sup>3</sup>H] hypoxanthine was added per well and the plates were incubated for an additional 24 h. Parasites were harvested onto glass-fiber filters, and radioactivity was counted using a Betaplate liquid scintillation counter (Wallac, Zurich). The results were recorded and expressed as a percentage of the untreated controls.<sup>43</sup> Fifty percent inhibitory concentrations (IC<sub>50</sub>) were estimated by linear interpolation. A summary of the results can be found in Table S3, ESI.†

#### Chemistry

All reagents and solvents were of commercial quality and used without further purification. Chemical yields were not optimised. Flash column chromatography (FCC) was performed for compounds packed in ISOLUTE® HM-N (Biotage AB, Uppsala, Sweden) using CombiFlash Rf+ (Teledyne Isco Ltd., Lincoln, NE, USA) equipped with RediSepRf silica columns (Axel Semrau GmbH, Sprockhövel, Germany). Low-



resolution mass analytics and purity control of final compounds was carried out using an Ultimate 3000-ISQ liquid-chromatography mass spectrometry (LCMS) system (Thermo Fisher Scientific AG, Dreieich, Germany), consisting of a Dionex UltiMate pump, an autosampler, DAD detector and an ESI quadrupole mass spectrometer. Preparative reverse phase-high performance liquid chromatography (RP-HPLC) was performed using an UltiMate 3000 semi-preparative system (Thermo Fisher Scientific AG, Dreieich, Germany) with a Nucleodur® C18 Gravity (250 mm × 10 mm, 5 μm) column. NMR spectra were recorded on a Bruker AV 500 (<sup>1</sup>H, 500 MHz; <sup>19</sup>F, 376 MHz; <sup>13</sup>C, 126 MHz) spectrometer. All spectra were measured in CDCl<sub>3</sub> or DMSO-*d*<sub>6</sub>, and chemical shifts were adjusted based on the residual proton of the internal standard in parts per million (ppm), (CDCl<sub>3</sub>, δ = 7.27, 77.00 and DMSO-*d*<sub>6</sub>, δ = 2.50, 39.51, <sup>1</sup>H and <sup>13</sup>C respectively). Coupling constants (*J*) are given in Hertz (Hz) and the following abbreviations were used for multiplicity (s = singlet, d = doublet, t = triplet, m = multiplet, br = broad or combinations of these). High-resolution mass spectrometry (HRMS) was determined by Thermo Scientific Q Exactive Focus Orbitrap system. The purity of all synthesised compounds used for biological testing was determined by UV tracing at 254 nm in the LCMS platform, being (≥95%) except compound **8** (93%). The reference compound **1** originated from a previous publication within the consortium.<sup>18</sup> Reference compounds **2** (Enamine Z26672805/CAS 2094230-26-7) and **3** (Enamine Z26672672/CAS 2391905-54-5) were commercially purchased compounds that were kindly provided by BASF. Synthetic derivatives were synthesised according to Schemes 1 and 2 using general procedures A and B as described in more detail in section S2, ESI†

### Computational methods

StarDrop v. 6.6.4.23412 (Optibrium, Ltd., Cambridge, UK) was used to calculate log*D*<sub>7,4</sub>, MW, TPSA, p*K*<sub>a</sub> and antibacterial scoring profile and to screen for PAINS showing no hits. The latter two were accessed *via* the Optibrium community (<http://www.optibrium.com/community/>). Dipole moment (PM3\_dipole), fraction of rotatable bonds (b\_rotB), predicted log of the octanol/water partition coefficients (log *P*<sub>(o/w)</sub>) and (S log *P*) and amphiphilic moment (vsurf\_A) were calculated with Molecular Operating Environment (MOE) 2018.01 software (Chemical Computing Group ULC, Montreal, Canada). MarvinSketch 20.8, ChemAxon, was used for calculating minimal projection area (<https://www.chemaxon.com>). The accordance to the eNTRY rules was predicted using eNTRYway, where *N*: presence of an ionisable primary amine, *T*: globularity and *R*: number of rotatable bonds.<sup>5,44</sup>

### Author contributions

H.-K. Ropponen: conceptualisation, data curation, formal analysis, investigation, software, visualisation, writing – original draft, writing – review & editing, E. Diamanti: investigation; supervision, writing – review & editing, A. Siemens: investigation, writing – review & editing, B. Illarionov:

data curation, formal analysis, investigation, writing – review & editing, J. Hauptenthal: formal analysis, supervision, validation, writing – review & editing, M. Fischer: resources, supervision, writing – review & editing, M. Rottmann: formal analysis, validation and writing – review & editing, M. Witschel: resources and writing – review & editing, A. K. H. Hirsch: conceptualisation, funding acquisition, project administration, resources, supervision and writing – review & editing.

### Conflicts of interest

There are no conflicts to declare.

### Acknowledgements

H.-K. Ropponen thanks Stiftung Stipendien-Fonds des Verbandes der Chemischen Industrie for the granted Kekulé Mobility Fellowship. A. K. H. Hirsch gratefully acknowledges funding from the Helmholtz Association's Initiative and Networking Fund. The authors thank Jeannine Jung and Dennis-Thomas Jener for excellent technical assistance, Dr. Jennifer Herrmann for kindly providing *E. coli* Δ*acrB* and Dr. Mostafa Hamed for critical proofreading of the manuscript (HIPS). The authors are also grateful to Prof. Dr. Jean-Marie Pagés for kindly providing *E. coli* BL21(DE3)omp8 strain.

### Notes and references

- U. Theuretzbacher, S. Gottwalt, P. Beyer, M. Butler, L. Czaplewski, C. Lienhardt, L. Moja, M. Paul, S. Paulin, J. H. Rex, L. L. Silver, M. Spiegelman, G. E. Thwaites, J. P. Paccaud and S. Harbarth, *Lancet Infect. Dis.*, 2019, **19**, e40–e50.
- A. L. Parkes, *Expert Opin. Drug Discovery*, 2020, **00**, 1–9.
- E. J. Lien, C. Hansch and S. M. Anderson, *J. Med. Chem.*, 1968, **11**, 430–441.
- R. O'Shea and H. E. Moser, *J. Med. Chem.*, 2008, **51**, 2871–2878.
- M. F. Richter, B. S. Drown, A. P. Riley, A. Garcia, T. Shirai, R. L. Svec and P. J. Hergenrother, *Nature*, 2017, **545**, 299–304.
- M. F. Richter and P. J. Hergenrother, *Ann. N. Y. Acad. Sci.*, 2019, **1435**, 18–38.
- S. Acosta-Gutiérrezgutiérrez, L. Ferrara, M. Pathania, M. Masi, J. Wang, I. Bodrenko, M. Zahn, M. Winterhalter, R. A. Stavenger, J.-M. Pagé, J. H. Naismith, B. Van Den Berg, M. G. P. Page and M. Ceccarelli, *ACS Infect. Dis.*, 2018, **4**, 1487–1498.
- B. Montefiore, F. Klingler and N. Foster, *Poster: A novel scoring profile for the design of antibacterials active against gram-negative bacteria*, 2018.
- S. J. Cooper, G. Krishnamoorthy, D. Wolloscheck, J. K. Walker, V. V. Rybenkov, J. M. Parks and H. I. Zgurskaya, *ACS Infect. Dis.*, 2018, **4**, 1223–1234.
- E. N. Parker, B. S. Drown, E. J. Geddes, H. Y. Lee, N. Ismail, G. W. Lau and P. J. Hergenrother, *Nat. Microbiol.*, 2019, **2019**(5), 1–9.
- P. A. Smith, M. F. T. Koehler, H. S. Girgis, D. Yan, Y. Chen, Y. Chen, J. J. Crawford, M. R. Durk, R. I. Higuchi, J. Kang, J. Murray, P. Paraselli, S. Park, W. Phung, J. G. Quinn, T. C.



- Roberts, L. Rougé, J. B. Schwarz, E. Skippington, J. Wai, M. Xu, Z. Yu, H. Zhang, M. W. Tan and C. E. Heise, *Nature*, 2018, **561**, 189–194.
- 12 B. Liu, R. E. Lee Trout, G.-H. Chu, D. McGarry, R. W. Jackson, J. C. Hamrick, D. M. Daigle, S. M. Cusick, C. Pozzi, F. De Luca, M. Benvenuti, S. Mangani, J.-D. Docquier, W. J. Weiss, D. C. Pevear, L. Xerri and C. J. Burns, *J. Med. Chem.*, 2020, **63**, 2789–2801.
- 13 Y. Hu, H. Shi, M. Zhou, Q. Ren, W. Zhu, W. Zhang, Z. Zhang, C. Zhou, Y. Liu, X. Ding, H. C. Shen, S. Frank Yan, F. Dey, W. Wu, G. Zhai, Z. Zhou, Z. Xu, Y. Ji, H. Lv, T. Jiang, W. Wang, Y. Xu, M. Verduyck, X. Yao, Y. Mao, X. Yu, K. Bradley and X. Tan, *J. Med. Chem.*, 2020, **63**, 9623–9649.
- 14 S. E. Motika, R. J. Ulrich, E. J. Geddes, Y. Lee, G. W. Lau and P. J. Hergenrother, *J. Am. Chem. Soc.*, 2020, **142**, 10856–10862.
- 15 L. D. Andrews, T. R. Kane, P. Dozzo, C. M. Haglund, D. J. Hilderbrandt, M. S. Linsell, T. Machajewski, G. Mckenroe, A. W. Serio, K. B. Wlasichuk, D. B. Neau, S. Pakhomova, G. L. Waldrop, M. Sharp, J. Pogliano, R. T. Cirz and F. Cohen, *J. Med. Chem.*, 2019, **62**, 7489–7505.
- 16 A. Frank and M. Groll, *Chem. Rev.*, 2017, **117**, 5675–5703.
- 17 T. Masini and A. K. H. Hirsch, *J. Med. Chem.*, 2014, **57**, 9740–9763.
- 18 A. K. H. Hirsch, M. S. Alphey, S. Lauw, M. Seet, L. Barandun, W. Eisenreich, F. Rohdich, W. N. Hunter, A. Bacher and F. Diederich, *Org. Biomol. Chem.*, 2008, **6**, 2719–2730.
- 19 F. Mjambili, M. Njoroge, K. Naran, C. De Kock, P. J. Smith, V. Mizrahi, D. Warner and K. Chibale, *Bioorg. Med. Chem. Lett.*, 2014, **24**, 560–564.
- 20 M. Yokoyama, M. Kurauchi and T. Imamoto, *Tetrahedron Lett.*, 1981, **22**, 4–45.
- 21 S. M. Devine, M. D. Mulcair, C. O. Debono, E. W. W. Leung, J. W. M. Nissink, S. S. Lim, I. R. Chandrashekar, M. Vazirani, B. Mohanty, J. S. Simpson, J. B. Baell, P. J. Scammells, R. S. Norton and M. J. Scanlon, *J. Med. Chem.*, 2015, **58**, 1205–1214.
- 22 C. Bolea, WO2011/86163A1, ADDEX PHARMA S.A., 2011.
- 23 B. Liu, G. Liu, L. Nelson, J. Patel, H. Sham, Z. Xin and H. Zhao, US20050014794A1, 2005.
- 24 F. Ruggiu, S. Yang, R. L. Simmons, A. Casarez, A. K. Jones, C. Li, J. M. Jansen, H. E. Moser, C. R. Dean, F. Reck and M. Lindvall, *ACS Infect. Dis.*, 2019, **5**, 1688–1692.
- 25 J. Vergalli, I. V. Bodrenko, M. Masi, L. Moynié, S. Acosta-Gutiérrez, J. H. Naismith, A. Davin-Regli, M. Ceccarelli, B. van den Berg, M. Winterhalter and J.-M. Pagès, *Nat. Rev. Microbiol.*, 2020, **18**, 164–176.
- 26 A. P. I., P. S. Phale, P. Van Gelder, J. P. Rosenbusch and R. Koebnik, 1998, 163, 65–72.
- 27 X. Shi, M. Chen, Z. Yu, J. M. Bell, H. Wang, I. Forrester, H. Villarreal, J. Jakana, D. Du, B. F. Luisi, S. J. Ludtke and Z. Wang, *Nat. Commun.*, 2019, **10**, 1–6.
- 28 H. Prochnow, V. Fetz, S. K. Hotop, M. A. García-Rivera, A. Heumann and M. Brønstrup, *Anal. Chem.*, 2019, **91**, 1863–1872.
- 29 J. Adler, Chemotaxis in bacteria, in *Surface Membrane Receptors*, NATO Advanced Study Institutes Series (Series A: Life Sciences), Springer, Boston, MA, 1975, p. 11.
- 30 M. D. Baker, P. M. Wolanin and J. B. Stock, *BioEssays*, 2006, **28**, 9–22.
- 31 J. A. Shapiro, *Annu. Rev. Microbiol.*, 1998, **52**, 81–104.
- 32 R. Mesibov and J. Adler, *J. Bacteriol.*, 1972, **112**, 315–326.
- 33 A. H. Delcour, B. Martinac, J. Adler and C. Kung, *Biophys. J.*, 1989, **56**, 631–636.
- 34 F. Hishinuma, K. Izaki and H. Takahashi, *Agric. Biol. Chem.*, 1969, **33**, 1577–1586.
- 35 Y. Yang, A. M. Pollard, C. Höfler, G. Poschet, M. Wirtz, R. Hell and V. Sourjik, *Mol. Microbiol.*, 2015, **96**, 1272–1282.
- 36 S. Heuston, M. Begley, C. G. M. Gahan and C. Hill, *Microbiology*, 2012, **158**, 1389–1401.
- 37 M. M. Alreshidi, R. H. Dunstan, M. M. Macdonald, J. Gottfries and T. K. Roberts, *Front Microbiol.*, 2020, **10**, 1–12.
- 38 H. Lüttgen, F. Rohdich, S. Herz, J. Wungsintawekul, S. Hecht, C. A. Schuhr, M. Fellermeier, S. Sagner, M. H. Zenk, A. Bacher and W. Eisenreich, *Proc. Natl. Acad. Sci. U. S. A.*, 2000, **97**, 1062–1067.
- 39 W. A. M. Elgaher, M. Fruth, M. Groh, J. Hauptenthal and R. W. Hartmann, *RSC Adv.*, 2014, **4**, 2177–2194.
- 40 J. Hauptenthal, C. Baehr, S. Zeuzem and A. Piiper, *Int. J. Cancer*, 2007, **121**, 206–210.
- 41 A. Dorn, R. Stoffel, H. Matile, A. Bubendorf and R. G. Ridley, *Nature*, 1995, **374**, 269–271.
- 42 W. Trager and J. B. Jensen, *Science*, 1976, **193**, 673–675.
- 43 W. Huber and J. C. Koella, *Acta Trop.*, 1993, **55**, 257–261.
- 44 Entryway, <http://www.entry-way.org/>, (accessed April 2020).

### 3.3 Chapter C:

#### Search for the Active Ingredients from a 2-Aminothiazole DMSO Stock Solution with Antimalarial Activity

H.-K. Ropponen, C. D. Bader, E. Diamanti B. Illarionov, M. Rottmann, M. Fischer, M. Witschel, R. Müller and A. K. H. Hirsch

This part of the thesis has been submitted to *ChemMedChem*.

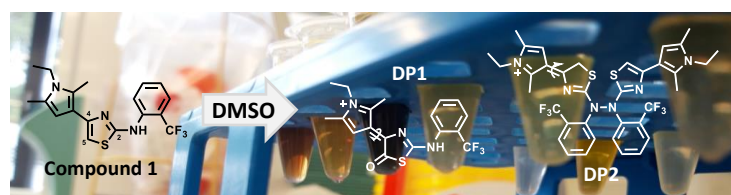
\*This part of the thesis was later accepted for publishing in *ChemMedChem*, **2021**, DOI: 10.1002/cmdc.202100067.

Copyright retained by the author to reuse here acceptably in accordance to Wiley guidelines.

**Abstract:** Chemical decomposition of DMSO stock solutions is a common incident that can mislead biological screening campaigns. Here, we share our case study of 2-aminothiazole **1**, originating from an antimalarial class that undergoes chemical decomposition in DMSO at room temperature. As previously measured biological activities observed against *Plasmodium falciparum* NF54 and for the target enzyme *PfIspE* were not reproducible for a fresh batch, we tackled the challenge to understand where the activity originated from. Solvent- and temperature-dependent studies using HRMS and NMR spectroscopy to monitor the decomposition led to the isolation and in vitro evaluation of several fractions against *PfIspE*. After four days of decomposition, we successfully isolated the oxygenated and dimerised compounds using SFC purification and correlated the observed activities to them. Due to the unstable nature of the two isolates, it is likely that they undergo further decomposition contributing to the overall instability of the compound.

**Keywords:** Antiprotozoal Agents • Decomposition • Drug Discovery • IspE • SFC

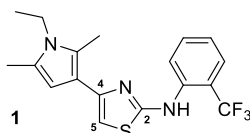
#### Graphical Abstract:



In the search for novel antimalarial compounds targeting the kinase IspE of the 2-C-methyl-D-erythritol 4-phosphate (MEP) pathway, we identified a new 2-aminothiazole class via an enzymatic high-throughput screening (HTS) campaign (unpublished results from the consortium). The MEP pathway is a key biosynthetic route for the production of universal isoprenoid precursors.<sup>[1]</sup> The HTS yielded compound **1** as a hit that was followed up due to its promising screening profile (Table 1), which was supported by some previously reported 2,4-substituted thiazoles with antiplasmodial activity.<sup>[2,3]</sup>

For a newly synthesised batch and the corresponding freshly prepared stock solution of compound **1**, no activity against *Plasmodium falciparum* (*Pf*) IspE was detected and cell-based activity against the plasmodial strain *Pf*NF54 resulted in a 20-fold reduction in activity (Table 1). Previous samples originated from older plates stored in DMSO, which had undergone several thawing cycles from  $-20\text{ }^{\circ}\text{C}$  storage. First evidence of the decomposition was visually observed due to a change in colour of the compound's stock solution from clear to dark. However, this colour change would only be obvious to someone familiar with the original colour of the parent compound. If such plates are sent to collaboration partners responsible for biological assays, as is often the case in medicinal chemistry projects, such alterations may not necessarily be observed or questioned. DMSO is a widely used solvent due to its amphiphilic nature, enabling higher solubility of many compounds and high viscosity improving the reproducibility in pipetting. Nevertheless, stability issues of chemical compounds kept as stock solutions in DMSO are also acknowledged and spontaneous reactions, such as oxidation, cyclisation and hydrolysis, in stock solutions may affect the biological activity.<sup>[4-6]</sup> Although reactivity of 2-aminothiazoles has not been directly ascribed to DMSO, we were concerned about it. 2-Aminothiazoles are frequently-hitting fragments in biophysical binding assays, as the so-called promiscuous 2-aminothiazoles (PrATs), and some sub-categories are classified as Pan-Assay Interference Compounds (PAINS).<sup>[7-9]</sup> The observed activity on target in vitro and in whole-cell systems prompted us to elucidate the structural changes of compound **1** in DMSO that accounted for the increased inhibitory activity.

**Table 1.** Starting point for the non-reproducible results of compound **1**.

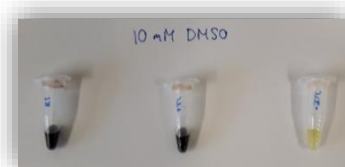


	<i>Pf</i> IspE IC <sub>50</sub> (μM)	<i>Pf</i> NF54 IC <sub>50</sub> (μM)
Old batch <sup>[a]</sup> (decomposed)	8.0 ± 2.8	0.43 ± 0.01
Fresh batch	>500	7.3 ± 0.8

[a] Cytotoxicity profile of the old sample before becoming aware of the decomposition; %-inh A549 =  $-0.3 \pm 4$ , HEK293 =  $28 \pm 13$  and HepG2. =  $44 \pm 7$ , all @100 μM. *Pf*: *Plasmodium falciparum*

Firstly, we performed a temperature-dependent decomposition study of compound **1** at 10 mM concentration in DMSO at room temperature (RT), +4 °C and –20 °C (SI, Section 2.3). After seven days, 64% of the sample stored at RT had decomposed (SI, Table S1). Besides visual inspection of the colour changes of the test sample (see Table 2), the decomposition was monitored by HRMS and NMR spectroscopy. The sample that was incubated at –20 °C underwent only minimal decomposition, whereas, the sample kept at RT was fully decomposed after two weeks (SI, Figure S10). Furthermore, all three samples were tested for their inhibitory activity against *PfIspE* after the incubation period. Only the samples incubated at RT and +4 °C showed measurable inhibitory activity in the *PfIspE* assay, which was not observable for the freshly prepared compound **1** (Table 2). This fact correlated with the degree of chemical transformation of compound **1** (Table S1). In the *IspE* assay, the activity of the target enzyme is coupled to the oxidation of NADH (which can be followed spectrophotometrically at 340 nm) via a cascade of the auxiliary enzymes pyruvate kinase and lactate dehydrogenase (PK/LDH).<sup>[10]</sup> Therefore, we next confirmed, whether the effects observed in the *IspE* assay are due to inhibition of the target enzyme or of the auxiliary enzymes. Three samples of compound **1** were tested in PK/LDH assay (Table 2). The resulting IC<sub>50</sub> values of 34 μM and 45 μM for compound **1** incubated at RT and +4 °C, respectively, are only about three times higher than the IC<sub>50</sub> values determined in the *PfIspE* assay (12 μM and 16 μM, respectively). From these results, it was impossible to evaluate the influence of inhibition of auxiliary enzymes on the IC<sub>50</sub> values determined in the *PfIspE* assay.

Another approach to address this issue is to perform the *IspE* assay with one or several orthologues of *PfIspE*. The inhibitory potency of samples incubated at different temperatures of compound **1** against *Escherichia coli* (*EcIspE*) are shown in the Table 2. The *IspE* assay setup was identical for both *Pf* and *EcIspE* orthologs except for the target enzyme used. One of the setup requirements was that the enzymatic activity of the auxiliary enzymes PK/LDH exceeded the activity of the target enzyme *IspE* not less than a factor of ten.<sup>[10]</sup> We investigated, if the inhibition of the auxiliary enzymes may substantially influence the IC<sub>50</sub> values obtained from the coupled *IspE* assay. The IC<sub>50</sub> values for the active batches (“RT” and “+4 °C”) of compound **1** observed in the *EcIspE* assay are eight- and three-fold less active in comparison to those observed in the *PfIspE* assay (Table 2). The fact that the inhibition of auxiliary enzymes in the *EcIspE* assay did not give rise to equally low IC<sub>50</sub> values in comparison to those from *PfIspE* assay means that the inhibition of auxiliary enzymes influenced only marginally the IC<sub>50</sub> values measured in the *PfIspE* assay.

**Table 2.** Temperature-dependent decomposition of compound **1**.

Activity measured after 3 months	RT <sup>[b]</sup>	+4 °C <sup>[b]</sup>	-20 °C <sup>[b]</sup>	<b>1 - Old sample</b> <sup>[c]</sup>
<i>Pf</i> IspE IC <sub>50</sub> (μM) <sup>[a]</sup>	12 ± 4	16 ± 7	>500	10 ± 3
PK/LDH IC <sub>50</sub> (μM) <sup>[a]</sup>	34 ± 4	45 ± 6	n.d.	40 ± 4
<i>Ec</i> IspE IC <sub>50</sub> (μM) <sup>[a]</sup>	101 ± 14	71 ± 10	>500	32 ± 6
<i>Degradation after 2 months</i>	100%	79%	18%	N/A

[a] Errors given as formal standard error. [b] HRMS chromatograms measured shortly before the assay are given in SI, Figure S7. [c] The control values for the old decomposed sample run at the same time. n.d.: not determined, N/A: not applicable, PK/LDH: pyruvate kinase and lactate dehydrogenase, *Pf*: *Plasmodium falciparum*, *Ec*: *Escherichia coli*, RT: room temperature.

Secondly, we analysed if spontaneous chemical transformation of compound **1** may depend on the solvent used for the preparation of its stock solutions. We incubated 10 mM stock preparations of compound **1** in DMSO, acetonitrile (ACN) and methanol (MeOH) at RT. Aliquots were taken during 16 days of incubation and tested against the enzyme *Pf*IspE (Table 3). Interestingly, no *Pf*IspE inhibitory activity for the ACN or MeOH aliquots was observed, meaning that no chemical transformation of compound **1** took place in ACN or MeOH, as supported by the HRMS and NMR data (SI, Section 2.4). For further decomposition incubation of compound **1**, only DMSO was used as solvent.

**Table 3.** Time-dependent decomposition of compound **1** at room temperature.

Days of incubation	<i>Pf</i> IspE IC <sub>50</sub> (μM) <sup>[a]</sup>			PK/LDH IC <sub>50</sub> (μM) <sup>[a]</sup>
	DMSO	ACN	MeOH	DMSO
<b>0</b>	>500	>500	>500	n.d.
<b>5</b>	19 ± 7	>500	>500	n.d.
<b>7</b>	24 ± 9	>500	>500	48 ± 16
<b>9</b>	10 ± 4	>500	>500	57 ± 22
<b>12</b>	1 ± 1	>500	>500	2 ± 1
<b>14</b>	10 ± 4	>500	>500	50 ± 11
<b>16</b>	11 ± 4	>500	>500	86 ± 17
<b>Solvent Blank</b>	>500	>500	>500	n.d.

[a] Errors given as formal standard error. PK/LDH: pyruvate kinase and lactate dehydrogenase, *Pf*: *Plasmodium falciparum*. n.d.: not determined

The HRMS chromatographic profile of the analytical sample of compound **1** after 16 days of incubation at RT showed decomposition into several peaks, as seen in the chromatographic profiles of the samples previously used for the biological testing (SI, Figure S13). For further analysis, we repeated the incubation in DMSO on a larger scale for two weeks and fractionated the mixture by semipreparative HPLC into 29 fractions. The inhibitory activities of the fractions were determined against *Pf*IspE (SI, Table S2). In the preparative sample, a peak ( $m/z$ : 426.12607) was detected and interestingly, the sample incubated in DMSO- $d_6$  included a peak at 4.86 min with the likely addition of the deuterated methyls to the mass ( $m/z$ : 432.16534), which initially attracted our attention due to a possible reaction with DMSO itself. However, this peak was isolated from the DMSO sample as fraction 4 in the semipreparative HPLC and it did not show any inhibitory activity against *Pf*IspE (SI, Table S2). Out of the isolated fractions, most of the active degradation products are very non-polar and poorly separable by rp-HPLC, showing dimerised masses as well as a mass of 380.10302 // 380.2 Da. The previous HRMS studies revealed that these signals appeared already after a couple of days of incubation at RT. In particular, we could observe that two peaks ( $m/z$ : 380.10257 and  $m/z$ : 365.11542) appeared after 15 hours and the latter becomes more prominent after four and a half days (SI, Figure S20).

Thus, we performed another round of large-scale decomposition in DMSO at RT for five days and optimised the semipreparative HPLC conditions (SI, Table S3). A second purification step with supercritical fluid chromatography (SFC) (SI, Section 2.6) finally yielded two main active degradation products in sufficient amount for NMR analysis: decomposition product (**DP1**) with the  $m/z$  value of 380.10376  $[M+H]^+$  or  $[M]^+$ , corresponding to the sum formula of  $C_{18}H_{16}F_3N_3OS$  or respectively  $C_{18}H_{17}F_3N_3OS^+$  (*Pf*IspE  $IC_{50}$  =  $199 \pm 26 \mu M$ ) and **DP2** with the  $m/z$  of 365.11542  $[M+2H]^{2+}$ , corresponding to the sum formula of  $C_{36}H_{35}F_6N_6S_2^+$  (*Pf*IspE  $IC_{50}$  =  $59 \pm 4 \mu M$ ) (Table 4, Figure 1).

**Table 4.** The biological data of the SFC-separated compounds and analytical samples over four days.

Days of incubation	$IC_{50}$ ( $\mu M$ ) <sup>[a]</sup>			
	<i>Pf</i> IspE <sup>[b]</sup>	<i>Ec</i> IspE	PK/LDH	<i>Pf</i> NF54
0	>500	>500	n.d.	n.d.
1	>500	>500	n.d.	n.d.
2	>500	>500	n.d.	$3.5 \pm 0.3$
3	$486 \pm 20$	$397^{[c]}$	n.d.	n.d.
4	$99 \pm 23$	$75 \pm 16$	$95 \pm 21$	$2.7 \pm 0.3$
<b>DP1 "380"</b>	$199 \pm 26$	n.d.	>500	n.i. (>20)
<b>DP2 "365"</b>	$59 \pm 4$	n.d.	$37 \pm 4$	$2.1 \pm 0.2$

[a] All compounds were dissolved in methanol shortly before the assay. [b] Freshly dissolved compound **1** (*Pf*IspE  $IC_{50}$  = >500  $\mu M$ ). [c] Error given as formal standard error. n.d.: not determined, n.i.: no inhibition at the highest concentration tested, PK/LDH: pyruvate kinase and lactate dehydrogenase, *Pf*: *Plasmodium falciparum*, *Ec*: *Escherichia coli*, DP: decomposition product.

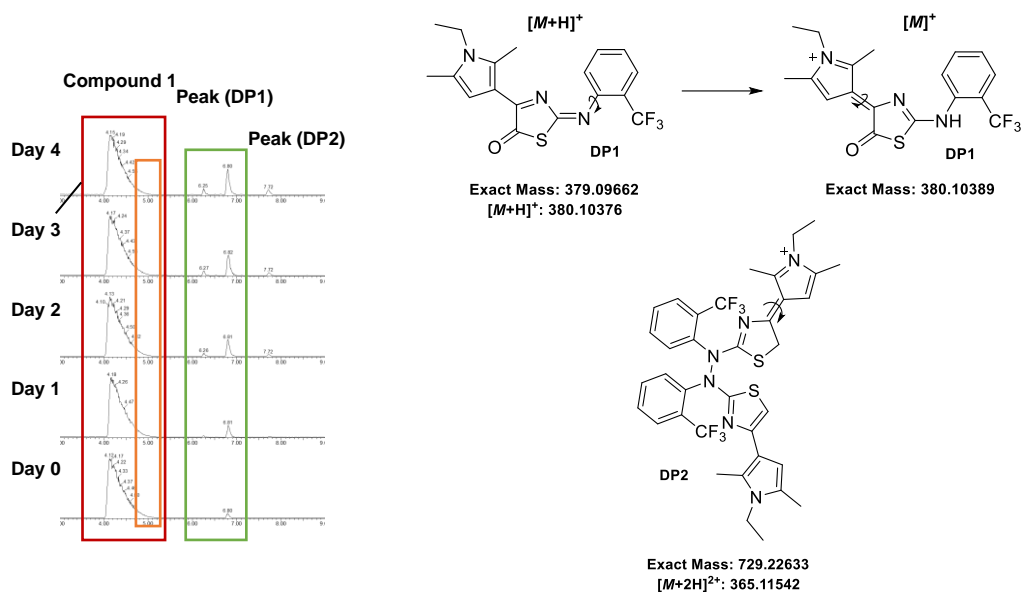


**Figure 1.** Characterised compounds isolated from the decomposition mixture. The shown chromatographic traces are base peak chromatograms generated with supercritical fluid chromatography.

**DP1** has a very distinct orange colour, supporting the formation of the formed oxygenated thiazolone core (UV<sub>max</sub> = 196, 223 and 457 nm), (SI, Figure S30). The addition of the oxygen atom was evident based on the MS data and the exact position was confirmed by the disappearance of the characteristic –CH proton signal of the thiazole position 5 at 6.54 ppm in the <sup>1</sup>H NMR spectrum (SI, Table S4, Figure S22–S23) supported by a change in chemical shift of the neighbouring carbon atom in 4-position from 141.3 ppm to 172.5 ppm. In the parent compound **1**, HMBC correlation of the thiazole carbon in 4-position (141.3 ppm) with the proton 5-position (6.52 ppm) is clear, whereas in the **DP1**, the thiazole carbon in 4-position (172.5 ppm) correlates with the nearest methyl of the pyrrole (2.83 ppm) (SI, Figure S26–S27). Detection by UV afforded a single peak, which, however, underwent isomerisation into a more polar derivative over time. In fact, the long-term stability of **DP1** became questionable as different stabilities were observed in acetone, MeOH, ACN, DMSO and CDCl<sub>3</sub>, (SI, Figure S31–35). Chloroform induces addition of chlorine as evidenced by the isotopic pattern, (*m/z*: 462.0 and 464.0 for <sup>35</sup>Cl and <sup>37</sup>Cl, respectively, Figure S33). The compound was most stable in acetone, in which we recorded NMR spectra and identified a mixture of compounds, as predicted based on the noticeable shift of the retention time in LCMS. The bond between the imine of the thiazolone core and the phenyl ring can rotate, as indicated in Figure 1, and thus, it is likely that **DP1** exists as either *E* or *Z* isomer. We calculated the energies of the lowest-energy conformations, pointing towards an *E* configuration of the isolated **DP1** (+29.4 for *E* vs +33.2 kcal/mol for *Z*). Additionally, the appearance of a broad singlet at 5.84 ppm for -NH and the changes in the pyrrole shifts supports the formation of a charged pyrrolium species that can also exist either as *E* or *Z* isomer (+66.1 vs +62.8 kcal/mol). Considering the overall reactivity of the 2,4-thiazole substitution, tautomerisation into a more stable conjugated form can occur due to the slightly



acidic and dipolar nature of DMSO. This would mean that we measure the charged form in the HRMS as 380.10376  $[M]^+$ . Due to the overall stability of **DP1**, further experiments to confirm the exact isomeric mixtures are cumbersome and were not pursued. Nevertheless, the oxygenated **DP1** in its isomeric mixture from the SFC separation showed moderate, yet selective, inhibitory activity against *Pf*IspeE ( $IC_{50} = 199 \pm 26 \mu\text{M}$ ) without PK/LDH inhibition ( $IC_{50} = >500 \mu\text{M}$ ), but showed no inhibition in the *Pf* cell-based assay at the highest tested concentration ( $IC_{50} > 20 \mu\text{M}$ ). Importantly, the cellular assay occurs over a longer time (72 hours) than the enzymatic assay (30 min), which may influence the overall stability of the compound.

Structure elucidation by NMR spectroscopy showed that the mass of **DP2** fits in fact to a dimer of **1** (Figure 1). We observed most often the doubly protonated species with  $m/z$  365.11542  $[M+2H]^{2+}$  more intensely than the charged mass  $[M]^+$ : 729.22633. With aid of the SFC, we found out that an isomer of **DP2** starts to form over the four days of incubation, as seen by the appearance of the minor peak, as highlighted in the green box in Figure 1. NMR measurements revealed its non-symmetry as one of the characteristic -CH peaks corresponding to the thiazole position 5 disappeared and a new peak appeared at 3.96 ppm, integrating for -CH<sub>2</sub> (SI, Table S5). This led us to question how the dimerisation would occur. Based on the NMR and MS data, we propose that an N–N bond formation occurs between the linker amines, as represented in the proposed reaction (SI, Scheme S1). N–N bonds are generally unstable, however, rather commonly occur in biological complexes.<sup>[11]</sup> Due to the slightly acidic nature of DMSO, it is likely that the conjugated pyrrolium species is present and the imine N, as in tautomer of compound **1**, is attacked by the nucleophilic linker amine forming the N–N bond. The charged pyrrolium may also undergo isomerisation between *E* and *Z* isomers as observed in the SFC conditions, (SI, Figure S36). *Z* being slightly more stable than *E* (+144.7 vs +148.5 kcal/mol), hampering the exact assignment of the pyrrolium NMR peaks. For **DP2**, we could reach a similar enzymatic activity profile as for the initial decomposed starting points (*Pf*IspeE  $IC_{50} = 59 \pm 4 \mu\text{M}$ ), although also inhibiting the auxiliary enzymes (PK/LDH  $IC_{50} = 37 \pm 4 \mu\text{M}$ ). The antimalarial activity (*Pf*NF54  $IC_{50} = 2.1 \pm 0.2 \mu\text{M}$ ) is also corresponding to an overall increase in activity as the decomposition occurs (Table 4). The dimerisation via N–N bond formation could also occur at other nitrogen atoms, supporting the other dimerised masses measured after the first rp-HPLC (SI, Table S2).

Lastly, we investigated, whether the decomposition would also occur in Cyrene<sup>TM</sup>, similarly dipolar and aprotic as DMSO, yet a green solvent.<sup>[12]</sup> Disappointingly, clear decomposition occurred even after one day incubation at RT, although showing different masses to the DMSO samples (SI, Figure S16). Interestingly, dominating peak ( $m/z$ : 476.16010, potentially with the addition of Cyrene<sup>TM</sup> and a loss of water) occurred at 4.68, where we previously observed the peak with DMSO ( $m/z$ : 426.12607) and DMSO-*d*<sub>6</sub> ( $m/z$ : 432.16534). This may be ascribed to the general reactivity of compound **1** and Cyrene<sup>TM</sup>, which may, nevertheless, still be an interesting choice for other compounds.



In conclusion, we analysed the collected data to understand what causes the antimalarial activity that evolved from compound **1** stored in DMSO. The *Pf*IspE activity can be partly ascribed to dimerised **DP2**, although it also inhibits PK/LDH. On the other hand, the oxygenated **DP1** may also play a role when in its active isomeric form. The isolated degradation products themselves are unstable. They undergo further degradation, leading to a mixture that may also account for the observed activities. Additionally, our study underlines the importance of appropriate storage conditions of DMSO stock solutions of 2-aminothiazoles. Based on the temperature-dependent studies, we confirmed that decomposition hardly occurs at  $-20\text{ }^{\circ}\text{C}$  over two months in DMSO. For the future, blocking the 5 position of the thiazole ring with a fluorine atom could be a feasible strategy to reduce the reactivity.<sup>[13]</sup> However, to avoid decomposition, working with such a class requires preparation of fresh stock solutions prior to biological assays. Furthermore, multiple freeze-thaw cycles should be avoided and alternative solvents should be considered. With this communication, we wish to remind the medicinal-chemistry community again that what is in the test well, might not be the compound one thought.

## Experimental Section

Details for chemical syntheses, analytical and biological methods together with characterisation data are described in the Supporting Information.

## Acknowledgements

H.-K.R. thanks Stiftung Stipendien-Fonds des Verbandes der Chemischen Industrie for the Kekulé Mobility Fellowship. A.K.H.H. gratefully acknowledges funding from the Helmholtz Association's Initiative and Networking Fund. The authors thank Daniel Andrews (BASF Intern, University of St. Andrews) for the initial synthesis and Dr. Jörg Hauptenthal (HIPS) for coordinating the initial cytotoxicity assays.

## References

- [1] A. Frank, M. Groll, *Chem. Rev.* **2017**, *117*, 5675–5703.
- [2] D. González Cabrera, F. Douelle, T. S. Feng, A. T. Nchinda, Y. Younis, K. L. White, Q. Wu, E. Ryan, J. N. Burrows, D. Waterson, M. J. Witty, S. Wittlin, S. A. Charman, K. Chibale, *J. Med. Chem.* **2011**, *54*, 7713–7719.
- [3] F. Mjambili, M. Njoroge, K. Naran, C. De Kock, P. J. Smith, V. Mizrahi, D. Warner, K. Chibale, *Bioorganic Med. Chem. Lett.* **2014**, *24*, 560–564.
- [4] K. V Balakin, Y. A. Ivanenkov, A. V Skorenko, Y. V Nikolsky, N. P. Savchuk, A. A. Ivashchenko, *J. Biomol. Screen.* **2004**, *9*, 22–31.
- [5] C. Engeloch, U. Schopfer, I. Muckenschnabel, F. Le Goff, H. Mees, K. Boesch, M. Popov, *J.*

- Biomol. Screen.* **2008**, *13*, 999–1006.
- [6] E. Zitha-Bovens, P. Maas, D. Wife, J. Tijhuis, Q. N. Hu, T. Kleinöder, J. Gasteiger, *J. Biomol. Screen.* **2009**, *14*, 557–565.
- [7] S. M. Devine, M. D. Mulcair, C. O. Debono, E. W. W. Leung, J. W. M. Nissink, S. S. Lim, I. R. Chandrashekar, M. Vazirani, B. Mohanty, J. S. Simpson, J. B. Baell, P. J. Scammells, R. S. Norton, M. J. Scanlon, *J. Med. Chem.* **2015**, *58*, 1205–1214.
- [8] J. B. Baell, J. M. Willem Nissink, *ACS Chem. Biol.* **2018**, *13*, 36–44.
- [9] J. B. Baell, L. Ferrins, H. Falk, G. Nikolakopoulos, *Aust. J. Chem.* **2013**, *66*, 1483–1494.
- [10] V. Illarionova, J. Kaiser, E. Ostrozhenkova, A. Bacher, M. Fischer, W. Eisenreich, F. Rohdich, *J. Org. Chem.* **2006**, *71*, 8824–8834.
- [11] C. Ferousi, S. H. Majer, I. M. Dimucci, K. M. Lancaster, *Chem. Rev.* **2020**, *120*, 5252–5307.
- [12] J. E. Camp, S. B. Nyamini, F. J. Scott, *RSC Med. Chem.* **2020**, *11*, 111–117.
- [13] A. S. Kalgutkar, *J. Med. Chem.* **2020**, *63*, 6276–6302.

## 4. Conclusions and Outlook

Various drug-discovery approaches were applied in this study to yield novel inhibitors of *Ec* and *Pf*IspE that serve as potential starting points for further optimisation. Although directly comparable cell- and enzyme-based activities are still being investigated for the presented series, this study has taken a step forward in the exploitation of the enzyme IspE, and the MEP pathway in general. Multidisciplinary methods were applied to bridge this translational gap and the study reports first attempts to approach this in a holistic way. The learnings from this study are hoped to bring new insights for future anti-infective drug-discovery campaigns focusing on the enzyme IspE. Going beyond the medicinal-chemistry focus, various chemical side reactions resulted in interesting findings, for instance [1,4]oxazepine and N–N bond formation, with the potential for further research in the light of synthesis. For each of the experimental chapters, the detailed conclusions and outlook are covered separately.

Beside the experimental studies, the literature research focusing on the Gram-negative bacteria led to the new concept of bacterial bioavailability. It urges to change the views of current anti-infective drug discovery to look at the target bacteria in a holistic way combining uptake, distribution, metabolism and efflux, as we regard oral bioavailability. We hope that it will spark future research to build suitable predictive experimental assays and computational models to speed up anti-infective drug discovery.

*Chapter A:* The virtual screening with *Ec*IspE provided a fragment-like hit that was further optimised to improve the antibacterial profile and increase the target engagement. The disadvantage of the series was its strong cytotoxicity. We suspected the primary amine selected using the eNTRY rules to be the cause, although further analysis demonstrated that the influence of the substituents of the diaryl ether and the positioning of halogens could have equally caused the cytotoxicity. In comparison, the secondary amine within the piperidine handle was shown to increase the activity against *P. aeruginosa*, which again pinpoints towards bacteria-specific uptake rules. Nevertheless, the halogen series provided the proof of concept of altering the amphiphilic moments in order to increase bacterial activity, as previously proposed by the eNTRY rules.<sup>70</sup> To examine the influence of the primary amine on different cell lines, for example the transformed human liver epithelial (THLE) cell line could be used that is less prone to acidic and neutral than to basic compounds. On the contrary, the same study reports HepG2 cells being more sensitive to basic compounds.<sup>108</sup> Furthermore, E. Lee *et al.* report primary amines to be less promiscuous *in vitro* and to cause less issues *in vivo* toxicity in comparison to secondary or tertiary amines.<sup>109</sup> We also observed this with the latest compounds, where the secondary amine **HIPS5990** (HepG2 IC<sub>50</sub> = 23 ± 4 μM) proved to be more toxic than the primary amine **HIPS6027** (HepG2 %.-inh. = 77 ± 20% @ 100 μM). The latest results with **HIPS6027** in fact show that the ideal amphiphilic moment is around 8 that should be taken into account together with an ideal pK<sub>a</sub> value around the physiological pH ~ 7.4 to balance out the cytotoxicity of the primary amine. This approach is already showing promising results of reduced

cytotoxicity with the ongoing follow-up series of **HIPS6027**. How the novel difluoromethyl handle, as a primary amine bioisoster, will influence bacterial uptake is still under investigation. Additionally, follow-up derivatives should aim for low  $\text{clogD}_{7.4}$ . In contrast, compounds with amphiphilic moment well below  $\sim 8$  seem to be more likely to undergo efflux in *E. coli*. Synthetic derivatives to decrease the  $\text{pK}_a$  of the more basic piperidine handle with, for instance fluorinated derivatives, could also circumvent its cytotoxicity, while retaining the activity against *P. aeruginosa*.<sup>110</sup> Additionally, the various handle derivatives could be tested more extensively against *A. baumannii*, which could help the design of an ideal broad-spectrum activity handle. The series also gathered many data against different *E. coli* mutant strains and human cell lines that could be of use to train future prediction models, in particular, in the light of the introduced bacterial bioavailability concept. Further studies with *P. aeruginosa* mutant strains could also provide interesting insights of the piperidine handles towards structure–permeation relationships whilst comparing the compound properties to recently reported predictive efflux rules of *P. aeruginosa*.<sup>111</sup> On the other hand, the physiological conditions of the infection site need to be taken into account in later optimisation. Further optimisation of the newly substituted diaryl core is ongoing beside co-crystallisation attempts. Based on a preliminary docking study, the new amide activity handle **HIPS6027** may provide a new binding mode to grow into the underexplored cavity, as illustrated with an example (Figure 4:1). The potential atropisomers of the follow-up diaryl derivatives should also be taken into account in future synthesis and their respective variation accounting for target engagement, keeping in mind the potential dual inhibition with ENR.<sup>112</sup>

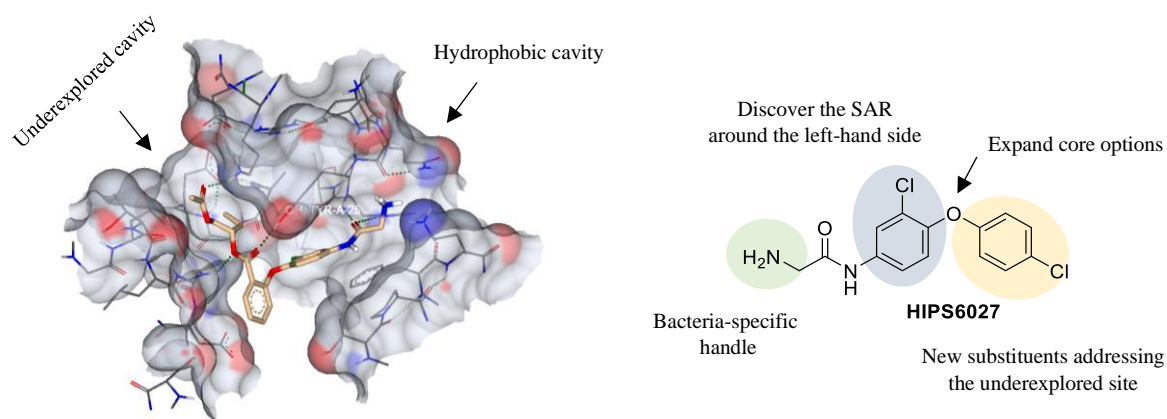


**Figure 4:1** - The follow-up series modelled in the binding site in *EcIspE*, occupying the underexplored cavity on the left-hand. Molecular modelling was performed in SeeSAR 10.3, and the figure was created in StarDrop 6.6.7.<sup>82</sup> The key optimisation strategies are summarised for **HIPS6027**.

Based on the destabilising effect on the melting point throughout the series, the mode of action is hypothesised to interfere with dimer formation by binding in the hydrophobic cavity. Successful crystallisation attempts could confirm the binding mode and provide new insights on the molecular recognition of the inhibitor by IspE. As seen in Figure 4:1, the cavities form a V-shaped

opening that could suggest that this gate is opened when requested by a correct molecular interaction. Alternatively, the previously reported MALDI-TOF MS<sup>52</sup> or SPR<sup>53</sup> assays could be used to confirm the interference of the PPI in the dimer interface. If the predicted binding site turns out to be in the catalytic site, there is a high chance to retain the activity for the series in other IspE enzymes of Gram-negative pathogens, as the sequence similarity is the highest in the catalytic site (red region highlighted in Figure 4:2). In order to move to the more pathogenic bacteria, it is also necessary to establish robust functional assays or to develop the metabolomics assay further (Appendix I). The metabolomics assay would open up the field to explore the necessity of the MEP pathway between fermenting or non-fermenting bacteria. The screening of future IspE inhibitors should also include testing against the GHMP kinase superfamily, to avoid selectivity issues. In addition, a first field-based virtual screening with the natural substrate CDP-ME was initiated. If successful, these ligands may also serve as interesting starting points to evaluate the translation across the IspE enzymes (Appendix II). Water-ligand observed *via* gradient spectroscopy (WaterLOGSY) based NMR screening could be of use to examine their interactions in the highly water-filled catalytic site.<sup>113,114</sup>

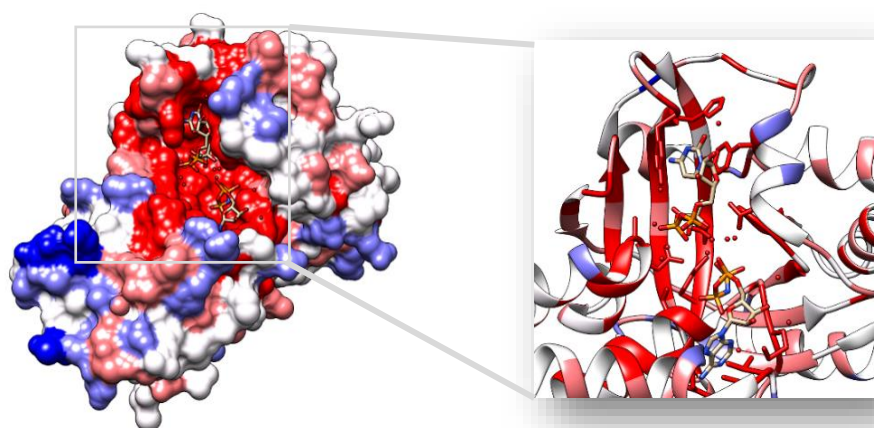


**Figure 4:2** - The Gram-negative ESKAPE pathogens from Table 1.2:1 overlaid onto *EcIspE* (PDB 1OJ4) showing high structural similarity, (red=1, white=0.6 and blue=0.2). The zoom-in shows the high conservation of the amino acid residues in the catalytic site. The figures were created in Chimera 1.15.<sup>115</sup>

*Chapter B:* We designed the underlying antimalarial compound class into a series with amino acids applying the rules, to gain antibacterial activity against Gram-negative bacteria. Although the series in general lacked antibacterial activity against wild-type *E. coli*, clear differences were observed between the Boc-protected and the corresponding free amine derivatives in the screening against *E. coli* mutant strains. In the enzyme assay testing against both *PfIspE* and *EcIspE*, the Boc-derivatives turned out to inhibit the IspE enzymes better than the free amines. These results could be used to examine the binding modes more closely between the two enzymes, implementing for example the established TSA assay to evaluate differences in (de)stabilisation of the protein. In addition, two of the Boc-derivatives turned out to also show comparable cell-based activity against

*Pf*NF54. Future studies should be conducted to understand, whether such amino acid handles could be used as recognition handles for cellular uptake in Gram-negative bacteria, which could be of equal interest in malaria parasites. Simultaneously, to understand the potential influence of the amino acid modifications on efflux, the compounds could be screened using recent computational tools to predict efflux issues.<sup>116,117</sup>

*Chapter C:* False positives are unfortunately part of medicinal-chemistry workflows. In Chapter C, we faced a decomposition issue with the parent inhibitor of *Pf*IspE. The 2-aminothiazole compound underwent chemical decomposition in a DMSO stock solution. Interestingly, this decomposition mixture led to both increased activity against the enzymatic target *Pf*IspE and in cell-based assays against *Pf*NF54. We made substantial efforts to isolate and characterise decomposition products causing the activity. Although these efforts did not result in a drug-like series, the investigation makes an important addition to the research on novel antimalarials targeting the underexplored enzyme IspE of the MEP pathway. It also reminds the medicinal-chemistry community to be always cautious of the stability of the compounds in DMSO stock solutions. Additionally, this study highlights the use of supercritical fluid chromatography (SFC) as an alternative to the traditional preparative HPLC.

## 5.) Supplementary Material

### 5.1 Supplementary Material of Introduction

#### 5.1.1 Section 1.2

The strain codes refer to the UNIPROT codes, unless specified, and the analysis was done in EMBOSS.<sup>60-62</sup>

#### Reference strain *E. coli* IspE<sup>118</sup>

```
>1OJ4_1|Chains A,B|4-DIPHOSPHOCYTIDYL-2-C-METHYL-D-ERYTHRITOL
KINASE|ESCHERICHIA COLI (217992)
```

```
MRTQWPSPAKLNLFYITGQRADGYHTLQTLFQFLDYGDTISIELRDDGDIRLLTPVEGVEHEDNLIVRAARL
LMKTAADSGRLPTGSGANISIDKRLPMGGGLGGSSNAATVLVALNHLWQCGLSMDELAEMGLTLGADVFPV
RGHAAFAEGVGEILTLPVDPEKWYLVVHPGVSIPTPVIFKDPPELPRNTPKRSIETLLKCEFSNDCEVIARKR
REVDAVLSWLLLEYAPSRLTGTGACVFAEFDTESEARQVLEQAPEWLNFGFVAKGVNLSPLHRAML
```

#### *E. coli* IspE vs *P. aeruginosa* IspE

```
sp|P42805|ISPE_PSEAE 4-diphosphocytidyl-2-C-methyl-D-erythritol kinase
OS=Pseudomonas aeruginosa (strain ATCC 15692 / DSM 22644 / CIP 104116 /
JCM 14847 / IMG 12228 / 1C / PRS 101 / PAO1) OX=208964 GN=ispE PE=3 SV=2
MSVRLSLPAPAKLNLFHLHILGRRDDGYHELQTLFQFLDHGDELHFEARQDGGVRLHTEIA
GVPHDSNLIVRAARGLQEASGSPQGVDIWLDKRLPMGGGIGGGSSDAATLLLALNHLWQL
GWDEDRIAALGLRLGADVVPVTRGRAAFVGEVGEKLTVPDIPEPWYLWVVPQVVLVSTAEI
FSDPLLTRDSPAIKVRTVLEGDSRNCQPVVERRYPEVRNALILLNKVFVSARLTGTGGCV
FGSFPNKAEADKVSALLPDHLQRFVAKGSNISMLHRKLETLV
```

# Aligned_sequences: 2		
# 1: <i>E. coli</i> (PDB 1OJ4)	1 MRTQWPSPAKLNLFYITGQRADGYHTLQTLFQFLDYGDTISIELRDDGD	50
# 2: <i>P. aeruginosa</i> (P42805)	3 VRLSLPAPAKLNLFHLHILGRRDDGYHELQTLFQFLDHGDELHFEARQDGG	52
# Matrix: EBLOSUM62		
# Gap_penalty: 14	51 IRLLTPEGVEHEDNLIVRAARLLMKTAADSGRLPTGSGANISIDKRLPM	100
# Extend_penalty: 4	53 VRLHTEIAGVPHDSNLIVRAARGLQEASGSP-----QGVDIWLKRLPM	96
#		
# Length: 282	101 GGGGGGGSSNAATVLVALNHLWQCGLSMDELAEMGLTLGADVVPVFRGH	150
# Identity: 154/282 (54.6%)	97 GGGGGGGSSDAATLLLALNHLWQLGWDEDRIAALGLRLGADVVPVTRGRA	146
# Similarity: 192/282 (68.1%)	151 AFAEGVGEILTLPVDPEKWYLVVHPGVSIPTPVIFKDPPELPRNTPKRSIE	200
# Gaps: 6/282 (2.1%)	147 AFAEGVGEKLTVPDIPEPWYLWVVPQVVLVSTAEIFSDPLLTRDSPAIKVR	196
# Score: 750		
	201 TLLKCEFSNDCEVIARKRFREVDVLSWLLLEYAPSRLTGTGACVFAEFD	250
	197 TVLEGDSRNCQPVVERRYPEVRNALILLNKVFVSARLTGTGGCVFGSFPN	246
	251 ESEARQVLEQAPEWLNFGFVAKGVNLSPLHRAM	282
	247 KAEADKVSALLPDHLQRFVAKGSNISMLHRKLE	278

### *E. coli* IspE vs *A. baumannii* IspE

>sp|B7GYQ7|ISPE\_ACIB3 4-diphosphocytidyl-2-C-methyl-D-erythritol kinase  
OS=*Acinetobacter baumannii* (strain AB307-0294) OX=557600 GN=ispE PE=3  
SV=1  
MIRVPSPAKLNLFHITGRRENGYHELQTFQLIDLYDWMFTTPISEDEIQIEGLGEVQL  
EQNLIYRAAQILRPHAQNPCGLHIKIEKNIPMGAGLGGSSNAATTLIVLNQLWQCGLTE  
EQLAQFGVKLGADVPIFIYGLNAWAEGIGEHLDFIDLDQKQFIVLKPDCFISTQLLFSQK  
TLTRDSKPTTFCAYQLEPSNFGNNFEPLARELYPEVEEAMQYLDQFGHAKLTGTGACVFA  
EVTDEMNVDDILKHAPCKAYLVHSLKESPLRHFVKVAS

```
# Aligned_sequences: 2
# 1: E. coli (PDB 1OJ4)
# 2: A. baumannii (B7GYQ7)
# Matrix: EBLOSUM62
# Gap_penalty: 14
# Extend_penalty: 4
#
# Length: 259
# Identity:      113/259 (43.6%)
# Similarity:   165/259 (63.7%)
# Gaps:         9/259 (3.5%)
# Score: 505

      6 PSPAKLNLFlyITGQRADGYHTLQTLFQFLDYGDTISIELRDDGDIRLLT    55
      5 PSPAKLNLFHITGRRENGYHELQTFQLIDLYDWMFTTPISEDEIQI-E      53

      56 PVEGVEHEDNLIVRAARLLMKTAADSGRLPTGSGANISIDKRLPMGGGLG    105
      54 GLGEVLEQNLIYRAAQILRPHAQNP-----CGLHIKIEKNIPMGAGLG      97

      106 GSSSNAATVLVALNHLWQCGLSMDELAEMGLTLGADVVPVVRGHAFAEAG    155
      98 GSSSNAATTLIVLNQLWQCGLTEEQLAQFGVKLGADVPIFIYGLNAWAEG    147

      156 VGEILTPVDPPEKWLVAHPGVSIPTPVIFKDPPELPRNTPKRSI--ETLL    203
      148 IGEHLDFIDLDQKQFIVLKPDCFISTQLLFSQKTLTRDSKPTTFCAYQLE    197

      204 KCEFSNDCEVIARKRFREVDVLSWLLLEYAPSRLTGTGACVFAEFDTESE    253
      198 PSNFGNNFEPLARELYPEVEEAMQYLDQFGHAKLTGTGACVFAEVTDEMN    247

      254 ARQVLEQAP      262
      ...:|:|
      248 VDDILKHAP      256
```

### *E. coli* IspE vs *K. pneumoniae* IspE

>sp|A6TAP2|ISPE\_KLEP7 4-diphosphocytidyl-2-C-methyl-D-erythritol kinase  
OS=*Klebsiella pneumoniae* subsp. *pneumoniae* (strain ATCC 700721 / MGH  
78578) OX=272620 GN=ispE PE=3 SV=1  
MMTRWPSPAKLNLFlyITGQRADGYHTLQTLFQFLDYGDTLTIEPRTDQQLRLLTPVAGV  
PDEENLIVRAARLLMHAASESDRLPAGSGADISIDKRLPMGGGLGGSSNAATVLVALNH  
LWGCGLSEDELATLGLQLGADVVPVVRGHAFAEAGVGEILTPVEPEEKWYLVAHPGVSIP  
TPIIFRDPELPRNTPRRSINTLLNCFESNDCELIARKRFREVDAAALSWLLEYAPSRLTGT  
GACVFAEFNTEESAARQVLDTAPAWLNGFVARGVNLSPKQALL

```
# Aligned_sequences: 2
# 1: E. coli (PDB 1OJ4)
# 2: K. pneumoniae (A6TAP2)
# Matrix: EBLOSUM62
# Gap_penalty: 14
# Extend_penalty: 4
#
# Length: 283
# Identity:      241/283 (85.2%)
# Similarity:   260/283 (91.9%)
# Gaps:         0/283 (0.0%)
# Score: 1271

      1 MRTQWPSPAKLNLFlyITGQRADGYHTLQTLFQFLDYGDTISIELRDDGD    50
      1 MMTRWPSPAKLNLFlyITGQRADGYHTLQTLFQFLDYGDTLTIEPRTDQQ    50

      51 IRLLTPEGVEHEDNLIVRAARLLMKTAADSGRLPTGSGANISIDKRLPM      100
      51 LRLLTPEVAGVPDEENLIVRAARLLMHAASESDRLPAGSGADISIDKRLPM    100

      101 GGLGGSSNAATVLVALNHLWQCGLSMDELAEMGLTLGADVVPVVRGHA      150
      101 GGLGGSSNAATVLVALNHLWGCGLSEDELATLGLQLGADVVPVVRGHA      150

      151 AFAEGVGEILTPVDPPEKWLVAHPGVSIPTPVIFKDPPELPRNTPKRISIE    200
      151 AFAEGVGEILTPVEPEEKWYLVAHPGVSIPTPVIFRDPELPRNTPRRSIN    200

      201 TLLKCEFSNDCEVIARKRFREVDVLSWLLLEYAPSRLTGTGACVFAEFDT    250
      201 TLLNCFESNDCELIARKRFREVDAAALSWLLEYAPSRLTGTGACVFAEFNT    250

      251 ESEARQVLEQAPEWLNFGVAKVNLSPHRAML      283
      ||:||||:|:|:|||||:|||||:|:|
      251 ESAARQVLDTAPAWLNGFVARGVNLSPKQALL      283
```



## *E. coli* IspE vs *Enterobacter* sp. IspE

```
>sp|A4WBC9|ISPE_ENT38 4-diphosphocytidyl-2-C-methyl-D-erythritol kinase
OS=Enterobacter sp. (strain 638) OX=399742 GN=ispE PE=3 SV=1
MMTQWPSPAKLNLFLYITGQRADGYHTLQTLFQFVDYGDITISIEPRQDGEIHLTPVDDV
ASEDNLIVRAARLLVQAAANSGRLEPEHYGADIGVEKRLPMGGGLGGSSNAATVLVALNH
LWGGCGFSQDELATLGLTLGADVPVFRGHAAFAEGVGEILTPVDPPEKWYLIHHPGVSIP
TPVIFNDPELPRNTPVRSIETLLKCEFGNDCEVIARKRFRKVDAAALSWLLEYAPSRLTGT
GSCVFAEFDTESAARQVLEQAPEWLHGFVARGMNTSPLQQTILAQTEFR
```

```
# Aligned_sequences: 2
# 1: E. coli (PDB 1OJ4)
# 2: Enterobacter sp. (A4WBC9)
# Matrix: EBLOSUM62
# Gap_penalty: 14
# Extend_penalty: 4
#
# Length: 283
# Identity: 241/283 (85.2%)
# Similarity: 259/283 (91.5%)
# Gaps: 0/283 (0.0%)
# Score: 1275

1 MRTQWPSPAKLNLFLYITGQRADGYHTLQTLFQFVDYGDITISIELRDDGD 50
.|||||:|||||:|||||:|||||:|||||:|||||:|||||:|||||:|||||:
1 MMTQWPSPAKLNLFLYITGQRADGYHTLQTLFQFVDYGDITISIEPRQDGE 50

51 IRLTPVEGVEHEDNLIVRAARLLMKTAAADSGRLPTGSGANISIDKRLPM 100
|.|||||.|||.|||||:|||||:|||||:|||||:|||||:|||||:
51 IHLTPVDDVASEDNLIVRAARLLVQAAANSGRLEPEHYGADIGVEKRLPM 100

101 GGGGGSSNAATVLVALNHLWQCGLSMDELAEMGLTLGADVPVFRGHA 150
|||||:|||||:|||||:|||||:|||||:|||||:|||||:|||||:
101 GGGGGSSNAATVLVALNHLWGGCGFSQDELATLGLTLGADVPVFRGHA 150

151 AFAEGVGEILTPVDPPEKWYLIHHPGVSIPTPVIFKDPPELPRNTPKRSIE 200
|||||:|||||:|||||:|||||:|||||:|||||:|||||:|||||:
151 AFAEGVGEILTPVDPPEKWYLIHHPGVSIPTPVIFNDPELPRNTPVRSIE 200

201 TLLKCEFSNDCEVIARKRFRFVDAVLSWLLEYAPSRLTGTGACVFAEFD 250
|||||:|||||:|||||:|||||:|||||:|||||:|||||:|||||:
201 TLLKCEFGNDCEVIARKRFRKVDAAALSWLLEYAPSRLTGTGSCVFAEFD 250

251 ESEARQVLEQAPEWLNGFVAKGVNLSPLHRAML 283
|.|||||:|||||:|||||:|||||:|||||:
251 ESAARQVLEQAPEWLHGFVARGMNTSPLQQTIL 283
```

## *E. coli* IspE vs *B. thailandensis* IspE

```
>sp| |ISPE_BURTA 4-diphosphocytidyl-2-C-methyl-D-erythritol kinase
OS=Burkholderia thailandensis (strain ATCC 700388 / DSM 13276 / CIP
106301 / E264) OX=271848 GN=ispE PE=3 SV=1
MTDTTRSLRDCLAPAKLNLFLHITGRRPDGYHELQSVFQLLDWGDRLHFTLRDDGKVS RK
TDVPGVPEETDLIVRAASLLKAHTGTAAGVDIEIDKRLPMGAGLGGGSSDAATLLALNR
LWKLDLPRATLQSLAVKLGADVPFFVFGKNAFAEGIGEALQAVELPTRWFLVVTPRVHVP
TAAIFSEKSLTRDSKPIITITDFLAQQDCNTGWPDSEFGRNDMQPVVTSKYAEVAKVVGWYF
NLTPTARMTGSGASVFAAFKSKAEAGAAQQLPAGWDSAVAESLGEHPLFAFAS
```

```
# Aligned_sequences: 2
# 1: E. coli (PDB 1OJ4)
# 2: B. thailandensis (Q2T1B6)
# Matrix: EBLOSUM62
# Gap_penalty: 14
# Extend_penalty: 4
#
# Length: 282
# Identity: 130/282 (46.1%)
# Similarity: 170/282 (60.3%)
# Gaps: 16/282 (5.7%)
# Score: 543

7 SPAKLNFLYITGQRADGYHTLQTLFQFVDYGDITISIELRDDGDIRLLTP 56
:|||||:|||||:|||||:|||||:|||||:|||||:|||||:|||||:
13 APAKLNFLHITGRRPDGYHELQSVFQLLDWGDRLHFTLRDDGKVS RKTD 62

57 VEGVEHEDNLIVRAARLLMKTAAADSGRLPTGSGANISIDKRLPMGGGLGG 106
|.|||||.|||.|||||:|||||:|||||:|||||:|||||:|||||:
63 VPGVPEETDLIVRAASLLK---AHTG---TAAGVDIEIDKRLPMGAGLGG 106

107 GSSNAATVLVALNHLWQCGLSMDELAEMGLTLGADVPVFRGHAAFAEGV 156
|||||:|||||:|||||:|||||:|||||:|||||:|||||:|||||:
107 GSSDAATLLALNRLWKLDLPRATLQSLAVKLGADVPFFVFGKNAFAEGI 156

157 GEILTPVDPPEKWYLIHHPGVSIPTPVIFKDPPELPRNTPKRSIETLLK-- 204
|.|||||.|||.|||||:|||||:|||||:|||||:|||||:|||||:
157 GEALQAVELPTRWFLVVTPRVHVPVTAIFSEKSLTRDSKPIITDFLAQQ 206

205 -CEFS-----NDCEVIARKRFRFVDAVLSWLLEYAPSRLTGTGACVFA 246
|... |...:|||||:|||||:|||||:|||||:|||||:
207 DCNTGWPDSEFGRNDMQPVVTSKYAEVAKVVGWYFNLTPTARMTGSGASVFA 256

247 EFDTESEARQVLEQAPEWLNGFVAKGVNLSPL 278
|.|||||:|||||:|||||:|||||:|||||:
257 AFKSKAEAGAAQQLPAGWDSAVAESLGEHPL 288
```

### *E. coli* IspE vs *M. tuberculosis* IspE

```
>sp|P9WKG7|ISPE_MYCTU 4-diphosphocytidyl-2-C-methyl-D-erythritol kinase
OS=Mycobacterium tuberculosis (strain ATCC 25618 / H37Rv) OX=83332
GN=ispE PE=1 SV=1
MPTGSVTVRVPGKVNLYLAVGDRREDGYHELTTVFHAVSLVDEVTVRNADVLSLELVGEG
ADQLPTDERNLAWQAAELMAEHVGRAPDVSIMIDKSI PVAGGMAGGSADAAAVLVAMNSL
WELNVPRRDLRMLAARLGS DVPFALHGGTALGTGRGEELATVLSRNTFHWVLA FADSGLL
TSAVYNELDRLREVGDPPRLGEPGPVLAALAAAGDPDQLAPLLGNEMQAAA VSLDPALARA
LRAGVEAGALAGIVSGSGPTCAFLCTSASSAIDVGAQLSGAGVCRTVVRVATGPVPGARVV
SAPTEV
```

```
# Aligned_sequences: 2
# 1: E. coli (PDB 1OJ4)
# 2: M. tuberculosis (P9WKG7)
# Matrix: EBLOSUM62
# Gap_penalty: 14
# Extend_penalty: 4
#
# Length: 158
# Identity: 58/158 (36.7%)
# Similarity: 84/158 (53.2%)
# Gaps: 8/158 (5.1%)
# Score: 207
8 PAKLNLFLYITGQRADGYHTLQTLFQFLDYGDITISIELRDDGDIRLLTPV 57
|.:.||:|.:.:.|.|||.|.:.|.:.:.|.:.:.|.:.:.|.:.:.|.:.|.:.
11 PGKVNLYLAVGDRREDGYHELTTVFHAVSLVDEVTVRNADVLSLELVGEG 60
58 EGV--EHEDNLIVRAARLLMKTAAADSGRLPTGSGANISIDKRLPMGGGLG 105
... ..|.||.:.|.:.|.:.|.:.|.:.|.:.|.:.|.:.|.:.|.:.|.:.
61 ADQLPTDERNLAWQAAELM---AEHVGRAPD---VSIIMIDKSI PVAGGM 104
106 GGSNAATVLVALNHLWQCGLSMDELAEMGLTLGADVVPVVRGHAFAEG 155
||:.|.|||.|.:.|.:.|.:.|.:.|.:.|.:.|.:.|.:.|.:.|.:.|.:.
105 GGSADAAAVLVAMNSLWELNVPRRDLRMLAARLGS DVPFALHGGTALGTG 154
156 VGEILTPV 163
. ||. |. |
155 RGEELATV 162
```

### *E. coli* IspE vs *P. falciparum* IspE

```
>tr|A0A1B1TK84|A0A1B1TK84_PLAFA 4-diphosphocytidyl-2c-methyl-D-erythritol
kinase OS=Plasmodium falciparum OX=5833 GN=IspE PE=3 SV=1
MNQFLNLKCVLFYFFCTHLLFFLHVITKHNLLKKEKGYIIRNDYKCKRKRKNNNLLKRSFFI
ICKNCRPNNNKFYIINNKGGENIYNVKKKKKACGYVRLNNEANVEKNNVNTNKEIEKLLL
DVLDRNWNWYDSKYFSPAKINLFLRLKEKKEKYNEVSTLMHSLNLGDDIFIRALKKEDQN
KLRHFLHPCESGDFLTIVRMEDKNRDKETLKEDCKIDVINKSDKDLFKHMKEDII IQEHE
KLPYEYNDYPINNDNII IKVLKRYREEFNISDDIRFLIHVNKRIP I FSGVGGGSSNGATV
FYFLENI FYKYFKGDNKANEF LKTIGSDISFFSSSGFAYCTDKGNVTDLKNIEANIKD
KDIYLFKIDEGLSKLVYKNVDYKRI IQYNPNVLLKCLINTSNDDI IKQIEEKEKKFANT
FISLDNRDNLQNVFVNDLEHS AFYLIK LKQLDLKEYLRSQNMFDVVSMMSGSSLSLFALSNK
KTQTHEISSSFQNERIKKLISDIKIKFNMNVRVYLC DALRKGLDVWYDPIKLAHEFK
```

```
# Aligned_sequences: 2
# 1: E. coli (PDB 1OJ4)
# 2: P. falciparum (A0A1B1TK84)
# Matrix: EBLOSUM62
# Gap_penalty: 14
# Extend_penalty: 4
#
# Length: 72
# Identity: 24/72 (33.3%)
# Similarity: 38/72 (52.8%)
# Gaps: 2/72 (2.8%)
# Score: 91
92 ISIDKRLPMGGGLGGSSNAATVLVALNHLWQCGLSMDELA--EMGLTLG 139
|:..||:|.:.|.|||.|||.|||.|||.|||.|||.|||.|||.|||.|||.
278 IHVNKRIP I FSGVGGGSSNGATV FYFLENI FYKYFKGDNKANEF LKTIG 327
140 ADVPVFVRGHAFAEGVGEILT 161
:|.:.|.:.|.:.|.:.|.:.|.:.|.:.|.:.|.:.|.:.|.:.|.:.|.:.
328 SDISFFSSSGFAYCTDKGNVVT 349
```

### 5.1.2 Section 1.3

## Supplementary Material to the Publication

### Mastering the Gram-Negative Bacterial Barrier – Chemical Approaches to Increase Bacterial Bioavailability of Antibiotics

Henni-Karoliina Ropponen\*, Robert Richter\*, Anna K. H. Hirsch#, Claus-Michael Lehr#

**Abstract:** To win the battle against resistant, pathogenic bacteria, novel classes of anti-infectives and targets are urgently needed. Bacterial uptake, distribution, metabolic and efflux pathways of antibiotics in Gram-negative bacteria determine what we here refer to as bacterial bioavailability. Understanding these mechanisms from a chemical perspective is essential for anti-infective activity and hence, drug discovery as well as drug delivery. A systematic and critical discussion of *in bacterio*, *in vitro* and *in silico* assays reveals that a sufficiently accurate holistic approach is still missing. We expect new findings based on Gram-negative bacterial bioavailability to guide future anti-infective research.

# E-mail: Anna.Hirsch@helmholtz-hips.de or Claus-Michael.Lehr@helmholtz-hips.de

## 2.2. Application of this concept to clinically approved antibiotic classes

**Table S1.** Classes of antibiotics for the treatment of Gram-negative infections and representatives

Antibiotic class		Panel
Aminoglycosides		Streptomycin, Tobramycin, Kanamycin, Amikacin
Penicillins		Ampicillin, Amoxicillin Piperacillin, Sultamicillin, Pivampicillin, Bacampicillin
Cephems		Cefuroxime, Ceftibuten, Flomoxef, Cefminox, Loracarbef
Carbapenems		Imipenem, Meropenem, Ertapenem, Doripenem, Thienamycin
Monobactams		Tabtoxin, Aztreonam, Carumonam Nocardicin A, Tigemonam
β-Lactamase inhibitors	1 <sup>st</sup> Generation	Clavulanic acid Enmetazobactam Sulbactam Tazobactam
	2 <sup>nd</sup> Generation	Avibactam Durlobactam Nacubactam Relebactam Zidebactam
	3 <sup>rd</sup> Generation	Taniborbactam Vaborbactam
Fluoroquinolones		Ciprofloxacin, Sparfloxacin, Gemifloxacin, Garenoxacin, Clinafloxacin, Prulifloxacin
Tetracyclines		Tetracycline, Minocycline, Tigecycline, Meclocycline, Lymecycline
Sulfonamides		Sulfamethoxazole, Sulfaguanidin, Sulfadimidin, Sulfadoxin
Polymyxins		Colistin A, Colistin B, Polymyxin A, Polymyxin B

## 5.2 Supplementary Material of Chapter A

### Table of Contents

<b>5.2.1) Structure-Based Virtual Screening .....</b>	<b>106</b>
5.2.1.1 General Workflow .....	106
5.2.1.2 Summary of Purchased Compounds .....	109
<b>5.2.2.) Biological Assays .....</b>	<b>114</b>
5.2.2.1 General Procedure for Enzymatic Assay .....	114
5.2.2.2 General Procedure for Antibacterial Assay .....	114
5.2.2.3 General Procedure for Cytotoxicity Assay .....	114
5.2.2.4 Summary of Biological Results .....	115
5.2.2.5 <i>Bacillus subtilis</i> Experiments .....	123
<b>5.2.3.) Biophysical Assays .....</b>	<b>128</b>
5.2.3.1 Thermal Shift Assay .....	128
5.2.3.2 Microscale Thermophoresis .....	129
5.2.3.3 Saturation-Transfer Difference Nucleomagnetic Resonance .....	130
<b>5.2.4.) SuFEx Probe.....</b>	<b>133</b>
<b>5.2.5.) Synthesis .....</b>	<b>136</b>
5.2.5.1 General Conditions.....	136
5.2.5.2 General Procedures .....	136
5.2.5.3 Synthesised Compounds .....	138

## 5.2.1. Structure-Based Virtual Screening

### 5.2.1.1 General Workflow

#### *Prediction of Druggable Pockets*

DoGSiteScorer was used to identify druggable pockets for *Escherichia coli* IspE (PDB 1OJ4).<sup>119,120</sup> Overall, only P\_0 with the druggability score of 0.81 was above the ideal druggability score (>0.80). Thus, pocket P\_0 was selected as the binding pocket, occupying the main catalytic region in monomer A (Figure 3.1:1).

#### **Descriptors of the P\_0 pocket**

##### **Size and shape descriptors**

volume = 809.93 Å<sup>3</sup>  
surface = 1210.48 Å<sup>2</sup>  
depth = 18.80 [Å]  
ellipsoid main axis ratio c/a = 0.17  
ellipsoid main axis ratio b/a = 0.43  
enclosure = 0.16

##### **Element descriptors**

# pocket atoms = 163  
# carbons = 108  
# nitrogens = 27  
# oxygens = 27  
# sulfurs = 1  
# other elements = 0

##### **Functional group descriptors**

# hydrogen bond donors = 23  
# hydrogen bond acceptors = 55  
# metals = 0  
# hydrophobic interactions = 65  
hydrophobicity ratio = 0.45

##### **Amino acid composition**

apolar amino acid ratio = 0.39  
polar amino acid ratio = 0.41  
positive amino acid ratio = 0.12  
negative amino acid ratio = 0.07

##### **Amino acid descriptors**

# ALA = 3  
# ARG = 0  
# ASN = 1  
# ASP = 2  
# CYS = 1  
# GLN = 1  
# GLU = 1  
# GLY = 9  
# HIS = 2  
# ILE = 1  
# LEU = 5  
# LYS = 3  
# MET = 0  
# PHE = 2  
# PRO = 2  
# SER = 1  
# THR = 3  
# TRP = 0  
# TYR = 1  
# VAL = 3

### *Virtual Screening Compounds*

The compound library was obtained from SPECS containing in total 106, 801 compounds. The library consisted of compounds with MW 250–500 Da fulfilling the Lipinski's rule of five<sup>121</sup> and any promiscuous compounds were filtering out by applying PAINS<sup>122</sup> and Eli Lilly rules.<sup>123,124</sup> Additionally, only compounds that were available (>2 mg) at the time of the library creation were included.

### *Protein Preparation*

The crystal structure of *Escherichia coli* IspE (PDB 1OJ4)<sup>118</sup> in the absence of the co-crystallised ligands, ATP and CDP-ME, was used for the virtual screening. The binding pocket was defined by selecting the following amino acids manually, as obtained in the druggability assessment: LYS10, ASN12, LEU15, GLN20, GLY24A, TYR25A, HIS26A, LEU28, THR30, PHE32, PRO99, GLY101, GLY102, GLY103, LEU104, GLY105, LEU136, GLY139, ALA140, ASP141, VAL144, ALA153, VAL156, GLY157, GLU158, LEU160, HIS174, VAL177, SER178, ILE179, THR181, PRO182, PHE185, LYS186, GLY239, THR240, GLY241, ALA242, CYS243, LYS76 (chain B) and ASP80 (chain B).

### *Virtual Screening*

The KNIME Analytics Platform<sup>125,126</sup> was used to run the virtual screening workflow using the following nodes (Generate 3D Coordinates, LeadIT, SeeSAR) from BioSolveIT. First, the 3D-coordinates were generated and then compounds were docked by using LeadIT (version 2.3.2).<sup>83</sup> The default settings were used for docking and for each molecule, ten poses were calculated. The resulting poses were then scored using the HYDE function in SeeSAR (version 8.1).<sup>82</sup> The compounds were filtered based on binding affinities, torsional angles and number of poses. Compounds with red-flagged torsional angles and compounds having a low binding affinity (>1 mM) were filtered out. For the remaining set of compounds, compounds only with a single pose fulfilling the stricter criteria were removed.

### *Filtering based on the eNTRY rules and StarDrop Antibacterial Scoring Profile*

Globularity and amphiphilic moment of the compounds was calculated using MOE (Molecular Operating Environment, version 2018.1). The compound filtering was completed using StarDrop (version 6.5.1) with the additional functions to calculate the number of rotatable bonds and filters to identify ionisable amines were performed in StarDrop. Compounds with high number of rotatable bonds (>5) and high globularity (>0.25) were filtered out. All 3D parameters were calculated for the docked poses. The Antibacterial Scoring Profile<sup>84</sup> was calculated in StarDrop and compounds with a score of 0.4–0.6 were considered ideal.

### Visual Inspection

Using the SeeSAR evaluation node in StarDrop, the poses were analysed visually for ideal interactions and consistency of the binding modes. Additionally, compounds were screened for PAINS and compounds with high similarity of ChEMBL (>0.9) and PDB (>0.7) were filtered out. The best compounds were clustered and a final selection of total 24 compounds was made. The compounds were purchased from SPECS and used for biological testing without further purification in DMSO stock solutions. The compound purchased were in >90% purity.

**Table S5.2.1.1:1** - The purchased compounds in their categories.

Category	Number of Compounds
Ionisable primary amine/globularity/rotatable bonds ( <i>1ry amine</i> )	3
Ionisable secondary amine/globularity/rotatable bonds ( <i>2ry amine</i> )	2
Ionisable tertiary amine/globularity/rotatable bonds ( <i>3ry amine</i> )	3
Non-ionisable primary amine/globularity/rotatable bonds ( <i>-sNH<sub>2</sub></i> )	7
Scoring Profile (0.4–06) ( <i>Scoring</i> )	4
High HYDE Affinity ( $\leq 500$ nM) ( <i>HYDE</i> )	6



## 5.2.1.2 Summary of Purchased Compounds

Table S5.2.1.2:1 - Virtual screening hits – Section 1.

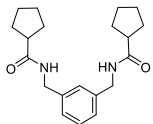
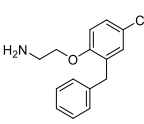
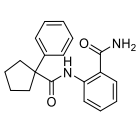
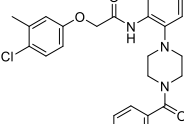
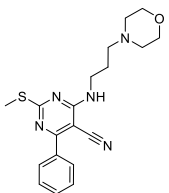
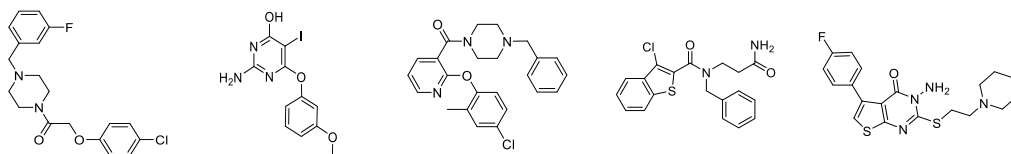
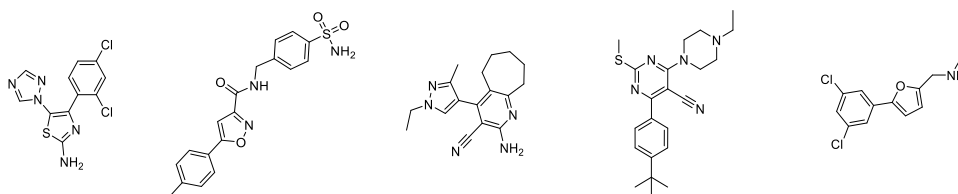
					
	HIPS5241	HIPS5242	HIPS5243	HIPS5244	HIPS5245
<b>Virtual Screening</b>					
<b>SPECS ID</b>	AK-968/ 41926654	AO-080/ 43442029	AP-970/ 43482379	AP-970/ 42444960	AS-871/ 43477312
<b>Filter category</b>	HYDE	1ry amine	HYDE	HYDE	HYDE
<b>HYDE estimated affinity lower boundary (nM)<sup>[a]</sup></b>	58.3	88.7	104.3	120.3	198.9
<b>HYDE estimated affinity upper boundary (nM)<sup>[a]</sup></b>	5794	8809	1.036e+04	1.196e+04	1.976e+04
<b>Torsion Quality<sup>[a]</sup></b>	yellow	yellow	yellow	yellow	yellow
<b>Docking E total<sup>[a]</sup></b>	-20.31	-13.53	-22.7	-25.45	-24.8
<b>Globularity<sup>[b]</sup></b>	0.1321	0.1085	0.1478	0.0800	0.0544
<b>Rotatable bonds<sup>[c]</sup></b>	6	5	4	6	7
<b>Ionisable amine<sup>[c]</sup></b>	N/A	1ry amine	N/A	N/A	3ry amine
<b>Amphiphilic Moment<sup>[b]</sup></b>	0.8374	4.7429	4.6133	2.8772	3.4566
<b>Gram-negative antibacterial scoring profile_Score<sup>[c]</sup></b>	0.0001381	1.073e-08	0.01162	0.01887	0.1664
<b>Enzyme Activity</b>					
<b><i>Ec</i>Ispe IC<sub>50</sub> (μM)</b>	>500	>500	>500	144 ± 7	>500
<b>PK/LDH IC<sub>50</sub> (μM)</b>	n.d.	n.d.	n.d.	39 ± 19	n.d.
<b>T<sub>m</sub>(°C) (ΔT<sub>m</sub>(°C))<sup>[d]</sup></b>	n.d.	50.42 ± 0.09 (-1.1)	n.d.	51.31 ± 0.37 (-0.2)	n.d.
<b>Antibacterial Activity (Minimum Inhibitory Concentration or Percentage inhibition @ 100 μM)</b>					
<b><i>E. coli</i> K12</b>	>50	99 ± 2	>100	>50	>50
<b><i>E. coli</i> Δ<i>tolC</i></b>	>50	97 ± 4	>100	>50	>50
<b><i>B. subtilis</i></b>	>50	>100 <sup>[e]</sup>	>100	>50	>50
<b><i>S. aureus</i></b>	n.d.	47 ± 8%	n.d.	n.d.	n.d.
<b><i>P. aeruginosa</i></b>	n.d.	52 ± 10%	n.d.	n.d.	n.d.
<b><i>A. baumannii</i></b>	n.d.	100 ± 0	n.d.	n.d.	n.d.
<b>Cytotoxicity</b>					
<b>HepG2</b>	n.d.	IC <sub>50</sub> = 21 ± 1 μM	n.d.	n.d.	n.d.
<b>Hek293</b>	n.d.	IC <sub>50</sub> = 14 μM*	n.d.	n.d.	n.d.
<b>A549</b>	n.d.	IC <sub>50</sub> = 29 μM*	n.d.	n.d.	n.d.
[a] BioSolveIT (LeadIT 2.3.2 and SeeSAR 8.1) [b] MOE 2018.01 [c] StarDrop v. 6.5.1 [d] See reference Table S5.2.3.1:1 for the blank protein. [e] Anomalous kinetics. Refer to Section 5.2.2.5 for more details. [f] <i>Klebsiella pneumoniae</i> MIC = 100 ± 0.0 μM, measured at MINS-HIPS. n.d.: not determined, N/A: not applicable. * Value of a single measurement.					

Table S5.2.1.2:2 - Virtual screening hits – Section 2.



	HIPS5246	HIPS5247	HIPS5248	HIPS5249	HIPS5250
<i>Virtual Screening</i>					
<b>SPECS ID</b>	AT-057/ 43313800	AG-670/ 11098007	AO-990/ 15068150	AN-329/ 43465228	AO-476/ 43417219
<b>Filter category</b>	3ry amine	Scoring (0.4-0.6)	HYDE	HYDE	3ry amine
<b>HYDE estimated affinity lower boundary (nM)<sup>[a]</sup></b>	416.8	741.2	7.529	11.24	516.3
<b>HYDE estimated affinity upper boundary (nM)<sup>[a]</sup></b>	4.141e+04	7.364e+04	748	1117	5.13e+04
<b>Torsion Quality<sup>[a]</sup></b>	green	green	yellow	yellow	yellow
<b>Docking E total<sup>[a]</sup></b>	-19.26	-26.96	-21.8	-19.66	-27.74
<b>Globularity<sup>[b]</sup></b>	0.03966	0.2713	0.08249	0.09595	0.07712
<b>Rotatable bonds<sup>[c]</sup></b>	5	3	5	6	5
<b>Ionisable amine<sup>[c]</sup></b>	3ry amine	N/A	3ry amine	N/A	3ry amine
<b>Amphiphilic Moment<sup>[b]</sup></b>	3.1070	5.1538	2.7088	1.5968	3.7062
<b>Gram-negative antibacterial scoring profile_Score<sup>[c]</sup></b>	1.224e-09	0.5045	1.609e-09	0.00199	0.005626
<i>Enzyme Activity</i>					
<b>EcIspE IC<sub>50</sub> (μM)</b>	>500	>500	>500	>500	239 ± 7
<b>PK/LDH IC<sub>50</sub> (μM)</b>	n.d.	n.d.	n.d.	n.d.	>500
<b>T<sub>m</sub>(°C) (ΔT<sub>m</sub> (°C))<sup>[d]</sup></b>	n.d.	n.d.	n.d.	n.d.	50.75 ± 0.08 (-0.8)
<i>Antibacterial Activity (Minimum Inhibitory Concentration or Percentage Inhibition @ 100 μM)</i>					
<b>E. coli K12</b>	>50	>100	>50	>50	10 ± 3%
<b>E. coli ΔtolC</b>	>50	>100	>50	>50	49 ± 6%
<b>B. subtilis</b>	>50	>100	>50	>50	>100
<b>S. aureus</b>	n.d.	n.d.	n.d.	n.d.	n.d.
<b>P. aeruginosa</b>	n.d.	n.d.	n.d.	n.d.	n.d.
<b>A. baumannii</b>	n.d.	n.d.	>50	n.d.	n.d.
<i>Cytotoxicity</i>					
<b>HepG2</b>	n.d.	n.d.	n.d.	n.d.	n.d.
<b>Hek293</b>	n.d.	n.d.	n.d.	n.d.	n.d.
<b>A549</b>	n.d.	n.d.	n.d.	n.d.	n.d.
[a] BioSolveIT (LeadIT 2.3.2 and SeeSAR 8.1) [b] MOE 2018.01 [c] StarDrop v. 6.5.1 [d] See reference Table S5.2.3.1:1 for the blank protein. n.d.: not determined, N/A: not applicable.					

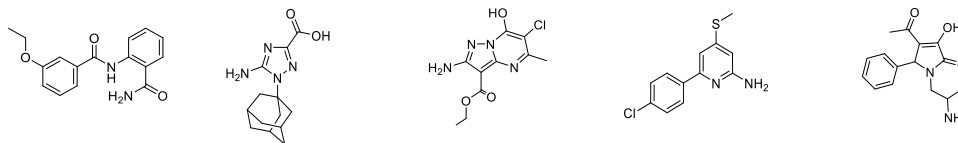
Table S5.2.1.2:3 - Virtual screening hits – Section 3.



	HIPS5251	HIPS5252	HIPS5253	HIPS5254	HIPS5255
<i>Virtual Screening</i>					
<b>SPECS ID</b>	AG-205/ 40649878	AS-871/ 43475260	AK-968/ 41017405	AS-871/ 43477283	AN-465/ 43411641
<b>Filter category</b>	-sNH <sub>2</sub>	-sNH <sub>2</sub>	-sNH <sub>2</sub>	3ry amine	2ry amine
<b>HYDE estimated affinity lower boundary (nM)<sup>[a]</sup></b>	790.8	808.7	1301	1608	1938
<b>HYDE estimated affinity upper boundary (nM)<sup>[a]</sup></b>	7.857e+04	8.035e+04	1.292e+05	1.597e+05	1.925e+05
<b>Torsion Quality<sup>[a]</sup></b>	green	yellow	green	green	green
<b>Docking E total<sup>[a]</sup></b>	-21.06	-31.89	-22.87	-21.27	-15.52
<b>Globularity<sup>[b]</sup></b>	0.0849	0.02412	0.1226	0.07662	0.05732
<b>Rotatable bonds<sup>[c]</sup></b>	2	5	2	5	3
<b>Ionisable amine<sup>[c]</sup></b>	N/A	N/A	N/A	3ry amine	2ry amine
<b>Amphiphilic Moment<sup>[b]</sup></b>	2.5254	7.1005	2.9562	2.6410	4.5464
<b>Gram-negative antibacterial scoring profile_Score<sup>[c]</sup></b>	0.02025	0.1208	0.05725	7.622e-09	4.249e-09
<i>Enzyme Activity</i>					
<b>EcIspE IC<sub>50</sub> (μM)</b>	>500	29 ± 5	>500	>500	356*
<b>PK/LDH IC<sub>50</sub> (μM)</b>	n.d.	21 ± 6	n.d.	n.d.	n.d.
<b>T<sub>m</sub>(°C) (ΔT<sub>m</sub> (°C))<sup>[d]</sup></b>	n.d.	51.79 ± 0.12 (+0.3)	n.d.	51.23 ± 0.09 (-0.3)	50.81 ± 0.09 (-0.7)
<i>Antibacterial Activity (Minimum Inhibitory Concentration or Percentage inhibition @ 100 μM)</i>					
<b><i>E. coli</i> K12</b>	>100	>50	>100	>50	71 ± 6%
<b><i>E. coli</i> ΔtolC</b>	>100	>50	>100	33 ± 16 (MIC)	74 ± 4%
<b><i>B. subtilis</i></b>	>100	>50	>100	91 ± 4%	>100 <sup>[e]</sup>
<b><i>S. aureus</i></b>	n.d.	n.d.	n.d.	>50	13 ± 16%
<b><i>P. aeruginosa</i></b>	n.d.	n.d.	n.d.	>100	25 ± 11%
<b><i>A. baumannii</i></b>	n.d.	n.d.	n.d.	>50	41 ± 28%
<i>Cytotoxicity</i>					
<b>HepG2</b>	n.d.	n.d.	n.d.	% inh. 85 ± 1 @ 50 μM	IC <sub>50</sub> 25 ± 2 μM
<b>Hek293</b>	n.d.	n.d.	n.d.	% inh. 81 ± 0 @ 50 μM	IC <sub>50</sub> 20 μM*
<b>A549</b>	n.d.	n.d.	n.d.	% inh. 22 ± 13 @ 50 μM	IC <sub>50</sub> 42 ± 2 μM

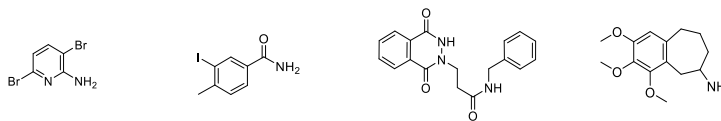
[a] BioSolveIT (LeadIT 2.3.2 and SeeSAR 8.1) [b] MOE 2018.01 [c] StarDrop v. 6.5.1 [d] See reference Table S5.2.3.1:1 for blank protein. [e] Anomalous kinetics. Refer to Section 5.2.2.5 for more details. n.d.: not determined, N/A: not applicable. \*Value of a single measurement.

Table S5.2.1.2:4 - Virtual screening hits – Section 4.



	HIPS5256	HIPS5257	HIPS5258	HIPS5259	HIPS5260
<i>Virtual Screening</i>					
<b>SPECS ID</b>	AP-970/ 41518174	AK-968/ 40064644	AE-641/ 11517590	AT-417/ 43484814	AQ-149/ 43285071
<b>Filter category</b>	-sNH <sub>2</sub>	Scoring (0.4-0.6)	Scoring (0.4-0.6)	-sNH <sub>2</sub>	1ry amine
<b>HYDE estimated affinity lower boundary (nM)<sup>[a]</sup></b>	2936	3447	5527	6472	9195
<b>HYDE estimated affinity upper boundary (nM)<sup>[a]</sup></b>	2.917e+05	3.425e+05	5.492e+05	6.43e+05	9.136e+05
<b>Torsion Quality<sup>[a]</sup></b>	green	green	green	yellow	green
<b>Docking E total<sup>[a]</sup></b>	-27.46	-15.34	-23.68	-18.23	-15.51
<b>Globularity<sup>[b]</sup></b>	0.01951	0.1926	0.05019	0.102	0.0847
<b>Rotatable bonds<sup>[c]</sup></b>	5	2	3	2	4
<b>Ionisable amine<sup>[c]</sup></b>	N/A	N/A	N/A	N/A	1ry amine
<b>Amphiphilic Moment<sup>[b]</sup></b>	4.1186	5.6843	3.4603	5.2405	4.6577
<b>Gram-negative antibacterial scoring profile_Score<sup>[c]</sup></b>	0.02997	0.4238	0.4706	6.881e-09	0.08908
<i>Enzyme Activity</i>					
<b>EcIspE IC<sub>50</sub> (μM)</b>	>500	>500	>500	349*	>500
<b>PK/LDH IC<sub>50</sub> (μM)</b>	n.d.	n.d.	n.d.	n.d.	n.d.
<b>T<sub>m</sub>(°C) (ΔT<sub>m</sub> (°C))<sup>[d]</sup></b>	n.d.	n.d.	n.d.	51.23 ± 0.13 (-0.3)	n.d.
<i>Antibacterial Activity (Minimum Inhibitory Concentration or Percentage inhibition @ 100 μM)</i>					
<b><i>E. coli</i> K12</b>	>100	>100	>100	>50	>50
<b><i>E. coli</i> ΔtolC</b>	>100	>100	>100	>50 (91% @ 100 μM*)	>50
<b><i>B. subtilis</i></b>	>100	>100	>100	>50	>50
<b><i>S. aureus</i></b>	n.d.	n.d.	n.d.	n.d.	n.d.
<b><i>P. aeruginosa</i></b>	n.d.	n.d.	n.d.	n.d.	n.d.
<b><i>A. baumannii</i></b>	n.d.	n.d.	n.d.	n.d.	n.d.
<i>Cytotoxicity</i>					
<b>HepG2</b>	n.d.	n.d.	n.d.	n.d.	n.d.
<b>Hek293</b>	n.d.	n.d.	n.d.	n.d.	n.d.
<b>A549</b>	n.d.	n.d.	n.d.	n.d.	n.d.
[a] BioSolveIT (LeadIT 2.3.2 and SeeSAR 8.1) [b] MOE 2018.01 [c] StarDrop v. 6.5.1 [d] See reference Table S5.2.3.1:1 for blank protein. n.d.: not determined, N/A: not applicable					

Table S5.2.1.2:5 - Virtual screening hits – Section 5.



	HIPS5261	HIPS5262	HIPS5263	HIPS5264
<i>Virtual Screening</i>				
<b>SPECS ID</b>	AC907/ 34104030	AN-329/ 41437602	AJ-292/ 41083380	AE-848/ 34162059
<b>Filter category</b>	-sNH <sub>2</sub>	-sNH <sub>2</sub>	Scoring (0.4–0.6)	1ry amine
<b>HYDE estimated affinity lower boundary (nM)<sup>[a]</sup></b>	1.108e+04	1.795e+04	1.291e+04	1.487e+04
<b>HYDE estimated affinity upper boundary (nM)<sup>[a]</sup></b>	1.101e+06	1.784e+06	1.283e+06	1.477e+06
<b>Torsion Quality<sup>[a]</sup></b>	not rotatable	green	green	green
<b>Docking E total<sup>[a]</sup></b>	-12.67	-17.13	-23.13	-14.23
<b>Globularity<sup>[b]</sup></b>	0.01404	0.02625	0.05944	0.0717
<b>Rotatable bonds<sup>[c]</sup></b>	0	1	5	3
<b>Ionisable amine<sup>[c]</sup></b>	N/A	N/A	N/A	1ry amine
<b>Amphiphilic Moment<sup>[b]</sup></b>	4.3979	5.8192	1.1035	4.2183
<b>Gram-negative antibacterial scoring profile_Score<sup>[c]</sup></b>	3.216e-08	2.54e-08	0.5087	3.398e-08
<i>Enzyme Activity</i>				
<b>EcIspE IC<sub>50</sub> (μM)</b>	>500	>500	>500	>500
<b>PK/LDH IC<sub>50</sub> (μM)</b>	n.d.	n.d.	n.d.	n.d.
<b>T<sub>m</sub>(°C) (ΔT<sub>m</sub> (°C))<sup>[d]</sup></b>	n.d.	n.d.	n.d.	n.d.
<i>Antibacterial Activity (Minimum Inhibitory Concentration or Percentage inhibition @ 100 μM)</i>				
<b><i>E. coli</i> K12</b>	>100	>100	>100	>100
<b><i>E. coli</i> ΔtolC</b>	>100	>100	>100	>100
<b><i>B. subtilis</i></b>	>100	>100	>100	>100
<b><i>S. aureus</i></b>	n.d.	n.d.	n.d.	n.d.
<b><i>P. aeruginosa</i></b>	n.d.	n.d.	n.d.	n.d.
<b><i>A. baumannii</i></b>	n.d.	n.d.	n.d.	n.d.
<i>Cytotoxicity</i>				
<b>HepG2</b>	n.d.	n.d.	n.d.	n.d.
<b>Hek293</b>	n.d.	n.d.	n.d.	n.d.
<b>A549</b>	n.d.	n.d.	n.d.	n.d.
[a] BioSolveIT (LeadIT 2.3.2 and SeeSAR 8.1) [b] MOE 2018.01 [c] StarDrop v. 6.5.1 [d] See reference Table S5.2.3.1:1 for blank protein. n.d.: not determined, N/A: not applicable				

## 5.2.2. Biological Assays

### 5.2.2.1 General Procedure for IspE Enzymatic Assay

The assay was performed as in Publication 2 (H.-K. Ropponen *et al.*, *RSC Med. Chem.*, **2021**, DOI: 10.1039/d0md00409j.)

### 5.2.2.2 General Procedure for Antibacterial Assays

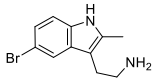
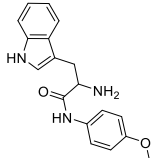
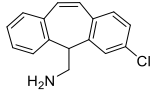
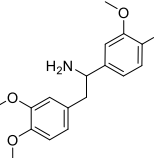
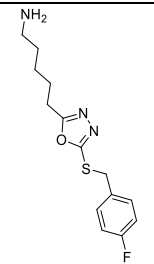
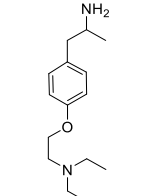
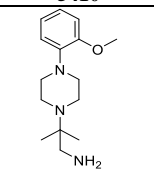
Assays regarding the determination of the minimum inhibitory concentration (MIC) were performed as described previously.<sup>127</sup> The experiments were based on a variety of *E. coli* strains/mutants (K12, D22,  $\Delta tolC$ ,  $\Delta acrB$  and BL21(DE3)omp8) as well as *B. subtilis*, *S. aureus* (Newman strains), *P. aeruginosa* (PA14,  $\Delta oprF$ ,  $\Delta ompH$ ,  $\Delta mexB$  and  $\Delta mexA$ ) and *A. baumannii* (DSM30007). In the case, no MIC value could be determined due to activity reasons, percentage (%) inhibition at 100  $\mu$ M (or lower, depending on the solubility of the compounds) was determined. While for these general MIC determinations the OD at 600 nm was determined after a final time point (16 h after inhibitor addition), we additionally recorded a time curve for *B. subtilis*. For this purpose, ODs were measured every 400 s over a period of 17 h in a CLARIOstar Platerereader (BMG Labtech, Ortenberg, Germany), followed by a graphical representation made with Python 3.8.3 using *Matplotlib* 3.2.2, *NumPy* 1.18.5, *xlrd* 1.2.0 and *re* 2.2.1 functions.<sup>128</sup> See Section 5.2.2.5.

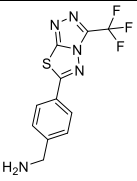
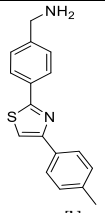
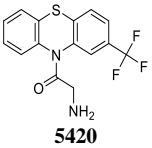
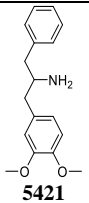
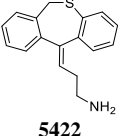
### 5.2.2.3 General Procedure for Cytotoxicity Assay

Cytotoxicity assays based on the human hepatocellular carcinoma (HepG2), human embryonic kidney (Hek293) and human lung adenocarcinoma (A549) cell lines were performed as described previously.<sup>129</sup>

## 5.2.2.4 Summary of Biological Results

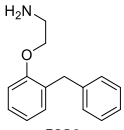
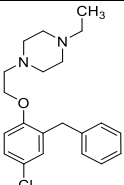
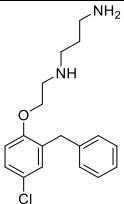
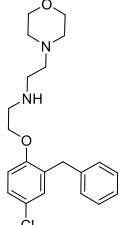
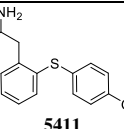
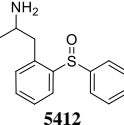
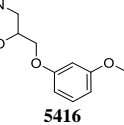
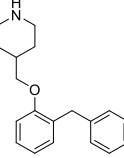
Table S5.2.2.4:1 - Other ordered primary amines from the SPECS library.

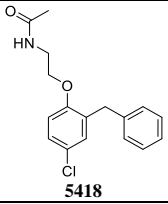
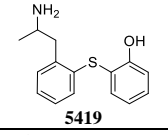
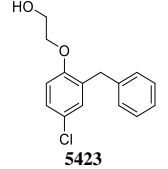
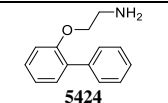
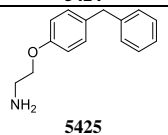
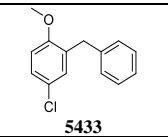
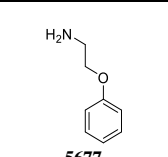
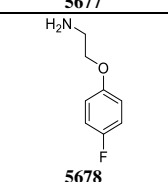
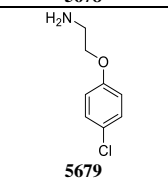
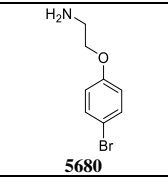
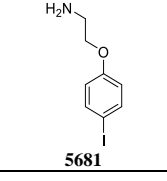
Structure and HIPS code	SPECS ID	<i>EcIspE</i> IC <sub>50</sub> (μM) <sup>[a]</sup>	PK/LDH IC <sub>50</sub> (μM)	Percentage Inhibition @ 100 μM			
				<i>E. coli</i> K12	<i>E. coli</i> Δ <i>tolC</i>	<i>P. aeruginosa</i>	<i>A. baumannii</i>
 <b>5405</b>	AG-205/ 14785177	>500	n.d.	21 ± 10	28 ± 3	12 ± 4	14 ± 1
 <b>5406</b>	AG-690/ 15435945	>500	n.d.	4 ± 1	40 ± 6	n.d.	6 ± 1
 <b>5407</b>	AE-641/ 06348040	>500	n.d.	50 ± 8	81 ± 0	23 ± 9	34 ± 4
 <b>5408</b>	AE-848/ 30721050	>500	n.d.	4 ± 7	6 ± 2	n.d.	n.d.
 <b>5409</b>	AS-871/ 43475867	>500	n.d.	9 ± 12	23 ± 5	n.d.	n.d.
 <b>5410</b>	AE-641/ 00601040	>500	n.d.	4 ± 0	14 ± 4	n.d.	n.d.
 <b>5413</b>	AS-871/ 43387350	>500	n.d.	-1 ± 6	6 ± 3	n.d.	n.d.

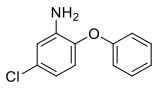
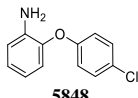
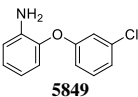
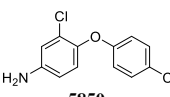
 <p><b>5414</b></p>	AP-970/ 43492176	>500	n.d.	6 ± 11	14 ± 1	n.d.	n.d.
 <p><b>5415<sup>[b]</sup></b></p>	AS-871/ 43475210	>500	n.d.	76 ± 16	MIC 98 ± 11	16 ± 4	9 ± 4 (@ 50 μM)
 <p><b>5420</b></p>	AG-690/ 13702538	>500	n.d.	7 ± 4	66 ± 6	8 ± 4	2 ± 0
 <p><b>5421</b></p>	AE-641/ 30115007	>500	n.d.	8 ± 1	13 ± 3	n.d.	n.d.
 <p><b>5422</b></p>	AE-641/ 30153055	>500	n.d.	57 ± 4	79 ± 1	24 ± 11	24 ± 3
<p>[a] Where <i>Ec</i>SpE activity was measured as IC<sub>50</sub> &gt;500 μM, no replicate or pyruvate kinase and lactate dehydrogenase (PK/LDH) inhibition was determined. [b] <b>HIPSS415</b> HepG2 IC<sub>50</sub> = 19 ± 3 μM and <i>S. aureus</i> MIC = 26 ± 1 μM. n.d.: not determined.</p>							



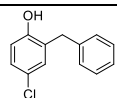
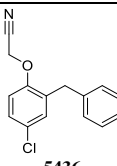
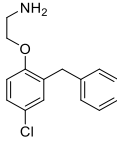
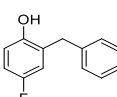
**Table S5.2.2.4:2** - Summary of biological data for the commercially available derivatives.

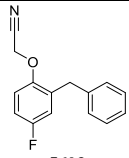
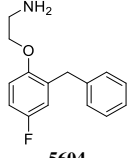
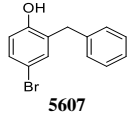
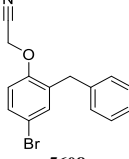
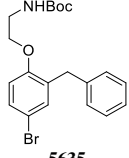
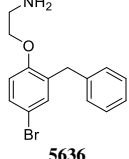
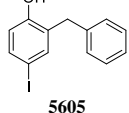
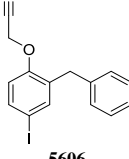
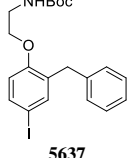
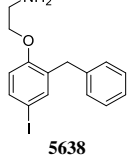
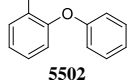
Structure and HIPS code	External code	EclspE IC <sub>50</sub> (μM) <sup>[a]</sup>	PK/LDH IC <sub>50</sub> (μM)	Percentage Inhibition @ 100 μM or Minimum Inhibitory Concentration (MIC)								
				<i>E. coli</i> K12	<i>E. coli</i> Δ <i>tolC</i>	<i>E. coli</i> Δ <i>acrB</i>	<i>E. coli</i> D22	<i>E. coli</i> Omp8	<i>A. baumannii</i>	<i>P. aeruginosa</i>	<i>S. aureus</i>	HepG2
 <b>5380</b>	Ambinter 6870079	>500	n.d.	31 ± 5	41 ± 0	42 ± 1	-3 ± 19	3 ± 1	22 ± 1	-2 ± 4	11 ± 7	88 ± 5
 <b>5381</b>	Ambinter 8604646	>500	n.d.	17 ± 8	MIC 48 ± 4	MIC 95*	40%*	n.d.	25 ± 5	5 ± 10	35 ± 16	94 ± 4
 <b>5382</b>	Ambinter 8612987	>500	n.d.	83 ± 4	MIC 80 ± 14	MIC 80 ± 0	MIC 93 ± 4	n.d.	MIC 100 ± 0	MIC 95 ± 0	MIC 103 ± 4	93 ± 5
 <b>5383</b>	Ambinter 8612833	>500	n.d.	16 ± 7	MIC 80 ± 7	MIC 95*	35%*	n.d.	14 ± 4	15 ± 5	33 ± 13	93 ± 4
 <b>5411</b>	SPECS AE-641/30177026	447 ± 95*	n.d.	33 ± 4	47 ± 20	n.d.	n.d.	n.d.	18 ± 2	5 ± 4	15 ± 8	79 ± 12 (IC <sub>50</sub> = 45 ± 6)
 <b>5412</b>	SPECS AE-641/30177033	>500	n.d.	12 ± 1	7 ± 2	n.d.	n.d.	n.d.	8 ± 0	3 ± 1	4 ± 5	-4 ± 20
 <b>5416</b>	SPECS AP-124/43382853	>500	n.d.	28 ± 5	40 ± 4	n.d.	n.d.	n.d.	12 ± 0	10 ± 8	-2 ± 2	85 ± 5
 <b>5417</b>	SPECS AN-329/43448394	>500	n.d.	13 ± 11	85 ± 8	MIC 108 ± 4	67 ± 4	58 ± 5	14 ± 6	43 ± 9	20 ± 10	93 ± 3 (IC <sub>50</sub> = 21 ± 4)

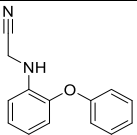
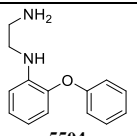
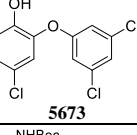
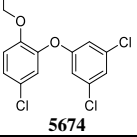
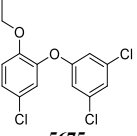
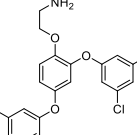
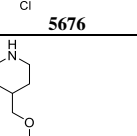
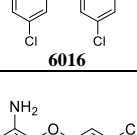
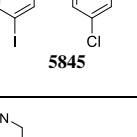
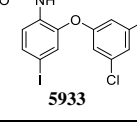
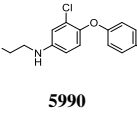
 <b>5418</b>	SPECS AO-080/ 43441925	>500	n.d.	8 ± 8	MIC 88 ± 11	30 ± 12 @50 μM	34 ± 6 @50 μM	-6 ± 7 @50 μM	2 ± 1 @50 μM	1 ± 1 @50 μM	22 ± 6	48 ± 4
 <b>5419</b>	SPECS AE-641/ 30177024	>500	n.d.	48 ± 3	MIC 57 ± 7	52 ± 3	7 ± 0	n.d.	19 ± 1	5 ± 1	14 ± 16	91 ± 2 (IC <sub>50</sub> = 47*)
 <b>5423</b>	Enamine Z1182353 799	>500	n.d.	27 ± 3	MIC 50 ± 0	MIC 103 ± 3	22 ± 4	MIC 104 ± 2	-2 ± 3 @50 μM	5 ± 2	32 ± 21	78 ± 13
 <b>5424</b>	Enamine Z5792159 5	>500	n.d.	42 ± 6	28 ± 11	n.d.	n.d.	n.d.	22 ± 4	6 ± 0	-1 ± 11	38 ± 2
 <b>5425</b>	Enamine Z2901973 293	>500	n.d.	41 ± 9	45 ± 15	n.d.	n.d.	n.d.	13 ± 4	12 ± 1	6 ± 10	51 ± 8
 <b>5433</b>	Enamine Z5418217 4	>500	n.d.	-2 ± 13 @50 μM	49 ± 1	n.d.	n.d.	n.d.	-2 ± 4 @50 μM	4 ± 1	36 ± 27	1 ± 10
 <b>5677</b>	CAS 17959-64- 7	n.d.	n.d.	3 ± 3	9 ± 7	n.d.	n.d.	n.d.	n.d.	n.d.	-6 ± 10	n.d.
 <b>5678</b>	CAS 263409- 81-0	n.d.	n.d.	4 ± 1	9 ± 4	n.d.	n.d.	n.d.	n.d.	n.d.	n.d.	n.d.
 <b>5679</b>	CAS 106038- 00-0	n.d.	n.d.	5 ± 0	5 ± 3	11 ± 3	n.d.	n.d.	n.d.	n.d.	n.d.	9 ± 1
 <b>5680</b>	CAS 663941- 79-5	n.d.	n.d.	-1 ± 6	8 ± 1	n.d.	n.d.	n.d.	n.d.	n.d.	n.d.	n.d.
 <b>5681</b>	CAS 151978- 97-1	n.d.	n.d.	-3 ± 1	10 ± 5	18 ± 2	n.d.	n.d.	n.d.	n.d.	-31 ± 8	-5 ± 3

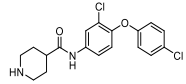
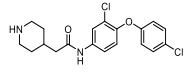
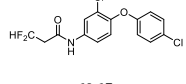
 <b>5847</b>	CAS 93-67-4	n.d.	n.d.	27 ± 5	MIC 100 ± 0	n.d.	n.d.	n.d.	n.d.	n.d.	n.d.	20 ± 8
 <b>5848</b>	CAS 2770-11-8	n.d.	n.d.	21 ± 0	29 ± 5	n.d.	n.d.	n.d.	n.d.	n.d.	n.d.	58 ± 5 (IC <sub>50</sub> = 92±18)
 <b>5849</b>	CAS 76838-73-8	n.d.	n.d.	4 ± 5	27 ± 6	n.d.	n.d.	n.d.	n.d.	n.d.	n.d.	51 ± 7
 <b>5850</b>	CAS 24900-79-6	n.d.	n.d.	28 ± 8	MIC 45 ± 1	n.d.	n.d.	n.d.	n.d.	n.d.	n.d.	-16 ± 9
[a] Only where <i>EcIspE</i> activity was measured as IC <sub>50</sub> >500 μM, no replicate pyruvate kinase and lactate dehydrogenase (PK/LDH) inhibition were determined. n.d.: not determined. *Value of a single measurement.												

**Table S5.2.2.4:3** - Summary of biological data for the synthesised derivatives.

Structure and HIPS code	<i>EcIspE</i> IC <sub>50</sub> (μM) <sup>[a]</sup>	PK/LDH IC <sub>50</sub> (μM)	<i>E. coli</i> K12	Percentage Inhibition @ 100 μM or Minimum Inhibitory Concentration (MIC)								
				<i>E. coli</i> Δ <i>tolC</i>	<i>E. coli</i> Δ <i>acrB</i>	<i>E. coli</i> D22	<i>E. coli</i> Omp8	<i>A. baumannii</i>	<i>P. aeruginosa</i>	<i>B. subtilis</i>	<i>S. aureus</i>	HepG2
 <b>5435</b>	>500	n.d.	50 ± 10	MIC 19 ± 1	MIC 33 ± 13	MIC 95 ± 0	n.d.	27 ± 4	46 ± 3	n.d.	MIC 95 ± 7	91 ± 6
 <b>5436</b>	>500	n.d.	13 ± 2	MIC 38 ± 1	54 ± 5	35 ± 5	n.d.	2* @50 μM	9 ± 5	n.d.	18 ± 24	80 ± 3
 <b>5242</b>	>500	n.d.	MIC 99 ± 2	MIC 97 ± 4	MIC 95 ± 0	MIC 105 ± 7	87 ± 7	MIC 100 ± 0	52 ± 10	MIC >100 *weird kinetics	47 ± 8	92 ± 0 (IC <sub>50</sub> : 21 ± 1)
 <b>5602</b>	n.d.	n.d.	30 ± 3	MIC 80 ± 14	n.d.	n.d.	n.d.	n.d.	n.d.	n.d.	82 ± 8	n.d.

 <b>5603</b>	n.d.	n.d.	4 ± 3 @50 μM	56 ± 27 @50 μM	n.d.	n.d.	n.d.	n.d.	5 ± 0 @50 μM	n.d.	1 ± 8 @100 μM	n.d.
 <b>5604</b>	n.d.	n.d.	38 ± 2	48 ± 6	44 ± 11	n.d.	8 ± 3	n.d.	11 ± 1	n.d.	7 ± 7	91 ± 10 (IC <sub>50</sub> = 58 ± 6)
 <b>5607</b>	n.d.	n.d.	18 ± 3	MIC 14 ± 0	n.d.	n.d.	n.d.	n.d.	n.d.	n.d.	MIC 85 ± 7	n.d.
 <b>5608</b>	n.d.	n.d.	8 ± 5 @50 μM	MIC 49 ± 2	n.d.	n.d.	n.d.	n.d.	n.d.	n.d.	5 ± 15	n.d.
 <b>5635</b>	n.d.	n.d.	9 ± 2 @50 μM	27 ± 4 @50 μM	n.d.	n.d.	n.d.	n.d.	7* @ 50 μM	n.d.	n.d.	n.d.
 <b>5636</b>	n.d.	n.d.	MIC 90 ± 0	MIC 93 ± 4	MIC 94 ± 0	n.d.	MIC 94 ± 1	n.d.	70 ± 3	n.d.	79*	98 ± 1
 <b>5605</b>	n.d.	n.d.	23 ± 6 @50 μM	MIC 12 ± 0	n.d.	n.d.	n.d.	n.d.	n.d.	n.d.	MIC 56 ± 33	n.d.
 <b>5606</b>	n.d.	n.d.	9 ± 8 @50 μM	MIC 65 ± 23	n.d.	n.d.	n.d.	n.d.	n.d.	n.d.	3 ± 5	n.d.
 <b>5637</b>	n.d.	n.d.	4 ± 1 @50 μM	15 ± 0 @25 μM	n.d.	n.d.	n.d.	n.d.	-0 ± 0	n.d.	n.d.	n.d.
 <b>5638</b>	n.d.	n.d.	MIC 53 ± 4	MIC 88 ± 4	MIC 84 ± 5	n.d.	MIC 75 ± 10	28 ± 13 @50 μM	52 ± 6	MIC 77 ± 20	86 ± 8	96 ± 2 (IC <sub>50</sub> = 17 ± 1)
 <b>5502</b>	n.d.	n.d.	12 ± 6	13 ± 4	-6 ± 3	11 ± 1	n.d.	n.d.	n.d.	n.d.	-0.2 ± 8	45 ± 4

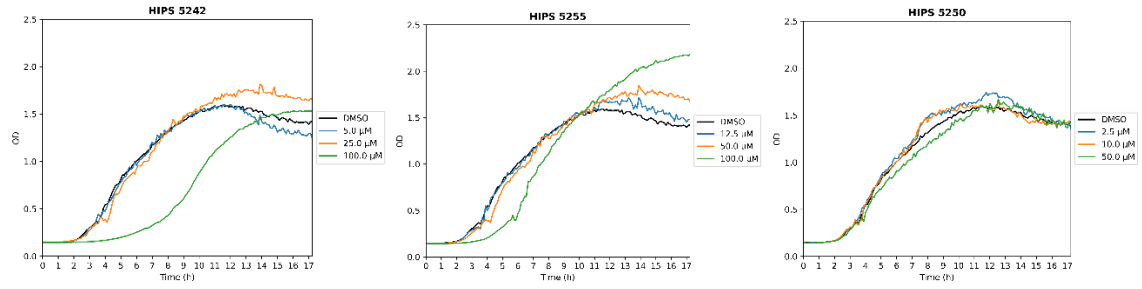
 <b>5503</b>	n.d.	n.d.	10 ± 1	44 ± 15	10 ± 25	14 ± 2	n.d.	n.d.	n.d.	n.d.	n.d.	-8 ± 19	n.d.
 <b>5504</b>	n.d.	n.d.	29 ± 2	24 ± 7	29 ± 20	1 ± 8	-14 ± 0	n.d.	n.d.	n.d.	n.d.	5 ± 2	48 ± 7
 <b>5673</b>	40 ± 6	46 ± 1	58 ± 6 @50 μM	MIC 3 ± 0	n.d.	n.d.	n.d.	n.d.	n.d.	n.d.	n.d.	MIC 5 ± 0	92 ± 3 (IC <sub>50</sub> = 33 ± 2)
 <b>5674</b>	130 ± 20	>500	-2 ± 5 @50 μM	3 ± 0 @50 μM	n.d.	n.d.	n.d.	22 ± 0 @50 μM	-1 ± 4 @50 μM	n.d.	33 ± 8 @50 μM	55 ± 3	
 <b>5675</b>	159 ± 4	>500	MIC 85 ± 6	MIC 41 ± 2	MIC 44 ± 1	MIC 86 ± 4	MIC 45 ± 2	MIC 64 ± 2	63 ± 8	MIC 46 ± 1	MIC 99 ± 6	93 ± 2 (IC <sub>50</sub> = 15 ± 3)	
 <b>5676</b>	4 ± 1	>500	16 ± 13 @50 μM	MIC 20 ± 6	MIC 20 ± 5	n.d.	n.d.	21* @50 μM	9 ± 6 @50 μM	MIC 22 ± 18	n.d.	95 @ 100 μM 95 @ 50 μM*	
 <b>6016</b>	n.d.	n.d.	MIC 98 ± 6	MIC 11 ± 0	n.d.	n.d.	n.d.	MIC 33*	MIC 107±12	n.d.	n.d.	97 ± 0	
 <b>5845</b>	n.d.	n.d.	10 ± 7 @50 μM	45 ± 7 @50 μM	n.d.	n.d.	n.d.	n.d.	n.d.	n.d.	n.d.	IC <sub>50</sub> = 15 ± 8	
 <b>5933</b>	n.d.	n.d.	MIC 47 ± 2	MIC 46 ± 1	n.d.	n.d.	n.d.	MIC 43 ± 4	64 ± 7	MIC 30 ± 9	87 ± 7	94 ± 0 (IC <sub>50</sub> = 9 ± 1)	
 <b>5990</b>	n.d.	n.d.	MIC 98 ± 6	MIC 46 ± 1	n.d.	n.d.	n.d.	n.d.	n.d.	n.d.	n.d.	96 ± 2 (IC <sub>50</sub> = 23 ± 4)	
 <b>6027</b>	n.d.	n.d.	MIC 48 ± 1	MIC 36 ± 11	n.d.	MIC 38*	MIC 44*	n.d.	MIC 95*	n.d.	MIC 100*	77 ± 18	

 <b>6017</b>	n.d.	n.d.	MIC 97 ± 2	MIC 45 ± 1	n.d.	n.d.	n.d.	86*.	86 ± 14	n.d.	n.d.	97 ± 0
 <b>6074</b>	n.d.	n.d.	MIC 94*	n.d.	n.d.	n.d.	n.d.	n.d.	MIC 92*	n.d.	n.d.	96 ± 0
 <b>6065</b>	n.d.	n.d.	25* @50 µM	MIC 12*	n.d.	53* @50 µM	MIC 35*	n.d.	44% @50 µM	n.d.	MIC 105*	65 ± 6

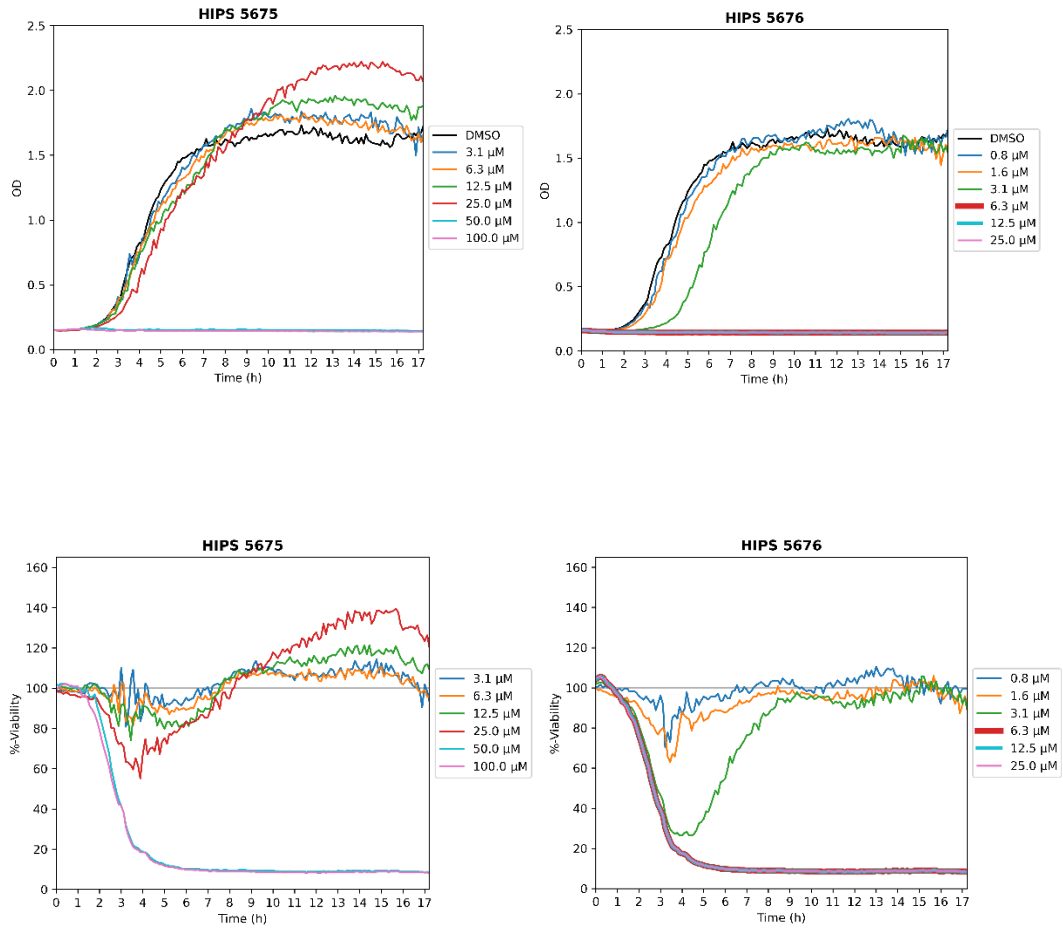
[a] The results are from at least two independent determinations. Only where *Ec*IspE activity was measured as IC<sub>50</sub> > 500 µM, no replicate pyruvate kinase and lactate dehydrogenase (PK/LDH) inhibition were determined. n.d.: not determined. \* Value of a single measurement.

## 5.2.2.5 *Bacillus subtilis* Experiments

Initial anomalous kinetics of *HIPS5242*, *HIPS5255* and *HIPS5250* (negative control)



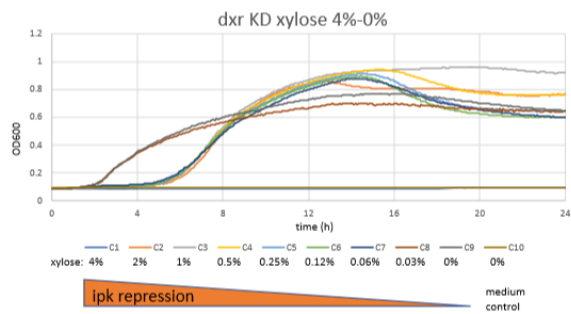
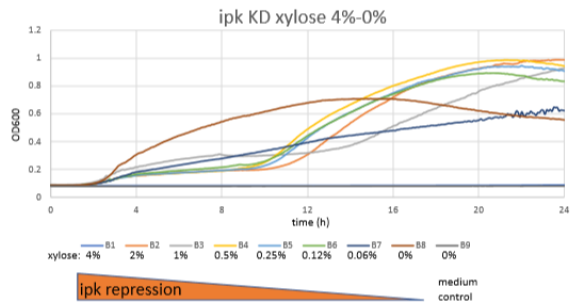
Comparison of *HIPS5675* and *HIPS5676*



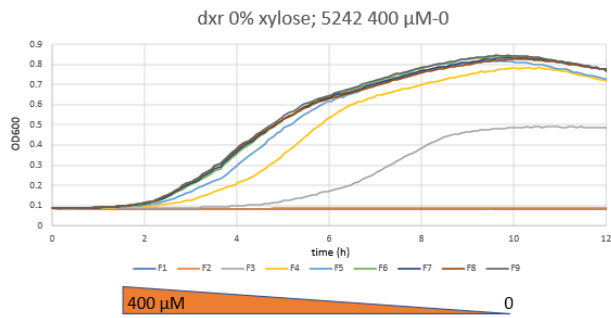




Effects of ipk and dxr knock-downs on growth



Effects of 5242 and 5255 on growth (dxr strain, not repressed)



Effects of 5242 and 5255 on growth (ipk strain, not repressed)

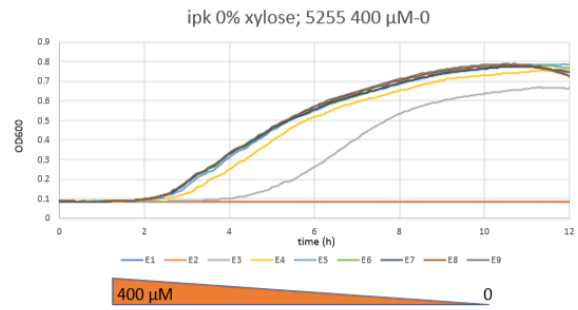
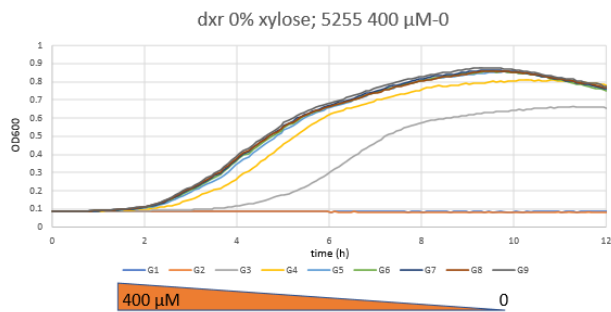
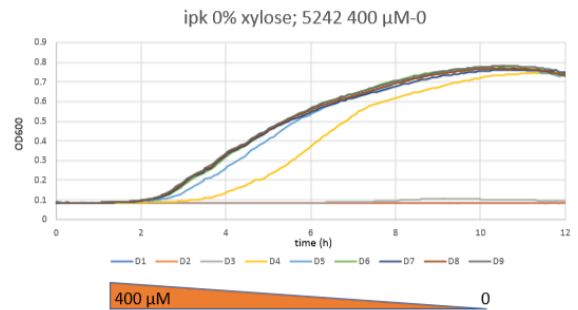
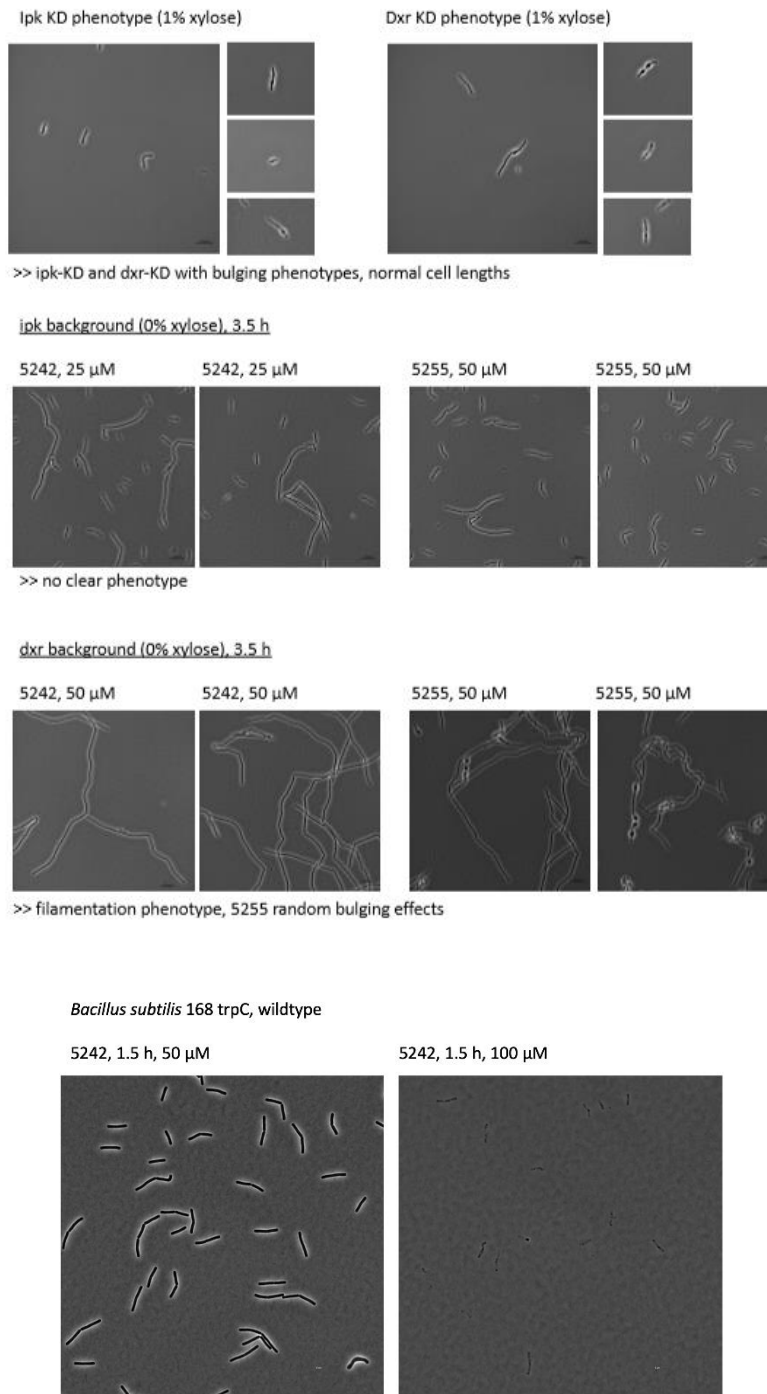
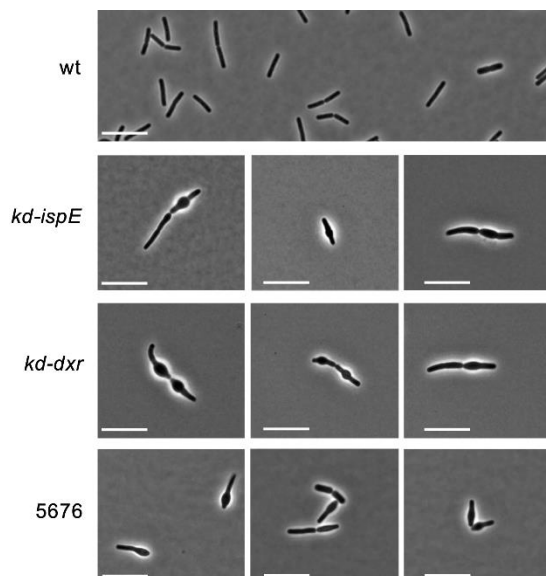


Figure S5.2.2.5:2 - HIPS5242 and HIPS5255 tested against the *Bacillus subtilis* dxr(dxs) and ipk(IspE) knockdown mutants.

Effects of ipk and dxr knock-downs on cell morphology  
(representative images are shown)



**Figure S5.2.2.5:3** - HIPS5242 and HIPS5255 tested against the *Bacillus subtilis* dxr(dxs) and ipk(IspE) knockdown and the respective cell morphology.



**Figure S5.2.2.5:4** - IspE depletion and **HIPS5676** treatment result in a bulging phenotype in *B. subtilis*. Exponentially growing cultures of *B. subtilis* mutant strains *kd-ispE* and *kd-dxr* were supplemented with 1% xylose to repress the expression of either IspE or Dxr, respectively. Accordingly, exponentially growing *B. subtilis* wild-type cells were treated with 6.25  $\mu\text{M}$  **HIPS5676**. After 90 minutes, cells were examined by phase contrast microscopy. In contrast to untreated control cells, both the depletion of IspE or Dxr as well as **HIPS5676** treatment led to cell lysis over time, which was often preceded by a characteristic bulging phenotype. Scale bars, 10  $\mu\text{m}$ . Images are representative of at least two biological replicate cultures.

### Method Microscopy

*Bacillus subtilis* cells were grown in lysogeny broth (LB) at 37 °C to an optical density at 600 nm ( $\text{OD}_{600}$ ) of 0.2. Then, the mutant strains *kd-ispE* (BEC00460) and *kd-dxr* (BEC16550)<sup>130</sup> were supplemented with 1% xylose to repress either IspE or Dxr expression. Similarly, *B. subtilis* 168 trpC2 wild-type cells were grown at 37 °C to an  $\text{OD}_{600}$  of 0.2 and were then treated with **HIPS5676** as indicated. Then, cultures were further grown for 90 minutes until sampling. For microscopy, cells were mounted on microscopy slides coated with 1% agarose in water to immobilize cells. Images were acquired using the Zeiss Axio Observer Z1 and ZEN image analysis software (Zeiss, Germany) and the Nikon Eclipse Ti equipped with Perfect Focus system (Nikon Instruments Europe BV, Netherlands), an Orca Flash 4.0 camera (Hamamatsu, Photonics, Japan) and CFI Plan-Apo DM $\times$ 100/1.45 Oil Ph3 objective (Nikon). Images were processed using the NIS elements AR software package (Nikon).

### 5.2.3. Biophysical Assays

#### 5.2.3.1 Thermal Shift Assay

The thermal shift assay (TSA) was performed in triplicates on a 96-well plate. Each well contained DMSO-ligand (200  $\mu$ M), *EcIspE* (2.5  $\mu$ M), 10% (V/V) x50 Protein Thermal Shift dye (LOT 1707029) and 75% (V/V) TBS-buffer (50 mM Tris-HCl, pH 7.6, 150 mM NaCl). The ligands were pipetted from a 4 mM DMSO stock solution. The protein stock in a concentration of 25  $\mu$ M was centrifuged at 4  $^{\circ}$ C, 14000 rpm for 5 min. The blank (protein-only) and the positive control (natural substrate CDP-ME) contained DMSO with the same volume as the ligand instead of the ligand (5% (V/V)). The positive control additionally contained 500  $\mu$ M CDP-ME (8 mM stock solution). The total sample volume in each well was 20  $\mu$ L. The well plate was covered with a PCR-membrane, centrifuged at 4  $^{\circ}$ C, 1400 rpm for 1 min and placed into a StepOnePlus Real-Time PCR System (Serial no. 272003367, Applied Biosystems). “Detect melting point” method was used with a temperature ramp over 20–90  $^{\circ}$ C proceeding in steps of 0.3  $^{\circ}$ C (1 min per step). Protein Thermal Shift Software Version 1.3 was used to determine melting points ( $T_m$ ) at least from two independent replicates.

**Table S5.2.3.1:1** - Summary of the thermal shift assay results.

Compound	$T_m$ ( $^{\circ}$ C)	$\Delta T_m$ ( $^{\circ}$ C) <sup>[a]</sup>
Protein only	51.52 $\pm$ 0.14	–
CDP-ME	52.28 $\pm$ 0.09	+0.8
HIPS5242	50.42 $\pm$ 0.09	–1.1
HIPS5244	51.31 $\pm$ 0.37	–0.2
HIPS5250	50.75 $\pm$ 0.08	–0.8
HIPS5252	51.79 $\pm$ 0.12	+0.3
HIPS5254	51.23 $\pm$ 0.09	–0.3
HIPS5255	50.81 $\pm$ 0.09	–0.7
HIPS5259	51.23 $\pm$ 0.13	–0.3
HIPS5411	50.82 $\pm$ 0.12	–0.7
HIPS5412	51.52 $\pm$ 0.10	0.0
HIPS5419	51.10 $\pm$ 0.08	–0.4
HIPS5674	51.31 $\pm$ 0.08	–0.2
HIPS5675	49.60 $\pm$ 0.20	–1.9
HIPS5676	49.75 $\pm$ 0.34	–1.8
HIPS5636	49.99 $\pm$ 0.09	–1.5

<b>HIPS5933</b>	48.38 ± 0.29	-3.1
<b>HIPS5990</b>	47.58 ± 0.31	-3.9
<b>SuFEx Probe<sup>[b]</sup></b>		
<b>Protein in HEPES</b>	51.52 ± 0.08	-
<b>CDP-ME in HEPES</b>	52.17 ± 0.08	+0.7
<b>HIPS5893</b> (after 72 h incubation)	50.35 ± 0.16	-1.2
<b>HIPS5893</b> (500 µM without incubation)	50.95 ± 0.15	-0.6
[a] $T_m(\text{EcIspE with compound}) - T_m(\text{EcIspE without compound})$ . [b] See details in Section 5.2.4.		

### 5.2.3.2 Microscale Thermophoresis

The microscale thermophoresis (MST) (Serial no. 201709-BR-N024, Monolith NT.115 Micro Scale Thermophoresis, NanoTemper Technologies GmbH.) was performed according to the standard protocol from the manufacturer NanoTemper Technologies GmbH using the Monolith His-Tag Labeling Kit RED-tris-NTA 2<sup>nd</sup> Generation kit (LOT #20L018-010). For **HIPS5242**, 1<sup>st</sup> Generation kit was used. The buffer used was HEPES (50 mM), pH 7.6, MgCl<sub>2</sub> (5 mM) and Tween (0.05%). The protein concentration of 50 nM was used and the ligand was tested at the highest soluble concentration, which was 0.5 mM for most of the compounds under the assay conditions. A 1:1 dilution of the ligand over 16 samples was performed using a stock of 10% DMSO ligand stock in HEPES buffer. Non-hydrophobic capillary tubes (LOT #20K022\_003) were used. A pretest to check for the labelling and compound fluorescence was performed before every sample, followed by a binding affinity ( $K_d$ ) determination. Each sample was measured after 15 min and 60 min incubation time at RT and analysed in MO Control version 1.6.

**Table S5.2.3.2:1** - Summary of the microscale thermophoresis results.

	Time	$K_d$ 1 [ $\mu$ M]	$K_d$ 2 [ $\mu$ M]	$K_d$ 3 [ $\mu$ M]	Average $K_d$ [ $\mu$ M]
<b>CDP-ME</b>	15 min	1.3	0.2	0.4	$0.3 \pm 0.2$
	1 h	(0.4)	0.1	0.1	$0.1 \pm 0.0$
<b>HIPS5242</b>	15 min	664.0 <sup>[a]</sup>	733.0 <sup>[a,b]</sup>	n.d.	$699 \pm 49$
	1 h	403.0 <sup>[a]</sup>	215.0 <sup>[a,b]</sup>	n.d.	$309 \pm 133$
<b>HIPS5675</b>	15 min	79.4	57.4	57.4	$65 \pm 13$
	1 h	60.6	60.0	60.0	$60 \pm 0$
<b>HIPS5676</b>	15 min	(-29.9)	116.0	n.d.	116*
	1 h	45.6	n.d.	n.d.	46*
<b>HIPS5933</b>	15 min	21.9	4.4	33.8	$20 \pm 15$
	1 h	(281)	12.0	17.3	$15 \pm 4$
<b>HIPS5990</b>	15 min	31.8	28.8	10.7	$24 \pm 11$
	1 h	37.7	61.1	17.7	$39 \pm 22$

[a] 1<sup>st</sup> Generation His-Tag Kit [b] Measured in Tris-HCl buffer. \*Value of a single measurement. n.d.: not determined

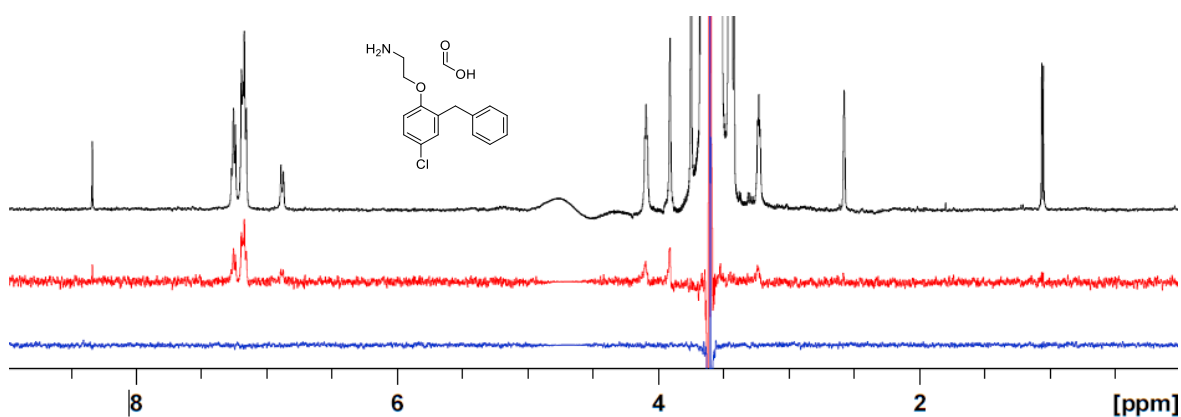
### 5.2.3.3 Saturation Transfer Difference-Nucleomagnetic Resonance

The STD experiments were recorded at 298 K on a Bruker Fourier spectrometer (500 MHz). The samples contained a 100- to 200-fold excess of compound (500  $\mu$ M) relative to *Ec*IspE (2.5  $\mu$ M or 5.0  $\mu$ M – see Table 5.2.3.3:1) in D<sub>2</sub>O buffer with Tris-HCl (50 mM) and MgCl<sub>2</sub> (5 mM) at pD = 7.6. The compounds were dissolved in DMSO-*d*<sub>6</sub> and added to the buffer to reach a final concentration of 2.4% DMSO-*d*<sub>6</sub>.

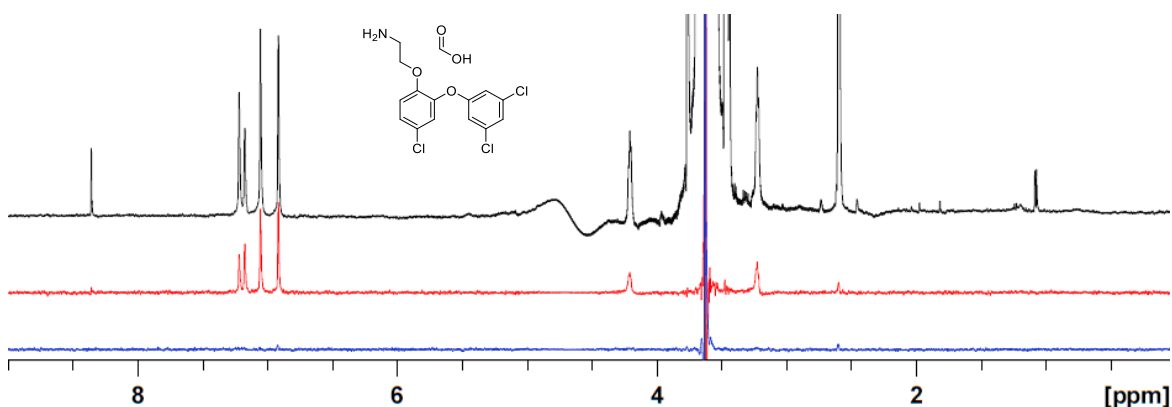
All experiments were performed using the *stdiffesgp.3* pulse program by Bruker. Blank spectra (compound in buffer without protein) were recorded to establish the parameters at which no residual compound signals were visible (Table 5.2.3.3:1). The screening experiments were all recorded with a carrier set at -2 or -3 ppm for the on-resonance and -40 ppm for the off-resonance irradiation. Selective protein saturation was carried out at 0.5 s or 1.0 s (d20 parameter in TopSpin) by using a train of 50 ms Gauss-shaped pulses, each separated by a 1 or 2 s delay (d1 parameter in TopSpin). In all cases, 256 scans were recorded. Binding was confirmed when a visible difference in peak intensity between off-resonance and STD spectrum could be observed.

**Table S5.2.3.3:1** - Measurement and experimental parameters that differed from general procedure.

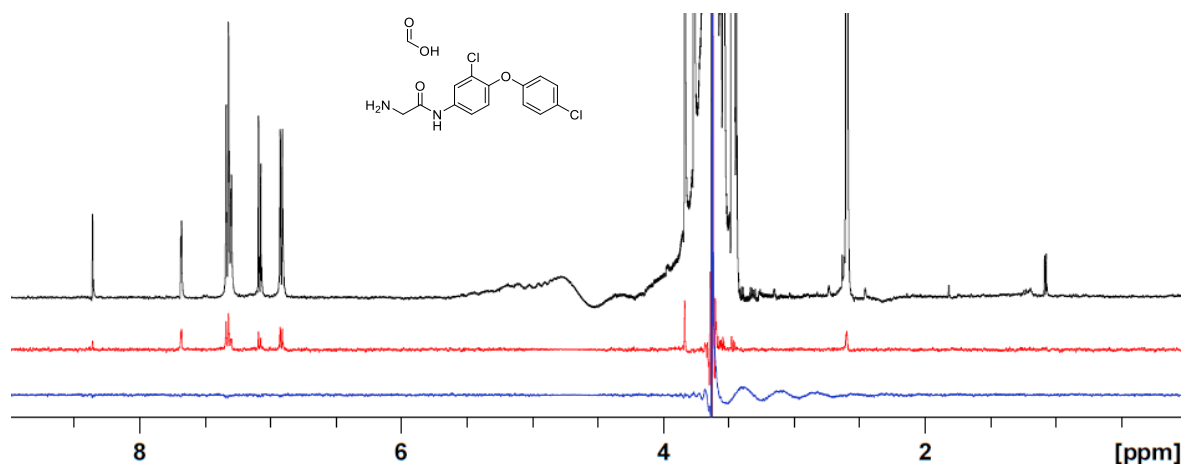
Compound	d1 (s)	d20 (s)	On-resonance frequency (ppm)	EcIspE ( $\mu\text{M}$ )
HIPS5242	2.0	0.5	-2	5.0
HIPS5675	1.0	0.5	-3	2.5
HIPS6027	1.0	1.0	-2	2.5
HIPS5990	1.0	0.5	-3	2.5



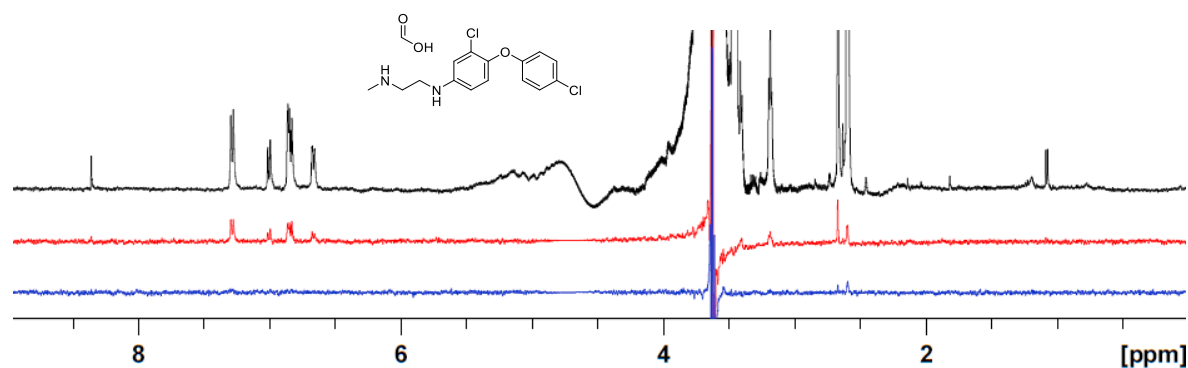
**Spectrum S5.2.3.3:1** - Blank (blue), STD (red) and off-resonance (black) spectrum of compound **HIPS5242**. Binding for all compound signals visible; differences in intensities confirm specific binding. Only weak binding of formic acid (8.3 ppm). Epitope mapping not possible, because peaks cannot be assigned unambiguously.



**Spectrum S5.2.3.3:2** - Blank (blue), STD (red) and off-resonance (black) spectrum of compound **HIPS5675**. Binding for all compound signals visible; differences in intensities confirm specific binding. Only weak binding of formic acid (8.3 ppm). Epitope mapping not possible, because peaks cannot be assigned unambiguously.



**Spectrum S5.2.3.3:3** - Blank (blue), STD (red) and off-resonance (black) spectrum of compound **HIPS6027**. Binding for all compound signals visible; differences in intensities confirm specific binding. Only weak binding of formic acid (8.3 ppm). Epitope mapping not possible, because peaks cannot be assigned unambiguously.



**Spectrum S5.2.3.3:4** - Blank (blue), STD (red) and off-resonance (black) spectrum of compound **HIPS5990**. Binding for all compound signals visible; differences in intensities confirm specific binding. Only weak binding of formic acid (8.3 ppm).



#### 5.2.4. SuFEx Probe

In an Eppendorf tube, *EcIspE* (23 mg/mL in Tris-HCl buffer), compound 4-phenoxybenzenesulfonyl fluoride **HIPS5893** (CAS 1368838-37-2) in DMSO and HEPES buffer (50 mM), pH 7.6, MgCl<sub>2</sub> (5 mM) were added to achieve final concentration: 10 μM *EcIspE*, 5% DMSO (including the compound solvent) and the desired compound concentration (*e.g.*, 1.38 μL of *EcIspE* 23 mg/mL in TRIS buffer + 4 μL of 10 mM **HIPS5893** + 1 μL DMSO + 93.62 μL buffer to achieve a final 400 μM concentration of the **HIPS5893**). A control experiment was performed using 5% DMSO without any compound. The Eppendorf tubes were incubated at RT on a shaking platform (IKA® Vibrax VXR basic) at 100 rpm for the given time. The subsequent temperature samples were incubated at 35 °C on a shaking platform (Eppendorf ThermoMixer F2.0) at 100 rpm. At the end of the incubation time, 10 μL of the samples was transferred to an LC-MS vial and diluted with 40 μL HEPES buffer for MS analysis that was carried out as previously reported.<sup>131</sup> The remaining samples were frozen in liquid nitrogen and stored at -80 °C until further MS measurements.

Initial trial with several samplings at 2 h, 4 h, 6 h, 8 h and 10 h

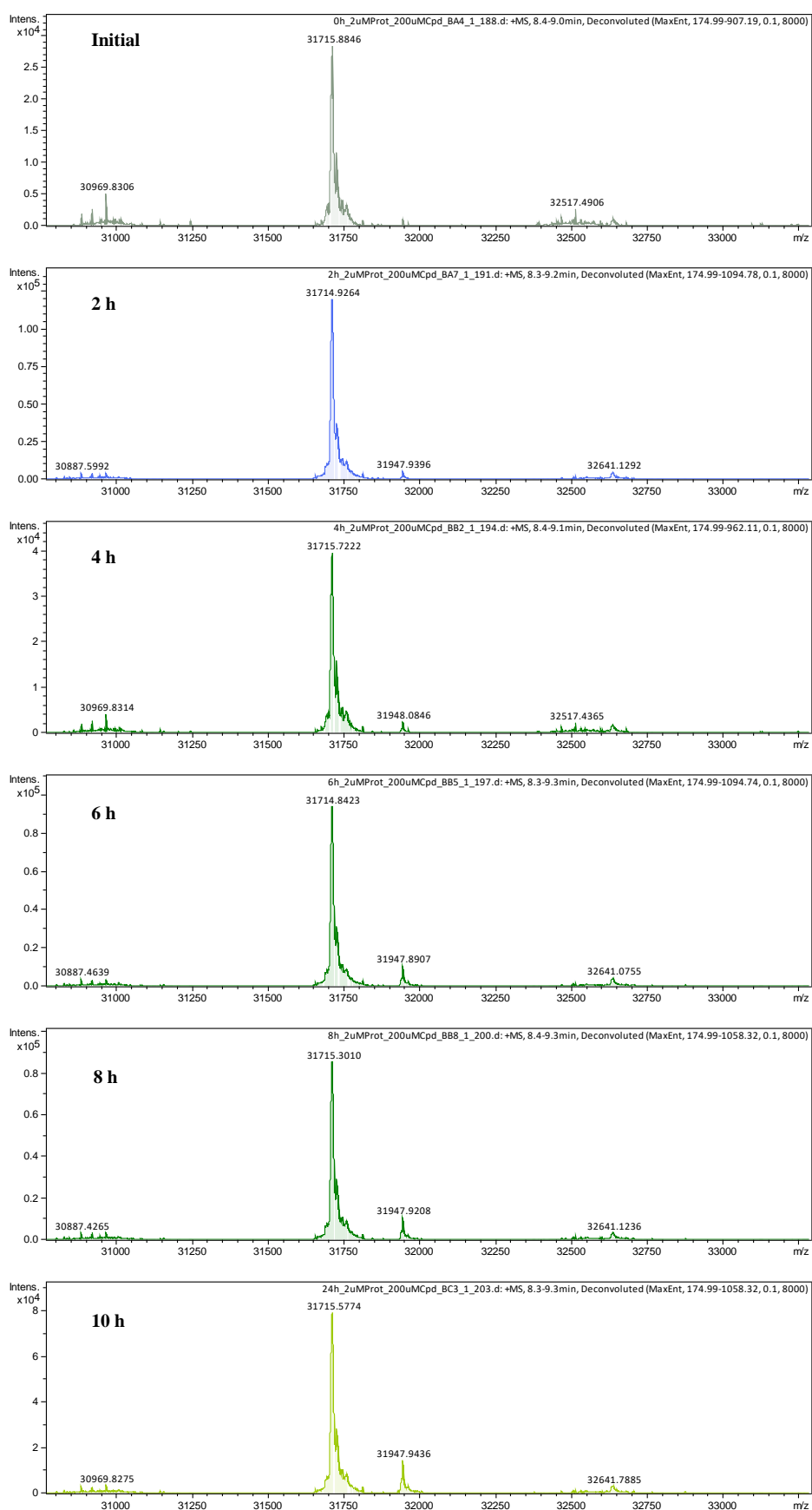


Figure S5.2.4:1 - Chromatograms of the deconvoluted *EcIspE* ( $m/z$ : 31715.5774) vs the singly substituted *EcIspE* + SuFEX probe **HIPS5893** ( $m/z$ : 31947.9436).

**Table S5.2.4:1** - MS results based on the increased compound concentration and incubation time.

<b>Compound Concentration (<math>\mu\text{M}</math>)</b>	<b>Time of incubation (h)</b>	<b>Bound Protein (%) Sample 1</b>	<b>Bound Protein (%) Sample 2</b>
200	24	17	17
200	48	22	22
400	24	0	19
400	48	0	31

**Table S5.2.4:2** - MS results based on the increased compound concentration at different buffer pH over 72 h.

<b>Compound Concentration (<math>\mu\text{M}</math>)</b>	<b>pH of Buffer</b>	<b>Monosubstituted Protein (%)</b>	<b>Bisubstituted Protein (%)</b>
400	7.2	17	0
600	7.2	22	0
400	7.6	31	4
600	7.6	40	8
400 <sup>[a]</sup>	8.0	42	10
600	8.0	59	25

[a] This sample was used for TSA (Section 5.2.3.1).

**Table S5.2.4:3** - MS results based on the increased temperature at different buffer pH over 22.5 h.

<b>Compound Concentration (<math>\mu\text{M}</math>)</b>	<b>pH of Buffer</b>	<b>Monosubstituted Protein (%)</b>	<b>Bisubstituted Protein (%)</b>
600	7.6	29	2
600	8.0	45	8

## 5.2.5. Synthesis

### 5.2.5.1 General Conditions

General conditions were same as in Publication 2 (H.-K. Ropponen *et al.*, *RSC Med. Chem.*, **2021**, DOI:10.1039/d0md00409j). Additionally, all spectra were measured in CDCl<sub>3</sub>, DMSO-*d*<sub>6</sub>, methanol-*d*<sub>4</sub> or acetone-*d*<sub>6</sub> and chemical shifts were adjusted based on the residual proton of the internal standard in parts per million (ppm), (CDCl<sub>3</sub>,  $\delta$  = 7.27, 77.00, DMSO-*d*<sub>6</sub>,  $\delta$  = 2.50, 39.51, methanol-*d*<sub>4</sub>,  $\delta$  = 4.87, 49.15 or acetone-*d*<sub>6</sub>,  $\delta$  = 2.05, 29.32, <sup>1</sup>H and <sup>13</sup>C, respectively). Compounds were purified by prep. HPLC eluting with an alternating gradient of 5–100% ACN with 0.05% FA in H<sub>2</sub>O with 0.05% FA.

### 5.2.5.2 General Procedures

#### General Procedure A<sup>105</sup>

The respective derivative of 2-benzyl-4-(*halogen*)phenol or 2-phenoxyaniline (1.0 eq.) was dissolved in dry acetone under N<sub>2</sub> flow. Anhydrous K<sub>2</sub>CO<sub>3</sub> (1.0 eq.) and NaI (0.2 eq.) were added followed by a dropwise addition of chloroacetonitrile (1.0 eq.). The mixture was refluxed for the given time, then cooled down to RT and diluted with acetone. The mixture was filtered through celite and the remaining filtrate was absorbed onto ISOLUTE® HM-N and purified by FCC with an alternating gradient of 0–10% EtOAc in petroleum benzene (40–60 °C) or cyclohexane to afford the title compounds.

#### General Procedure B<sup>96</sup>

In a pressure sealed vial, the specific halogen derivative of 1-(benzyloxy)-4-(*halogen*)benzene (1.0 eq.) was flushed with N<sub>2</sub>. TFA (4 mL) was added under N<sub>2</sub> flow and the pressure vial was sealed. The mixture was stirred at 80 °C for 1 h. After 1 h, aq. 2M HCl (4 mL) was added dropwise and stirred at 80 °C for 1 h. The reaction mixture was cooled down to RT and carefully extracted with DCM (2 x 10 mL). The organic layers were then dried over anhydrous Na<sub>2</sub>SO<sub>4</sub>, filtered and evaporated to dryness. The crude was absorbed onto ISOLUTE® HM-N and purified by FCC with an alternating gradient of 0–10% EtOAc in petroleum benzene (40–60 °C) leaving TFA traces. The crude was dissolved in (aq. 2M HCl), basified with aq. sat. NaHCO<sub>3</sub> and finally extracted with DCM. The organic layer was then dried over anhydrous Na<sub>2</sub>SO<sub>4</sub>, filtered and evaporated to dryness. The crude was absorbed onto ISOLUTE® HM-N and purified by FCC with an alternating gradient of 0–10% EtOAc in petroleum benzene (40–60 °C) or cyclohexane, affording the respective title compounds.

### General Procedure C1<sup>132</sup>

To a stirred solution of the respective derivative of 2-benzyl-4-(*halogen*)phenol derivative (1.0 eq.) in dry DMF under N<sub>2</sub> flow, CsCO<sub>3</sub> (3.0 eq.) and TBAI (0.1 eq.) were added. The mixture was stirred at RT for 1 h followed by the addition of *tert*-butyl (2-chloroethyl)carbamate (2.5 eq.). The reaction was stirred overnight, and where not complete, followed by another addition of *tert*-butyl (2-chloroethyl)carbamate (2.5 eq.). The mixture was quenched with water and extracted with EtOAc. The combined organic layers were washed with brine, dried over anhydrous Na<sub>2</sub>SO<sub>4</sub>, filtered and evaporated to dryness. The crude was absorbed onto ISOLUTE® HM-N and purified by FCC with an alternating gradient of 0–100% EtOAc in petroleum benzene (40–60 °C) to afford the respective title compounds.

### General Procedure C2<sup>133</sup>

To a solution of 4-chloro-2-(3,5-dichlorophenoxy)phenol (1 eq.) in dry DMF, K<sub>2</sub>CO<sub>3</sub> (3 eq.) was added and the mixture was stirred for 20 min. The corresponding Boc-protected chloroamine (in excess) and KI (2 eq.) were added and the reaction mixture was stirred at 80 °C. The mixture was cooled to RT, poured into water and extracted with EtOAc (3 x 10 mL). The organic layers were washed with water (5 x 5 mL) and brine (2 x 5 mL), dried over anhydrous Na<sub>2</sub>SO<sub>4</sub> and concentrated *in vacuo*. The crude was purified by FCC as described in detail to afford the respective title compounds.

### General Procedure D1

To a stirred solution of Boc-derivative (1.0 eq.) in THF, aq. 6M HCl (4.0 eq.) was added. The mixture was stirred at RT for 1.5 h. The reaction mixture was basified with saturated aq. NaHCO<sub>3</sub> and extracted with DCM. The combined organic layers were concentrated and purified with prep. HPLC to afford the respective title compounds.

### General Procedure D2<sup>134</sup>

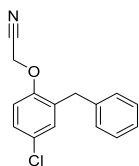
To a solution of Boc-protected derivative (1 eq.) in dioxane, 4M HCl/dioxane (10 eq.) was added dropwise at 0 °C and the reaction solution was stirred at RT until full conversion. The mixture was then concentrated *in vacuo* and dissolved in water. The aqueous phase was basified with saturated aq. NaHCO<sub>3</sub> and extracted with diethyl ether. The organic layers were washed with brine, dried over anhydrous Na<sub>2</sub>SO<sub>4</sub> and concentrated *in vacuo* to afford the desired compounds as crudes that were purified as described in detail to afford the respective title compounds.

## General Procedure E

To a solution of the corresponding handle as carboxylic acid (1.0 eq.) in dry DMF, DIPEA (1.1 eq.) was added. After 10 min, HATU (1.2 eq.) was added to the solution and the reaction mixture was stirred for further 10 min. Then 3-chloro-4-(4-chlorophenoxy)aniline **HIPS5850** (1.1 eq.) was added and the mixture was heated to reflux. The reaction mixture was cooled down to RT, quenched with  $\text{NH}_4\text{Cl}$  and extracted with EtOAc (x3). The organic layers were washed with water (x5), saturated aq.  $\text{NaHCO}_3$  (x1) and brine (x2). The combined organic layers were dried over anhydrous  $\text{Na}_2\text{SO}_4$  and concentrated *in vacuo* to afford the desired compounds as crude products that were further purified as described in detail for each compound.

### 5.2.5.3 Synthesised of Compounds

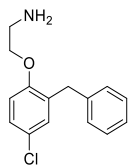
#### 2-(2-Benzyl-4-chlorophenoxy)acetonitrile (**HIPS5436**)<sup>135</sup>



Using general procedure A, 2-benzyl-4-chlorophenol (1.0 eq., 0.500 g, 2.286 mmol) was refluxed for 8 h with anhydrous  $\text{K}_2\text{CO}_3$  (1.0 eq., 0.316 g, 2.286 mmol), NaI (0.2 eq., 0.069 g, 0.457 mmol) and chloroacetonitrile (1.0 eq., 2.286 mmol, 140  $\mu\text{L}$ ) in dry acetone (5 mL) to afford FCC purified compound **HIPS5436** as a clear oil (0.474 g, 80%). Further prep. HPLC purification (0.040 g) afforded compound **HIPS5436** as a beige powder, (0.028 g).

$^1\text{H}$  NMR ( $\text{DMSO-}d_6$ , 500 MHz)  $\delta$  7.34 (dd,  $J=8.8, 2.8$  Hz, 1 H) 7.26 - 7.29 (m, 2 H) 7.25 - 7.28 (m, 1 H) 7.21 - 7.23 (m, 2 H) 7.17 - 7.23 (m, 1 H) 7.15 (d,  $J=8.8$  Hz, 1 H) 5.21 (s, 2 H) 3.91 (s, 2 H).  $^{13}\text{C}$  NMR ( $\text{DMSO-}d_6$ , 126 MHz)  $\delta$  153.4, 140.2, 132.8, 130.6, 129.1, 128.9, 127.7, 126.6, 126.5, 116.9, 114.6, 54.4, 35.2. HRMS (ESI+) calcd. for  $\text{C}_{15}\text{H}_{12}\text{ClNO}$  [ $\text{M} - \text{H}$ ] $^-$ : 256.05346, found: 256.05315.

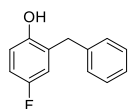
## 2-(2-Benzyl-4-chlorophenoxy)ethan-1-amine (HIPS5242)<sup>105</sup>



2-(2-Benzyl-4-chlorophenoxy)acetonitrile **HIPS5436** (1.0 eq., 0.200 g, 0.776 mmol) was dissolved in dry diethyl ether (1.0 mL) and flushed with N<sub>2</sub>. LiAlH<sub>4</sub> (2.0 eq., 0.059 g, 1.552 mmol) was carefully dissolved in another flask in dry diethyl ether (2.5 mL) under N<sub>2</sub> flow. The solution of **HIPS5436** was then added dropwise to the LiAlH<sub>4</sub> mixture and let to stir at RT for 2 h. The reaction mixture was quenched with ice and let to cool down on an ice bath forming a white precipitate. The white precipitate was filtered off, dissolved in EtOAc and concentrated *in vacuo*. The crude was purified with prep. HPLC to afford compound **HIPS5242** as a white powder one FA salt form, (0.039 g, 17%).

<sup>1</sup>H NMR (DMSO-*d*<sub>6</sub>, 500 MHz)  $\delta$  8.34 (s, 1 H) 7.26 - 7.29 (m, 2 H) 7.23 - 7.25 (m, 2 H) 7.21 - 7.23 (m, 1 H) 7.16 - 7.20 (m, 1 H) 7.14 - 7.16 (m, 1 H) 6.98 (d, *J*=8.7 Hz, 1 H) 4.02 (t, *J*=5.3 Hz, 3 H) 3.94 - 3.95 (m, 2 H) 3.02 (t, *J*=5.3 Hz, 3 H). <sup>13</sup>C NMR (DMSO-*d*<sub>6</sub>, 126 MHz)  $\delta$  164.9, 154.7, 140.2, 132.0, 129.5, 128.9, 128.4, 127.0, 126.0, 124.2, 113.3, 67.8, 39.5, 34.9. HRMS (ESI+) calcd. for C<sub>15</sub>H<sub>16</sub>ClNO [M + H]<sup>+</sup>: 262.09932, found: 262.09867.

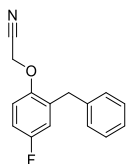
## 2-Benzyl-4-fluorophenol (HIPS5602)



Using general procedure B, 1-(benzyloxy)-4-fluorobenzene (1.0 eq., 0.209 g, 1.035 mmol) was reacted accordingly to afford FCC purified compound **HIPS5602** as a yellow oil, (0.064 g, 34%).

<sup>1</sup>H NMR (DMSO-*d*<sub>6</sub>, 500 MHz)  $\delta$  9.42 (br s, 1 H) 7.24 - 7.29 (m, 2 H) 7.20 - 7.24 (m, 2 H) 7.15 - 7.19 (m, 1 H) 6.83 - 6.86 (m, 1 H) 6.80 - 6.86 (m, 1 H) 6.75 - 6.80 (m, 1 H) 3.84 (s, 2 H). <sup>13</sup>C NMR (DMSO-*d*<sub>6</sub>, 126 MHz)  $\delta$  155.8, 151.7, 141.0, 129.6, 129.1, 128.7, 126.3, 116.8, 116.1, 113.6, 35.6. <sup>19</sup>F NMR (DMSO-*d*<sub>6</sub>, 470 MHz,)  $\delta$  ppm -125.96 (s, 1 F). HRMS (ESI+) calcd. for C<sub>13</sub>H<sub>11</sub>FO [M - H]<sup>-</sup>: 201.07211, found: 201.07115.

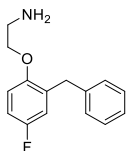
## 2-(2-Benzyl-4-fluorophenoxy)acetonitrile (HIPS5603)



Using general procedure A, 2-benzyl-4-fluorophenol (1.0 eq., 0.050 g, 0.247 mmol) was refluxed overnight with anhydrous  $K_2CO_3$  (1.0 eq., 0.034 g, 0.247 mmol), NaI (0.2 eq., 0.007 g, 0.049 mmol) and chloroacetonitrile (1.0 eq., 20  $\mu$ L, 0.247 mmol) in dry acetone (0.5 mL) to afford FCC purified compound **HIPS5603** as a colourless oil, (0.045 g, 76%).

$^1H$  NMR (DMSO- $d_6$ , 500 MHz)  $\delta$  7.26 - 7.30 (m, 2 H) 7.21 - 7.24 (m, 2 H) 7.17 - 7.21 (m, 1 H) 7.13 - 7.15 (m, 1 H) 7.10 - 7.13 (m, 2 H) 7.06 - 7.10 (m, 1 H) 5.18 (s, 2 H) 3.91 (s, 2 H).  $^{13}C$  NMR (DMSO- $d_6$ , 126 MHz)  $\delta$  157.7, 150.8, 140.2, 132.8, 129.1, 128.9, 126.6, 117.7, 117.1, 114.5, 114.1, 54.8, 35.4.  $^{19}F$  NMR (DMSO- $d_6$ , 470 MHz)  $\delta$  -121.37 (s, 1 F). HRMS (ESI+) calcd. for  $C_{15}H_{12}FNO$  [M - H]: 240.08301, found: 240.08250.

## 2-(2-Benzyl-4-fluorophenoxy)ethan-1-amine (HIPS5604)

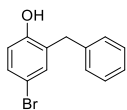


2-(2-Benzyl-4-fluorophenoxy)acetonitrile **HIPS5603** (1.0 eq., 0.025 g, 1.1096 mmol) was dissolved in dry THF (2 mL) under  $N_2$  flow.  $LiAlH_4$  (2.4M in THF) (2.0 eq., 100  $\mu$ L, 0.207 mmol) was added dropwise to the mixture. The mixture was stirred at RT for 2 h. The mixture was quenched with aq. 2M NaOH (2 mL) under ice bath. The mixture was extracted with THF (2 x 5 mL). The organic layers were combined and concentrated *in vacuo*. The crude was purified with prep. HPLC to afford compound **HIPS5242** as a crystalline, colourless powder one FA salt form, (0.005 g, 14%).

$^1H$  NMR (Methanol- $d_4$ , 500 MHz)  $\delta$  8.43 (br s, 1 H) 7.22 - 7.27 (m, 2 H) 7.19 - 7.21 (m, 1 H) 7.13 - 7.17 (m, 3 H) 7.13 - 7.18 (m, 1 H) 6.92 - 6.95 (m, 1 H) 6.87 - 6.91 (m, 1 H) 6.76 (dd,  $J=9.2, 2.9$  Hz, 1 H) 4.09 - 4.12 (m, 2 H) 3.98 - 4.00 (m, 2 H) 3.22 - 3.25 (m, 2 H).  $^{13}C$  NMR (Methanol- $d_4$ , 126 MHz)  $\delta$  156.6, 151.5, 140.3, 132.2, 128.4, 128.1, 125.8, 116.6, 113.0, 112.9, 64.8, 38.8, 35.1.  $^{19}F$  NMR (Methanol- $d_4$ , 470 MHz)  $\delta$  ppm -124.49 (s, 1 F). HRMS (ESI+) calcd. for  $C_{15}H_{16}FNO$  [M + H] $^+$ : 246.12887, found: 246.12816.



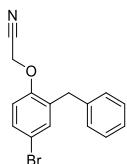
## 2-Benzyl-4-bromophenol (HIPS5607)



Using general procedure B, 1-(benzyloxy)-4-bromobenzene (1.0 eq., 0.210 g, 0.798 mmol) was reacted accordingly to afford FCC purified compound **HIPS5607** as a colourless oil, (0.054 g, 26%).

$^1\text{H}$  NMR (DMSO- $d_6$ , 500 MHz)  $\delta$  9.80 (br s, 1 H) 7.24 - 7.29 (m, 2 H) 7.21 - 7.23 (m, 2 H) 7.15 - 7.19 (m, 3 H) 6.73 - 6.78 (m, 1 H) 3.84 (s, 2 H).  $^{13}\text{C}$  NMR (DMSO- $d_6$ , 126 MHz)  $\delta$  154.4, 140.5, 132.4, 130.4, 129.7, 128.7, 128.3, 125.9, 117.1, 109.9, 34.8. HRMS (ESI+) calcd. for  $\text{C}_{13}\text{H}_{11}\text{BrO}$  [ $\text{M} - \text{H}$ ] $^-$ : 260.99205, found: 260.99173.

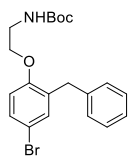
## 2-(2-Benzyl-4-bromophenoxy)acetonitrile (HIPS5608)



Using general procedure A, 2-benzyl-4-bromophenol **HIPS5607** (1.0 eq., 0.045 g, 0.171 mmol) was refluxed for 8 h with anhydrous  $\text{K}_2\text{CO}_3$  (1.0 eq., 0.024 g, 0.171 mmol), NaI (0.2 eq., 0.005 g, 0.034 mmol) and chloroacetonitrile (1.0 eq., 10  $\mu\text{L}$ , 0.171 mmol) in dry acetone (0.5 mL) to afford FCC purified compound **HIPS5608** as a colourless oil, (0.039 g, 75%).

$^1\text{H}$  NMR (acetone- $d_6$ , 500 MHz)  $\delta$  7.43 (dd,  $J=8.7, 2.3$  Hz, 1 H) 7.36 (d,  $J=2.3$  Hz, 1 H) 7.22 - 7.31 (m, 4 H) 7.17 - 7.22 (m, 1 H) 7.11 - 7.14 (m, 1 H) 5.15 (s, 2 H) 3.99 (s, 2 H).  $^{13}\text{C}$  NMR (DMSO- $d_6$ , 126 MHz)  $\delta$  153.4, 139.7, 133.0, 132.7, 130.2, 128.6, 128.4, 126.2, 116.4, 114.6, 114.0, 53.9, 34.7. HRMS (ESI+) calcd. for  $\text{C}_{15}\text{H}_{12}\text{BrNO}$  [ $\text{M} - \text{H}$ ] $^-$ : 300.00295, found: 300.00269.

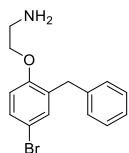
### ***Tert*-butyl (2-(2-benzyl-4-bromophenoxy)ethyl)carbamate (HIPS5635)**



Using general procedure C1, into a solution of 2-benzyl-4-bromophenol **HIPS5607** (1.0 eq., 0.100 g, 0.380 mmol) in anhydrous DMF (4 mL), CsCO<sub>3</sub> (3.0 eq., 0.375 g, 1.140 mmol) and TBAI (0.1 eq., 0.014 g, 0.038 mmol) were added. The mixture was stirred at RT for 1 h followed by the addition of *tert*-butyl (2-chloroethyl)carbamate (2.5 eq., 0.171 g, 0.950 mmol). The reaction was stirred overnight followed by another addition of *tert*-butyl (2-chloroethyl)carbamate (2.5 eq., 0.171 g, 0.950 mmol) with a total reaction time of 36 h to afford FCC purified compound **HIPS5635** as a yellow oil, (0.080 g, 52%). Further prep. HPLC purification (0.040 g) afforded compound **HIPS5635** as a white powder, (0.013 g).

<sup>1</sup>H NMR (Methanol-*d*<sub>4</sub>, 500 MHz)  $\delta$  7.22 - 7.24 (m, 1 H) 7.19 - 7.22 (m, 2 H) 7.14 - 7.17 (m, 2 H) 7.09 - 7.14 (m, 2 H) 6.79 (d, *J*=8.7 Hz, 1 H) 4.60 (br s, 1 H) 3.91 (t, *J*=5.5 Hz, 2 H) 3.88 (s, 2 H) 3.36 (t, *J*=5.5 Hz, 2 H) 1.38 (s, 9 H). <sup>13</sup>C NMR (Methanol-*d*<sub>4</sub>, 126 MHz)  $\delta$  158.6, 157.2, 141.9, 134.0, 131.3, 130.1, 129.6, 127.3, 114.5, 113.9, 80.4, 68.5, 41.1, 36.8, 28.9. HRMS (ESI+) calcd. for C<sub>20</sub>H<sub>24</sub>BrNO<sub>3</sub> [M + H]<sup>+</sup>: 406.10124, found: 306.04829 without Boc-group.

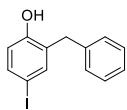
### **2-(2-Benzyl-4-bromophenoxy)ethan-1-amine (HIPS5636)**



Using general procedure D1, to a stirred solution of *tert*-butyl (2-(2-benzyl-4-bromophenoxy)ethyl)carbamate **HIPS5635** (1.0 eq., 0.020 mg, 0.049 mmol) in THF (1 mL), aq. 6M HCl (1 mL) was added. The mixture was stirred at RT for 1 h to afford prep. HPLC purified compound **HIPS5636** as a white powder one FA salt form, (0.002 g, 14%).

<sup>1</sup>H NMR (Methanol-*d*<sub>4</sub>, 500 MHz)  $\delta$  8.50 (br s, 1 H) 7.26 - 7.30 (m, 1 H) 7.20 - 7.25 (m, 2 H) 7.16 - 7.18 (m, 1 H) 7.12 - 7.15 (m, 3 H) 6.82 - 6.85 (m, 1 H) 3.98 - 4.03 (m, 2 H) 3.93 (s, 2 H) 3.02 - 3.08 (m, 2 H). <sup>13</sup>C NMR (Methanol-*d*<sub>4</sub>, 126 MHz)  $\delta$  156.9, 141.9, 134.4, 133.8, 131.5, 129.9, 129.7, 127.4, 114.6, 114.4, 68.5, 41.1, 36.9. HRMS (ESI+) calcd. for C<sub>15</sub>H<sub>16</sub>BrNO [M + H]<sup>+</sup>: 306.04881, found: 306.04807.

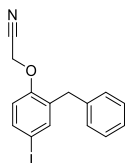
## 2-Benzyl-4-iodophenol (HIPS5605)



Using general procedure B, 1-(benzyloxy)-4-iodobenzene (1.0 eq., 0.210 g, 0.677 mmol) was reacted accordingly to afford FCC purified compound **HIPS5605** as a colourless oil, (0.053 g, 25%).

$^1\text{H}$  NMR (DMSO- $d_6$ , 500 MHz)  $\delta$  9.77 (br s, 1 H) 7.30 - 7.33 (m, 1 H) 7.29 - 7.34 (m, 1 H) 7.23 - 7.29 (m, 2 H) 7.19 - 7.23 (m, 2 H) 7.14 - 7.19 (m, 1 H) 6.64 (br d,  $J=9.2$  Hz, 1 H) 3.81 (s, 2 H).  $^{13}\text{C}$  NMR (DMSO- $d_6$ , 126 MHz)  $\delta$  155.6, 141.1, 138.7, 136.1, 131.3, 129.1, 128.8, 126.3, 118.2, 81.3, 35.2. HRMS (ESI+) calcd. for  $\text{C}_{13}\text{H}_{11}\text{IO}$  [ $\text{M} - \text{H}$ ] $^-$ : 308.97818, found: 308.97791.

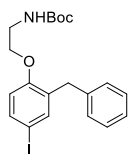
## 2-(2-Benzyl-4-iodophenoxy)acetonitrile (HIPS5606)



Using general procedure A, 2-benzyl-4-iodophenol **HIPS5605** (1.0 eq., 0.045 g, 0.145 mmol) was refluxed for 8 h with anhydrous  $\text{K}_2\text{CO}_3$  (1.0 eq., 0.020 g, 0.145 mmol), NaI (0.2 eq., 0.004 g, 0.029 mmol) and chloroacetonitrile (1.0 eq., 10  $\mu\text{L}$ , 0.145 mmol) in dry acetone (0.45 mL) to afford FCC purified compound **HIPS5606** as a colourless oil, (0.038 g, 75%).

$^1\text{H}$  NMR (acetone- $d_6$ , 500 MHz)  $\delta$  7.60 - 7.74 (m, 1 H) 7.51 - 7.57 (m, 1 H) 7.15 - 7.33 (m, 4 H) 6.93 - 7.02 (m, 1 H) 5.13 (s, 2 H) 3.96 (s, 2 H).  $^{13}\text{C}$  NMR (DMSO- $d_6$ , 126 MHz)  $\delta$  154.1, 138.8, 138.3, 136.1, 132.9, 128.6, 128.4, 126.1, 126.1, 116.4, 115.0, 85.8, 53.7, 34.5. HRMS (ESI+) calcd. for  $\text{C}_{15}\text{H}_{12}\text{INO}$  [ $\text{M} - \text{H}$ ] $^-$ : 347.98908, found: 347.9888.

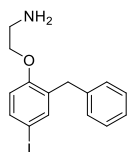
### ***Tert*-butyl (2-(2-benzyl-4-iodophenoxy)ethyl)carbamate (HIPS5637)**



Using general procedure C1, 2-benzyl-4-iodophenol **HIPS5605** (1.0 eq., 0.120 g, 0.387 mmol) was reacted with CsCO<sub>3</sub> (3.0 eq., 0.382 g, 1.161 mmol) and TBAI (0.1 eq., 0.039 g, 0.014 mmol) in dry DMF (4 mL). The mixture was stirred at RT for 1 h followed by the addition of *tert*-butyl (2-chloroethyl)carbamate (2.5 eq., 0.174 g, 0.967 mmol). The reaction was stirred overnight followed by another addition of *tert*-butyl (2-chloroethyl)carbamate (2.5 eq., 0.174 g, 0.967 mmol) with a total reaction time of 36 h to afford FCC purified compound **HIPS5637** as a yellow oil, (0.090 g, 51%). Further prep. HPLC purification (0.045 g) afforded compound **HIPS5637** as a white powder, (0.015 g).

<sup>1</sup>H NMR (Methanol-*d*<sub>4</sub>, 500 MHz)  $\delta$  7.41 (dd, *J*=8.5, 2.3 Hz, 1 H) 7.31 (d, *J*=2.3 Hz, 1 H) 7.18 - 7.23 (m, 2 H) 7.13 - 7.18 (m, 2 H) 7.09 - 7.13 (m, 1 H) 6.68 (br d, *J*=8.5 Hz, 1 H) 4.60 (br s, 4 H) 3.91 (br t, *J*=5.4 Hz, 2 H) 3.85 (s, 2 H) 3.35 (br t, *J*=5.4 Hz, 2 H), 1.34 - 1.41 (m, 9 H). <sup>13</sup>C NMR (Methanol-*d*<sub>4</sub>, 126 MHz)  $\delta$  157.9, 152.6, 142.0, 140.0, 137.6, 134.4, 130.1, 129.6, 127.2, 115.0, 83.7, 80.4, 68.3, 41.0, 36.7, 28.9. HRMS (ESI+) calcd. for C<sub>15</sub>H<sub>12</sub>INO [M + H]<sup>+</sup>: 454.08737, found: 354.03433 without Boc-group.

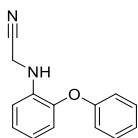
### **2-(2-Benzyl-4-iodophenoxy)ethan-1-amine (HIPS5638)**



Using general procedure D1, to a stirred solution of *tert*-butyl (2-(2-benzyl-4-iodophenoxy)ethyl)carbamate **HIPS5637** (1.0 eq., 0.030 mg, 0.063 mmol) in THF (1.1 mL), aq. 6M HCl (1.1 mL) was added. The mixture was stirred at RT for 1 h to afford prep. HPLC purified compound **HIPS5638** as a white powder one FA salt form, (0.002 g, 7%).

<sup>1</sup>H NMR (Methanol-*d*<sub>4</sub>, 500 MHz)  $\delta$  8.49 (br s, 1 H) 7.46 (br d, *J*=8.7 Hz, 1 H) 7.33 - 7.37 (m, 1 H) 7.20 - 7.25 (m, 2 H) 7.10 - 7.15 (m, 3 H) 6.72 (d, *J*=8.5 Hz, 1 H) 4.01 (t, *J*=4.5 Hz, 2 H) 3.91 (s, 2 H) 3.06 (br t, *J*=4.5 Hz, 2 H). <sup>13</sup>C NMR (Methanol-*d*<sub>4</sub>, 126 MHz)  $\delta$  170.4, 157.6, 141.9, 140.4, 137.8, 134.2, 129.9, 129.7, 127.4, 115.2, 84.3, 68.0, 41.0, 36.8. HRMS (ESI+) calcd. for C<sub>15</sub>H<sub>16</sub>INO [M + H]<sup>+</sup>: 354.03494, found: 354.03393.

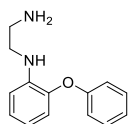
## 2-((2-Phenoxyphenyl)amino)acetonitrile (HIPS5503)



Using general procedure A, 2-phenoxyaniline (1.0 eq., 0.500 g, 2.699 mmol) was refluxed for 16 h with anhydrous  $K_2CO_3$  (1.0 eq., 0.373 g, 2.699 mmol), NaI (0.2 eq., 0.081 g, 0.540 mmol) and chloroacetonitrile (1.0 eq., 170  $\mu$ L, 2.699 mmol) in dry acetone (5 mL). After 16 h, the reaction was reloaded with  $K_2CO_3$  (0.5 eq.), NaI (0.1 eq.) and chloroacetonitrile (1.0 eq.) and the mixture was refluxed for 60 h in total to afford FCC purified compound **HIPS5503** as a light yellow oil, (0.200 g, 33%). Additional prep. HPLC purified compound **HIPS5503** was afforded from the unreacted starting material from the following step (**HIPS5504**) as a light beige powder, (0.023 g).

$^1H$  NMR (DMSO- $d_6$ , 500 MHz)  $\delta$  7.32 - 7.36 (m, 2 H) 7.11 (td,  $J=7.7$ , 1.4 Hz, 1 H) 7.05 - 7.09 (m, 1 H) 6.89 - 6.94 (m, 3 H) 6.84 (dd,  $J=7.7$ , 1.4 Hz, 1 H) 6.73 (td,  $J=7.7$ , 1.4 Hz, 1 H) 5.97 (t,  $J=6.9$  Hz, 1 H) 4.25 (d,  $J=6.9$  Hz, 2 H).  $^{13}C$  NMR (DMSO- $d_6$ , 126 MHz)  $\delta$  157.3, 143.0, 138.5, 129.8, 125.1, 122.7, 119.7, 118.5, 118.2, 117.1, 112.3, 31.5. HRMS (ESI+) calcd. for  $C_{14}H_{12}N_2O$   $[M + H]^+$ : 225.10224, found: 225.10184.

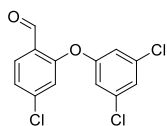
## $N^1$ -(2-Phenoxyphenyl)ethane-1,2-diamine (HIPS5504)



2-((2-phenoxyphenyl)amino)acetonitrile **HIPS5503** (1.0 eq., 0.156 g, 0.696 mmol) was dissolved in dry diethyl ether (1.0 mL) and flushed with  $N_2$ .  $LiAlH_4$  (2.0 eq., 0.053 g, 1.391 mmol) was carefully dissolved in another flask in dry diethyl ether (1.8 mL) under  $N_2$  flow. The solution of **HIPS5503** was then added dropwise to the  $LiAlH_4$  mixture and let to stir at RT for 2 h. LCMS control revealed a side product formation ( $m/z$  (ESI+): 200  $[M + H]^+$ ). The mixture was quenched with aq. 2M NaOH (2 mL) under ice bath. The aqueous layer was extracted with diethyl ether (2 x 10 mL). The organic phase was concentrated *in vacuo* and purified with prep. HPLC to afford compound **HIPS5504** as an off-white powder one FA salt form, (0.005 g, 2%).

$^1H$  NMR (DMSO- $d_6$ , 500 MHz)  $\delta$  8.41 (br s, 1 H) 7.29 - 7.38 (m, 2 H) 6.98 - 7.09 (m, 1 H) 6.98 - 7.04 (m, 1 H) 6.92 (br d,  $J=8.4$  Hz, 2 H) 6.74 - 6.78 (m, 1 H) 6.73 - 6.80 (m, 1 H) 6.55 - 6.61 (m, 1 H) 5.39 (br s, 1 H) 3.21 - 3.27 (m, 2 H) 2.80 - 2.91 (m, 2 H).  $^{13}C$  NMR (DMSO- $d_6$ , 126 MHz)  $\delta$  157.4, 142.6, 140.3, 129.8, 125.0, 122.6, 119.3, 117.3, 116.1, 111.2, 42.3, 38.7. HRMS (ESI+) calcd. for  $C_{14}H_{16}N_2O$   $[M + H]^+$ : 229.13354, found: 229.13301.

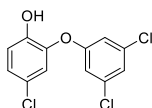
#### 4-Chloro-2-(3,5-dichlorophenoxy)benzaldehyde (HIPS5673-precursor)<sup>136</sup>



To a stirred solution of 4-chloro-2-fluorobenzaldehyde (1.0 eq., 0.500 g, 3.153 mmol) and 3,5-dichlorophenol (1.1 eq., 0.585 g, 3.469 mmol) in DMSO (6.5 mL), K<sub>2</sub>CO<sub>3</sub> (1.2 eq., 0.523 g, 3.784 mmol) was added. The mixture was stirred overnight at 100 °C. The reaction mixture was cooled down to RT and quenched with aq. 1M HCl (15 mL) and extracted with diethyl ether (2 x 20 mL). The combined organic layers were washed with brine (20 mL), dried over anhydrous Na<sub>2</sub>SO<sub>4</sub>, filtered and evaporated to dryness. The crude was absorbed onto ISOLUTE® HM-N and purified by FCC with an alternating gradient of 0–20% acetone in hexane to afford compound **HIPS5673-precursor** as a white sticky solid, (0.743 g, 78%).

<sup>1</sup>H NMR (DMSO-*d*<sub>6</sub>, 500 MHz) δ 10.23 (s, 1 H) 7.88 (d, *J*=8.2 Hz, 1 H) 7.50 (t, *J*=1.8 Hz, 1 H) 7.44 - 7.48 (m, 1 H) 7.32 (d, *J*=1.7 Hz, 2 H) 7.27 (d, *J*=1.8 Hz, 1 H). <sup>13</sup>C NMR (DMSO-*d*<sub>6</sub>, 500 MHz) δ 188.1, 158.0, 157.3, 140.5, 135.1, 130.6, 125.7, 125.3, 124.5, 119.8, 118.4. LCMS *m/z* (ESI+) 300.9 [M – H]<sup>+</sup>.

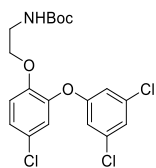
#### 4-Chloro-2-(3,5-dichlorophenoxy)phenol (HIPS5673)<sup>136</sup>



To a stirred solution of 4-chloro-2-(3,5-dichlorophenoxy)benzaldehyde **HIPS5673-precursor** (1.0 eq., 0.594 g, 1.970 mmol) in chloroform (7 mL), *m*-CPBA (purity ~75%) (5.0 eq., 2.266 g, 9.849 mmol) was added. The mixture was refluxed for 2 h. The mixture was then cooled down, quenched with aq. 10% Na<sub>2</sub>S<sub>2</sub>O<sub>3</sub> (10 mL) and extracted with DCM (3 x 15 mL). The combined organic layers were washed with brine, dried over anhydrous Na<sub>2</sub>SO<sub>4</sub>, filtered and evaporated to dryness. The crude was dissolved in MeOH (15 mL) and K<sub>2</sub>CO<sub>3</sub> (3 eq., 0.716 g, 5.181 mmol) was added. The mixture was stirred at RT for 30 min followed by filtration. The filtrate was absorbed onto ISOLUTE® HM-N and purified by FCC with an alternating gradient of 0–10% acetone in cyclohexane to afford compound **HIPS5673** as a light yellow sticky solid, (0.215 g, 38%).

<sup>1</sup>H NMR (CDCl<sub>3</sub>, 500 MHz) δ 7.17 (t, *J*=1.9 Hz, 1 H) 7.10 (dd, *J*=8.6, 2.4 Hz, 1 H) 7.01 (d, *J*=8.6 Hz, 1 H) 6.92 - 6.93 (m, 3 H) 5.35 (s, 1 H). <sup>13</sup>C NMR (CDCl<sub>3</sub>, 126 MHz) δ 157.2, 145.9, 142.3, 135.8, 125.7, 124.2, 119.5, 117.4, 116.4, 115.8. HRMS (ESI+) calcd. for C<sub>12</sub>H<sub>7</sub>Cl<sub>3</sub>O<sub>2</sub> [M – H]<sup>+</sup>: 286.94388, found: 286.94381.

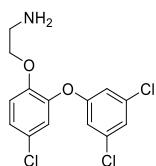
***Tert*-butyl (2-(4-chloro-2-(3,5-dichlorophenoxy)phenoxy)ethyl)carbamate (HIPS5674)**



Using general procedure C2, into a solution of 4-chloro-2-(3,5-dichlorophenoxy)phenol **HIPS5673** (1.0 eq., 0.157 g, 0.542 mmol) in anhydrous DMF (2 mL),  $K_2CO_3$  (3.0 eq., 0.225 g, 1.627 mmol) was added. The mixture was stirred at RT for 30 min followed by the addition of KI (2.0 eq., 0.180 g, 1.084 mmol) and *tert*-butyl (2-chloroethyl)carbamate (1.2 eq., 0.117 g, 0.651 mmol). The mixture was refluxed for 4 h. The reaction mixture was cooled down to RT, diluted with water (10 mL) and extracted with EtOAc (3 x 15 mL). The combined organic layers were washed with brine (3 x 5 mL), dried over anhydrous  $Na_2SO_4$ , filtered and evaporated to dryness. The crude was absorbed onto ISOLUTE® HM-N and purified by FCC with an alternating gradient of 0–10% EtOAc in cyclohexane to afford compound **HIPS5674** as a light yellow oil, (0.165 g, 70%). Further prep. HPLC purification (0.065 g) afforded compound **HIPS5674** as a white powder, (0.031 g).

$^1H$  NMR ( $CDCl_3$ , 500 MHz)  $\delta$  7.02 - 7.06 (m, 2 H) 6.99 - 7.01 (m, 2 H) 6.79 (d,  $J=1.6$  Hz, 2 H) 4.47 (br s, 1 H) 3.99 (t,  $J=5.0$  Hz, 2 H) 3.39 (q,  $J=5.0$  Hz, 2 H) 1.44 (s, 9 H).  $^{13}C$  NMR ( $CDCl_3$ , 126 MHz)  $\delta$  152.1, 150.9, 149.1, 141.9, 135.5, 123.3, 122.8, 121.8, 115.0, 114.9, 79.8, 68.6, 53.7, 28.3. HRMS (ESI+) calcd. for  $C_{19}H_{20}Cl_3NO_4$   $[M + H]^+$ : 432.05307, found: 332.00007 without Boc-group.

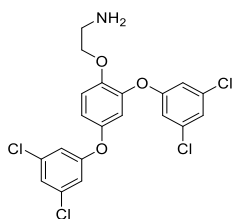
## 2-(4-Chloro-2-(3,5-dichlorophenoxy)phenoxy)ethan-1-amine (HIPS5675)



To a stirred solution of *tert*-butyl (2-(4-chloro-2-(3,5-dichlorophenoxy)phenoxy)ethyl)carbamate **HIPS5674** (1.0 eq., 0.100 g, 0.231 mmol) in dioxane (0.5 mL), 4M HCl/dioxane (10 eq., 0.58 mL, 2.311 mmol) was added. The mixture was stirred at RT overnight (14 h) resulting in the desired compound and a side product formation ( $m/z$ : 460). The mixture was concentrated to dryness and the crude was partitioned between water and diethyl ether. The organic layer was washed with aq. 1M HCl. The aqueous layer was basified with aq. 2M NaOH and extracted with DCM (2 x 5 mL). The combined organic layers were dried over anhydrous  $\text{Na}_2\text{SO}_4$ , filtered and evaporated to dryness. The crude was purified by prep. HPLC to afford compound **HIPS5675** as a white powder one FA salt form, (0.008 g, 9%).

$^1\text{H}$  NMR (DMSO- $d_6$ , 500 MHz,)  $\delta$  8.28 (s, 1 H) 7.33 (d,  $J=2.4$  Hz, 1 H) 7.31 (t,  $J=1.6$  Hz, 1 H) 7.22 (d,  $J=8.5$  Hz, 1 H) 7.09 (dd,  $J=8.5, 2.4$  Hz, 1 H) 6.95 (d,  $J=1.6$  Hz, 2 H) 4.05 (t,  $J=5.5$  Hz, 9 H) 2.81 (t,  $J=5.5$  Hz, 2 H).  $^{13}\text{C}$  NMR (DMSO- $d_6$ , 126 MHz)  $\delta$  164.3, 159.0, 150.9, 141.7, 134.7, 130.3, 123.5, 122.3, 121.5, 115.4, 115.2, 69.5 (one peak under DMSO- $d_6$ ). HRMS (ESI+) calcd. for  $\text{C}_{14}\text{H}_{12}\text{Cl}_3\text{NO}_2$   $[\text{M} + \text{H}]^+$ : 332.00064, found: 331.99998.

## 2-(2,4-Bis(3,5-dichlorophenoxy)phenoxy)ethan-1-amine (HIPS5676)

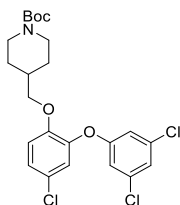


Isolated side product from the reaction affording **HIPS5676**, (0.002 g).

$^1\text{H}$  NMR (DMSO- $d_6$ , 500 MHz,)  $\delta$  7.74 (br s, 2 H), 7.39 - 7.41 (m, 1 H) 7.31 - 7.34 (m, 1 H) 7.25 (d,  $J=8.6$  Hz, 1 H) 7.14 - 7.16 (m, 2 H) 7.12 (d,  $J=2.7$  Hz, 1 H) 7.00 - 7.03 (m, 2 H) 6.81 (dd,  $J=8.6, 2.7$  Hz, 1 H) 4.14 - 4.21 (m, 2 H) 3.04 - 3.14 (m, 2 H).  $^{13}\text{C}$  NMR (DMSO- $d_6$ , 126 MHz)  $\delta$  159.3, 158.7, 152.8, 151.0, 140.0, 135.0, 134.8, 123.5, 123.1, 122.3, 117.0, 115.5, 113.2, 108.1, 66.2, 38.2. HRMS (ESI+) calcd. for  $\text{C}_{20}\text{H}_{15}\text{Cl}_4\text{NO}_3$   $[\text{M} + \text{H}]^+$ : 457.98788, found: 457.98757.



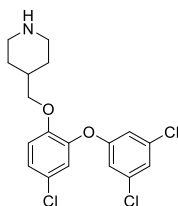
**Tert-butyl 4-((4-chloro-2-(3,5-dichlorophenoxy)phenoxy)methyl)piperidine-1-carboxylate (HIPS6016-precursor)**



Using general procedure C2, into a solution of 4-chloro-2-(3,5-dichlorophenoxy)phenol **HIPS5673** (1 eq., 0.110 g, 0.400 mmol) in dry DMF (4 mL),  $K_2CO_3$  (3 eq., 0.166 g, 1.2 mmol), *tert*-butyl 4-(chloromethyl)piperidine-1-carboxylate (1.2 eq., 0.112 g, 0.480 mmol) and KI (2 eq., 0.133 g, 0.800 mmol) were added. The mixture was stirred at 80 °C for 4 h followed by an addition of *tert*-butyl 4-(chloromethyl)piperidine-1-carboxylate (1 eq., 0.094 g, 0.400 mmol). The reaction was stirred overnight followed by another addition of *tert*-butyl 4-(chloromethyl)piperidine-1-carboxylate (0.2 eq., 0.019 g, 0.080 mmol) with a total reaction time of 30 h. The crude was absorbed onto silica 0.063–0.200 mm and purified by FCC with an alternating gradient of 0–10% EtOAc in cyclohexane to afford compound **HIPS6016-precursor** as a colourless oil, (0.100 g, 51%).

$^1H$  NMR (DMSO- $d_6$ , 500 MHz)  $\delta$  7.24 - 7.29 (m, 3 H) 7.07 (dd,  $J=8.5, 2.3$  Hz, 1 H) 6.89 (d,  $J=1.7$  Hz, 2 H) 3.86 (br d,  $J=6.3$  Hz, 5 H) 3.54 (d,  $J=6.3$  Hz, 1 H) 1.63 - 1.73 (m, 2 H) 1.36 - 1.38 (m, 9 H) 0.89 (br dd,  $J=12.3, 3.9$  Hz, 2 H).  $^{13}C$  NMR (DMSO- $d_6$ , 126 MHz)  $\delta$  159.3, 153.8, 151.1, 141.1, 134.7, 130.5, 123.7, 122.0, 121.0, 114.9, 114.8, 78.6, 78.5, 72.5, 49.8, 37.8, 35.0, 28.1. LCMS  $m/z$  (ESI+) 386.1  $[M + H]^+$  without Boc-group.

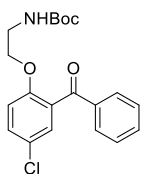
#### 4-((4-Chloro-2-(3,5-dichlorophenoxy)phenoxy)methyl)piperidine (HIPS6016)



Using general procedure D2, into a solution of *tert*-butyl 4-((4-chloro-2-(3,5-dichlorophenoxy)phenoxy)methyl)piperidine-1-carboxylate **HIPS6016-precursor** (1 eq., 0.100 g, 0.210 mmol) in dioxane (0.5 mL), 4M HCl/dioxane (10 eq., 0.53 mL, 2.100 mmol) was added and the reaction was stirred at RT for 7 h to afford a crude product as an oil, (0.070 g, 86%). Further prep. HPLC purification (0.060 g) afforded compound **HIPS6016** as a beige powder one FA salt, (0.025 g).

$^1\text{H}$  NMR (DMSO- $d_6$ , 500 MHz)  $\delta$  8.38 (br s, 1 H) 7.28 - 7.31 (m, 2 H) 7.24 (d,  $J=8.5$  Hz, 1 H) 7.07 (dd,  $J=8.5, 2.4$  Hz, 1 H) 6.91 (d,  $J=1.8$  Hz, 2 H) 3.85 (d,  $J=6.7$  Hz, 3 H) 3.03 (br d,  $J=12.4$  Hz, 3 H) 2.58 - 2.65 (m, 3 H) 1.74 (br s, 2 H) 1.47 (br d,  $J=12.4$  Hz, 3 H) 1.12 (br d,  $J=10.1$  Hz, 3 H).  $^{13}\text{C}$ - NMR (DMSO- $d_6$ , 126 MHz)  $\delta$  159.3, 151.0, 141.2, 134.7, 130.5, 123.7, 122.1, 121.1, 115.0, 114.9, 72.5, 43.2, 33.8, 26.3. HRMS (ESI+) calcd. for  $\text{C}_{18}\text{H}_{18}\text{Cl}_3\text{NO}_2$   $[\text{M} + \text{H}]^+$ : 386.04759, found: 386.04760.

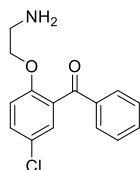
#### *Tert*-butyl (2-(2-benzoyl-4-chlorophenoxy)ethyl)carbamate (Benzophenone probe precursor)



Using general procedure C1, (5-chloro-2-hydroxyphenyl)(phenyl)methanone (1.0 eq., 0.150 g, 0.645 mmol) was reacted with  $\text{CsCO}_3$  (3.0 eq., 0.636 g, 1.934 mmol) and TBAI (0.02 eq., 0.004 g, 0.013 mmol) in dry DMF (6 mL). The mixture was stirred at RT for 1 h followed by the addition of *tert*-butyl (2-chloroethyl)carbamate (2.5 eq., 0.174 g, 0.967 mmol). The reaction was stirred overnight in total for 4 days to afford FCC purified **Benzophenone probe precursor** compound as a light yellow powder, (0.110 g, 48%).

HRMS (ESI+) calcd. for  $\text{C}_{20}\text{H}_{22}\text{ClNO}_4$   $[\text{M} + \text{H}]^+$ : 376.13102, found: 276.07809 without Boc-group.

### (2-(2-Aminoethoxy)-5-chlorophenyl)(phenyl)methanone (Benzophenone probe)

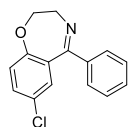


Using general procedure D1, to a stirred solution of *tert*-butyl (2-(2-benzoyl-4-chlorophenoxy)ethyl)carbamate **Benzophenone probe precursor** (1.0 eq., 0.015 mg, 0.038 mmol) in THF (1.5 mL), aq. 6M HCl (8 eq., 2 mL) was added. The mixture was stirred at RT for 1.5 h to afford prep. HPLC purified compound **Benzophenone probe** as a white powder one FA salt, (0.007 g, 55%). The compound however underwent *in situ* reaction partly into the compound **Benzophenone probe – side product** ( $m/z$ : 258.2) as observed with LCMS (Figure 5.2.5.3:1). The shift was also clearly seen in NMR (Figure 5.2.5.3:2).

To briefly investigate the *in situ* reaction, Boc-deprotection was tried using a mixture of 1:10 (TFA:DCM) in an analytical scale showing slower conversion to the compound ( $m/z$ : 258.2). Prep. HPLC was done with 0.1% TFA, affording compound **HKR194** as a white powder one TFA salt. The NMR measurement was repeated after 6.5 h hours showing the formation of the side product.

HRMS (ESI+) calcd. for  $C_{15}H_{14}ClNO_2$   $[M + H]^+$ : 276.07859, found: 276.07797.

### 7-Chloro-5-phenyl-2,3-dihydrobenzo[f][1,4]oxazepine (Benzophenone probe – side product)



HRMS (ESI+) calcd. for  $C_{15}H_{12}ClNO$   $[M + H]^+$ : 258.06802, found: 258.06750.

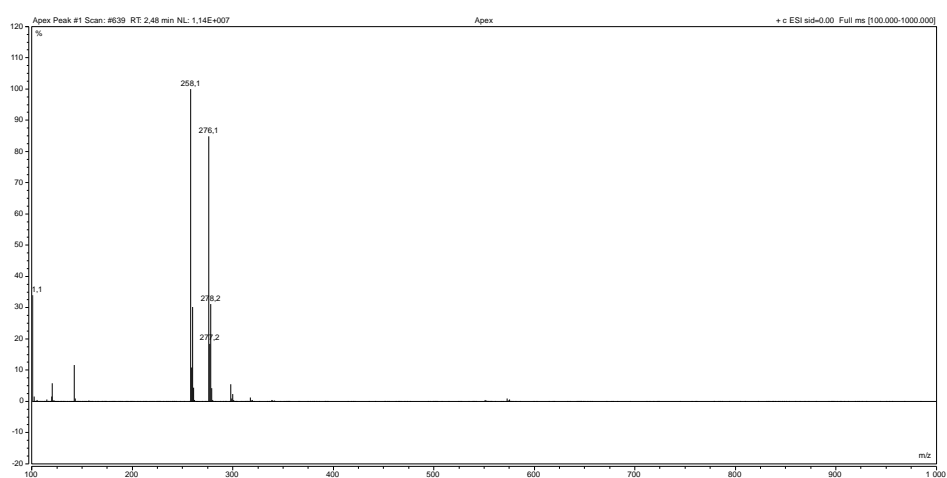
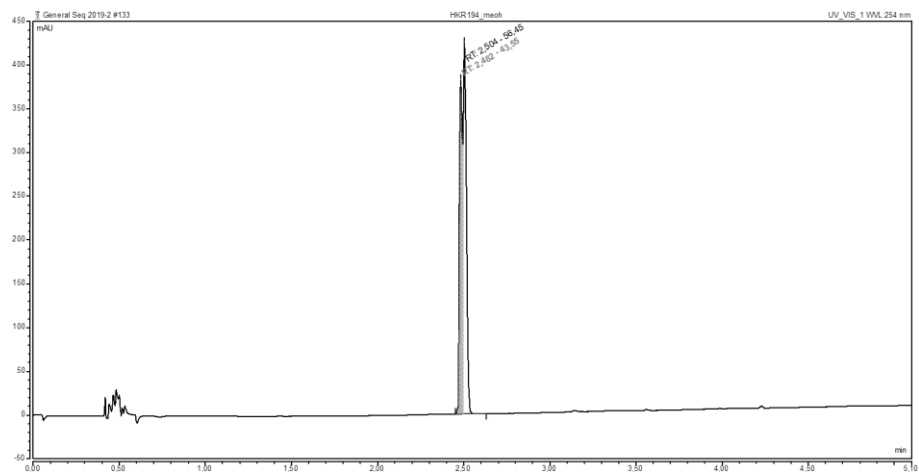


**Figure 5.2.5.3:1** - Side product formation from **Benzophenone probe** (right-hand side peak) into the **Benzophenone probe – side product** (left-hand side peak) in MeOH sample.

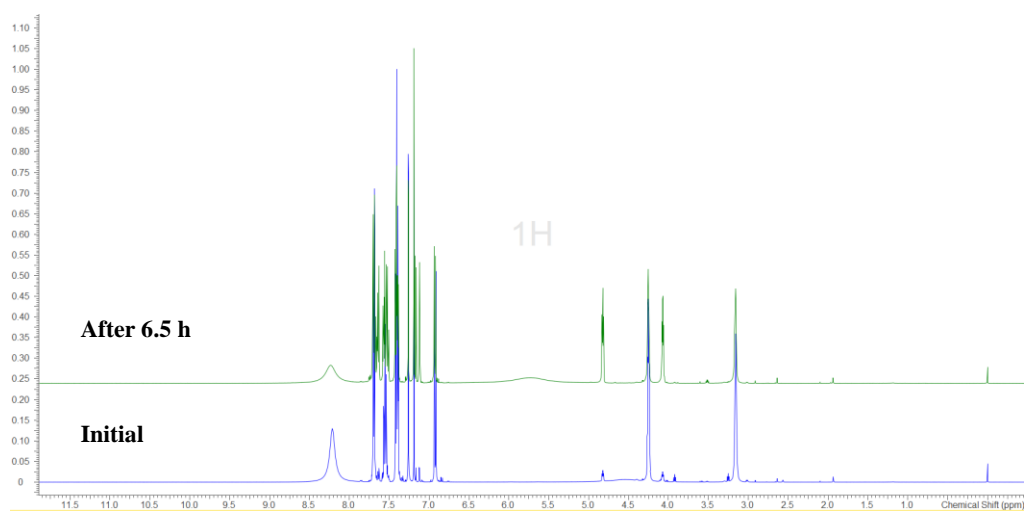


**Figure 5.2.5.3:2** -  $^1\text{H-NMR}$  spectrum of the mixture as a TFA salt in  $\text{CDCl}_3$ .

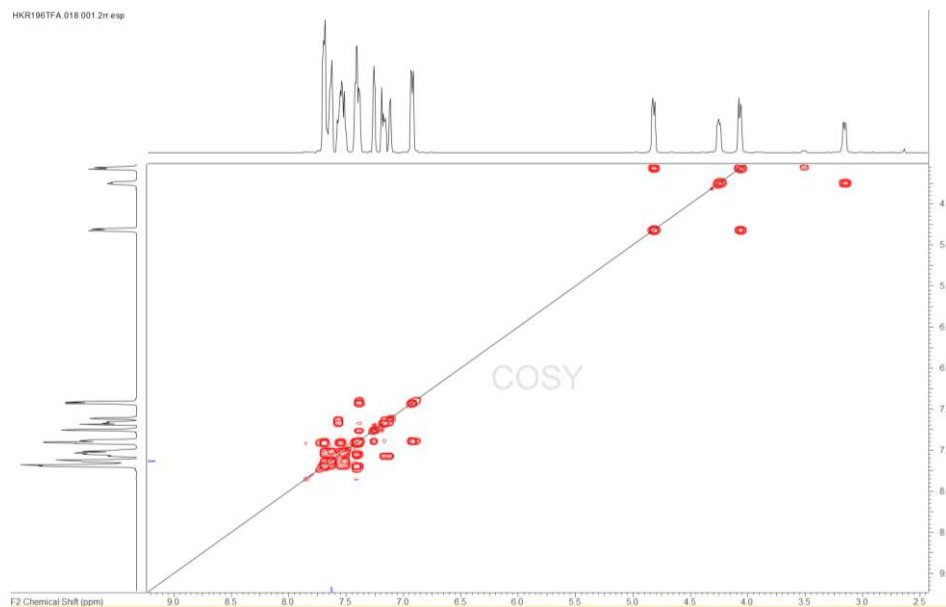


**Figure 5.2.5.3:3** - [ $^1\text{H}, ^1\text{H}$ ]-COSY NMR spectrum of the mixture as a TFA salt in  $\text{CDCl}_3$ .

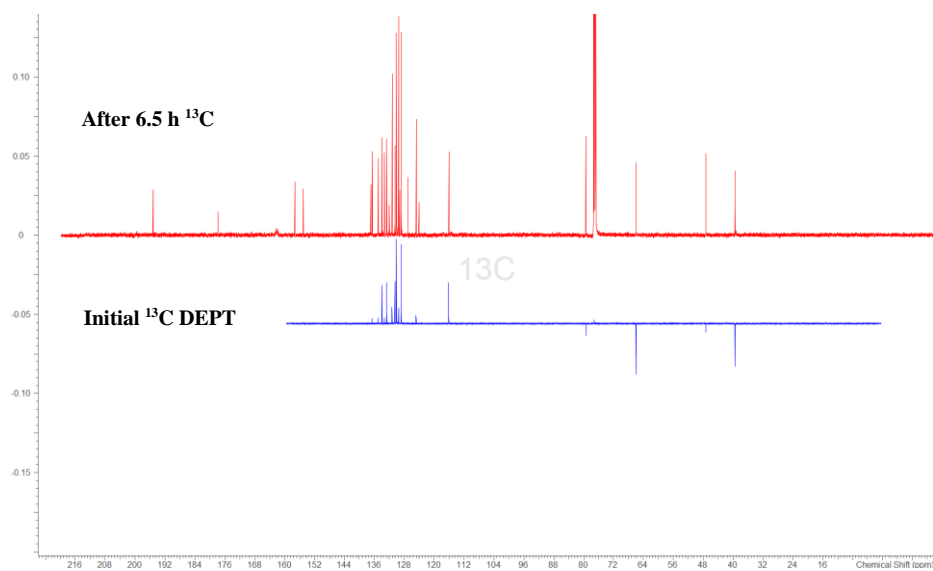
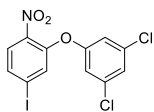


**Figure 5.2.5.3:4** -  $^{13}\text{C}$  NMR spectrum of the mixture as a TFA salt in  $\text{CDCl}_3$ .

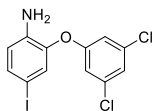
## 2-(3,5-Dichlorophenoxy)-4-iodo-1-nitrobenzene (HIPS5845-precursor)



A solution of 3,5-dichlorophenol (1.0 eq., 0.305 g, 1.87 mmol) and  $K_2CO_3$  (1.2 eq., 0.310 g, 2.24 mmol) was stirred in DMSO (9.35 mL) at RT for 30 min. Then 2-fluoro-4-iodo-1-nitrobenzene (1.0 eq., 0.500 g, 1.87 mmol) was added and the mixture was refluxed for 3 h. The mixture was quenched with water and extracted with EtOAc (3x). The organic layers were combined and concentrated *in vacuo* to afford **HIPS5845-precursor** as crude yellow powder, (0.700 g, 91%).

$^1H$  NMR (DMSO- $d_6$ , 500 MHz)  $\delta$  7.85 - 7.90 (m, 2 H), 7.77 (d,  $J=1.4$  Hz, 1 H), 7.46 (t,  $J=1.8$  Hz, 1 H), 7.22 (d,  $J=1.8$  Hz, 2 H).  $^{13}C$  NMR (DMSO- $d_6$ , 126 MHz)  $\delta$  157.4, 147.8, 141.0, 135.1, 134.8, 131.0, 127.4, 124.1, 117.2, 103.1.

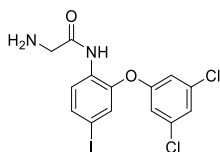
## 2-(3,5-Dichlorophenoxy)-4-iodoaniline (HIPS5845)



2-(3,5-Dichlorophenoxy)-4-iodo-1-nitrobenzene **HIPS5845-precursor** (1.0 eq., 0.700 g, 1.71 mmol) and Fe (5.0 eq., 0.477 g, 8.55 mmol) were mixed with  $NH_4Cl$  (1.0 eq., 0.09 g, 1.71 mmol) in EtOH/ $H_2O$  (2:1, 18 mL). The mixture was refluxed for 2 h and then filtered through celite. The remaining filtrate was concentrated *in vacuo* to afford **HIPS5845** as a crude brown solid, (0.600 g, 92%).

$^1H$  NMR (DMSO- $d_6$ , 500 MHz)  $\delta$  7.27 - 7.30 (m, 2 H), 7.20 - 7.22 (m, 1 H), 6.87 (d,  $J=1.8$  Hz, 2 H), 6.66 (d,  $J=8.4$  Hz, 1 H), 5.30 (s, 2 H).  $^{13}C$  NMR (DMSO- $d_6$ , 126 MHz)  $\delta$  158.8, 141.0, 140.6, 134.9, 134.6, 129.4, 122.0, 118.2, 115.3, 75.0. HRMS (ESI+) calcd. for  $C_{12}H_8Cl_2INO$  [ $M + H$ ] $^+$ : 379.91004, found: 379.90918.

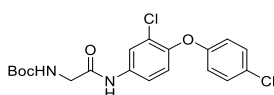
## 2-Amino-N-(2-(3,5-dichlorophenoxy)-4-iodophenyl)acetamide (HIPS5933)



*N*-Boc glycine (0.115 g, 0.656 mmol) was refluxed with SOCl<sub>2</sub> (3 mL) for 2 h. After evaporation of the solvent, the formed acid chloride was added to a mixture of **HIPS5845** (1 eq., 0.100 g, 0.260 mmol) in DMF (3 mL) under dry condition. The mixture was stirred at RT overnight. The mixture was quenched with water and extracted with EtOAc (3x). The organic layers were combined, concentrated and purified with prep. HPLC to afford **HIPS5933** as a white powder one FA salt, (0.030 g, 26%).

<sup>1</sup>H NMR (DMSO-*d*<sub>6</sub>, 500 MHz) δ 8.18 (s, 1 H) 8.06 (d, *J*=8.6 Hz, 1 H) 7.60 (dd, *J*=8.6, 1.9 Hz, 1 H) 7.43 (t, *J*=1.7 Hz, 1 H) 7.41 (d, *J*=1.7 Hz, 1 H) 7.10 (d, *J*=1.9 Hz, 2 H) 3.41 (s, 4 H). <sup>13</sup>C NMR (DMSO-*d*<sub>6</sub>, 126 MHz) δ 169.7, 163.6, 157.8, 145.5, 135.0, 134.2, 129.8, 128.0, 123.7, 123.4, 117.2, 87.5, 43.6. HRMS (ESI+) calcd. for C<sub>14</sub>H<sub>11</sub>Cl<sub>2</sub>IN<sub>2</sub>O<sub>2</sub> [M + H]<sup>+</sup>: 436.93151, found: 436.93052.

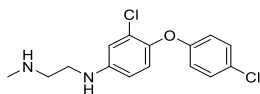
## *Tert*-butyl 2-((3-chloro-4-(4-chlorophenoxy)phenyl)amino)-2-oxoethyl)carbamate (HIPS6027-precursor)



Using general procedure E, into a solution of *N*-Boc-glycine (1.0 eq., 0.125 g, 0.715 mmol) in dry DMF (3.5 mL), DIPEA (1.1 eq., 0.14 mL, 0.787 mmol), HATU (1.2 eq., 0.326 g, 0.858 mmol) and 3-chloro-4-(4-chlorophenoxy)aniline **HIPS5850** (1.1 eq., 0.200 g, 0.787 mmol) were added. The reaction was stirred for 48 h. The crude was absorbed onto silica 0.063–0.200 mm and purified by FCC with an alternating gradient of 0–30% EtOAc in cyclohexane to afford compound **HIPS6027-precursor** as a white solid, (0.220 g, 75%).

<sup>1</sup>H NMR (DMSO-*d*<sub>6</sub>, 500 MHz) δ 10.17 (s, 1 H) 7.95 (d, *J*=2.4 Hz, 1 H) 7.49 (dd, *J*=8.9, 2.4 Hz, 1 H) 7.37 - 7.42 (m, 2 H) 7.18 (d, *J*=8.9 Hz, 1 H) 7.10 (t, *J*=6.0 Hz, 1 H) 6.90 - 6.94 (m, 2 H) 3.72 (d, *J*=6.0 Hz, 2 H) 1.39 (s, 9 H). <sup>13</sup>C NMR (DMSO-*d*<sub>6</sub>, 126 MHz) δ 168.6, 156.1, 155.9, 145.8, 136.8, 129.8, 126.6, 125.1, 122.6, 120.6, 119.4, 118.2, 78.1, 54.9, 43.8, 28.2. HRMS (ESI+) calcd. for C<sub>19</sub>H<sub>20</sub>Cl<sub>2</sub>N<sub>2</sub>O<sub>4</sub> [M + H]<sup>+</sup>: 411.08729, found: 311.03470 without Boc-group.

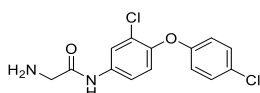
## 2-Amino-N-(3-chloro-4-(4-chlorophenoxy)phenyl)acetamide (HIPS5990)



To a solution of **HIPS6027-precursor** (1.0 eq., 0.227 g, 0.551 mmol) in dry THF (2 mL) in a 2-neck round flask flushed with nitrogen, a suspension of LiAlH<sub>4</sub> (3.0 eq., 0.062 g, 1.652 mmol) in anhydrous THF (2 mL) was added. The reaction mixture was refluxed for 4 h followed by an addition of a new suspension of LiAlH<sub>4</sub> (3.0 eq., 0.062 g, 1.652 mmol) in anhydrous THF (4 mL). The mixture was refluxed for 1.5 h, resulting in the conversion of the side product under LCMS control. The reaction was quenched with ice and aq. 2 M HCl was added dropwise. The mixture was diluted with water and extracted with EtOAc. The crude was concentrated *in vacuo*, (0.140 g, 82%). Further prep. HPLC purification (0.041 g) yielded pure compound **HIPS5990** as a honey-like oil, (0.010 g).

<sup>1</sup>H NMR (DMSO-*d*<sub>6</sub>, 500 MHz)  $\delta$  8.30 (br s, 1 H) 7.35 (d, *J*=9.0 Hz, 2 H) 7.01 (d, *J*=8.9 Hz, 1 H) 6.79 - 6.83 (m, 2 H) 6.74 (d, *J*=2.8 Hz, 1 H) 6.61 (dd, *J*=8.9, 2.8 Hz, 1 H) 5.99 - 6.12 (m, 1 H) 3.14 - 3.23 (m, 5 H) 2.82 - 2.86 (m, 1 H) 2.43 (s, 1 H). <sup>13</sup>C NMR (DMSO-*d*<sub>6</sub>, 126 MHz)  $\delta$  164.6, 157.2, 147.2, 139.7, 129.6, 126.3, 125.7, 123.8, 117.1, 112.4, 48.6, 41.0, 34.2. HRMS (ESI+) calcd. for C<sub>15</sub>H<sub>16</sub>Cl<sub>2</sub>N<sub>2</sub>O [M + H]<sup>+</sup>: 311.07125, found: 311.07080.

## 2-Amino-N-(3-chloro-4-(4-chlorophenoxy)phenyl)acetamide (HIPS6027)

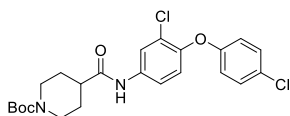


Using general procedure D2, into a solution of *tert*-butyl (2-(3-chloro-4-(4-chlorophenoxy)phenyl)amino)-2-oxoethyl)carbamate **HIPS6027-precursor** (1 eq., 0.090 g, 0.219 mmol) in dioxane (0.5 mL), 4M HCl/dioxane (10 eq., 0.55 mL, 2.190 mol) was added and the reaction was stirred at RT for 2 h. The crude was purified by prep. HPLC to afford compound **HIPS6027** as a white powder one FA salt, (0.028 g, 36%).

<sup>1</sup>H NMR (Methanol-*d*<sub>4</sub>, 500 MHz)  $\delta$  8.51 (s, 1 H) 7.93 (d, *J*=2.6 Hz, 1 H) 7.46 (dd, *J*=8.8, 2.5 Hz, 1 H) 7.29 - 7.34 (m, 2 H) 7.08 (d, *J*=8.8 Hz, 1 H) 6.85 - 6.89 (m, 2 H) 3.78 (s, 2 H). <sup>13</sup>C NMR (Methanol-*d*<sub>4</sub>, 126 MHz)  $\delta$  170.0, 167.3, 157.9, 149.3, 137.1, 130.9, 129.2, 127.7, 123.4, 123.1, 120.9, 119.5, 42.9. HRMS (ESI+) calcd. for C<sub>14</sub>H<sub>12</sub>Cl<sub>2</sub>N<sub>2</sub>O<sub>2</sub> [M + H]<sup>+</sup>: 311.03486, found: 311.03450.



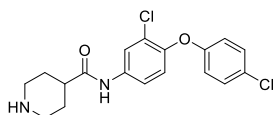
***Tert*-butyl 4-((3-chloro-4-(4-chlorophenoxy)phenyl)carbamoyl)piperidine-1-carboxylate (HIPS6017-precursor)**



Using the general procedure E, into a solution of 1-(*tert*-butoxycarbonyl)piperidine-4-carboxylic acid (1.0 eq., 0.123 g, 0.536 mmol) in dry DMF (3 mL), DIPEA (1.1 eq., 0.1 mL, 0.590 mmol), HATU (1.2 eq., 0.245 g, 0.643 mmol) and 3-chloro-4-(4-chlorophenoxy)aniline **HIPS5850** (1.1 eq., 0.150 g, 0.590 mmol) were added. The crude was absorbed onto silica 0.063–0.200 mm and purified by FFC with an alternating gradient of 0–30% EtOAc in cyclohexane to afford compound **HIPS6017-precursor** as a white solid, (0.160 g, 64%).

$^1\text{H}$  NMR ( $\text{CDCl}_3$ , 500 MHz)  $\delta$  7.77 (d,  $J=2.4$  Hz, 1 H) 7.36 (dd,  $J=8.8$ , 2.4 Hz, 1 H) 7.21 - 7.33 (m, 2 H) 6.99 (d,  $J=8.8$  Hz, 1 H) 6.81 - 6.90 (m, 2 H) 4.20 (br s, 2 H) 2.81 (br s, 2 H) 2.35 - 2.44 (m, 1 H) 1.91 (br d,  $J=12.2$  Hz, 2 H) 1.71 - 1.81 (m, 2 H) 1.48 (s, 9 H).  $^{13}\text{C}$  NMR ( $\text{CDCl}_3$ , 126 MHz)  $\delta$  172.6, 155.9, 154.7, 148.1, 134.8, 129.7, 128.1, 126.6, 122.3, 121.7, 119.6, 118.4, 79.8, 44.3, 28.4. LCMS  $m/z$  (ESI+) 365.1  $[\text{M} + \text{H}]^+$  without Boc-group.

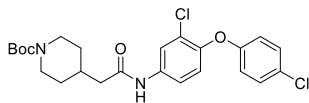
***N*-(3-chloro-4-(4-chlorophenoxy)phenyl)piperidine-4-carboxamide (HIPS6017)**



Using the general procedure D2, into a solution of *tert*-butyl-((3-chloro-4-(4-chlorophenoxy)phenyl)carbamoyl)piperidine-1-carboxylate **HIPS6017-precursor** (1 eq., 0.100 g, 0.215 mmol) in dioxane (0.5 mL), 4M HCl/dioxane (10 eq., 0.54 mL, 2.150 mmol) was added and the reaction was stirred at RT for 2 h to the reaction was stirred at RT for 2 h. The crude was purified by prep. HPLC to afford compound **HIPS6017** as a white powder one FA salt, (0.025 g, 19%).

$^1\text{H}$  NMR ( $\text{DMSO-}d_6$ , 500 MHz)  $\delta$  7.99 (d,  $J=2.5$  Hz, 2 H), 7.51 (dd,  $J = 8.8$ , 2.5 Hz, 2 H), 7.51 (dd,  $J = 8.8$ , 2.5 Hz, 2 H), 7.36-7.41 (m, 2 H), 7.17 (d,  $J=8.8$  Hz), 6.88 - 6.93 (m, 2 H), 3.10 - 3.18 (m, 3 H), 2.65 - 2.73 (m, 2 H), 1.78 - 1.84 (m, 2 H), 1.81 (m, 2 H), 1.61 - 1.71 (m, 2 H).  $^{13}\text{C}$  NMR ( $\text{DMSO-}d_6$ , 126 MHz)  $\delta$  173.1, 156.2, 145.8, 137.2, 129.8, 126.6, 125.1, 122.7, 120.7, 119.5, 118.1, 43.3, 41.3, 26.6. HRMS (ESI+) calcd. for  $\text{C}_{18}\text{H}_{18}\text{Cl}_2\text{N}_2\text{O}_2$   $[\text{M} + \text{H}]^+$ : 365.08181, found: 365.08170.

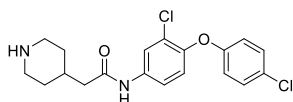
***Tert*-butyl 4-(2-((3-chloro-4-(4-chlorophenoxy)phenyl)amino)-2-oxoethyl)piperidine-1-carboxylate (HIPS6074-precursor)**



Using the general procedure E, into a solution of 2-(1-(*tert*-butoxycarbonyl)piperidin-4-yl)acetic acid (1.0 eq., 0.130 g, 0.536 mmol) in dry DMF (2 mL), DIPEA (1.1 eq., 0.1 mL, 0.590 mmol), HATU (1.2 eq., 0.245 g, 0.643 mmol) and 3-chloro-4-(4-chlorophenoxy)aniline **HIPS5850** (1.1 eq., 0.150 g, 0.590 mmol) were added. The reaction was stirred for 18 h. The crude was absorbed onto silica 0.063–0.200 mm and purified by FFC with an alternating gradient of 10–100% EtOAc in cyclohexane to afford compound **HIPS6074-precursor** (0.205 g, 80%). Further prep. HPLC purification (0.050 g) afforded compound **HIPS6074-precursor** as a light yellow powder one FA salt (0.042 g).

<sup>1</sup>H NMR (DMSO-*d*<sub>6</sub>, 500 MHz)  $\delta$  10.14 (s, 1 H) 7.98 (d, *J*=2.4 Hz, 1 H) 7.48 (dd, *J*=8.9, 2.4 Hz, 1 H) 7.37 - 7.41 (m, 2 H) 7.17 (d, *J*=8.9 Hz, 1 H) 6.89 - 6.93 (m, 2 H) 3.83 - 3.97 (m, 2 H) 2.65 - 2.79 (m, 2 H) 2.25 (d, *J*=7.0 Hz, 2 H) 1.86 - 2.01 (m, 1 H) 1.65 (br d, *J*=11.1 Hz, 2 H) 1.39 (s, 9 H) 1.01 - 1.13 (m, 2 H). <sup>13</sup>C NMR (DMSO-*d*<sub>6</sub>, 126 MHz)  $\delta$  170.3, 156.1, 153.9, 145.7, 137.0, 129.8, 126.6, 125.1, 122.6, 120.6, 119.3, 118.1, 78.5, 43.1, 32.9, 28.1. HRMS (ESI+) calcd. for C<sub>24</sub>H<sub>28</sub>Cl<sub>2</sub>N<sub>2</sub>O<sub>4</sub> [M + H]<sup>+</sup>: 479.14989, found 379.09630 without Boc-group.

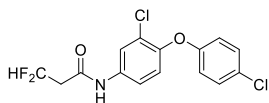
***N*-(3-chloro-4-(4-chlorophenoxy)phenyl)-2-(piperidin-4-yl)acetamide (HIPS6074)**



Using the general procedure D2, into a solution of *tert*-butyl 4-(2-((3-chloro-4-(4-chlorophenoxy)phenyl)amino)-2-oxoethyl)piperidine-1-carboxylate **HIPS6074-precursor** (1 eq., 0.155 g, 0.323 mmol) in dioxane (3 mL), 4M HCl/dioxane (10 eq., 0.81 mL, 3.230 mmol) was added and the reaction was stirred at RT for 2 h. The crude was purified by prep. HPLC to afford compound **HIPS6074** as a white powder one FA salt form, (0.070 g, 51%).

<sup>1</sup>H NMR (DMSO-*d*<sub>6</sub>, 500 MHz)  $\delta$  10.29 (s, 1 H) 8.42 (s, 1 H) 7.99 (d, *J*=2.4 Hz, 1 H) 7.49 (dd, *J*=8.9, 2.4 Hz, 1 H) 7.37 - 7.41 (m, 2 H) 7.17 (d, *J*=8.9 Hz, 1 H) 6.89 - 6.93 (m, 2 H) 3.07 - 3.19 (m, 2 H) 2.72 (br t, *J*=11.6 Hz, 4 H) 2.27 (d, *J*=7.0 Hz, 3 H) 1.73 (br d, *J*=12.5 Hz, 2 H) 1.26 - 1.37 (m, 2 H). <sup>13</sup>C NMR (DMSO-*d*<sub>6</sub>, 126 MHz)  $\delta$  170.2, 156.1, 145.7, 137.1, 129.8, 126.6, 125.1, 122.6, 120.6, 119.3, 118.1, 43.6, 43.1, 31.6, 29.4. HRMS (ESI+) calcd. for C<sub>19</sub>H<sub>20</sub>Cl<sub>2</sub>N<sub>2</sub>O<sub>2</sub> [M + H]<sup>+</sup>: 379.09746, found 379.09670.

***N*-(3-chloro-4-(4-chlorophenoxy)phenyl)-3,3-difluoropropanamide (HIPS6065)**



To a solution of 3,3-difluoropropanoic acid (1.0 eq., 0.03 g, 0.273 mmol) in dry DMF (0.3 mL), DIPEA (1.1 eq., 0.052 mL, 0.300 mmol) was added. After 10 min, HATU (1.2 eq., 0.125 g, 0.328 mmol) was added to the solution and it was stirred for further 10 min. 3-chloro-4-(4-chlorophenoxy)aniline **HIPS5850** (1.1 eq., 0.076 g, 0.300 mmol) was added. The reaction was stirred at RT for 4 h, then heated to 50 °C and stirred for 2 h. The reaction mixture was cooled down to RT, quenched with NH<sub>4</sub>Cl and extracted with EtOAc (3 x 10 mL). The combined organic layers were washed with water (5 x 5 mL), saturated aq. NaHCO<sub>3</sub> (1 x 5 mL), brine (2 x 10 mL), dried over anhydrous Na<sub>2</sub>SO<sub>4</sub> and concentrated *in vacuo* to afford a crude product as a brown solid. The crude was purified by prep. HPLC to afford compound **HIPS6065** as a light yellow powder, (0.012 g, 13%).

<sup>1</sup>H NMR (DMSO-*d*<sub>6</sub>, 500 MHz) δ 10.46 (s, 1 H), 7.95 (d, *J*=2.6 Hz, 1 H), 7.48 (dd, *J*=8.9, 2.6 Hz, 1 H), 7.39 - 7.43 (m, 2 H), 7.20 (d, *J*=8.9 Hz, 1 H), 6.92 - 6.96 (m, 2 H), 6.38 (tt, *J*=55.8, 4.8 Hz, 1 H), 3.08 (td, *J*=16.8, 4.8 Hz, 2 H). <sup>13</sup>C NMR (DMSO-*d*<sub>6</sub>, 126 MHz) δ 165.3, 156.4, 146.7, 136.8, 130.3, 127.2, 125.6, 123.1, 121.3, 120.0, 118.8, 116.0, 41.8. <sup>19</sup>F NMR (DMSO-*d*<sub>6</sub>, 470 MHz) -115.79 (s). HRMS (ESI+) calcd. for C<sub>15</sub>H<sub>11</sub>Cl<sub>2</sub>F<sub>2</sub>NO<sub>2</sub> [M - H]<sup>-</sup>: 344.00621, found: 344.00560.

## 5.3 Supplementary Material of Chapter B

---

### Electronic Supplementary Information to the Publication

#### Assessment of the rules related to gaining activity against Gram-negative bacteria

Henni-Karoliina Ropponen<sup>a,b</sup>, Eleonora Diamanti<sup>a</sup>, Alexandra Siemens<sup>c</sup>, Boris Illarionov<sup>c</sup>, Jörg Hauptenthal<sup>a</sup>, Markus Fischer<sup>c</sup>, Matthias Rottmann<sup>d,e</sup>, Matthias Witschel<sup>f</sup>, Anna K. H. Hirsch<sup>a,b\*</sup>

<sup>a</sup>. Helmholtz Institute for Pharmaceutical Research Saarland (HIPS) – Helmholtz Centre for Infection Research (HZI), Campus Building E8.1, 66123 Saarbrücken, Germany.

<sup>b</sup>. Department of Pharmacy, Saarland University, Campus Building E8.1, 66123 Saarbrücken, Germany.

<sup>c</sup>. Hamburg School of Food Science, University of Hamburg, Grindelallee 117, 20146 Hamburg, Germany.

<sup>d</sup>. Swiss Tropical and Public Health Institute, Socinstrasse 57, 4002 Basel, Switzerland.

<sup>e</sup>. Universität Basel, Petersplatz 1, 4003 Basel, Switzerland.

<sup>f</sup>. BASF-SE, Carl-Bosch-Strasse 38, 67056 Ludwigshafen, Germany.

\* Corresponding author: Anna K. H. Hirsch, [Anna.Hirsch@helmholtz-hips.de](mailto:Anna.Hirsch@helmholtz-hips.de)

## Table of Contents

<b>1.) Biological Results</b> .....	<b>S3</b>
1.1 Cloning, Expression and Purification of <i>Plasmodium falciparum</i> IspE.....	S3
1.2 Summary of Enzymatic Results.....	S4
1.3 Summary of Cellular Results.....	S5
<b>2.) Synthetic Procedures</b> .....	<b>S7</b>
2.1 General Procedures .....	S7
2.2 Reference Compounds .....	S8
2.3 Right-Hand Side Synthesis (Compounds <b>4–17</b> from Scheme 1).....	S8
2.4 Left-Hand Side Synthesis (Compounds <b>18–26</b> from Scheme 2).....	S14
<b>3.) References</b> .....	<b>S17</b>

## 1.) Biological Results

### 1.1 Cloning, Expression and Purification of *Plasmodium falciparum* IspE

**Table S1** Primers used for amplification of the DNA fragment coding for the IspE of *P. falciparum*.

Primer	Primer sequence (5' → 3')
<i>Pf</i> IspE-NcoI-cHis6-fw	ATAATAATACCATGGGACATCATCACCACCATCATGGCAGCAATGTGGAAAAGAACAACG
<i>Pf</i> IspE-cHis6-HindIII-bw	TGTTGTTGAAGCTTACTGAACTCATGCGCTAGCTTGATCGGGTCCG

CCATGGGAAATGTGGAAAAGAACAACGTGGTTAACACTAATAAGGAGATCGAGAACTGCTCTAGATGATTGGACAACCGTAATAACTGGTACGATTC  
 AAAAGTACTTCTCCGGCGAAAATTAATCTGTTTCTGCGCTTGAAGGAAAAGAAAGAGACGTACAATGAAGTATCAACCTCATGCATTTCACTGAATTTGG  
 GCGATGACATCTTCAATTCGCGCCTTGAAGAAAGAGATCAGAATAAGCTGCGCCATTTCTTACACCCGTGCGAGTCTGGCGACTTCTTGACAATTGTACGT  
 ATGGAGATAAGAACCAGCGATAAGGAAACGTTAAAGAAAGACTGCAAGATCGATGTGATCAATAAGAGTGATAAGGACTTGTTTAAACACATGAAAAGAG  
 GACATCATTATCCAAGAACACGAGAAATTACCGTACGAGTACAATGACTACCCGATCAATAACGATAATATCATCATTAAAGGTGTTAAAGCGCTATCGTGA  
 GGAATTCAATATCAGTGATGACATCCGCTTCTGATCCACGTGAATAAGCGCATCCCGATCTTTAGTGCGTGGGTGGTGGGAGCTCTAATGGTGGCGACC  
 GTTTTCTATTTCTTAGAGAACATCTTTTACAAGTATTTTAAAGGCGACAATATCAAAAGCGAACGAGTTCTTAAAGACTATCGGCAGCGACATCTCTTTTCA  
 GTAGCTCGGGCTTTCGCTATTGCACGGATAAGGGCAATAACGTGACGGATTTAAAAACATCGAAGCGAATATCAAGGACAAAGATATCTATTTATTCAA  
 GATTGATGAGGGCTTATCTTCGAACTAGTATACAAAATGTCGACTACAAGCGCATTATCCAATATAACCCGGTGAATCTGCTTAAAGTCTTAATTAACAC  
 ATCAAAATGATGACATCATCAACAGATCGAGGAAAAGGAGAAGAAATTTGCCAACCTTTCATTTTCGCTGGATAATCGGATAACCTGCAAAAATGTGTTTC  
 GTGAATGACCTCGAGCACTCAGCGTTTACTTAATCAAAAAGCTGCAGGATTTAAAGGAATATCTGCGCAGTCAAAACATGTTTGACGTGCTGTCATGAG  
 CGGCAAGTGGCTCTTCGCTGTTTGCCTTGTCCAACAAGAAAACGCAACTCATGAGATCTCTCATCGTTTCAAACGAACGCATTAAGAAACTCATCAGCG  
 ACATCAAGATTAATTAACATGAATGTACGCGTCTATCTGTGCGATGCGCTCCGTAAGGCGCTTGTGTGGTACGACCCGATCAAGTAGCGCATGA  
 GTTCAAGGGCAGC**CATCATCACCACCATCAT**AAGCTT

**Fig. S1** The nucleotide sequence of the DNA fragment coding for IspE from *P. falciparum*. The restriction sites NcoI and HindIII are underlined. The sequence coding for the His<sub>6</sub>-Tag is shown in bold.

## 1.2. Summary of Enzymatic Results

**Table S2** Inhibitory activities against IspE enzymes and auxiliary enzymes PK/LDH.

Compound	<i>E</i> clspE IC <sub>50</sub> (μM)	<i>P</i> flspE IC <sub>50</sub> (μM)	PK/LDH IC <sub>50</sub> (μM)
1	1 ± 0	>500	>500
2	91 ± 21	57 ± 12	65 ± 15
3	68 ± 13	35 ± 6	56 ± 11
8	200 ± 62	33 ± 11	200 ± 9
9	>500	61 ± 7	>500
10	>500	37 ± 2	159 ± 28
11	>500	196 ± 44	>500
12	>500	113 ± 40	>500
13	200 ± 35	>500	>500
14	>500	>500	n.d.
15	>500	>500	n.d.
16	>500	>500	n.d.
17	>500	>500	n.d.
21	>500	>500	n.d.
22	>500	>500	n.d.
23	>500	>500	n.d.
24	>500	>500	n.d.
25	>500	>500	n.d.
26	>500	>500	n.d.

\* The results are from at least two independent determinations. Only where *P*flspE or *E*clspE activity was measured as >500, no replicate was determined. PK/LDH: pyruvate kinase and lactate dehydrogenase and n.d.: not determined.

### 1.3. Summary of Cellular Results

**Table S3** Inhibitory activities against a panel of *Escherichia coli* strains, *Staphylococcus aureus*, *Plasmodium falciparum* and the human hepatoma cell line HepG2, from at least two independent determinations.

Compound	Percentage Inhibition @ given concentration							IC <sub>50</sub>	
	<i>E. coli</i>					<i>S. aureus</i> Newman	HepG2		P <sub>1</sub> NF54
	K12	$\Delta$ tolC	$\Delta$ acrB	D22	(DE3) omp8				
<b>1</b>	6 ± 1 (@100 μM) 1 μg/mL PMBN	n.d.	n.d.	n.d.	n.d.	n.d.	n.d.	n.d.	
<b>2</b>	5 ± 6 (@25 μM)	30 ± 16 (@25 μM)	2 ± 5 (@25 μM)	9 ± 7 (@25 μM)	-4 ± 3 (@25 μM)	6 ± 1 (@25 μM)	19 ± 2 (@25 μM)	5.3 ± 0.6	
<b>3</b>	2 ± 11 (@50 μM)	33 ± 3 (@50 μM)	6 ± 7 (@50 μM)	3 ± 4 (@50 μM)	-22 ± 19 (@25 μM)	7 ± 5 (@50 μM)	-3 ± 5 (@50 μM)	5.5 ± 0.3	
<b>8</b>	n.d.	9 ± 13 (@50 μM)	n.d.	n.d.	n.d.	3 ± 11 (@50 μM)	n.d.	n.d.	
<b>9</b>	n.d.	14 ± 10 (@50 μM)	n.d.	n.d.	n.d.	21 ± 1 (@50 μM)	n.d.	1.9 ± 0.4	
<b>10</b>	n.d.	5 ± 8 (@50 μM)	n.d.	n.d.	n.d.	8 ± 4 (@50 μM)	n.d.	n.d.	
<b>11</b>	1 ± 9 (@100 μM)	46 ± 12 (@100 μM)	-29 ± 3 (@100 μM)	-2 ± 1 (@100 μM)	-36 ± 4 (@100 μM)	11 ± 1 (@100 μM)	n.d.	5.1 ± 0.5	
<b>12</b>	1 ± 9 (@50 μM)	41 ± 17 (@50 μM)	14 ± 3 (@50 μM)	1 ± 7 (@100 μM)	-29 ± 24 (@50 μM)	-2 ± 12 (@50 μM)	n.d.	n.d.	
<b>13</b>	-1 ± 1 (@100 μM)	38 ± 14 (@100 μM)	n.d.	n.d.	n.d.	10 ± 0 (@100 μM)	n.d.	n.d.	
<b>14</b>	-2 ± 0 (@100 μM)	42 ± 15 (@100 μM)	n.d.	n.d.	n.d.	12 ± 10 (@100 μM)	n.d.	n.d.	
<b>15</b>	2 ± 2 (@100 μM)	58 ± 17 (@100 μM)	n.d.	n.d.	n.d.	52 ± 15 (@100 μM)	n.d.	n.d.	
<b>16</b>	13 ± 0 (@100 μM)	57 ± 2 (@100 μM)	4 ± 8 (@100 μM)	3 ± 3 (@100 μM)	18 ± 1 (@100 μM)	6 ± 3 (@100 μM)	19 ± 12 (@50 μM)	n.d.	
<b>17</b>	13 ± 2 (@100 μM)	55 ± 14 (@100 μM)	65 ± 1 (@100 μM)	20 ± 4 (@100 μM)	16 ± 10 (@100 μM)	14 ± 3 (@50 μM)	23 ± 5 (@100 μM)	n.d.	
<b>21</b>	8 ± 1 (@100 μM)	21 ± 2 (@100 μM)	n.d.	n.d.	n.d.	17 ± 2 (@100 μM)	n.d.	n.d.	
<b>22</b>	2 ± 3 (@100 μM)	-3 ± 1 (@100 μM)	n.d.	n.d.	n.d.	10 ± 12 (@100 μM)	n.d.	n.d.	



<b>23</b>	15 ± 2 (@100 µM)	34 ± 10 (@100 µM)	n.d.	n.d.	n.d.	16 ± 4 (@100 µM)	n.d.	n.d.
<b>24</b>	10 ± 13 (@100 µM)	17 ± 1 (@100 µM)	1 ± 2 (@100 µM)	14 ± 1 (@100 µM)	-3 ± 16 (@100 µM)	5 ± 3 (@100 µM)	n.d.	n.d.
<b>25</b>	18 ± 11 (@100 µM)	32 ± 1 (@100 µM)	11 ± 6 (@100 µM)	18 ± 3 (@100 µM)	30 ± 7 (@100 µM)	11 ± 1 (@100 µM)	n.d.	n.d.
<b>26</b>	22 ± 4 (@100 µM)	10 ± 5 (@100 µM)	6 ± 1 (@100 µM)	15 ± 3 (@100 µM)	-20 ± 19 (@100 µM)	-2 ± 5 (@100 µM)	17 ± 17 (@100 µM)	n.d.

\* PMBN: polymyxin B nonapeptide, n.d.: not determined.

**Table S4** Inhibitory activities against a panel of *Pseudomonas aeruginosa* and *Acinetobacter baumannii*, from at least two independent determinations.

Compound	Percentage Inhibition @ 100 µM	
	<i>P. aeruginosa</i>	<i>A. baumannii</i>
<b>17</b>	11 ± 7	31 ± 17
<b>26</b>	3 ± 9	12 ± 9

## 2.) Synthetic Procedures

### 2.1 General Procedures

#### General Procedure A: Amide Couplings<sup>1</sup>

Respective *N*-Boc protected amino acid (1.0 eq.), amine as either 2-aminothiazole derivative **6** or **7**, or 4-aminothiazole derivative **20** (1.0 eq.) and HBTU (1.2 eq.) were stirred under N<sub>2</sub> flow in DMF (1.5 mL) for 5 min, followed by an addition of triethylamine (3.0 eq.). The reaction mixture was stirred for 18 h. The mixture was quenched with saturated aq. NaHCO<sub>3</sub> and extracted with EtOAc. The combined organic layers were washed with aq. 2 M HCl and brine. The organic layer was then dried over anhydrous Na<sub>2</sub>SO<sub>4</sub>, filtered and evaporated to dryness. The crude product was absorbed onto ISOLUTE® HM-N and purified by FCC with an alternating gradient of 0–80% EtOAc in cyclohexane to afford the title compounds **8–12** and **21–23**. Compounds **8–12** were further purified by prep. HPLC eluting with a gradient of 5–100% MeCN with 0.05% FA in H<sub>2</sub>O with 0.05% FA. Collected fractions were lyophilised to afford the respective title compounds.

#### General Procedure B: Boc-deprotections

Boc-protected intermediates **8–12** and **21–23** was dissolved in DCM and TFA was added dropwise, in ratio of 5:1 or 10:1. The reaction mixture was stirred at room temperature for 30 min and then evaporated to dryness under reduced pressure. The obtained crude product was purified by prep. HPLC eluting with a gradient of 5–100% MeCN with 0.1% TFA in H<sub>2</sub>O with 0.1% TFA. Collected fractions were lyophilised to afford the respective title compounds **13–17** and **24–26** as TFA salts. The TFA salt form of the compounds was measured using 4-(trifluoromethyl)phenylacetonitrile as an internal spike control.

General Abbreviations: aq. = aqueous, DCM = dichloromethane, DMF = dimethylformamide, eq. = equivalent, EtOAc = ethyl acetate, EtOH = ethanol, FA = formic acid, HCl = hydrochloric acid, HBTU = (2-(1H-benzotriazol-1-yl)-1,1,3,3-tetramethyluronium hexafluorophosphate, MeCN = acetonitrile, NaHCO<sub>3</sub> = sodium bicarbonate, NaOH = sodium hydroxide, Na<sub>2</sub>SO<sub>4</sub> = sodium sulfate, prep. = preparative, TEA = triethylamine and TFA = trifluoroacetic acid.

## 2.2 Reference Compounds

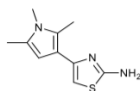
The reference compound **1** originated from previous publication within the consortium. Reference compounds **2** and **3** were commercially available compounds that were kindly provided by BASF. The purity of compounds was confirmed with LCMS.

**Table S5** Reference compounds.

Compound	MW	LCMS [M+H] <sup>+</sup>	UV-purity	Origin
<b>1</b>	354.44	355.1	>99%	Ref. 2
<b>2</b>	329.42	330.2	92%	Enamine Z26672805 (CAS 2094230-26-7)
<b>3</b>	345.48	346.1	~80%	Enamine Z26672672 (CAS 2391905-54-5)

## 2.3 Right-Hand Side Synthesis (Compounds 4–17 from Scheme 1)

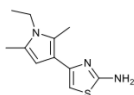
### 4-(1,2,5-Trimethyl-1H-pyrrol-3-yl)thiazol-2-amine (**6**)<sup>3</sup>



To a stirred solution of 2-chloro-1-(1,2,5-trimethyl-1H-pyrrol-3-yl)ethan-1-one **4** (0.500 g, 2.702 mmol) in EtOH (5 mL), thiourea (0.206 g, 2.702 mmol) was added. The mixture was refluxed for 16 h with an addition of thiourea (0.2 eq.) after 7 h. The reaction was quenched with water (35 mL) and washed with DCM (2 x 25 mL). The aqueous phase was concentrated *in vacuo*. The crude was dissolved in minimum amount of water (10 mL) and basified to pH 8 with aq. 2 M NaOH. The precipitate was filtered and vacuum dried to afford compound **6** as a brown sticky oil, (0.278 g, 50%).

<sup>1</sup>H NMR (DMSO-*d*<sub>6</sub>, 500 MHz) δ 6.76 (s, 2H), 6.14 (s, 1H), 5.92 (s, 1H), 3.34 (s, 3H), 2.40 (s, 3H), 2.12 (s, 3H). <sup>13</sup>C NMR (DMSO-*d*<sub>6</sub>, 126 MHz) δ 167.1, 148.2, 126.4, 124.7, 114.6, 104.7, 96.4, 29.8, 12.2, 11.4. m/z (ESI<sup>+</sup>) 208.1 [M + H]<sup>+</sup>.

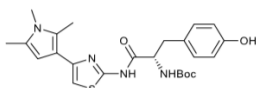
#### 4-(1-Ethyl-2,5-dimethyl-1H-pyrrol-3-yl)thiazol-2-amine (7)<sup>3</sup>



To a stirred solution of 2-chloro-1-(1-ethyl-2,5-dimethyl-1H-pyrrol-3-yl)ethan-1-one **5** (0.500 g, 2.504 mmol) in EtOH (5 mL), thiourea (0.191 mg, 2.504 mmol) was added. The mixture was refluxed for 16 h with an addition of thiourea (0.2 eq.) after 7 h. The reaction was quenched with water (35 mL) and washed with DCM (2 x 25 mL). The aqueous phase was concentrated *in vacuo*. The crude was dissolved in minimum amount of water (10 mL) and basified to pH 8 with aq. 2 M NaOH. The precipitate was filtered and vacuum dried to afford compound **7** as a brown sticky oil, (0.135 g, 24%).

<sup>1</sup>H NMR (DMSO-*d*<sub>6</sub>, 500 MHz)  $\delta$  6.77 (s, 2H), 6.16 (s, 1H), 5.92 (d, 1H, *J*=0.9), 3.79 (q, 2H, *J*=7.2 Hz), 2.43 (s, 3H), 2.16 (s, 3H), 1.15 (t, 3H, *J*=7.2 Hz). <sup>13</sup>C NMR (DMSO-*d*<sub>6</sub>, 126 MHz)  $\delta$  167.1, 148.2, 125.6, 123.8, 114.9, 105.2, 96.4, 37.4, 15.9, 11.9, 11.1. *m/z* (ESI+) 222.1 [M + H]<sup>+</sup>.

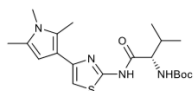
#### Tert-butyl (S)-3-(4-hydroxyphenyl)-1-oxo-1-((4-(1,2,5-trimethyl-1H-pyrrol-3-yl)thiazol-2-yl)amino)propan-2-yl)carbamate (8)



Using general procedure A with heating at 80 °C, *N*-Boc-L-tyrosine (0.060 g, 0.213 mmol) was coupled with 4-(1,2,5-trimethyl-1H-pyrrol-3-yl)thiazol-2-amine **6** (0.044 g, 0.213 mmol), HBTU (0.097 g, 0.256 mmol) and TEA (9  $\mu$ L, 0.640 mmol) in DMF (1.5 mL) to afford FCC purified compound **8** as a brown sticky oil (0.035 g, 35%). Further prep. HPLC purification (0.015 g) afforded compound **8** as a beige powder, (0.005 g).

<sup>1</sup>H NMR (CDCl<sub>3</sub>, 500 MHz)  $\delta$  6.98 (br d, 2H, *J* = 7.6 Hz), 6.70 (br d, 2H, *J* = 7.6 Hz), 6.63 (s, 1H), 6.11 (s, 1H), 5.07 (br d, 1H, *J* = 5.2 Hz), 4.4-4.6 (m, 1H), 3.41 (s, 3H), 3.05-3.12 (m, 1H), 2.95-3.03 (m, 1H), 2.39 (s, 3H), 2.22 (s, 3H), 1.41 (br s, 9H). <sup>13</sup>C NMR (DMSO-*d*<sub>6</sub>, 126 MHz)  $\delta$  171.1, 163.0, 156.5, 155.4, 147.2, 130.2, 127.7, 126.9, 125.0, 114.8, 113.9, 104.8, 103.3, 78.2, 56.2, 36.2, 29.9, 28.1, 12.2, 11.4. HRMS (ESI+) calcd. for C<sub>24</sub>H<sub>30</sub>N<sub>4</sub>O<sub>4</sub>S [M + H]<sup>+</sup>: 471.20606, found: 471.20422.

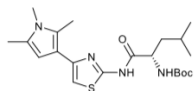
**Tert-butyl (S)-(3-methyl-1-oxo-1-((4-(1,2,5-trimethyl-1H-pyrrol-3-yl)thiazol-2-yl)amino)butan-2-yl)carbamate (9)**



Using general procedure A, *N*-Boc-L-valine (0.050 g, 0.230 mmol) was coupled with 4-(1,2,5-trimethyl-1H-pyrrol-3-yl)thiazol-2-amine **6** (0.048 g, 0.230 mmol), HBTU (0.105 g, 0.276 mmol) and TEA (10  $\mu$ L, 0.690 mmol) in DMF (1.5 mL) to afford FCC purified compound **9** as a brown sticky oil (0.037 g, 40%). Further prep. HPLC purification (0.017 g) afforded compound **9** as a beige powder, (0.004 g).

$^1\text{H}$  NMR (DMSO- $d_6$ , 500 MHz)  $\delta$  12.03 (s, 1H), 7.06 (br d, 1H,  $J=8.4$  Hz), 6.77 (s, 1H), 6.01 (s, 1H), 4.05 (br t, 1H,  $J=7.1$  Hz), 3.36 (br s, 3H), 2.44 (s, 3H), 2.15 (s, 3H), 1.9-2.0 (m, 1H), 1.37 (s, 9H), 0.87 (br t, 6H,  $J=7.1$  Hz).  $^{13}\text{C}$  NMR (DMSO- $d_6$ , 126 MHz)  $\delta$  170.6, 155.3, 147.0, 126.6, 124.8, 113.6, 104.5, 103.0, 77.9, 59.5, 29.8, 29.6, 27.9, 18.8, 18.2, 11.9, 11.1. HRMS (ESI+) calcd. for  $\text{C}_{20}\text{H}_{30}\text{N}_4\text{O}_3\text{S}$  [ $\text{M} + \text{H}$ ] $^+$ : 407.21114, found: 407.20929.

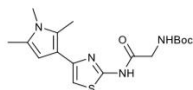
**Tert-butyl (S)-(4-methyl-1-oxo-1-((4-(1,2,5-trimethyl-1H-pyrrol-3-yl)thiazol-2-yl)amino)pentan-2-yl)carbamate (10)**



Using general procedure A, *N*-Boc-L-leucine (0.050 g, 0.216 mmol) was coupled with 4-(1,2,5-trimethyl-1H-pyrrol-3-yl)thiazol-2-amine **6** (0.045 g, 0.216 mmol), HBTU (0.099 g, 0.259 mmol) and TEA (9  $\mu$ L, 0.649 mmol) in DMF (1.5 mL) to afford FCC purified compound **10** as a brown sticky oil (0.055 g, 60%). Further prep. HPLC purification (0.025 g) afforded compound **10** as a light beige powder, (0.007 g).

$^1\text{H}$  NMR (DMSO- $d_6$ , 500 MHz)  $\delta$  12.06 (s, 1H), 7.16 (br d, 1H,  $J=7.6$  Hz), 6.77 (s, 1H), 6.02 (s, 1H), 4.2-4.3 (m, 1H), 2.44 (s, 3H), 2.15 (s, 3H), 1.6-1.7 (m, 1H), 1.5-1.6 (m, 1H), 1.40-1.45 (m, 1H), 1.36 (s, 9H), 0.88 (br t, 6H,  $J=5.4$  Hz).  $^{13}\text{C}$  NMR (DMSO- $d_6$ , 126 MHz)  $\delta$  171.8, 156.4, 155.4, 147.1, 126.8, 125.0, 113.8, 104.7, 103.2, 78.1, 52.6, 29.8, 28.1, 24.3, 22.9, 21.2, 12.1, 11.3. HRMS (ESI+) calcd. for  $\text{C}_{21}\text{H}_{32}\text{N}_4\text{O}_3\text{S}$  [ $\text{M} + \text{H}$ ] $^+$ : 421.22679, found: 421.22486.

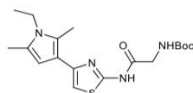
**Tert-butyl (2-oxo-2-((4-(1,2,5-trimethyl-1H-pyrrol-3-yl)thiazol-2-yl)amino)ethyl)carbamate (11)**



Using general procedure A, *N*-Boc-glycine (0.040 g, 0.228 mmol) was coupled with 4-(1,2,5-trimethyl-1H-pyrrol-3-yl)thiazol-2-amine **6** (0.047 g, 0.228 mmol), HBTU (0.104 g, 0.274 mmol) and TEA (10  $\mu$ L, 0.685 mmol) in DMF (1.5 mL) to afford FCC purified compound **11** as a brown sticky oil (0.038 g, 46%). Further prep. HPLC purification (0.018 g) afforded compound **11** as a beige-rosa powder, (0.005 g).

$^1\text{H}$  NMR (DMSO- $d_6$ , 500 MHz)  $\delta$  12.01 (br s, 1H), 7.14 (t, 1H,  $J=6.1$  Hz), 6.78 (s, 1H), 6.02 (s, 1H), 3.83 (d, 2H,  $J=6.1$  Hz), 3.37 (s, 3H), 2.44 (s, 3H), 2.15 (s, 3H), 1.40 (s, 9H).  $^{13}\text{C}$  NMR (DMSO- $d_6$ , 126 MHz)  $\delta$  168.5, 156.6, 156.1, 147.4, 127.1, 125.2, 114.1, 105.0, 103.3, 78.4, 43.1, 30.1, 28.4, 12.4, 11.6. HRMS (ESI+) calcd. for  $\text{C}_{17}\text{H}_{24}\text{N}_4\text{O}_3\text{S}$  [ $\text{M} + \text{H}$ ] $^+$ : 365.16419, found: 365.16255.

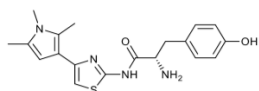
**Tert-butyl (2-((4-(1-ethyl-2,5-dimethyl-1H-pyrrol-3-yl)thiazol-2-yl)amino)-2-oxoethyl)carbamate (12)**



Using general procedure A, *N*-Boc-glycine (0.035 g, 0.200 mmol) was coupled with 4-(1-ethyl-2,5-dimethyl-1H-pyrrol-3-yl)thiazol-2-amine **7** (0.044 g, 0.200 mmol), HBTU (0.091 g, 0.240 mmol) and TEA (8  $\mu$ L, 0.599 mmol) in DMF (1.5 mL) to afford FCC purified compound **12** as a brown sticky oil (0.062 g, 82%). Further prep. HPLC purification (0.022 g) afforded compound **12** as a white powder, (0.005 g).

$^1\text{H}$  NMR (DMSO- $d_6$ , 500 MHz)  $\delta$  12.00 (br s, 1H), 7.14 (br t, 1H,  $J=6.0$  Hz), 6.78 (s, 1H), 6.01 (s, 1H), 3.8-3.9 (m, 4H), 2.46 (br s, 3H), 2.15-2.20 (m, 3H), 1.3-1.4 (m, 9H), 1.16 (br t, 3H,  $J=7.1$  Hz).  $^{13}\text{C}$  NMR (DMSO- $d_6$ , 126 MHz)  $\delta$  168.2, 156.3, 155.8, 147.1, 126.0, 124.1, 114.0, 105.1, 103.1, 78.1, 42.8, 37.4, 28.1, 15.8, 11.8, 11.0. HRMS (ESI+) calcd. for  $\text{C}_{18}\text{H}_{26}\text{N}_4\text{O}_3\text{S}$  [ $\text{M} + \text{H}$ ] $^+$ : 379.17984, found: 379.17789.

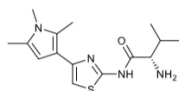
**(S)-2-Amino-3-(4-hydroxyphenyl)-N-(4-(1,2,5-trimethyl-1H-pyrrol-3-yl)thiazol-2-yl)propanamide (13)**



Using general procedure B, compound **8** (0.020 g, 0.186 mmol) was Boc-deprotected in DCM (1 mL) with TFA (0.2 mL) to afford prep. HPLC purified compound **13** as a purple powder one TFA salt form, (0.003 g, 17%).

$^1\text{H}$  NMR (DMSO- $d_6$ , 500 MHz)  $\delta$  12.54 (br s, 1H), 9.3-9.5 (m, 1H), 8.2-8.4 (m, 4H), 7.04 (d, 2H,  $J=8.4$  Hz), 6.88 (s, 1H), 6.71 (d, 2H,  $J=8.4$  Hz), 6.02 (s, 1H), 4.16-4.22 (m, 1H), 3.37 (s, 3H), 3.08-3.13 (m, 1H), 2.9-3.0 (m, 1H), 2.54 (s, 3H), 2.43 (s, 3H), 2.15 (s, 3H).  $^{13}\text{C}$  NMR (DMSO- $d_6$ , 126 MHz)  $\delta$  166.9, 158.1, 157.8, 156.5, 154.4, 130.3, 126.9, 125.0, 124.2, 115.3, 104.6, 103.9, 53.9, 35.9, 29.8, 12.0, 11.2. HRMS (ESI+) calcd. for  $\text{C}_{19}\text{H}_{22}\text{N}_4\text{O}_2\text{S}$  [ $\text{M} + \text{H}$ ] $^+$ : 371.15363, found: 371.15204.

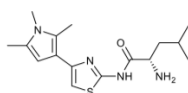
**(S)-2-Amino-3-methyl-N-(4-(1,2,5-trimethyl-1H-pyrrol-3-yl)thiazol-2-yl)butanamide (14)**



Using general procedure B, compound **9** (0.020 g, 0.049 mmol) was Boc-deprotected in DCM (1 mL) with TFA (0.2 mL) to afford prep. HPLC purified compound **14** as a light pink powder one TFA salt form, (0.014 g, 68%).

$^1\text{H}$  NMR (DMSO- $d_6$ , 500 MHz)  $\delta$  12.60 (br s, 1H), 8.34 (br s, 4H), 6.90 (s, 1H), 6.03 (m, 1H), 3.86-3.89 (m, 2H), 3.37 (s, 3H), 2.44 (s, 3H), 2.2-2.3 (m, 1H), 2.15 (s, 3H), 0.97 (dd, 6H,  $J=6.9, 10.8$  Hz).  $^{13}\text{C}$  NMR (DMSO- $d_6$ , 126 MHz)  $\delta$  158.3, 158.0, 147.7, 127.1, 125.3, 113.6, 104.8, 104.1, 57.6, 29.9, 18.5, 17.6, 12.2, 11.4. HRMS (ESI+) calcd. for  $\text{C}_{15}\text{H}_{22}\text{N}_4\text{O}\text{S}$  [ $\text{M} + \text{H}$ ] $^+$ : 307.15871, found: 307.15727.

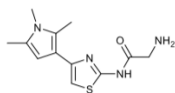
**(S)-2-Amino-4-methyl-N-(4-(1,2,5-trimethyl-1H-pyrrol-3-yl)thiazol-2-yl)pentanamide (15)**



Using general procedure B, compound **10** (0.030 g, 0.071 mmol) was Boc-protected in DCM (1.5 mL) with TFA (0.3 mL) to afford prep. HPLC purified compound **15** as a rosa powder one TFA salt form, (0.013 g, 41%).

<sup>1</sup>H NMR (DMSO-*d*<sub>6</sub>, 500 MHz)  $\delta$  12.68 (br s, 1H), 8.35 (br s, 4H), 6.90 (s, 1H), 6.04 (s, 1H), 4.07-4.10 (m, 1H), 3.38 (s, 3H), 2.45 (s, 3H), 2.16 (s, 3H), 1.6-1.7 (m, 3H), 0.94 (br d, 6H, *J*=4.0 Hz). <sup>13</sup>C NMR (DMSO-*d*<sub>6</sub>, 126 MHz)  $\delta$  158.2, 158.0, 127.1, 125.3, 115.3, 104.8, 104.1, 51.1, 30.0, 23.7, 22.7, 21.6, 12.2, 11.4. HRMS (ESI+) calcd. for C<sub>16</sub>H<sub>24</sub>N<sub>4</sub>OS [M + H]<sup>+</sup>: 321.17436, found: 321.17288.

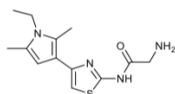
**2-Amino-N-(4-(1,2,5-trimethyl-1H-pyrrol-3-yl)thiazol-2-yl)acetamide (16)**



Using general procedure B, compound **11** (0.020 g, 0.055 mmol) was Boc-protected in DCM (1 mL) with TFA (0.2 mL) to afford prep. HPLC purified compound **16** as a rosa powder one TFA salt form, (0.008 g, 39%).

<sup>1</sup>H NMR (DMSO-*d*<sub>6</sub>, 500 MHz)  $\delta$  12.46 (br s, 1H), 8.18 (br s, 4H), 6.88 (s, 1H), 6.02 (d, 1H, *J*=0.8 Hz), 3.89 (br d, 2H, *J*=5.5 Hz), 3.37 (s, 3H), 2.44 (s, 3H), 2.15 (s, 3H). <sup>13</sup>C NMR (DMSO-*d*<sub>6</sub>, 126 MHz)  $\delta$  157.9, 127.1, 125.2, 113.7, 104.8, 103.8, 40.7, 30.0, 12.2, 11.4. HRMS (ESI+) calcd. for C<sub>12</sub>H<sub>16</sub>N<sub>4</sub>OS [M + H]<sup>+</sup>: 265.11176, found: 265.11059.

**2-Amino-N-(4-(1-ethyl-2,5-dimethyl-1H-pyrrol-3-yl)thiazol-2-yl)acetamide (17)**



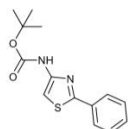
Using general procedure B, compound **12** (0.040 g, 0.106 mmol) was Boc-protected in DCM (2 mL) with TFA (0.4 mL) to afford prep. HPLC purified compound **17** as a pink powder one TFA salt form, (0.006 g, 14%).

<sup>1</sup>H NMR (DMSO-*d*<sub>6</sub>, 500 MHz)  $\delta$  12.44 (br s, 1H), 8.19 (br s, 4H), 6.87 (s, 1H), 6.02 (s, 1H), 3.87-3.91 (m, 2H), 3.82 (q, 3H, *J*=7.1 Hz), 2.46 (s, 3H), 2.18 (s, 3H), 1.17 (br t, 4H, *J*=7.1 Hz). <sup>13</sup>C NMR (DMSO-*d*<sub>6</sub>, 126 MHz)  $\delta$  158.2, 157.9, 126.3, 124.4, 113.7, 105.2, 103.8, 40.7, 37.6, 15.9, 11.9, 11.1. HRMS (ESI+) calcd. for C<sub>13</sub>H<sub>18</sub>N<sub>4</sub>OS [M + H]<sup>+</sup>: 279.12741, found: 279.12604.



## 2.4 Left-Hand Side Synthesis (Compounds 18-26 from Scheme 2)

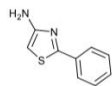
### **Tert-butyl (2-phenylthiazol-4-yl)carbamate (19)<sup>4</sup>**



To a suspension of 2-phenylthiazole-4-carboxylic acid **18** (0.500 g, 2.439 mmol) in *t*BuOH (6.8 mL), DPPA (0.63 mL, 2.926 mmol) and TEA (0.41 mL, 2.926 mmol) were added. The mixture was stirred in a pressure vial at 80 °C for 16 h. The reaction mixture was cooled down to room temperature and concentrated to dryness. The crude was dissolved in EtOAc (10 mL), washed with water (5 mL) and saturated aq. NaHCO<sub>3</sub> (5 mL). The organic layer was dried over anhydrous Na<sub>2</sub>SO<sub>4</sub>, filtered and evaporated to dryness. The crude product was absorbed onto ISOLUTE® HM-N and purified by FCC with a gradient of 0–20% EtOAc in cyclohexane to afford the compound **19** as an off-white powder, (0.345 g, 51%).

<sup>1</sup>H NMR (CDCl<sub>3</sub>, 500 MHz)  $\delta$  7.86-7.92 (m, 2H), 7.53 (br s, 1H), 7.4-7.5 (m, 3H), 7.24 (br s, 1H), 1.54 (s, 9H). <sup>13</sup>C NMR (CDCl<sub>3</sub>, 126 MHz)  $\delta$  165.5, 152.6, 148.4, 133.3, 130.4, 129.2, 126.3, 98.5, 28.5, 27.2. *m/z* (ESI+) 277.1 [M + H]<sup>+</sup>.

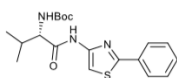
### **2-Phenylthiazol-4-amine (20)<sup>4</sup>**



To a solution of *tert*-butyl (2-phenylthiazol-4-yl)carbamate **19** (0.300 g, 1.086 mmol) in dioxane (2.4 mL), 4M HCl/dioxane solution (3.9 mL) was added. The mixture was stirred at room temperature for 16 h. Organic phase was evaporated leaving the acidic aqueous layer that was extracted with Et<sub>2</sub>O (2 x 10 mL). Combined organic layers were further washed with aq. 1 M HCl solution (15 mL). The combined aqueous layers were basified with 10% NaOH (aq.) and extracted with DCM (2 x 20 mL). The organic layers were then combined, dried over anhydrous Na<sub>2</sub>SO<sub>4</sub>, filtered and evaporated to dryness to afford compound **20** as an orange-brown oil, (0.181 g, 95%).

<sup>1</sup>H NMR (DMSO-*d*<sub>6</sub>, 500 MHz)  $\delta$  7.80-7.83 (m, 2H), 7.4-7.5 (m, 3H), 5.92 (s, 1H), 5.45 (s, 2H). <sup>13</sup>C NMR (DMSO-*d*<sub>6</sub>, 126 MHz)  $\delta$  163.2, 158.8, 133.2, 129.2, 128.8, 124.9, 87.1. *m/z* (ESI+) 177.1 [M + H]<sup>+</sup>.

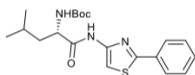
**Tert-butyl (S)-(3-methyl-1-oxo-1-((2-phenylthiazol-4-yl)amino)butan-2-yl)carbamate (21)**



Using general procedure A, *N*-Boc-L-valine (0.045 g, 0.207 mmol) was coupled with 2-phenylthiazol-4-amine **20** (0.037 g, 0.207 mmol), HBTU (0.095 g, 0.249 mmol) and TEA (9  $\mu$ L, 0.621 mmol) in DMF (1.5 mL) with addition of *N*-Boc-L-valine, HBTU and TEA (1.0 eq.) after 16 h continued in total reaction time of 48 h at room temperature to afford FCC purified compound **21** as a yellow oil (0.011 g, 15%).

$^1\text{H}$  NMR ( $\text{CDCl}_3$ , 500 MHz)  $\delta$  9.01 (br s, 1H), 7.89-7.93 (m, 2H), 7.69 (s, 1H), 7.5-7.5 (m, 3H), 5.0-5.1 (m, 1H), 4.1-4.2 (m, 1H), 2.3-2.4 (m, 1H), 1.48 (s, 9H), 1.05 (d, 3H,  $J=6.7$  Hz), 0.98 (d, 3H,  $J=6.7$  Hz).  $^{13}\text{C}$  NMR ( $\text{CDCl}_3$ , 126 MHz)  $\delta$  169.8, 165.7, 156.2, 147.3, 133.3, 130.5, 129.3, 126.4, 102.3, 80.7, 60.6, 28.5, 27.1, 19.6. HRMS (ESI+) calcd. for  $\text{C}_{19}\text{H}_{25}\text{N}_3\text{O}_3\text{S}$  [ $\text{M} + \text{H}$ ] $^+$ : 376.16894, found: 376.16869.

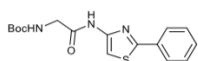
**Tert-butyl (S)-(4-methyl-1-oxo-1-((2-phenylthiazol-4-yl)amino)pentan-2-yl)carbamate (22)**



Using general procedure A, *N*-Boc-L-leucine (0.045 g, 0.195 mmol) was coupled with 2-phenylthiazol-4-amine **20** (0.034 g, 0.195 mmol), HBTU (0.089 g, 0.233 mmol) and TEA (8  $\mu$ L, 0.584 mmol) in DMF (1.5 mL) with addition of *N*-Boc-L-leucine, HBTU and TEA (1.0 eq.) after 16 h, continued in total reaction time of 48 h at room temperature to afford FCC purified compound **22** as a yellow oil (0.017 g, 22%).

$^1\text{H}$  NMR ( $\text{CDCl}_3$ , 500 MHz)  $\delta$  9.02 (br s, 1H), 7.89-7.93 (m, 2H), 7.65 (s, 1H), 7.4-7.5 (m, 3H), 4.8-5.0 (m, 1H), 4.3-4.4 (m, 1H), 1.7-1.9 (m, 2H), 1.55-1.62 (m, 1H), 1.48 (s, 9H), 0.97-1.01 (m, 6H).  $^{13}\text{C}$  NMR ( $\text{CDCl}_3$ , 126 MHz)  $\delta$  170.5, 165.3, 151.2, 146.9, 132.6, 130.4, 129.1, 126.2, 101.9, 80.7, 53.5, 41.2, 29.7, 28.3, 24.8, 23.0. HRMS (ESI+) calcd. for  $\text{C}_{20}\text{H}_{27}\text{N}_3\text{O}_3\text{S}$  [ $\text{M} + \text{H}$ ] $^+$ : 390.18459, found: 390.18440.

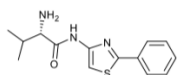
**Tert-butyl (2-oxo-2-((2-phenylthiazol-4-yl)amino)ethyl)carbamate (23)**



Using general procedure A, *N*-Boc-glycine (0.035 g, 0.200 mmol) was coupled with 2-phenylthiazol-4-amine **20** (0.035 g, 0.200 mmol), HBTU (0.091 g, 0.240 mmol) and TEA (8  $\mu$ L, 0.599 mmol) in DMF (1.5 mL) to afford FCC purified compound **23** as a yellow oil (0.024 g, 35%).

$^1\text{H}$  NMR ( $\text{CDCl}_3$ , 500 MHz)  $\delta$  8.94 (br s, 1H), 7.87-7.92 (m, 2H), 7.66 (s, 1H), 7.4-7.5 (m, 3H), 5.22 (br s, 1H), 4.03 (br s, 2H), 1.50 (s, 9H).  $^{13}\text{C}$  NMR ( $\text{CDCl}_3$ , 126 MHz)  $\delta$  167.0, 165.1, 155.8, 146.5, 132.5, 130.1, 128.8, 126.0, 101.9, 80.5, 44.5, 28.0. HRMS (ESI+) calcd. for  $\text{C}_{16}\text{H}_{19}\text{N}_3\text{O}_3\text{S}$  [ $\text{M} + \text{H}$ ] $^+$ : 334.12199, found: 334.12169.

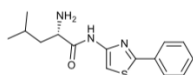
**(S)-2-Amino-3-methyl-N-(2-phenylthiazol-4-yl)butanamide (24)**



Using general procedure B, compound **21** (0.008 g, 0.021 mmol) was Boc-deprotected in DCM (0.9 mL) with TFA (0.1 mL) to afford prep. HPLC purified compound **24** as a white powder one TFA salt form, (0.005 g, 58%).

$^1\text{H}$  NMR ( $\text{DMSO-}d_6$ , 500 MHz)  $\delta$  11.64 (br s, 1H), 8.2-8.3 (m, 3H), 7.90-7.94 (m, 2H), 7.74 (s, 1H), 7.5-7.6 (m, 3H), 3.8-3.9 (m, 1H), 3.7-3.8 (m, 1H), 2.1-2.2 (m, 1H), 0.99 (t, 6H,  $J=7.2$  Hz).  $^{13}\text{C}$  NMR ( $\text{DMSO-}d_6$ , 126 MHz)  $\delta$  172.2, 157.6, 147.6, 131.0, 130.1, 129.8, 129.5, 126.2, 103.5, 58.1, 30.4, 25.9, 18.8, 18.1. HRMS (ESI+) calcd. for  $\text{C}_{14}\text{H}_{17}\text{N}_3\text{OS}$  [ $\text{M} + \text{H}$ ] $^+$ : 276.11651, found: 276.11639.

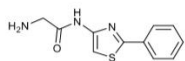
**(S)-2-Amino-4-methyl-N-(2-phenylthiazol-4-yl)pentanamide (25)**



Using general procedure B, compound **22** (0.014 g, 0.036 mmol) was Boc-deprotected in DCM (1.1 mL) with TFA (0.11 mL) to afford prep. HPLC purified compound **25** as an off-white powder one TFA salt form, (0.006 g, 40%).

$^1\text{H}$  NMR ( $\text{DMSO-}d_6$ , 500 MHz)  $\delta$  11.74 (br s, 1H), 8.2-8.3 (m, 3H), 7.90-7.94 (m, 2H), 7.73 (s, 1H), 7.51-7.54 (m, 3H), 4.0-4.1 (m, 1H), 1.6-1.7 (m, 3H), 0.94 (t, 6H,  $J=6.3$  Hz).  $^{13}\text{C}$  NMR ( $\text{DMSO-}d_6$ , 126 MHz)  $\delta$  168.0, 165.1, 147.7, 132.9, 130.9, 129.7, 126.1, 103.4, 51.6, 24.1, 23.0, 22.1. HRMS (ESI+) calcd. for  $\text{C}_{15}\text{H}_{19}\text{N}_3\text{OS}$  [ $\text{M} + \text{H}$ ] $^+$ : 290.13216, found: 290.13187.

### 2-Amino-N-(2-phenylthiazol-4-yl)acetamide (**26**)



Using general procedure B, compound **23** (0.018 g, 0.054 mmol) was Boc-deprotected in DCM (1.8 mL) with TFA (0.2 mL) to afford prep. HPLC purified compound **26** as a beige powder one TFA salt form, (0.009 g, 45%).

$^1\text{H}$  NMR (DMSO- $d_6$ , 500 MHz)  $\delta$  11.54 (s, 1H), 8.15 (br s, 3H), 7.89-7.93 (m, 2H), 7.68 (s, 1H), 7.50-7.55 (m, 3H), 3.83 (s, 2H).  
 $^{13}\text{C}$  NMR (DMSO- $d_6$ , 126 MHz)  $\delta$  165.2, 165.1, 147.9, 133.0, 131.0, 129.9, 126.2, 102.9, 41.2. HRMS (ESI+) calcd. for  $\text{C}_{11}\text{H}_{11}\text{N}_3\text{OS}$  [M + H] $^+$ : 234.06956, found: 234.06944.

### 3.) References

- 1) B. Liu, G. Liu, L. Nelson, J. Patel, H. Sham, Z. Xin, H. Zhao, US20050014794 A1, 2005.
- 2) A. K. H. Hirsch, M. S. Alphey, S. Lauw, M. Seet, L. Barandun, W. Eisenreich, F. Rohdich, W. N. Hunter, A. Bacher and F. Diederich, *Org. Biomol. Chem.*, 2008, **6**, 2719–2730.
- 3) F. Mjambili, M. Njoroge, K. Naran, C. De Kock, P. J. Smith, V. Mizrahi, D. Warner and K. Chibale, *Bioorganic Med. Chem. Lett.*, 2014, **24**, 560–564.
- 4) C. Bolea, WO2011/86163A1, ADDEX PHARMA S.A., 2011.

## Supporting Information

### Search for the Active Ingredients from a 2-Aminothiazole

#### DMSO Stock Solution with Antimalarial Activity

Henni-Karoliina Ropponen,<sup>[a,b]</sup> Chantal D. Bader,<sup>[a,b]</sup> Eleonora Diamanti,<sup>[a]</sup> Boris Illarionov,<sup>[c]</sup> Matthias Rottmann,<sup>[d,e]</sup> Markus Fischer,<sup>[c]</sup> Matthias Witschel,<sup>[f]</sup> Rolf Müller,<sup>[a,b]</sup> and Anna K. H. Hirsch\*<sup>[a,b]</sup>

**Abstract:** Chemical decomposition of DMSO stock solutions is a common incident that can mislead biological screening campaigns. Here, we share our case study of 2-aminothiazole **1**, originating from an antimalarial class that undergoes chemical decomposition in DMSO at room temperature. As previously measured biological activities observed against *Plasmodium falciparum* NF54 and for the target enzyme *Pf*IspE were not reproducible for a fresh batch, we tackled the challenge to understand where the activity originated from. Solvent- and temperature-dependent studies using HRMS and NMR spectroscopy to monitor the decomposition led to the isolation and in vitro evaluation of several fractions against *Pf*IspE. After four days of decomposition, we successfully isolated the oxygenated and dimerised compounds using SFC purification and correlated the observed activities to them. Due to the unstable nature of the two isolates, it is likely that they undergo further decomposition contributing to the overall instability of the compound.

## Table of Contents

<b>1.) Biological Assays .....</b>	<b>179</b>
1.1 General Procedure for Enzymatic Assay .....	179
1.2 General Procedure for Antimalarial Assay .....	179
1.3 General Procedure for Cytotoxicity Assay .....	179
<b>2.) Decomposition Study Procedures .....</b>	<b>180</b>
2.1 General Conditions .....	180
2.2 Synthesis of Compound <b>1</b> .....	181
2.3 Temperature-Dependent Study .....	186
2.4 Solvent-Dependent Study .....	187
2.5 Preparative HPLC Purification .....	191
2.6 SFC Purification .....	194
2.7 Characterisation of Decomposition Product <b>1</b> .....	196
2.8 Characterisation of Decomposition Product <b>2</b> .....	206
<b>3.) References .....</b>	<b>215</b>
<b>4.) Appendix .....</b>	<b>215</b>
4.1 Appendix I – Calibration of the HRMS Data .....	215
4.2 Appendix II – Extra NMR Spectra of the Other Isolated Fractions .....	216

## 1.) Biological Assays

### 1.1 General Procedure for Enzymatic Assay

The cloning, expression and purification of *Plasmodium falciparum* (Publication 2, H.-K. Ropponen *et al. RSC Med. Chem.*, **2021**, DOI:10.1039/d0md00409j) and *Escherichia coli*.<sup>[1,2]</sup> and their subsequent assays (Publication 2, H.-K. Ropponen *et al. RSC Med. Chem.*, **2021**, DOI:10.1039/d0md00409j) followed the previously reported procedures. Due to the nature of the study, some decomposition samples were only tested once and thus, for some formal standard error, determined from one IC<sub>50</sub> curve with 5 to 10 data points, is given. For the final purified compounds, replicates were measured and standard deviation was calculated at least from two replicates.

### 1.2 General Procedure for Antimalarial Assay

*Plasmodium falciparum* drug-sensitive NF54 (airport strain from The Netherlands, provided by F. Hoffmann-La Roche Ltd) was cultivated in a variation of the medium consisting of RPMI 1640 supplemented with 0.5% ALBUMAX® II, 25 mM Hepes, 25 mM NaHCO<sub>3</sub> (pH 7.3), 0.36 mM hypoxanthine, and 100 µg/ml neomycin, as previously described.<sup>[3,4]</sup> Human erythrocytes served as host cells. Cultures were maintained in an atmosphere of 3% O<sub>2</sub>, 4% CO<sub>2</sub>, and 93% N<sub>2</sub> in humidified modular chambers at 37 °C. Compounds were dissolved in MeOH (10 mM), diluted in hypoxanthine-free culture medium and titrated in duplicates over a 64-fold range in 96 well plates. Infected erythrocytes (1.25% final hematocrit and 0.3% final parasitemia) were added into the wells. After 48 h incubation, 0.25 µCi of [<sup>3</sup>H]hypoxanthine was added per well and plates were incubated for an additional 24 h. Parasites were harvested onto glass-fiber filters and radioactivity was counted using a Betaplate liquid scintillation counter (Wallac, Zurich). Chloroquine (IC<sub>50</sub> = 3.1 ± 0.8 ng/mL) and artesunate (IC<sub>50</sub> = 4.0 ± 1.7 ng/mL) were used as controls. The results were recorded and expressed as a percentage of the untreated controls. Fifty percent inhibitory concentrations (IC<sub>50</sub>) were estimated by linear interpolation.<sup>[5]</sup>

### 1.3 General Procedure for Cytotoxicity Assay

Cytotoxicity assays based on the human lung adenocarcinoma (A549), human embryonic kidney (Hek293) and human hepatocellular carcinoma (HepG2) cell lines were performed as described previously.<sup>[6]</sup>

## 2.) Decomposition Study Procedure

### 2.1 General Conditions

All reagents and solvents were of commercial quality and used without further purification. Chemical yields were not optimised and the yields for the compounds isolated from the decomposition mixtures were not calculated. Low resolution mass analytics and purity controls were carried out using an Ultimate 3000-ISQ liquid-chromatography mass spectrometry (LCMS) system (Thermo Fisher Scientific, Dreieich, Germany) consisting of a Dionex UltiMate pump, an autosampler, DAD detector and an ESI quadrupole mass spectrometer. NMR spectra were recorded on a Bruker AV 500 or Ascend 700 ( $^1\text{H}$ , 500 MHz or 700 MHz;  $^{13}\text{C}$ , 126 MHz or 175 MHz;  $^{19}\text{F}$ , 470 MHz) spectrometer. All spectra were measured in DMSO- $d_6$ , methanol- $d_4$ , acetone- $d_6$  or acetonitrile- $d_3$  to which reported chemical shifts in parts per million (ppm), where adjusted based on the residual protons as the internal standards, (DMSO- $d_6$ ,  $\delta = 2.50, 39.51$ , methanol- $d_4$ ,  $\delta = 4.87, 49.1$ , acetone- $d_6$ ,  $\delta = 2.05, 29.32$  or acetonitrile- $d_3$ ,  $\delta = 1.94, 1.39$ ,  $^1\text{H}$  and  $^{13}\text{C}$  respectively). Coupling constants ( $J$ ) are given in Hertz (Hz) and following abbreviations were used for multiplicity (s = singlet, d = doublet, t = triplet, m = multiplet, br = broad and combinations of these). High-resolution mass spectra (HRMS) were obtained using a Thermo Scientific Q Exactive Focus Orbitrap system or a maXis 4G UHR-TOF (Bruker Daltonics) both coupled to a Dionex Ultimate 3000 RSLC and equipped with a standard electrospray ion (ESI) source. An Acquity UPLC® BEH C8, 150 x 2.1 mm, 1.7  $\mu\text{m}$  column equipped with a VanGuard Pre-Column BEH C8, 5 x 2.1 mm, 1.7  $\mu\text{m}$  (Waters, Germany) was used for measurements with the Orbitrap system, using a flow rate of 250  $\mu\text{L}/\text{min}$ . The gradient of [A]  $\text{H}_2\text{O} + 0.1\% \text{FA}$  and [B]  $\text{ACN} + 0.1\% \text{FA}$  was kept at 10% B for 1 min and then increased to 95% B over 4 min and kept at 95% B for 1.2 min, before returning to 10% B over 0.3 min and equilibration for 1 min. For measurements with the TOF system, an Acquity UPLC® BEH C18, 100 x 2.1 mm, 1.7  $\mu\text{m}$  column equipped with a VanGuard Pre-Column BEH C18, 5 x 2.1 mm, 1.7  $\mu\text{m}$  (Waters, Germany) was used. The flow rate was set to 600  $\mu\text{L}/\text{min}$  using the same solvents as for the Orbitrap system and the column thermostated at 45  $^\circ\text{C}$ . The gradient started at 5% B for one minute, before increasing to 100% B in 9 minutes. The amount of B was kept at 100% B for one minute before returning to initial conditions and equilibration. The flow was split to 75  $\mu\text{L min}^{-1}$  before entering the mass spectrometer, which was externally calibrated to a mass accuracy below 1 ppm. Mass spectra were acquired in centroid mode ranging from 150–2500  $m/z$  at a 2 Hz scan rate. All mass spectra were measured in positive ionisation mode in a range from 120–500  $m/z$  for the Orbitrap and 150-2500  $m/z$  for the TOF. UV spectra were recorded by a DAD in the range from 200 to 600 nm.

Preparative reverse phase-high performance liquid chromatography (rp-HPLC) was performed using an UltiMate 3000 Semi-Preparative System (Thermo Fisher Scientific, Dreieich, Germany) equipped with a Phenomenex Luna® 5  $\mu\text{m}$  C18(2) 100 Å LC Column (250 x 10 mm) thermostated at 45  $^\circ\text{C}$ .

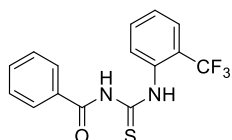


Separation was achieved using a linear gradient from 60% (A) ddH<sub>2</sub>O to 100% (B) acetonitrile over 22.5 minutes. Before ramping the gradient, an equilibration step at 40% B was performed for 1 min. The B content was kept for 1 min at 100% after the gradient, before returning to 40% in 0.5 min and a final equilibration for 5 min. The compounds were detected by UV absorption at 210 and 280 nm.

The compounds were separated on a Waters Prep 15 SFC System coupled to an Acquity QDa mass spectrometer equipped with a 5  $\mu$ m Torus Diol 130 Å OBD Prep Column 250 x 19 mm thermostated at 40 °C. Separation was achieved using a linear gradient of 25–45% ACN as a cosolvent over 10 minutes, after a 1 min equilibration step at 25% in the beginning. The percentage of cosolvent was kept at 45 % for 1 minute before returning to 25 % in 1 minute and reequilibration for 3 minutes. Flow rate was set to 15 mL/min and backpressure to 120 bar. Analytical measurements were conducted on a 5  $\mu$ m Torus Diol 130 Å OBD Prep Column 150 x 2.1 mm with a gradient from 5–55% ACN and a flow rate of 3 mL/min. All other parameters resemble the preparative measurements.

## 2.2 Synthesis of Compound 1

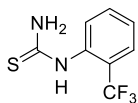
### *N*-((2-(trifluoromethyl)phenyl)carbamothioyl)benzamide



To a stirred solution of 2-(trifluoromethyl)aniline (1 eq., 0.77 g, 4.77 mmol) in acetone (16 mL), benzoyl isothiocyanate (1 eq., 0.64 mL, 4.77 mmol) was added and the reaction mixture was stirred to reflux for 1.5 h. The mixture was then poured into ice to obtain a yellowish precipitate (1.5 g, 99%). The compound was used without any further purification in the next step.

<sup>1</sup>H NMR (500 MHz, DMSO-*d*<sub>6</sub>):  $\delta$  = 12.65 (s, 1H), 11.91 (s, 1H), 8.01 (dd, *J* = 8.4, 1.2 Hz, 2H), 7.79-7.83 (m, 1H), 7.81 (s, 1H), 7.74-7.79 (m, 1H), 7.73-7.78 (m, 1H), 7.66-7.71 (m, 1H), 7.52-7.59 ppm (m, 3H). *m/z* (ESI+) 325.06 [*M*+H]<sup>+</sup>

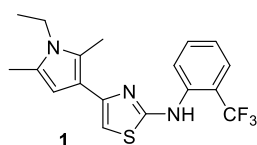
### 1-(2-(Trifluoromethyl)phenyl)thiourea



A solution of *N*-((2-(trifluoromethyl)phenyl)carbamothioyl)benzamide (1 eq., 1.5 g, 4.6 mmol) is refluxed in an aq. 10% NaOH solution (15 mL) for 1 hour. The reaction mixture was cooled to RT, acidified with aq. HCl 0.1 M and extracted with EtOAc (3 x 20 mL). The combined organic layers were dried over Na<sub>2</sub>SO<sub>4</sub>, filtered, concentrated in vacuo to afford as yellowish powder (0.57 g, 56%).

<sup>1</sup>H NMR (500 MHz, DMSO-*d*<sub>6</sub>): δ = 9.26 (s, 1H), 7.95 (m, 1H), 7.70 (m, 1H), 7.66 (t, *J* = 7.7 Hz, 1H), 7.51 (m, 2H), 7.49- 7.43 (m, 1H). *m/z* (ESI+) 221.04 [*M*+H]<sup>+</sup>

### 4-(1-Ethyl-2,5-dimethyl-1*H*-pyrrol-3-yl)-*N*-(2-(trifluoromethyl)phenyl)thiazol-2-amine



2-chloro-1-(1-ethyl-2,5-dimethyl-1*H*-pyrrol-3-yl)ethan-1-one (1 eq., 0.100 g, 0.501 mmol) and 1-(2-(trifluoromethyl)phenyl)thiourea (1 eq., 0.110 g, 0.501 mmol) were dissolved in ethanol and heated to reflux for 6 h. The reaction mixture was cooled and the solvent removed under reduced pressure. The crude product was recrystallised from propan-2-ol to yield the pure compound **1** as light beige powder, (0.114 g, 0.312 mmol, 31%).

<sup>1</sup>H NMR (500 MHz, DMSO-*d*<sub>6</sub>): δ = 9.52 (br s, 1H), 7.98-8.13 (m, 1H), 7.73 (d, *J* = 7.8 Hz, 1H), 7.67 (br t, *J* = 7.5 Hz, 1H), 7.33 (br t, *J* = 7.5 Hz, 1H), 6.51 (br s, 1H), 5.96-5.99 (m, 1H), 3.80 (q, *J* = 7.2 Hz, 2H), 2.37 (s, 3H), 2.17 (s, 3H), 1.14 ppm (t, *J* = 7.2 Hz, 3H). <sup>13</sup>C NMR (126 MHz, DMSO-*d*<sub>6</sub>): δ = 166.2, 138.0, 133.9, 126.9, 126.5, 125.9, 125.3, 124.8, 122.6, 111.5, 105.2, 99.2, 37.7, 15.9, 11.8, 10.9 ppm. <sup>19</sup>F NMR (470 MHz, DMSO-*d*<sub>6</sub>): δ = -59.41 (s, 3F). HRMS (ESI+) calcd. for C<sub>18</sub>H<sub>18</sub>F<sub>3</sub>N<sub>3</sub>S [*M*+H]<sup>+</sup>: 366.12463, found: 366.12292.

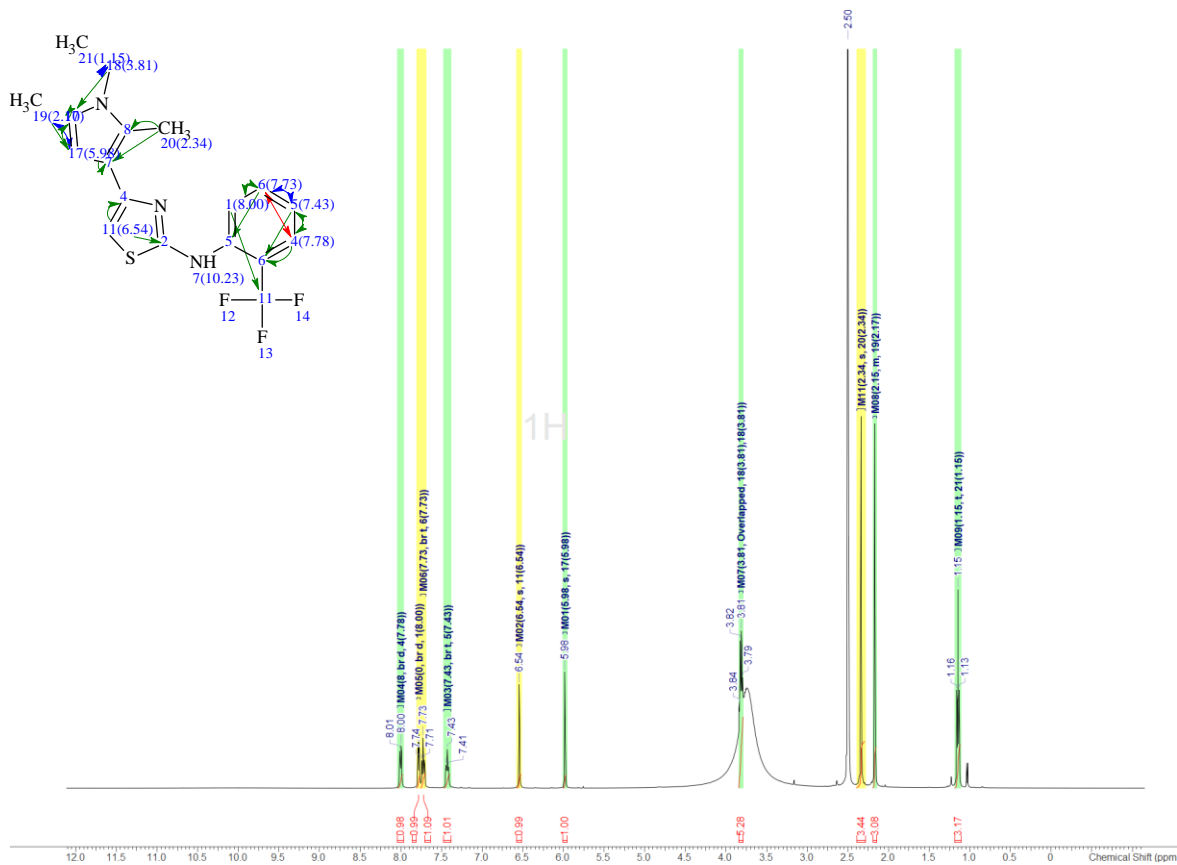


Figure S1. <sup>1</sup>H-NMR spectrum of compound 1 in DMSO-*d*<sub>6</sub>.

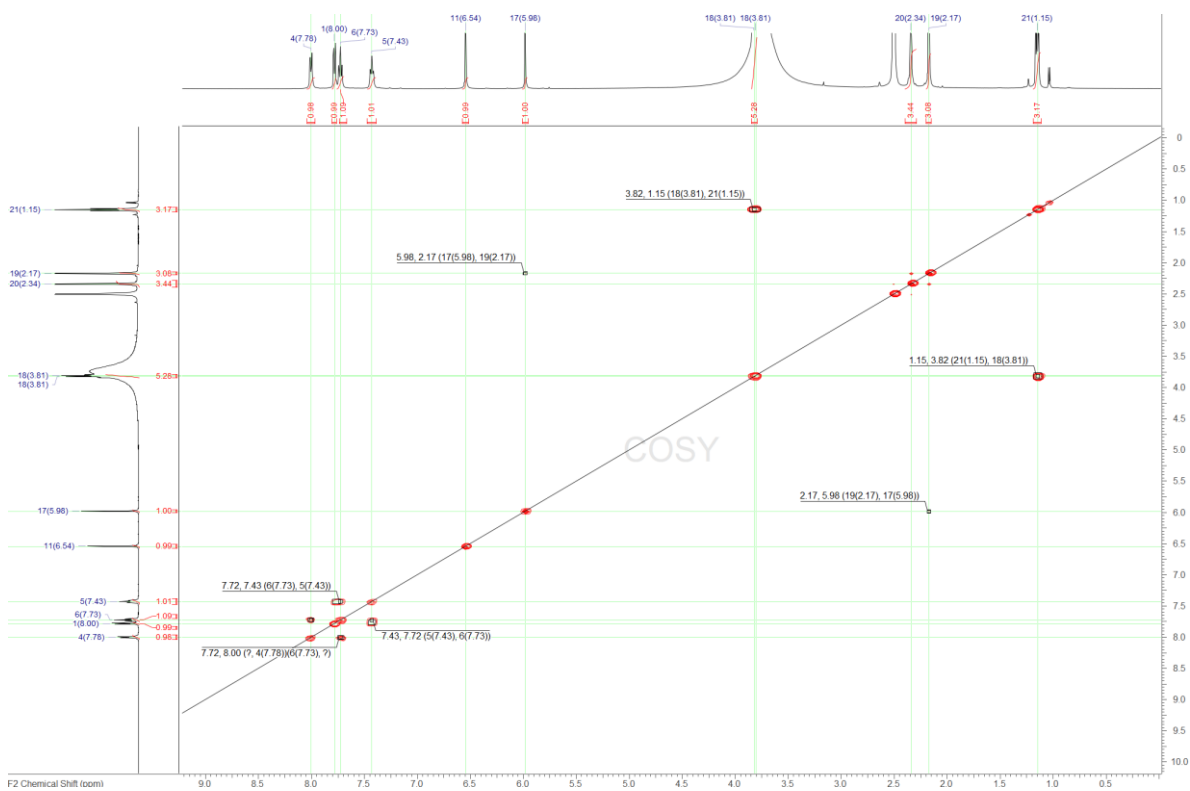


Figure S2. [<sup>1</sup>H,<sup>1</sup>H]-COSY NMR spectrum of compound 1 in DMSO-*d*<sub>6</sub>.





### 2.3 Temperature-Dependent Study

Compound **1** was dissolved in DMSO to afford 10 mM stock solution, in the scale of 3.65 mg in 1 mL. Three aliquots were prepared and one each was stored inside a light-protecting box at different temperatures: room temperature (RT), +4 °C and –20 °C. Samples were only taken to RT for the minimum time required for sampling. Samples were further diluted with acetonitrile to 10 μM (1:1000) for HRMS analysis. For calibration, a fresh stock solution of the compound **1** was prepared shortly before the analysis. The concentration range used for the calibration was from 10 μM to 20 nM, including 10 samples with 1:1 dilutions starting from the highest concentration (Appendix I). In all of the calibration points and samples, diphenhydramine ( $m/z$ : 256.16907 [ $M+H$ ]<sup>+</sup>) was included as an internal standard at the concentration of 500 nM. The results were analysed using Thermo Xcalibur Quan Browser. Similarly, three NMR samples of compound **1** were prepared in DMSO- $d_6$  and each stored at different temperatures; RT, +4 °C and –20 °C, (Figure S8).

**Table S1.** Summary of the decomposition of compound **1** at different temperatures with the corresponding enzymatic activities measured after three months.

Temperature	The Percentage of Compound <b>1</b> Left After Degradation <sup>[a]</sup>			Enzymatic activities after 3 months of decomposition <sup>[b]</sup>		
	Day 7	1 month	2 months	<i>Pf</i> /IspE IC <sub>50</sub> (μM)	<i>Ec</i> IspE IC <sub>50</sub> (μM)	PK/LDH IC <sub>50</sub> (μM)
RT	36%	1%	0%	12 ± 4	101 ± 14	34 ± 4
+4 °C	96%	48%	21%	16 ± 7	71 ± 10	45 ± 6
–20 °C	96%	91%	82%	>500	>500	n.d.

[a] The decomposition percentages are reported as the average of two values given in Tables S6. [b] Errors given as formal standard error. n.d.: not determined, PK/LDH: pyruvate kinase and lactate dehydrogenase, *Pf*: *Plasmodium falciparum*, *Ec*: *Escherichia coli*.

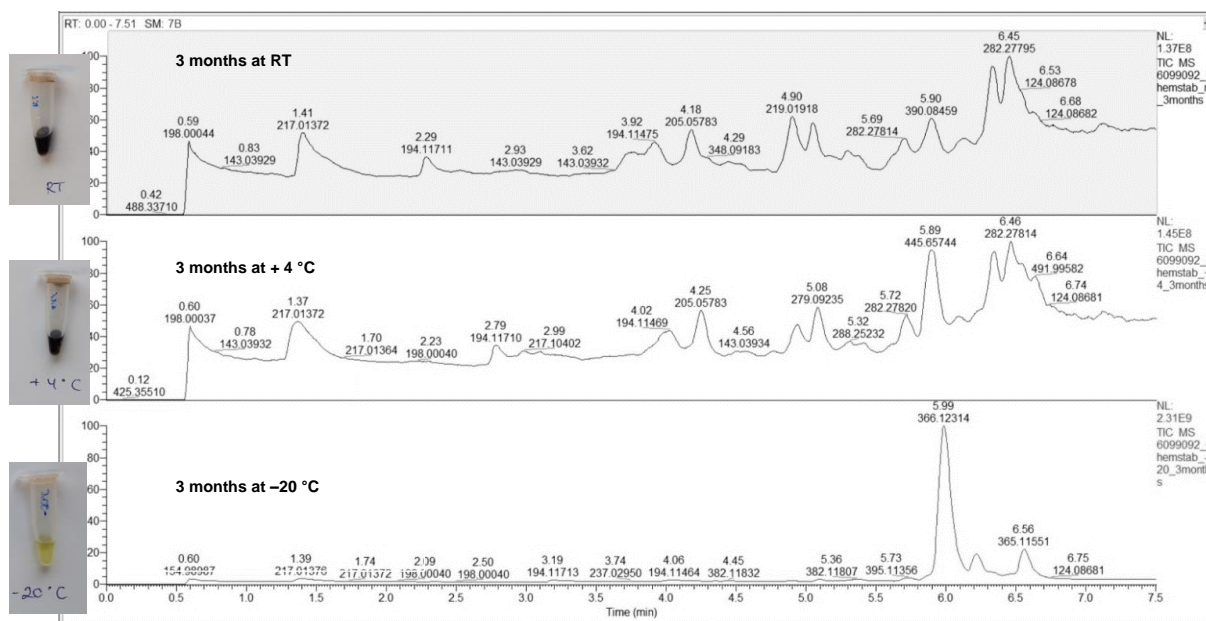


**Figure S7.** The HRMS recorded for the samples submitted to the enzyme assay after 3 months of decomposition with the corresponding colour differences.

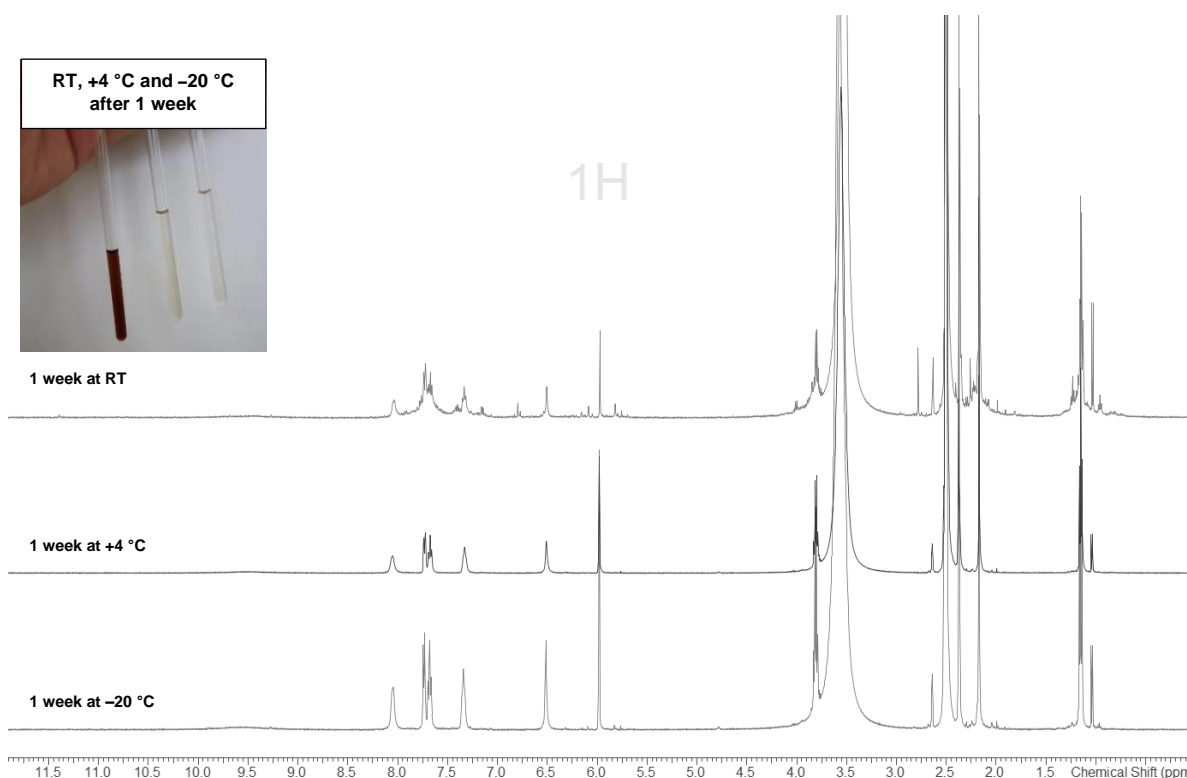


**Figure S8.** Decomposition of compound **1** in DMSO-*d*<sub>6</sub> samples at RT, +4 °C and –20 °C recorded with NMR after one week.

## 2.4 Solvent-Dependent Study

As in the Section 2.3, stock solutions of compound **1** were prepared in DMSO, ACN and MeOH and stored at RT for 16 days in a box protected from light. Samples were collected during this time and the enzymatic activity was analysed for them as in main text, Table 3. The samples were also diluted in ACN (1:1000) affording 10 μM solution and measured with HRMS, where no decomposition of compound **1** for ACN or MeOH was detectable (Figures S11–12). Similarly, the old samples of compound **1** used for enzyme and cell assays were analysed with HRMS (Figure S13). Additionally, NMR sample in MeOH was prepared and measured over time while stored at RT. As a follow-up experiment, the stability of compound **1** was determined for its 10 mM stock solution in Cyrene™ with HRMS (Figure S16).



**Figure S9.** Colour differences of the decomposition samples in different solvent stored at RT.

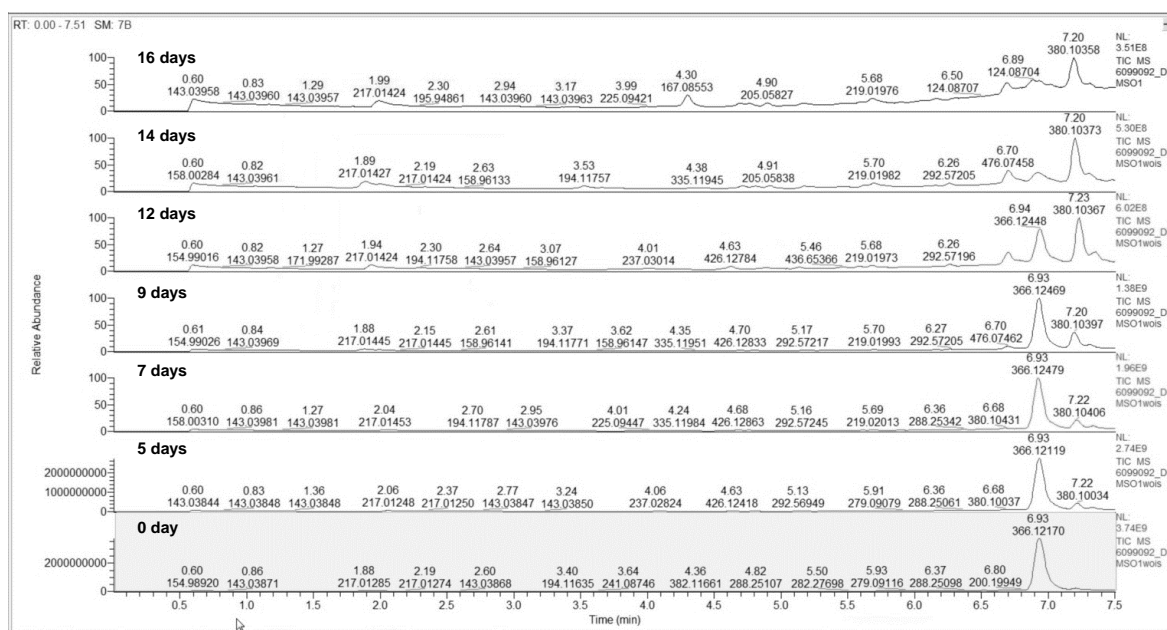


Figure S10. Decomposition of compound 1 studied in DMSO.

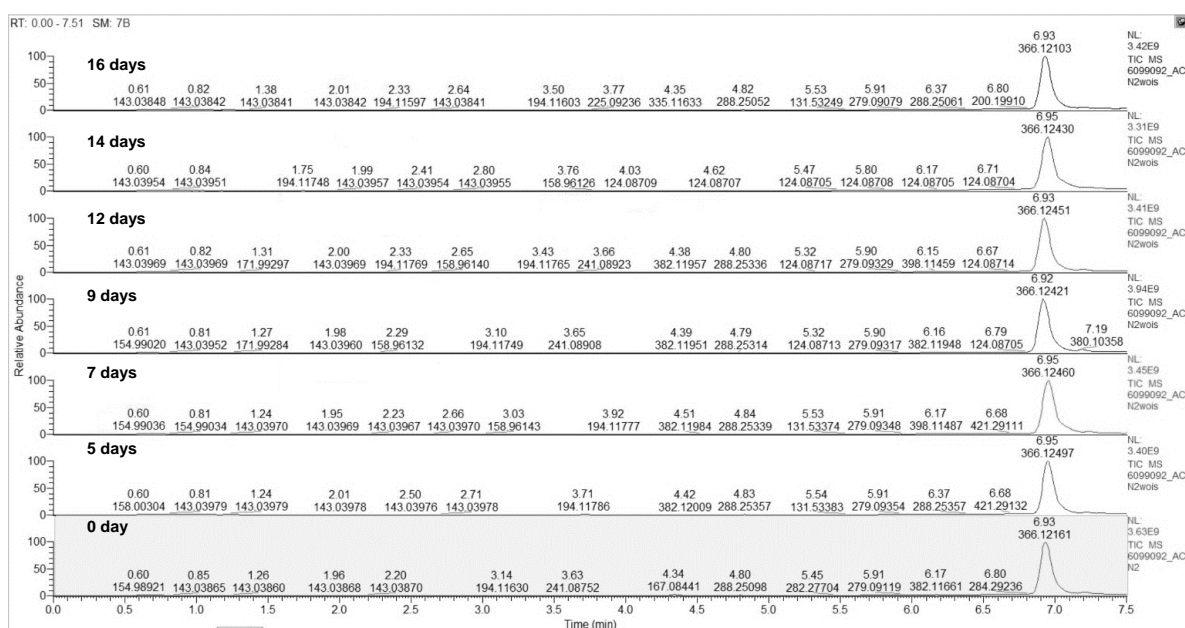
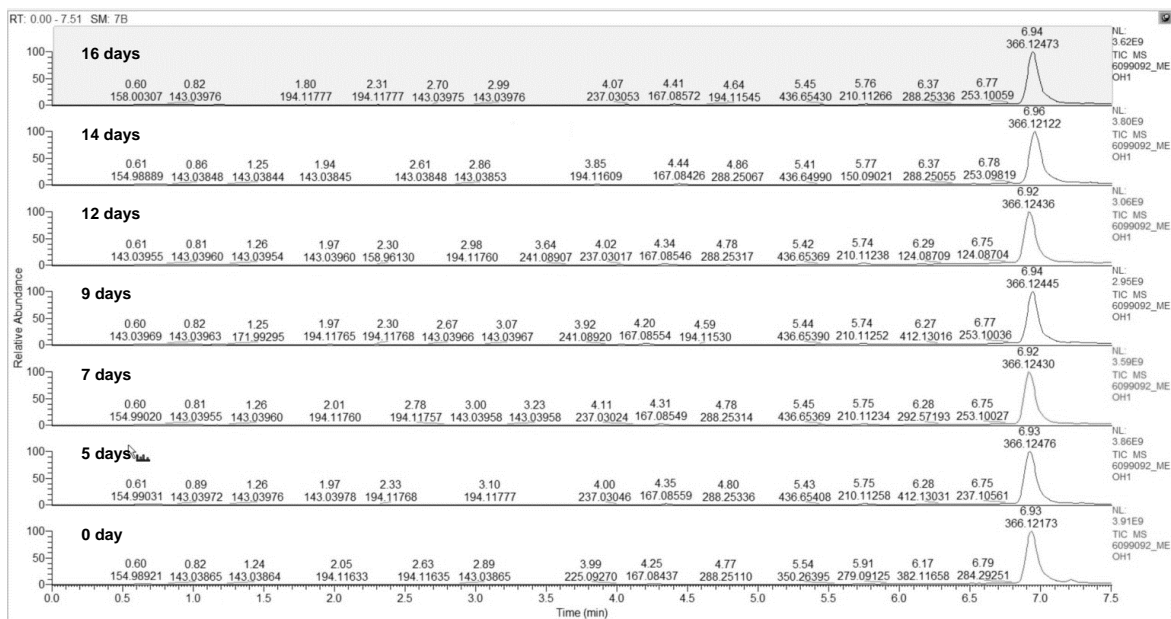
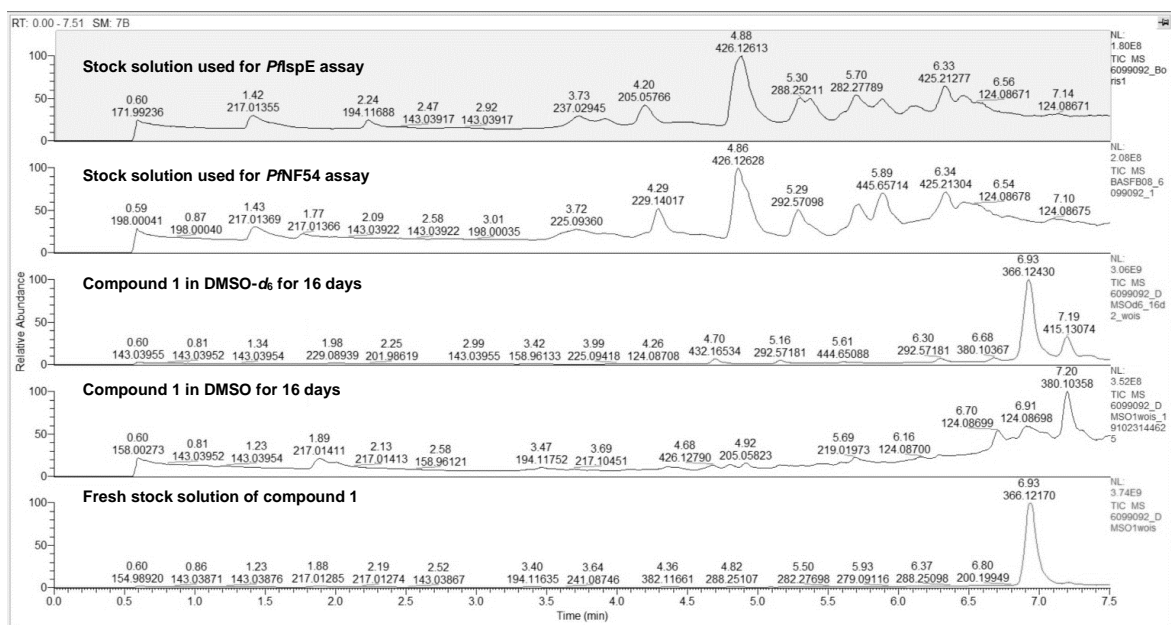


Figure S11. Decomposition of compound 1 studied in ACN.





**Figure S12.** Decomposition of compound **1** studied in MeOH



**Figure S13.** Comparison of the chromatographic profile of different samples. Note that the column conditions had changed in between the measurements.

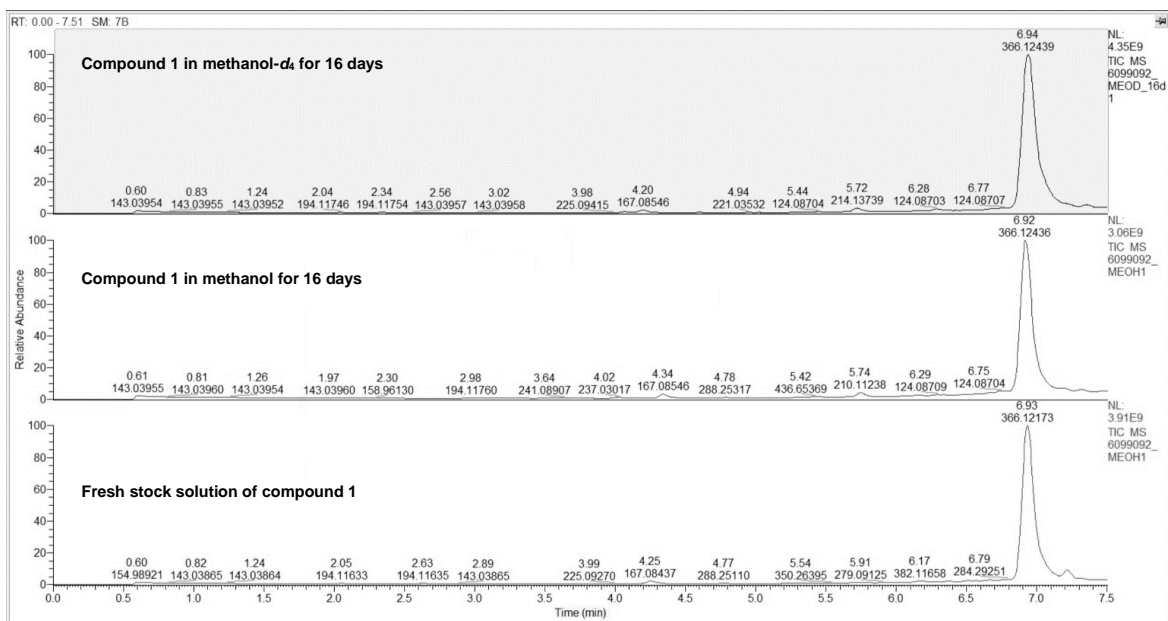


**Figure S14.** Decomposition of compound **1** studied in methanol- $d_4$ .

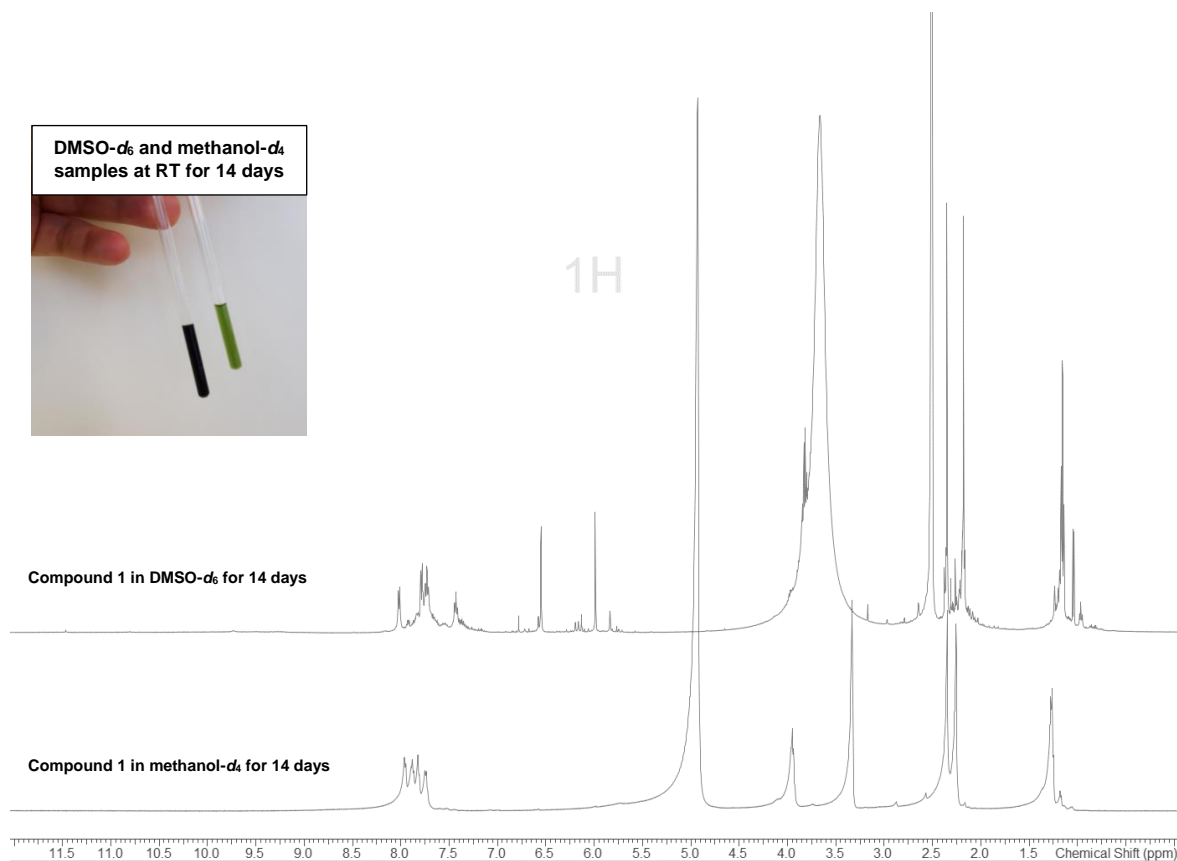


**Figure S15.** Decomposition of compound **1** studied in methanol- $d_4$  and DMSO- $d_6$ .

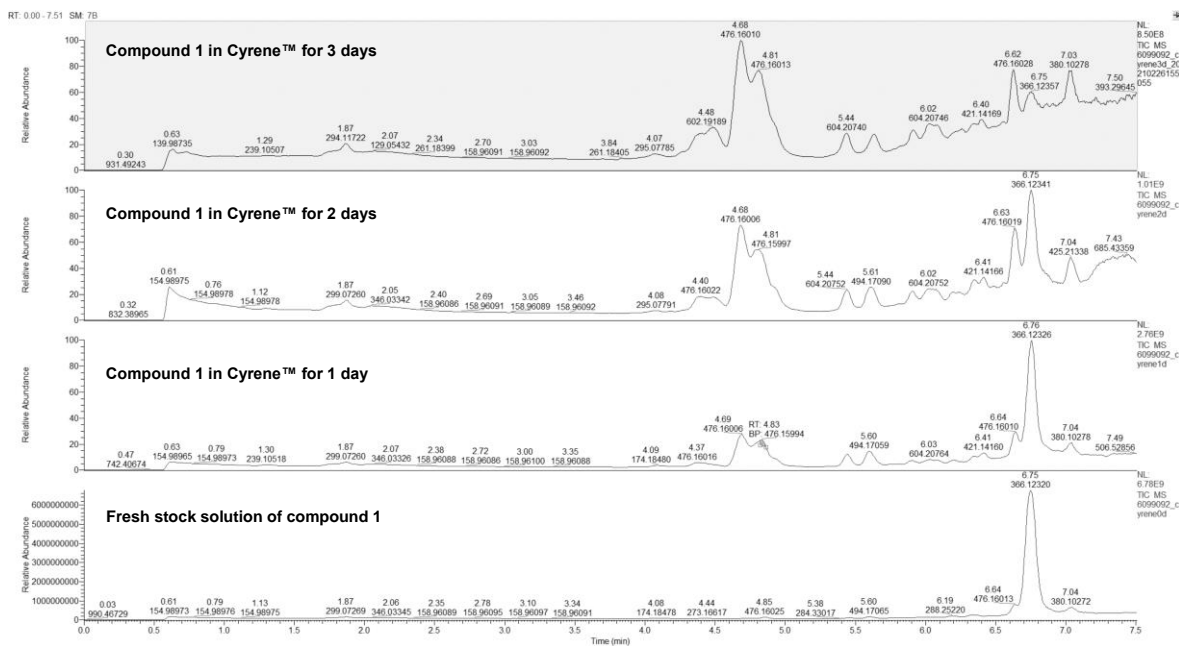


**Figure S16.** Decomposition of compound **1** studied in Cyrene™. The compound was incubated at RT in 10 mM stock solution.

## 2.5 Preparative HPLC Purification

Stock solution of 10 mM DMSO (in the scale of 3.65 mg in 1 mL, x3) was decomposed at RT for 2.5 weeks after which it was purified with prep. HPLC. The same was repeated for another set of samples after five days of decomposition of compound **1** in DMSO at RT. ....

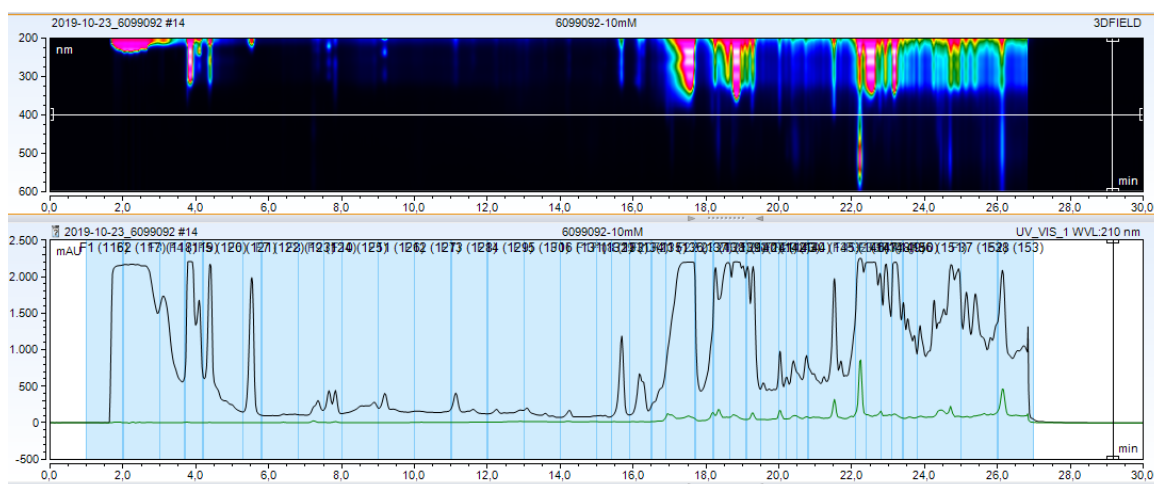


**Figure S17.** Chromatogram of the separation with the corresponding 3D-field.

**Table S2.** Separated fractions from the first prep. HPLC purification with the corresponding enzymatic activities.

Fraction	Weight (mg)	MS [M+H] <sup>+</sup>	HRMS [M+H] <sup>+</sup>	<i>Pf</i> IspE IC <sub>50</sub> (µg/mL) <sup>[a,c]</sup>	PK/LDH IC <sub>50</sub> (µg/mL) <sup>[a,c]</sup>
1_3	0.6	-	n.d.	>500	n.d.
4 <sup>[d]</sup>	0.4	426.1 // 205.1	426.12723 // 205.05789	>500	n.d.
5	0.2	426.1	426.12754	>500	n.d.
6	0.2	-	n.d.	>500	n.d.
7	0.4	-	n.d.	>500	n.d.
8	0.2	-	n.d.	>500	n.d.
9_10	0.3	426.1 // 210.0	426.12753 // 219.01955	>500	n.d.
11_12	0.5	426.1 // 472.1	426.12733 // 472.11520	>500	n.d.
13_17	3.9	472.1	472.11464	>500	n.d.
18	0.5	476.1	476.07387	>500	n.d.
19	0.6	-	n.d.	>500	n.d.
20_21	0.8	366.1 // 380.1 // 729.1 (364.1 [M+2H] <sup>2+</sup> )	366.12414 // 380.10388 // 727.20965 // 729.22360	22 ± 7	n.d.
22	0.3	584.1 // 757.1	584.13629 // 757.18403	>500	n.d.
23	0.5	584.1 // 380.1	584.13619 // 380.10333	>500	n.d.
24	1.1	584.1 // 412.1	584.13688 // 412.11331	>500	n.d.
25	0.5	380.1 // 428.1 // 743.2	380.10338 // 428.10676 // 743.20462	>500	n.d.
26	0.3	725.1	725.19351	>500	n.d.
27	0.4	725.1	725.19397	>500	n.d.
28	0.4	-	n.d.	>500	n.d.
29	0.3	-	n.d.	264 ± 250	n.d.
30	1.2	359.1 // 380.1 // 375.2	359.20286 // 380.10354 // 375.19847	66 ± 26	n.d.
31 <sup>[d]</sup>	0.4	741.2	741.22560	14 ± 2	>500
32	1.6	373.2 // 586.4 // 380.1	373.23288 // 586.36900 // 380.10347	53 ± 16	n.d.
33	1.3	-	n.d.	>500	n.d.
34	0.4	775.2 // (388.1 [M+2H] <sup>2+</sup> )	775.21228	41 ± 9	
35	0.4	-	380.10329	18 ± 3 <sup>[b]</sup>	>500
36	0.6	-	380.10327 // 725.19059	7 ± 2 <sup>[b]</sup>	>500
37	0.6	-	380.10302 // 725.18974	7 ± 2	26 ± 3
38	0.5	-	380.10338 // 725.18974	20 ± 3	240 ± 114

[a] All fractions were dissolved in DMSO as 1 mg/mL. [b] *Ec*IspE IC<sub>50</sub> (µg/mL) = >500. [c] Errors given as formal standard error. [d] NMR recorded for these two fractions (Appendix II). n.d.: not determined, PK/LDH: pyruvate kinase and lactate dehydrogenase, *Pf*: *Plasmodium falciparum*. *Ec*: *Escherichia coli*.

**Table S3.** Separated fractions from the second purification with the corresponding enzymatic activities.

Fraction	Weight (mg)	MS [M+H] <sup>+</sup>	<i>Pf</i> IspE IC <sub>50</sub> (µg/mL) <sup>[a]</sup>	<i>Ec</i> IspE IC <sub>50</sub> (µg/mL) <sup>[a]</sup>	PK/LDH IC <sub>50</sub> (µg/mL)
1	0.05	745.3	>500 (ACN) >500 (MeOH)	>500 (ACN) >500 (MeOH)	n.d.
2	0.05	380.1	>500 (ACN) >500 (MeOH)	>500 (ACN) >500 (MeOH)	n.d.
3	0.03	363.3	>500 (ACN) >500 (MeOH)	>500 (ACN) >500 (MeOH)	n.d.
4	0.10	365.2	>500 (ACN) 47 ± 17 (MeOH)	>500 (ACN) 123 ± 35 (MeOH) <sup>[b]</sup>	10 ± 2 (MeOH) <sup>[b]</sup>
5	0.05	381.3	>500 (ACN) <sup>[c]</sup>	>500 (ACN) <sup>[c]</sup>	n.d.

[a] All fractions were dissolved either in methanol (MeOH) or acetonitrile (ACN) to avoid further decomposition. [b] Errors given as formal standard error. [c] Only enough material for acetonitrile samples. n.d.: not determined, PK/LDH: pyruvate kinase and lactate dehydrogenase, *Pf*: *Plasmodium falciparum*. *Ec*: *Escherichia coli*.

## 2.6 SFC Purification

A stock solution of compound **1** in 10 mM DMSO (in the scale of 3.65 mg in 1 mL, x4) was decomposed at RT for four days after which it was purified with SFC.

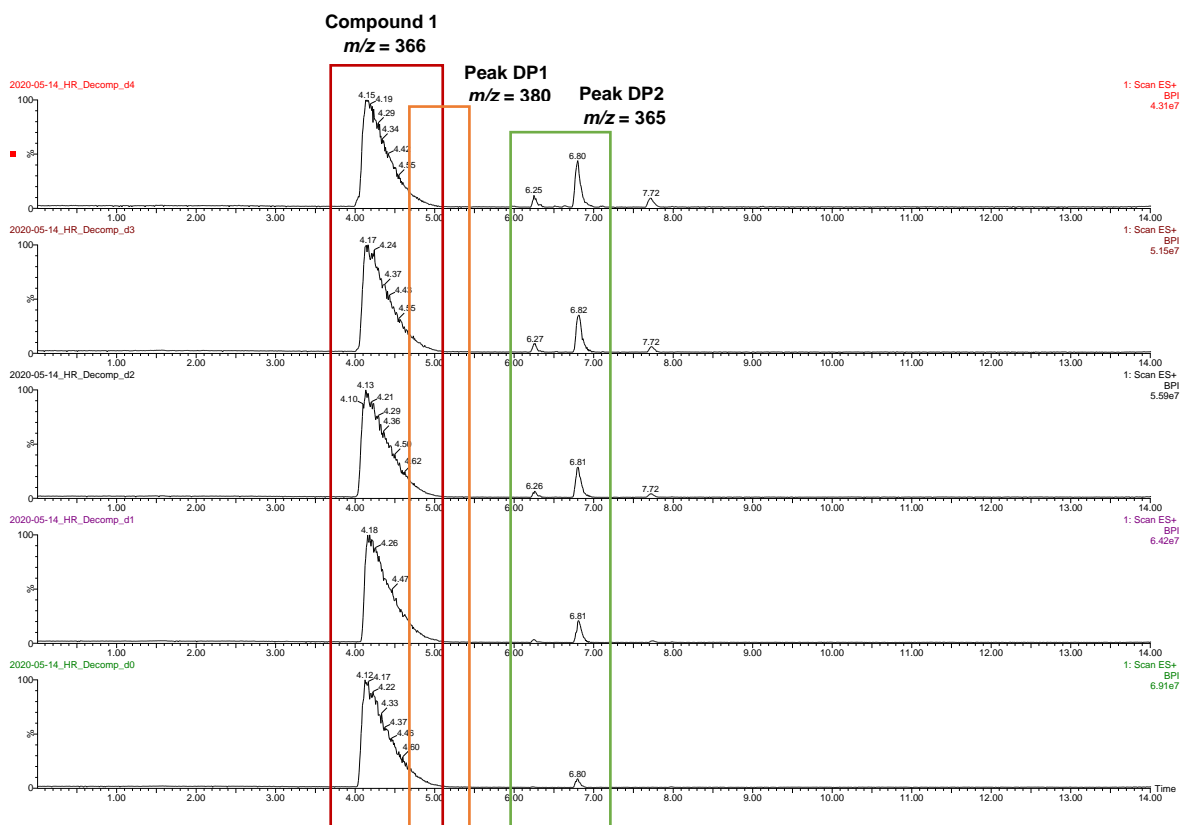


**Figure S18.** SFC chromatograms of the decomposition samples in DMSO over four days. The peak DP1 380 is co-eluting with the parent compound.

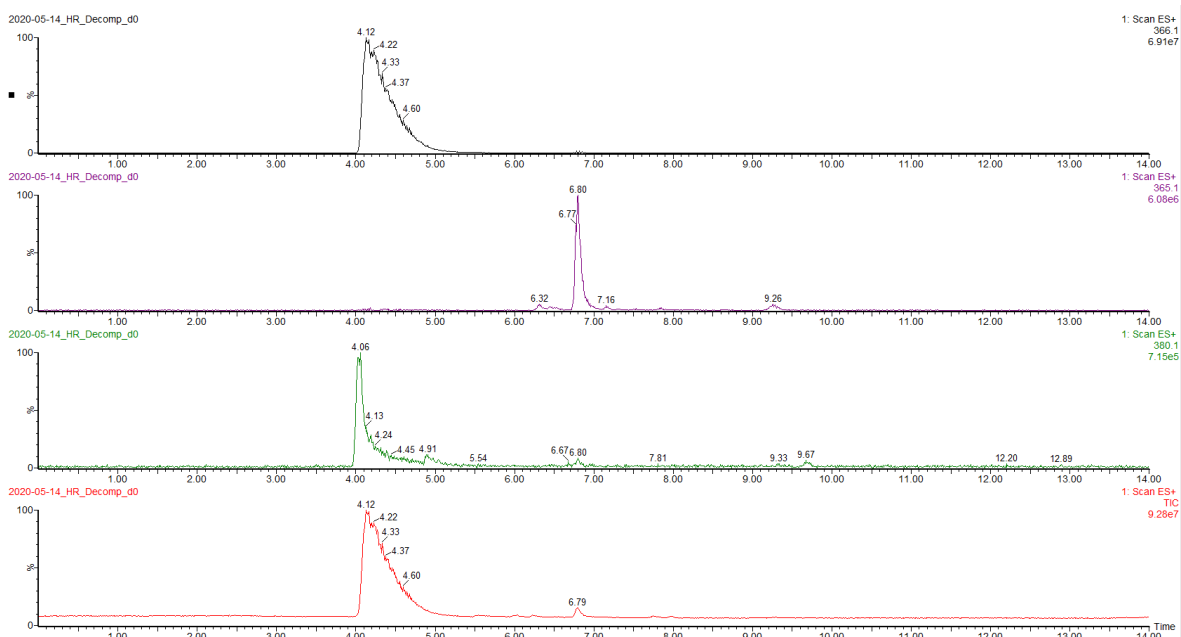


**Figure S19a.** SFC chromatograms of the decomposition samples in DMSO at d0. Black = EIC 366.1, purple = EIC 365.1, green = 380.1, red = TIC.

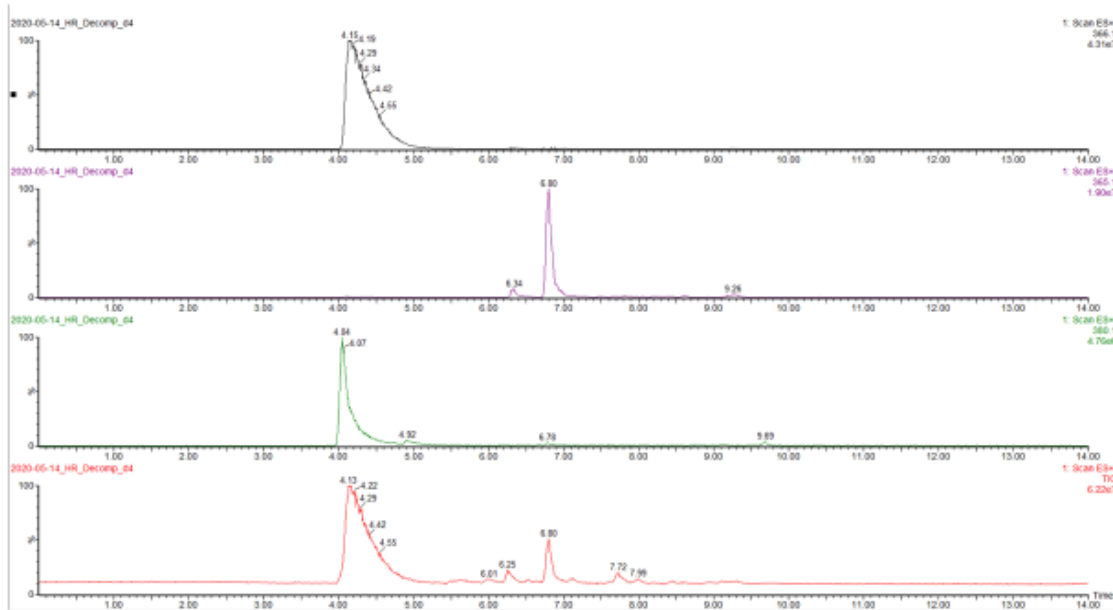


**Figure S19b.** SFC chromatograms of the decomposition samples in DMSO at d4. Black = EIC 366.1, purple = EIC 365.1, green = 380.1, red = TIC.

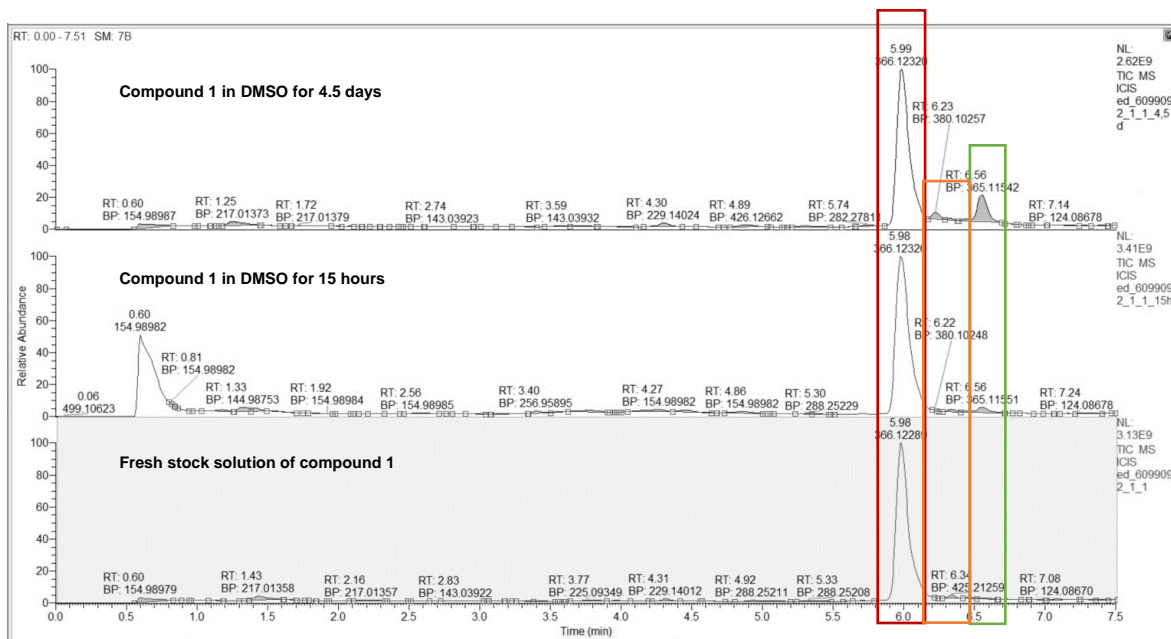
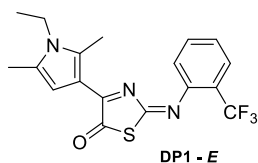


**Figure S20.** HRMS chromatograms of the decomposition samples in DMSO over to compare the visibility of the separation.

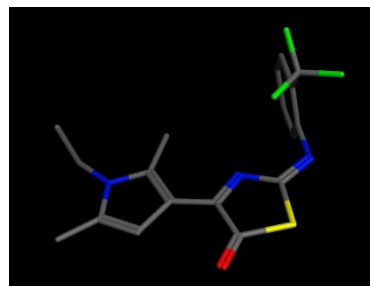
## 2.7 Characterisation of Decomposition Product 1

### (E)-4-(1-Ethyl-2,5-dimethyl-1H-pyrrol-3-yl)-2-((2-(trifluoromethyl)phenyl)imino)thiazol-5(2H)-one

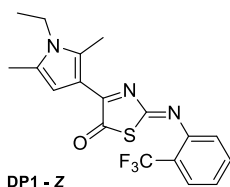


Chemical Formula:  $C_{18}H_{16}F_3N_3OS$   
Exact Mass: 379.09662

E = +29.4 kcal/mol of the lowest-energy conformation

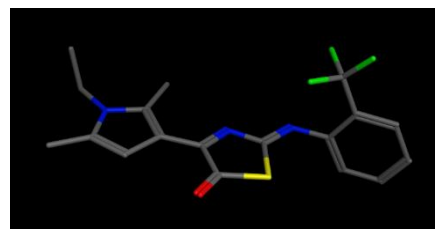


### (Z)-4-(1-Ethyl-2,5-dimethyl-1H-pyrrol-3-yl)-2-((2-(trifluoromethyl)phenyl)imino)thiazol-5(2H)-one

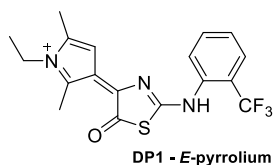


Chemical Formula:  $C_{18}H_{16}F_3N_3OS$   
Exact Mass: 379.09662

E = +33.2 kcal/mol of the lowest-energy conformation

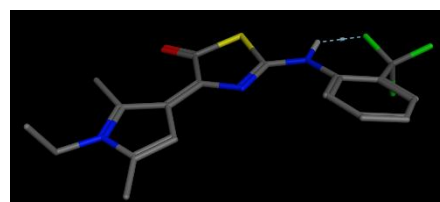


### (E)-1-Ethyl-2,5-dimethyl-3-(5-oxo-2-((2-(trifluoromethyl)phenyl)amino)thiazol-4(5H)-ylidene)-3H-pyrrol-1-ium

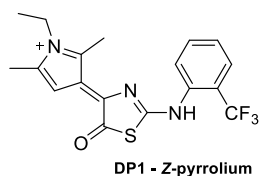


Chemical Formula:  $C_{18}H_{17}F_3N_3OS^+$   
Exact Mass: 380.10389

E = +66.1 kcal/mol of the lowest-energy conformation

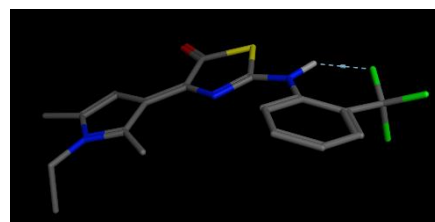


### (Z)-1-Ethyl-2,5-dimethyl-3-(5-oxo-2-((2-(trifluoromethyl)phenyl)amino)thiazol-4(5H)-ylidene)-3H-pyrrol-1-ium



Chemical Formula:  $C_{18}H_{17}F_3N_3OS^+$   
Exact Mass: 380.10389

E = +62.8 kcal/mol of the lowest-energy conformation



(MOE 2018.01 was used to calculate the lowest energy conformation in MMFF94X force field)



## DP1

Colour: bright red-orange

Isolated amount after SFC: 0.3 mg

HRMS (ESI+) calcd. for  $C_{18}H_{16}F_3N_3OS$   $[M+H]^+$ : 379.09662 or  $C_{18}H_{17}F_3N_3OS^+$   $[M]^+$ : 380.10389,

found: 380.10376 for the mixture of compounds.

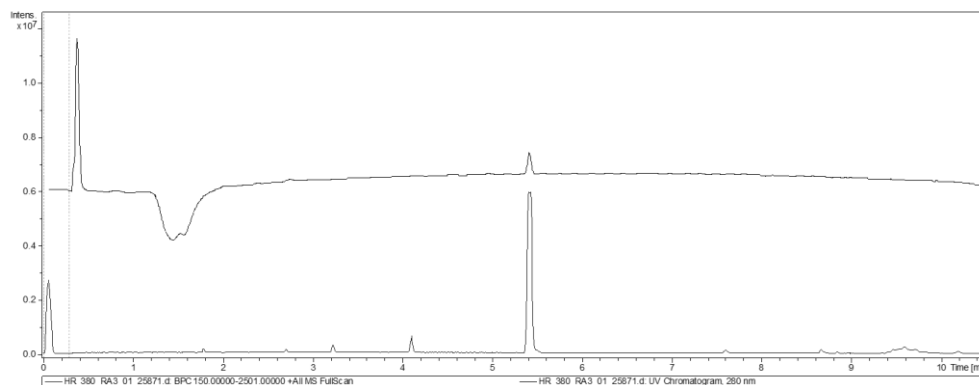
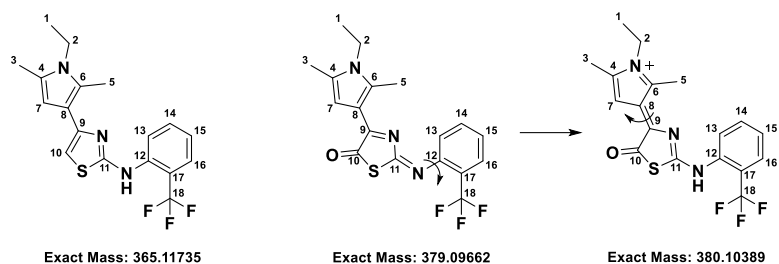


**Figure S21.** Chromatogram of the isolated **DP1**.

**Table S4.** Summary of the NMR shifts for **DPI** mixture.



#	Parent compound		Non-charged pyrrole		Charged pyrrolium	
	<sup>1</sup> H 366	<sup>13</sup> C 366	<sup>1</sup> H 380	<sup>13</sup> C 380	<sup>1</sup> H 380	<sup>13</sup> C 380
1 – CH <sub>3</sub>	1.24	15.3	1.34	14.3	1.36	n.d.
2 – CH <sub>2</sub>	3.93	37.9	4.09	38.7	4.09	38.7
3 – CH <sub>3</sub>	2.24	11.3	2.31	11.1	2.32	n.d.
4 – C	x	127.4	x	133.4	x	n.d.
5 – CH <sub>3</sub>	2.44	10.6	2.83	12.6	2.46	n.d.
6 – C	x	126.2	x	144.8	x	n.d.
7 – CH	6.23	105.1	6.87	108.8	6.99	108.9
8 – C	x	110.1	x	109.5	x	n.d.
9 – C	x	141.3	x	172.5	x	n.d.
10 – C	6.54	96.4	x	n.d.	x	n.d.
11 – C	x	168.7	x	n.d.	x	n.d.
12 – C	x	136.5	x	132.7	x	n.d.
13 – CH	7.88	127.2	7.78	130.0	7.13	121.5
14 – CH	7.58	127.4	7.61	132.2	7.70	133.4
15 – CH	7.83	134.2	7.86	133.4	7.41	125.1
16 – CH	8.13	126.2	7.93	127.0	7.73	126.2
17 – C	x	124.1	x	n.d.	x	n.d.
18 – CF <sub>3</sub>	x	122.2	x	n.d.	x	n.d.

- Measured in acetone-*d*<sub>6</sub> n.d.: not determined

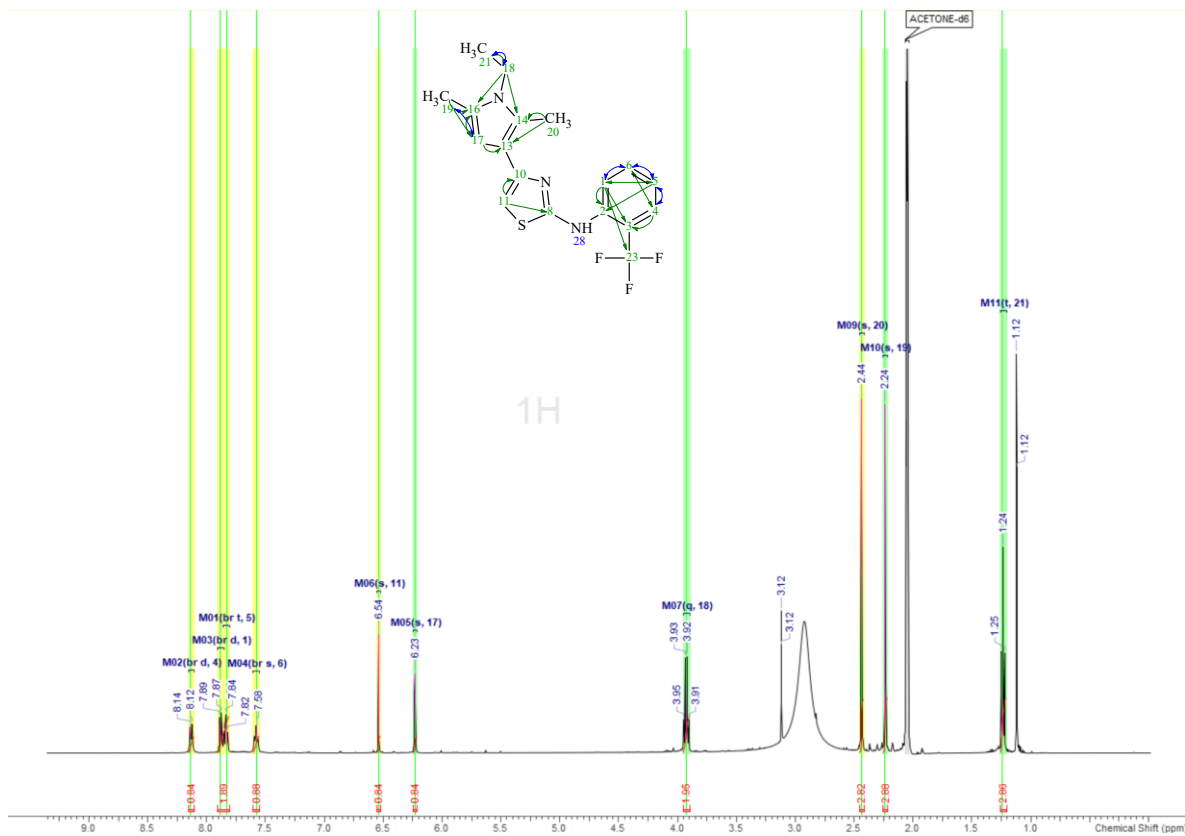


Figure S22.  $^1\text{H-NMR}$  spectrum of compound **1** in acetone- $d_6$ .

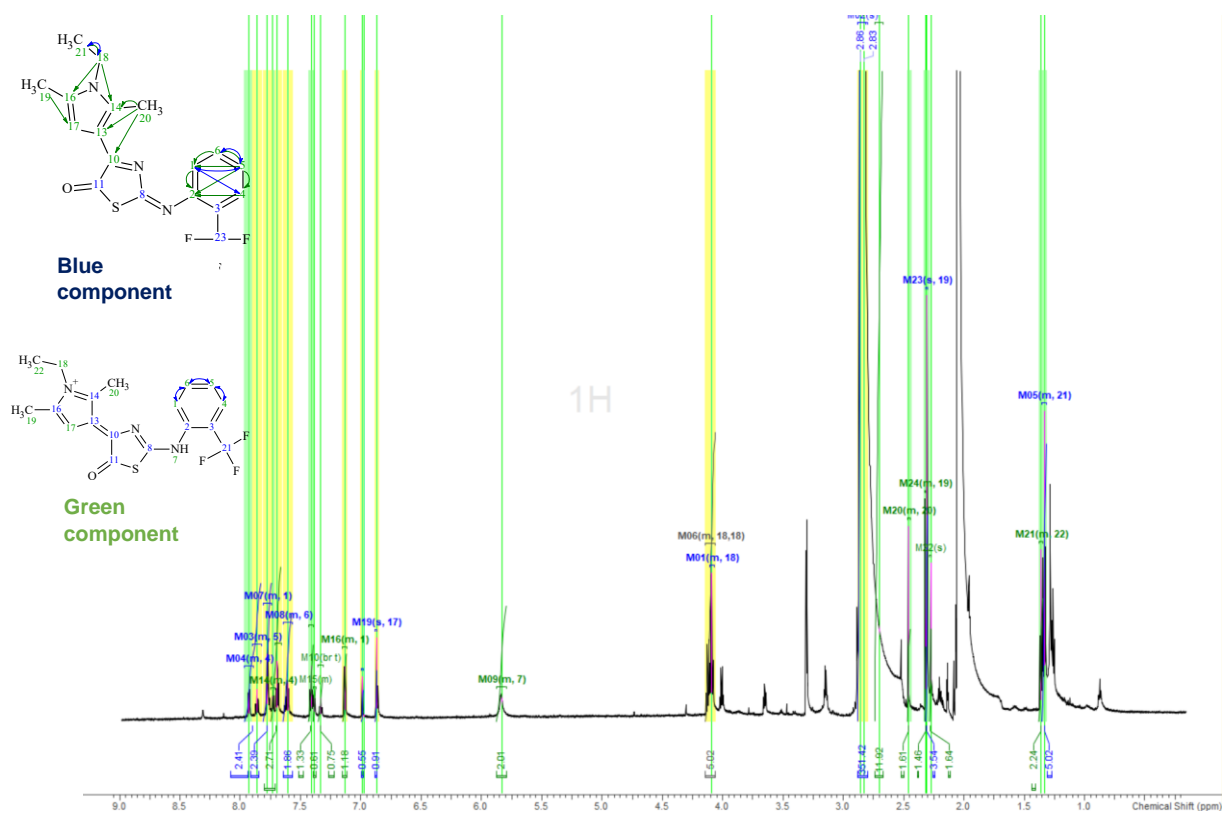
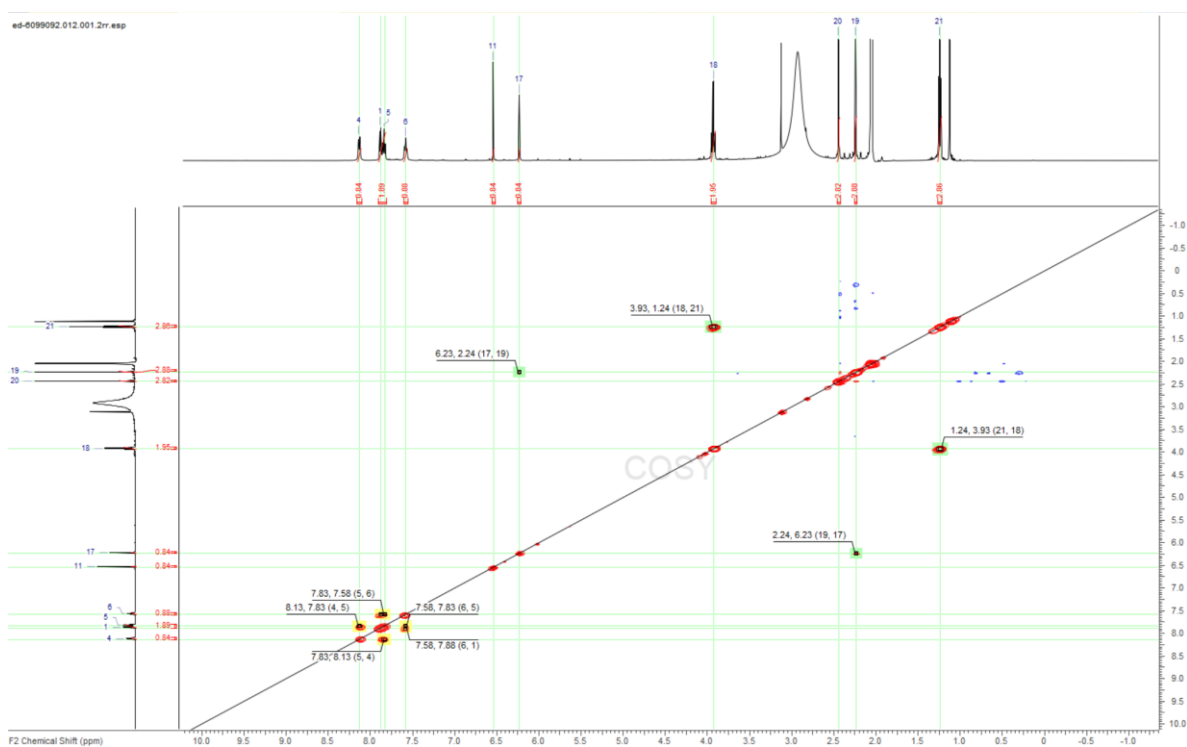
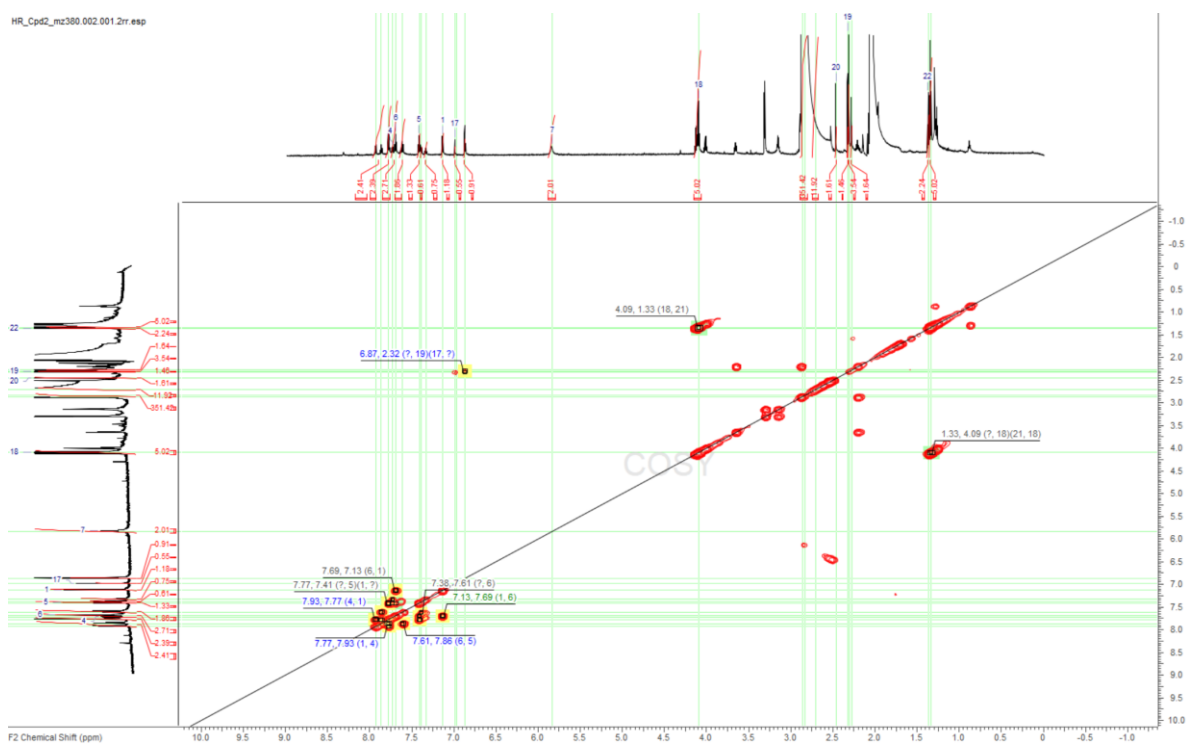


Figure S23.  $^1\text{H-NMR}$  spectrum of DP1 mixture in acetone- $d_6$ .



**Figure S24.**  $^1\text{H}$ ,  $^1\text{H}$ -COSY NMR spectrum of compound **1** in acetone- $d_6$ .



**Figure S25.**  $^1\text{H}$ ,  $^1\text{H}$ -COSY NMR spectrum of **DP1** mixture in acetone- $d_6$ .

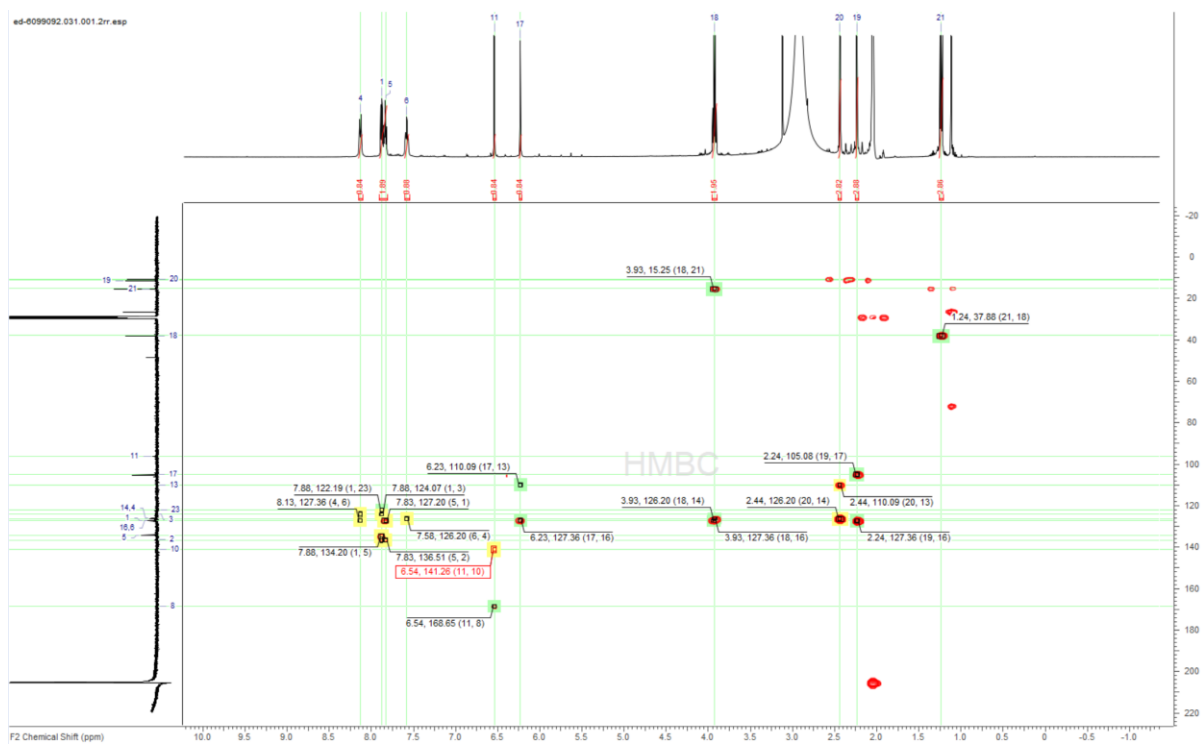


Figure S26.  $^1\text{H}$ ,  $^{13}\text{C}$ -HMBC spectrum of compound **1** in acetone- $d_6$ .

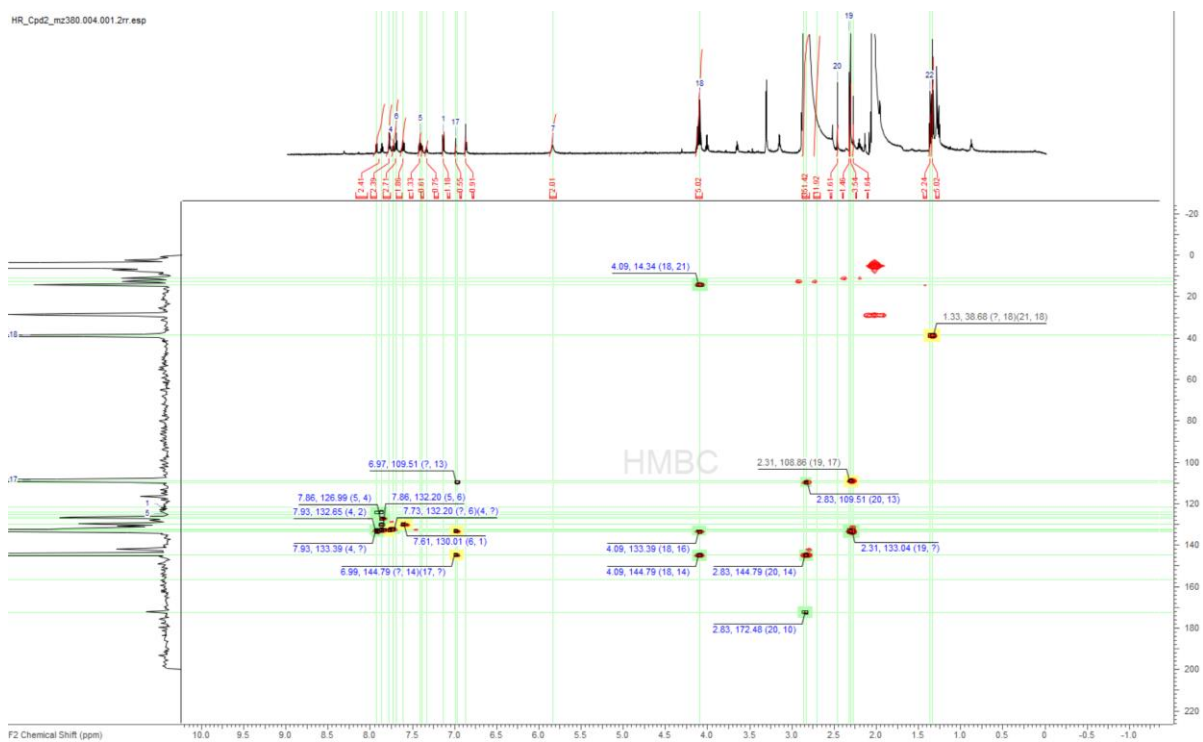


Figure S27.  $^1\text{H}$ ,  $^{13}\text{C}$ -HMBC spectrum of DP1 mixture in acetone- $d_6$ .

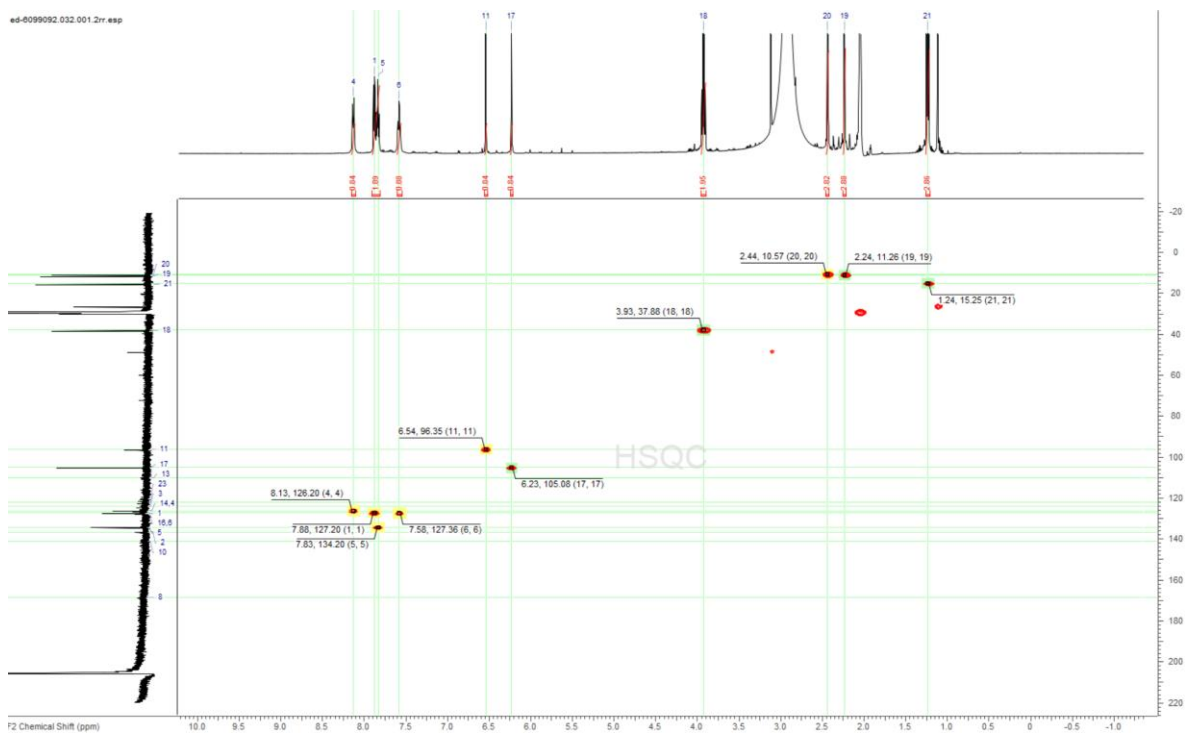


Figure S28.  $^1\text{H}$ ,  $^{13}\text{C}$ -HSQC spectrum of compound 1 in acetone- $d_6$ .

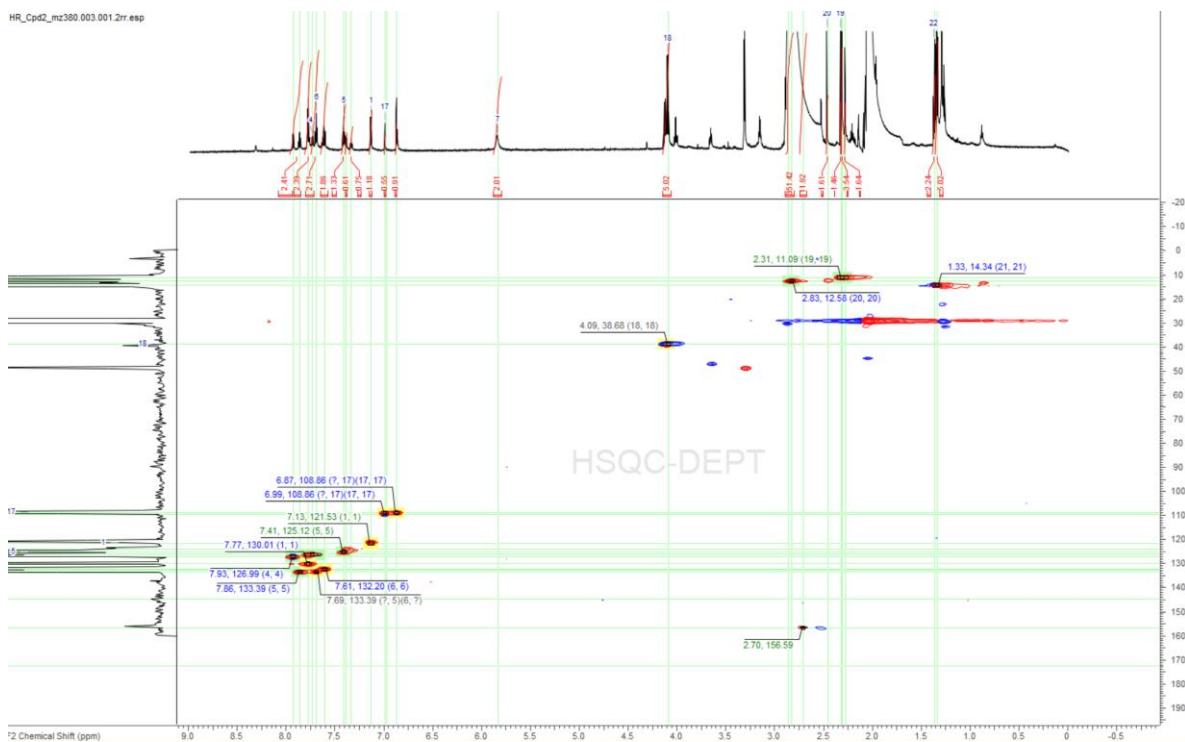
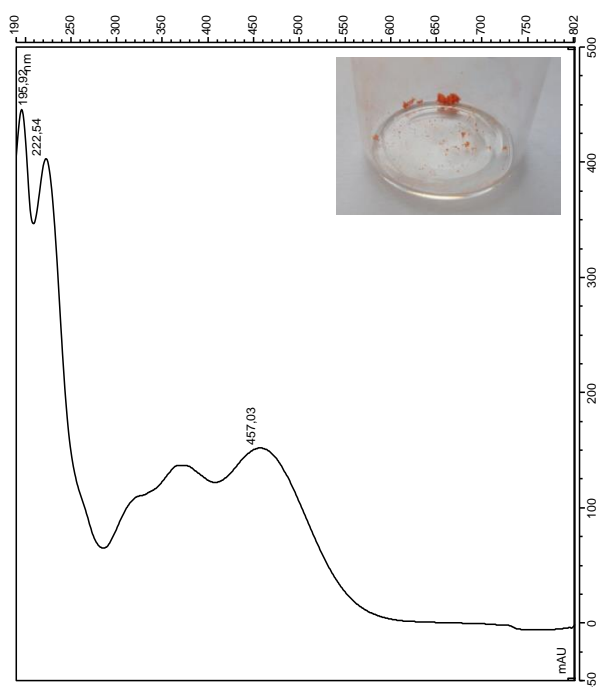
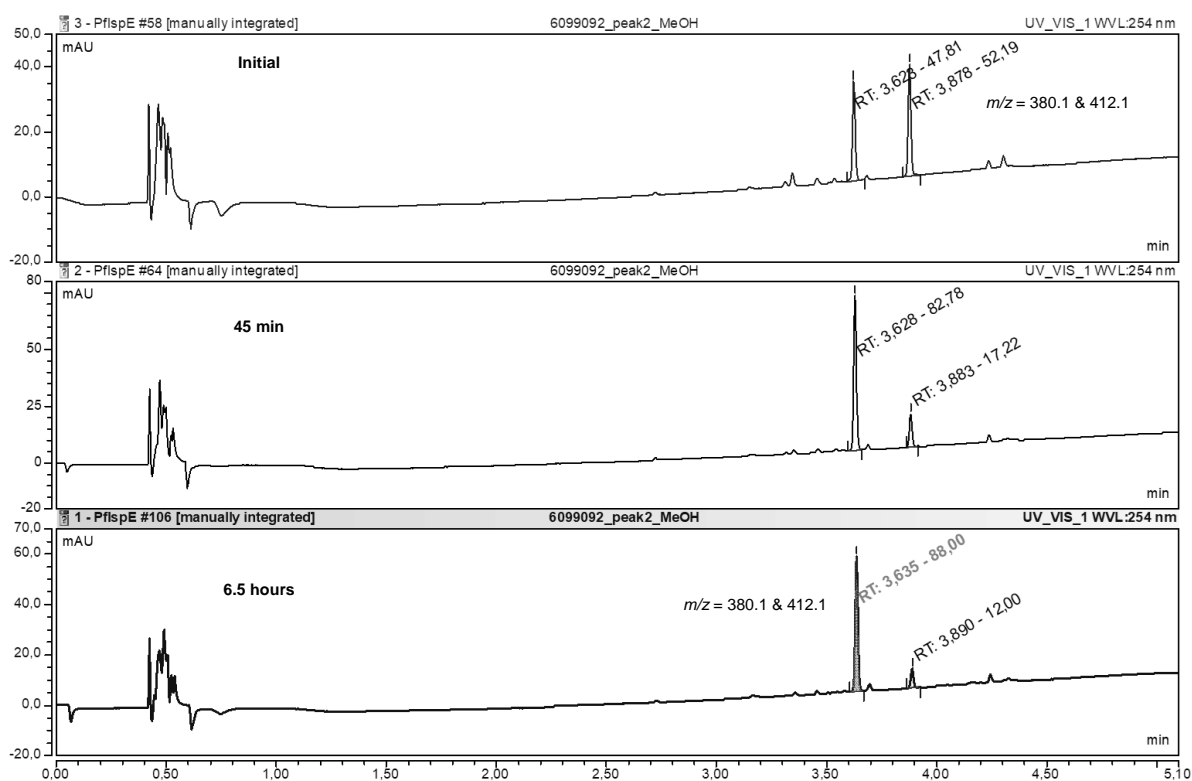


Figure S29.  $^1\text{H}$ ,  $^{13}\text{C}$ -HSQC-DEPT spectrum of DP1 mixture in acetone- $d_6$ .



**Figure S30.** UV-spectra of **DP1** mixture with the distinct colour.



**Figure S31.** Stability of **DP1** in MeOH and the observed shift in retention time.

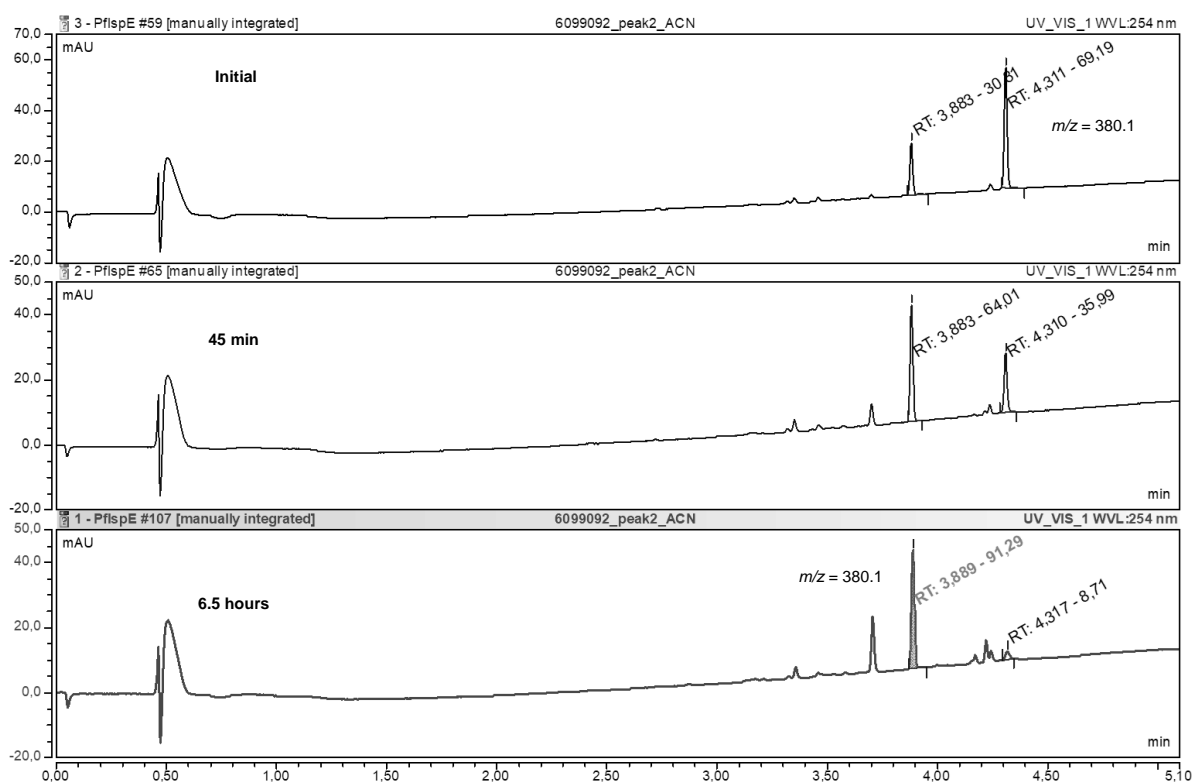


**Figure S32.** Stability of DP1 in ACN and the observed shift in retention time.

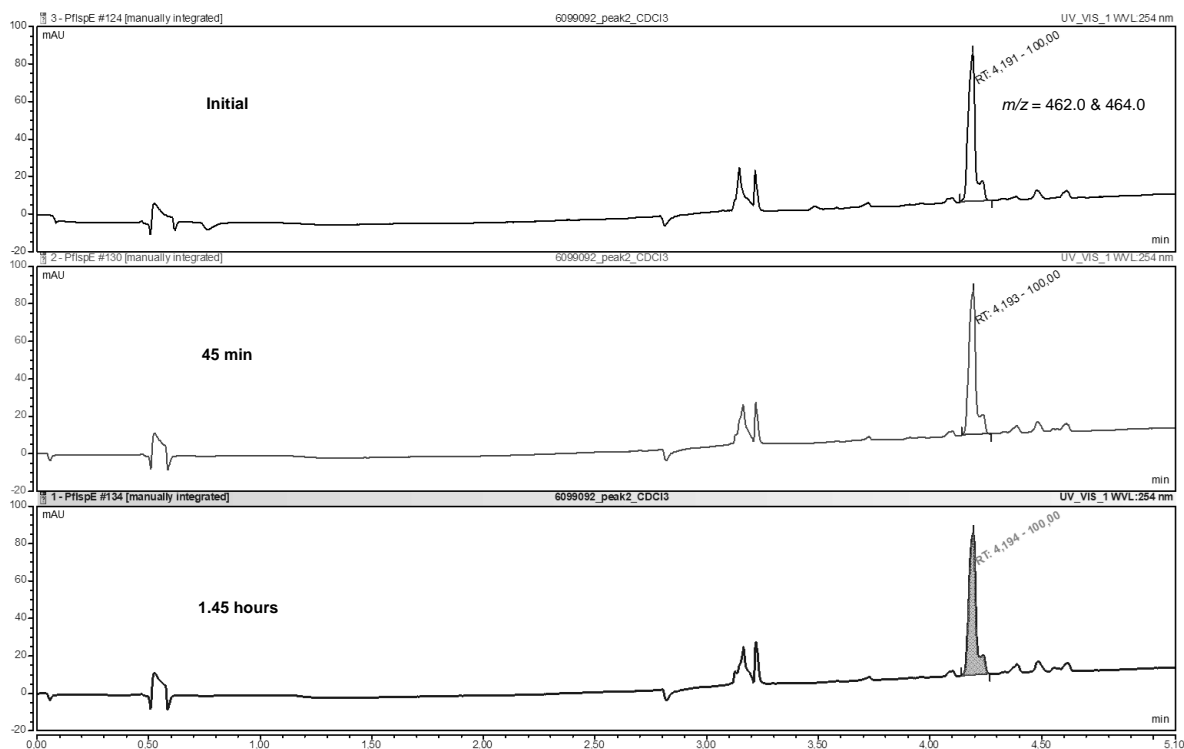


**Figure S33.** Stability of DP1 in CDCl<sub>3</sub>.



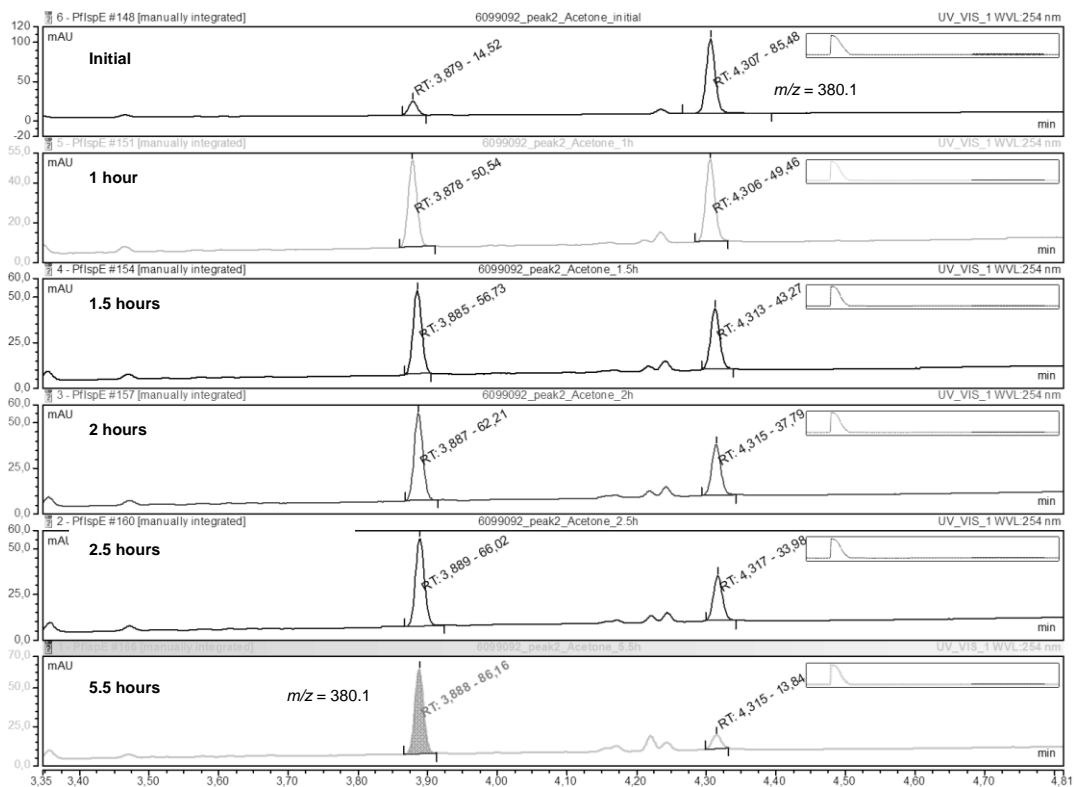


Figure S34. Stability of DP1 in acetone and the observed shift in retention time.

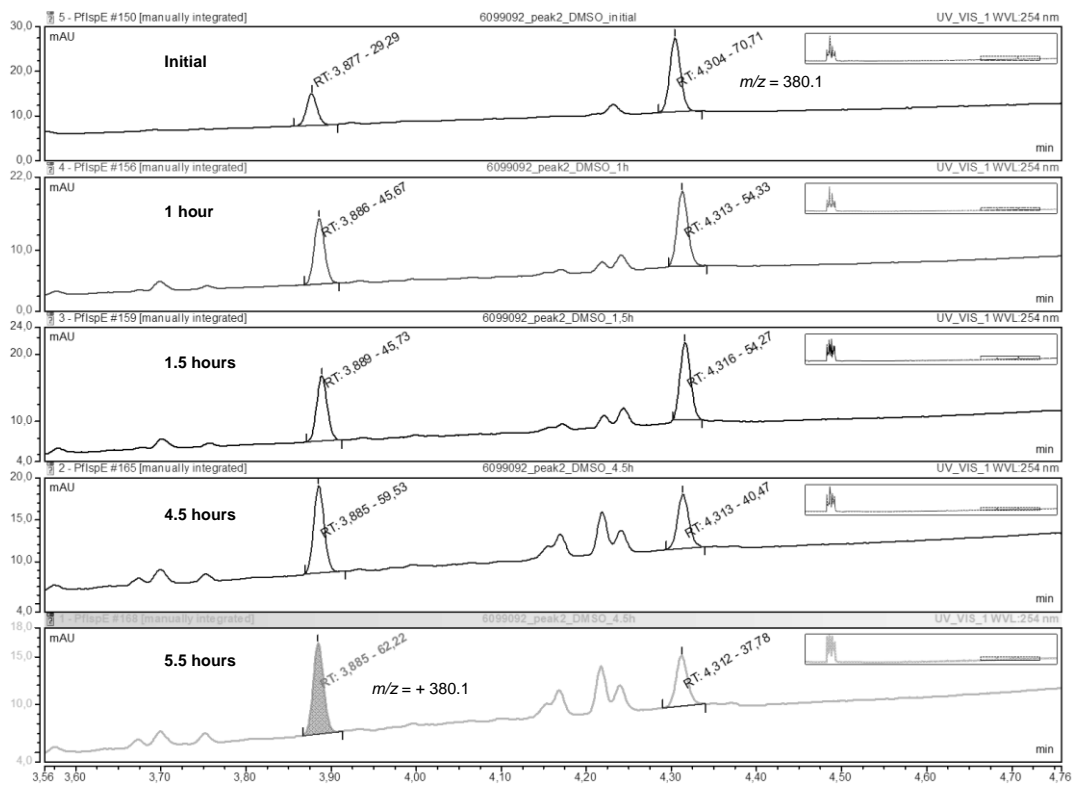
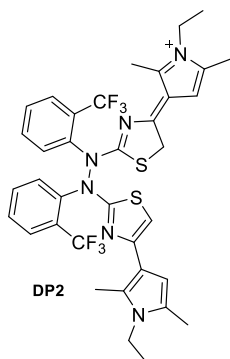


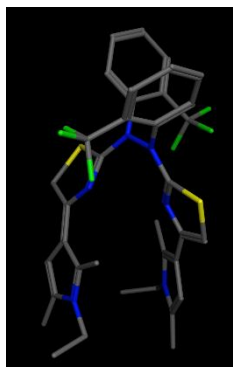
Figure S35. Stability of DP1 in DMSO and the observed shift in retention time.

## 2.8 Characterisation of Decomposition Product 2

**(Z)-1-Ethyl-3-(2-(2-(4-(1-ethyl-2,5-dimethyl-1H-pyrrol-3-yl)thiazol-2-yl)-1,2-bis(2-(trifluoromethyl)phenyl)hydrazineyl)thiazol-4(5H)-ylidene)-2,5-dimethyl-3H-pyrrol-1-ium**

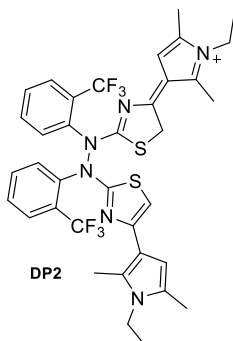


Exact Mass: 729.22633

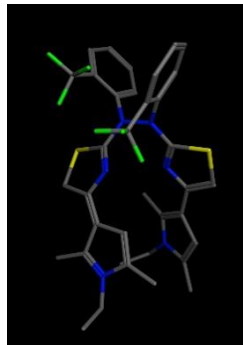


E = +144.7 kcal/mol of the lowest-energy conformation

**(E)-1-Ethyl-3-(2-(2-(4-(1-ethyl-2,5-dimethyl-1H-pyrrol-3-yl)thiazol-2-yl)-1,2-bis(2-(trifluoromethyl)phenyl)hydrazineyl)thiazol-4(5H)-ylidene)-2,5-dimethyl-3H-pyrrol-1-ium**



Exact Mass: 729.22633



E = +148.5 kcal/mol of the lowest-energy conformation

*(MOE 2018.01 was used to calculate the lowest energy conformation in MMFF94X force field)*

## DP2

Colour: beige brown powder

Isolated amount after SFC: 0.9 mg

HRMS (ESI+) calcd. for  $C_{36}H_{35}F_6N_6S_2^+$   $[M]^+$ : 729.22633, found: 729.22473; and  $[M+2H]^{2+}$ : 365.11681, found: 365.11642.

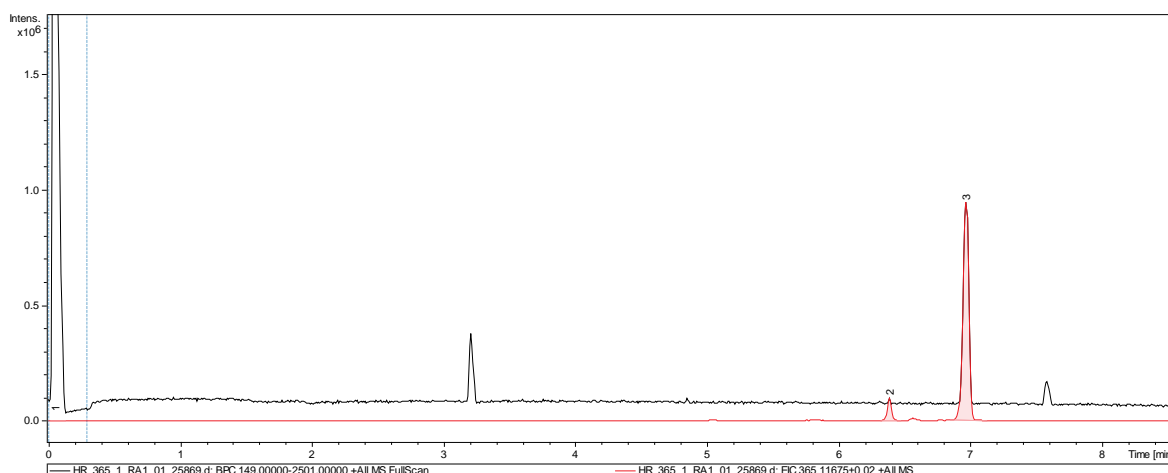
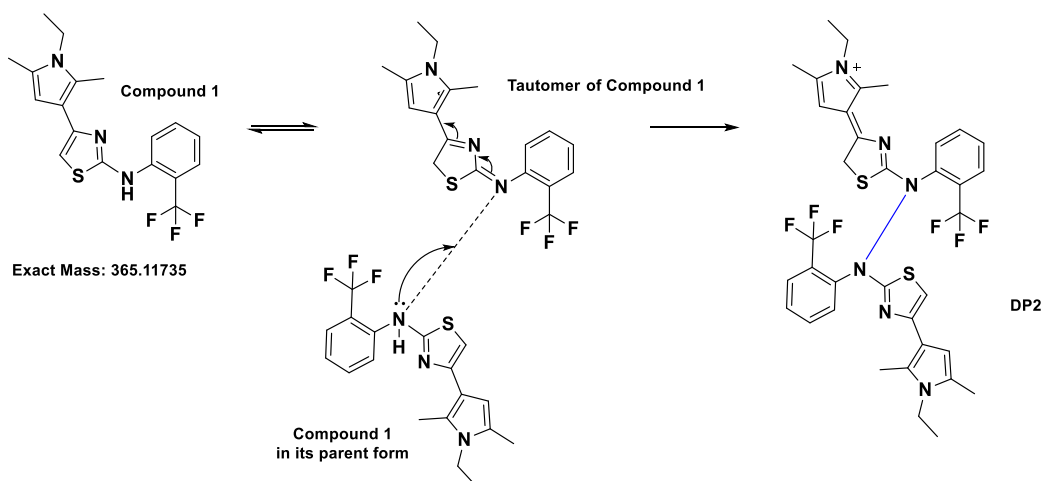
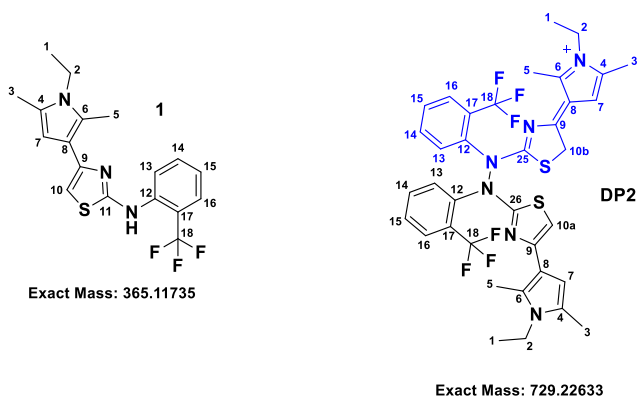


**Figure S36.** Chromatogram of the isolated **DP2**. Red = EIC at  $365.11 \pm 0.02$ , Black = BPC.



**Scheme S1.** Proposed reaction mechanism for the formation of **DP2**.

**Table S5.** Summary of the **DP2** NMR shifts.



#	Parent compound		Dimer	
	$^1\text{H}$ 366	$^{13}\text{C}$ 366	$^1\text{H}$ DP2 <sup>[a]</sup>	$^{13}\text{C}$ DP2
1 – CH <sub>3</sub>	1.22	16.5	1.23	16.1
	-	-	b - 1.01	b - 16.1
2 – CH <sub>2</sub>	3.88	39.4	3.87	38.9
	-	-	b - 3.68	b - 38.9
3 – CH <sub>3</sub>	2.23	12.5	2.22	11.9
	-	-	b - 2.15	b - 11.4
4 – C	x	128.7	x	127.4
	-	-	b - x	b - 129.1
5 – CH <sub>3</sub>	2.38	11.9	2.27	11.4
	-	-	b - 2.42	b - 11.4
6 – C	x	127.4	x	126.6
	-	-	b - x	b - 175.6
7 – CH	6.14	106.3	5.87	107.2
	-	-	b - 6.09	b - 106.5
8 – C	x	110.6	x	114.1
	-	-	b - x	b - 131.2
9 – C	x	141.5	x	149.5
	-	-	b - x	b - 121.1
10a – C	6.36	98.3	6.48	100.98
10b – CH <sub>2</sub>	-	-	b - 3.96	b - 25.4
11/26 – C	x	169.5	x	164.2
(11)25 – C	-	-	b - x	b - 143.8
12 – C	x	137.6	x	140.1
	-	-	b - x	b - 140.8
13 – CH	7.83	128.7	7.68	127.4
	-	-	b - 7.64	b - 127.3

<b>14 – CH</b>	7.51	128.9	7.22	123.9
	-	-	b - 7.17	b - 123.8
<b>15 – CH</b>	7.74	135.6	7.60	134.2
	-	-	b - 7.56	b - 134.1
<b>16 – CH</b>	7.91	127.4	8.20	123.9
	-	-	b - 8.09	b - 123.6
<b>17 – C</b>	x	125.9	x	x <sup>[b]</sup>
	-	-	b - n.d. <sup>[b]</sup>	b - 126.01
<b>18 – CF<sub>3</sub></b>	x	123.7	x	x
	-	-	b - n.d. <sup>[b]</sup>	b - 124.5 <sup>[b]</sup>

- Measured in acetonitrile-*d*<sub>3</sub>, n.d.: not determined [a]; Peaks “b” corresponding to the blue part of the dimer  
[b]: Overlapping with the other dimer part.

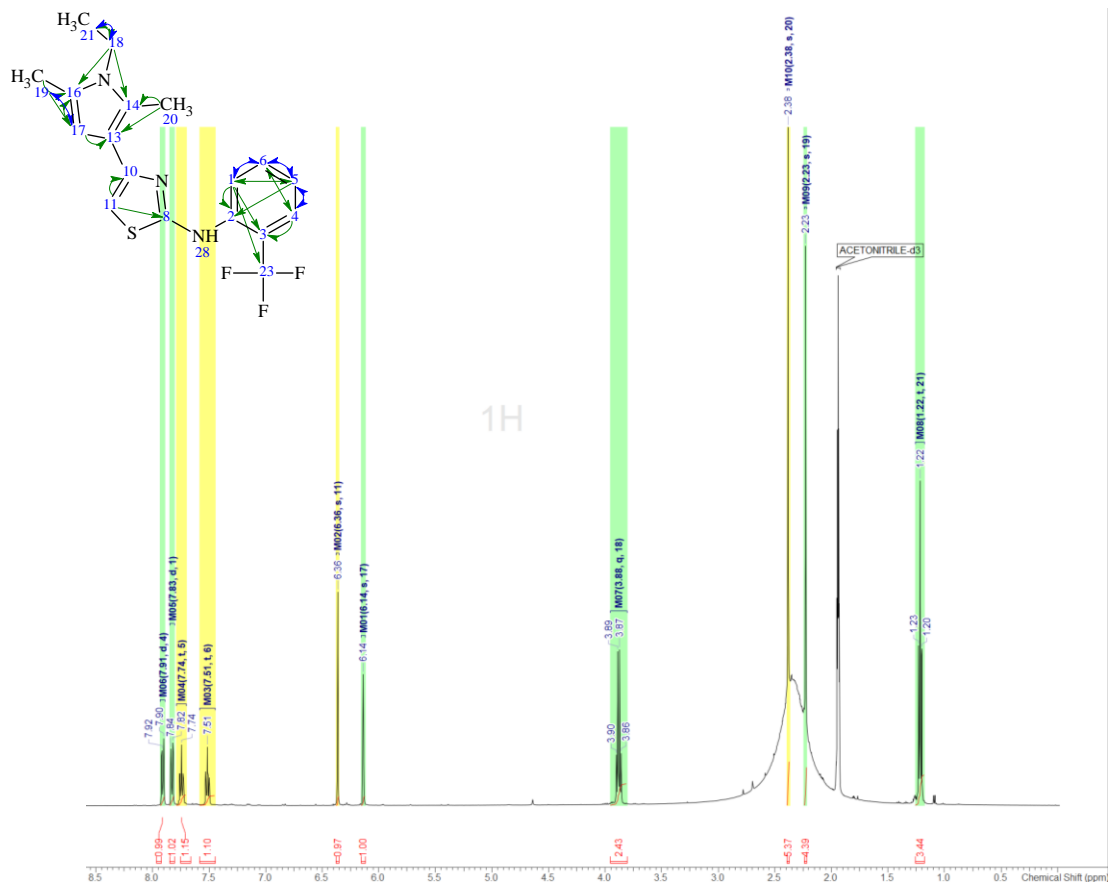


**Figure S37.**  $^1\text{H-NMR}$  spectrum of compound **1** in acetonitrile- $d_3$ .

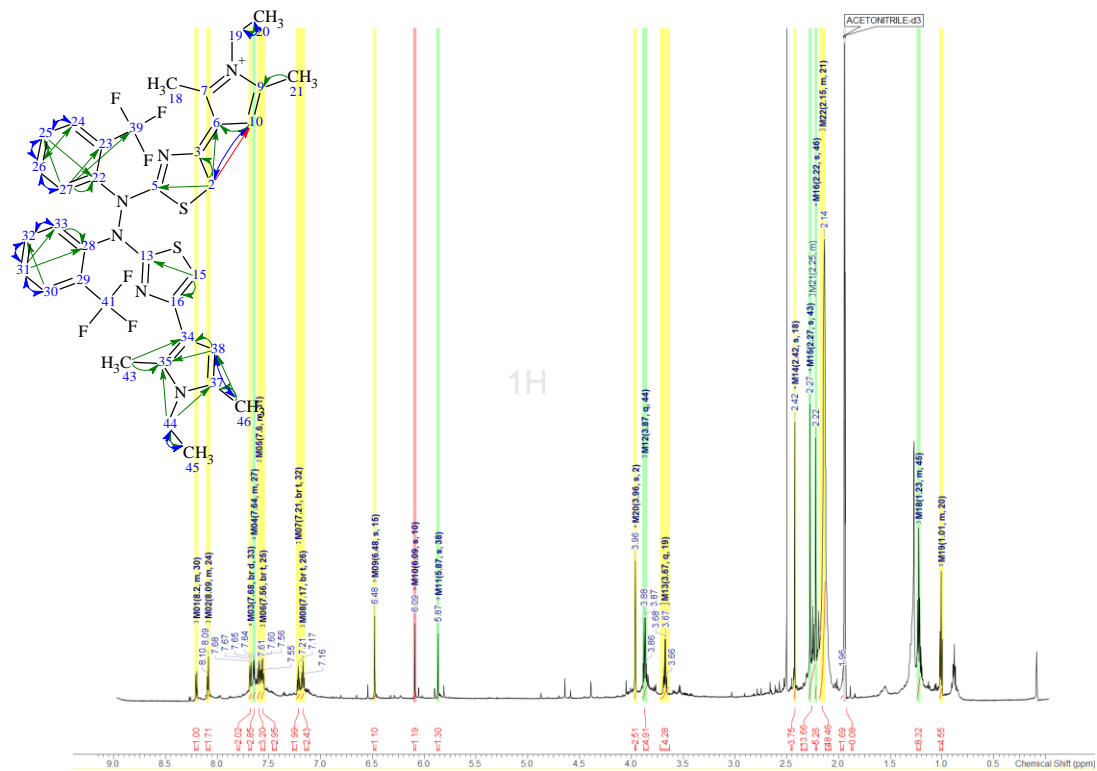


**Figure S38.**  $^1\text{H-NMR}$  spectrum of DP2 in acetonitrile- $d_3$ .

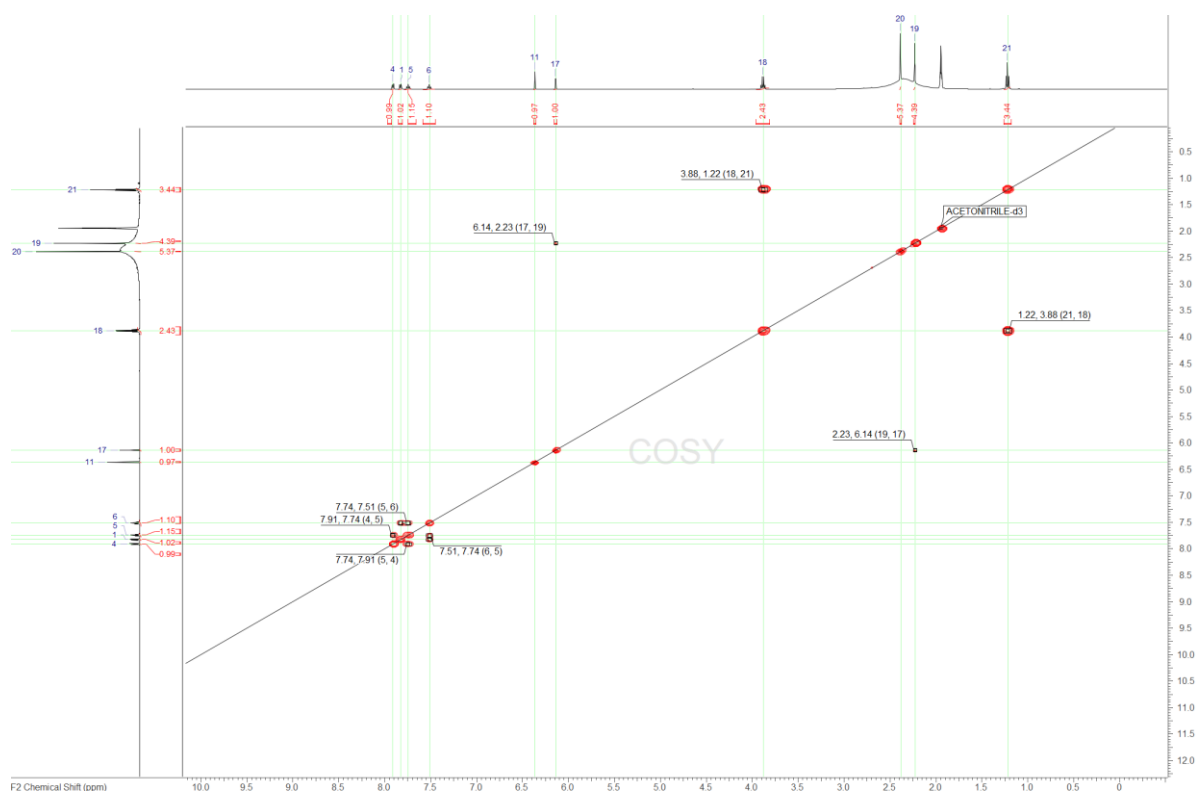


Figure S39.  $^1\text{H}$ ,  $^1\text{H}$ -COSY NMR spectrum of compound **1** in acetonitrile- $d_3$ .

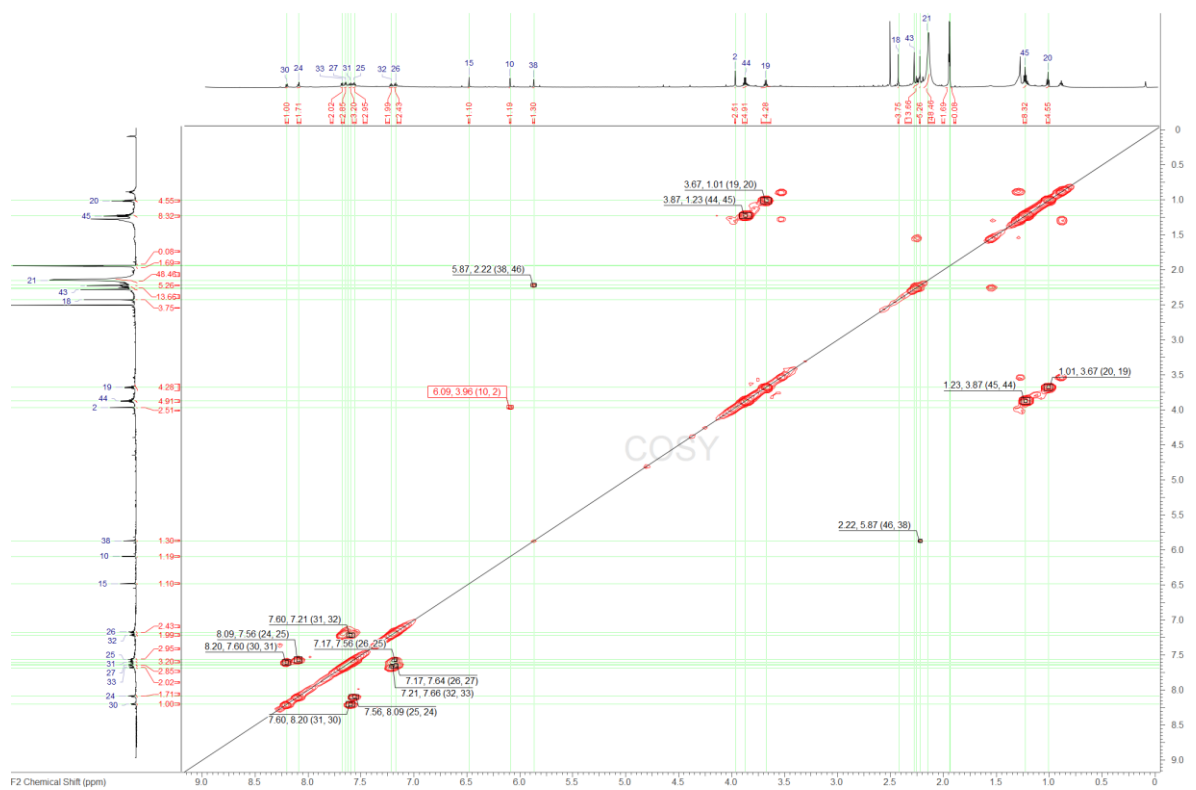


Figure S40.  $^1\text{H}$ ,  $^1\text{H}$ -COSY NMR spectrum of DP2 in acetonitrile- $d_3$ .

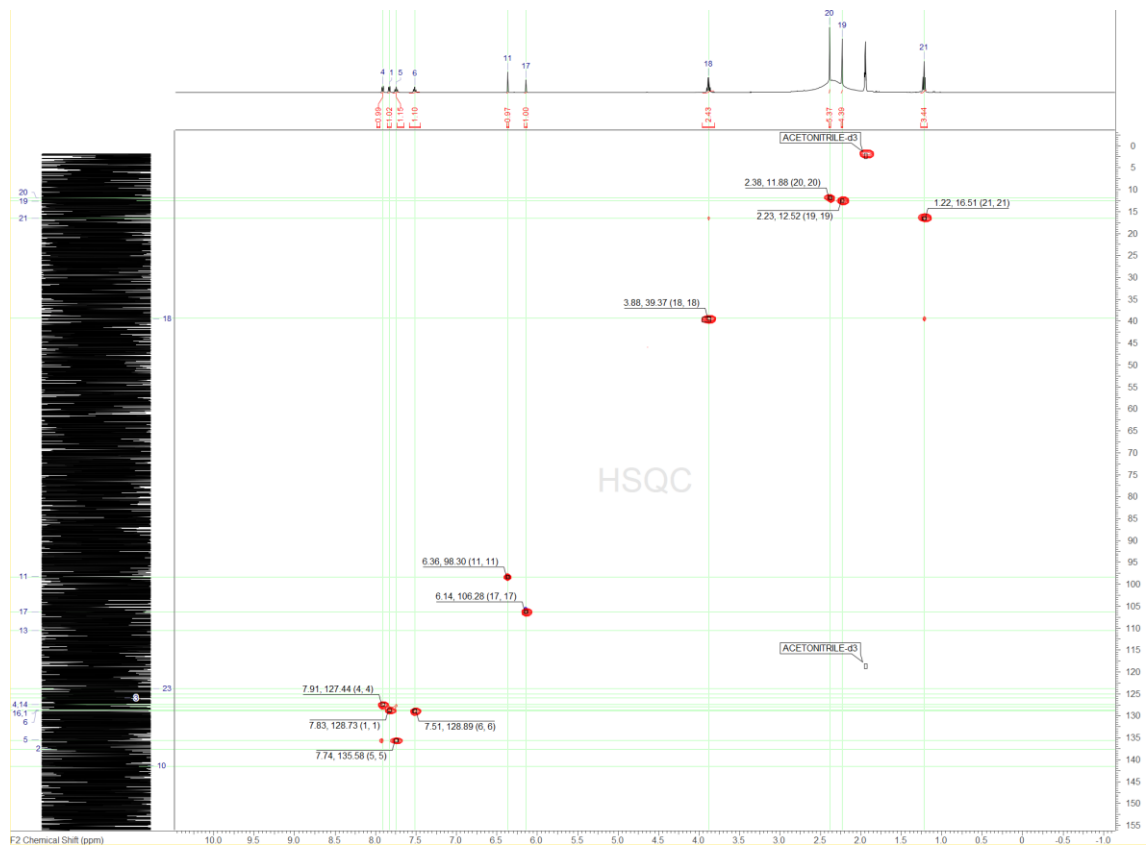


Figure S41.  $^1\text{H}$ ,  $^{13}\text{C}$ -HSQC spectrum of compound 1 in acetonitrile- $d_3$ .

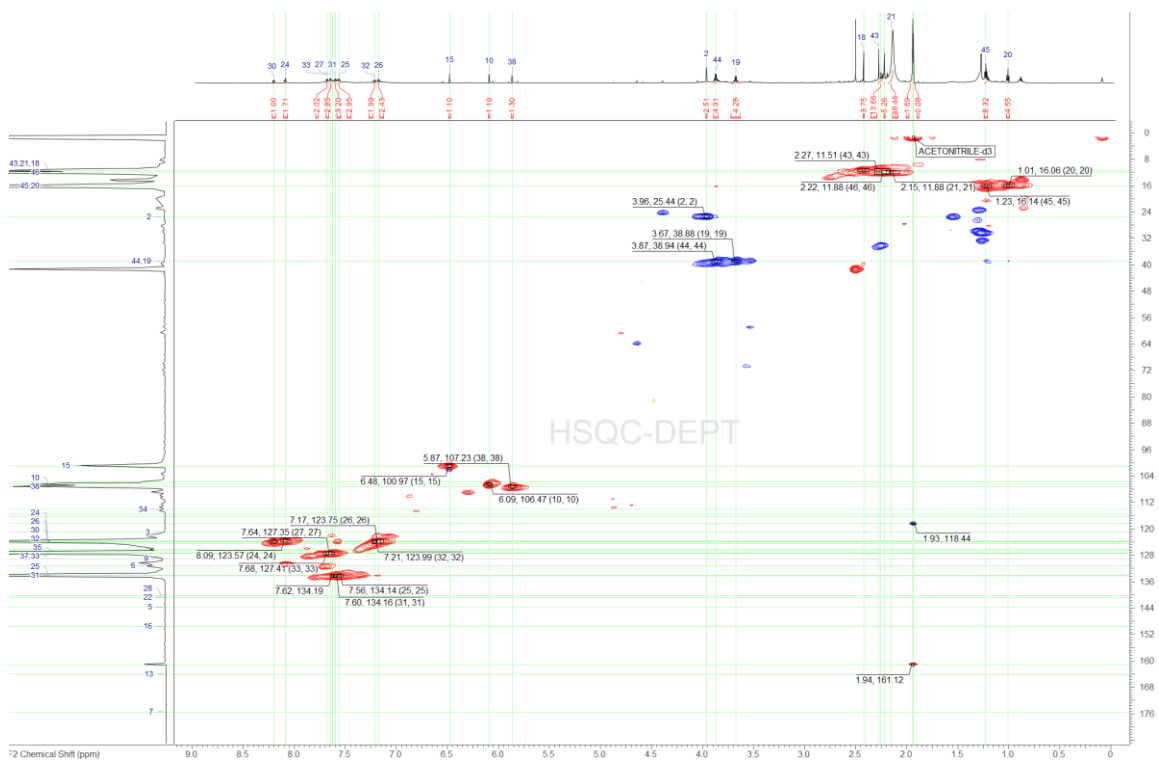


Figure S42.  $^1\text{H}$ ,  $^{13}\text{C}$ -HSQC-DEPT spectrum of DP2 in acetonitrile- $d_3$ .



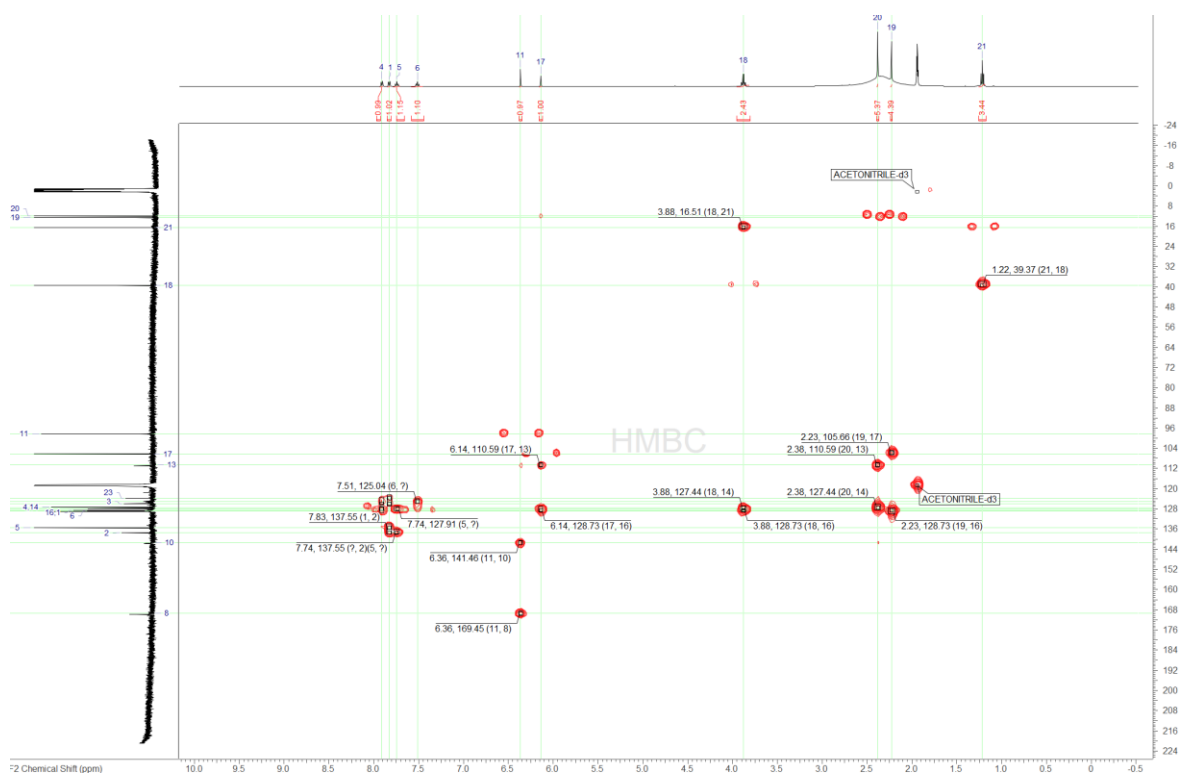


Figure S43.  $^1\text{H}$ ,  $^{13}\text{C}$ -HMBC spectrum of compound **1** in acetonitrile- $d_3$ .

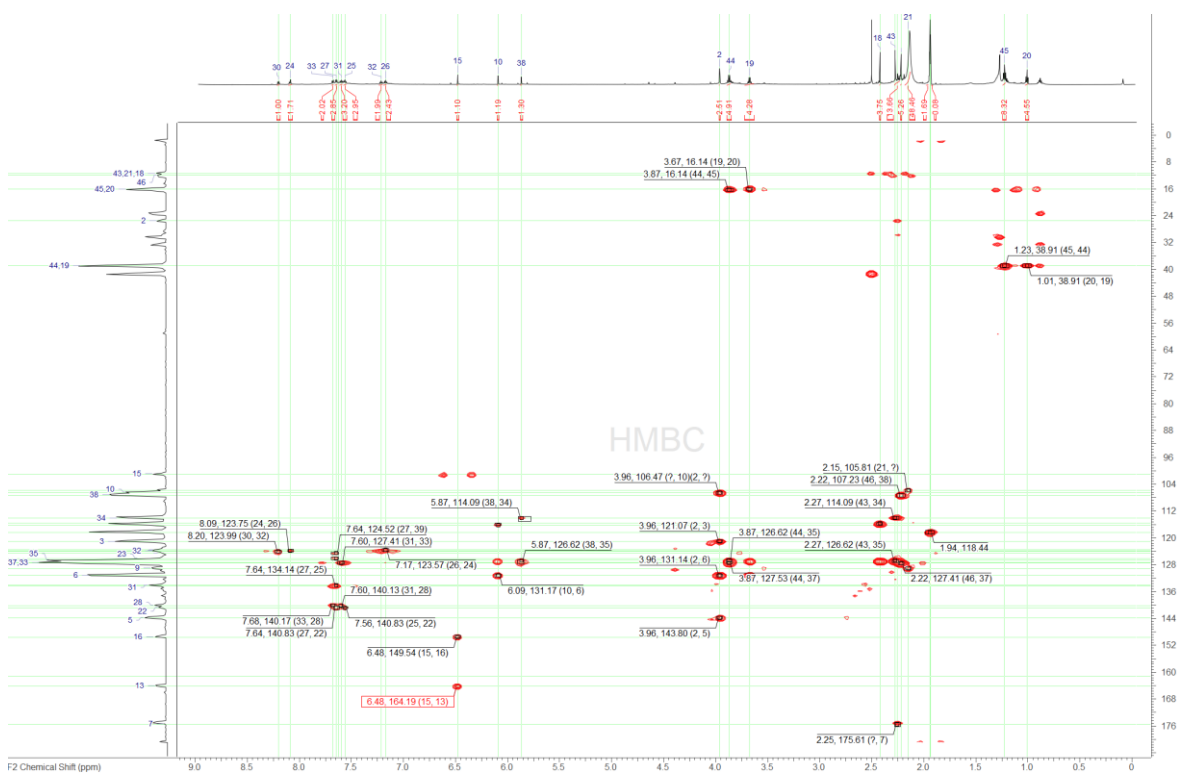


Figure S44.  $^1\text{H}$ ,  $^{13}\text{C}$ -HMBC spectrum of **DP2** in acetonitrile- $d_3$ .

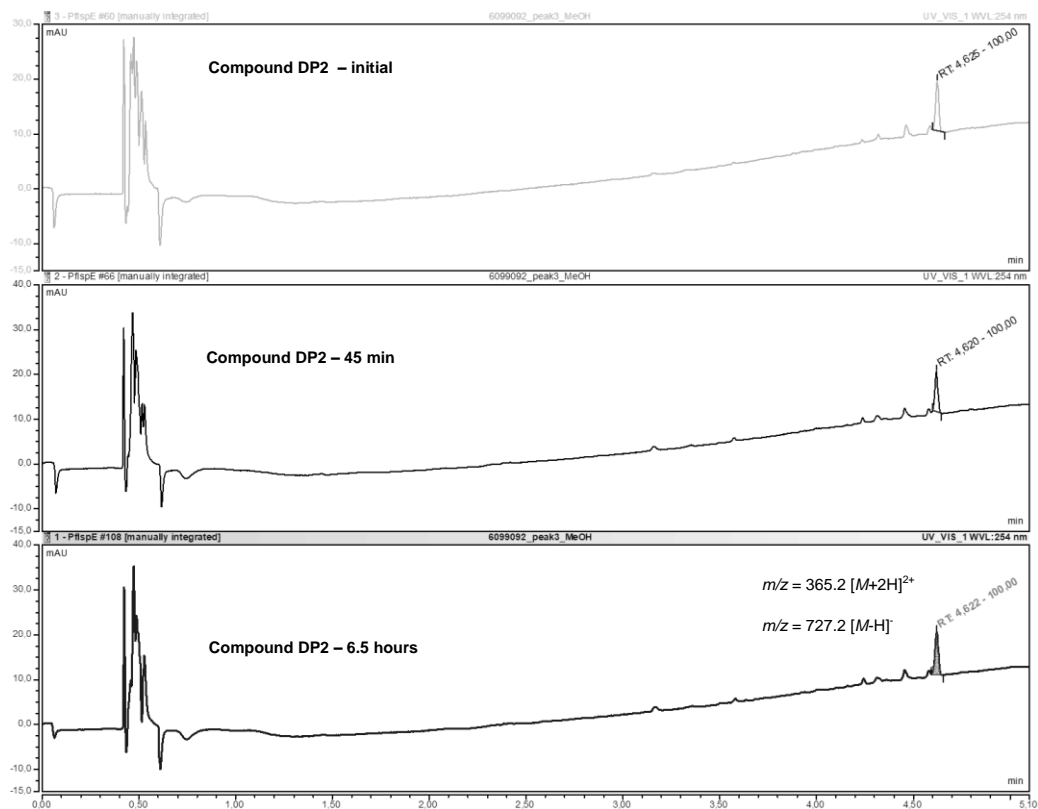


Figure S45. Stability of DP2 in MeOH and stability check over time.

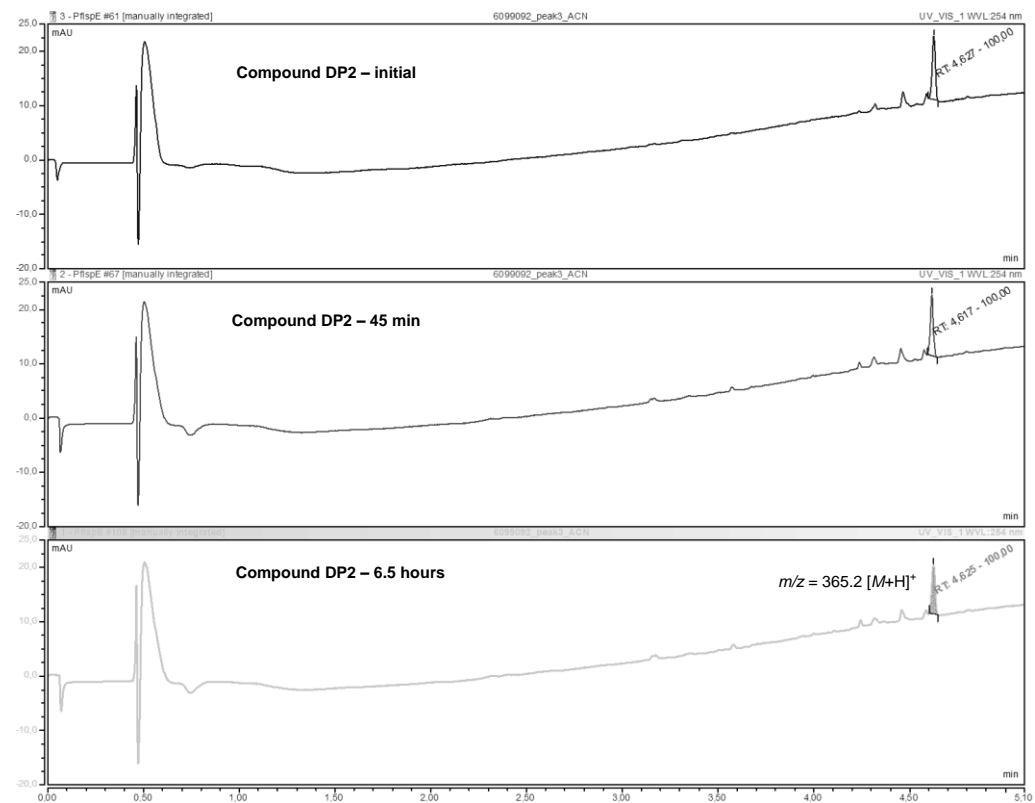


Figure S46. Stability of DP2 in ACN and stability check over time.

### 3. References

- [1] H. Lüttgen, F. Rohdich, S. Herz, J. Wungstintaweekul, S. Hecht, C. A. Schuhr, M. Fellermeier, S. Sagner, M. H. Zenk, A. Bacher, W. Eisenreich, *Proc. Natl. Acad. Sci. U. S. A.* **2000**, *97*, 1062–1067.
- [2] A. K. H. Hirsch, M. S. Alphey, S. Lauw, M. Seet, L. Barandun, W. Eisenreich, F. Rohdich, W. N. Hunter, A. Bacher, F. Diederich, *Org. Biomol. Chem.* **2008**, *6*, 2719–2730.
- [3] A. Dorn, R. Stoffel, H. Matile, A. Bubendorf, R. G. Ridley, *Nature* **1995**, *374*, 269–271.
- [4] W. Trager, J. B. Jensen, *Science (80-. )*. **1976**, *193*, 673–675.
- [5] W. Huber, J. C. Koella, *Acta Trop.* **1993**, *55*, 257–261.
- [6] J. Haupenthal, C. Baehr, S. Zeuzem, A. Piiper, *Int. J. Cancer* **2007**, *121*, 206–210.

### 4. Appendix

#### Appendix I – Calibration of the HRMS Data

**Table S6.** Calibration curve of the compound **1** with an internal standard at different incubation temperatures.

Component Name	Curve Index	Weighting Index	Origin Index	Equation	Specified				
Compound 1	Linear	1/X <sup>2</sup>	Ignore	Y = -0.375618+9.90624*X R <sup>2</sup> = 0.9890					
Filename	Area	ISTD Area	Area Ratio	Amount calculated present (µM)	Amount present (µM)	%Diff	%RSD-AMT	Retention Time	Notes
Cal1	1015020937	108024178	93.965	10.000	9.523	-5%	0.0%	5.74	
Cal2	5529194612	108615825	50.906	5.000	5.177	4%	0.0%	5.73	
Cal3	2950165560	111027345	26.572	2.500	2.720	9%	0.0%	5.73	
Cal4	1490851206	113101576	13.182	1.250	1.369	9%	0.0%	5.74	
Cal5	708935183	116652524	6.060	0.625	0.650	4%	0.0%	5.74	
Cal6	309216919	118907216	2.599	0.313	0.300	-4%	0.0%	5.73	
Cal7	124517300	12453478	0.942	0.156	0.133	-15%	0.0%	5.74	
Cal8	39000722	126381297	0.309	0.078	0.089	-11%	0.0%	5.73	
Cal9	5921925	127751015	0.046	0.039	0.043	9%	0.0%	5.73	
Cal10	2121888	131737338	0.016	0.020	0.040	102%	NA	5.73	Excluded
Percentage of 7.653									
Initial Compound 1	8415425965	111503864	75.472	NA	7.657	100%	NA	5.72	
Initial Compound 1	8550587377	113394813	75.405	NA	7.650	100%	NA	5.73	
					Average=	7.653			
Average of Two Samples									
1week RT1	3975188172	147432193	26.963	NA	2.780	36%	36%	5.74	
1week RT2	3841533630	144556254	26.575	NA	2.721	36%		5.73	
1week +4 °C1	10527675861	144236464	72.989	NA	7.406	97%	96%	5.74	
1week +4 °C2	10246397426	144141113	71.986	NA	7.214	94%		5.74	
1week -20 °C1	10460128182	144477062	72.400	NA	7.346	96%	96%	5.73	
1week -20 °C2	10664148926	147035848	72.528	NA	7.359	96%		5.73	
1week -20 °C solid1	11336006749	144593718	78.399	NA	7.952	104%	101%	5.73	
1week -20 °C solid2	10450815845	140225592	74.529	NA	7.561	99%		5.73	
1week +4 °C solid1	10077684135	140341550	71.808	NA	7.287	95%	98%	5.73	
1week +4 °C solid2	10705408284	141361442	75.731	NA	7.683	100%		5.73	
1week RT solid1	10929237063	144443787	75.684	NA	7.676	100%	99%	5.73	
1week RT solid2	10341923364	141166150	73.261	NA	7.433	97%		5.72	
Lower IS amount, dilution factor x100 used									
1month RT1	921036	1901671	0.484	NA	0.087	1%	1%	5.82	
1month RT2	1446146	1689226	0.856	NA	0.124	2%		5.71	
1month +4 °C1	7005299232	1745394	4013.593	NA	4.052	53%	48%	5.74	
1month +4 °C2	6110709717	1854816	3294.509	NA	3.326	43%		5.71	
1month -20 °C1	11311078789	1610313	7024.151	NA	7.091	93%	91%	5.72	
1month -20 °C2	11148102857	1643267	6784.027	NA	6.849	89%		5.72	
Column conditions changed, RT shifted									
2months RT1	1918627	1531601	1.253	NA	0.164	0%	0%	5.57	
2months RT2	2022446	1576658	1.283	NA	0.167	0%		5.56	
2months +4C1	30239658	1721642	17.564	NA	1.811	24%	21%	5.80	
2months +4C2	21706730	1643370	13.209	NA	1.371	18%		5.78	
2months -20C1	12136948119	1900005	6192.305	NA	6.251	82%	82%	5.79	
2months -20C2	10261734758	1657331	6191.721	NA	6.251	82%		5.80	
Original Decomposed Sample	28364982	1591587	17.822	NA	1.837	24%	28%	5.80	
Original Decomposed Sample	37865473	1537328	24.631	NA	2.524	33%		5.80	

IS = Diphenhydramine (500 nM)  
Retention Time 4.1 min

## Appendix II – Extra NMR Spectra of the Other Isolated Fractions

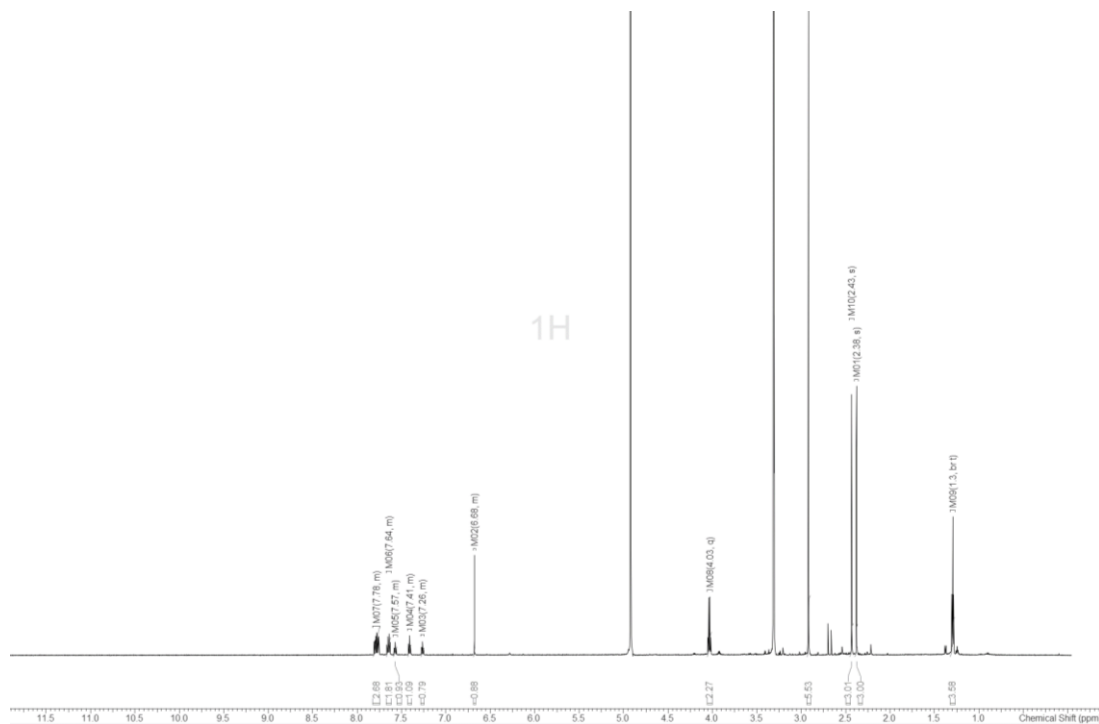


Figure S47. Fraction 4 of the first prep. HPLC separation in methanol- $d_4$ .

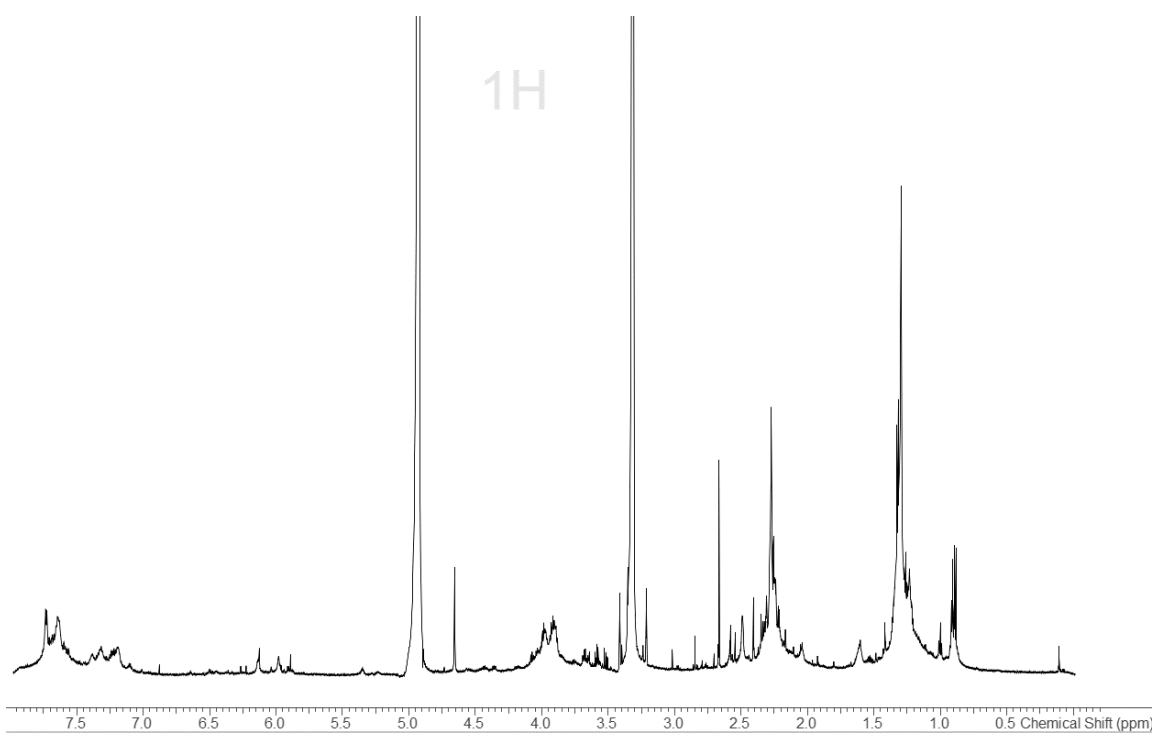
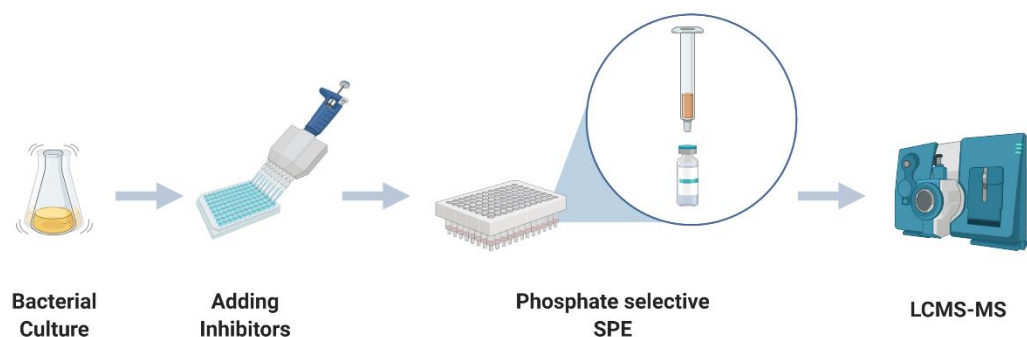


Figure S48. Fraction 31 of the first prep. HPLC separation in methanol- $d_4$ .

## 6. Appendix

### 6.1 Appendix I - MS-MEP

As discussed in the Introduction Section 1.2, one of the challenges with the previous *E. coli* inhibitors has been the lack of antibacterial activity. In order to speed up the process, we started the implementation of a metabolomics approach in order to measure simultaneously activity on target and in the cellular assay. A recent example of such targeted metabolomics in Gram-negative bacteria was published for CoaD inhibitors by C. M. Rath *et al.*<sup>137</sup> With respect to IspE, the idea was to quantify the amount of the natural substrate CDP-ME with MS. So-called isoprenoid rescue assays have been used for target validation of inhibitors of *Plasmodium falciparum* and *Escherichia coli*, namely for fosfidomycin.<sup>138–140</sup> Additionally, (GC)-MS-based methods to measure the natural substrates of the MEP pathway have been reported for *E. coli* and other bacteria, as well as plants.<sup>141–144</sup> To the author's knowledge, none of them had been particularly implemented to serve the needs of medicinal chemistry workflows to measure target engagement or cellular inhibition simultaneously. Therefore, the previous methods were customised to fit the possibilities of the existing laboratory. Additionally, to selectively separate the phosphate containing natural substrates, solid-phase extraction (SPE) was used for cell cultures, as sketched in Figure 6.1:1.



**Figure 6.1:1** - The simplified flow for establishing the metabolomics assay for the MEP pathway with the solid phase extraction (SPE) integration in an automated fashion. Figure was created with BioRender.com.

Suitable column and eluent conditions were found to ensure a sufficient difference in retention time between MEP and CDP-ME in order to quantify both within one MS run. A first attempt with SPE was made, using Strata® Strata-X-AW minicolumns from Phenomenex. Using the known inhibitors of several different MEP enzymes with antibacterial activity as control compounds, one may reach a more thorough understanding when the concentration of the natural substrate is increased and what is the resulting effect. For example quantifying the CDP-ME concentration, one would expect to see the decreased concentration for IspD inhibitors or increased concentration

for IspE inhibitors. As the natural substrates are  $^{13}\text{C}$ -labelled, a complimentary approach *via* quantification of stable isotope labelled standards could be used for the calibration.<sup>145</sup> With further optimisation, this metabolomics approach accompanied with phosphate-selective SPE may result in a high-throughput assay to measure the target engagement and cellular inhibition from the same well in one sample, in particular being of benefit for the more pathogenic bacteria.

### Brief Method Description

[1,3,4- $^{13}\text{C}_3$ ]1-Deoxy-D-xylulose-5-phosphate (MEP) and [1,3,4- $^{13}\text{C}_3$ ]4-diphosphocytidyl-2C-methyl-D-erythritol (CDP-ME) were purified, as previously described.<sup>44</sup> They were kindly provided by the Fischer Lab from the MEP consortium. [1,3,4- $^{13}\text{C}_3$ ]-MEP and [1,3,4- $^{13}\text{C}_3$ ]-CDP-ME were dissolved in MeOH from 97 mM and 84 mM water-based stock solutions, respectively. The MS analyses were done using a negative ionisation in a TF UltiMate 3000 binary RSLC UHPLC (Thermo Fisher, Dreieich, Germany) equipped with a degasser, a binary pump, an autosampler, and a thermostated column compartment and a MWD, coupled to a TF TSQ Quantum Access Max mass spectrometer with heated electrospray ionization source (HESI-II). The method was created with the following modifications: (1) Phenyl-Hexyl 2.7  $\mu\text{m}$ , 100x3 mm (Macherey-Nagel, Düren, Germany), (2) flow rate of 0.5 mL/min, (3) eluent gradient with A = ACN and B = H<sub>2</sub>O (98% solvent B from 0 to 2.5 min, 90% B for 2.8 min, 2% B for 5.0 min, 98% B for 5.1 min and column equilibration for 1.4 min), (4) column compartment at 30 °C, (5) UV detection at 290, 270, 254 and 212 nm and (6) autosamples injection volume of 5  $\mu\text{L}$  of [1,3,4- $^{13}\text{C}_3$ ]-MEP at 10  $\mu\text{M}$  and [1,3,4- $^{13}\text{C}_3$ ]-CDP-ME at 8  $\mu\text{M}$ . A test run with SPE Strata® Strata-X-AW (weak anion-exchange & reversed phase) was done for *E. coli* DH5 $\alpha$  – *pca108-2  $\Delta$ pqsR*. The cultivate was centrifuged (4 °C, 2.5 min, 12,500 rpm) and the supernatant was removed. Remaining pellets were rinsed with ammonium acetate (25 mM), resuspended with an ultrasound stick (30 sec, 10% power) and centrifuged (4 °C, 2.5 min, 12,500 rpm). The SPE was done with the suggested protocol from Phenomenex.<sup>146</sup>

**Table 6.1:1** - Summary of the [1,3,4- $^{13}\text{C}_3$ ]-MEP and [1,3,4- $^{13}\text{C}_3$ ]-CDP-ME.

Compound	Exact Mass for $^{12}\text{C}$	[M – H] <sup>-</sup> / [M – 2H] <sup>-</sup>	Product Mass	Retention Time (min)
[1,3,4- $^{13}\text{C}_3$ ]-MEP	214.02534	217.998/ 79.280	79.280	1.74
[1,3,4- $^{13}\text{C}_3$ ]-CDP-ME	519.06662	523.037/ 321.940	321.940	4.24

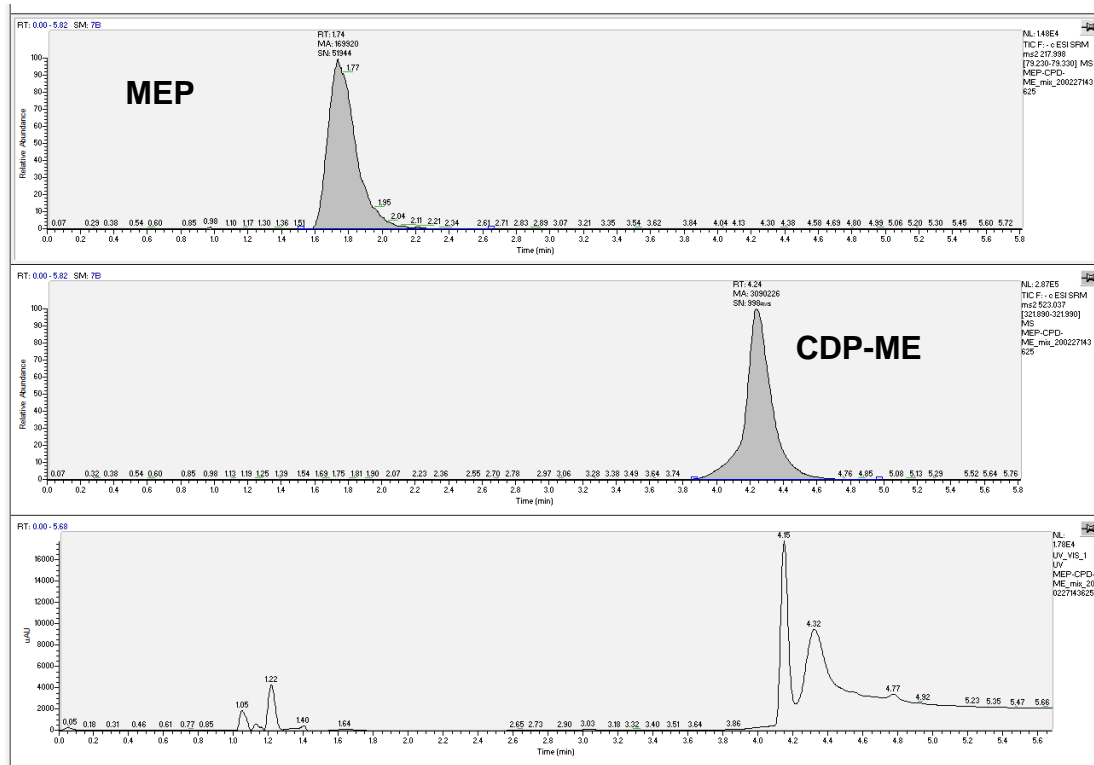


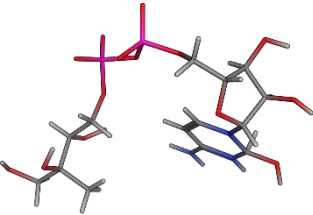
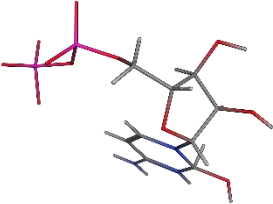
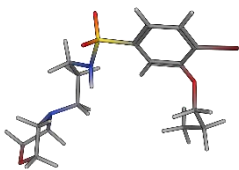
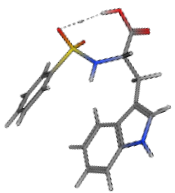
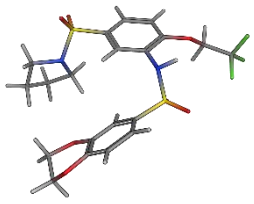
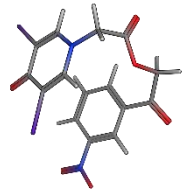
**Figure 6.1:2** - Chromatograms of [1,3,4-<sup>13</sup>C<sub>3</sub>]-MEP and [1,3,4-<sup>13</sup>C<sub>3</sub>]-CDP-ME measured from their mixture.

*With thanks to Dr. Teresa Röhrig and Dr. Stefan Boettcher for the helpful advice.*

## 6.2. Appendix II - Field-Based Screening with CDP-ME

As an alternative approach to the SBDD as described in Section 3.1, we initiated a field-based virtual screening, as a subtype of ligand-based virtual screening, with Pharmacelera software.<sup>147</sup> This strategy focuses on the occupied hydrophobic properties of a reference ligand. The natural substrate CDP-ME was selected as the reference ligand in its 3D-conformation as in the co-crystal structure (PDB 1OJ4).<sup>120</sup> A comparison screening was also done for the fragmented CDP-ME, as in Table 6.2:1. At the time of writing this thesis, a SPECS library, as used in Chapter A, and a Enamine library with the filters (MW >500 Da) were screened. The screening was run with the standardised virtual screening settings from Pharmacelera within the KNIME platform.<sup>126</sup> Further biological evaluation of the virtual hits is ongoing.

**Table 6.2:1** - The best hits from the corresponding library. Similarity score given in reference to CDP-ME or the fragmented CDP-ME. Figures of the molecules were created in MOE 2018.01.

	<b>CDP-ME</b> 	<b>Fragmented CDP-ME</b> 
<b>SPECS</b>	 ID = AP-263/43411934 Similarity = 0.54	 ID = AF-399/40881368 Similarity = 0.56
<b>Enamine</b>	 ID = Z45739335 Similarity = 0.53	 ID = Z56919617 Similarity = 0.53

*With thanks to Pharmacelera for our collaboration.*



### 6.3 Appendix III - COVID-19 Virtual Screenings

*Due to the ongoing project, structural and experimental details are not yet reported in this thesis.*

During this PhD thesis, the world was hit hard by the current coronavirus (COVID-19) pandemic. At the time of writing this thesis on the 15<sup>th</sup> January 2021, more than 93 million COVID-19 cases and over 2 million deaths were reported all over the world.<sup>148</sup> We did our part to overcome this crisis and initiated multiple virtual screenings to identify novel inhibitors to treat COVID-19. For our primary targets of the severe acute respiratory disease corona-virus 2 (SARS-CoV-2), we selected the well-established RNA-dependent RNA polymerase (RdRp), or in other words the nonstructural protein (nsp12), as well as the underexplored nsp10/nsp14 complex. The nsp14 complex has two functions; proofread exoribonuclease and methyl transferase of guanine-N7. This is activated by complexation of nsp10. Overall, they all account for the cascade of events that is essential for viral replication and transcription, as summarised in Figure 6.3:1.<sup>149</sup> In an ideal case, a potential combination of inhibitors targeting RdRp and the protein–protein interaction (PPI) could lead to synergetic effects. Substantial efforts were made to screen available in-house and commercial libraries. In the following subchapters, the workflows related to each virtual screening are described. The published biological procedures are referenced or otherwise still under work.

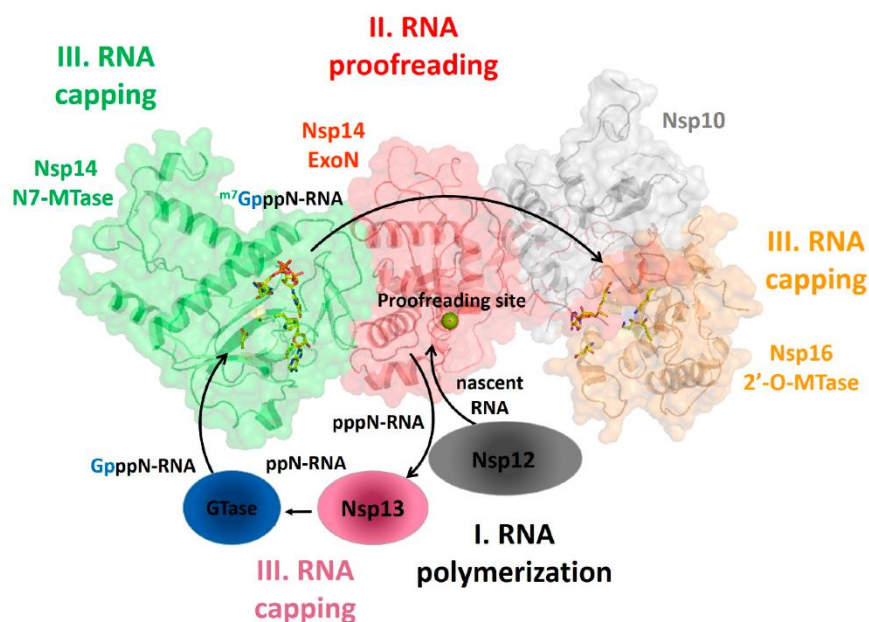


**Figure 6.3:1** - The summary of the cascade of the non-structural proteins (nsp) in the viral RNA formation.<sup>149</sup> Taken from Ref.<sup>149</sup> without extra permission under the copyright of open access Creative Commons Attribution License.

## nsp12

At the time of the screening, a cryo-electron microscopy structure of the SARS-CoV-2 RdRP was published (2.95 Å – PDB 7BTF).<sup>150</sup> The crystal structure was energy minimised by HIPS-WIBI. We defined two binding sites, one focusing on the so-called “Active Site”, where remdesivir binds, and an allosteric pocket in close proximity, red and cyano pockets, respectively in Figure 6.3:2. Overall, about 120,000 compounds were screened for both pockets using LeadIT 2.3.2 and BioSolveIT 9.2 on the KNIME platform.<sup>82,83,125,126</sup> For each compound, ten poses were calculated and only selected further if the compound had at least two poses with green or orange torsional angles and HYDE binding affinity of less than 1 mM. StarDrop 6.6.4 was used for the final visual inspection of the compounds. The biological evaluation of the hits was done in collaboration with the Götte Group, using their published gel-based assay.<sup>151</sup> At the time of writing this thesis, the hit validation was still ongoing.

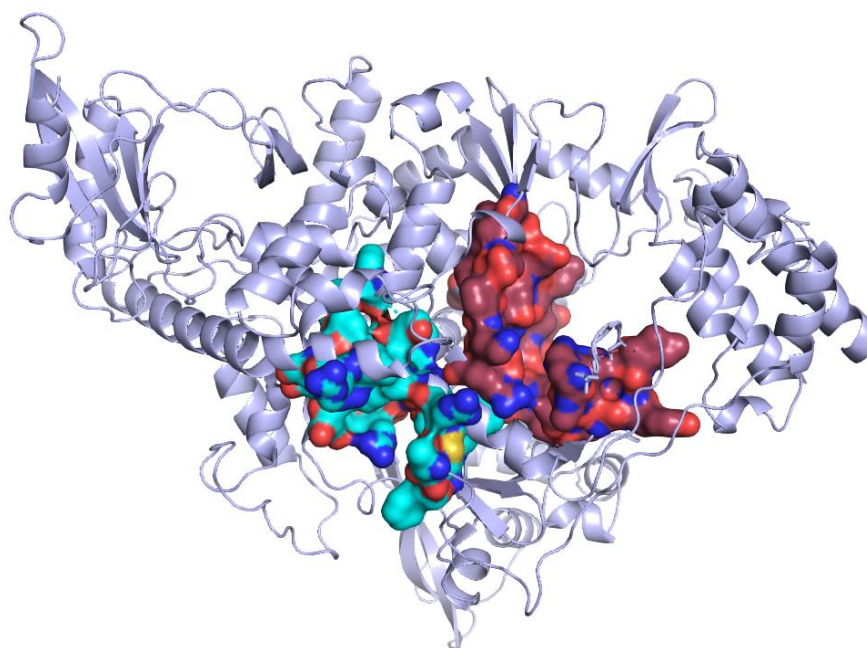


**Figure 6.3:2** - The selected binding pockets highlighted for nsp12 (PDB 7BTF). The “Active remdesivir Site” pocket in red includes residues 545–548, 553–558, 616–624, 680–693, and 757–762 (PDB 7BTF). The cyano “allosteric” pocket includes the residues 172, 173, 176, 243, 246, 247, 249, 315, 318, 318, 319, 350, 394–396, 456, 457, 459–462, 627–629, 675–677, 788 and 791. The figure was created with PyMOL Molecular Graphics System 4.6.0, courtesy of Spyridon Bousis.

**Table 6.3:1** - Summary of the hits in the testing with nsp12.

<b>Library</b>	<b>Binding site</b>	<b>Number of compounds through the first filters</b>	<b>Number of compounds selected for testing</b>	<b>Hit validation ongoing</b>
<b>DDOP Hartmann</b> ~2,500 compounds	Active	80	20	<b>HIPS1771, HIPS708</b>
	Allosteric	132 (*HYDE <50 $\mu$ M)	52	<b>HIPS1906, HIPS1493</b>
<b>DDOP Hirsch</b> ~700 compounds	Active	6	4	none
	Allosteric	64 (*HYDE <50 $\mu$ M)	35	<b>HIPS5327</b>
<b>MINS Myxo</b> ~500 compounds	Active	6	3	none
	Allosteric	35	9	none
<b>Enamine Antibacterial</b> ~9,000 compounds	Active	16	15	<b>HIPS5720</b>
	Allosteric	211	not included	none
<b>Enamine Antiviral</b> ~4,000 compounds	Active	21	21	none
	Allosteric	446	not included	none
<b>SPECS</b> ~106,000 compounds	Active	791	13	<b>HIPS5853</b>
	Allosteric	197 (*HYDE <10 $\mu$ M)	10	none

## nsp10

No previous inhibitors for nsp10 have been reported and therefore, it was selected as a novel target with the aim to interrupt the PPI with nsp14 complex. First test runs were done with an older crystal structure of SARS-CoV-1 (3.2 Å - PDB 5C8T) applying the filters and workflows from the nsp12 section.<sup>152</sup> Later on, we moved to an automated workflow in KNIME using only SeeSAR 10.1 with a new crystal structure of SARS-CoV-2 (1.6 Å - PDB 6ZPE) with higher resolution.<sup>82,125,126,153</sup> For each compound, ten poses were generated and docked and only selected further if the compound had at least two poses with green or orange torsional angles and a HYDE binding affinity of less than 1 mM. StarDrop 6.6.4 was used for the final visual inspection of the compounds. At the time of writing, in-house SPR, functional (DDOP) and MS-based (MINS) assays were under development and their details are not reported here.

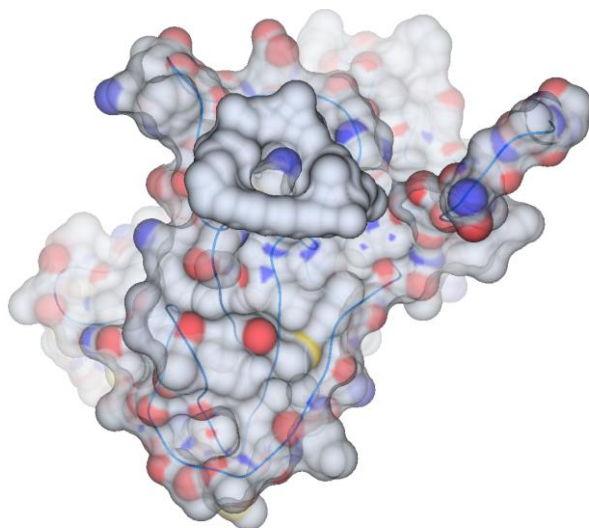


**Figure 6.3:3** - The binding pocket highlighted for nsp10 (3 Å - PDB 5C8T) including residues 5, 6, 14–16, 18, 40–42, 71, 72, 77–91 and 93. The binding site illustration with a macrocycle (opaque) was created in StarDrop 6.6.4.

**Table 6.3:2** - Summary of the hits in the testing with nsp10.

<b>Library</b>	<b>Crystal Structure</b>	<b>Through the first filters</b>	<b>Selected for testing</b>	<b>Hit validation ongoing</b>
<b>DDOP Hartmann</b> ~2,500 compounds	6ZPE	258	5	ongoing
<b>DDOP Hirsch</b> ~700 compounds	6ZPE	70	5	ongoing
<b>MINS Myxo</b> ~500 compounds	5C8T	6	4	1 (MS-assay)
	6ZPE	11	5	ongoing
<b>SpiroChem</b> ~700 compounds	6ZPE	66	13	ongoing
<b>SPECS</b> ~106,000 compounds	6ZPE	6926	ongoing	ongoing

*With thanks to HIPS-COVID team and  
in particular, Dr. Ravindra Jumde and Spyridon Bousis from the COVID VS team.*

## 7. References

- (1) Fleming, A. Penicillin's Finder Assays Its Future. *New York Times*. July 26, 1945, p 21.
- (2) Chellat, M. F.; Raguž, L.; Riedl, R. Targeting Antibiotic Resistance. *Angew. Chemie - Int. Ed.* **2016**, *55* (23), 6600–6626. <https://doi.org/10.1002/anie.201506818>.
- (3) Årdal, C.; Balasegaram, M.; Laxminarayan, R.; McAdams, D.; Outtersson, K.; Rex, J. H.; Sumpradit, N. Antibiotic Development — Economic, Regulatory and Societal Challenges. *Nat. Rev. Microbiol.* **2020**, *18* (5), 267–274. <https://doi.org/10.1038/s41579-019-0293-3>.
- (4) Cassini, A.; Högberg, L. D.; Plachouras, D.; Quattrocchi, A.; Hoxha, A.; Simonsen, G. S.; Colomb-Cotinat, M.; Kretzschmar, M. E.; Devleeschauwer, B.; Cecchini, M.; Ouakrim, D. A.; Oliveira, T. C.; Struelens, M. J.; Suetens, C.; Monnet, D. L.; Strauss, R.; Mertens, K.; Struyf, T.; Catry, B.; Latour, K.; Ivanov, I. N.; Dobрева, E. G.; Tambic Andrašević, A.; Soprek, S.; Budimir, A.; Paphitou, N.; Žemlicková, H.; Schytte Olsen, S.; Wolff Sönksen, U.; Märtin, P.; Ivanova, M.; Lyytikäinen, O.; Jalava, J.; Coignard, B.; Eckmanns, T.; Abu Sin, M.; Haller, S.; Daikos, G. L.; Gikas, A.; Tsiodras, S.; Kontopidou, F.; Tóth, Á.; Hajdu, Á.; Guólaugsson, Ó.; Kristinsson, K. G.; Murchan, S.; Burns, K.; Pezzotti, P.; Gagliotti, C.; Dumpis, U.; Liuimiene, A.; Perrin, M.; Borg, M. A.; de Greeff, S. C.; Monen, J. C.; Koek, M. B.; Elstrøm, P.; Zabicka, D.; Deptula, A.; Hryniewicz, W.; Caniça, M.; Nogueira, P. J.; Fernandes, P. A.; Manageiro, V.; Popescu, G. A.; Serban, R. I.; Schréterová, E.; Litvová, S.; Štefkovicová, M.; Kolman, J.; Klavs, I.; Korošec, A.; Aracil, B.; Asensio, A.; Pérez-Vázquez, M.; Billström, H.; Larsson, S.; Reilly, J. S.; Johnson, A.; Hopkins, S. Attributable Deaths and Disability-Adjusted Life-Years Caused by Infections with Antibiotic-Resistant Bacteria in the EU and the European Economic Area in 2015: A Population-Level Modelling Analysis. *Lancet Infect. Dis.* **2019**, *19* (1), 56–66. [https://doi.org/10.1016/S1473-3099\(18\)30605-4](https://doi.org/10.1016/S1473-3099(18)30605-4).
- (5) Getahun, H.; Smith, I.; Trivedi, K.; Paulin, S.; Balkhy, H. H. Tackling Antimicrobial Resistance in the COVID-19 Pandemic. *Bull. World Health Organ.* **2020**, *98* (7), 442–442A. <https://doi.org/10.2471/BLT.20.268573>.
- (6) Rice, L. B. Federal Funding for the Study of Antimicrobial Resistance in Nosocomial Pathogens: No ESKAPE. *J. Infect. Dis.* **2008**, *197* (8), 1079–1081. <https://doi.org/10.1086/533452>.
- (7) Gram, H. Ueber Die Isolirte Faerbung Der Schizomyceten : In Schnitt-Und Trockenpraeparaten. *Dtsch Med Wochenschr* **1884**, *10* (15), 234–235. <https://doi.org/10.1055/s-0029-1209285>.
- (8) Gilbert, D. N.; Guidos, R. J.; Boucher, H. W.; Talbot, G. H.; Spellberg, B.; Edwards, J. E.;

- Michael Scheld, W.; Bradley, J. S.; Bartlett As, J. G. The 10 X 20 Initiative: Pursuing a Global Commitment to Develop 10 New Antibacterial Drugs by 2020. *Clin. Infect. Dis.* **2010**, *50* (8), 1081–1083. <https://doi.org/10.1086/652237>.
- (9) Boucher, H. W.; Talbot, G. H.; Benjamin, D. K.; Bradley, J.; Guidos, R. J.; Jones, R. N.; Murray, B. E.; Bonomo, R. A.; Gilbert, D. 10 × '20 Progress - Development of New Drugs Active against Gram-Negative Bacilli: An Update from the Infectious Diseases Society of America. *Clin. Infect. Dis.* **2013**, *56* (12), 1685–1694. <https://doi.org/10.1093/cid/cit152>.
- (10) Five-Year Analysis Shows Continued Deficiencies in Antibiotic Development | The Pew Charitable Trusts <https://www.pewtrusts.org/en/research-and-analysis/data-visualizations/2019/five-year-analysis-shows-continued-deficiencies-in-antibiotic-development> (accessed Jan 28, 2021).
- (11) O'Neill, J. *Tackling Drug-Resistant Infections Globally: Final Report and Recommendations / the Review on Antimicrobial Resistance*; 2016.
- (12) Tacconelli, E.; Magrini, N. *Global Priority List of Antibiotic-Resistant Bacteria to Guide Research, Discovery, and Development of New Antibiotics*; 2017. <https://doi.org/10.1590/S0100-15742013000100018>.
- (13) WHO. *Antibacterial Agents in Clinical Development: An Analysis of the Antibacterial Clinical Development Pipeline*; 2019.
- (14) Global Antibiotic Research and Development Partnership <https://gardp.org/> (accessed Jan 28, 2021).
- (15) CARB-X <https://carb-x.org/> (accessed Jan 28, 2021).
- (16) AMR Action Fund <https://www.amractionfund.com/contact-us/> (accessed Jan 28, 2021).
- (17) World Antimicrobial Awareness Week 2020 <https://www.who.int/news-room/events/detail/2020/11/18/default-calendar/world-antimicrobial-awareness-week-2020> (accessed Jan 27, 2021).
- (18) WHO. *Technical Brief on Water, Sanitation, Hygiene and Wastewater Management to Prevent Infections and Reduce the Spread of Antimicrobial Resistance*; 2020.
- (19) McAdams, D.; Waldetoft, K. W.; Tedijanto, C.; Lipsitch, M.; Brown, S. P. Resistance Diagnostics as a Public Health Tool to Combat Antibiotic Resistance: A Modelbased Evaluation. *PLoS Biol.* **2019**, *17* (5), e3000250. <https://doi.org/10.1371/journal.pbio.3000250>.
- (20) Lewis, K. The Science of Antibiotic Discovery. *Cell* **2020**, *181* (1), 29–45.

- <https://doi.org/10.1016/j.cell.2020.02.056>.
- (21) Schwartz, D. J.; Langdon, A. E.; Dantas, G. Understanding the Impact of Antibiotic Perturbation on the Human Microbiome. *Genome Med.* **2020**, *12* (1), 82. <https://doi.org/10.1186/s13073-020-00782-x>.
- (22) Marchant, J. When Antibiotics Turn Toxic. *Nature* **2018**, *555* (7697), 431–433. <https://doi.org/10.1038/d41586-018-03267-5>.
- (23) Ribeiro, C. F. A.; Silveira, G. G. D. O. S.; Cândido, E. D. S.; Cardoso, M. H.; Espínola Carvalho, C. M.; Franco, O. L. Effects of Antibiotic Treatment on Gut Microbiota and How to Overcome Its Negative Impacts on Human Health. *ACS Infect. Dis.* **2020**, *6* (10), 2544–2559. <https://doi.org/10.1021/acsinfecdis.0c00036>.
- (24) Theuretzbacher, U.; Outtersson, K.; Engel, A.; Karlén, A. The Global Preclinical Antibacterial Pipeline. *Nat. Rev. Microbiol.* **2020**, *18*, 275–285. <https://doi.org/10.1038/s41579-019-0288-0>.
- (25) Encyclopaedia – REVIVE <https://revive.gardp.org/resources/encyclopaedia/> (accessed Jan 28, 2021).
- (26) Wagner, S.; Sommer, R.; Hinsberger, S.; Lu, C.; Hartmann, R. W.; Empting, M.; Titz, A. Novel Strategies for the Treatment of Pseudomonas Aeruginosa Infections. *J. Med. Chem.* **2016**, *59* (13), 5929–5969. <https://doi.org/10.1021/acs.jmedchem.5b01698>.
- (27) WHO Strategic Advisory Group on Malaria Eradication. *Malaria Eradication: Benefits, Future Scenarios and Feasibility. A Report of the Strategic Advisory Group on Malaria Eradication*; 2019.
- (28) WHO. *World Malaria Report 2020: 20 Years of Global Progress and Challenges*; 2020.
- (29) WHO. *WHO Malaria Terminology*; 2019.
- (30) Belete, T. M. Recent Progress in the Development of New Antimalarial Drugs with Novel Targets. *Drug Des. Devel. Ther.* **2020**, *14*, 3875–3889. <https://doi.org/10.2147/DDDT.S265602>.
- (31) Tse, E. G.; Korsik, M.; Todd, M. H. The Past, Present and Future of Anti-Malarial Medicines. *Malar. J.* **2019**, *18* (1), 1–21. <https://doi.org/10.1186/s12936-019-2724-z>.
- (32) WHO. *Guidelines for the Treatment of Malaria - 3rd Edition*; 2015.
- (33) IUPHAR/MMV Guide to Malaria Pharmacology <https://www.guidetomalariapharmacology.org/malaria/> (accessed Jan 28, 2021).
- (34) Rohmer, M.; Knani, M.; Simonin, P.; Sutter, B.; Sahm, H. Isoprenoid Biosynthesis in



- Bacteria: A Novel Pathway for the Early Steps Leading to Isopentenyl Diphosphate. *Biochem. J.* **1993**, 295 (2), 517–524. <https://doi.org/10.1042/bj2950517>.
- (35) Eisenreich, W.; Bacher, A.; Arigoni, D.; Rohdich, F. Biosynthesis of Isoprenoids via the Non-Mevalonate Pathway. *Cell. Mol. Life Sci.* **2004**, 61 (12), 1401–1426. <https://doi.org/10.1007/s00018-004-3381-z>.
- (36) Hedl, M.; Taberner, L.; Stauffacher, C. V.; Rodwell, V. W. Class II 3-Hydroxy-3-Methylglutaryl Coenzyme A Reductases. *J. Bacteriol.* **2004**, 186 (7), 1927–1932. <https://doi.org/10.1128/JB.186.7.1927-1932.2004>.
- (37) Heuston, S.; Begley, M.; Gahan, C. G. M.; Hill, C. Isoprenoid Biosynthesis in Bacterial Pathogens. *Microbiol. (United Kingdom)* **2012**, 158 (6), 1389–1401. <https://doi.org/10.1099/mic.0.051599-0>.
- (38) Patrick, G. L. Chapter 9 - Drug Targets in the Apicoplast. *Antimalar. Agents* **2020**, 319–374. <https://doi.org/10.1016/B978-0-08-101210-9.00009-3>.
- (39) DeColli, A. A.; Johnston, M. L.; Freel Meyers, C. L. Recent Insights Into Mechanism and Structure of MEP Pathway Enzymes and Implications for Inhibition Strategies. *Compr. Nat. Prod. III* **2020**, 4, 287–322. <https://doi.org/10.1016/b978-0-12-409547-2.14710-9>.
- (40) Frank, A.; Groll, M. The Methylerythritol Phosphate Pathway to Isoprenoids. *Chem. Rev.* **2017**, 117 (8), 5675–5703. <https://doi.org/10.1021/acs.chemrev.6b00537>.
- (41) Masini, T.; Hirsch, A. K. H. Development of Inhibitors of the 2C-Methyl-D-Erythritol 4-Phosphate (MEP) Pathway Enzymes as Potential Anti-Infective Agents. *J. Med. Chem.* **2014**, 57 (23), 9740–9763. <https://doi.org/10.1021/jm5010978>.
- (42) Bork, P.; Sander, C.; Valencia, A. Convergent Evolution of Similar Enzymatic Function on Different Protein Folds: The Hexokinase, Ribokinase, and Galactokinase Families of Sugar Kinases. *Protein Sci.* **1993**, 2 (1), 31–40. <https://doi.org/10.1002/pro.5560020104>.
- (43) Lange, B. M.; Croteau, R. Isopentenyl Diphosphate Biosynthesis via a Mevalonate-Independent Pathway: Isopentenyl Monophosphate Kinase Catalyzes the Terminal Enzymatic Step. *Proc. Natl. Acad. Sci. U. S. A.* **1999**, 96 (24), 13714–13719. <https://doi.org/10.1073/pnas.96.24.13714>.
- (44) Illarionova, V.; Kaiser, J.; Ostrozhenskova, E.; Bacher, A.; Fischer, M.; Eisenreich, W.; Rohdich, F. Nonmevalonate Terpene Biosynthesis Enzymes as Antiinfective Drug Targets: Substrate Synthesis and High-Throughput Screening Methods. *J. Org. Chem.* **2006**, 71 (23), 8824–8834. <https://doi.org/10.1021/jo061466o>.
- (45) Hirsch, A. K. H.; Alphey, M. S.; Lauw, S.; Seet, M.; Barandun, L.; Eisenreich, W.;

- Rohdich, F.; Hunter, W. N.; Bacher, A.; Diederich, F. Inhibitors of the Kinase IspE: Structure-Activity Relationships and Co-Crystal Structure Analysis. *Org. Biomol. Chem.* **2008**, *6* (15), 2719–2730. <https://doi.org/10.1039/b804375b>.
- (46) Crane, C. M.; Hirsch, A. K. H.; Alphey, M. S.; Sgraja, T.; Lauw, S.; Illarionova, V.; Rohdich, F.; Eisenreich, W.; Hunter, W. N.; Bacher, A.; Diederich, F. Synthesis and Characterization of Cytidine Derivatives That Inhibit the Kinase IspE of the Non-Mevalonate Pathway for Isoprenoid Biosynthesis. *ChemMedChem* **2008**, *3* (1), 91–101. <https://doi.org/10.1002/cmdc.200700208>.
- (47) Hirsch, A. K. H.; Lauw, S.; Gersbach, P.; Schweizer, W. B.; Rohdich, F.; Eisenreich, W.; Bacher, A.; Diederich, F. Nonphosphate Inhibitors of IspE Protein, a Kinase in the Non-Mevalonate Pathway for Isoprenoid Biosynthesis and a Potential Target for Antimalarial Therapy. *ChemMedChem* **2007**, *2* (6), 806–810. <https://doi.org/10.1002/cmdc.200700014>.
- (48) Tidten-Luksch, N.; Grimaldi, R.; Torrie, L. S.; Frearson, J. A.; Hunter, W. N. IspE Inhibitors Identified by a Combination of In Silico and In Vitro High-Throughput Screening. *PLoS One* **2012**, *7* (4), 35792. <https://doi.org/10.1371/journal.pone.0035792>.
- (49) Tang, M.; Wierenga, K.; Elsas, L. J.; Lai, K. Molecular and Biochemical Characterization of Human Galactokinase and Its Small Molecule Inhibitors. *Chem. Biol. Interact.* **2010**, *188* (3), 376–385. <https://doi.org/10.1016/j.cbi.2010.07.025>.
- (50) Tang, M.; Odejinmi, S. I.; Allette, Y. M.; Vankayalapati, H.; Lai, K. Identification of Novel Small Molecule Inhibitors of 4-Diphosphocytidyl-2-C-Methyl-d-Erythritol (CDP-ME) Kinase of Gram-Negative Bacteria. *Bioorg. Med. Chem.* **2011**, *19* (19), 5886–5895. <https://doi.org/10.1016/j.bmc.2011.08.012>.
- (51) Wierenga, K. J.; Lai, K.; Buchwald, P.; Tang, M. High-Throughput Screening for Human Galactokinase Inhibitors. *J. Biomol. Screen.* **2008**, *13* (5), 415–423. <https://doi.org/10.1177/1087057108318331>.
- (52) Giménez-Oya, V.; Villacañas, Ó.; Fernández-Busquets, X.; Rubio-Martinez, J.; Imperial, S. Mimicking Direct Protein-Protein and Solvent-Mediated Interactions in the CDP-Methylerythritol Kinase Homodimer: A Pharmacophore-Directed Virtual Screening Approach. *J. Mol. Model.* **2009**, *15* (8), 997–1007. <https://doi.org/10.1007/s00894-009-0458-5>.
- (53) Giménez-Oya, V.; Villacañas, Ó.; Obiol-Pardo, C.; Antolin-Llovera, M.; Rubio-Martinez, J.; Imperial, S. Design of Novel Ligands of CDP-Methylerythritol Kinase by Mimicking Direct Protein-Protein and Solvent-Mediated Interactions. *J. Mol. Recognit.* **2011**, *24* (1), 71–80. <https://doi.org/10.1002/jmr.1024>.

- (54) Hoerchler, K. B. Evaluation of IspE for Inhibitor Design in the Non-Mevalonate Pathway, 2018.
- (55) Goshu, G. M.; Ghose, D.; Bain, J. M.; Pierce, P. G.; Begley, D. W.; Hewitt, S. N.; Udell, H. S.; Myler, P. J.; Meganathan, R.; Hagen, T. J. Synthesis and Biological Evaluation of Pyrazolopyrimidines as Potential Antibacterial Agents. *Bioorganic Med. Chem. Lett.* **2015**, 25 (24), 5699–5704. <https://doi.org/10.1016/j.bmcl.2015.10.096>.
- (56) Goshu, G. M. Design and Synthesis of IspD, IspE and IspF Enzyme Inhibitors of the Methylerythritol Phosphate Pathway, 2016.
- (57) Witschel, M.; Röhl, F.; Niggeweg, R.; Newton, T. In Search of New Herbicidal Inhibitors of the Non-Mevalonate Pathway. *Pest Manag. Sci.* **2013**, 69 (5), 559–563. <https://doi.org/10.1002/ps.3479>.
- (58) Mombelli, P.; Witschel, M. C.; van Zijl, A. W.; Geist, J. G.; Rottmann, M.; Freymond, C.; Röhl, F.; Kaiser, M.; Illarionova, V.; Fischer, M.; Siepe, I.; Schweizer, W. B.; Brun, R.; Diederich, F. Identification of 1,3-Diiminoisoindoline Carbohydrazides as Potential Antimalarial Candidates. *ChemMedChem* **2012**, 7 (1), 151–158. <https://doi.org/10.1002/cmdc.201100441>.
- (59) Kadian, K.; Vijay, S.; Gupta, Y.; Rawal, R.; Singh, J.; Anvikar, A.; Pande, V.; Sharma, A. Structural Modeling Identifies Plasmodium Vivax 4-Diphosphocytidyl-2C-Methyl-D-Erythritol Kinase (IspE) as a Plausible New Antimalarial Drug Target. *Parasitol. Int.* **2018**, 67 (4), 375–385. <https://doi.org/10.1016/j.parint.2018.03.001>.
- (60) Bateman, A. UniProt: A Worldwide Hub of Protein Knowledge. *Nucleic Acids Res.* **2019**, 47 (D1), D506–D515. <https://doi.org/10.1093/nar/gky1049>.
- (61) EMBOSS: matcher <https://www.bioinformatics.nl/cgi-bin/emboss/matcher> (accessed Dec 22, 2020).
- (62) Rice, P.; Longden, L.; Bleasby, A. EMBOSS: The European Molecular Biology Open Software Suite. *Trends Genet.* **2000**, 16 (6), 276–277. [https://doi.org/10.1016/S0168-9525\(00\)02024-2](https://doi.org/10.1016/S0168-9525(00)02024-2).
- (63) Jin, Y.; Liu, Z.; Li, Y.; Liu, W.; Tao, Y.; Wang, G. A Structural and Functional Study on the 2-C-Methyl-d-Erythritol-4-Phosphate Cytidyltransferase (IspD) from Bacillus Subtilis. *Sci. Rep.* **2016**, 6 (1), 1–11. <https://doi.org/10.1038/srep36379>.
- (64) Huttner, B. D.; Catho, G.; Pano-Pardo, J. R.; Pulcini, C.; Schouten, J. COVID-19: Don't Neglect Antimicrobial Stewardship Principles! *Clin. Microbiol. Infect.* **2020**, 26 (7), 808–810. <https://doi.org/10.1016/j.cmi.2020.04.024>.

- (65) Collignon, P.; Beggs, J. J. CON: COVID-19 Will Not Result in Increased Antimicrobial Resistance Prevalence. *JAC-Antimicrobial Resist.* **2020**, *2* (3).  
<https://doi.org/10.1093/jacamr/dlaa051>.
- (66) Lu, J.; Guo, J. Disinfection Spreads Antimicrobial Resistance. **2021**, *371* (6528), 474.  
[https://doi.org/DOI: 10.1126/science.abg4380](https://doi.org/DOI:10.1126/science.abg4380).
- (67) Parkes, A. L. Antibacterial Medicinal Chemistry—What Can We Design For? *Expert Opin. Drug Discov.* **2020**, *00* (00), 1–9. <https://doi.org/10.1080/17460441.2020.1767065>.
- (68) Vergalli, J.; Bodrenko, I. V.; Masi, M.; Moynié, L.; Acosta-Gutiérrez, S.; Naismith, J. H.; Davin-Regli, A.; Ceccarelli, M.; van den Berg, B.; Winterhalter, M.; Pagès, J.-M. Porins and Small-Molecule Translocation across the Outer Membrane of Gram-Negative Bacteria. *Nat. Rev. Microbiol.* **2020**, *18*, 164–176. <https://doi.org/10.1038/s41579-019-0294-2>.
- (69) Richter, M. F.; Drown, B. S.; Riley, A. P.; Garcia, A.; Shirai, T.; Svec, R. L.; Hergenrother, P. J. Predictive Compound Accumulation Rules Yield a Broad-Spectrum Antibiotic. *Nature* **2017**, *545* (7654), 299–304. <https://doi.org/10.1038/nature22308>.
- (70) Richter, M. F.; Hergenrother, P. J. The Challenge of Converting Gram-Positive-Only Compounds into Broad-Spectrum Antibiotics. *Ann. N. Y. Acad. Sci.* **2019**, *1435* (1), 18–38. <https://doi.org/10.1111/nyas.13598>.
- (71) Parker, E. N.; Drown, B. S.; Geddes, E. J.; Lee, H. Y.; Ismail, N.; Lau, G. W.; Hergenrother, P. J. Implementation of Permeation Rules Leads to a FabI Inhibitor with Activity against Gram-Negative Pathogens. *Nat. Microbiol.* **2020**, *5*, 67–75. <https://doi.org/10.1038/s41564-019-0604-5>.
- (72) Smith, P. A.; Koehler, M. F. T.; Girgis, H. S.; Yan, D.; Chen, Y.; Chen, Y.; Crawford, J. J.; Durk, M. R.; Higuchi, R. I.; Kang, J.; Murray, J.; Paraselli, P.; Park, S.; Phung, W.; Quinn, J. G.; Roberts, T. C.; Rougé, L.; Schwarz, J. B.; Skippington, E.; Wai, J.; Xu, M.; Yu, Z.; Zhang, H.; Tan, M. W.; Heise, C. E. Optimized Arylomycins Are a New Class of Gram-Negative Antibiotics. *Nature* **2018**, *561* (7722), 189–194. <https://doi.org/10.1038/s41586-018-0483-6>.
- (73) Liu, B.; Lee Trout, R. E.; Chu, G.-H.; McGarry, D.; Jackson, R. W.; Hamrick, J. C.; Daigle, D. M.; Cusick, S. M.; Pozzi, C.; De Luca, F.; Benvenuti, M.; Mangani, S.; Docquier, J.-D.; Weiss, W. J.; Pevear, D. C.; Xerri, L.; Burns, C. J. Discovery of Taniborbactam (VNRX-5133): A Broad-Spectrum Serine- and Metallo- $\beta$ -Lactamase Inhibitor for Carbapenem-Resistant Bacterial Infections. *J. Med. Chem.* **2020**, *63*, 2789–2801. <https://doi.org/10.1021/acs.jmedchem.9b01518>.
- (74) Hu, Y.; Shi, H.; Zhou, M.; Ren, Q.; Zhu, W.; Zhang, W.; Zhang, Z.; Zhou, C.; Liu, Y.;

- Ding, X.; Shen, H. C.; Frank Yan, S.; Dey, F.; Wu, W.; Zhai, G.; Zhou, Z.; Xu, Z.; Ji, Y.; Lv, H.; Jiang, T.; Wang, W.; Xu, Y.; Vercruyssen, M.; Yao, X.; Mao, Y.; Yu, X.; Bradley, K.; Tan, X. Discovery of Pyrido[2,3-b]Indole Derivatives with Gram-Negative Activity Targeting Both DNA Gyrase and Topoisomerase IV. *J. Med. Chem.* **2020**, *63*, 9623–9649. <https://doi.org/10.1021/acs.jmedchem.0c00768>.
- (75) Motika, S. E.; Ulrich, R. J.; Geddes, E. J.; Lee, Y.; Lau, G. W.; Hergenrother, P. J. Gram-Negative Antibiotic Active Through Inhibition of an Essential Riboswitch. *J. Am. Chem. Soc.* **2020**, *142*, 10856–10862. <https://doi.org/10.1021/jacs.0c04427>.
- (76) Andrews, L. D.; Kane, T. R.; Dozzo, P.; Haglund, C. M.; Hilderbrandt, D. J.; Linsell, M. S.; Machajewski, T.; Mcenroe, G.; Serio, A. W.; Wlasichuk, K. B.; Neau, D. B.; Pakhomova, S.; Waldrop, G. L.; Sharp, M.; Pogliano, J.; Cirz, R. T.; Cohen, F. Optimization and Mechanistic Characterization of Pyridopyrimidine Inhibitors of Bacterial Biotin Carboxylase. *J. Med. Chem.* **2019**, *62*, 7489–7505. <https://doi.org/10.1021/acs.jmedchem.9b00625>.
- (77) Fosmidomycin <https://drugs.ncats.io/drug/5829E3D9I9> (accessed Sep 30, 2020).
- (78) Mombo-Ngoma, G.; Remppis, J.; Sievers, M.; Zoleko Manego, R.; Endamne, L.; Kabwende, L.; Veletzky, L.; Nguyen, T. T.; Groger, M.; Lötsch, F.; Mischlinger, J.; Flohr, L.; Kim, J.; Cattaneo, C.; Hutchinson, D.; Duparc, S.; Moehrle, J.; Velavan, T. P.; Lell, B.; Ramharter, M.; Adegnika, A. A.; Mordmüller, B.; Kremsner, P. G. Efficacy and Safety of Fosmidomycin-Piperaquine as Nonartemisinin-Based Combination Therapy for Uncomplicated Falciparum Malaria: A Single-Arm, Age De-Escalation Proof-of-Concept Study in Gabon. *Clin. Infect. Dis.* **2018**, *66* (12), 1823–1830. <https://doi.org/10.1093/cid/cix1122>.
- (79) Davey, M. S.; Tyrrell, J. M.; Howe, R. A.; Walsh, T. R.; Moser, B.; Toleman, M. A.; Eberl, M. A Promising Target for Treatment of Multidrug-Resistant Bacterial Infections. *Antimicrob. Agents Chemother.* **2011**, *55* (7), 3635–3636. <https://doi.org/10.1128/AAC.00382-11>.
- (80) Volkamer, A.; Kuhn, D.; Rippmann, F.; Rarey, M. DoGSiteScorer: A Web Server for Automatic Binding Site Prediction, Analysis and Druggability Assessment. *Bioinformatics* **2012**, *28* (15), 2074–2075. <https://doi.org/10.1093/bioinformatics/bts310>.
- (81) Volkamer, A.; Kuhn, D.; Grombacher, T.; Rippmann, F.; Rarey, M. Combining Global and Local Measures for Structure-Based Druggability Predictions. In *Journal of Chemical Information and Modeling*; American Chemical Society, 2012; Vol. 52, pp 360–372. <https://doi.org/10.1021/ci200454v>.

- (82) BioSolveIT - SeeSAR <https://www.biosolveit.de/SeeSAR/> (accessed Oct 1, 2020).
- (83) BioSolveIT - LeadIT <https://www.biosolveit.de/LeadIT/> (accessed Oct 1, 2020).
- (84) Montefiore, B.; Klingler, F.; Foster, N. A Novel Scoring Profile for the Design of Antibacterials Active against Gram-Negative Bacteria. 2018.
- (85) Slade, J. A.; Brockett, M.; Singh, R.; Liechti, G. W.; Maurelli, A. T. Fosmidomycin, an Inhibitor of Isoprenoid Synthesis, Induces Persistence in Chlamydia by Inhibiting Peptidoglycan Assembly. *PLoS Pathog.* **2019**, *15* (10), e1008078. <https://doi.org/10.1371/journal.ppat.1008078>.
- (86) Klarmann, E. DE649172, 1937.
- (87) Kindler, K.; Stobbe, H. DE824058, 1951.
- (88) Ciba Specialty Chemicals Holding Inc. WO 2007/009879 A1, 2007.
- (89) Cocker chemical Co. Ltd. DE2211266A1, 1972.
- (90) Chevalier, S.; Bouffartigues, E.; Bodilis, J.; Maillot, O.; Lesouhaitier, O.; Feuilloley, M. G. J.; Orange, N.; Dufour, A.; Cornelis, P. Structure, Function and Regulation of Pseudomonas Aeruginosa Porins. *FEMS Microbiol. Rev.* **2017**, *020*, 698–722. <https://doi.org/10.1093/femsre/fux020>.
- (91) Fernández, L.; Hancock, R. E. W. Adaptive and Mutational Resistance: Role of Porins and Efflux Pumps in Drug Resistance. *Clin. Microbiol. Rev.* **2012**, *25* (4), 661–681. <https://doi.org/10.1128/CMR.00043-12>.
- (92) Dötsch, A.; Becker, T.; Pommerenke, C.; Magnowska, Z.; Jänsch, L.; Häussler, S. Genomewide Identification of Genetic Determinants of Antimicrobial Drug Resistance in Pseudomonas Aeruginosa. *Antimicrob. Agents Chemother.* **2009**, *53* (6), 2522–2531. <https://doi.org/10.1128/AAC.00035-09>.
- (93) Richter, M. F.; Drown, B. S.; Riley, A. P.; Garcia, A.; Shirai, T.; Svec, R. L.; Hergenrother, P. J. Predictive Compound Accumulation Rules Yield a Broad-Spectrum Antibiotic. *Nature* **2017**, *545* (7654), 299–304. <https://doi.org/10.1038/nature22308>.
- (94) Mannhold, R. .; Kubinyi, H. .; Folkers, G. .; Cruciani, G. *Molecular Interaction Fields: Applications in Drug Discovery and ADME Prediction*; John Wiley & Sons, 2006.
- (95) Nikaido, H.; Thanassi, D. Penetration of Lipophilic Agents with Multiple Protonation Sites into Bacterial Cells: Tetracyclines and Fluoroquinolones as Examples. *Antimicrob. Agents Chemother.* **1993**, *37* (7), 1393–1399.
- (96) Chavan, S. P.; Lasonkar, P. B. One-Pot Migration-Formylation of Benzyl Aryl Ethers under

- Duff Reaction Condition. *Tetrahedron Lett.* **2013**, *54* (35), 4789–4792.  
<https://doi.org/10.1016/j.tetlet.2013.06.133>.
- (97) Cimperman, P.; Baranauskienė, L.; Jachimovičiute, S.; Jachno, J.; Torresan, J.; Michailoviene, V.; Matuliene, J.; Sereikaite, J.; Bumelis, V.; Matulis, D. A Quantitative Model of Thermal Stabilization and Destabilization of Proteins by Ligands. *Biophys. J.* **2008**, *95* (7), 3222–3231. <https://doi.org/10.1529/biophysj.108.134973>.
- (98) Chen, T.; Xiong, H.; Yang, J.-F.; Zhu, X.-L.; Qu, R.-Y.; Yang, G.-F. Diaryl Ether: A Privileged Scaffold for Drug and Agrochemical Discovery. *Cite This J. Agric. Food Chem* **2020**, *68*, 9839–9877. <https://doi.org/10.1021/acs.jafc.0c03369>.
- (99) Shrestha, P.; Zhang, Y.; Chen, W. J.; Wong, T. Y. Triclosan: Antimicrobial Mechanisms, Antibiotics Interactions, Clinical Applications, and Human Health. *J. Environ. Sci. Heal. Part C Toxicol. Carcinog.* **2020**, *38* (3), 245–268.  
<https://doi.org/10.1080/26896583.2020.1809286>.
- (100) Khan, R.; Zeb, A.; Choi, K.; Lee, G.; Lee, K. W.; Lee, S. W. Biochemical and Structural Insights Concerning Triclosan Resistance in a Novel YX7K Type Enoyl-Acyl Carrier Protein Reductase from Soil Metagenome. *Sci. Rep.* **2019**, *9* (1), 1–11.  
<https://doi.org/10.1038/s41598-019-51895-2>.
- (101) Wu, D. W.; Chen, T. C.; Huang, H. S.; Lee, H. TC-N19, a Novel Dual Inhibitor of EGFR and CMET, Efficiently Overcomes EGFR-TKI Resistance in Non-Small-Cell Lung Cancer Cells. *Cell Death Dis.* **2016**, *7* (6), e2290–e2290. <https://doi.org/10.1038/cddis.2016.192>.
- (102) Shrestha, N.; Nimick, M.; Dass, P.; Rosengren, R. J.; Ashton, J. C. Mechanisms of Suppression of Cell Growth by Dual Inhibition of ALK and MEK in ALK-Positive Non-Small Cell Lung Cancer. *Sci. Rep.* **2019**, *9* (1), 1–12. <https://doi.org/10.1038/s41598-019-55376-4>.
- (103) Zeng, X.; Yan, W.; Zacate, S. B.; Cai, A.; Wang, Y.; Yang, D.; Yang, K.; Liu, W. Copper-Catalyzed Deaminative Difluoromethylation. *Angew. Chemie Int. Ed.* **2020**, *59* (38), 16398–16403. <https://doi.org/10.1002/anie.202006048>.
- (104) Dormán, G.; Nakamura, H.; Pulsipher, A.; Prestwich, G. D. The Life of Pi Star: Exploring the Exciting and Forbidden Worlds of the Benzophenone Photophore. *Chem. Rev.* **2016**, *116* (24), 15284–15398. <https://doi.org/10.1021/acs.chemrev.6b00342>.
- (105) Gunawardana, I. W. K. Synthesis of Some Benzoxaza and Benzodioxaza Heterocycles: Use of the Meisenheimer Rearrangement Route to Fused Medium-Ring Systems, 1982.
- (106) Shaabani, S.; Shaabani, A.; Kucerakova, M.; Dusek, M. A One-Pot Synthesis of Oxazepine-

Quinazolinone Bis-Heterocyclic Scaffolds via Isocyanide-Based Three-Component Reactions. *Front. Chem.* **2019**, *7*, 623. <https://doi.org/10.3389/fchem.2019.00623>.

- (107) Jones, L. H.; Kelly, J. W. Structure-Based Design and Analysis of SuFEx Chemical Probes. *RSC Med. Chem.* **2020**, *11* (1), 10–17. <https://doi.org/10.1039/c9md00542k>.
- (108) Shah, F.; Louise-May, S.; Greene, N. Chemotypes Sensitivity and Predictivity of in Vivo Outcomes for Cytotoxic Assays in THLE and HepG2 Cell Lines. *Bioorganic Med. Chem. Lett.* **2014**, *24* (12), 2753–2757. <https://doi.org/10.1016/j.bmcl.2014.04.039>.
- (109) Lee, E. C. Y.; Steeno, G.; Wassermann, A. M.; Zhang, L.; Shah, F.; Price, D. A. Amine Promiscuity and Toxicology Analysis. *Bioorganic Med. Chem. Lett.* **2017**, *27* (3), 653–657. <https://doi.org/10.1016/j.bmcl.2016.11.085>.
- (110) Meanwell, N. A. Fluorine and Fluorinated Motifs in the Design and Application of Bioisosteres for Drug Design. *J. Med. Chem.* **2018**, *61* (14), 5822–5880. <https://doi.org/10.1021/acs.jmedchem.7b01788>.
- (111) Mehla, J.; Mallocci, G.; Mansbach, R.; López, C. A.; Tsivkovski, R.; Haynes, K.; Leus, I. V.; Grindstaff, S. B.; Cascella, R. H.; D’cunha, N.; Herndon, L.; Hengartner, N. W.; Margiotta, E.; Atzori, A.; Vargiu, A. V.; Manrique, P. D.; Walker, J. K.; Lomovskaya, O.; Ruggerone, P.; Gnanakaran, S.; Rybenkov, V. V.; Zgurskaya, H. I. Predictive Rules of Efflux Inhibition and Avoidance in *Pseudomonas Aeruginosa*. *MBio* **2021**, *12* (1), 1–19. <https://doi.org/10.1128/mBio.02785-20>.
- (112) Gustafson, J. Louis; Cardenas, M. M.; Nguyen, A. D.; Brown, Z. E.; Heydari, B. S.; Heydari, B. S.; Vaidya, S. D. Atropisomerism as Inspiration for New Chemistry. *Arkivoc* **2021**, *2021* (1). <https://doi.org/10.24820/ark.5550190.p011.382>.
- (113) Sugiki, T.; Furuita, K.; Fujiwara, T.; Kojima, C. Current NMR Techniques for Structure-Based Drug Discovery. *Molecules* **2018**, *23* (1), 1–27. <https://doi.org/10.3390/molecules23010148>.
- (114) Raingeval, C.; Cala, O.; Brion, B.; Le Borgne, M.; Hubbard, R. E.; Krimm, I. 1D NMR WaterLOGSY as an Efficient Method for Fragment-Based Lead Discovery. *J. Enzyme Inhib. Med. Chem.* **2019**, *34* (1), 1218–1225. <https://doi.org/10.1080/14756366.2019.1636235>.
- (115) Pettersen, E. F.; Goddard, T. D.; Huang, C. C.; Couch, G. S.; Greenblatt, D. M.; Meng, E. C.; Ferrin, T. E. UCSF Chimera - A Visualization System for Exploratory Research and Analysis. *J. Comput. Chem.* **2004**, *25* (13), 1605–1612. <https://doi.org/10.1002/jcc.20084>.
- (116) Pandey, D.; Kumari, B.; Singhal, N.; Kumar, M. BacEffluxPred: A Two-Tier System to



- Predict and Categorize Bacterial Efflux Mediated Antibiotic Resistance Proteins. **2020**.  
<https://doi.org/10.1038/s41598-020-65981-3>.
- (117) El Zahed, S. S.; French, S.; Farha, M. A.; Kumar, G.; Brown, E. D. Physicochemical and Structural Parameters Contributing to the Antibacterial Activity and Efflux Susceptibility of Small Molecule Inhibitors of Escherichia Coli . *Antimicrob. Agents Chemother.* **2021**, No. January. <https://doi.org/10.1128/aac.01925-20>.
- (118) Miallau, L.; Alphey, M. S.; Kemp, L. E.; Leonard, G. A.; McSweeney, S. M.; Hecht, S.; Bacher, A.; Eisenreich, W.; Rohdich, F.; Hunter, W. N. Biosynthesis of Isoprenoids: Crystal Structure of 4-Diphosphocytidyl-2C-Methyl-D-Erythritol Kinase. *Proc. Natl. Acad. Sci. U. S. A.* **2003**, *100* (16), 9173–9178. <https://doi.org/10.1073/pnas.1533425100>.
- (119) Volkamer, A.; Griewel, A.; Grombacher, T.; Rarey, M. Analyzing the Topology of Active Sites: On the Prediction of Pockets and Subpockets. *J. Chem. Inf. Model.* **2010**, *50* (11), 2041–2052. <https://doi.org/10.1021/ci100241y>.
- (120) Miallau, L.; Alphey, M. S.; Kemp, L. E.; Leonard, G. A.; McSweeney, S. M.; Hecht, S.; Bacher, A.; Eisenreich, W.; Rohdich, F.; Hunter, W. N. Biosynthesis of Isoprenoids: Crystal Structure of 4-Diphosphocytidyl-2C-Methyl-D-Erythritol Kinase. *Proc. Natl. Acad. Sci. U. S. A.* **2003**, *100* (16), 9173–9178. <https://doi.org/10.1073/pnas.1533425100>.
- (121) Lipinski, C. A.; Lombardo, F.; Dominy, B. W.; Feeney, P. J. Experimental and Computational Approaches to Estimate Solubility and Permeability in Drug Discovery and Development Settings. *Adv. Drug Deliv. Rev.* **2001**, *46*, 3–26.  
<https://doi.org/10.1016/j.addr.2012.09.019>.
- (122) Baell, J. B.; Willem Nissink, J. M. Seven Year Itch: Pan-Assay Interference Compounds (PAINS) in 2017—Utility and Limitations. *ACS Chem. Biol* **2018**, *13* (1), 36–44.  
<https://doi.org/10.1021/acscchembio.7b00903>.
- (123) Bruns, R. F.; Watson, I. A. Rules for Identifying Potentially Reactive or Promiscuous Compounds. *J. Med. Chem.* **2012**, *55* (22), 9763–9772. <https://doi.org/10.1021/jm301008n>.
- (124) GitHub - IanAWatson/Lilly-Medchem-Rules: Implementation of Lilly Medchem Rules - J Med Chem 2012 <https://github.com/IanAWatson/Lilly-Medchem-Rules> (accessed Oct 14, 2020).
- (125) BioSolveIT - KNIME Interfaces <https://www.biosolveit.de/KNIME/> (accessed Oct 14, 2020).
- (126) Berthold, M. R.; Cebren, N.; Dill, F.; Gabriel, T. R.; Kötter, T.; Meinl, T.; Ohl, P.; Sieb, C.; Thiel, K.; Wiswedel, B. *Studies in Classification, Data Analysis, and Knowledge*

*Organization - KNIME The {K}onstanz {I}nformation {M}iner*; Springer, 2007.

- (127) Elgaher, W. A. M.; Fruth, M.; Groh, M.; Hauptenthal, J.; Hartmann, R. W. Expanding the Scaffold for Bacterial RNA Polymerase Inhibitors: Design, Synthesis and Structure-Activity Relationships of Ureido-Heterocyclic-Carboxylic Acids. *RSC Adv.* **2014**, *4* (5), 2177–2194. <https://doi.org/10.1039/c3ra45820b>.
- (128) Van Rossum, G.; Drake, F. L. *Python 3 Reference Manual*; Scotts Valley, CA: CreateSpace, 2009.
- (129) Hauptenthal, J.; Baehr, C.; Zeuzem, S.; Piiper, A. RNase A-like Enzymes in Serum Inhibit the Anti-Neoplastic Activity of SiRNA Targeting Polo-like Kinase 1. *Int. J. Cancer* **2007**, *121* (1), 206–210. <https://doi.org/10.1002/ijc.22665>.
- (130) Peters, J. M.; Colavin, A.; Shi, H.; Czarny, T. L.; Larson, M. H.; Wong, S.; Hawkins, J. S.; Lu, C. H. S.; Koo, B. M.; Marta, E.; Shiver, A. L.; Whitehead, E. H.; Weissman, J. S.; Brown, E. D.; Qi, L. S.; Huang, K. C.; Gross, C. A. A Comprehensive, CRISPR-Based Functional Analysis of Essential Genes in Bacteria. *Cell* **2016**, *165* (6), 1493–1506. <https://doi.org/10.1016/j.cell.2016.05.003>.
- (131) Gierse, R. M.; Reddem, E. R.; Alhayek, A.; Baitinger, D.; Hamid, Z.; Jakobi, H.; Laber, B.; Lange, G.; Hirsch, A. K. H.; Groves, M. R. Identification of a 1-Deoxy-D-Xylulose-5-Phosphate Synthase (DXS) Mutant with Improved Crystallographic Properties. *Biochem. Biophys. Res. Commun.* **2021**, *539*, 42–47. <https://doi.org/10.1016/j.bbrc.2020.12.069>.
- (132) Green, K.; Fosso, M.; Garneau-Tsodikova, S. Multifunctional Donepezil Analogues as Cholinesterase and BACE1 Inhibitors. *Molecules* **2018**, *23* (12), 3252. <https://doi.org/10.3390/molecules23123252>.
- (133) Manasieva, L. I.; Maria, B. U.; Prandi, A.; Brasili, L.; Franchini, S. Synthesis of Heteroaryl Ortho -Phenoxyethylamines via Suzuki Cross-Coupling: Easy Access to New Potential Scaffolds in Medicinal Chemistry. *Synth.* **2015**, *47* (23), 3767–3775. <https://doi.org/10.1055/s-0035-1560456>.
- (134) ADDEX PHARMA S.A. WO2011/86163, 2019.
- (135) Rai, N. P.; Venu, T. D.; Manuprasad, B. K.; Shashikanth, S.; Arunachalam, P. N.; Firdouse, A. Synthesis of Some Novel 2-[2-(Aroyl-Aroxy)-Methyl]-4-Phenyl-1,3-Thiazoles as Potent Anti-Inflammatory Agents: Research Letter. *Chem. Biol. Drug Des.* **2010**, *75* (4), 400–406. <https://doi.org/10.1111/j.1747-0285.2009.00932.x>.
- (136) Eli Lilly and Company. WO2005019151, 2005.
- (137) Rath, C. M.; Benton, B. M.; De Vicente, J.; Drumm, J. E.; Geng, M.; Li, C.; Moreau, R. J.;

- Shen, X.; Skepper, C. K.; Steffek, M.; Takeoka, K.; Wang, L.; Wei, J. R.; Xu, W.; Zhang, Q.; Feng, B. Y. Optimization of CoaD Inhibitors against Gram-Negative Organisms through Targeted Metabolomics. *ACS Infect. Dis.* **2018**, *4* (3), 391–402.  
<https://doi.org/10.1021/acsinfectdis.7b00214>.
- (138) Yeh, E.; DeRisi, J. L. Chemical Rescue of Malaria Parasites Lacking an Apicoplast Defines Organelle Function in Blood-Stage Plasmodium Falciparum. *PLoS Biol.* **2011**, *9* (8), e1001138. <https://doi.org/10.1371/journal.pbio.1001138>.
- (139) Zhang, B.; Watts, K. M.; Hodge, D.; Kemp, L. M.; Hunstad, D. A.; Hicks, L. M.; Odom, A. R. A Second Target of the Antimalarial and Antibacterial Agent Fosmidomycin Revealed by Cellular Metabolic Profiling. *Biochemistry* **2011**, *50* (17), 3570–3577.  
<https://doi.org/10.1021/bi200113y>.
- (140) Edwards, R. L.; Brothers, R. C.; Wang, X.; Maron, M. I.; Ziniel, P. D.; Tsang, P. S.; Kraft, T. E.; Hruz, P. W.; Williamson, K. C.; Dowd, C. S.; Odom John, A. R. MEPicides: Potent Antimalarial Prodrugs Targeting Isoprenoid Biosynthesis. *Sci. Rep.* **2017**, *7*.  
<https://doi.org/10.1038/s41598-017-07159-y>.
- (141) Vickers, C. E.; Bongers, M.; Bydder, S. F.; Chrysanthopoulos, P.; Hodson, M. P. Protocols for the Production and Analysis of Isoprenoids in Bacteria and Yeast. In *Hydrocarbon and Lipid Microbiology Protocols. Springer Protocols Handbooks*; Springer, Berlin, Heidelberg, 2015; pp 23–52. [https://doi.org/10.1007/8623\\_2015\\_107](https://doi.org/10.1007/8623_2015_107).
- (142) Zhou, K.; Zou, R.; Stephanopoulos, G.; Too, H.-P. Metabolite Profiling Identified Methylerythritol Cyclodiphosphate Efflux as a Limiting Step in Microbial Isoprenoid Production. *PLoS One* **2012**, *7* (11), e47513. <https://doi.org/10.1371/journal.pone.0047513>.
- (143) Bongers, M.; Chrysanthopoulos, P. K.; Y H Behrendorff, J. B.; Hodson, M. P.; Vickers, C. E.; Nielsen, L. K. Systems Analysis of Methylerythritol-Phosphate Pathway Flux in E. Coli: Insights into the Role of Oxidative Stress and the Validity of Lycopene as an Isoprenoid Reporter Metabolite. *Microb. Cell Fact.* **2015**, *14* (1). <https://doi.org/10.1186/s12934-015-0381-7>.
- (144) Li, Z.; Sharkey, T. D. Metabolic Profiling of the Methylerythritol Phosphate Pathway Reveals the Source of Post-Illumination Isoprene Burst from Leaves. *Plant, Cell Environ.* **2013**, *36* (2), 429–437. <https://doi.org/10.1111/j.1365-3040.2012.02584.x>.
- (145) Häubl, G.; Berthiller, F.; Krska, R.; Schuhmacher, R. Suitability of a Fully <sup>13</sup>C Isotope Labeled Internal Standard for the Determination of the Mycotoxin Deoxynivalenol by LC-MS/MS without Clean Up. *Anal. Bioanal. Chem.* **2006**, *384* (3), 692–696.  
<https://doi.org/10.1007/s00216-005-0218-z>.

- (146) Phenomenex. *The Complete Guide to Solid Phase Extraction (SPE): A Method Development and Application Guide*; 2017.
- (147) Vázquez, J.; Deplano, A.; Herrero, A.; Ginex, T.; Gibert, E.; Rabal, O.; Oyarzabal, J.; Herrero, E.; Luque, F. J. Development and Validation of Molecular Overlays Derived from Three-Dimensional Hydrophobic Similarity with PharmScreen. *J. Chem. Inf. Model.* **2018**, *58* (8), 1596–1609. <https://doi.org/10.1021/acs.jcim.8b00216>.
- (148) Coronavirus Update (Live): 93,688,066 Cases and 2,005,773 Deaths from COVID-19 Virus Pandemic - Worldometer <https://www.worldometers.info/coronavirus/> (accessed Jan 15, 2021).
- (149) Romano, M.; Ruggiero, A.; Squeglia, F.; Maga, G.; Berisio, R. A Structural View of SARS-CoV-2 RNA Replication Machinery: RNA Synthesis, Proofreading and Final Capping. *Cells* **2020**, *9* (5), 1267. <https://doi.org/10.3390/cells9051267>.
- (150) Gao, Y.; Yan, L.; Huang, Y.; Liu, F.; Zhao, Y.; Cao, L.; Wang, T.; Sun, Q.; Ming, Z.; Zhang, L.; Ge, J.; Zheng, L.; Zhang, Y.; Wang, H.; Zhu, Y.; Zhu, C.; Hu, T.; Hua, T.; Zhang, B.; Yang, X.; Li, J.; Yang, H.; Liu, Z.; Xu, W.; Guddat, L. W.; Wang, Q.; Lou, Z.; Rao, Z. Structure of the RNA-Dependent RNA Polymerase from COVID-19 Virus. *Science* (80-. ). **2020**, *368* (6492), 779–782. <https://doi.org/10.1126/science.abb7498>.
- (151) Gordon, C. J.; Tchesnokov, E. P.; Feng, J. Y.; Porter, D. P.; Götte, M. The Antiviral Compound Remdesivir Potently Inhibits RNA-dependent RNA Polymerase from Middle East Respiratory Syndrome Coronavirus. *J. Biol. Chem.* **2020**, *295* (15), 4773–4779. <https://doi.org/10.1074/jbc.AC120.013056>.
- (152) Ma, Y.; Wu, L.; Shaw, N.; Gao, Y.; Wang, J.; Sun, Y.; Lou, Z.; Yan, L.; Zhang, R.; Rao, Z. Structural Basis and Functional Analysis of the SARS Coronavirus Nsp14-Nsp10 Complex. *Proc. Natl. Acad. Sci. U. S. A.* **2015**, *112* (30), 9436–9441. <https://doi.org/10.1073/pnas.1508686112>.
- (153) Rogstam, A.; Nyblom, M.; Christensen, S.; Sele, C.; Talibov, V. O.; Lindvall, T.; Rasmussen, A. A.; André, I.; Fisher, Z.; Knecht, W.; Kozielski, F. Crystal Structure of Non-Structural Protein 10 from Severe Acute Respiratory Syndrome Coronavirus-2. *Int. J. Mol. Sci.* **2020**, *21* (19), 7375. <https://doi.org/10.3390/ijms21197375>.

## 8. Conference Contributions

### *Oral Presentations*

H.-K. Ropponen, "Design and Synthesis of Inhibitors of the Anti-Infective Target Enzyme IspE", Regionales Fonds-Stipendiatentreffen, December 2019, Karlsruhe, Germany.

Issued by W. M. Klopper, *Nachrichten aus der Chemie*, **2020**, DOI:10.1002/nadc.20204096381.

H.-K. Ropponen, "Design and Synthesis of Inhibitors of the Anti-Infective Target Enzyme IspE", Sommersymposium der Graduierten Naturstoffforschung, July 2019, Saarbrücken, Germany.

### *Poster Presentations*

#### **Hit-Identification Strategies for the Anti-Infective Target Enzyme IspE**

H.-K. Ropponen, E. Diamanti, B. Illarionov, J. Hauptenthal, K. Rox, M. Brönstrup, M. Fischer, M. Rottmann, F. Diederich, M. Witschel and A. K. H. Hirsch

Presented at

- 10<sup>th</sup> International HIPS Symposium, June 2019, Saarbrücken, Germany.
- RSC Medicinal Chemistry Residential School 2019, June 2019, Loughborough, UK.
- Frontiers in Medicinal Chemistry, March 2019, Würzburg, Germany.

#### **Anti-Infective Target Enzyme IspE**

– *Optimising the balance between enzymatic and cellular activity*

H.-K. Ropponen, E. Diamanti, B. Illarionov, J. Hauptenthal, M. Fischer and A. K. H. Hirsch

Presented at

- 2<sup>nd</sup> Anglo-Swiss Symposium on MedChem, February 2020, Basel, Switzerland.
- TTU NAB Treffen, Oktober 2019, Saarbrücken, Germany.
- (Accepted for an oral presentation FJS Cologne, March 2020, cancelled due to COVID-19)

## 9. Curriculum Vitae

### **Henni-Karoliina Ropponen**

born on 25<sup>th</sup> September 1994 in Varkaus, Finland

#### **Education**

- 2018–2021** PhD in the group of Prof. Dr. Anna K. H. Hirsch  
Helmholtz Institute for Pharmaceutical Research Saarland,  
Saarbrücken, Germany  
*awarded with the Kekulé Mobility Fellowship (2019–2021)*
- 2013–2018** Master of Chemistry with Drug Discovery  
University of Strathclyde, Glasgow, UK  
*graduated with the Andersonian Centenary Medal Prize*
- 2010–2013** International Baccalaureate (IB)  
Kuopion Lysen lukio, Kuopio, Finland
- 2011–2012** Scottish Highers (High School Exchange)  
Peebles High School, Peebles, UK
- 2000–2011** Finnish Primary Education  
Puurtilan ala-aste & Päiviönsaaren yläaste, Varkaus, Finland

#### **Research Experiences**

- 2017–2018** Master's Thesis in the group of Dr. Vânia Moreira,  
University of Strathclyde, Glasgow, UK
- 2016–2017** Roche Internship in Medicinal Chemistry (RiCH)  
F. Hoffmann-La Roche, Basel, Switzerland
- 2015 & 2016** Laboratory Analyst  
Savo-Karjalan Ympäristötutkimus Oy, Kuopio, Finland